

# EXTRUSION OF ALUMINIUM ALLOYS

# **EXTRUSION OF ALUMINIUM ALLOYS**

---

**PROFESSOR T. SHEPPARD**

D.Sc, Ph.D., F.I.M., C.Eng., F.I.Mech.E.

Department of Product Design and Manufacture,  
Bournemouth University



**SPRINGER-SCIENCE+BUSINESS MEDIA, B.V.**

A C.I.P. Catalogue record for this book is available from the Library of Congress

ISBN 978-1-4419-4728-4      ISBN 978-1-4757-3001-2 (eBook)  
DOI 10.1007/978-1-4757-3001-2

All Rights Reserved

© 1999 Springer Science+Business Media Dordrecht  
Originally published by Kluwer Academic Publishers in 1999  
Softcover reprint of the hardcover 1st edition 1999

No part of the material protected by this copyright notice may be reproduced or utilized in any form or by any means, electronic or mechanical, including photocopying, recording, or by information storage and retrieval system, without written permission from the copyright owner.

# Contents

Preface	xi
<b>1 Introduction</b>	<b>1</b>
1.1 Brief history of the extrusion process	1
1.1.1 The origin of extrusion	2
1.1.2 Extrusion presses for sheathing electric cables	3
1.1.3 Application of extrusion to copper alloys	3
1.2 The thermomechanical process	6
1.3 Direct and indirect extrusion	7
1.3.1 Direct extrusion	8
1.3.2 Indirect extrusion	11
1.4 Extrusion of rods and solid shapes	12
1.5 Extrusion of hollow sections	14
1.6 The extrusion press	16
1.6.1 Direct presses	16
1.6.2 Indirect presses	20
<b>2 Continuum principles</b>	<b>24</b>
2.1 Yielding and ductility	24
2.2 Constitutive equations	27
2.3 The extrusion pressure	29
2.3.1 Bulk analysis	30
2.3.2 The upper-bound theorem	31
2.3.3 Finite-element solutions	37
2.3.4 Comparison of finite-element modelling with upper-bound and slip-line field techniques	38
2.4 The friction coefficient	48
2.5 Temperature models	49
2.5.1 Temperature profile in the heated billet	49
2.5.2 Heat balance in extrusion	50
2.5.3 Finite-element modelling predictions	53



2.5.4	Thermal balance during extrusion predicted by integral profile techniques	55
2.6	Diffusion	61
2.6.1	Fick's laws of diffusion	62
2.6.2	Solutions to the diffusion equation	63
2.6.3	Problems in which $D$ varies with composition	66
<b>3</b>	<b>Metallurgical features affecting the extrusion of aluminium alloys</b>	<b>69</b>
3.1	Aluminium-alloy systems	69
3.1.1	The 1XXX system	69
3.1.2	The 2XXX system	70
3.1.3	The 3XXX system	72
3.1.4	The 4XXX system	72
3.1.5	The 5XXX system	72
3.1.6	The AA6XXX system	76
3.1.7	The AA7XXX system	81
3.1.8	Aluminium–lithium alloys	86
3.2	The DC cast state	90
3.3	Homogenization	93
3.3.1	Atomic movements and $D$	95
3.3.2	Metallurgical consideration of homogenization	102
3.4	Thermal activation	110
3.5	Recovery and recrystallization	113
3.5.1	Dynamic recovery and dynamic recrystallization	114
3.5.2	Microstructure	115
3.6	Recrystallization and layer thickness after solution soaking	116
3.7	Quench sensitivity	119
<b>4</b>	<b>Extrusion processing</b>	<b>127</b>
4.1	Introduction	127
4.2	The Zener–Hollomon parameter and flow stress	127
4.2.1	Flow stress	127
4.2.2	Theoretical considerations	129
4.2.3	Comparison of compression and torsion in material assessment	130
4.3	Material flow in extrusion	136
4.3.1	The three types of flow	136
4.4	The pressure/displacement diagram	140
4.5	The strain rate during extrusion	141
4.6	Extrusion pressure – practical considerations	143
4.6.1	The effect of friction	144
4.6.2	The effect of the temperature-compensated strain rate	144
4.6.3	The effect of section shape	146
4.7	Surface quality considerations	151

4.8	Process–structure relationships	156
4.9	Recrystallization	160
4.9.1	Structure after extrusion	160
4.9.2	Volume fraction recrystallization in the F-temper and after solution soaking	166
4.10	The relationship between process parameters and properties	170
4.11	Material flow and inhomogeneity – structural considerations	176
4.11.1	Development of structure in the extrusion container	176
4.11.2	Substructural considerations	179
4.11.3	Extrudate structure	183
4.11.4	Subgrain size	184
4.11.5	Development of dislocation structure related to peak pressure	185
4.12	Press quenching and press solutionizing	186
4.12.1	Introduction	186
4.12.2	Metallurgical aspects	188
4.12.3	Technological problems	191
4.13	Limit diagrams	198
<b>5</b>	<b>Homogenization and extrusion conditions for specific alloys</b>	<b>205</b>
5.1	Introduction	205
5.2	1XXX alloys	206
5.3	2XXX alloys	208
5.4	3XXX alloys	216
5.5	4XXX alloys	219
5.6	5XXX alloys	221
5.7	6XXX alloys	227
5.8	7XXX alloys	227
5.8.1	Al–Zn–Mg alloys	227
5.8.2	Al–Zn–Mg–Cu alloys	232
5.9	Aluminium–lithium alloys	236
5.10	Extrudability, limit and productivity diagrams	238
5.10.1	Extrudability	238
5.10.2	Limit diagrams	240
5.10.3	Productivity diagrams	245
<b>6</b>	<b>Processing of 6XXX alloys</b>	<b>253</b>
6.1	Homogenization	253
6.1.1	General principles of heat treatment	253
6.2	Alloys for specific applications	261
6.2.1	High extrudability, general purpose alloys	261
6.2.2	Medium-strength alloys	263
6.3	Factors affecting quench sensitivity	267
6.3.1	Cooling rate	267

6.3.2	Recrystallization inhibitors	269
6.3.3	Toughness	270
6.3.4	Structural sensitivity	270
6.3.5	Quench sensitivity in welding	270
6.4	Surface problems and surface generation	272
6.4.1	Introduction	272
6.4.2	Surface features	274
6.4.3	Extrusion topology (limit) diagrams	291
6.4.4	Summary	293
6.5	Alternative metallurgical diagrams	295
6.5.1	Possible phase transformations	296
6.6	Texture	301
6.7	Extrusion defects	303
6.7.1	Metallurgical factors affecting press productivity	303
6.7.2	Recovery related defects	307
6.7.3	Metallurgical defects visible after anodizing	317
<b>7</b>	<b>Plant utilization</b>	<b>323</b>
7.1	Introduction	323
7.2	The modern extrusion plant	323
7.2.1	The extrusion press	324
7.2.2	Ancillary equipment	327
7.2.3	The extrusion process and parameter optimizing	330
7.3	Press requirements	331
7.3.1	Reliability	332
7.3.2	Mechanics	332
7.3.3	Hydraulics	335
7.3.4	Control and monitoring	335
7.4	Isothermal extrusion	340
7.4.1	Process optimization	342
7.4.2	Features required in a comprehensive process optimization	343
7.4.3	Results of process optimization	345
7.5	Expert systems	351
7.5.1	An expert system applied to an extrusion press	353
7.5.2	A typical system description	354
7.6	Aspects of die design and correction	357
7.6.1	Die stack considerations	360
7.6.2	Die design steps	360
7.6.3	Process factors to consider before modifying the die	370
7.7	Tool failure	374
7.7.1	Characteristics	374
7.7.2	Preventative measures	374
7.8	Scrap losses	375
7.8.1	Extrusion losses	376

7.8.2 Billet scrap	378
7.9 Extrusion control in manufacturing profiles of complex shapes	380
7.9.1 Classification of complex shapes	380
7.9.2 Improvement of billet quality	381
7.9.3 Extrusion press alignment	381
7.9.4 Extrusion condition	382
7.10 Product tolerance	382
7.10.1 Die section	382
7.10.2 Extrusion section	384
7.10.3 Billet section	385
7.10.4 Extrusion conditions	385
7.10.5 Improvements in yield	385
<b>Appendix 1</b> International alloy designations and chemical composition limits for wrought aluminium and wrought aluminium alloys	<b>389</b>
<b>Appendix 2</b> Conversion factors for some common units	<b>401</b>
<b>Appendix 3</b> Temper designations	<b>405</b>
<b>Index</b>	<b>409</b>

# Preface

Aluminium extrusions have become much more widely used in the last decade. The largest expansion being in the architectural field but in both aerospace and in automotive applications significant advances have been achieved. Significantly this expansion has been accompanied by a demand for increased quality both in dimensional tolerance and in property specification. Much research has been published especially in Germany and the United Kingdom and the research groups at SINTEF, Trondheim and at Imperial College, London have been recognized as producing significant contributions. The large extrusion companies have also published and the author recognizes the excellent work published by Norsk-Hydro, Alcan International, Alussuisse, Reynolds Pechenet and Alcoa. Individuals in each of these companies have been invaluable in discussions on various topics and for this I express my sincere thanks.

The aim of this book is to view the extrusion process as a thermomechanical event: hence individual press design is not considered although the more important and relevant features of both design and essential practice are discussed at length in the final chapter. I also consider it necessary to give the reader the opportunity to study the continuum plasticity, metallurgy and diffusion background theory and to show how this may be applied in practice. Hence individual chapters are introduced to cover these subjects. Extrusion may now be considered in a theoretical manner and I am hopeful that this text will assist the practical extruder as well as those working in research centres and Universities to approach the process to achieve the required dimensional and property requirements.

Each group of aluminium alloys are considered separately with a separate chapter devoted to the 6XXX alloys which are the most widely produced. I am deeply indebted to Dr Nick Parsons of Alcan International and to Dr Mike Clode for assistance in preparing this chapter. In this context I also recognize the contribution of Comalco research laboratories in Melbourne where I was fortunate to spend several months stretched over three years.

Each of my research students have contributed via their thesis, but special thanks are due to Dr. A.F. Castle, Dr. M.G. Tutchter, Dr. S.J. Patterson and to the input of Professor H M Flower to the theses.

I must also recognize the very important role played by the Aluminum Association, Washington DC who, together with the American Extruders Council, have organized conferences every four years. In the same context, the input of Bob Werner to these conferences has been outstanding. The proceedings of these conferences have provided a rich source of reference material.

Finally my thanks to all the countless journals for permission to use illustrations and to SMS Schloemann for their assistance with Chapter 7.

Terry Sheppard, Bournemouth, June 1998.

# Introduction

1

## 1.1 BRIEF HISTORY OF THE EXTRUSION PROCESS

Although extrusion is a modern process (rolling and forging being much older) it precedes the development of aluminium which was only commercially available following the invention in 1886, concurrently by Hall and Heroult, of the electrolytic process to extract the metal from bauxite. Among the industrial methods by which aluminium billets can be transformed to exceedingly complex shapes, extrusion has no rival and has firmly established itself as a major industrial process. The process converts a cast billet of solid metal into a continuous length of generally uniform cross-section by forcing it to flow through a die which is shaped to produce the required form of product. Generally it is a hot working operation, the metal being heated to give it a suitable flow stress (i.e. degree of softness and ductility); but it can also, in some instances, be carried out in the cold. In the modern process, cast billets of cylindrical shape, loaded into a composite cylinder (the container), are extruded through the die under pressure exerted by a ram, actuated hydraulically.

Figure 1.1 illustrates the essential principle of the process, and, at the same time, the distinction between two methods of working, known as direct and indirect extrusion. These depend on the arrangement of the tools. In direct extrusion, the die is located at one end of the container and the metal to be extruded is pushed towards it, hence moving relative to the container. In the case of indirect extrusion, the die is placed on the end of the ram, which is bored out to allow passage of the extruded section, and moves through the container from one end, the opposite end being closed. It is, in fact, generally more convenient, in using the indirect process, for the container to travel and for the die to be attached to a stationary ram or, as it now becomes, a die assembly which is attached to a fixed crosshead on the press frame.

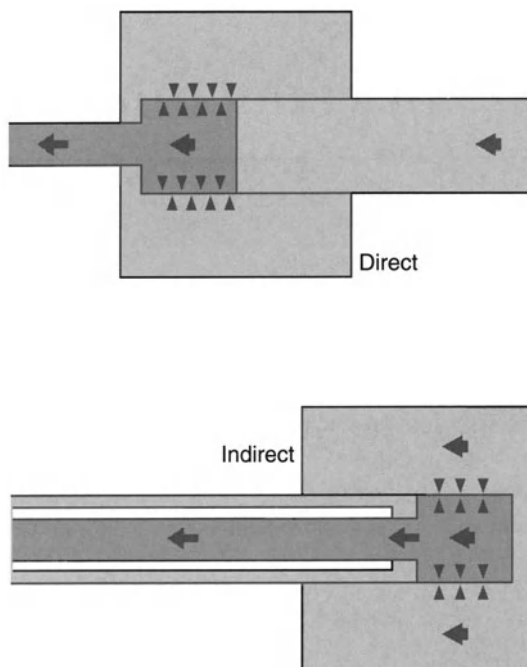


Fig. 1.1 Direct and indirect extrusion.

### 1.1.1 The origin of extrusion

The earliest consideration of the principles of extrusion was due to Joseph Bramah, the famous hydraulic engineer, who, in a patent granted in 1797, described a press in which lead, maintained molten in an iron pot, was forced by a pump into a long projecting tube, which served as a die. A tapered mandrel was supported concentrically with the tube by a bridge in its enlarged end. The lead passing through the annular space between the tube and mandrel was kept molten by the fuel gases inside the outer casing until it approached the outlet, where it was chilled to cause it to solidify so that it emerged in the form of a pipe. Though it is doubtful whether any such machine ever operated satisfactorily, it claims attention in providing the first record of a machine which clearly contains the idea of extrusion, whilst also suggesting the idea of die-casting. It was not until 1820, when Thomas Burr, a Shrewsbury plumber, constructed a press operated by hydraulic power, that the manufacture of lead pipes by extrusion came into actual operation.

In 1863, Shaw used a press in which precast hollow billets of lead, with an internally cast sleeve of tin, were charged cold into the container. Several billet presses of this kind were designed, but records show that very considerable difficulty was



met in arriving at the correct shape of sleeve to give a uniform lining of tin in the pipe. A remarkable press for this work, invented in France by Hamon in 1867, showed many advanced features. The principal points of interest were:

- A fixed mandrel bar was used, into which could be screwed tips of different sizes, over which the extrusion ram travelled.
- The container was made with ducts in its outer jacket through which steam or hot gases could be circulated to raise its temperature to about 210°C. This provides the first example of the use of a heated container. Pointing out the necessity for careful adjustment of the temperature to avoid melting the tin sleeve, Hamon suggested the use of a pyrometer.
- An auxiliary hydraulic ram was used to bring the die and die-holder into position against the container, where it was locked.
- An accumulator was introduced into the hydraulic system. Although the hydraulic accumulator had been invented by Sir William Armstrong in 1840, it does not appear to have been used before this in connection with extrusion.

The next stage in the evolution of the pipe press came with the introduction by Haines, and by J. and W. Weems, both in 1870, of the indirect mode of extrusion. On the application of this method to copper alloys at a much later date, it was shown to have the effect of altering the deformation flow in the billet and thus exaggerating the back-end defect common to this material. We will return to this later, but it is of interest to note that the Weems', even at that time, claimed that since relative displacement of the billet and walls of the container was avoided, the metal was concentrated in the neighbourhood of the die, thus making it possible to produce a more even coating of tin in the pipe.

### **1.1.2 Extrusion presses for sheathing electric cables**

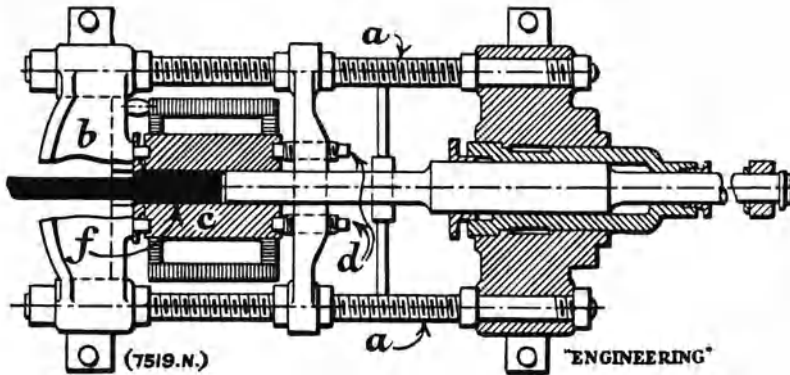
In 1879, Borel in France and Wesslau in Germany developed the first methods by which a lead sheath could be directly extruded onto cables. In both cases vertical extrusion presses were used in which hollow-cast billets of lead were extruded as a tubular sheath over an insulated conductor, which was passed into the press through a hollow mandrel and exited through the tubular ram. With the ram swung aside, a billet heated to 120°C was placed in the container and extruded as a tube through the annulus between a die carried on the nose of the extrusion ram and the conical end of a mandrel tube. Although the press worked successfully, it had the disadvantage that a continuous length of cable could not be sheathed due to the necessity of cutting to allow a fresh billet to be inserted.

### **1.1.3 Application of extrusion to copper alloys**

The advanced state to which extrusion had been brought in the lead industry, and the advantages which it offered, naturally directed attention to the possibility of its utilization for other metals possessing better mechanical properties, such as

the brass alloys, which, while much harder than lead at ordinary temperatures (i.e. 200°C), were capable of being extruded when the temperature was raised. Records exist of several efforts to do this during the last century. A report of one trial states surprisingly that 'it was anxiously and unexpectedly found that when the brass block came to be subjected to pressure, the zinc left the copper, thereby producing a zinc pipe and leaving the copper behind ... proving that the atoms of brass composition, united by fusion, were only mechanically arranged, not chemically combined'. Thus at this stage some of the essential metallurgical features of the process (although erroneous) were recognized. The main difficulty when compared with previous practice was that even the brasses most susceptible to hot work are not sufficiently plastic to undergo the heavy deformations involved in extrusion until they are heated to a temperature of at least 600°C; hence the problem was by no means only that of providing a powerful press. Not only had the temperature of the metal to be maintained within the working range where it could be dealt with under the pressures available during the extrusion stroke, but the question also arose of providing dies, containers and other parts of composition and design to withstand the unusually severe thermal and stress conditions, and that at a time when little development of the special steels that are now available for use had taken place. It is therefore hardly possible to overestimate the achievement of Alexander Dick in successfully overcoming the obstacles involved. On his inventive genius has been laid the foundation of the modern hot extrusion process, which has now been extended far beyond its original limitations to a stage where it covers most of the technical non-ferrous alloys, and where it has become one of the major metal-working processes in the field. Dick's first patent for an extrusion press was obtained in 1894 and was followed in the next few years by several others as experience was gained.

One of Dick's early designs is shown in Fig. 1.2. The horizontal frame was tied together by four rods (a). A heavy crosshead (b) formed one end of the press and supported the die, which was held in position against the container by a pair of jaws, pivoted at the base of the crosshead. The container (c), held and centred by the set-screws (d), was surrounded by a furnace jacket heated by coke or gas. The billet (f) heated to a plastic state was fed into the container from the front. With the object of preventing the ram from becoming wedged by the escape of metal past its sides, a dished or corrugated disc (the modern dummy block) was placed between it and the billet. At the end of the extrusion, the jaws were opened to allow the die and discard to be pushed out. A persistent source of trouble was encountered in that the heat given up by the billet caused unequal heating of the thick-walled container so that it frequently cracked. To meet this, compound containers were introduced. One of the first of these had a thin tapered inner liner surrounded by castings, with the annular space between them packed with material such as crushed granite or asbestos to give a measure of heat insulation; the complete assembly was carried in a strong outer shell. The idea of this was that although the inner liner became hot it would suffer less damage from heat stresses than a thicker one, and would moreover be easily replaced, while the outer shell



**Fig. 1.2** Early design of extrusion press by Alexander Dick. (This diagram was originally shown in an address to the Newcomen Society by C.E. Pearson.)

being at a much lower temperature would retain its strength and therefore be capable of resisting the pressure. In addition, as the heat was more carefully controlled, the billet could be extruded much more readily. This construction did away with the need for external heating of the container, though it had to be warmed up to begin with by a gas-burner or by inserting a hot block of iron. For a time, as an alternative to the use of preheated billets, the practice was also followed of casting the metal directly in the container, which was mounted for this purpose on trunnions so that it could be turned into an upright position for casting. A plate closed the bottom of the container during this operation. An improved method of supporting the die in a holder placed in a diehead was soon adopted, and this assembly was locked during operation by a transverse slide buttressed against the cross-head of the press.

The production of round rod and other solid sections was soon augmented by the manufacture of tubes from hollow-cast billets, though considerable difficulty had to be met, owing to the inadequate material available for the mandrel, in keeping it cool enough to prevent breaking, and in securing tubes of concentric bore. Many of these troubles yielded only slowly as steps were taken to improve machinery and materials, and as technique and experience were gathered, but Dick must be credited with many of the first steps which opened the way to progress, as, for instance, in his experiments with various types of fixed and floating mandrels. Such possibilities, too, as the application to copper alloys of inverted extrusion through a hollow ram, and the use of an electrically heated container, were also envisaged by him. In concluding this historical survey it may be said that although radical changes in design and accessory equipment have taken place during the last ninety years, extrusion presses at the present time are essentially constructed to the principles laid down by Dick.

## 1.2 THE THERMOMECHANICAL PROCESS

Historically, mechanical working has been used as the primary means of changing the size and shape of materials while transforming the cast structure of an ingot into what is generically referred to as a wrought product. Extrusion is one of the major processes by which this has been achieved. The process is typically conducted at relatively high temperatures because the lower flow stress of the material permits larger section reductions to be achieved; lowering the power requirements and processing times.

It is now generally recognized that the structure of the material also requires careful control and hence the integrated process must be considered. For extrusion, the integrated process (the thermomechanical process or TMP) will consist of the unit processes involved: homogenization, heating to working temperature, extrusion, stretching, solution treatment and ageing. Microstructural features of importance for property control of aluminium alloys include: (a) the coherency and distribution of strengthening precipitates; (b) the degree of recrystallization; (c) the grain and/or subgrain size and shape; (d) crystallographic texture and (e) size and distribution of intermetallic particles including the dispersoids (present by design) and constituent phases (which result from iron and silicon impurities). The ability to understand the effect of these features on the properties of aluminium alloys has led to efforts to upgrade product performance by modifications in conventional primary processing methods. Beginning with the as-cast ingot which exhibits a heterogeneous morphology, processing includes a homogenization treatment, to reduce segregation, remove the low melting point phases and thus improve workability. This thermal treatment also serves to precipitate dispersoid-forming elements such as chromium, manganese and zirconium, so that they may perform their role of grain control during processing. Reheating to an appropriate working temperature may produce further changes to the structure, usually involving precipitation.

The extrusion process breaks down the billet and effects the required shape change. Since aluminium and its alloys have a high stacking fault energy, sufficient dynamic recovery normally occurs during hot deformation, i.e. at temperatures above  $0.5 T_h$ , to give rise to a stable polygonized substructure. It is convenient to express the temperature as the homologous temperature  $T_h$ , which is defined as the extrusion temperature divided by the temperature of the lowest melting phase. The subgrains remain equiaxed during hot working although the grains elongate in the direction of flow and do not recrystallize. Some of the alloying additions are in solution during hot working but the dispersoid-forming transition elements have already precipitated and may become strung out in the working direction. A fine distribution of dispersoids delays or prevents static recrystallization and aids in retaining the elongated or 'fibrous' grains during subsequent processing. The wrought product may be heat treated to develop the desired microstructure, i.e. solutionized, quenched, stretched and aged.

The homogenization process involves holding the metal at an elevated temperature for a sufficient time to allow the concentration gradients to diminish to an acceptable level. The controlling factor is thus the diffusivity of the alloying elements dictating the speed at which mass transfer may occur. Thus the homogenization process is a mass-transfer problem and we would expect the controlling equations to be of the Arrhenius type involving an exponential term. Similarly precipitation during reheating will be a mass-transfer problem. A typical example of this is in the reheating of 6XXX alloys in which the  $Mg_2Si$  phase changes from  $\beta$  to  $\beta'$  to  $\beta''$  under certain heating conditions. Extrusion is a deformation process in which atomic planes slip over each other (assisted by dislocations) and in which atomic bonds are individually broken and new bonds formed. Plastic flow is the consequence of this action and the macroscopically observed change is the summation of individual atomic events. The two most important features of plastic flow are incorporated in the concept of dislocations, which provide high-energy atomic configurations in association with lowered energy barriers and vacancies into which material may move. Plastic flow may thus also be regarded as a mass-transfer problem. Solutionizing and ageing are also controlled by diffusion and we may thus conclude that the thermomechanical process is a mass-transfer problem. This is dealt with in more detail in Chapter 5.

### 1.3 DIRECT AND INDIRECT EXTRUSION

We have noted in section 1.1 that almost since the inception of the extrusion process there have been two modes of operation; we shall now consider the difference between the two modes in greater detail.

The basic processes are shown in Fig. 1.3 with the relevant sequence of operations in direct extrusion being illustrated in Fig. 1.4(a) and indirect in Fig. 1.4(b). The major difference is that in the indirect mode there is no friction between the billet and container whereas in the direct mode the outer shell of the billet moves relative to the container as extrusion proceeds. Thus in direct extrusion the surface of the billet is sheared at, or slides along, the container wall. The ease with which this is carried out is dependent on the selection and application of the lubricant. In every case, part of the extrusion load, depending on the length of the billet, is expended in overcoming the friction between the billet and the container, or in shearing the inner material from the slower-moving peripheral layer adjacent to the container wall. As would be expected, this results in considerable variation in flow behaviour which is considered in detail in Chapter 4.

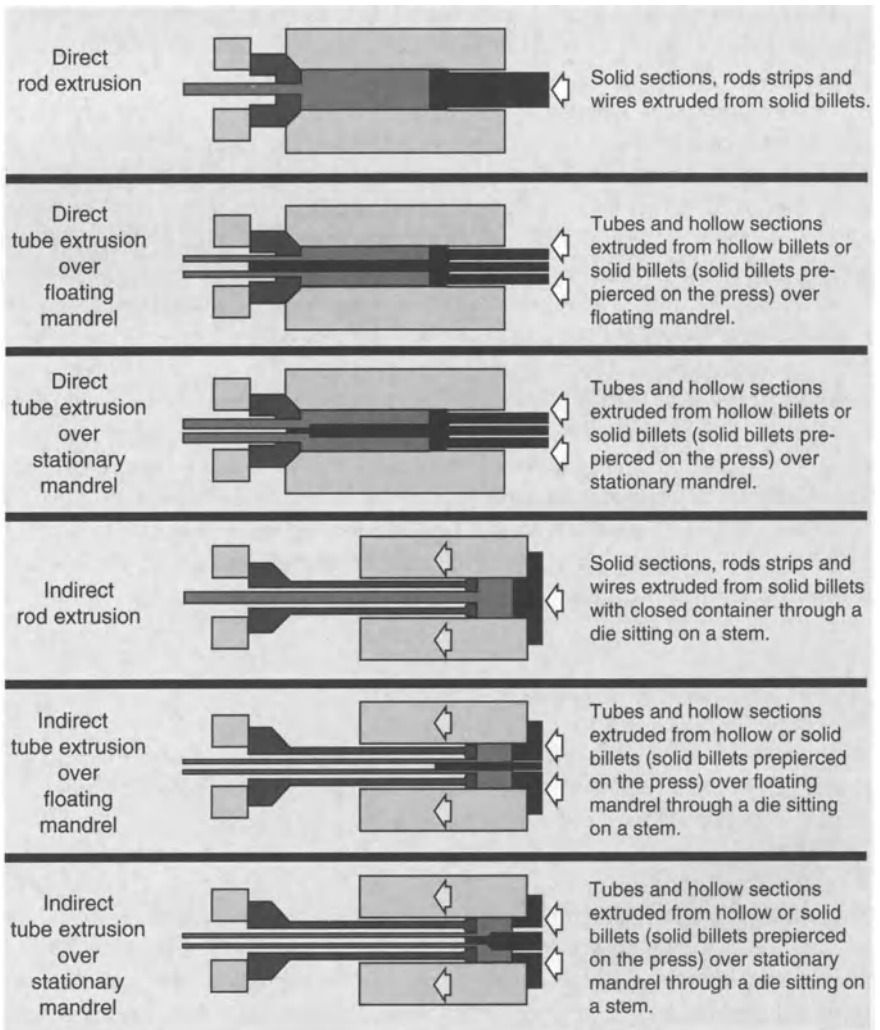
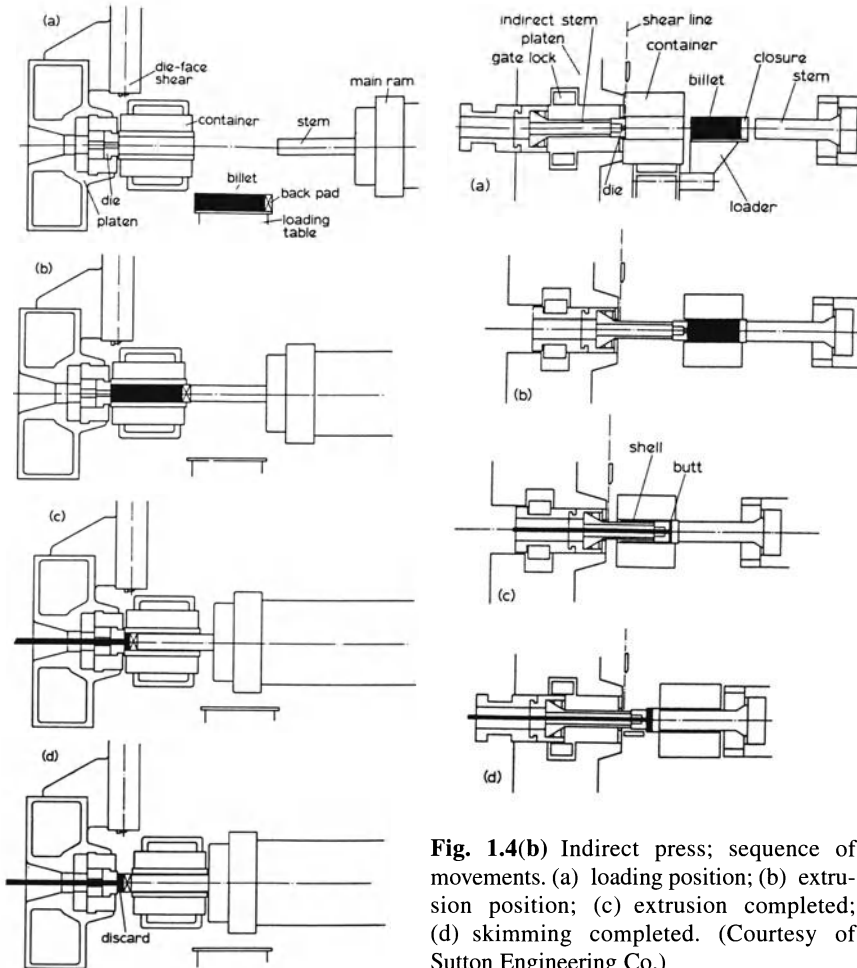


Fig. 1.3 Methods of extrusion. (Courtesy of SMS Schloemann.)

### 1.3.1 Direct extrusion

The more widely utilized method is the direct process. This is because of the difficulties in ram construction for the indirect process and the greater circumscribing circle diameter available for the extrudate in the direct mode. The sequence of operation of the press in the direct mode, shown in Fig. 1.4(a) is:

1. Loading of the billet and dummy block into the press;
2. Extrusion of the billet;
3. Decompression of the press and opening of the container to expose the discard and the dummy block (often referred to as stripping);
4. Shearing the discard;
5. Returning the shear, container and ram to the loading position.



**Fig. 1.4(b)** Indirect press; sequence of movements. (a) loading position; (b) extrusion position; (c) extrusion completed; (d) skimming completed. (Courtesy of Sutton Engineering Co.)

**Fig. 1.4(a)** Sequence of movements for aluminium extrusion of 16 MN press; four positions (a)–(d). (Courtesy of Fielding and Platt Ltd.)

Figure 1.4(b) illustrates the sequence of operations in the indirect mode in which there is relative movement between die and container but none between billet and container. The individual steps are:

1. Loading of the die holder and die (on modern presses the die is more frequently held in the stem);
2. Loading of the billet;
3. Extrusion;
4. Separation of the (die holder with the die) and the discard from the extrusion.

Direct extrusion is the simplest production mode, can be carried out with or without a lubricant and, in the latter case, with or without a shell. Almost all metals will tend to shear at the container interface, adding to the force required to extrude the metal and depositing a layer at that interface. This material will be pushed backwards during the extrusion and will be extruded at the end of the ram stroke. In many metals this leads to a central pipe forming at the rear of the extrudate which is largely composed of oxides, dross, etc. Thus it is common to utilize a dummy block which is about 2 mm less than the container diameter such that a shell remains and must be removed by a separate action of the main ram. Clearly this prolongs the cycle time and is undesirable. The process, if practised in this way, is also known as Dick's method of extrusion. Aluminium alloys are generally extruded using a dummy block with a very close fit in the container. Consequently, hardly any shell remains and the surface is not drawn into the billet because, in contrast to heavy metals (which are generally extruded using some form of lubricant), aluminium sticks to the container wall and impurities on the surface are held there, eventually entering the rear of the billet in the 'discard'.

Generally there is only a small temperature difference between the billet and the container, and the difference in velocity between the centre of the billet and the periphery is much less than in the case of heavy metals. As the dummy block advances, impurities on the billet surface and the peripheral segregation are sheared off and collect in the discard, which must therefore be large enough to ensure that impurities do not appear in the product. Although there are many potential advantages, little use is made of lubricated extrusion for aluminium and the only lubricant used is usually a token of graphite based grease on the face of the die and of the dummy block or ram. This is because the surface is a very important feature of the product and is formed from the interior of the billet by the shear occurring in the conical zone adjacent to the die known as the dead metal zone. If too much or too little lubricant is used, several types of surface defects occur that are not encountered in the usual method of unlubricated extrusion.

Figure 1.5 shows that the load in direct extrusion initially increases very rapidly as the billet upsets to fill the container. There is a further increase in pressure until extrusion commences. The cone-shaped deformation zone then develops in front of the die aperture and the maximum strain rate is developed in this zone. After the peak pressure has been reached the extrusion pressure falls as



the billet length decreases until rapidly increasing as the dummy block interferes with flow and the metal has to move radially towards the die aperture.

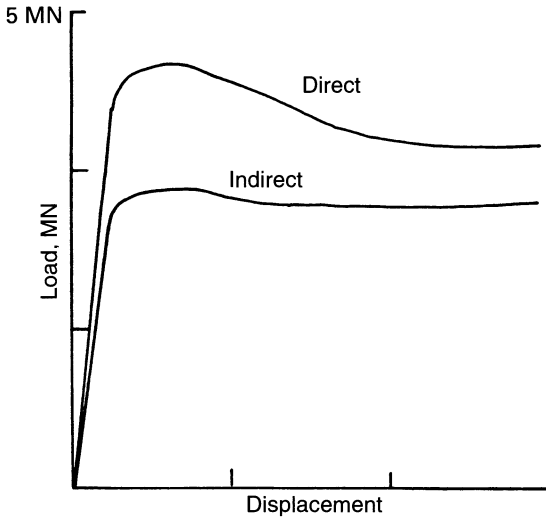


Fig. 1.5 Extrusion load/displacement curves for direct and indirect extrusion.

### 1.3.2 Indirect extrusion

In indirect extrusion of aluminium alloys the process is characterized by the absence of friction between the billet surface and the container. The load required is therefore always decreased compared with the direct mode as illustrated in Fig. 1.5 and can be reduced by as much as 50%. The advantages of indirect extrusion are partly related to the lower load needed and partly to the more uniform flow pattern developed because of the absence of relative motion between the billet and the container such that no heat is produced by friction.

The main advantages are:

- There is a 25–50% reduction in peak load compared with direct extrusion.
- The resultant higher extrusion load available can be used either to extrude smaller cross-sections or to decrease the billet temperatures, permitting the use of higher speeds.
- The extrusion pressure is not a function of the billet length, because there is no relative displacement of the billet centre relative to the peripheral region. The billet length is therefore not limited by the load required for this displacement but only by the length and stability of the hollow stem needed for a given container length.

- No heat is produced by friction between the billet and the container, and consequently there is less temperature increase at the billet surface towards the end of extrusion, as is typical in the direct extrusion of aluminium alloys. Therefore, there is less tendency for the surfaces and edges to crack in the indirect process and significantly higher extrusion speeds can be used.
- The service life of the tooling is increased, especially that of the inner liner, because of the almost total absence of friction.
- There is a more uniform deformation of the complete billet cross section with no tendency to form an extrusion defect or a coarse-grained peripheral zone.

The disadvantage of indirect extrusion is that, because of the modified flow in this mode, impurities or defects on the billet surface affect the surface of the extrusion and are not automatically retained as a shell or discard in the container. Therefore, machined billets have to be used. In addition, the cross sectional area of the extrusion is limited by the size of the hollow stem, although recent developments using segmented discs held in a retainer ring partly overcome this difficulty. One disadvantage which is not easily overcome is that the product must travel the length of the stem before it is possible to quench. In many aluminium alloys, press quenching replaces a separate solution treatment. Because of these limiting factors indirect extrusion has not found the same extensive application as the direct process.

#### **1.4 EXTRUSION OF RODS AND SOLID SHAPES**

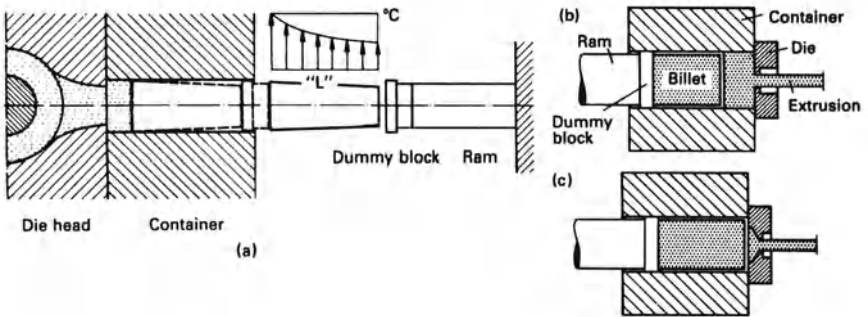
The direct extrusion of rods and solid shapes is the simplest production method in use. Nevertheless, in order to achieve an acceptable tolerance and desired properties throughout the extrude the process must be considered as complex. The metallurgical problems involved in rod and section extrusion will be discussed in Chapter 5; Chapter 3 describes the methods used for various alloys and the problems of achieving satisfactory quality. Rods and sections are extruded with a separate dummy block and a discard, the length depending on the complexity of shape, the material flow stress and homogenization and the nature of the shear occurring at the container/billet interface. Billet-to-billet extrusion is very suitable for continuous lengths of coiled products. The design of the tooling is a decisive factor in rod and solid shape extrusion particularly for sections for which the spacing of the orifices in multi-hole extrusion must be designed to give even flow through each. The die land must also be designed such that the section extrudes correctly and correct tool assemblies must take care of the inevitable deflections. At the same time, the shrinkage of the extrusion upon cooling has to be considered, together with the influence of the material flow through the die land. This flow is of particular importance when extruding complicated sections to close tolerances, and is considered in more detail in Chapter 5.

Sections with gradual variations in cross-section along the length of the extrusion can be manufactured by interrupting the extrusion stroke after a certain ram displacement and changing the die. Extrusion begins with the smallest cross section; the die, which is made up of two or more sections, is then replaced by a larger one and the ram stroke is continued. This process is used in the United States for aircraft sections and saves on machining. Stepped posts for street lamps and the like are produced in the same way. Dies have also been developed to give a continuous increase in the size of the aperture and allow conical sections to be extruded.

Billet-to-billet extrusion is a special method for alloys that easily weld together at the extrusion temperature. Using this process, continuous lengths can be produced by discontinuous extrusion. Initially, it was of particular importance in cable sheathing with lead or aluminium, where the aim was a continuous metallic casing around the cable. Billet-to-billet extrusion is also a viable process in the production of coiled semifinished products for further processing—for example, wire and tube production. The aluminium alloys that easily weld together during extrusion, 1XXX and 6XXX series, some of the more dilute 3XXX and 5XXX and the Al–Mg–Zn alloys of the 7XXX series are suitable. Perfect welding of the billet in the container with the following billet must take place as the junction passes through the deformation zone, and therefore the following requirements have to be fulfilled:

- good weldability at the temperature of deformation;
- accurate temperature control;
- clean, but not necessarily machined, billet surfaces with no impurities, porosity or surface defects (brush cleaning immediately before billet heating);
- sawn, clean billet ends free of grease;
- bleeding the air from the container at the start of extrusion to avoid the problem of pockets of compressed air that later re-expand to form blisters and other defects.

A very simple and efficient method used for bleeding, especially in aluminium extrusion, is illustrated in Fig. 1.6. After the billet has reached a uniform 'base' temperature, an axial temperature gradient of about 90–100°C over its length is produced by rapidly heating the front of the billet. It is then quickly loaded into the container (Fig. 1.6(a)). As the billet upsets, it fills the container from the front to the back and the air is squeezed out of the container (Fig. 1.6(a)) past the stem. Two methods of billet-to-billet extrusion have been developed. In the first method (Fig. 1.6(b)), the discard is removed and the following billet is welded to the one remaining in the feeder plate. The second method (Fig. 1.6(c)) does not need a discard: the subsequent billet is pressed directly onto the billet still in the container. In this case a separate dummy block cannot be used. The dummy block shears an aluminium ring from the container during each return stroke, and this has to be removed from the ram. With aluminium the return load in this cleaning operation can be as high as 10% of the press capacity.



**Fig. 1.6** Removal of air from the container in billet-to-billet extrusion (a) temperature gradient; (b) normal die; (c) feeder plate die. (Courtesy of Schloemann-Siemag AG.)

## 1.5 EXTRUSION OF HOLLOW SECTIONS

In order to extrude tubes, the billet has to be pressed through a die that determines the outside diameter, and over a centrally located mandrel that determines the inside diameter. The metal must, therefore, flow through an annular gap. The various methods of producing tubes are characterized by the following points:

1. Type of mandrel location
  - (a) on the extrusion stem
  - (b) on the die (welding chamber die).
2. Method of axial movement of the mandrel (for those fitted to the stem)
  - (a) fixed mandrel screwed to the stem
  - (b) moving mandrel controlled independently of the ram displacement
  - (c) stationary mandrel controlled independently of the ram displacement.
3. Method of billet piercing
  - (a) solid billet pierced in the press
  - (b) hollow billets
  - (c) pre-drilled billets.

Extrusion may be conducted with the mandrel solidly attached to the main ram and for many years this was the usual method of producing tube using a hollow billet. Currently the mandrel has two main functions: the first is to pierce the solid billet in the container by pushing the mandrel axially through the billet; the whole billet is plastically deformed. The volume of metal displaced by the mandrel moves roughly axially, and there is a corresponding increase in the billet length. At the end of the piercing process, the mandrel is centrally located in the die. The pierced billet is then extruded to a tube. The axial position of the mandrel relative to the die and its variation during extrusion, and hence during the deformation of

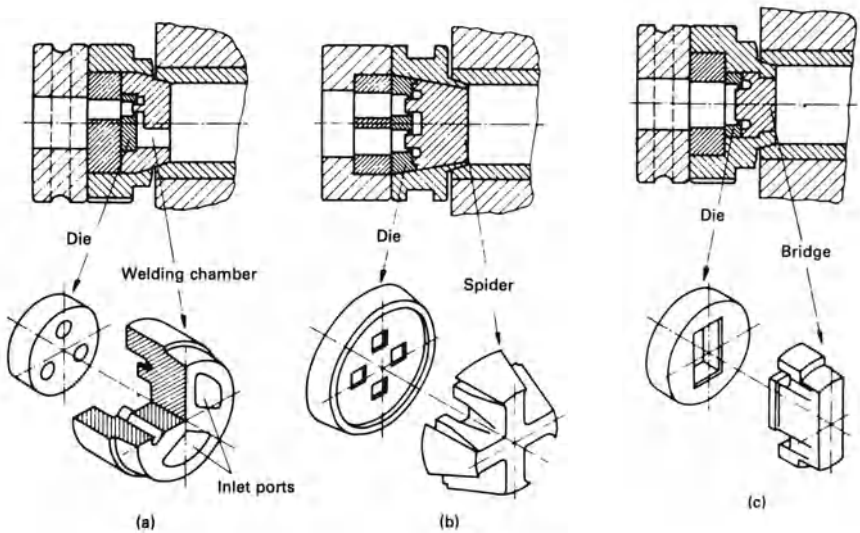
the pierced or bored billet, are important for a number of reasons; the largest being to ensure concentricity along the length of the extrude. In the original process the mandrel was constructed such that it was integral with the stem thus producing problems in maintaining concentricity and demanding a large stroke on the cylinder with the concomitant extended press frame but with the continuing development of the extrusion process, control of the mandrel location and its movement has kept pace with the requirements of tube production. Methods which have been utilized, and still are by those extruders lacking a specialized tube press, are (a) the use of a floating mandrel which is attached to the dummy block (usually with a taper fitting ) and hence excluding the possibility of piercing and (b) by use of a mandrel fitted within the main ram which has a fixed and thus limited stroke but can be used for billet piercing. Modern tube production is either using a mandrel in which the movement is completely independent of the main ram or by the use of bridge or porthole dies. The former is usually a dedicated tube press whilst the latter involves a mandrel fixed to the die and is discussed below. The advantages of a fully dedicated press are:

- Solid billets can be pierced.
- The piercing load is independent of the load applied by the extrusion stem.
- Extrusion can be carried out with a moving, leading or stationary mandrel. In the last instance, the position of the mandrel is adjusted so that its tip remains stationary during extrusion whilst the ram advances. This is termed 'extrusion over the tip'.
- The use of a stationary mandrel allows both tubes and hollow sections to be produced to close tolerances. The mandrel tip conforms to the internal shape of the section, and hollow billets are used in the case of shaped sections.

Tubes and hollow sections are also produced by the use of a welding chamber concept in which the stream of flowing metal is first divided into distinct streams and subsequently rejoined by a pressure weld. The die sets used are termed either bridge or porthole. This process has found a wide range of application within the aluminium industry and is probably the most widely used method for the production of complex and often thin-walled sections. The process is applicable only to dilute alloys in which the extrusion temperatures possible are relatively high and thus excludes the high strength aerospace alloys. Nevertheless alloys in the 1XXX and 6XXX series, some of the more dilute 3XXX and 5XXX and the Al-Mg-Zn alloys of the 7XXX series are each amenable to this form of extrusion. Tubes are extruded by this method and if long lengths are required can be extruded using billet-to-billet extrusion. The same precautions must be taken as in the production of solid bars. The welding chamber process represents a great advance in the production of the very complicated sections used in architecture, instrument construction and vehicle manufacture.

The internal shape of the tube or hollow section is formed by a short mandrel supported on two or more arms by the die and its support tooling. The metal is divided by the arms into several strands of large cross-section and, as deformation

continues, these enter the inlets, flow around the arms and are rewelded in the welding chamber to form the section. The metal flows out between the tip of the mandrel and the die aperture to form a tube or a hollow section according to the shape selected. This method of extrusion requires dies of a very high quality, precise control of the extrusion parameters, recognition of the complexity of the shape and special attention to the die land design for thin-walled sections. Three types of die are illustrated in Fig. 1.7(a)–(c). The main difference between them is the method of supporting the mandrel. The individual aspects of the design of the die are discussed in more detail in Chapter 7.

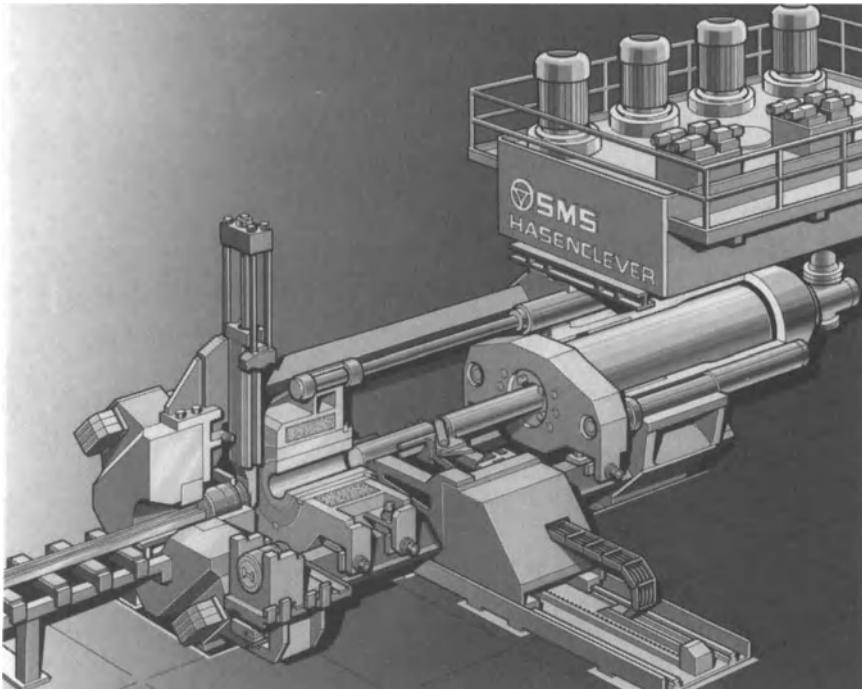


**Fig. 1.7** Construction of dies for the welding chamber process (a) porthole; (b) spider; (c) bridge.

## 1.6 THE EXTRUSION PRESS

### 1.6.1 Direct presses

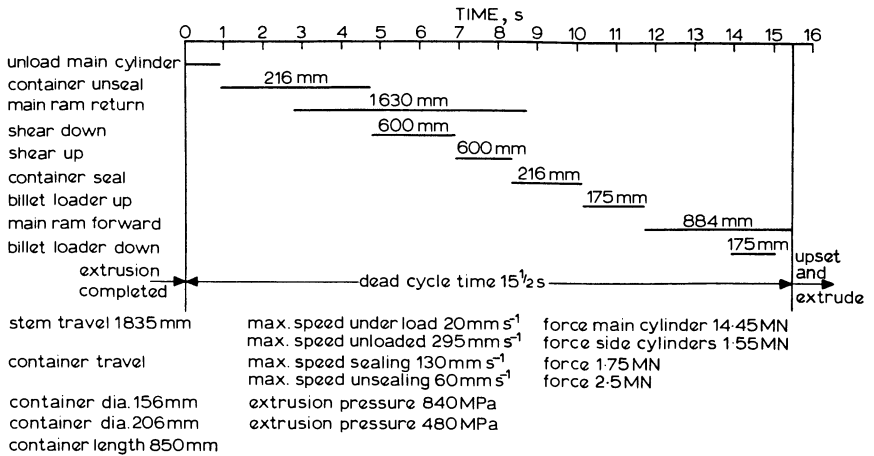
A schematic section drawing of a modern aluminium press is illustrated in Fig. 1.8. The basic design is unchanged from that of earlier presses and really does not differ in essence from the original design of Alexander Dick. The ram, on which is mounted the pressing stem, which transmits the load to extrude the billet, is actuated during extrusion by the main cylinder powered by direct pumping from constant-speed variable-delivery oil-hydraulic pumps. Backward movement of the ram crosshead, and also forward movement when not under load, is by two smaller rams on either side which can also reinforce the main ram during extrusion. The container is moved away from the fixed platen by columns operated by cylinders mounted on the platen, allowing space for the introduction of the die and die-backing tools, and for a shear or saw to sever the



**Fig. 1.8** Modern extrusion press (schematic). (Courtesy of SMS Schoemann.)

extrusion from the unextruded butt. The sealing of the container against the die during extrusion is reinforced by a separate pump. The mechanism for loading the billet is again powered by a separate pumping system, the billet being introduced between the stem and container, along with a back pad, pressing disc or dummy block. The sequence of movements for extrusion have been discussed in section 1.3. A time/cycle diagram incorporating the various movements on a typical 16 MN press, together with data relating to the forces involved, distances travelled, and operating speeds, are shown in Fig. 1.9. The reader should note that the dead cycle time (i.e. that part of the cycle when the press is not extruding) must be optimized to a minimum and this will be further discussed in Chapter 7.

The simplest arrangement for changing dies is by a die-face slide. The pre-heated die assembly is placed in a horseshoe holder, and is moved into position by a hydraulic cylinder, the discarded die assembly being removed, and replaced, on the opposite side of the press. The inconvenience of changing dies on both sides of the press can be avoided by having the die-holders carried on a rotating head, trunnion mounted on the platen. The loading position is then at  $180^\circ$  to the centreline of the press, with a hole for dealing with stickers placed at  $90^\circ$ . An elaboration is the die shuffle in which the dies are mounted in individual carriers located on a table which can be moved backwards and forwards parallel to the



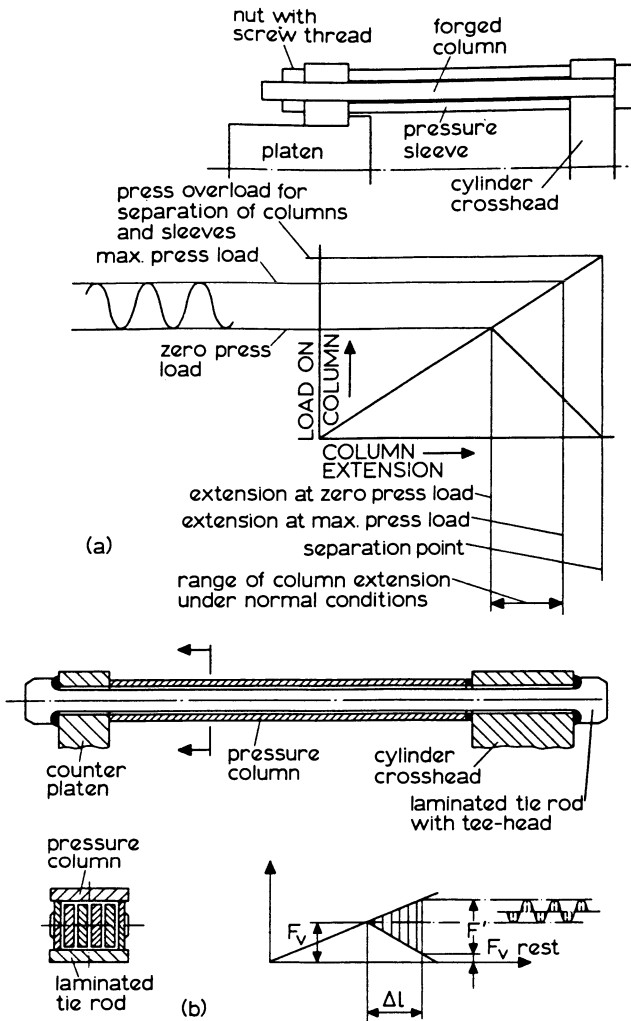
**Fig. 1.9** Time cycle diagram for 16 MN press.

press axis. The used die is moved back on to the table by a hydraulic ram, the table position re-adjusted, and a new die selected, the operation being carried out by remote control from the main panel. Ideally, the storage boxes are heated, so that any die is immediately available as required.

A feature not seen in the Dick press is the prestressing of the columns tying together the platen and main cylinder. The compression member is a cast steel sleeve accurately bored to a clearance over the columns. Prestressing is arranged to be some 20% greater than the maximum load available from the combined main and auxiliary rams. As can be seen from Fig. 1.10(a), the stress fluctuations in the columns are reduced and fatigue life is thereby increased. Prestressing also provides a stiffer construction, and more accurately controlled press movements are possible. An alternative system of prestressing employs an assembly of flat plates for both tie bars and compression members (Fig. 1.10(b)). Spade ends on the tie bars avoid the weakening effect of threads on a conventional round tie bar. The greater rigidity of a press with prestressed columns makes it possible to dispense with a base plate, at least in presses of up to about 20 MN, the main crosshead and container sliding on the accurately machined surfaces of the lower stress-members, and guided by the upper stress-members, with an overall saving in weight.

The oil reservoir is normally located above the main cylinder assembly at the rear of the press, the large prefill pipe from the tank to the main cylinder providing the oil flow for rapid movement of the unloaded ram before and after extrusion. Often, to reduce noise level in the plant, the pumps are in a separate room, where they are mounted on rubber supports with flexible pipe connections to still further attenuate noise and vibration. The modern practice is to locate the control console at the press mouth, since it is here that the operator can exercise the most immediate control over the emerging product.





**Fig. 1.10** Prestressing of main columns (a) conventional forged and machined columns (courtesy of Fielding and Platt Ltd); (b) laminated plate columns. (Courtesy of Schloemann-Siemag AG.)

For billet preheating, both mains-frequency induction and fuel-fired furnaces are employed. In the USA the latter is generally preferred because of the lower running cost. In Europe it is more common to see induction furnaces, which are often more precise in temperature determination and, perhaps just as importantly, in reproducibility. Spray cooling of the back end of the billet may be employed as an alternative to taper heating, in order to compensate for the increased energy input to the back end of the billet during extrusion. To avoid the necessity of

emptying and recharging the billet furnace when a change in programme calls for a different billet length, and to keep the scrap arising to a minimum, furnaces can be arranged to preheat full-length cast logs. A measured length is then cut off by a hot shear, and delivered to the press table, the remaining portion being returned to the furnace.

Both container and liners are of 5%Cr hot-work steels. Wear is normally greater at the die end, and the liner is designed to be reversible within its supporting shell. Heating may be provided by induction elements embedded within the container, but this causes some weakening, and it is more usual to employ resistance elements within the container housing. Two, or sometimes three, separate heating zones may be provided, each with its independent thermostatic control based on embedded thermocouples. Most presses are equipped with at least two containers of differing diameter, so as to be capable of achieving maximum output from a range of aluminium alloys, some difficult (such as 2024 and 7075) and others (such as 6063) easy to extrude. In order to speed changeover, both container and press stem are equipped with quick-action locking devices. Generally, replacement of these items and rechecking alignment can be carried out within an hour or so.

### 1.6.2 Indirect presses

In conventional direct extrusion, the die seals the container at the front end, while the billet is pushed through the container from the back end by the press stem. In moving the billet through the container as much as 50% of the work done may be expended in shearing a layer of metal near the container wall. The heavy deformation in this outer layer leads to the formation, in strong alloys such as 2024 and 7075, of a coarse-grain outer zone of low mechanical strength in the extruded and heat-treated product. By indirect extrusion, in which the die is pushed through the billet, there is no relative movement between billet and container, with a consequent saving of energy, while the uniform deformation of the billet results in a uniform fine-grain structure throughout the cross-section of the extruded and heat-treated product.

Here, the die is a sliding fit in the container, and is supported on a fixed hollow stool. In designing a horizontal indirect press it is evident that a loose die is not admissible, and provision must be made for fixing the die rigidly on the indirect stem through which the extruded product must pass.

Indirect presses are designed with oil-hydraulic variable delivery power units and full automation of movement sequencing, to give a performance comparable with that of a direct press, but with advantages in operation and in quality of product:

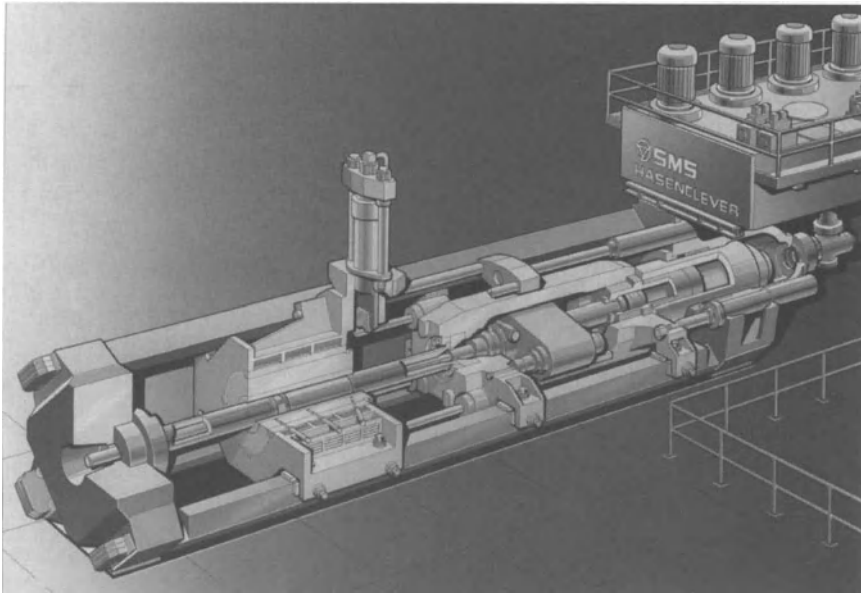
- less extrusion force is required, so that a larger-diameter billet can be extruded with a given main-ram force;
- faster extrusion is possible, but only with hard alloys such as 2XXX and 7XXX where very low speeds are possible in direct extrusion;

- more uniform deformation giving the possibility of zero recrystallisation in the solution treated product. More uniform mechanical properties, and closer dimensional tolerances are obtained in the product.

Disadvantages are:

- the maximum size of extrusion is limited because of the space inside the container occupied by the hollow indirect stem supporting the die;
- press sequencing and die handling is more complex.

Figure 1.11 shows the schematic arrangement of an indirect press.



**Fig. 1.11** Indirect press for rod and tube extrusion (schematic). (Courtesy of SMS Schloemann.)

The main difference in construction to provide for indirect extrusion lies in the considerably increased length between the main cylinder and platen to accommodate the extended travel of the container, with a concomitant increase in main-ram travel. For indirect extrusion the die stem is held in a gate-lock mechanism, with run-out travel of extended length for die changing and servicing. A die-face shear is in a similar position to that of a direct press, as is also the mechanism for the separation and recovery of the discard and dummy block. As in a direct press the container movement is from cylinders mounted on the platen.

A comparison of the main characteristics and capabilities of direct and indirect presses is given in Table 1.1. The most obvious advantage of the indirect press is that the weight of billet extruded is more than double compared with a

**Table 1.1** Extrusion of aluminium alloys by direct and indirect presses

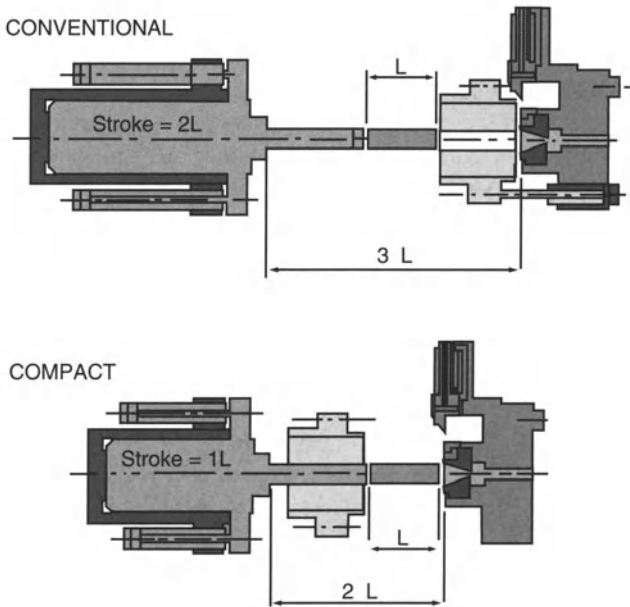
	<i>20 MN direct</i>	<i>20/23<sup>a</sup>MN</i>	<i>50 MN direct</i>	<i>50/55<sup>a</sup>MN indirect</i>
<b>Soft alloys</b>				
<b>Billet</b>				
diameter (mm)	250	320	420	500
<b>Billet</b>				
length (mm)	900	200	1200	2000
Length/diameter ratio	3.6	3.7	2.85	4.0
Weight (kg)	125	270	465	1100
Circumscribing circle diameter <sup>b</sup> (mm)	210	220	330	325
<b>Container</b>				
diameter (mm)	256	326	426	506
Pressure (MPa)	385	240/275	350	245/270
<b>Hard alloys</b>				
<b>Billet</b>				
diameter (mm)	170	195	270	300
<b>Billet</b>				
length (mm)	750	1200	1000	2000
Length/diameter ratio	4.4	6.15	3.7	6.7
Weight (kg)	48	100	160	395
Circumscribing circle diameter <sup>b</sup> (mm)	140	70	220	100
<b>Container</b>				
diameter (mm)	176	201	276	306
Pressure (MPa)	820	630/725	835	680/745

<sup>a</sup> Including container advance force. <sup>b</sup> Circumscribing circle gives the diameter within which tooling must normally be confined. This depends upon the type of section, and is approximate only.

direct press of the same force. Although the back-end discard is greatly reduced as compared with the direct method, there is metal loss owing to the billet being machined or die scalped. Yield overall is therefore about the same as in direct extrusion, although in direct extrusion of strong alloys back-end rejections of product have to be taken into account. Because of the limitation in die area imposed by the scalping/skull and indirect stem, as well as the limited available space for a conventional die stack, it is evident that the indirect press cannot take over the main production programme of the average direct press extruding mainly thin-walled sections of easily extruded aluminium alloys such as 6063. The indirect press is particularly suited to the single-hole extrusion of heavy bars, tubes

and structural sections. In either soft or hard alloys there is the advantage of being able to extrude at higher speeds, and to produce larger and heavier single pieces. This advantage is particularly great with the strong aircraft alloys, such as 2014, 2024, 7050 and 7075, where superior metallurgical structure and more consistent mechanical properties are achieved, and it seems likely that indirect presses will be used to an increasing extent in this particular application.

In the case of both indirect and direct presses there are many variations claimed by the manufacturer to yield particular advantages. This book is concerned primarily with the extrusion process rather than press design and hence cannot deal with this aspect of the plant. However it is, perhaps, worthwhile noting that there is a tendency towards more compact presses thus shortening the overall stroke and hence the dead time. Such an arrangement is shown schematically in Fig. 1.12. together with a conventional press to illustrate the saving in space. It will be obvious to the reader that if the run-out tables and handling mechanisms were added to the diagrams the space saving would not be spectacular.



**Fig. 1.12** Modern compact press. (Courtesy of Clecim.)

## 2.1 YIELDING AND DUCTILITY

It has long been established that the type of failure exhibited in materials is a function, not only of the magnitude of the applied stress or the basic material characteristics, but also of the way in which they are applied. Thus for annealed EC grade aluminium we might expect an elongation of ~30% if tested in tension, of ~400% if cold rolled and several 1000% if extruded. It was Von Karman [1] who first demonstrated the effect of hydrostatic stresses on the mode of yielding when he demonstrated the ductility of marble under the application of high compressive hydrostatic stresses and this has since been confirmed by observing other more typical cases such as notched bars where the ductility appears to be reduced in the presence of high tensile hydrostatic stresses. In both rolling and extrusion the stresses are in each case predominantly compressive and in extrusion are compressive in all three directions.

Deformation can be defined exactly by referring the stresses in the deformation zone to the axis of a three-dimensional coordinate system. Stress components in each of the three directions occur in the planes normal to each other – a normal stress  $\sigma_{ii}$  and two shear stresses  $\tau_{ij}$  perpendicular to each other (Fig. 2.1). If the coordinates are taken parallel to the directions of the maximum normal stresses (the principal stresses), the stress system can be represented simply by the three normal stresses  $\sigma_{11}$ ,  $\sigma_{22}$  and  $\sigma_{33}$  (Fig. 2.2) and the resultant stress on any other plane consists of the hydrostatic stress OP and the deviatoric or shear component PN. The hydrostatic component does not contribute to deformation but may increase ductility; thus it is the stress component PN which dictates deformation. Analysis shows that the cubic equation solving the problem for the principal stresses is:

$$\sigma^3 - J_1\sigma^2 - J_2\sigma - J_3 = 0$$

where  $J_1$ ,  $J_2$  and  $J_3$  are termed the invariants of the stress tensor  $\sigma_{ij}$ .

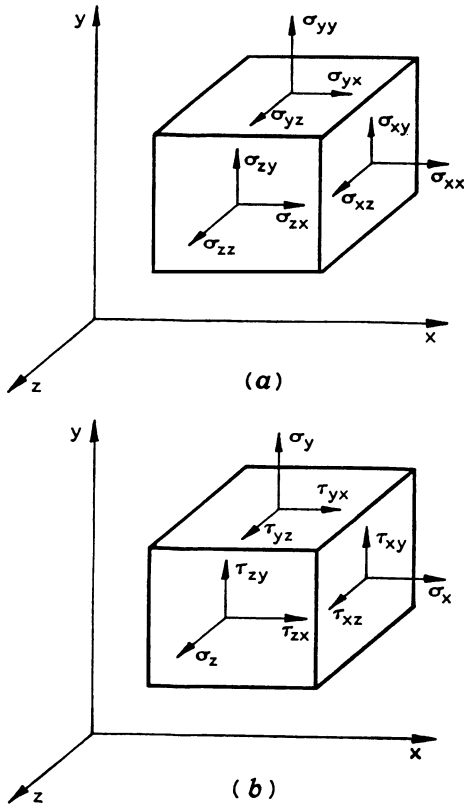


Fig. 2.1 Three-dimensional stress coordinate system.

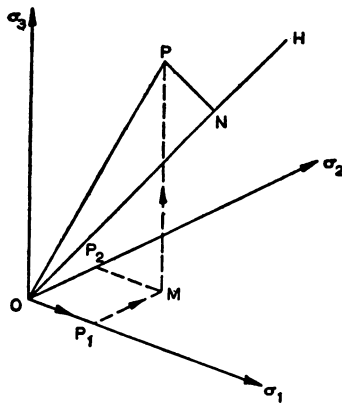


Fig. 2.2 Three-dimensional stress coordinate system with principal stresses as axes.

Tresca proposed that yielding would occur when the maximum principal stress reached a critical value equal to the shear yield stress  $k$ . Thus:

$$(\sigma_1 - \sigma_3) \geq 2k = \bar{\sigma}$$

where

$$\sigma_1 > \sigma_2 > \sigma_3$$

The value  $\bar{\sigma}$  is termed the mean equivalent stress and is a very important feature of plastic flow and is discussed in detail below.

The Tresca yield criterion states that plastic flow can be initiated by either compressive or tensile stresses, provided the stress gradient is maintained at the value  $\bar{\sigma}$  or  $2k$ . However, an important feature of extrusion is that all three principal stresses are compressive, in contrast to most other deformation processes. The axial stress  $\sigma_x$  has the greatest magnitude. The radial and tangential stresses ( $\sigma_r$  and  $\sigma_\theta$ ) have approximately the same magnitude in a cylindrical billet, but are less than  $\sigma_x$ .

All three principal stresses are compressive and  $\sigma_x > \sigma_r \cong \sigma_\theta$ , and hence:

$$\sigma_x - \sigma_r \geq 2k = \bar{\sigma}$$

We can see that the axial stress is given by  $\sigma_x = \bar{\sigma} - \sigma_r$  and even if the radial stress is only 50% that of the axial stress then the stress on the extrusion ram will be  $2\bar{\sigma}$  before adding the effect of friction.

As discussed above, the ductility increases with hydrostatic pressure at least for the case of compression. In three-dimensional stress systems the hydrostatic component of stress is given by the first invariant  $J_1/3$ :

$$\sigma_m = \frac{\sigma_x + \sigma_r + \sigma_\theta}{3}$$

In mathematical analyses the Tresca yield criterion is often used because the form is easily manipulated. However experiments show that the Von Mises criteria are closer to observed results. Von Mises proposed that yielding occurred when the second invariant of the stress tensor assumed a critical value. This invariant reduces to:

$$(\sigma_r - \sigma_x)^2 + (\sigma_x - \sigma_\theta)^2 + (\sigma_\theta - \sigma_r)^2$$

which can be shown to represent the shear strain energy stored when divided by the constant  $12G$  where  $G$  is the shear modulus. Thus in tension the shear strain energy stored will be  $2\bar{\sigma}^2/12G$  and the Von Mises criteria is written:

$$(\sigma_r - \sigma_x)^2 + (\sigma_x - \sigma_\theta)^2 + (\sigma_\theta - \sigma_r)^2 = 2\bar{\sigma}^2$$

For the case of pure shear in a stress system defined by principal stresses  $\sigma_1, \sigma_2, \sigma_3$  then  $\sigma_3 = 0, \sigma_1 = k$  and  $\sigma_2 = -k$ . Under these conditions the Von Mises criteria give the plastic relationship:

$$6k^2 = 2\bar{\sigma}^2 \quad \text{or} \quad k = \frac{\bar{\sigma}}{\sqrt{3}}$$



## 2.2 CONSTITUTIVE EQUATIONS

It is a fundamental tenet of materials science that the current properties of a material depend entirely upon its current metallurgical structure and that changes in property result from changes in structure. The structure may, however, change as the property is being tested, for example by ageing. The dislocation structure occupies a special place in its relation to mechanical properties because it necessarily changes during the test. This is obviously true in a dynamic sense since it is dislocation motion that causes the deformation; but it is also true in a dynamic sense when the material strain hardens.

The macroscopic variables of deformation are the prescribed mean equivalent flow stress  $\bar{\sigma}$ , the temperature  $T$ , the mean equivalent strain-rate  $\dot{\bar{\epsilon}}$  and the strain  $\epsilon$  at time  $t$ . If the material is at low temperatures ( $< 0.1T_m$ ) where  $T_m$  is the lowest melting point of the material (in K) then the material work-hardens until the flow stress just equals the applied stress. In doing so its structure changes; the dislocation density (a 'state variable') increases, obstructing further dislocation motion, and the strain rate falls to zero. If, instead,  $\dot{\bar{\epsilon}}$  and  $T$  are prescribed, the stress rises as the dislocation density increases. However, for a given set of values of this and the other state variables  $S_i$  (dislocation density and arrangement, cell size, grain size, precipitate spacing etc.), the strength is determined by  $T$  and  $\dot{\bar{\epsilon}}$  or, alternatively, the strain rate is determined by  $\bar{\sigma}$  and  $T$ .

At higher temperatures ( $< 0.5T_m$ ), after some transient during which the state variables change, a steady state may be reached in which the material continues to deform with no significant change in the  $S_i$ . At very high temperatures ( $< 0.9T_m$ ), the state variables, instead of tending to the steady state may oscillate (because of dynamic recrystallization), but only about steady values so that stress temperature and strain rate may be related.

Clearly either stress or strain rate may be treated as the independent variable. If strain rate is chosen then each mechanism of deformation can be described by a rate equation which relates  $\dot{\bar{\epsilon}}$  to  $\bar{\sigma}$ ,  $T$  and  $S_i$ . If stress is treated as the independent variable then there exists a rate equation relating  $\bar{\sigma}$  to  $\dot{\bar{\epsilon}}$ ,  $T$  and  $S_i$ . Thus the equation may be written:

$$\bar{\sigma} = f(\dot{\bar{\epsilon}}, T, S_i, P_j) \quad (2.1)$$

where  $S_i$  are the state variables and  $P_j$  are the material properties invariant to the specific material.

The state variables  $S_i$  change during deformation. A second equation describes this rate of change in the form:

$$\frac{dS_i}{dt} = f(\dot{\bar{\epsilon}}, T, S_i, P_j) \quad (2.2)$$

This coupled set of equations are the constitutive law for a mechanism. Satisfactory forms exist for the rate equations 2.1 but the evolution of structure with time is less well understood. For a simple phenomenological theory it is

prudent to choose the list of variables to contain a single member,  $s$ , which is a non-zero positive valued scalar with the dimensions of stress. Such an internal variable may be considered variously as a ‘drag stress’, ‘hardness’, or ‘mechanical threshold’. The assumption that only a scalar characterizes the internal structure is, of course, a gross simplification. It will in general be inadequate, except (possibly) for certain special classes of loading histories such as uniaxial loading of constant sign. Nevertheless classical rate-independent theory assumes isotropic hardening and the approach is worth pursuing. Various models have been proposed, generally designating a single state variable, frequently the dislocation density or some function of this parameter, or even by using strain as a substitute for the state variable.

In the extrusion process the deformation is continuous and the strains are large throughout most of the deformation zone. We are therefore able to assume steady state and in these conditions:

$$\frac{dS_i}{dt} = 0$$

and the constitutive law reduces to:

$$\bar{\sigma} = f(\dot{\bar{\epsilon}}, T) \quad (2.3)$$

Clearly we may not make this assumption if we are using the equation in an incremental model (F.D or FEM) because the elements at the entry to the deformation zone cannot be correctly described, leading to instabilities of the solution.

However for all practical operations we may assume that the Zener–Hollomon equation as modified by Sheppard [2] will suffice to describe the behaviour of aluminium alloys:

$$\bar{\sigma} = \frac{1}{\alpha} \ln \left\{ \left( \frac{Z}{A} \right)^{1/n} + \sqrt{\left[ \left( \frac{Z}{A} \right)^{2/n} + 1 \right]} \right\} \quad (2.4)$$

where  $Z = \dot{\bar{\epsilon}} \exp \left( \frac{\Delta H}{GT} \right)$

and  $\dot{\bar{\epsilon}}$  is the strain rate,  $\Delta H$  is the activation energy for deformation,  $T$  is the temperature (discussed in detail below),  $\alpha$  and  $n$  are material constants and  $G$  is the universal gas constant which indicates that the process is essentially one of mass transfer. The most common equation used to represent the strain rate  $\dot{\bar{\epsilon}}$  is that proposed by Feltham [3] and is given by:

$$\dot{\bar{\epsilon}} = \frac{6D_B^2 V_R \ln R}{D_B^3 - D_E^3}$$

where  $D_B$  and  $D_E$  are the billet and extrude diameters  $V_R$  is the ram speed and  $R$  is the extrusion ratio  $D_B^2/D_E^2$ . Useful modifications have been introduced to this equation from work in the upper bound and finite-element analyses and these are described in subsequent sections.

### 2.3 THE EXTRUSION PRESSURE

The first estimation of extrusion pressure was probably made by Siebel and Fangmeir [4] and was based on the assumption of uniform deformation. Thus it is a *lower bound* representing the minimum energy required to achieve deformation. All extrusion pressure calculations are based upon steady-state pressures and hence represent a lower pressure than is actually required.

$$\text{internal work done per unit volume} = \bar{\sigma} \, d\bar{\epsilon}$$

Assuming  $\bar{\sigma}$  to be independent of strain rate and steady-state extrusion to occur at constant temperature:

$$\text{work done per unit volume} = \bar{\sigma} \int \frac{dL}{L}$$

where  $L$  is the billet length.

$$\bar{\sigma} \int \frac{dL}{L} = \bar{\sigma} \ln \frac{L_2}{L_1} = \bar{\sigma} \ln \frac{A_1}{A_2} = \bar{\sigma} \ln R$$

where  $R$  is the extrusion ratio.

$$R = \frac{A_1}{A_2}$$

external work done by the ram =  $pAL$  where  $A$  and  $L$  are the area and length of the billet and  $p$  is the required pressure.

$$\text{external work done per unit volume} = p$$

Hence: 
$$p = \bar{\sigma} \ln R \quad (2.5)$$

This formula underestimates the extrusion pressure by about 60% because it ignores the peak in the pressure curve and, more importantly, ignores friction and redundant deformation.

The practical situation can be analysed by:

- local stress evaluation;
- upper bound theory;
- slip line field theory;
- finite element analysis.

The results of these analyses all agree with the experimental observation and each yields formulae of the form:

$$p = \bar{\sigma} (a + b \ln R + cL) \quad (2.6)$$

where the  $a$  term in this equation is assumed to be due to the contribution of the massive redundant work associated with this form of deformation whilst the  $c$  term is the friction coefficient and the  $b$  term is also an indication that deformation is far from the homogenous event assumed by Siebel and Fangmeir.

### 2.3.1 Bulk analysis

If the pressure anywhere within the container is the same at all points across any transverse plane, as shown in Fig. 2.3, then considering the force equilibrium in the  $x$  direction we may write:

$$d\sigma_x \frac{\pi D_B^2}{4} = \mu \sigma_r \pi D_B dx$$

where  $\sigma_x$  is the pressure in the billet at a distance  $x$  from the ram,  $\mu$  is the coefficient of friction,  $D_B$  is the diameter of the billet or container and  $R$  is the extrusion ratio. The values of  $\sigma_x$  at  $x = 0$  and  $x = L$  are  $p$  and  $p_r$ , respectively.

Rearranging we obtain:

$$D_B d\sigma_x = 4\mu\sigma_r dx$$

If we assume that  $\sigma_x = \sigma_r$

$$D_B d\sigma_x = 4\mu\sigma_x dx$$

which may be integrated from  $x = 0$  to  $x = L$  to give:

$$\left[ \ln \sigma_x \right]_p^{p_r} = \left[ \frac{4\mu x}{D_B} \right]_0^L$$

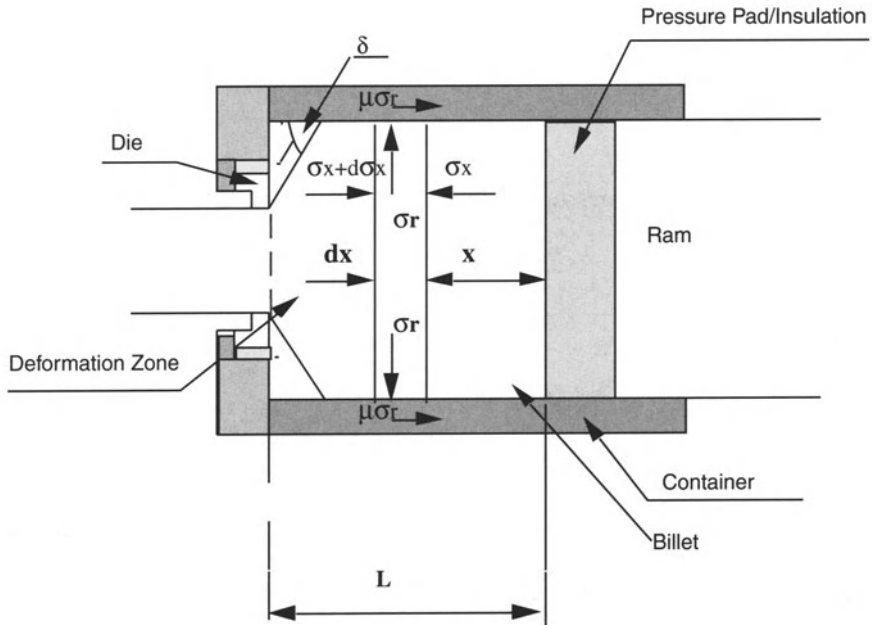


Fig. 2.3 Stresses on a plane in the direct extrusion process.

Hence:

$$\ln \left\{ \frac{p_T}{p} \right\} = \frac{4\mu L}{D_B}$$

and

$$p_T = p \exp \left( \frac{4\mu L}{D_B} \right) = \bar{\sigma} (a + b \ln R) \exp \left( \frac{4\mu L}{D_B} \right)$$

which is of the same form as equation 2.6.

If, as is normally the case, sticking friction conditions are assumed to obtain then the equilibrium equation is:

$$D_B d\sigma_x = 4\mu k dx$$

giving

$$D_B d\sigma_x = \frac{4\bar{\sigma}}{\sqrt{3}} dx$$

which on integration yields

$$p_T = p + \frac{4\bar{\sigma}L}{D_B\sqrt{3}} = \bar{\sigma} (a + b \ln R) + \frac{4\bar{\sigma}L}{D_B\sqrt{3}}$$

such that

$$p_T = p + \frac{4\bar{\sigma}L}{D_B\sqrt{3}} = \bar{\sigma} (a + b \ln R) + \frac{4\bar{\sigma}L}{D_B\sqrt{3}}$$

or

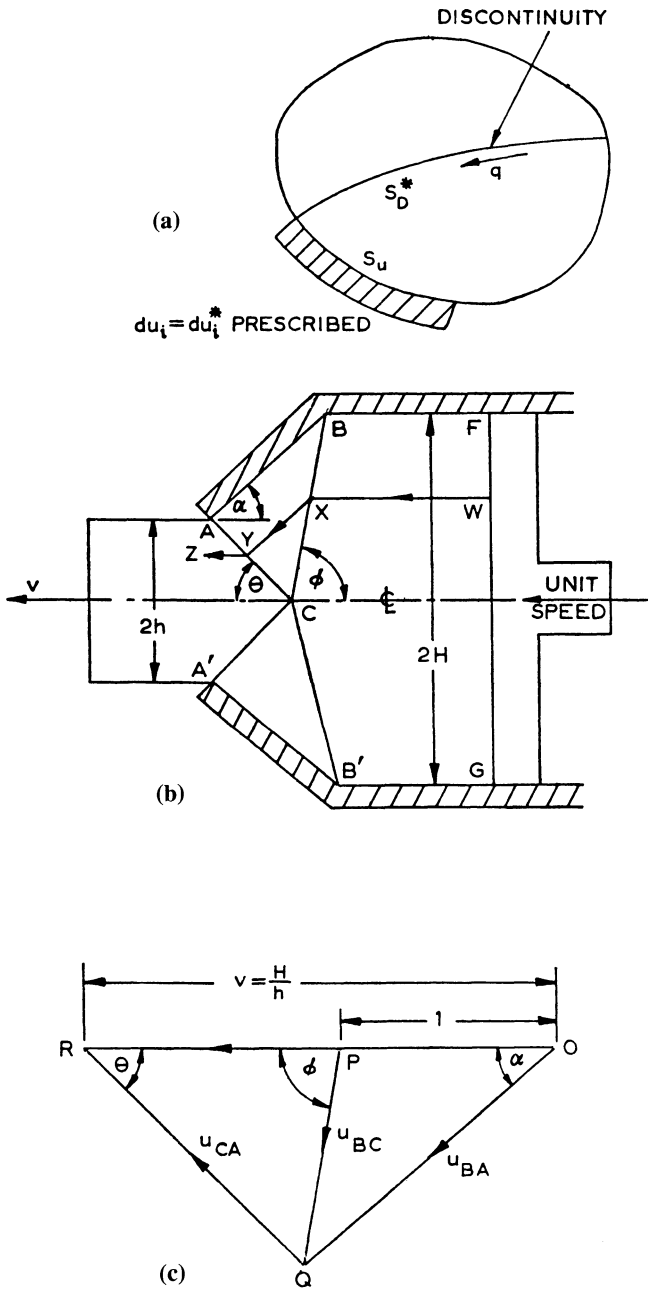
$$p_T = \bar{\sigma} \left( a + b \ln R + \frac{4mL}{D_B\sqrt{3}} \right) \tag{2.7}$$

where  $m$  is a friction coefficient to account for the observation that the stress at the container/billet interface is rarely observed to be the shear yield stress  $k$ . We would expect, however, that the value for  $m$  should be close to 1. Equation 2.7 is once more similar to the empirical equation 2.6.

### 2.3.2 The upper-bound theorem [5]

Suppose an actual displacement field is denoted by  $du_i$  and any other different or assumed field by  $du_i^*$  such that  $du_i^* = du_i$  on  $S_u$  i.e.  $du_i$  is prescribed over the part of the boundary  $S_u$  as shown in Fig. 2.4. Both fields are required to fulfil the incompressibility condition  $du_i^*/dx = 0$  and  $du_i/dx = 0$  otherwise the spherical components of stress would do work.

A kinematically admissible displacement incremental field may have discontinuities in the tangential direction along certain surfaces  $S_D$  but normal components must be the same on each side of the surface in order that there should be no plastic volume change.



**Fig. 2.4** Upper-bound plain strain (a) generalized physical field; (b) physical field (direct extrusion); (c) hodograph.

Denoting by  $d\epsilon_{ij}^*$  the assumed plastic strain increments derivable from  $du_i^*$  in accord with standard elasticity theory, and applying the principle of virtual work to the kinematically admissible displacement incremental field and the actual stress field  $\sigma_{ij}$  then

$$\int_S T_i du_i dS = \int_V \sigma_{ij} d\epsilon_{ij}^* dV + \sum \int_{S_D} q (dV^*) dS_D \quad (2.8)$$

where  $dV^*$  is the displacement incremental discontinuity on  $S_D^*$  and  $q$  is the shearing stress component of  $\sigma_{ij}^*$  in the direction of the discontinuity. If  $\sigma_{ij}^*$  is a stress field not necessarily statically admissible but derivable from the strain increment field  $d\epsilon_{ij}^*$  then:

$$\int_V (\sigma_{ij}^* - \sigma_{ij}) dV \geq 0$$

$$\int_V (\sigma_{ij}^* d\epsilon_{ij}^*) dV \geq \int_V (\sigma_{ij} d\epsilon_{ij}^*) dV \quad (2.9)$$

Substituting in equation 2.8 we obtain:

$$\int_S T_i du_i dS \leq \int_V (\sigma_{ij}^* d\epsilon_{ij}^*) dV + \sum \int_{S_D} q (dV^*) dS_D$$

since the shear yield stress  $k > q$ .

Associated with the fictitious surface stresses  $T_i^*$  acting through the same incremental displacements as those undergone on the surface of the real body, is an amount of plastic or internal work equal to that associated with the fictitious stress distribution.

Now 
$$\int_S T_i du_i^* dS = \int_{S_U} T_i du_i^* dS_U + \int_{S_T} T_i du_i^* dS_T$$

because  $T_i$  is prescribed as being equal to  $T_i^*$  on  $S_T$ . Consequently:

$$\int_{S_U} T_i du_i^* dS_U \leq \int_V (\sigma_{ij}^* d\epsilon_{ij}^*) dV + \sum \int_{S_D} q (dV^*) dS_D - \int_{S_T} T_i du_i^* dS_T$$

The RHS is an upper bound for the increment of work of the unknown surface tractions acting on  $S_U$ .

For plane strain conditions:

$$\int_V (\sigma_{ij}^* d\epsilon_{ij}^*) dV = \int_V k d\gamma^* dV$$

where  $k$  is the shear yield stress and  $d\gamma^*$  is the maximum engineering shear strain increment. If we consider only cases where  $d\gamma^* = 0$ , i.e. modes of deformation composed of rigid blocks of material separated by lines of discontinuity, then  $\int_V k d\gamma^* dV = 0$ . Further, in every instance the term  $\int_{S_T} T_i du_i^* dS_T = 0$  and then:

$$\int_{S_U} T_i du_i dS_U \leq \sum \int_{S_D} k d\gamma^* dS_D \quad (2.10)$$

stating that the external work done is equal to the internal energy consumed.

Originally only plane strain upper-bound solutions existed usually utilizing hodographs involving discontinuities which were linear. It is, perhaps easier to understand the method by considering a simple solution first proposed by Johnson and Kudo [6].

Figure 2.4(b), (c) shows a solution for extrusion through perfectly smooth cone shaped dies. Material originally moving with unit speed in the direction WX encounters the velocity discontinuity BC and is constrained to move in direction XY parallel to the die face AB. On exit to the die, the metal encounters a further discontinuity at AC and is forced to exit the die in the prescribed horizontal direction. The hodograph in Fig. 2.4(c) is constructed by:

1. ensuring that  $V = H/h =$  extrusion ratio  $R$ ;
2. adjusting the angles  $\theta$  and  $\phi$  until condition 1. is achieved. Since  $\theta$  and  $\phi$  are not independently variable the best solution is the least pressure calculated. This may be achieved by straightforward differentiation or by minimization techniques.

The internal dissipation of energy is given by:

$$\dot{E} = k (BC U_{BC} + CA U_{CA})$$

whilst the external work done  $= p 1 H$

$$\text{Hence:} \quad \frac{p}{2k} = \frac{(BC U_{BC} + CA U_{CA})}{2H}$$

It is usually not necessary to draw the hodograph because the lengths presented inside the brackets can be expressed in terms of the extrusion ratio and the angles  $\theta$ ,  $\phi$  and  $\alpha$ . Note that for the case of frictionless extrusion  $\alpha$  is fixed and  $\phi = f(\theta)$ .

This solution is, of course, impractical because it does not recognize that, in general, a dead metal zone is formed and shearing occurs along the container/billet interface. If we assume, that in Fig. 2.4(c), BA represents the dead metal zone and the length of the billet is  $L$  it is obvious that the resulting equation will be:

$$\frac{p}{2k} = \frac{[BC U_{BC} + CA U_{CA} + BA U_{BA} + 2(L - BA \cos \alpha)]}{2H}$$

which when optimized for the angles and regressed again yields an approximately linear function in  $\ln R$  giving:

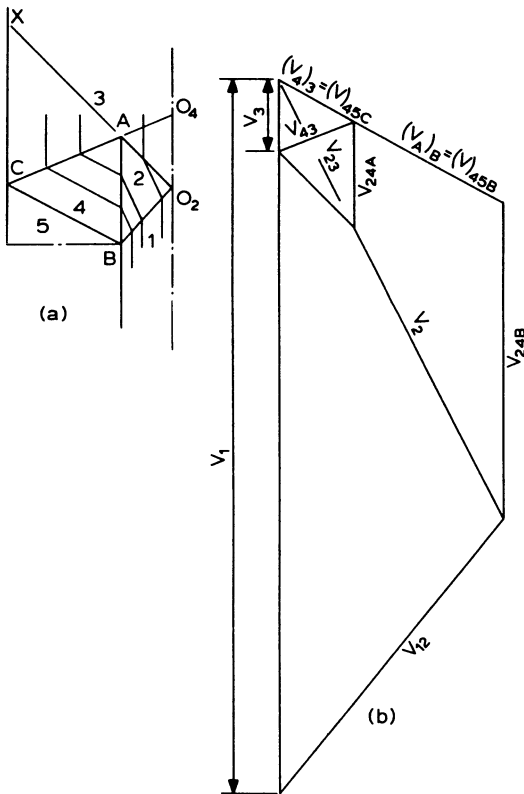
$$\frac{p}{2k} = a + b \ln R + cL$$



*Axisymmetric upper bound*

Upper-bound techniques have been extended to the axisymmetric case. The most accurate results were obtained using a minimized axisymmetric solution of the type first proposed by Adie and Alexander [7], Halling and Mitchell [8,9] and subsequently modified by Sheppard *et al.* [10]. This approach has allowed the consideration of large extrusion ratios, particularly important when considering the industrial process. The majority of empirical formulae used by industry have been developed from mathematical and experimental data generally obtained at extrusion ratios less than 10.

The diagrams presented are based upon a double-triangle velocity field, which with its corresponding kinematically admissible hodograph, is shown in Fig. 2.5. Flow takes place in region 2 as if velocity discontinuities formed the triangle  $BXO_2$  and in region 4 as if velocity discontinuities formed the triangle  $BCO_4$ . Streamlines are thus parallel to  $BX$  and  $BC$  in regions 2 and 4 respectively. The velocity vectors in regions 2 and 4 are constant on lines through  $O_2$  and  $O_4$ .



**Fig. 2.5** Axisymmetric upper bound (a) physical field; (b) hodograph.

The best upper-bound solution will minimize the expression for the internal rate of energy dissipation:

$$\dot{E} = \dot{E}_{12} + \dot{E}_{23} + \dot{E}_{34} + \dot{E}_{45} + \dot{E}_{24} + \dot{E}_4 + \dot{E}_2 = pV_B A_B / 2 \quad (2.11)$$

where  $\dot{E}_{ij}$  is the energy expended in crossing a discontinuity,  $\dot{E}_{ii}$  is the work done in the  $i$ th domain and  $V_B$  and  $A_B$  are the billet velocity and area, respectively. This yields the solution:

$$\dot{E} = \sum_{ij=1}^n \left( \int_V \bar{\sigma} \dot{\bar{\epsilon}} dV + \int_S T_{ij} V_{ij} dS \right) \quad (2.12)$$

For each deforming region, the velocity along a streamline,  $v$ , is constant along a radius drawn from the origin such as  $O_2$ ,  $O_4$  etc. When the deforming region is specified in spherical coordinates from that origin, then  $E_i$  can be reduced to a function in  $r$  and  $\beta$  only. This function may then be integrated and minimized using an adaptation of the quasi-Newton method [14] by selecting angles not fixed by the geometry of the problem. Energy input is the product of the pressure and ram velocity; thus the required external pressure may be calculated. This pressure can be represented in the form:

$$\frac{P_b}{\sigma} = a + b \ln R$$

Here  $p_b$ , representing what may be regarded as a base pressure, is not immediately useful to the industrial processor, because it represents the pressure required at the end of the ram stroke with no temperature rise. Further pressure will be required to overcome friction or cylinder wall shear and the additional pressure is necessary to ensure initial product breakthrough. When the term for friction is included this formula is similar to equation 2.7 above and yields:

$$p = \bar{\sigma} \left( 0.171 + 1.86 \ln R + \frac{4mL_b}{D_B \sqrt{3}} \right)$$

The strain rate varies from point to point throughout the deformation zone during the extrusion process. It is thus necessary to define some average value for this parameter. There are two techniques which appear to be acceptable in order to perform this calculation; the finite-element technique and the minimized upper-bound extrusion solution. The latter technique requires less computer time and when coupled with piecewise integration can consider variations occurring in the flow stress and strain rate during extrusion.

Having obtained the minimized solution it is possible to evaluate the strain rate at any point in the deformation zone since  $\dot{\bar{\epsilon}}$  reduces to a function in  $\theta$  only where  $\theta$  defines the lines bounding the region  $i$ . The mean equivalent strain rate may then be evaluated by piecewise integration and time averaging along a streamline coupled with area averaging over the deformation zone. It is this analysis which has been used in the calculation of the temperature compensated strain rate,  $Z$ , in the relationships presented in this chapter. Regression analysis yields a modified solution of Felthams' equation which may be written:

$$\dot{\bar{\epsilon}} = \frac{6V_R D_b^3 (0.171 + 1.86 \ln R) \tan (38.7 + 6.9 \ln R)}{D_B^2 - D_E^2}$$

### 2.3.3 Finite-element solutions

The application of numerical techniques to the continuum mechanics problem, developed over the last decade, has improved the capability for an integrated treatment of both tool-load demands and internal micromechanics [11–18]. Their implementation as computer codes, with thermomechanical balance and kinematic compatibility built in, has introduced a modelling tool driven only by the external boundary conditions and the material behaviour. Thus, additional assumptions such as the pre-setting of discontinuity lines – as in U.B. techniques – are not necessary. Because of their flexibility in reproducing almost any required geometry, finite-element techniques must be regarded as *potentially* the most practical tool presently available. Although offering great potential, there are two main problems when applying the analysis to the hot extrusion of rate-sensitive alloys: (a) re-meshing when dealing with large reductions (in practice extrusion ratios of up to 100:1 may be encountered); (b) the absence of any accepted procedure using a well-defined material constitutive equation which will result in the accurate prediction of both mechanical and microstructural development over the large variations in loading conditions expected in the metallurgical three-dimensional extrusion process.

In the real process, each elementary volume in the cross-section of extruded product is known to be subjected to a different deformation history during its path through the deformation zone. Such deformation histories reveal very complex situations of dynamic loading involving yielding, strain and strain rate hardening. Unloading is also complex, encompassing thermally activated recovery and recrystallization, time softening and relaxation of the hydrostatic stress. However, evidence from analysis of grids obtained from billets which have been partially extruded suggests that a quasi-steady state exhibiting little alteration in flow pattern at spatially fixed locations (i.e. referred to the container) may be obtained after the breakthrough pressure has been reached and before the ram advances to the point at which the vicinity of the container and die will change the flow. This is an indication that both the competitive metallurgical changes and the influence of stress gradients on material flow achieve an equilibrium such that further spatial alterations do not occur. Both load displacement traces and partial extrude examination reveal that the flow pattern is predominantly defined by the mode of operation (e.g. direct or indirect extrusion), the lubricating conditions obtaining at the boundaries and the geometry of the tooling. Reported viscoplastic-penalty finite-element solutions have been validated for scattered case studies, mainly in terms of tooling load and velocity distributions and for low extrusion ratios. Even for such cases, it can be observed that the proximity of the macroparameters to slip-line solutions does not always guarantee a consistency between achieved

stresses and imposed boundary conditions. Furthermore, even less attention has been paid to both large reductions and the resulting strain rate localisations, which can be of critical importance when attempting to predict the product microstructure. These problems are considered in this section, identifying typical flow and deformation patterns for both direct and indirect extrusion through flat-faced dies under different geometrical and frictional conditions. The influence of the boundary conditions upon the kinematic definition is explored assuming a constant flow stress material.

Since a perfectly plastic material is assumed, alternative solutions are available using slip-line field and upper-bound techniques and the results can be compared. Alterations in the flow stress due to geometrical effects cannot be considered, but it is possible to examine large axisymmetric extrusion ratios which are more representative of the actual process.

#### 2.3.4 Comparison of finite-element modelling with upper-bound and slip-line field techniques

The major problem connected with FEM solutions is in determining whether the solution provides an answer corresponding to the physical extrusion parameters being investigated [19]. It will therefore be useful, at the outset, to debate the methodology as simply as possible and to compare simple solutions with slip-line field analysis which is mathematically sound and with upper-bound solutions which may be derived with substantially less computer effort. We shall also see that simpler and very rapid temperature solutions may be comparable to FEM. In fact, we shall present temperature solutions which are sufficiently rapid to use in an on-line mode.

For reference purposes it will be useful to summarize the method of analysis. The description of viscoplastic incompressible flow assumes that the deviatoric components of the stress tensor are described by the constitutive law:

$$\sigma'_{ij} = 2\mu \dot{\epsilon}_{ij} \quad (2.13a)$$

where

$$\mu = \frac{\bar{\sigma}}{(\sqrt{3})\dot{\bar{\epsilon}}_{ij}} \quad (2.13b)$$

the bar indicating effective values with  $\sigma = \sigma_0$  for a perfectly plastic material. The hydrostatic components are:

$$\sigma_i^h = \alpha \dot{\bar{\epsilon}}_i^v \quad (2.14a)$$

where  $\alpha$  is analogous to the bulk modulus in elastic problems and if designated of sufficient magnitude allows the enforcement of the incompressibility condition  $\dot{\bar{\epsilon}}_i^v = 0$ . Application of the virtual work principle based on the energy rate density  $(\sigma' + \sigma_h) \dot{\bar{\epsilon}}$  over the deformation volume discretized by finite elements produces a non-linear algebraic system of equations:

$${}^1K_{ij} + {}^2K_{ij}v_j + f_i = 0 \quad (2.14b)$$

in which the stiffness matrix coefficients  $K_{ij}(u)$  are integrals numerically computed by selective integration and  $u$  and  $f$  are, respectively, nodal velocities and nodal forces. Alternative treatments of boundary conditions and mesh geometry are possible and are discussed below.

The numerical simulation of the extrusion process may also be based on a two-dimensional Eulerian description (as opposed to Lagrangian) with thermomechanical coupling in the time domain. A finite element discretization is applied and the space of the billet, container, die and ram is divided into small elements of triangular shape [20]. Container and die are assembled into one mesh. The aluminium mesh is refined close to the outlet where the strain rate gradients are steep and a high degree of accuracy is wanted. Since the metal is effectively flowing through the mesh no penalty function need be applied since the incompressibility relationship may be maintained by normal means (i.e.  $\bar{\epsilon}_{ij} = 0$ ). However a further effect of the material flowing through the mesh is that it is not possible to predict material structural changes.

Two-dimensional triangular finite elements are used to discretize the aluminium, container, die and ram. Along the boundary between the aluminium and the surrounding container, die and ram, one-dimensional bar elements may be inserted to describe velocity boundary conditions different from 'full stick' or 'full slip' and heat flux governed by heat transfer.

Velocities are interpolated within each element using a complete quadratic polynomial through corner and midside nodes. The pressure is linear within each element. In the case of temperature calculations, the elements are split into four linear equally shaped subtriangles in order to obtain a simple upwinding formulation of the convective part of the heat balance differential equation.

The incremental finite-element equations for the individual elements are obtained from an integrated incremental form of the governing equations, following a traditional Galerkin procedure. The corresponding finite-element equations of the total system are established through a straightforward procedure where the individual finite elements are assembled, yielding two systems for the aluminium mesh (material flow and temperature), one system for the container and die mesh (temperature) and one system for the ram mesh (temperature).

The time is divided into a number of steps and the final set of equations has to be satisfied at the end of each step by equilibrium iterations.

The total acceleration will be dominated by the convective part and therefore a simplified time domain analysis is sufficient for the velocity and pressure system of the aluminium. The local acceleration at the end of a time step is therefore given by an approximation to the mean value within the time step. In the temperature case, a full implicit formulation in the time domain is used with constant mean value of the temperature change during a time step. The coupling within the total system is very similar to the Integral Profile solution shown in Fig. 2.14.

The velocity and pressure field in the aluminium are coupled to the temperature field through a temperature dependent viscosity factor and through heat generation by stresses and strain rates and also by the convective part of the temperature change.

When the ram is close to the die, the original mesh will be severely compressed and may not be representative of the real problem. It is therefore possible to change the mesh topology at certain user-defined ram positions. If the mesh topology is changed at a ram position, then the basic variables are found at the new nodal positions by interpolation in the old mesh. Obviously, equilibrium will not be satisfied by the interpolated values and therefore equilibrium iterations have to be performed in the new mesh. Two sets of results are then found at the time for which the mesh topology has been changed.

Conservation of energy implies that the rate of change of internal energy in the material equals the work produced by the stresses and the heat generated. It is assumed that the internal energy is a function of temperature only and that Fourier's law of heat conduction applies. The final expression for the heat balance may then be written as:

$$\frac{\partial}{\partial X_i} \left( k_{ij} \frac{\partial T}{\partial X_j} \right) + \bar{\sigma}_{ij} \dot{\epsilon}_{ij} = \rho c \left[ \frac{\partial T}{\partial t} + (u_i - u_0) \frac{\partial T}{\partial X_i} \right] \quad (2.15)$$

where  $c$  is the heat capacity,  $k_{ij}$  is the heat conduction parameter and  $T$  the temperature. Usually the time is divided into convenient steps and the equation expressed in incremental form.

In classical two-dimensional plastic flow the principal stresses within the body must satisfy:

$$\sigma_{1,2} = \sigma^h \pm \left[ \left( \frac{\sigma_x - \sigma_y}{2} \right)^2 + \tau_{xy}^2 \right]^{1/2} \quad (2.16)$$

$$\tan(x,1) = \frac{2\tau_{xy}}{\sigma_x - \sigma_y} \quad (2.17)$$

where  $(x,1)$  is a set of local axes normal-tangential to the tool.

Thus, when container shear is ignored (i.e. perfect lubrication) the numerical solution must yield principal stresses which have not rotated with respect to the  $(x,y)$  frame. As soon as deviatoric deformation occurs the angle  $(x,1)$  must depart from zero. In the limit, the magnitude of the shear  $\tau_{xy}$  should reach the value of the yield surface radius with  $\sigma_x = \sigma_y$  and  $(x,1) = 45^\circ$ . These properties of principal stress axes, although simple, are an invaluable tool in detecting discrepancies between the solution and the imposed boundary conditions, which are not easily recognizable from other computed data such as overall load or pressure, or even from the velocity fields.

*Treatment of friction*

The boundary conditions imposed can often only deal with extreme friction situations involved in either fully lubricated or sticking interfaces. In the practical case the conditions are likely to lie somewhere between these extremes. These conditions may initially be dealt with following the method suggested by Zienkiewicz *et al.* [16] in which a thin boundary element is introduced having outer nodes firmly restrained at the container interface. The flow stress in equation 2.13b for this element changes from hydrostatic control:

$$\sigma = m |\sigma^h| = m\alpha |\dot{\epsilon}^v| \quad \text{for } \sigma \leq \sigma_0 \quad (2.18a)$$

to sticking shear

$$\sigma = \sigma_0 \quad \text{when } \sigma \geq \sigma_0 \quad (2.18b)$$

However, the use of this condition for an extrusion ratio of say  $R = 20$  cannot differentiate between load requirements even when the  $m$  factor varies between 0.2 and 1.0. For high axisymmetric extrusion ratios there are very large hydrostatic stresses which tend to predominate over shear, thus forcing equation 2.18 to degenerate to the sticking condition  $\sigma = \sigma_0$  regardless of the value of the  $m$  parameter. A more pragmatic approach must therefore be adopted, suggested by upper-bound techniques in which the flow stress in equation 2.18b for the interface element is written:

$$\bar{\sigma} = m\sigma_0 \quad (2.19)$$

Thus, when  $m = 1$  the boundary layer material cannot be distinguished from the rest of the billet and perfect sticking friction obtains, whilst  $m = 0$  allows for infinite sliding along the interface without any frictional resistance.

*Axisymmetric rod extrusion*

The die wall reactions computed for direct extrusion with correct frictional treatment, show little scatter under both change of billet length and change of frictional  $m$  parameter. Therefore this property can be used to assess the load which would be required for the zero friction condition  $m = 0$  from the  $m \neq 0$  solutions. In order to do that, we define a ram-equivalent to the die wall pressure as:

$$p^* = \frac{\text{total reaction at the container face}}{\text{ram area}} \quad (2.20)$$

Thus,  $p^*$  provides an estimation of the frictionless component of the total ram pressure  $p$ . Some normalized  $p^*/\sigma$  results for low extrusion ratios are shown in Table 2.1 and compare favourably with reported upper-bound solutions using both linear and curved discontinuities as well as experimental results for fully lubricated extrusion of lead. At higher extrusion ratios' model predictions for  $p^*$  are lower than those produced using either single or double triangle minimized upper bounds (Fig. 2.5(a)), a result which is expected given the better definition

of the localisation's of high shearing areas in the FE model. It must be recalled that here the major strain lines M1 and M2 arise as a consequence of boundary conditions and are not preset *a priori* as the discontinuity lines of rigid upper-bound constructions.

**Table 2.1** Some comparative results from extrusion analysis

$r = 1 - \left( \frac{R_2}{R_1} \right)^2$	<i>Kobayashi and Thomsen</i> [12]	<i>Halling and Mitchell</i> [9]	<i>Adie</i> [7]	<i>Johnson</i> [6]	<i>Bianchi</i> $FE \frac{p^*}{\sigma}$ [18]	<i>Onate</i> $FE \frac{p}{\sigma}$ [16]
0.8	3.05	3.19	3.19	3.21	3.00	5.05
0.9	3.79	4.32	4.23	4.25	3.58	5.99

The FEM normalized pressure predictions are also lower than those calculated using Johnson's empirical fit to experiments. Results from hot extrusions of steel [19] and titanium [21] also reveal that, in practice, lubrication is rarely efficient enough to completely eliminate friction, particularly at the die entry; in Child's [19] viscoplasticity solution the directions of principal strain rates at the surface in contact with the die entry are not normal-tangential as would be expected from equations 2.16 and 2.17 for frictionless sliding, but exhibit tilting indicating the presence of shear. In spite of good lubrication elsewhere, this die entry shear can be significant, resulting in pronounced wear and die damage [21].

The total ram pressure  $p$  for axisymmetric unlubricated extrusion also shows both flow stress and billet length dependence (equation 2.7). The latter feature is clearly the result of container friction since  $p^*$  is invariant. For any given  $\sigma_0$  and billet length, the pressure  $p$  is a linear function of the logarithm of the extrusion ratio  $R$  and is parallel to the slope of the  $p^*$  line, a condition which would only hold for a perfectly plastic material. The finite-element predictions of ram pressure for unlubricated extrusion are also lower than those obtained by single and double triangle minimized upper-bound solutions.

Complete sticking between billet and tool can also be treated by tangential force specification where the magnitude is calculated from the maximum shear stress and the direction specified. This calls for extra predictor capabilities if the possibility of a neutral point exists (e.g. recirculating flow at the dead metal zone corner). Hence, sticking friction is more easily dealt with by constraining the tangential velocity to be zero and embedding the border nodes at the tool interface (Fig. 2.7(a)). This restriction implies that normal strain rates at the surface are not permissible,  $\dot{\gamma}_{xy}$  is the only strain rate component, and must produce a pure shear stress state at the interface. At the free surface of the extrusion there are no forces operating and therefore for the solution to be consistent the stress field must vanish.

Examination of the internal fields for the case of sticking friction clarifies some features of mesh dependency; the maximum strain rate line M2 (Figs. 2.7(b) and (c)) intersects both the 2nd and 5th rows, a situation which does not



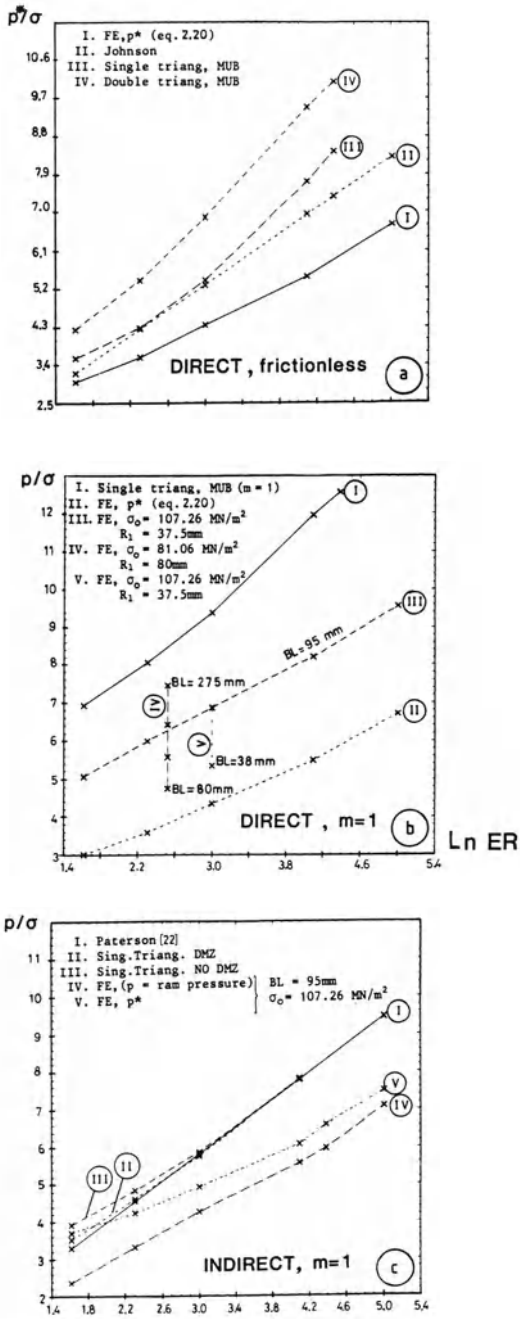


Fig. 2.6 Comparison of finite-element method and upper-bound results.

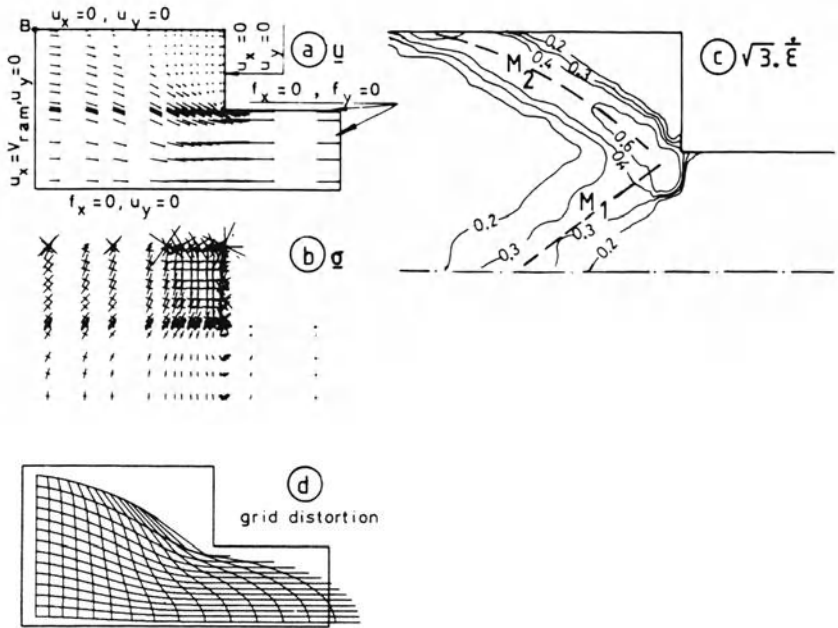


Fig. 2.7 Prediction by finite-element method of the principal slip lines M1 and M2.

occur when the extrusion is fully lubricated. Thus, general reductions of the critical mesh when sticking friction obtains is imperative in order to ensure that the gradients of the strain rate are spatially confined within very few elements, otherwise the resulting internal out of balance forces readily become unbounded producing deficient tool reactions (and overall pressures). Both maximum strain rate loci agree with the predictions of slip-line field theory.

A mean strain rate for the extrusion process can be calculated by averaging along the cylindrical surface defined by the median radial line of the  $3 \times 3$  element Gauss points.

Comparison with the Feltham estimation of  $\langle \bar{\epsilon} \rangle$  which is frequently used in metallurgical calculations indicates that FEM models give a reasonable approximation but that the variance with  $\ln R$  is parabolic rather than linear as suggested by the Feltham model (Fig. 2.8). At constant extrusion ratio both the FEM prediction and the Feltham estimate lie within the bounds set by the peaks achieved at the outer L3 and inner L1, L2 streamlines Figs. 2.9(a) and (b). This agreement deteriorates very considerably at higher extrusion ratios due to an absence of any spin correction in the  $\bar{\epsilon}$  measure.

The observations presented above clearly emphasize the non-homogeneous nature of the deformation, with strain rate and hydrostatic stress in particular exhibiting pronounced gradients. Although there is general agreement with slip-line

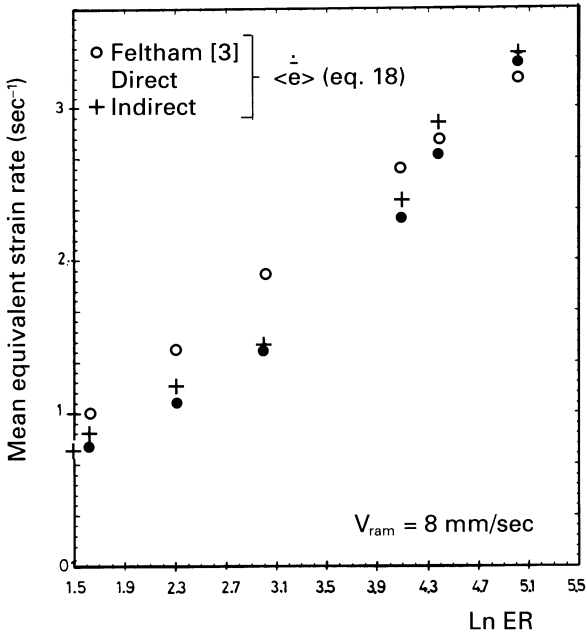


Fig. 2.8 Variation of mean strain rate with extrusion ratio.

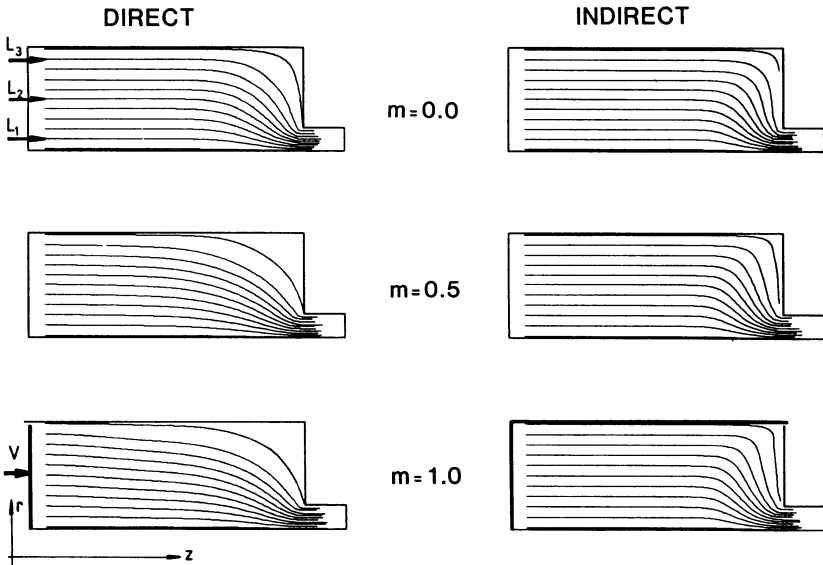


Fig. 2.9(a) Effect of friction conditions on the flow pattern.

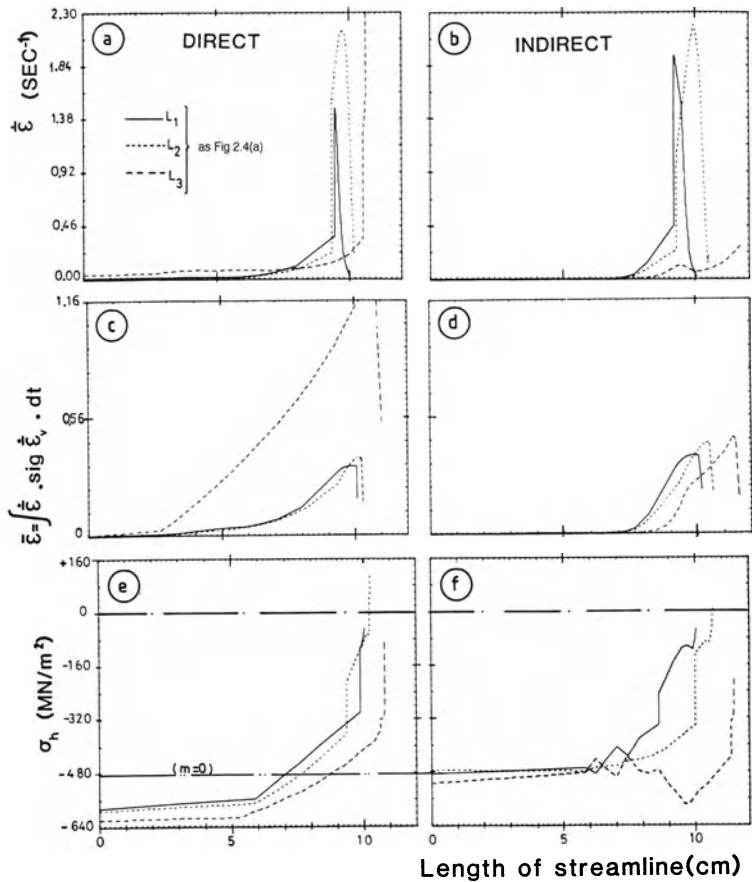


Fig. 2.9(b) Deformation history along streamlines.

field theory both in terms of the deformation zone and the principal stress orientation, the numerical solution is more complete and identifies maximum strain rate loci M1 which are simultaneously lines of maximum shear and maximum  $\dot{\bar{\epsilon}}$ . The line M1 is the most significant and is present in both direct and indirect extrusion under all lubrication conditions. As the material crosses this line it is subjected to a large strain rate sensitive deviatoric loading occurring simultaneously with a hydrostatic stress release which quenches the metallurgical microstructure developed at the  $\dot{\bar{\epsilon}}$  peak. *This explains the success of hot working theories in relating the product microstructure to the maximum  $\dot{\bar{\epsilon}}$  and temperature reached in the process at the discontinuity line M1.*

In fully lubricated direct extrusion, most of the external energy supplied is dissipated at the M1 line. This feature persists throughout the steady state flow even although the material experiences large dynamic loading as it crosses this region. The proximity of both total ram force and die reaction predicted by the numerical

results support that conclusion, which is also reflected in terms of the true ram pressure  $p$  and die pressure converted to ram area  $p^*$ .

On the other hand, the very well known dependence of ram load on displacement which is a characteristic of unlubricated direct extrusion can immediately be associated with the shortening of the high shearing line M2 as the ram advances. Significantly, the die reactions remain virtually independent of ram displacement and, furthermore, they almost coincide with the frictionless value. Therefore, as  $p^*$  is regarded as the frictionless component associated with the steady state achieved at M1, the fraction  $(p - p^*)$  represents the frictional forces varying with the length of M2. The resulting billet length dependency reported for  $p$  is related to a perfectly plastic plateau which corresponds to a slow rate loading along M2 where strain hardening and thermal softening balance each other with a resulting microstructural state parameter almost constant. Such behaviour would be expected to deviate in alloys exhibiting both large strain rate sensitivity of the flow stress and a high activation energy, when significant history dependency on the loading along M2 would result. The strain rate localization at M2 also introduces a characteristic strain accumulation at the border streamline L3 which is a unique feature of unlubricated direct extrusion. Also, because of the slow velocity loading rate along M2 and locking of the hydrostatic state, the strain accumulation at the border is more likely to achieve sufficiently high values to promote static recrystallization after the material has traversed the high temperature zone at M1. Thus, peripheral recrystallization is more likely to occur, introducing heterogeneity across the product section which is undesirable.

The fact that, regardless of the lubricating conditions, the indirect ram load is much lower than its direct counterpart, is related to the configuration of the M2 line, and its localization with respect to the container boundary. Friction, however, is not completely eliminated as shown by the presence of the line M3 which indicates the presence of a high shear in the material which even at extremely slow velocity manages to flow along the die wall. For a given extrusion ratio the length of the line M3 is constant and hence the die wall forces are independent of billet length. The forces at the ram face exhibit reduced scatter with the billet length due to some M2 influence, but it is very much smaller than in the direct extrusion case.

For unlubricated extrusion, a hydrostatic stress gradient can be detected across the streamlines at the rear of the billet, with the central line L1 (Fig. 2.9(a)) in a less compressive stress state than the flow lines L2 and L3 (Fig. 2.9(b)). If the forces resulting from that distribution were allowed to operate, they would promote flow towards the less compressed axial line, thus generating a void at the end of the ram stroke producing the well-known 'piping' defect. Because the absolute pressure and the hydrostatic gradient are both greater in the direct extrusion mode this defect is more likely to be observed in that mode.

We must conclude that FEM solutions are, in fact, upper-bound solutions and require experimental verification if they are to be utilized to model the practical extrusion process. We must also recognize that only two-dimensional analysis

have been presented and it may be easier to adapt other forms of solution to deal with the complex and three-dimensional flow which we would normally encounter. We will return to specific solutions and comparisons below.

## 2.4 THE FRICTION COEFFICIENT

The effect of friction in the direct extrusion process is important in the commercial process because it determines the billet size, either by pressure limitation or by surface limitation at the end of the ram stroke. One method used to evaluate the friction effect expresses the stress at the friction wall as a fraction of the shear stress as shown above of the material as:

$$\tau = \frac{4m\bar{\sigma}}{\sqrt{3}} \quad (2.21a)$$

For perfect lubrication  $m = 0$  and for sticking friction  $m = 1$ . This is a convenient way to express mathematically the magnitude of the pressure required to overcome friction, but assumes that all the force is absorbed in an infinitely thin layer at the surface, which is clearly incorrect. In effect, there is a shear zone with a finite depth at the container/billet interface in which the strain rate varies from zero at the shear zone/billet interface to some higher value at the container/billet interface. Thus the  $m$  value can give only an approximate guide to the friction conditions.

An alternative method is to define the shear stress in terms of a friction coefficient  $\mu$  and the applied pressure  $p$ , such that:

$$\tau = \mu p \quad (2.21b)$$

The friction coefficient is more quantitative than the stress coefficient  $m$  (but theoretically less reliable) and may be evaluated either by extruding billets of varying length or by considering the gradient of the pressure–displacement trace. Variation of pressure with billet length have been investigated for 1100 and 2014 [22] alloys by extruding billets of varying lengths under identical extrusion conditions. It was observed that the peak pressure/billet length relationship in each case was linear. The statistical data are given in Table 2.2 and the value of  $m$  determined from the data at 300°C was 0.88 for the 1100 alloy and 0.8 for the 2014 alloy, indicating that friction conditions are near the sticking point. Values of  $\mu$  were also determined from the experimental data, and are given in Table 2.2. They are of the same order as those found by numerous workers, but for both alloys the coefficient increased with temperature, which is contrary to previous observations.

**Table 2.2** Friction data for 1100 and 2014 alloys, using equations 2.21a and b;  $R = 30:1$ ,  $P = aL + C$

Alloy	Ram speed ( $\text{mm s}^{-1}$ )	Temperature ( $^{\circ}\text{C}$ )	a	c	Correlation	Constants	
						m	$\mu$
1100	8	300	1.88	320	0.9520	0.88	0.075
		400					0.092
2014	5	300	2.47	746	0.9965	0.88	0.048
		400	2.31	506	0.9937	0.88	0.055
		475	1.32	155	0.9633	0.88	0.098

Clearly neither of these methods of determining the friction coefficient is satisfactory, although for design purposes the use of  $m \approx 0.85$  would suffice. It would be theoretically possible to calculate friction using FD or FEM techniques but, in general, the definition of the container/billet interface friction is one of the boundary conditions required for a solution to the problem. It would thus require considerable experimentation coupled with an inverted solution in order to explain the friction phenomenon. We can, however, see that in effect the mechanism is a shearing of a layer of material at the interface; the thickness of the layer can be calculated as of the order of 40–100  $\mu\text{m}$ .

## 2.5 TEMPERATURE MODELS

### 2.5.1 Temperature profile in the heated billet

During induction heating the surface of the billet is rapidly heated, the depth of penetration depending on the frequency used and the alloy characteristics. It is usual to use mains frequency heaters (50 Hz) which in aluminium gives a penetration depth of about 18  $\mu\text{m}$ . Induction heating gives an excellent heat distribution around the circumference and under normal operating conditions the billet will leave the heater with not more than 3–4% variation between centre and surface. Hence by the time the billet reaches the press the temperature throughout the billet is uniform. Induction heating has the additional advantage that a predetermined taper can also be induced into the billet yielding the possibility of isothermal extrusion by these means.

Uniformity of heating in gas furnaces depends on the type of furnace and heat transfer. The heat is not developed internally but is transferred to the billet surface by radiation and convection. This can cause large temperature variations if the billet location and method of heat transfer are not carefully controlled. However, in modern gas furnaces the billet is heated, in effect, from all sides and a temperature profile as uniform as that obtained with an induction furnace is developed with a heating cycle of 15–20 min.

### 2.5.2 Heat balance in extrusion

Complex thermal changes commence as soon as the hot billet is loaded into the usually preheated container and extrusion started. They consist of the following individual processes:

- production of heat by deformation proceeding in front of the die in the deformation zone;
- production of heat by friction between the billet and the container and by shearing at the dead metal zone;
- transfer of heat as the billet moves towards the die;
- conduction of heat to the tooling (container, ram, die);
- conduction of heat to the billet;
- conduction of heat to the extrusion;
- production of heat by friction through the die.

With a knowledge of these factors it should be possible to calculate the mean exit temperature and several mathematical models have been developed. However, all these models involve certain assumptions to simplify the analysis and these are detailed in the individual references [23–30].

The decisive temperature in extrusion is the exit temperature of the extruded product which depends on all the above factors. It increases if the heat produced by deformation and friction exceeds the heat losses and decreases if the reverse is true. Heat conduction requires a definite time and therefore, depending on the alloy and the extrusion conditions, heat production predominates above a certain ram speed. This explains the dependence of the temperature profile along the length of the extrusion on the ram speed. In extremely rapid extrusion adiabatic extrusion could occur; no heat lost to the surroundings and all the heat developed retained in the deformed material. We would not normally experience these conditions. The laws governing heat balance must be known if the extrusion process is to be under optimal control (a constant exit temperature maintained). Several methods of calculating temperature rise during extrusion have been developed.

Akeret [23,30] developed an approximate numerical method in which the temperatures are calculated point by point or cell by cell. The billet is assumed to be divided into a number of uniform discs and the work done and heat transferred calculated as each disc is extruded.

The partial numerical solutions for the heat produced and the heat lost can be combined linearly and the temperature profile along the billet in the container and the extrusion obtained. The method is almost as time consuming as an FEM solution and does not appear to function well unless the container is hotter than the billet, a condition seldom encountered in practice.

In comparison with other theoretical methods a simple estimation of the temperature changes during extrusion can be made using the approximate equations of Stuwe [31]. He assumed that the increase in temperature of the emerging extrusion consisted of three components:



1. A temperature increase caused by the work of deformation that is almost entirely converted into heat (adiabatic):

$$\Delta T_1 = \frac{\bar{\sigma} \ln R}{\sqrt{3}(\rho_{al} C_{p(al)})}$$

where  $\rho$  is the density,  $C_p$  is the thermal conductivity,  $\bar{\sigma}/\sqrt{3}$  is the shear stress and  $R$  the extrusion ratio.

2. A temperature increase at the billet surface caused by friction at the container wall, taking the temperature balance within a given surface layer of the billet into account but assuming adiabatic deformation:

$$\Delta T_2 = \frac{\bar{\sigma}}{4\sqrt{3}(\rho_{al} C_{p(al)})} \sqrt{\left( \frac{V_R L_B}{\alpha_{al}} \right)}$$

where  $V_R$  is the ram velocity,  $L_B$  the billet length and  $\alpha$  the thermal diffusivity equal to  $k/\rho C_p$ .

This equation assumes that the heat developed by friction is divided equally and uniformly between the billet and the container to a depth of:

$$y \approx \sqrt{\left( \frac{\alpha_{al} L_B}{V_R} \right)}$$

3. A temperature increase at the extrusion surface caused by friction at the die land:

$$\Delta T_3 = \frac{\bar{\sigma}}{4\sqrt{3}(\rho_{al} C_{p(al)})} \sqrt{\left( \frac{V_E L_D}{\alpha_{al}} \right)}$$

where  $V_E$  is the exit speed and  $L_D$  the die length .

The depth of heating caused by this temperature difference is:

$$y_D = \sqrt{\left( \frac{\alpha_{al} L_D}{V_E} \right)}$$

The temperature rise caused by friction in the die land area indicates that this source of heat cannot be ignored – a statement borne out by the integral profile results shown below. It clearly has a significant influence on the maximum admissible billet temperature and extrusion speed for the following reasons:

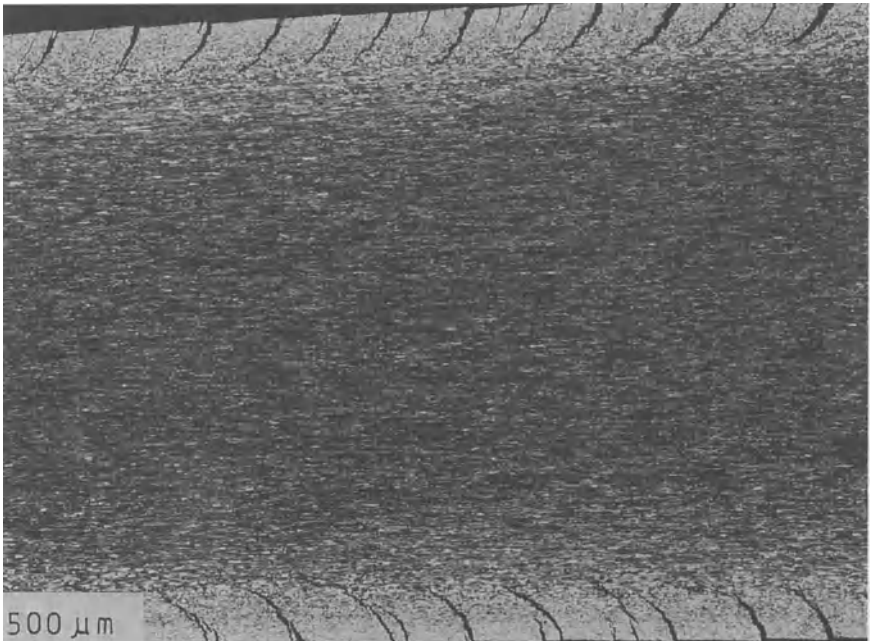
- The relatively high exit speed during extrusion of 6XXX alloys and the related brief contact time (< 0.005 s) mean that the temperature increase is concentrated in a thin surface layer, which is critical to the generation of an acceptable surface.
- The heating of the outside regions leads to a concentration of heat, especially at sharp edges on the extrusion, which increases the chances of undesirable surface defects.
- The temperature of the surface regions is already higher than that of the inside, because of the shearing and friction in the container [32].

In practice, if the exit temperature or speed is too high, tearing initially starts at the edges of the extrusion and then develops over the remainder of the surface (Fig. 2.10). The press operator has traditionally used these observations to regulate the press speed but, as we shall discuss, this duty should by now be in the more capable hands of a computer. Lange [32] has also attempted to calculate the temperature increase at the surface of rectangular extrudes, especially at the edges. Sections that are not too small are extruded at relatively high speeds, and therefore the temperature at the centre remains almost constant. Based on experience, Lange [32] assumes the temperature rise at the edges to be twice that at the midpoint of the sides, and this arrives at:

$$T = \frac{2.26b_e\tau}{(b_d + b_e)\lambda} \sqrt{(\alpha_{al}V_E L_D)}$$

$V_E$  is the maximum dimension of the extrude,  $L_D$  the die length,  $\alpha_{al}$  the thermal diffusivity of aluminium and  $\lambda$  a shape factor.

The temperature increase at the edges of a square section was calculated using this equation, and the results are shown in Fig. 2.11. The importance of the length of the die land on the temperature rise is also illustrated in Fig. 2.11.



**Fig. 2.10** Mechanism of tearing of surface.

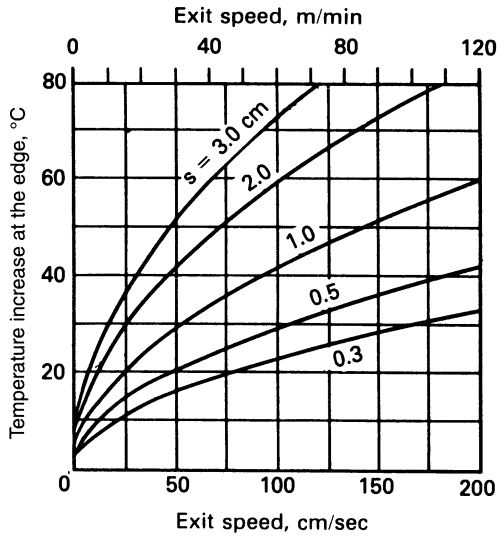
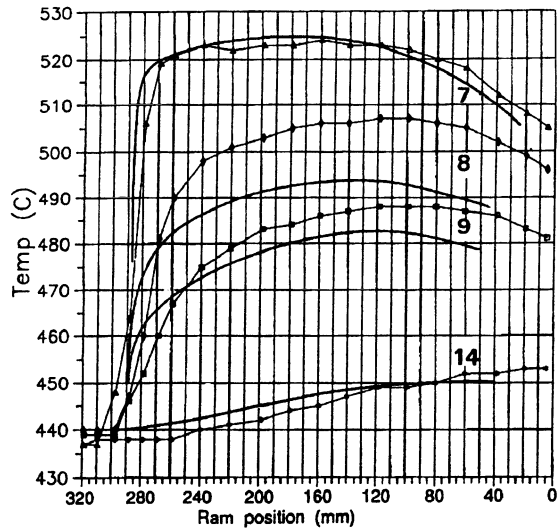


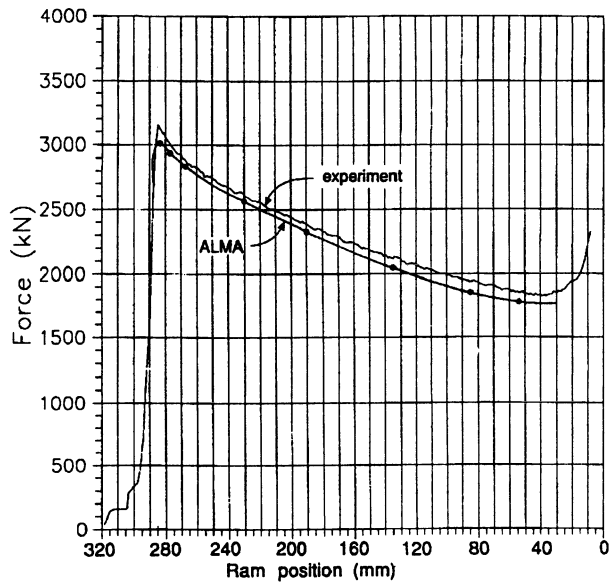
Fig. 2.11 Temperature increase at the edge of a square bar [31].

### 2.5.3 Finite-element modelling predictions

Numerous temperature linked FEM models have been proposed. However, few give any experimental verification. It is also apparent that the cost and complexity in developing FEM modelling techniques preclude their use by all but the largest companies [33,34]. Generic deformation models are, however, available and a number of publications have used the French developed FORGE2 software [35,36]. In general the authors have not presented details of the temperature changes occurring which questionably is the most important feature of the extrusion process but Dashwood and McShane [35] have presented details of temperature rises during the extrusion of 7075 alloy and compared them with experimental data. Their results are compared in Figs. 2.19 and 2.21 below. The temperature was not measured but the results agree with observations made on the onset of cracking and the incipient melting point. The calculated loads agree quite closely with those observed experimentally. Another two-dimensional model by Grasmø *et al.* [33] considering only the steady state, presented much experimental evidence to justify their model; typical results for temperature and pressure correlations are shown in Figs 2.12 and 2.13. We shall compare these results with axisymmetric upper-bound/integral profile results below, bearing in mind the expense and computer time required to process the FEM models.



**Fig. 2.12** Comparison of finite-element method and experimental temperatures [33]. Heavy lines are the calculated results.



**Fig. 2.13** Comparison of finite-element method and experimental ram force [33].

### 2.5.4 Thermal balance during extrusion predicted by integral profile techniques

The integral profile approach proposed by Sheppard and Wood [24,25] and subsequently modified by the author assumes a heat profile surrounding the heat source to be given by the expression  $\Delta T = a + bx + cx^2$  which has to satisfy the pertaining boundary conditions and where  $\Delta T$  is the temperature differential driving the heat conduction. In most cases this involves integrating to determine the various heat flows; hence the term 'Integral Profile'. The advantage of the method lies in its simple approach and the fact that the calculation can be achieved on a normal PC in real time. It has the potential to provide an on-line prediction of the exit temperature and could allow ram speed changes to be activated automatically during the process in order to achieve, for example, isothermal extrusion. The thermal balance between the deforming material and the extrusion tools dictates the temperature rise occurring in the extrudate. This may be quantified by placing control volumes around the deformation zone and equating the heat leaving this volume to the work generated by the deformation process. Similar control volumes must be inserted wherever there is a significant heat flow. For example, in the model presented, a second control volume is placed around the non-deforming part of the billet since significant heat flow may occur between the billet and the cooler container. Back conduction into the pressure pad or the lubricated ram is included in the analysis as is the heat generated in the die land area. The heat flows and extrusion geometry are shown in Fig. 2.14 and assuming that 95% of the work is converted into heat then by considering control volume 1 we may write:

$$0.95V_B P_t = Q_1 + Q_2 + Q_4 + Q_7 + Q_{acc1} \quad (2.22)$$

$Q_4$  is determined by considering the heat balance in control volume 2, giving:

$$Q_4 + Q_{acc4} + Q_{WD2} = Q_5 + Q_6 \quad (2.23)$$

Finally, consideration of control volume 3 gives the exit surface temperature from the equation:

$$Q_{accs} + Q_{WDs} + Q_7 = Q_7 + Q_8 \quad (2.24)$$

It is assumed the work of extrusion is absorbed as heat in control volume 1 and that the work done in control volume 2 is simple compression. In each volume  $Q_{acc}$  is the heat accumulated in the time interval  $\Delta t$  giving the temperature differential  $\Delta T$ .

In each case:

$$Q_i = K_i (\Delta t)^n \Delta T_i$$

where  $K_i = f(k, \rho, C_p, CV_{geom})$  and where  $k, \rho$  and  $C_p$  are the corresponding thermal conductivity, density and specific heat of the materials and  $CV_{geom}$  represents the geometry of the control volume.

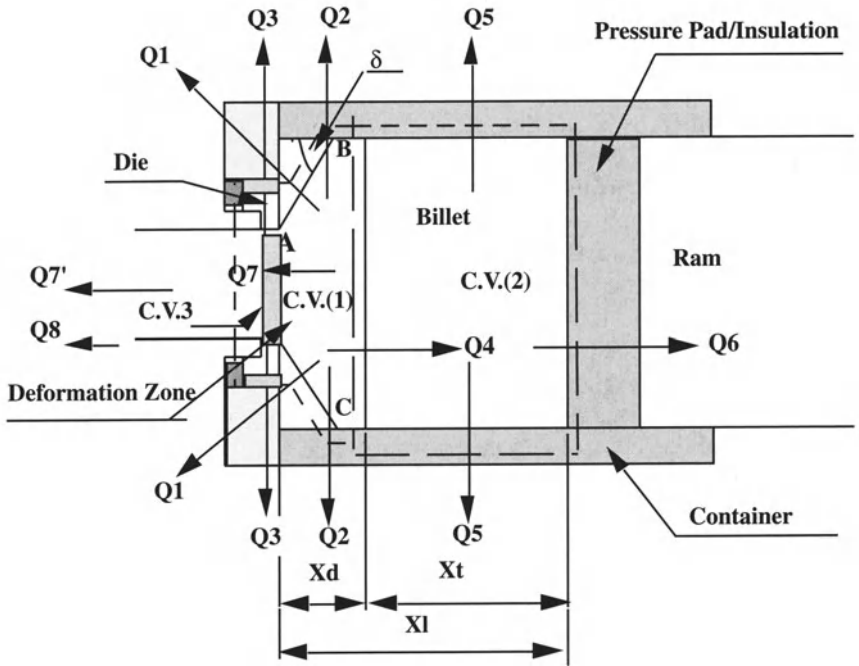


Fig. 2.14 Heat balance during the extrusion process.

The interface temperature between the billet and the extrusion, container, ram etc. is the major drive for heat conduction and these may be obtained by assuming a linear temperature distribution in the subcutaneous layers of each which will, of course, assume heat flows governed by the Fourier equation, and equating the total heat losses and gains by the billet and container respectively. Such an approach gives:

$$\left( \frac{T_B - T_I}{T_I - T_c} \right) = \sqrt[3]{\left( \frac{k_c \rho_c C_{p(c)}}{k_a \rho_a C_{p(a)}} \right)} \quad (2.25)$$

where  $T_B$ ,  $T_I$ ,  $T_c$  are the initial temperatures of the billet, billet/container interface and container respectively and  $k$ ,  $\rho$  and  $C_p$  are the corresponding thermal conductivity, density and specific heat of the materials. For Al-alloys and the normal Cr-V tooling steels the appropriate values are:

$$k_c = 32.65 \text{ W m}^{-1} \text{ K}^{-1}, \rho_c = 7860 \text{ kg m}^{-3}, C_{p(c)} = 489.76 \text{ J kg}^{-1} \text{ K}^{-1}, \\ k_a = 201 \text{ W m}^{-1} \text{ K}^{-1}, \rho_a = 2800 \text{ kg m}^{-3}, C_{p(a)} = 1063.9 \text{ J kg}^{-1} \text{ K}^{-1}.$$

Referring to Fig. 2.14 the remaining data required are  $P$  the load in newtons,  $V_R$  the ram speed in  $\text{m s}^{-1}$ , the deformation depth,  $X_d$ , and the semi-cone angle,  $\delta$ . These may be obtained from a suitable axisymmetric upper-bound analysis described above. Utilizing the results from a double triangle hodograph of such a solution coupled with multiregression yields:

$$p = \bar{\sigma} \left[ 0.171 + 1.86 \ln R + \frac{4m \left( \frac{D_B - D_E}{2 \tan \delta} \right)}{D_B \sqrt{3}} \right] \quad (2.26)$$

for the extrusion pressure where  $m$  assumes the average value of 0.88 as shown above.

We would normally utilize the load displacement loci to feed this information to the program. If this is not available then we are aware that an additional increment of pressure is required to set up the deformation load. Sheppard and his co-workers [25,37] have shown that this increment may be expressed in terms of (a) the constants in the constitutive equation and given by:

$$\Delta p = 6.62 + 0.921 \frac{\ln Z/A}{\alpha n} \quad (2.27)$$

and the upper bound solution yields

$$X_D = 0.35D_B(1 + 0.15\sqrt{R} - 0.0145R) \quad (2.28)$$

and the semi-angle, which is normally assumed to be 45°:

$$\delta = 38.7 + 6.9 \ln R \quad (2.29)$$

If the temperature in the deformation zone rises by an amount  $\Delta T_i$  in the time interval  $i$  then the temperature in the deformation zone is  $T_{Bi} + \Delta T_i$ . The temperature differential between the tools and the periphery of the billet is  $T_i - T_s = \Delta T_d$  where  $T_s$  is the surface temperature. Then the temperature differential between the deformation zone and the tooling is  $\Delta T_d + \Delta T_i$  or  $\Delta T_i^*$ . Similarly the temperature of the non-deforming zone will be  $T_{Bi} + \Delta T_{Bi}$  ( $\Delta T_{Bi}$  being close to zero).

$Q_1$  to  $Q_8$  are now estimated by assuming that the temperature profile around a heat source may be assumed to be represented by  $\Delta T(x,t) = a_0 + a_1x + a_2x^2$  where  $\Delta T(x,t)$  is the temperature at a distance  $x$  from the heat source at a time  $t$ . The constants  $a_0$ ,  $a_1$  and  $a_2$  may be found by consideration of the boundary conditions.

In summary:

$$\begin{aligned} Q_1 &= (\Delta T^*)k_1t^{1/2} & Q_2 &= (\Delta T^*) (k_2t^{2/3} + k_3t^{1/3}) \\ Q_3 &= (\Delta T^*) (k_4t^{2/3} + k_5t^{1/3}) & Q_4 &= (\Delta T_b)k_6t^{1/2} \\ Q_5 &= X_i(\Delta T_d) (k_7t^{2/3} + k_8t^{1/3}) & Q_6 &= (\Delta T_r)k_9t^{1/2} \\ Q_7 &= (\Delta T)k_{10}t & Q_7 &= (\Delta T)k_{11}t \\ Q_8 &= (\Delta T_s)k_{12}t \end{aligned}$$

$k_i$  are constants involving the thermal diffusivity, and the exponent of the time interval  $t$  is determined by the integration operation. For a more detailed analysis the reader should investigate references 24 and 25.

Hence the energy balance equation may be written in terms of the temperature differentials and the temperature rise in the deformation zone:

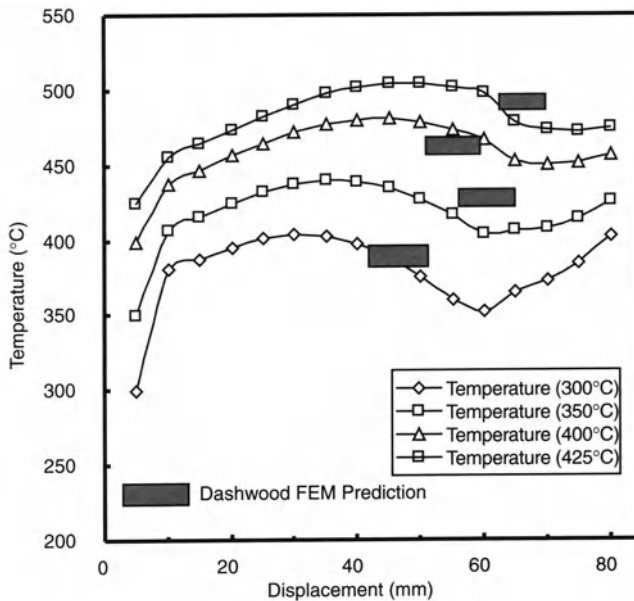
$$\Delta T = \left\{ \frac{0.95 V_b P - \left[ \Delta T_d \left( \sum_1^3 k_n t^{t_i} \right) + \Delta T_b k_6 t^{t_6} \right]}{\sum_1^3 k_n t^{t_i} + (k_{10} + k_{acc1})} \right\} \quad (2.30)$$

and the surface temperature becomes:

$$\Delta T_s = \frac{\hat{f} \left( \frac{\dot{\sigma}}{\sqrt{3}}, X_D \right) + (k_{accs} + k_{10} + k_{11})}{k_{12}} \quad (2.31)$$

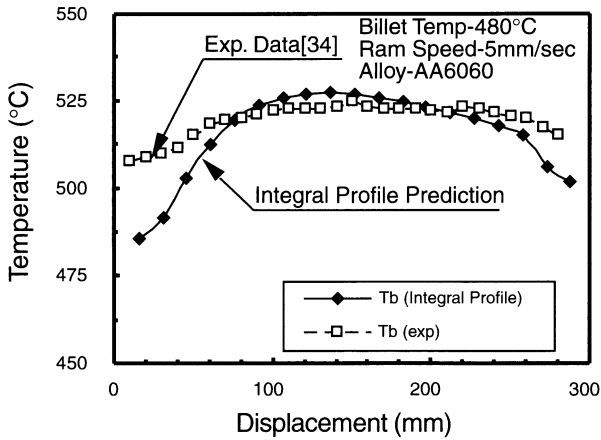
where  $T_s$  is the surface temperature.

Figure 2.15 shows the output from an integral profile analysis for extrusion of AA7075 at an extrusion ratio of 30 and ram speed of  $3 \text{ mm s}^{-1}$  for billet temperatures from  $300\text{--}425^\circ\text{C}$ . In this case load/displacement loci were not available and theoretical pressures have been used. It is clear that in this case the pressures have been overestimated and, consequently, the temperatures are slightly greater than those calculated by the FEM technique. A further comparison of the two methods is shown in Fig. 2.17 from which it can be concluded the results are extremely close. Nevertheless the agreement between the techniques could be more contiguous since, in practice, we would use the actual pressure curve (note that the IP programme operates in real time) and we might expect the temperature predicted to be slightly higher and close to that measured. For example Fig. 2.16 compares the predicted temperature with those measured by



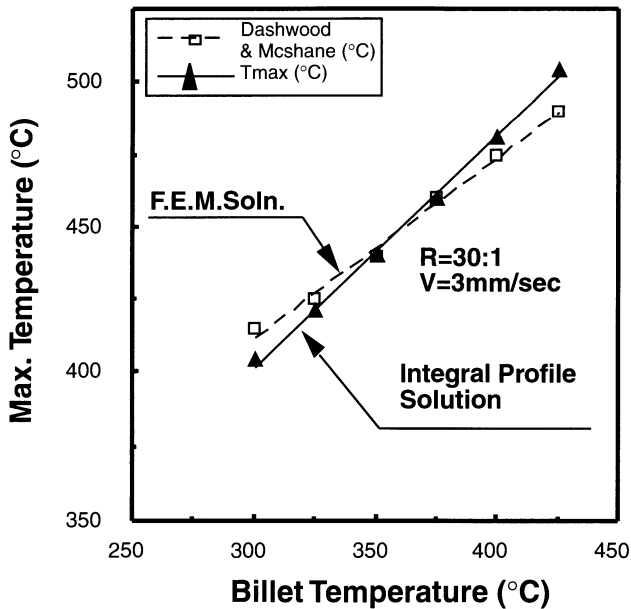
**Fig. 2.15** Comparison of finite-element method [35] and integral profile models.





**Fig. 2.16** Comparison of experimental data [36] with integral profile model.

Grasmo [34] at a point of entry to the die land area. In general the agreement is satisfactory; it is perhaps surprising that the experimental results increase quite so rapidly at commencement of extrusion with a billet temperature of 480°C, an extrusion ratio of 40 and a ram speed of only 5 mm s<sup>-1</sup>. The author does, however, explain that there may have been some uncertainty of the placement of the thermocouple and of the die and container properties.



**Fig. 2.17** Comparison of maximum temperature predicted by finite-element method and integral profile.

Figures 2.18 and 2.19 show the separate effects of extrusion ratio and ram speed on the exit temperature. The slope of each of these graphs is steep indicating the requirement of close control of each parameter if precise exit conditions are to remain as required.

Finally in this section we compare the rise in temperature (Fig. 2.20) due to friction in the die land when extruding AA6063 speeds of 25 and 55 mm s<sup>-1</sup>. It is very clear that the die has a significant effect on the exit temperature and we must therefore assume that both the die land length and the choke will be important variables when designing the integral process.

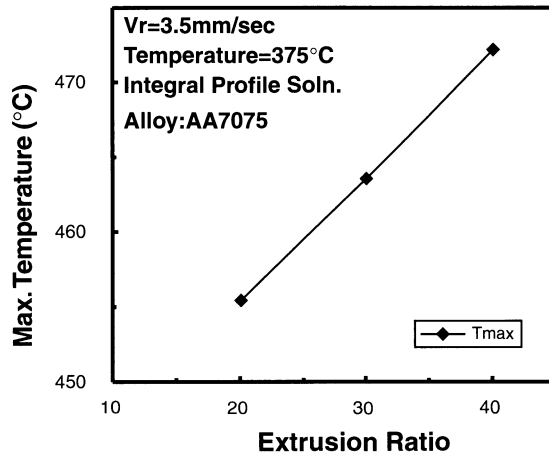


Fig. 2.18 The effect of extrusion ratio on the exit temperature.

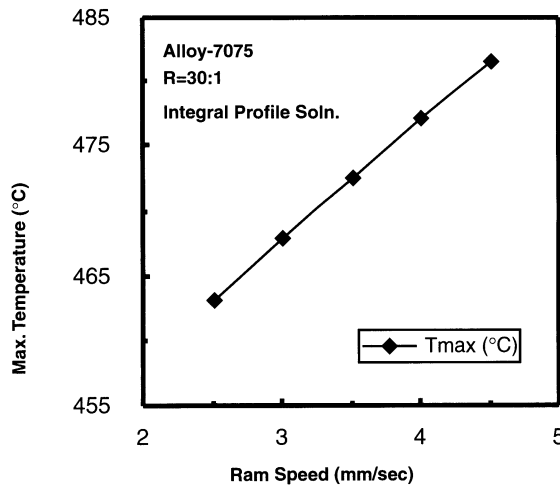


Fig. 2.19 The effect of ram speed on exit temperature when extruding hard alloy.

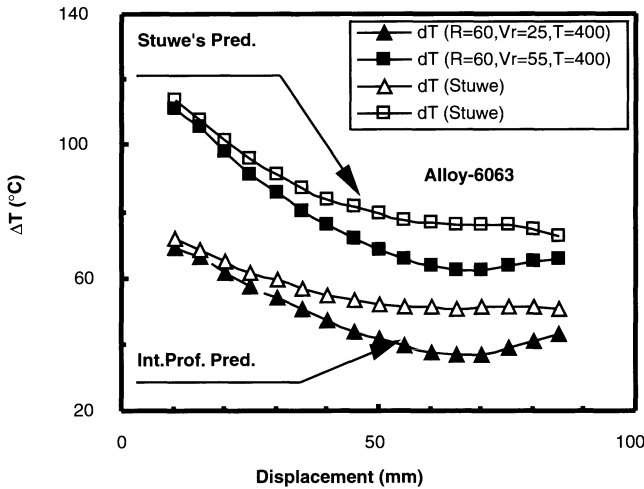


Fig. 2.20 Comparison of temperature rise due to die friction.

## 2.6 DIFFUSION

From thermodynamics, or practical experience, one can deduce that any single-phase system which is at equilibrium will be homogeneous. For example, a gin and tonic or a smoke-filled room will both become homogeneous over a period of time. Although it is not as easily observed in solids, the same effect is found there. For example, if a binary alloy becomes inhomogeneous upon solidification, the alloy can be homogenized by annealing at a temperature near the solidus. This occurs by the atoms of each component moving (diffusing) through the solid from regions of high concentration toward regions of lower concentration. The study of diffusion in metals is concerned with how fast, and how, the atoms move through the lattice.

The uses made of diffusion studies fall roughly into two categories. The first is concerned primarily with how fast the atoms move; the mechanism of movement is unimportant. Examples are: how fast will a casting homogenize?; how fast will a metal oxidize?; how fast will one phase precipitate from another? These questions and many others arise in practical and theoretical metallurgical problems.

The second category of diffusion problems is concerned with the atomic mechanism of diffusion; that is, the relation between the random movement of atoms between sites only a few Ångström apart, and the microscopic flow of matter which is experimentally measured. Diffusion is intimately related to the study of the simplest defects in a crystalline solid. These defects influence many properties of solids, and their properties, concentrations and formation are best studied by diffusion measurements.

### 2.6.1 Fick's laws of diffusion

We start with a discussion of the mathematics of diffusion in solids. These equations were first applied to diffusion by Adolph Fick in 1858, though they are quite similar to the equations developed a decade earlier by Fourier in his classic analysis of heat flow. It was pointed out above that atoms move from a region of high concentration to one of lower concentration, and that when there is no longer a concentration gradient this net flow of atoms ceases. If the  $x$  axis is parallel to the concentration gradient, an equation for the flow of matter which is consistent with these conditions is:

$$J = -D \left( \frac{dc}{dx} \right) \quad (2.32)$$

where  $J$  is the flux of atoms across unit area of a plane at any instant,  $(dc/dx)$ , is the concentration gradient normal to the plane at the same instant and  $D$  is a constant equal to minus the flux per unit concentration gradient. This is the first law of diffusion. Note that when  $dc/dx = 0$ ,  $J = 0$ , which satisfies the requirement that there is no net flow of atoms in a homogeneous system.

Equation 2.32 is referred to as Fick's first law. The commonly used dimensions for the terms in equation 2.32 are:

$$\frac{\text{N}}{\text{m}^2 \text{ s}} = \frac{\text{m}}{\text{s}} \left( \frac{\text{N m}^{-3}}{\text{m}} \right)$$

Thus  $D$  must be in units of  $(\text{length})^2 \text{ time}^{-1}$ , and is usually expressed in  $\text{m}^2 \text{ s}^{-1}$ . The second law needed to describe diffusion is derived from equation 2.32 and the fact that matter is conserved. Consider the region between the two planes  $[(x_1), (x_1 + dx)]$  shown in Fig. 2.21. Figure 2.21(a) shows the solute concentration ( $c$ ) vs. distance ( $x$ ). Since  $dc/dx$  at  $x_1$  is greater than  $(dc/dx)$  at  $x_1 + dx$ ,  $J(x_1)$  will be greater than  $J(x_1 + dx)$ . This is shown in Fig. 2.21(b), where the flux resulting from  $c(x)$  in part (a) is shown. But, if  $J(x_1) > J(x_1 + dx)$  and matter is conserved, the solute concentration in the region between  $x_1$  and  $x_1 + dx$  must increase.

Considering a volume element of unit area normal to the  $x$  axis and  $dx$  in thickness, the rate of change of concentration ( $dc/dt$ ) is:

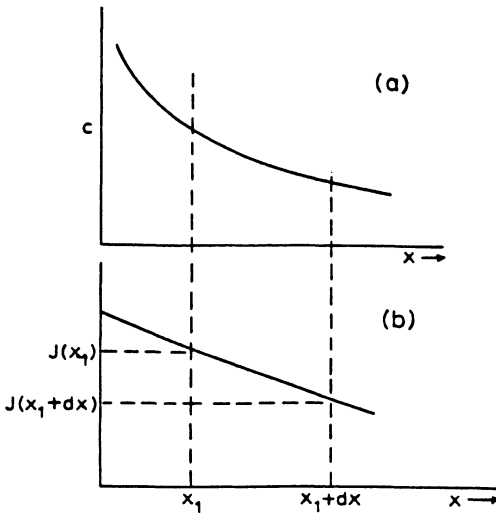
$$\left( \frac{dc}{dt} \right)_{x_1} dx = J(x_1) - J(x_1 + dx) \quad (2.33)$$

But, if  $dx$  is small,  $J(x_1 + dx)$  can be related to  $J(x)$  by the equation:

$$J(x_1 + dx) = J(x_1) + \left( \frac{dJ}{dx} \right)_{x_1} dx \quad (2.34)$$

Thus

$$\frac{dc}{dt} = - \frac{dJ}{dx} = \frac{d}{dx} \left( D \frac{dc}{dx} \right) \quad (2.35)$$



**Fig. 2.21** Plots of (a) concentration  $c$  versus distance; (b) resulting flux  $J$  versus distance.

where the second equality comes from substituting equation 2.32 for  $J$ . This is the second law of diffusion. A similar derivation could be given for two- (or more) dimensional problems in cartesian, cylindrical or polar coordinates. However, for simplicity, the discussion here will be limited to one-dimensional problems.

### 2.6.2 Solutions to the diffusion equation

There are several large books written on the solutions to equation 2.32 for various conditions [38,39]. In this section, examples are given of three classes of solutions which are particularly useful.

#### *Steady state*

Consider a thin sheet which has a high, constant concentration of an impurity maintained in the metal on one side, and a low constant concentration maintained in the metal on its other side. Material may be added or removed from the sheet initially, but after some period material will leave any given element of volume at the same rate as it enters. Under these conditions,  $dc/dt = 0$  at each point and the sheet is said to be at steady state. If  $dc/dt = 0$ , then

$$\frac{d}{dx} \left( D \frac{dc}{dx} \right) = 0 \quad \text{or} \quad D \frac{dc}{dx} = \text{constant}$$

If  $D$  is independent of composition, then  $dc/dx$  is the same throughout and it can be replaced by  $\Delta c/\Delta x$ , that is, the concentration drop across the entire sheet ( $\Delta c$ ) divided by the sheet thickness ( $\Delta x$ ).

*Infinite systems*

Consider a diffusion couple consisting of a bar of composition 40%A and 60%B welded to a bar of 55%A and 45%B. Over this composition range the diffusivity may be assumed to be constant and provided the length in the diffusion direction is sufficient to ensure that the composition of the ends remains constant then Fick's second law may be written:

$$\frac{dc_A}{dt} = -\frac{dJ}{dx} = D\left[\frac{d^2c_A}{dx^2}\right] \quad (2.36)$$

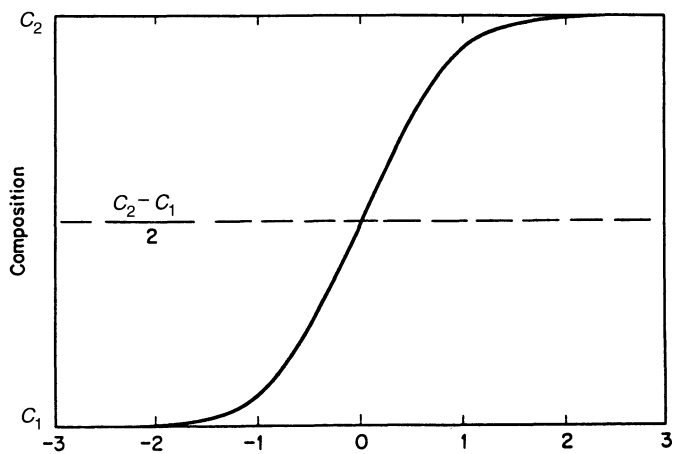
The solution of this equation for the two alloys, one having the concentration of A (atomic %)  $c_1$  and the other  $c_2$  at the start of the diffusion process, is:

$$c_A = \frac{c_1 + c_2}{2} \left[ 1 + \operatorname{erf} \frac{x}{2\sqrt{(Dt)}} \right] \quad \text{for } -\infty \leq x \leq \infty \quad (2.37)$$

where  $c_A$  is the concentration at a distance  $x$  (in cm) from the original interface,  $t$  is the time in seconds and  $D$  is the diffusivity. The symbol  $\operatorname{erf} x/2\sqrt{(Dt)}$  represents the error function, or probability integral with the argument  $y = x/2\sqrt{(Dt)}$ . This function is defined by the equation:

$$\operatorname{erf}(y) = \frac{2}{\pi} \int_0^y e^{-y^2} dy$$

Figure 2.22 shows the theoretical penetration curve when this solution of Fick's equation is plotted as a function of the variable  $x/2\sqrt{(Dt)}$ . This curve is obtained under the assumption that  $D$  is constant or that  $D$  varies only slightly within the A composition interval  $c_1$  to  $c_2$ . Thus the concentration is a single-valued function of the variable  $x/2\sqrt{(Dt)}$ .



**Fig. 2.22** Plot of composition versus the argument of the error function.

Rearranging equation 2.37 will give:

$$\frac{c_A - c_1}{c_1 - c_2} = 1 - \operatorname{erf} \frac{x}{2\sqrt{(Dt)}} \quad (2.38)$$

Note that a constant value of  $x/2\sqrt{(Dt)}$  requires that the left side of the equation must be a constant. This means that any particular value of  $c_A$  corresponds to a particular value of  $x/2\sqrt{(Dt)}$ . For example, if  $(c_A - c_1)/(c_1 - c_2) = 1/2$ ,  $x/2\sqrt{(Dt)}$  must equal 0.52; that is,  $x$  for this composition is given by the equation  $x_{(1/2)} = 1.04\sqrt{(Dt)}$  for all times. Since  $x$  increases in proportion to  $t^{1/2}$  this means that the time of soak must be quadrupled to get double the depth of penetration ( $x$ ).

In addition to varying the time of soak, the value of  $D$  might be changed. Since the composition range is fixed, the only practical way to do this is to change the temperature. The magnitude of the temperature dependence of  $D$  is given by the equation:

$$D = D_0 \exp \left\{ \frac{-Q}{GT} \right\} \quad (2.39)$$

Here  $T$  is the absolute temperature,  $Q$  is the activation energy for self diffusion (and is sometimes represented by the symbol  $\Delta H$ ) and  $D_0$  is a temperature independent constant. Some values of the constants  $D_0$  and  $Q$  are given in Table 2.3.

**Table 2.3** Diffusivities of some elements in aluminium at 475°C

<i>Element</i>	$D_0$ ( $m^2s^{-1}$ )	$Q$ ( $kJ mol^{-1}$ )	$D_x$ ( $m^2s^{-1}$ ) at 475°C
Cu	$0.29 \times 10^{-4}$	125.6	$4.9 \times 10^{-14}$
Zn	$0.11 \times 10^{-4}$	83.7	$1.6 \times 10^{-11}$
Mg	$0.11 \times 10^{-3}$	117.2	$7.2 \times 10^{-13}$
Mn	$0.22 \times 10^{-4}$	121.4	$7.3 \times 10^{-14}$
Cr	$3.00 \times 10^{-11}$	62.8	$1.2 \times 10^{-15}$
Zr	$7.28 \times 10^{-2}$	240.8	$1.1 \times 10^{-18}$
Si	$0.90 \times 10^{-4}$	125.6	$1.5 \times 10^{-13}$
Fe	$0.41 \times 10^{-14}$	58.6	$3.3 \times 10^{-19}$

### *Rate of homogenization*

Another type of solution to Fick's second law applies to cases in which the concentration at each point relaxes toward the same constant value; that is, the system becomes completely homogenized. Rates of homogenization are of interest in many metallurgical problems. Though we will not discuss it here, similar solutions apply to the kinetics of precipitation since here the matrix becomes homogeneous as solute diffuses from the matrix to the precipitate particles.

In any inhomogeneous metal, the concentration will vary in a roughly periodic manner along any given straight line. For simplicity, let us assume that this variation occurs in only one direction so that the initial concentration can be described by the equation:

$$c(x) = c_0 + c_m \cos \left\{ \pi \frac{x}{l} \right\} \quad (2.40)$$

This corresponds to a concentration that varies from a maximum concentration of  $c_0 + c_m$  to a minimum of  $c_0 - c_m$  in moving a distance  $l$  along the  $x$ -axis. These concentration gradients will tend to be relieved by the flowing of solute from the regions of higher concentration toward regions of lower concentration.

If  $D$  does not vary with composition, the solution to this diffusion problem is:

$$c(x,t) = c_0 + c_m \cos \left\{ \pi \frac{x}{l} \right\} \exp \left\{ \frac{-\pi^2 D t}{l^2} \right\} \quad (2.41)$$

This shows that the relaxation of  $c$  at any point toward the final value  $c_0$  is given by an equation of the form:

$$c - c_0 \approx \exp \left( \frac{-t}{\tau} \right) \quad (2.42)$$

where  $\tau$  is a constant called the relaxation time and is given by the equation  $\tau = l^2/\pi^2 D$ . It has the dimensions of time and is a useful parameter for discussing the effect of various operations on the rate of homogenization. The variation of  $c(x,t)$  in equation 2.41 with the parameter  $t/\tau$  is shown in Fig. 2.22.

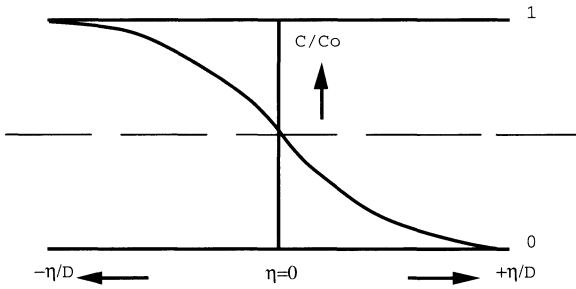
As an application of the above, consider the problem of increasing the rate of homogenization of a casting. An actual mathematical solution for the variation of  $c$  with  $x$ ,  $y$ ,  $z$  and  $t$  could be quite complicated. However, the solution would consist of a group or series of groups of terms identical to those found in equation 2.42; that is, the final composition ( $c_0$ ) plus a function of position multiplied by a term of the form  $\exp(-t/\tau)$ . Thus, no matter how complicated the problem becomes, insight can be gained into how fast the relaxation will proceed simply by determining the effect of various operations on the relaxation time,  $\tau$ .

Consider the measures that would be most effective in decreasing  $\tau$  for a casting. Raising the temperature will help since as  $D$  increases  $\tau$  decreases. However, the melting point sets an upper limit on this approach, and a more useful approach is to vary the mean distance between maxima and minima in the concentration ( $l$ ). Since this distance enters as  $l^2$ , it has a strong effect. Thus, if  $l$  can be decreased by a factor of 4 by more rapid cooling, or some other means, the time for homogenization is reduced by a factor of 16. This also indicates one reason why a wrought product should be more easily homogenized, and thus usually more homogeneous, than a cast product. The mechanical working presses the high and low concentration regions closer together thus decreasing  $l$ . This approach will, of course, not be viable since the principal objectives of the process are to improve workability prevent the formation of voids and control dynamic recovery.

### 2.6.3 Problems in which $D$ varies with composition

A case of great practical interest is that in which the diffusion coefficient depends only on the concentration of diffusing substance. Such a concentration dependence





**Fig. 2.23** Penetration curve when  $D$  varies with composition.

exists in most systems but often, for example in dilute alloys, the dependence is slight and the diffusion coefficient can be assumed to be constant for all practical purposes. In other cases, however, the concentration dependence is a very strong characteristic feature. A number of methods have been used to obtain numerical solutions, some applicable to any type of concentration dependence and others restricted to particular types, e.g. exponential or linear dependence.

Fick's second equation for one dimensional diffusion when the diffusion is a function of the concentration  $c$  is:

$$\frac{dc}{dt} = \frac{d}{dx} \left( D \frac{dc}{dx} \right)$$

In 1894 Boltzmann showed that for certain boundary conditions, provided  $D$  is a function of  $c$  only,  $c$  may be expressed in terms of a single variable  $x/2\sqrt{t}$  and that Fick's equation may therefore be reduced to an ordinary differential equation by the introduction of a new variable  $\eta$ , where:

$$\eta = \frac{x}{2\sqrt{t}} \tag{2.43}$$

Thus we have: 
$$\frac{dc}{dx} = \frac{1}{2\sqrt{t}} \frac{dc}{d\eta} \tag{2.44}$$

and 
$$\frac{dc}{dt} = -\frac{x}{4\sqrt{t}} \frac{dc}{d\eta} \tag{2.45}$$

and hence 
$$\frac{d}{dx} \left( D \frac{dc}{dx} \right) = \frac{d}{dx} \left( \frac{D}{2\sqrt{t}} \frac{dc}{d\eta} \right) = \frac{1}{4t} \frac{d}{d\eta} \left( D \frac{dc}{d\eta} \right) \tag{2.46}$$

so that finally Fick's equation may be written:

$$-2\eta \frac{dc}{d\eta} = \frac{d}{d\eta} \left( D \frac{dc}{d\eta} \right) \tag{2.47}$$

This equation shows that  $c$  is a function of  $\eta$  only. Thus all concentration profiles can be plotted on a single curve showing  $c/c_0$  as a function of  $\eta$  or  $\eta/D$  (Fig. 2.23).

## REFERENCES

1. von Karman, Th. (1909) *Göttinger Nachrichten*, Math.-phys. Klasse, 204.
2. Sheppard, T. and Wright, D.S. (1979) *Met. Tech.*, **6**, 215.
3. Feltham, P. (1956) *Metal Treatment*, **23**, 440.
4. Siebel, E. and Fangmeier, E. (1931) *Mitt. Kais. Wilh. Eisenf.*, **13**, 28.
5. Johnson, W. and Mellor, P.B. (1962) *Plasticity for Mechanical Engineers*, Van Nostrand, London.
6. Johnson, W. and Kudo, H. (1960) *Int. J. Mech. Sci.*, **1**, 57.
7. Adie, J.F. and Alexander, J.M. (1967) *Int. J. Mech. Sci.*, **9**, 349.
8. Halling, J. and Mitchell L. (1965) *Int. J. Mech. Sci.*, **7**, 227.
9. Halling, J. and Mitchell L. (1965) *Int. J. Prod. Res.*, **4**, 141.
10. Sheppard, T., McShane, H.B. and Tutchter, M.G. (1978) *Powder Met.*, **21**, 47.
11. Thomsen, E.G. (1957) Proc. Conf. *Prop. Mat. at High Rates of Strain*, I. Mech. E., London.
12. Shabaik, A.H., Kobayashi, S. and Thomson, E.G. (1967) *J. Eng. Ind. Trans., ASME, Series B*, **89**, 343.
13. Iwata, K., Osakada, K. and Fujino, S. (1972) *J. Eng. Ind. Trans., ASME, Series B*, **94**, 397.
14. Nagpal, V. and Altan, T. (1975) Proc. 3rd. NAMRC, 26.
15. Zienkiewicz, O.C. and Godbole, P.N. (1974) *Int. J. Num. Meth. Eng.*, **8**, 3.
16. Zienkiewicz, O.C., Jain, P.C. and Onate, E. (1978) *Int. J. Solids Struct.*, **14**, 15.
17. Kato, K., Okada, T., Murota, T. and Itoh, H. (1987) *Advanced Technology of Plasticity*, (ed. K. Lange) Springer-Verlag, Heidelberg, 523.
18. Sheppard, T. and Bianchi, J.H. (1987) *J. Mech. Phys. Sol.*, **29**, 61.
19. Childs, T.H. (1974) *Met. Tech.*, **1**, 305.
20. Dawson, P.R. and Thompson, E.G. (1977) in *Numerical Modelling of Manufacturing Processes*, ASME, PVP-PB-025, 167–182.
21. Norley, J. (1979) Ph.D. Thesis, University of London.
22. Sheppard, T. and Paterson, S.J. (1982) *J. Mech. Work. Tech.*, **4**, 39–56.
23. Akeret, R. (1980) *Metal*, **34**, 737–741.
24. Sheppard, T. and Wood, E.P. (1980) *Met. Tech.*, **7**, 58–66.
25. Sheppard, T. and Wood, E.P. (1978) Proc. 17th Int. MTDR Conf., **411**(1), Macmillan & Co., London.
26. Akeret, R. (1967) *J.I.M.*, **95**, 204–211.
27. Lange, G. (1971) *Z. Metallkd.*, **62**, 571–579.
28. Lange, G. and Stuwe, H.P. (1971) *Z. Metallkd.*, **62**, 580–584.
29. Bishop, J.F.W. (1966) *J. Mech. Appl. Math.*, **9**, 236.
30. Akeret, R. (1968) *Aluminium*, **44**, 412.
31. Stuwe, H.P. (1968) *Metall.*, **22**, 1197.
32. Lange, G. (1971) *Z. Metallkd.*, **62**, 571.
33. Macey, G.E. and Salim, M. (1988) Proc. 4th International Extrusion Technology Seminar, Chicago, USA, 247.
34. Grasmø, G., *et al.* (1992) Proc. 5th International Extrusion Technology Seminar, Chicago, USA, **1**, 367.
35. Dashwood, R.J. and McShane, H.B. (1996) Proc. 6th International Extrusion Technology Seminar, Chicago, USA, **1**, 331.
36. Chenot, J.L. (1992) *J. Mat. Proc. Tech.*, **24**, 9.
37. Castle, A.F. and Sheppard, T. (1976) *Met. Tech.*, **2**, 465–475.
38. Carslaw, H.S. and Jaeger, J.C. (1959) *Conduction of Heat in Solids*, Clarendon, Oxford.
39. Crank, J. (1950) *Mathematics of Diffusion*, Oxford University Press, London.

# Metallurgical features affecting the extrusion of aluminium alloys

3

Wrought alloys are divided into seven major classes according to their principal alloy elements. Each class demonstrates a different type of microstructure because of these alloy differences. Typical microstructural features are described in this chapter for each class and show how microstructure progressively develops from the as-cast ingot to the final wrought form (although this is treated in more detail in Chapter 4). Furthermore, alloy classes can be divided into two categories according to whether they are strengthened by work hardening only or by heat treatment (precipitation hardening). The former applies to 1XXX, 3XXX, 4XXX and 5XXX alloys, while the latter applies to 2XXX, 6XXX and 7XXX alloys. We shall also consider some of the more recently developed Al–Li alloys.

## 3.1 ALUMINIUM-ALLOY SYSTEMS

### 3.1.1 The 1XXX system

*1XXX or commercially pure aluminium*

Because iron and silicon are ever-present impurity elements and the solid solubility of iron in aluminium is very small, phases of aluminium–iron or aluminium–iron–silicon are seen in microstructures of all but refined, super-purity aluminium. In the as-cast condition, all of the phases that come into equilibrium with aluminium may be found –  $\text{FeAl}_3$ ,  $\text{Fe}_3\text{SiAl}_2$  or  $\text{Fe}_2\text{Si}_2\text{Al}_9$ . In addition, a number of metastable nonequilibrium phases may be formed when solidification is rapid.  $\text{FeAl}_6$ , a phase that has the same crystal structure as  $\text{MnAl}_6$ , is one example. Minor impurity or addition elements such as copper and manganese that are not in sufficient quantity to form their own phases influence the

type and quantity of less stable phases. Subsequent thermal processes generally revert these phases back to the equilibrium types.

### *1100 alloy*

In the as-cast state the typical constituent in 1100 aluminium is Si in the dendrite interstices whilst when homogenized  $\text{Fe}_3\text{Si}$  is normally present which is redistributed in a typical worked structure. The grain structure of annealed material shows a slight departure from equiaxiality because of alignment of iron-rich particles. The apparent volume fraction of second-phase particles is almost a direct function of iron content.

## **3.1.2 The 2XXX system**

### *Al–Cu wrought alloys*

These commenced with the development of the Al–4.5%Cu alloy 2025 in North America [1]. This alloy contained deliberate additions of Si and Mn which do not contribute to age hardening. The alloy is still used for some aerospace forgings. Alloy 2219 which was introduced in 1954 [2] will yield all the properties of 2025 but with superior weldability, stress corrosion and fracture toughness. Originally introduced because of its superior high temperature strength it is now used primarily because of its excellent weldability. The Al–Cu alloy 2011, containing lead, exhibits good chipping and cutting characteristics which are a necessity for high speed production of screw machine parts and has no stringent requirements in its extrusion characteristics.

### *Al–Cu–Mg*

These systems have been known for over half a century since their discovery by Wilm [3].

Following the discovery of this first heat treatable alloy, now designated 2017, research efforts extended the principles of age hardening to other alloy systems. Few alloys available in the 1920s and 1930s remain in use today but the results of developments during this period are reflected in 2014 and 2024 which are now the most widely used alloys of this system.

The development of 2014 alloy utilized the effect of silicon to produce an Al–Cu–Mg alloy that is more susceptible to artificial ageing than 2017 and provides a desirable high level of strength unobtainable in naturally aged 2017 or 2014. Alloy 2024 was introduced in the 1930s as a higher strength natural ageing alloy to replace 2017 in the airframe industry. The response of 2024 to artificial ageing is accelerated by strain hardening of the heat-treated material and is available in a number of naturally and artificially aged tempers that reflect several degrees of strain hardening [4]. Tempers of 2014 are usually limited to the naturally and artificially aged conditions.

These two alloys have widespread applications in the aircraft industry but improved versions have recently been introduced. 2214 and 2124, the purer derivatives of 2014 and 2024, are often used, essentially because they offer better fracture toughness properties [5]. AA2048 also has improved toughness; 2618 (Concorde alloy – RR58) was developed for use at elevated service temperatures and 2219 has improved weldability.

### *Effect of alloying elements*

Copper is one of the most important alloying constituents for aluminium because of its appreciable solubility and strengthening effect, the strength increasing with increasing copper content up to a maximum of approximately 6%. Magnesium is used in combination with copper to accelerate and increase the age hardening at room temperature. The equilibrium compounds for this system are  $\text{CuAl}_2$  ( $\theta$ -phase) and  $\text{CuMgAl}_2$  (S-phase) [6–8]. These are soluble in the matrix during solution heat treatment.

The addition of silicon improves the response to artificial ageing and has some strengthening effect [9], especially at higher temperatures, but at the expense of ductility. It combines with magnesium to form the compound  $\text{Mg}_2\text{Si}$  in preference to the formation of other compounds such as  $\text{CuMgAl}_2$ ,  $\text{CuMg}_4\text{Al}_6$ ,  $\text{Cu}_2\text{Mg}_8\text{Si}_6\text{Al}_5$  and  $(\text{CuFeMn})_3\text{Si}_2\text{Al}_{15}$  [8].

The presence of iron has a beneficial strengthening effect, especially at high temperatures, but also causes embrittlement and must be kept to a minimum [10]. It forms such compounds as  $(\text{CuFe})\text{Al}_6 + \text{Cu}_2\text{FeAl}_7$ .

The addition of manganese has a marked strengthening effect [6,9] partly because of its solubility and partly because of the formation of intermetallic compounds. Manganese additions remain in solution during casting but combine with iron during homogenization to form small intermetallic particles such as  $(\text{CuFeMn})_3\text{Si}_2\text{Al}_{15}$  and  $(\text{CuFeMn})\text{Al}_6$  [11,8,12]. This reduces the embrittling effect of iron. The effect of manganese in solution is to retard the onset of recrystallization [12,13] and the manganese-rich intermetallic compounds, which tend to be associated with the sub-boundary dislocation network, inhibit grain growth [11]. The size and spacing of these particles therefore have an important effect on the mechanical properties of the material. The addition of transition metals such as manganese and iron does not influence the mechanism of age hardening [13].

Small amounts of titanium or boron are added to aluminium and alloys to form the compounds  $\text{TiAl}_3$  and  $\text{AlB}_2$  which are very effective as grain refiners [13]. The grain refining effect is intensified and prolonged by the formation of the compound  $\text{TiB}_2$  when both elements are present. Chromium has no detectable influence on recrystallization and consequently is not used in these alloys.

### 3.1.3 The 3XXX system

The first and only Al–Mn alloy, AA3003 [14], consists of the addition of manganese to what is basically 1100 aluminium. The dominant phases become  $(\text{Mn,Fe})\text{Al}_6$  and  $(\text{Fe,Mn})\text{SiAl}_{12}$ . In the as-cast structure, the former phase predominates; subsequent heating causes a transformation to the latter phase by a delayed peritectic reaction. Manganese also supersaturates the cored solid solution of the primary dendrites and subsequently precipitates as a dispersoid. Grains formed by recrystallization after the extrusion process are more elongated than those of 1100, principally because of the dispersoid. Some manganese remains in solid solution. A few alloys in this class also contain magnesium (the most common being 3004 developed as a container alloy) which, because of its affinity for silicon, tends to shift the phase proportioning toward  $(\text{Mn,Fe})\text{Al}_6$  [15].

Several lower strength alloys were added to the Al–Mn–Mg group; notably AA3005 in 1953 and 3105 in 1960. These alloys offer desirable combinations of strength, formability and corrosion resistance for application in the building and automotive sectors.

### 3.1.4 The 4XXX system

#### *4XXX or aluminum–silicon alloys*

Except for some architectural applications and forged pistons, most wrought 4XXX alloys are used for welding and brazing filler materials where they are remelted. However, good joining characteristics may depend on having a uniform and fine initial wrought structure. The as-cast phases are usually elemental silicon and  $\text{Fe}_2\text{Si}_2\text{Al}_9$ . Thermal treatment causes silicon to coalesce and spheroidize, while the insoluble iron-rich phase is not altered.

### 3.1.5 The 5XXX system

#### *Commercial aluminium–magnesium alloys*

The Aluminium Association 5XXX series alloys represent the most important commercial non heat treatable alloys. Their hot working range is limited because they are stiff throughout the working range and hence prone to incipient melting at higher extrusion temperatures. Their main use is for applications in which corrosion resistance as good as that of pure aluminium is needed, but higher strength is imperative. They have extensive use in the aerospace, shipbuilding, transport and forged components industries. For wrought products, 5–6% Mg is seldom exceeded because the alloys with higher Mg are difficult to form and are susceptible to intergranular and stress corrosion or exfoliation [16]. The higher strength alloys show good welding response with joint efficiencies of up to 80–90% of the annealed strength, leading to their use in engineering structures, pressure vessels and chemical plants.

The Mg atom is approximately 12% larger than the Al atom and the lattice distortion contributes considerably to the strain hardening of the alloy. An added bonus is the weight reduction compared with pure aluminium of  $9.7 \text{ kg m}^{-3}$  for every weight percentage Mg added. In the binary Al–Mg system, the solubility of Mg in Al varies from approximately 1.5 wt% at room temperature up to 17.4 wt% at  $450^\circ\text{C}$  [8]. (In the following text a percentage implies a weight percentage unless stated otherwise.) The aluminium corner of the Al–Mg binary phase diagram is shown in Fig. 3.1. It has been indicated by previous work that Mg does not significantly modify the stacking fault energy of aluminium [17–19] and therefore the cross-slip and climb characteristics of the alloys are similar to aluminium itself.

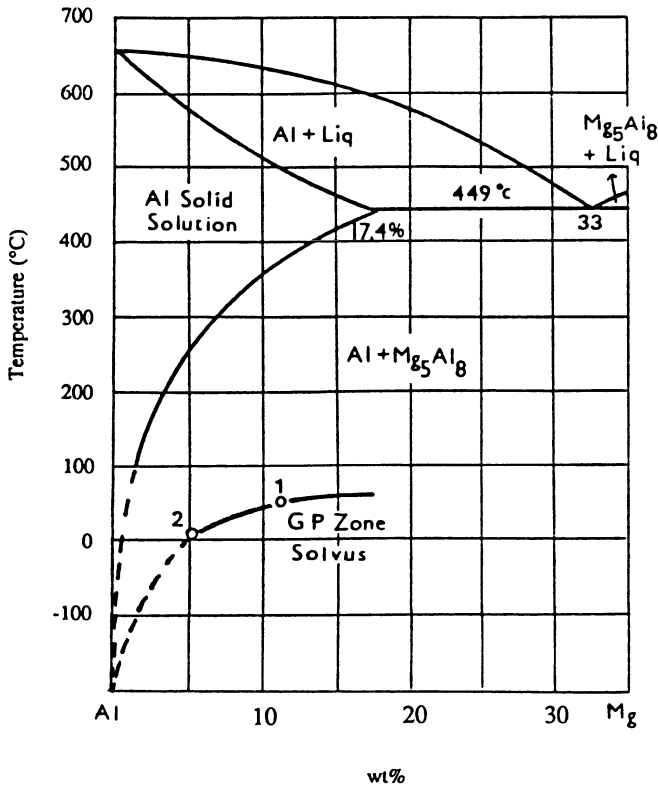


Fig. 3.1 Al–Mg equilibrium diagram with the GP zone metastable boundary added.

Despite the substantial solid solubility of Mg in Al, there are no appreciable precipitation hardening characteristics below 7% Mg [6]. Alloys below this composition are generally utilized as wrought alloys characterized by substantial

substitutional solid solution strengthening and high work-hardening rates. The amount of Mg soluble at the annealing temperature for alloys such as 5456 and 5083 is higher than that retained in solid solution at room temperature. Long storage at room temperature or exposure to elevated temperatures results in precipitation along grain boundaries or along slip planes. This precipitation promotes intergranular attack and stress cracking in corrosive atmospheres, because it is anodic to the remainder and so preferentially attacked. This situation resulted in the development of specific tempers to eliminate or minimize this instability [6]. The treatments most used for wrought products are stress relief treatments or low temperature anneals to stabilize the structure and thus eliminate a tendency to stress corrosion and exfoliation.

As-cast and homogenized microstructure cast microstructures are influenced by solidification conditions and by the alloy composition. The typical microstructure resulting can usually be considered in terms of the two morphological forms i.e. dendritic and eutectic, although a mixture of both morphologies will often be present. The most common microstructures are:

1. pure aluminium, which solidifies in a dendritic manner;
2. solid solution dendritic (with or without interdendritic precipitates);
3. dendrites plus interdendritic eutectic;
4. eutectic.

A binary Al–5% Mg alloy can be characterized by dendrites and interdendritic eutectics during solidification if sufficiently slowly cooled as shown in Fig. 3.1, which is an equilibrium diagram for binary Al–Mg [20], exhibiting extensive solid solubility at the Al-rich end.

Solidification under non-uniform conditions (cooling rate of more than  $5 \times 10^{-6} \text{ }^\circ\text{C h}^{-1}$ ) leads to coring, which is defined as composition differences within the primary Al-rich phase ( $\alpha$  solid solution) with the  $\beta \text{ Mg}_5\text{Al}_8$  phase appearing at Mg contents as low as 5% Mg. Sufficiently rapid cooling rates during solidification can alter the composition range of cooperative eutectic growth, eutectic constituents and their morphologies to produce, for example, degenerate eutectic structures.

In practice, the main microstructural features in commercial Al alloys are more complicated, because of alloying additions or Fe and Si impurities interrelating with the very fast cooling rates that are normally used in ‘direct chill’ (DC) casting. As a result, the normal components of the microstructure probably consist of  $\alpha$  solid solution supersaturated with Mn, Cr, Fe and Si, some mixture of degenerate eutectics and various precipitates in the interdendritic regions. The presence of these secondary phases arises through numerous mechanisms. Some of the more common ones are non-equilibrium constitutional solidification, solid-state reactions (precipitation reactions and phase changes) and direct dispersion [21,22].

When the Fe content is greatly in excess of the equilibrium solubility (maximum solubility in Al; 0.05% at 665°C), substantial supersaturation occurs due to



the rapid cooling rate. Si is added to control the amount of Fe available in solution. This leads to formation of a ternary Al–Fe–Si compound which precipitates more rapidly than the binary  $\text{FeAl}_3$  intermetallic [25]. In the presence of Mn, added for strength and grain control in commercial Al–5% Mg alloys,  $\text{FeAl}_3$  and Al–Fe–Si compounds transform into  $(\text{Fe,Mn})\text{Al}_6$  and  $\text{Al}_{12}(\text{Fe,Mn})_3\text{Si}$ , respectively. These impurity particles are coarse, insoluble intermetallic compounds which form interdendritically during solidification and are usually rich in Fe or Si. They would cause ‘mechanical anisotropy’ by tending to align as stringers in the fabrication direction and promote premature fracture. Typically they are fractured to a size of  $10\ \mu\text{m}$  during hot deformation [26] and can act as stress concentrators. Also, it has been reported [23] that recrystallization nucleation during annealing occurs preferentially in deformation zones adjacent to these large particles where the lattice is substantially misoriented.

On the other hand, smaller intermetallic compounds or submicron particles (the so-called ‘dispersoids’), which contain combinations of transition metals (Cr, Mn, Fe) and Si form from solid-state precipitation reactions and precipitate in interdendritic regions, usually showing non-uniformity. It is necessary for the precipitates to be uniformly distributed. They serve primarily to retard recrystallization and grain growth in the alloys and also assist in improving ductility in the final product by increasing strain hardening which delays localized deformation and necking.

Microstructurally, commercial Al alloys are characterized by the presence of large impurity particles at the grain boundaries and fine dispersoids within grains. Dispersoids adjacent to the large grain boundary particles or original grain boundaries are generally not found [28,29] (the so-called ‘precipitate free zone’ (PFZ)). These zones are formed by depletion of vacancies during rapid cooling, the excess vacancies in the region adjacent to the grain boundaries migrating to the boundaries, which serve as effective sinks. These areas represent regions where dislocation motion and boundary migration is relatively more easy than in the regions of densely distributed particles.

Additionally, as the GP zone solvus occurs at about  $0^\circ\text{C}$  for Al–5% Mg alloys and the room temperature solid solubility of Mg in Al is only about 1%, little or no response to age hardening can be exhibited due to the difficulty of nucleation of the finely distributed particles and hence precipitation hardening effects are not marked.

In general, the identification of the above phases has been mainly carried out [27,30–32] using X-ray diffraction (with powder samples), energy dispersive X-ray method (EDX) and transmission electron method (using dark field imaging). The measurement of concentration distribution is performed by electron microprobe analysis and differential scanning calorimetry (DSC). Naturally, homogenization is required for the purpose of the elimination of solute concentration gradients that form during casting and the reprecipitation, in a suitable form, of elements from supersaturated solid solution which are precipitated, mainly, at interdendritic sites or sometimes at grain boundaries.

The various changes in precipitation and solute level with different homogenisation treatments of DC cast commercial purity Al have been studied [28] and will be dealt with in Chapter 4.

### 3.1.6 The AA6XXX system

#### *Aluminium–magnesium–silicon*

The use of magnesium (Mg) and silicon (Si) as alloying elements can be traced to 1918 with several Swiss experiments. Eight years later in 1926, the commercial beginning of Al–Mg–Si alloys was marked by the introduction of ‘Aldur’. Today, the Al–Mg–Si system, designated the  $Mg_2Si$  alloys, are the most widely used in the extruded products market. The AA6XXX series alloys have the following qualities: good corrosion resistance, surface finish, formability and medium strength, thus making them suitable for decorative architectural sections and structural applications.

The formation of the stoichiometric compound, magnesium silicide ( $Mg_2Si$ ), makes the AA6XXX series alloys heat treatable and capable of achieving medium strength in the T6 condition. There are two main alloys of the AA6XXX series used to meet consumer demands. These are AA6061, for medium strength, structural applications, and AA6063 for architectural applications. The other major alloys of the series include AA6351, AA6005 and AA6082.

Of the alloys mentioned above, AA6063 is considered to be the ‘bread and butter’ [33] of the extrusion industry, possessing excellent extrusion characteristics and finishing capabilities. The Aluminium Association’s chemical composition limits of AA6063 have a broad range for alloy and impurity elements from which a spectrum of strength and finishing properties can be developed. Three main divisions are offered by aluminium founders: these have magnesium silicide contents of 1%, 0.8% and 0.7%, for high strength, general purpose and high extrudability, respectively. The effects of magnesium silicide content and other alloying elements are discussed in the following sections.

#### *The effect of alloying elements*

##### *Magnesium silicide ( $Mg_2Si$ )*

Magnesium and silicon are the main alloying elements in the AA6XXX series and combine to form the stoichiometric constituent magnesium silicide ( $Mg_2Si$ ), which is the primary hardening phase. The proportion of magnesium to silicon required for equilibrium magnesium silicide is 1.73:1. In a balanced alloy, aluminium and magnesium silicide can be treated as a quasi-binary system, thereby simplifying the phase diagram representation (Fig. 3.2). The diagram shows that the maximum solubility of  $Mg_2Si$  in aluminium is 1.85% at 600°C.

An increase in the  $Mg_2Si$  content results in improved tensile properties [34–39], but is accompanied by a loss of extrudability. For example, Traenkner

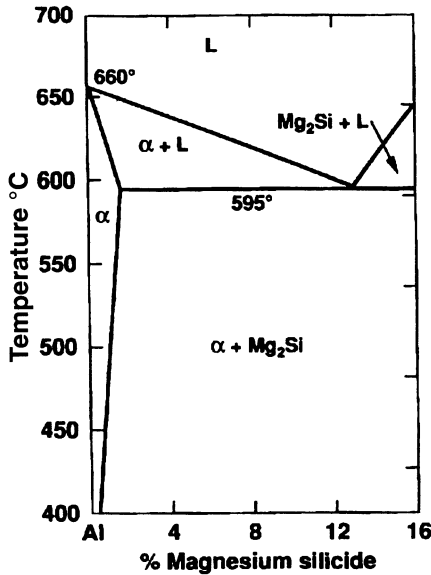


Fig. 3.2 Al-Mg<sub>2</sub>Si phase diagram.

[40] found that by increasing the Mg<sub>2</sub>Si content from 0.5% to 0.95% and 1.35%, ram speed reductions of 40% and 70% respectively were necessary. However, when overall productivity is considered, increased Mg<sub>2</sub>Si content can improve productivity by reducing the storage time required between extrusion and artificial ageing [41]. For example, it has been reported [42] that for alloys with low content (<0.35% Mg<sub>2</sub>Si) the storage time may be several days, which is not feasible with the high production requirements of modern extrusion plants. The reason for the storage time is not fully understood but it is believed to be associated with the growth of very fine precipitates during this period [43].

To obtain full T6 age hardened properties, without the need of a separate solution treatment [44], the Mg<sub>2</sub>Si must dissolve into solution during extrusion as the deforming material passes through the deformation zone. The Mg<sub>2</sub>Si can then be retained in solution by quenching directly after extrusion. To ensure all the Mg<sub>2</sub>Si dissolves during extrusion the precipitates must be fine and uniformly dispersed, as large precipitates require extended soak times for complete dissolution. A fine and uniform distribution of Mg<sub>2</sub>Si can be obtained by good casting processes [45], homogenization (and subsequent cooling practices) [35,44,46] and rapid reheating to the extrusion temperature [32]. Minor alloying elements [36,37,44] which form nucleation sites for Mg<sub>2</sub>Si, also aid a fine distribution of precipitates.

Rapid precipitation of Mg<sub>2</sub>Si occurs in the temperature range, 316°C to 417°C [39] and will result in coarse precipitates unless this temperature range is traversed rapidly on reheating to extrusion temperature. Coarse Mg<sub>2</sub>Si particles

cause low hardness [45], increased pick-up [47] on the extrude surface, and a cloudy finish upon anodizing [47–49].

For best strength and anodized brightness a fine and uniformly distributed  $Mg_2Si$  precipitate size of approximately  $0.25\ \mu m$  is recommended [49].

An  $Mg_2Si$  precipitate size of  $0.5\ \mu m$  is reported [48–50] to give the best compromise of extrusion pressure, ram speed, surface finish, aged strength and anodized brightness when extruded at  $450^\circ C$ .

#### *Silicon (Si)*

Silicon combines with iron in preference to magnesium [36] to form an  $AlFeSi$  phase. The silicon available for magnesium silicide is therefore given by [40]:  $\%Si - 0.25(\%Fe + \%Mn)$ .

An excess of silicon over that required for magnesium silicide and iron phases will increase the strength [34,36,37,40,45,48,49] but decrease the extrudability [34,45,48,50]. The influence of silicon on extrusion speed, for alloys with constant levels of 0.4% and 0.5% Mg, has been shown [33] to decrease the ram speed by  $0.4\ m\ min^{-1}$  per 0.01% Si increase.

Notch sensitivity [35] and brittleness [36,44,45] are reported to increase with excess silicon. The loss of ductility is considered [33] to be due to Si and  $Mg_2Si$  precipitates in the grain boundary. Loss of toughness [35,47,48] can be controlled, however, with minor additions of manganese and/or chromium [35,44,48,50].

The surface finish of extrudates produced with excess silicon alloys may display deleterious dark spots [45] which are caused by silicon precipitates.

#### *Magnesium (Mg)*

An excess of magnesium in the AA6XXX series alloys is much more detrimental to the extrudability [45,48] than an equal amount of excess silicon, and contributes little to strength [48]. For a constant 0.43% and 0.5% silicon level and magnesium content  $<0.55\%$ , extrusion speed is decreased by  $0.4\ m\ min^{-1}$  per 0.01% Mg increase [33]. At levels of magnesium  $>0.55\%$  the speed decrease is more rapid. This is because there is a change in the mechanism of tear initiation. This phenomenon is discussed later.

Corrosion resistance is reported [49] to improve with excess magnesium.

#### *Iron (Fe)*

Iron is present in AA6XXX series alloys as a controlled impurity [39], hence, even the most simple of AA6XXX alloys may be considered as a quaternary alloy of the  $Al-Fe-Mg-Si$  system.

Silicon combines with iron in preference to magnesium [48] to form an  $AlFeSi$  phase. An increase in the iron content can therefore decrease the strength of the alloy by removing excess silicon (especially when there is inadequate silicon remaining to combine with magnesium). This is often a cause of low mechanical properties in AA6063-T5 [40]. However, a secondary effect of the iron phase is

to refine the magnesium silicide precipitate thus producing an increase in the T6 strength [36], this being more prevalent in higher excess silicon alloys.

The  $\beta$ -AlFeSi phase, which is present in as-cast billets, has an adverse effect on the hot working characteristics [52]. To permit higher extrusion speeds [38], without the appearance of intermittent finite white fleck surface tears [48], a homogenization treatment must be used to refine and transform the  $\beta$ -AlFeSi into the preferred  $\alpha$ -AlFeSi. A typical industrial homogenization treatment [44] is 6 hours at 565°C.

Iron is also reported to cause a reduction in corrosion resistance [48] and improve toughness [50].

### *Copper (Cu)*

Europe does not approve the additions of copper to AA6XXX series alloys due to the alleged poor corrosion resistance [34,48,53]. This is contrary to the findings of some workers [34,48,49] who have shown that, in balanced alloys, small additions of copper have no detrimental effect. However, in alloys with excess silicon, low levels of copper have been found [48] to significantly decrease corrosion resistance under severe conditions.

Small additions of copper enter aluminium solid solution and iron-rich phases [48], with copper phases only occurring at levels greater than 1%. Minor copper additions improve strength [34,36,37,48,52,57] by entering solid solution and also by refining the  $Mg_2Si$  precipitate [34,35,48,51]. The refining effect of copper is additive to that produced by excess silicon [36].

A low level of copper has no noticeable effect on toughness. However, it does to some extent inhibit grain boundary precipitation and influences deformation within the grains [36].

Copper is added to alloys AA6063 and AA6463 to enhance brightness on bright dipping and anodizing [40].

### *Manganese (Mn), chromium (Cr) and zirconium (Zr)*

The three minor additions Mn, Cr and Zr are added to improve toughness [34,44,58] by forming fine, stable incoherent dispersoids during homogenization [35,48,54]. However, these additions increase quench sensitivity [51] by providing nucleation sites for the  $Mg_2Si$ . Increasing the Mn and Cr beyond that required for adequate toughness will further decrease extrudability [34,35]. Mn is preferred over Cr because it is far less detrimental to extrusion speed and finish [51,55]. However, it is more harmful to quench sensitivity [56,57].

Recrystallization is inhibited with the addition of Mn and Cr by forming intermetallic particles which are capable of pinning grain boundaries.

Small percentages of Mn reduce pick-up [59] and improve surface finish by promoting a fine distribution of  $Mg_2Si$ . The introduction of Mn also accelerates the transformation of the non-equilibrium  $\beta$  to the equilibrium  $\alpha$  iron phase, during homogenization [42].

*Other minor additions*

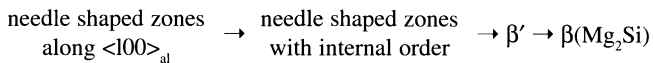
Vanadium (V) may be added to promote a fine grain size on casting [60], this leads to improved strength, toughness and formability.

Lead (Pb) is sometimes added to improve machinability [52] by entering solid solution.

Titanium (Ti) and boron (B) control grain size [39,52] and increase the solidification rate [49].

*Phase transformations in Al–Mg–Si alloys*

The majority of phase transformation studies in this alloy have been undertaken on so-called ‘balanced alloys’ where solute additions are such that the alloys may be considered as a pseudo-binary (Al–Mg<sub>2</sub>Si) system. The decomposition of supersaturated solid solution in Al–Mg–Si alloys has been studied extensively by X-ray [61–63] and transmission electron microscopy [43,52,64,65] investigations. The precipitation sequence in this alloy has been proposed [66] as:



The  $\beta'$  rods were determined [65] to be hexagonal ( $a = 7.05 \pm 0.5$ ,  $c = 4.05 \pm 0.05$ ) and form in the cube direction. The equilibrium  $\beta(\text{Mg}_2\text{Si})$  phase forms as platelets with an f.c.c. (CaF<sub>2</sub>) structure ( $a = 6.39$ ).

In AA6063 alloy the second phase dissolution is of considerable importance, as its overall process economics relies on attaining sufficient dissolution during hot extrusion. This eliminates (with a suitable quench rate immediately after extrusion) the need for a separate solution treatment before artificial ageing treatments. Therefore, the homogenization treatment must render the Mg<sub>2</sub>Si in a form suitable for rapid dissolution during the short excursion above the solvus temperature, when extruded. Under common (industrial) practices the short homogenisation treatments and cooling conditions produce  $\beta'$  rods which dissolve more readily than equilibrium  $\beta$ , during billet preheat and subsequent extrusion at 450°C to 480°C.

The use of stepped cooling has been observed [46] to increase dissolution of  $\beta'$  rods by the precipitation of  $\alpha$ -phase on the  $\beta'$  interface which on reheating was thought to provide local sink sites for the solute fluxes driving the dissolution process. However, these experimental findings were confined to small sample sizes and carefully controlled furnace temperatures, which probably could not be reproduced on industrial scale production. Also there was no comparison made between step-cooling and normal continuous cooling treatments during and after extrusion in order to justify the additional thermal processing.

Another important phase transformation to be made, especially when considering surface finish, is that of the iron phase. This is discussed in the following chapter.

### 3.1.7 The AA7XXX system

#### *Al–Zn–Mg alloys*

From the limited data on strictly ternary alloys it appears that there is little difference between the mechanical properties of high-purity ternary alloys and their commercial equivalents, the strengths being 20–30 N mm<sup>-2</sup> lower and the elongations correspondingly higher. The maximum strengths in both the naturally and artificially aged tempers correspond to the alloys close to the Al–MgZn<sub>2</sub> line with 8–10% Zn and 3–4% Mg. These alloys are also the most susceptible to stress corrosion, especially when treated to maximum strength. Somewhat lower strengths but better toughness at low temperature, better formability and better fatigue strength are obtained in the alloys with lower Zn:Mg ratios, especially with lowered alloy content. The alloys in this system have relatively low high-temperature resistance: overaging is very rapid at temperatures above 500 K. Thus, the high strength of the aged alloys disappears very rapidly with exposure at high temperatures. Persistent slip bands form in an alloy with 7.5% Zn, 2.5% Mg, aged and then subjected to torsion fatigue. These bands are accompanied by resolution of the precipitate and formation of fatigue cracks. Stacking faults can form as a result of cold work, increasing as the amount of zinc plus magnesium increases.

Rates of diffusion of magnesium and zinc in ternary alloys do not differ substantially from the binary ones.

The resistance to normal corrosion of the aluminium–magnesium–zinc alloys is very good, but the alloys are particularly susceptible to stress corrosion.

Most ternary alloys are age hardenable. Four groups [8] can be distinguished:

1. Alloys in which Mg<sub>3</sub>Al<sub>8</sub> predominates. These alloys have a Mg:Zn ratio of 6:1 or higher.
2. Alloys in which Mg<sub>3</sub>Zn<sub>3</sub>Al<sub>2</sub> predominates. These alloys represent a wide range of compositions, from a Mg:Zn ratio of 6:1 to one of 3:7.
3. Alloys in which MgZn<sub>2</sub> is the precipitating phase, at least at the lower temperatures. The exact range of these alloys is not ascertained, but alloys with ratios 2:5 to 1:7 should fall within it. In alloys with the higher Mg:Zn ratios the ternary compound may be the precipitating phase at higher temperatures.
4. Alloys with Mg:Zn < 1:10. In these alloys Mg<sub>2</sub>Zn<sub>11</sub>, should be the precipitating phase.

The limits given for the ranges are only approximate and refer to the free magnesium and zinc, not necessarily the total. Impurities that combine with magnesium or zinc, or affect their solid solubility, shift the boundaries of the ranges. Most of the commercial alloys fall in groups 2 and 3. The alloys in group 1 behave approximately as the binary aluminium–magnesium alloys. There is an acceleration of the rate of ageing but the amount of change remains the same [67,68]. This acceleration is attributed to the absorption of zinc in the Guinier–Preston zones [69]. The addition of 1% zinc to alloys with 7–9% Mg is reported to reduce the susceptibility to intergranular corrosion after annealing at

350–500 K [70], but to increase the susceptibility to stress corrosion. Mechanical properties obtained in these alloys by age hardening treatments are far from exceptional and do not differ appreciably from those obtained in binary aluminium–magnesium alloys of similar alloying content.

The range in group 2 is very wide, but most of the work is on complex commercial alloys [71–74]. Zone formation starts with more or less spherical zinc clusters, which, upon ageing at 500 K for a few hours, have a diameter of the order of  $1000 \times 10^{-10}$  m [8]. An intermediate lattice,  $T'$ , cubic, with  $a = 14.50 \times 10^{-10}$  m, is formed, with orientation relationship

$$(100)_{T'} \parallel (111)_{Al} \quad [010]_{T'} \parallel [112]_{Al}$$

The orientation relationship for the final phase is given as

$$(100)_T \parallel (112)_{Al} \quad [001]_T \parallel [110]_{Al}$$

The higher the Mg:Zn ratio the slower the zone formation, but the faster the latter stages.

The group of alloys in which  $Mg_2Zn_{11}$  should be the precipitating phase require a zinc content well above 30% Zn, and do not have properties that will make them commercially attractive.

#### *Al–Zn–Mg–Cu alloys*

The class of alloy most frequently encountered contains magnesium and copper, as well as additives such as chromium, manganese or zirconium, and the ever-present iron and silicon. In cast ingot form, alloy 7075 forms one or more variants of  $(Fe, Cr)_3SiAl_2$ ,  $Mg_2Si$ , and a pseudobinary eutectic made up of aluminium and  $MgZn_2$ . The latter phase contains aluminium and copper as substitutes for zinc and can be written  $Mg(Zn, Cu, Al)_2$ . Subsequent heating causes the iron-rich phases to transform to  $Al_7Cu_2Fe$ .  $Mg_2Si$  is relatively insoluble and tends to spheroidize somewhat;  $Mg(Zn, Cu, Al)_2$  rapidly begins to dissolve, and at the same time some  $Al_2CuMg$  precipitates, which then requires high temperatures and lengthy soaking to become completely dissolved. Chromium is precipitated from supersaturated solution as  $Cr_2Mg_3Al_8$  dispersoid, concentrated heavily in the primary dendrite regions. A well-solutionized wrought alloy contains only  $Al_7Cu_2Fe$ ,  $(Fe, Cr)_3SiAl_2$  and  $Mg_2Si$ , along with the dispersoid. Recrystallized grains are extremely elongated or flattened because of dispersoid banding, and unrecrystallized regions are not unusual even in sheet. The unrecrystallized regions are made up of very fine subgrains in which boundaries are decorated by hardening precipitate. This is more obvious in hot worked structures, especially in the more highly worked regions near the surface, where critical deformation has caused coarse recrystallized grains to form. The dispersoids inhibit recrystallization and foster formation of the fine subgrain structures.  $ZrAl_3$  is coherent with the matrix, and has similar effects.



Other high- and moderate-strength 7XXX alloys represent variants from 7075. Alloy 7050, with higher copper and zinc, has more  $\text{Al}_2\text{CuMg}$  to be dissolved at the solutionizing temperature. More dilute alloys can readily dissolve all of the zinc-rich phases. Signs of overheating in 7XXX alloys are usually related to segregated regions with unusual concentrations of  $\text{Al}_2\text{CuMg}$ . The homogeneous alloy has an equilibrium solidus that is well above the solution heat treating temperature range. If  $\text{Al}_2\text{CuMg}$  is present, however, very rapid heating rates can result in the appearance of rosettes, because of the inadequate time for diffusion and particle dissolution before exceeding the non-equilibrium eutectic temperature.

A given alloy cannot be characterized by a single microstructural aspect. The initial size of second-phase particles formed during solidification depends on the rate of heat removal. The degree of comminution and randomization of less soluble second-phase particles depends upon the total accumulation of mechanical working. The amount of excess soluble phase depends on the individual alloy composition, within specification limits, and upon the thermal treatment. The quantity and size of the dispersoid depends on the individual composition and the total thermal history, supplemented by severity of mechanical deformation. The degree of recovery and recrystallization and the size and shape of recrystallized grains depend in large measure on all of the above, as well as on factors such as rate of heating. An understanding of these interactions is important for correct interpretation of microstructural features.

Development of the Al–Mg–Zn–Cu quaternary system was initiated in the 1940s with the introduction of the alloy AA7075. This quaternary alloy also contained additions of such elements as Cr, Ti, Fe and Si. The aim of this alloy was to increase strengths beyond the range exhibited by the Al–Cu alloys of the time. Later, improvements based on this alloy led to the introduction of AA7X49 alloys, which utilize higher zinc contents for increased strengths. More recently, alloys of the AA7X50 type have been developed, which use zirconium as a substitute for the chromium additions in AA7075, to further improve the performance characteristics of the AA7XXX alloy system.

The main use of AA7XXX alloys is either as large forgings or as extruded sections, and their main applications arise where a combination of high strength and low mass is required (e.g. the aerospace industry).

### *The effects of alloying additions*

#### *Zinc and magnesium*

The respective zinc:magnesium ratio is the most significant factor with these additions. This ratio affects mechanical properties, precipitation during ageing, quench sensitivity and stress corrosion resistance.

An increase in either zinc or magnesium will increase the tensile strength and hardness of the alloys [75]. A magnesium addition exhibits approximately 3 to 4 times the effect of a zinc addition. Separately these elements increase the strength

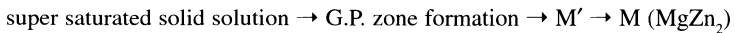
via a solid solution hardening mechanism. If these elements combine they form the hardening  $\text{MgZn}_2$  precipitate phase. The increased strength of either mechanism corresponds to a reduction in ductility and elongation [76].

The quench sensitivity of these alloys is found to increase with a decrease in the Zn:Mg ratio. A decrease in this ratio corresponds to a greater amount of free magnesium in the alloy matrix. This free magnesium could therefore increase the kinetics of precipitate nucleation and growth with respect to magnesium-containing precipitates. This free magnesium increase in the matrix is also thought to be responsible for the fact that stress corrosion cracking susceptibility increases as the Zn:Mg ratio decreases [77].

### *Copper*

The addition of copper to these alloys has a direct effect upon all alloy properties. Copper increases the strength of the alloy via a solid solution strengthening mechanism and not via precipitation. When Cu is present in precipitate form it is combined with other alloying elements forming coarse  $\text{S}(\text{Al-Cu-Mg})$  and  $\text{T}(\text{Al-Zn-Mg-Cu})$  phases which are detrimental to both strength and toughness. The formation of these coarse particles is usually deterred by utilizing a slow heat up during homogenization to take these phases into solid solution thus increasing strength and toughness [78].

In post-working heat treatments, the precipitation of  $\text{MgZn}_2$  is thought to follow the sequence:



Copper helps to stabilize and accelerate G.P. zone formation which in turn helps to retain peak strength in the final product [8]. For the ageing process, there is a critical temperature below which the G.P. zones can act as the  $\text{MgZn}_2$  phase nucleation sites and above which the zones dissolve. Copper additions raise this critical temperature and hence enable peak strengths to become attainable with higher temperature ageing treatments. This is advantageous to the alloy because higher temperature treatments increase stress corrosion resistance. Copper also has an electrochemical effect on stress corrosion and additions of  $\text{Cu} > 1\text{wt}\%$  improve the resistance significantly. There is however a quench rate criterion to be considered for the corrosion resistance. Slow quench rates lead to coarse copper-containing particles being precipitated at the grain boundaries with a subsequent dramatic increase in stress corrosion susceptibility.

Copper additions can also have other adverse effects in the alloy. In particular, the addition of copper reduces the castability of  $\text{Al-Mg-Zn-Cu}$  alloys. High copper contents lead to high residual stresses and cracking in the ingot. The weldability of the alloy is also severely decreased even for small copper additions but fatigue resistance, however, is increased, particularly in an overaged condition.

*Chromium, manganese and zirconium*

Such transition element additions are primarily added as recrystallization inhibitors to retain as much of the fine grain (i.e. worked) structure as possible after the solution heat treatments. Recent improved alloy designs based upon the original AA7075 system have utilized zirconium as an alloy addition. One example of such a modified AA7075 alloy is designated as AA7150. The effectiveness of these additions as inhibitors are in the order  $Zr > Mn > Cr$ . Stress corrosion resistance is enhanced in extrusions with little or no surface recrystallization, because it is extremely difficult to propagate intergranular stress corrosion cracks perpendicular to a highly elongated grain structure. This then explains the benefits of transition elements for stress corrosion resistance in these alloys.

This order also applies to the quench sensitivity of the alloy, with zirconium again being the most effective in reducing quench sensitivity, especially in thick sections. The mechanism operating during precipitation for manganese and chromium containing phases is the same. The dispersoid particles formed by these elements ( $CrAl_7$ ,  $AlCrMg$ ,  $MnAl_6$  and  $AlMnSi$ ) have planes in common with the precipitate phase (M) and hence lower the activation barrier for precipitation. This then increases the rate of precipitation and thus a slower cool results in coarser precipitates, and consequently lower mechanical properties. Zirconium, however, forms no ternary phases leaving more solute available for hardening. The binary  $ZrAl_3$  has no planes in common with the ageing precipitates, resulting in much lower quench sensitivity and hence much better properties at slower cooling rates (e.g. thick sections).

The toughness properties are affected by a combination of finer grain size and dispersoid/dislocation interaction. Here zirconium additions again show greater improvements over manganese and chromium additions. These transition elements do form, however, coarse particles during casting (for zirconium this occurs at concentrations of  $Zr > 0.15wt\%$ ), which need to be eliminated for optimum properties in the final product. Zirconium also has the particular disadvantage of poisoning the grain refining properties of the titanium and boron present in the casting alloy, and, hence, excess titanium and boron usually need to be added to counteract this.

Zirconium can also adversely affect the homogenization of the alloy performed prior to hot working. Zirconium precipitates out more slowly than most other additions during homogenization at high temperatures and must be precipitated as  $ZrAl_3$  by heating slowly between 380°C and 420°C [70]. It thus increases the time of this process.

Chromium also has deleterious properties in the alloy [79]. Such additions decrease the exfoliation resistance of the alloy and can also reduce the strengthening effects of copper additions. Exfoliation corrosion is a form of selective subsurface attack that proceeds along multiple narrow paths parallel to the metal's surface. The attack is generally intergranular but has been observed along striations of insoluble constituents. In AA7XXX alloys exfoliation is generally only observed in heavily worked thin sections. Extrusion products, however, generally

exhibit surface recrystallization and hence are quite resistant to this type of attack. Thus chromium (and other transition elements) by inhibiting recrystallization enhance exfoliation susceptibility but reduce stress corrosion susceptibility. Therefore, transition element additions need to be assessed with regard to the predominant corrosion mechanism of the final product [80]. Chromium and manganese decrease the strengthening effects of copper additions by aiding the precipitation of coarse  $\text{MgZn}_2$ , thereby counteracting the formation of fine dispersions by precipitation on copper containing G.P. zones.

#### *Iron and silicon*

These elements are present as impurities in commercial alloys and are not deliberately added because their effects are detrimental to alloy properties in every respect. They form as coarse dispersoids reducing toughness and maximum strength in the alloy. The effect of iron is more detrimental than that of silicon and concentrations of  $\text{Fe} > 0.15\%$  can lead to severe toughness problems.

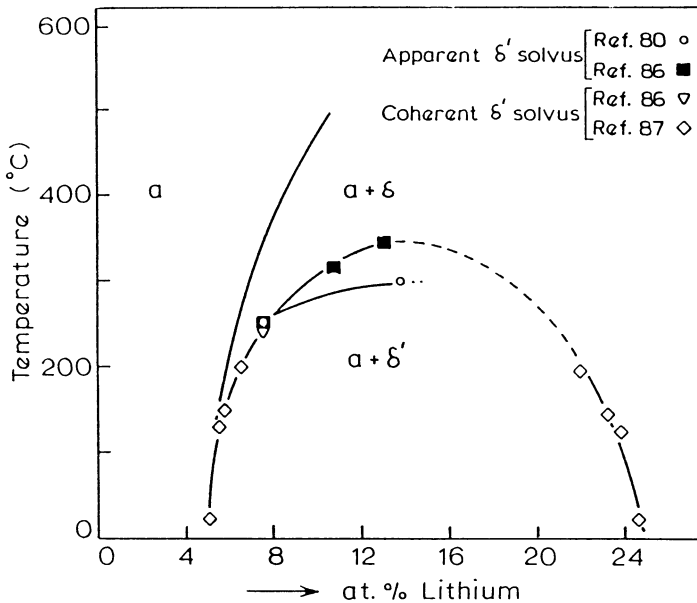
As regards quench sensitivity their detrimental effects are not as great. It is thought that iron also decreases exfoliation resistance [75]. As a consequence iron and silicon are reduced to the lowest possible levels in AA7075 and generally in all Al–Mg–Zn–Cu type alloys.

### **3.1.8 Aluminium–lithium alloys**

In common with conventional heat-treatable aluminium alloys, e.g. Al–Cu–Mg, Al–Zn–Mg–Cu, Al–Mg–Si etc., Al–Li alloys rely upon the ageing heat treatments producing precipitation hardening behaviour for increased strength. The aluminium rich corner of the equilibrium Al–Li phase diagram reviewed in detail by McAlister [79] is presented in Fig. 3.3(a). The figure shows that a simple eutectic reaction, liquid  $\rightarrow \alpha(\text{Al}) + \delta(\text{AlLi})$ , takes place at about  $600^\circ\text{C}$ ; additionally, the solubility of lithium in aluminium decreases rapidly with decrease in temperature such that an alloy containing more than about 6 at.% lithium may be quenched from the single phase field and aged in the two phase field to obtain the whole amount of excess lithium available in the form of precipitates.

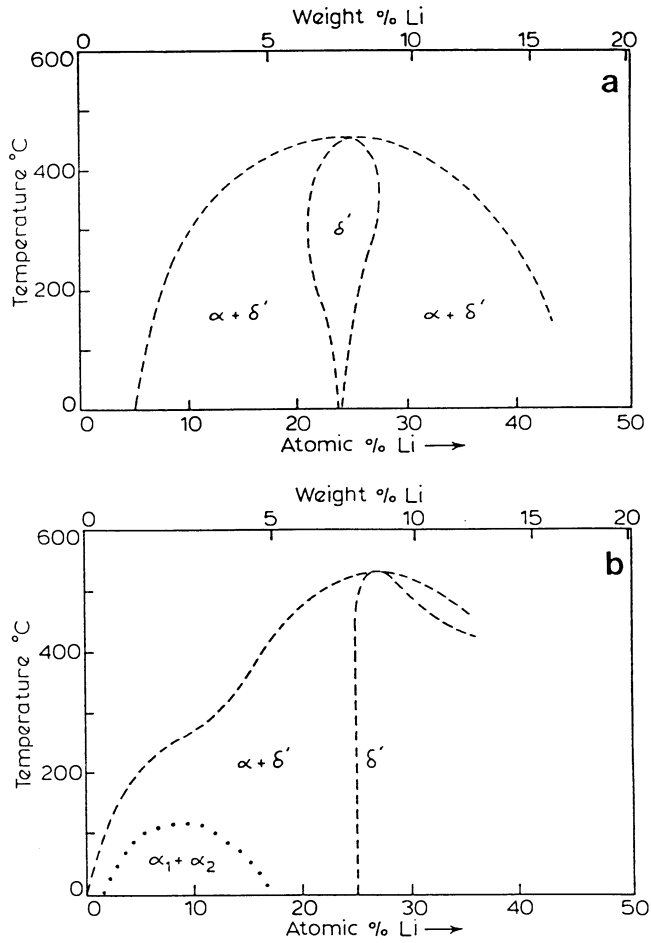
In the early 1960s Silcock [80] detected the presence of  $\delta(\text{AlLi})$  phase in Al–9 at.% Li alloys aged at  $240^\circ\text{C}$ . At a lower ageing temperature of  $165^\circ\text{C}$ , a simple L12 superlattice of the face centred cubic matrix occurred; it was identified to be due to  $\delta'(\text{Al}_3\text{Li})$  phase. This precipitate is spherical and yields a very low  $\alpha/\delta'$  mismatch value  $\sim 0.3\%$  [82]. It is coherent with the matrix and is responsible for age hardening in the binary Al–Li system.

Although  $\delta'$  was extensively studied by both X-ray diffraction [82] and transmission electron microscopy [80,81] it was not until 1971 that the  $\delta'$  solvus was first defined by Noble and Thompson [83] using transmission electron microscopy and resistivity measurements. Their work together with that of Costas and Marshall [84], Nozato and Nakai [85] and Williams and Edington [88] is



**Fig. 3.3(a)** Phase diagram of Al-Li showing the  $\delta$  solvus and the apparent and coherent  $\delta'$  solvus lines.

included in Fig. 3.3(a) showing the solvus lines for both  $\delta$  and  $\delta'$ . In addition to the metastable solvus line, Williams and Edington inferred the presence of a coherent solvus line just below the  $\delta'$  solvus from the heterogeneous precipitation of  $\delta'$  on dislocations and the absence of homogeneously precipitated matrix  $\delta'$ . Additional SAXS work by Ceresara *et al.* [87] extended the thermodynamic  $\delta'$  solvus line to define the coherent miscibility gap over the full range of the  $\delta'$  phase field to ~25 at.% lithium. The full Al-Li phase diagram showing the  $\delta$  solvus and the apparent coherent  $\delta'$  solvus lines as determined by TEM [85,88] and SAXS [90,91] is shown in Fig. 3.3(b). The metastable  $\alpha + \delta'$  solvus plays a significant role ensuring that heat treatment of alloys of commercial interest involves compositions and temperatures lying within it. A simple miscibility gap, produced by connecting the experimentally determined  $\alpha$  and  $\delta'$  solvi (Fig. 3.3), was generally accepted until recently. However, Gayle and Vandersande [89] pointed out that such a miscibility gap involving two distinct crystal structures (disordered  $\alpha$  and L12 ordered  $\delta'$ ) violates thermodynamic restrictions. These authors and others have proposed several possible forms of metastable phase diagrams [90,95] the latest being shown in Fig. 3.3(b). A theoretical model concerning the stable and metastable Al-Li phase diagram has been recently developed by Papazian, Sigli and Sanchez and others [91-93].



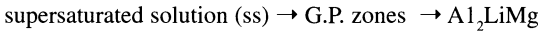
**Fig. 3.3(b)** The metastable  $\alpha$ - $\delta'$  system (a) as proposed by Gayle and Vandersande [90]; (b) as proposed by Sigli and Sanchez [91].

#### *Ternary Al-Li-Mg system*

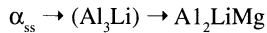
In the early stages of the development of lithium-containing aluminium alloys, basically ternary additions e.g. copper and magnesium by Jones and Das [96] were made with the aim of increasing the strength without sacrificing much ductility and density; promising results were obtained, though it is now apparent that those developments were carried out with an incomplete understanding of the strengthening mechanism and the role of the metastable  $\delta'$  phase.

A detailed study on the equilibrium phase relations in the Al-Li-Mg system was initially carried out by Levinson and McPherson [97]. Friedlander *et al.* [103] studied the phase equilibria and mechanical properties of Al-Mg-Li alloys and

their work finally resulted in an alloy designated 01420 in the mid-1960s with a nominal composition of Al-5%Mg-2%Li-0.5% Mn. The authors explained the precipitation sequence of the following type:



Little strengthening was associated with the zone formation but ageing at 160–180°C produced a substantial increase in strength. The Al<sub>2</sub>LiMg phase was claimed to be the major strengthening phase in this alloy system. The exact precipitation reactions in this alloy system were not known until Thompson and Noble [99] examined in detail the precipitation characteristics of Al-(1.5–2.0 wt%)Li-(6 wt%)Mg alloys and showed the precipitation sequence to be:



They suggested that the primary contribution of magnesium to strength is in its solid solution hardening. Also, it has been suggested [100,101] that magnesium reduces the solubility of lithium, thereby increasing the volume fraction of  $\delta'$  for a given lithium content. Additional strengthening involving possible incorporation of magnesium into  $\delta'$  has also been suggested [101–102].

#### *Ternary Al–Li–Cu system*

Addition of copper to binary Al–Li alloys produces phases which are partly related to the Al–Cu system and partly to the Al–Li system; also, formation of several ternary phases is feasible depending on the alloy composition. In the early stages of the development of these alloys, the studies by Hardy and Silcock [104] concerning phase relationships in aluminium-rich Al–Cu–Li alloys were most encouraging.

In the USA, a commercial alloy 2020 of the Al–Cu–Li alloy series was developed following Silcock's work with a composition Al-4.5%Cu-1.1%Li-0.5% Mn-0.2%Cd. Peak strength in this series of alloys has been attributed to the formation of  $\theta''$  and  $\delta'$ .

In the former USSR, the commercial alloy VAD 23 based on the Al–Cu–Li system was developed at the same time but with increased copper and lithium content. The phases present within these alloys were found to be similar to those found by Silcock, but the major strengthening of VAD 23 was attributed to the phases T<sub>B</sub> and T<sub>I</sub>.

The influence of additional phases from the ternary Al–Li–Cu system on the  $\delta'$  precipitation has been studied by several investigators. Tosten *et al.* [105], and Huang and Ardell [106] have shown that  $\delta'$  can grow on the faces of  $\delta'$  plates. Tosten *et al.* have also shown that at low Li:Cu ratio, T<sub>I</sub> can compete with  $\delta'$  for available lithium such that heterogeneous precipitation of T<sub>I</sub> phase at the grain boundaries resulted in a  $\delta'$  precipitation free zone within the Al-2%Li-3%Cu alloy whereas no such PFZs were observed within the alloy

containing 2.6% lithium and 1% copper. The formation of PFZ in this manner has been shown to be related to the copper:lithium ratio of the Al–Li–Cu alloys.

#### *Al–Li–Cu–Mg system*

Magnesium addition to a ternary Al–Li–Cu system forms the basis for today's commercial Li-containing Al-based alloys. The precipitation reactions within the Al–Li–Cu–Mg system are complex and also the phase diagram of the quaternary system has not been determined. However, studies [107–111] have shown that the phases present within the quaternary Al–Li–Cu–Mg system are similar to those present within the ternary Al–Li–Cu, Al–Li–Mg and Al–Cu–Mg systems and the choice of phases may be obtained via optimization of the alloy composition and the ageing conditions.

The beneficial effect of Mg addition is twofold: first, it can replace some percentage of copper which is advantageous from density consideration and secondly precipitation of additional phases *viz.*  $\text{Al}_2\text{CuMg}$ -based S phase and  $\text{Al}_6\text{CuMg}_4$ -based T phase in the Al–Cu–Mg system are feasible. Precipitation of T phase requires a high supersaturation of magnesium and so to allow it to form would also simultaneously encourage formation of  $\text{Al}_2\text{LiMg}$  phase in the Al–Li–Mg system. In lithium-containing Al–Cu–Mg alloys, at the typical ageing temperature the  $\text{Al}_2\text{CuMg}$ -based precipitate is generally termed S' phase.

In commercial Al–Li–Mg–Cu alloys the major matrix precipitates observed are  $\delta'(\text{Al}_3\text{Li})$ , T1( $\text{Al}_2\text{CuLi}$ ) and S'( $\text{Al}_2\text{CuMg}$ ). Since both T1 and S' phases involve copper a critical balance between copper and magnesium concentration is a deciding factor for the optimization of a particular phase within the aged microstructure. Peel [109] suggested that the balance between T1 and S' phases was dependent on the Cu:Mg ratio and from the commercial point of view it is important to maintain a Mg content of 0.7wt% in order to ensure the optimum distribution of the S' phase which may be produced during extrusion as the S' phase is considered to homogenize the slip process.

### **3.2 THE DC CAST STATE**

In a volume dedicated to extrusion it is not possible to fully cover the cast state for each of the alloys, nor would it be advisable. In the cast state all of the alloys are to a greater or lesser extent heterogeneous and the features are most exaggerated in the 7XXX Al–Zn–Mg–Cu alloys. It may therefore be helpful to consider the alloy 7075.

In the industrial casting of AA7075, it is common to find the employment of direct chill casting moulds for the production of ingot material. Such a practice usually induces non-equilibrium freezing within the ingot. Non-equilibrium solidification introduces segregation in the casting, as well as enhancing the possibility of non-equilibrium reactions as solidification proceeds.



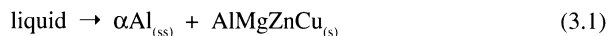
Segregation has a number of effects upon the as-cast microstructure, one of which is the production of a 'cored structure' within the solidified primary aluminium grains. Due to the high cooling rate associated with chill casting, the solid state diffusion of solute within the primary, solid aluminium dendrites is not fast enough to maintain an even distribution of solute concentration throughout the solid. This results in a solute concentration gradient (from edge to grain centre) across the primary aluminium grains of the final solid ingot. Such grains are said to be 'cored'. Another effect of segregation is to congregate more of the low melting point phases in the centre of the casting. This occurs because the advancing, primary wall of solid effectively sweeps these phases (in a liquid form) before it. Ultimately they are trapped between the solidification fronts combining in the ingot centre, and solidify as the ingot cools.

The non-equilibrium reactions occurring within a solidifying AA7XXX type casting will be discussed in relation to the actual solidifying sequence.

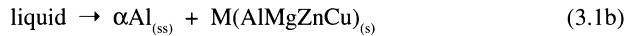
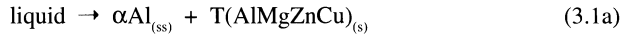
The quaternary Al–Mg–Zn–Cu system was investigated [112] by Strawbridge *et al.* It was shown by this research that only the phases found in the respective ternary systems are present in the quaternary system; no new quaternary phase was found. We can therefore consider the following phases with respect to the major alloy additions:

- $\theta(\text{CuAl}_2)$  – This phase can take up to 1–2wt% Zn into solid solution.
- $\text{S}(\text{Al}_2\text{CuMg})$  – This phase dissolves little or no zinc. Thus in ( $\alpha$ +S) type structure quaternary alloys all of the Zn is held in Al solid solution.
- $\text{T}(\text{AlMgZnCu})$  – The isomorphous  $\text{T}(\text{Al}_2\text{Mg}_3\text{Zn}_3)$  and  $\text{T}(\text{Al}_6\text{CuMg}_4)$  phases present give rise to quaternary  $\text{T}(\text{AlMgZnCu})$  solid solutions.
- $\text{M}(\text{AlMgZnCu})$  – There are two isomorphous M phases namely  $\text{M}(\text{MgZn}_2)$  and  $\text{M}(\text{AlCuMg})$ . These may give  $\text{M}(\text{AlMgZnCu})$  solid solutions in quaternary alloys when wt% Zn is high enough.
- $\text{Z}(\text{AlMgZnCu})$  – There are two isomorphous Z phases namely  $\text{Z}(\text{MgZn}_5)$  and  $\text{Z}(\text{Al}_{10}\text{Cu}_7\text{Mg}_3)$ . These give  $\text{Z}(\text{AlMgZnCu})$  quaternary solid solutions.

The solidification of an actual Al–Mg–Zn–Cu alloy proceeds with the precipitation of primary aluminium solid solution crystals ( $\alpha$ ). Ignoring, for the moment, the minor alloy additions, the solidification is concluded by the formation of a quasi-binary eutectic by the reaction:



This reaction has added complexity because it represents the parallel solidification of two quasi-binary eutectics denoted as reactions 3.1a and 3.1b.



Thus the majority of the microstructure within cast AA7XXX material will consist of large grains of primary Al (with alloying additions held in solid solution) surrounded by an intergranular eutectic network, consisting of Al solid solution, the T(AlMgZnCu) phase and the M(AlMgZnCu) phase.

This microstructure is modified by the presence of the alloy additive/impurity precipitated phases. These minor alloying elements precipitate out of solution in the form of intermetallic phases which solidify eutectically within the interdendritic/intercellular regions.

One characteristic of the minor alloy additions is that attaining equilibrium is strongly retarded for all phases. Another characteristic is the pronounced tendency these elements have for supersaturation within the Al solid solution. There are added considerations because small amounts of one element can considerably lower the solubility of another element in aluminium. One example of such behaviour is the effect of iron upon the solubility of manganese in aluminium; the presence of iron significantly lowers the solubility of manganese in aluminium.

The equilibrium (slow cooling) reactions of these minor alloy elements were investigated by Sperry [113] for alloy AA2024 (i.e. Al–Cu alloy) and the results can be directly applied to AA7XXX alloys. From this work it was possible to formulate the schematic Table 3.1 showing the sequence in which these impurity reactions took place during solidification.

None of the reactions listed in Table 3.1 occur to completion under commercial, non-equilibrium casting conditions. At low cooling rates, those phases with high solidification (reaction) temperatures will dominate in the microstructure, whereas, under high cooling rate conditions, the eutectic reactions at lower temperatures will predominate. Therefore, at low cooling rates the phases  $\text{Al}_6(\text{Mn,Fe})$  and  $\text{Al}_3\text{Fe}$  predominate, and at faster cooling rates mainly  $\text{Al}(\text{Fe,Mn})\text{Si}$  is formed.

**Table 3.1** Solidification sequence of minor element additions [113]

(a)		liq.	$\rightarrow$	primary $\alpha\text{Al}_{(\text{ss})}$
(b)		liq.	$\xrightarrow{\text{e}}$	$\alpha\text{Al}_{(\text{ss})} + \text{Al}_6(\text{Mn,Fe})$
(c)		liq.	$\xrightarrow{\text{e}}$	$\alpha\text{Al}_{(\text{ss})} + \text{Al}_3\text{Fe}$
(d)	$\alpha\text{Al}_{(\text{ss})}$	+ liq.	$\xrightarrow{\text{p}}$	$\text{Al}(\text{Fe,Mn})\text{Si}$
(e)		liq.	$\xrightarrow{\text{e}}$	$\alpha\text{Al}_{(\text{ss})} + \text{Al}(\text{Fe,Mn})\text{Si}$
(f)	$\text{Al}_3\text{Fe}$	+ liq.	$\xrightarrow{\text{p}}$	$\text{Al}(\text{Fe,Mn})\text{Si}$
(g)	$\text{Al}_6(\text{Mn,Fe})$	+ liq.	$\xrightarrow{\text{p}}$	$\text{Al}_7\text{Cu}_2\text{Fe}$
(h)	$\text{Al}_3\text{Fe}$	+ liq.	$\xrightarrow{\text{p}}$	$\text{Al}_7\text{Cu}_2\text{Fe}$
(i)	$\text{Al}(\text{Fe,Mn})\text{Si}$	+ liq.	$\xrightarrow{\text{p}}$	$\text{Al}_7\text{Cu}_2\text{Fe}$
(j)		liq.	$\xrightarrow{\text{e}}$	$\alpha\text{Al}_{(\text{ss})} + \text{Al}_7\text{Cu}_2\text{Fe}$

The reactions (a)–(j) are listed in order of decreasing reaction temperature. The superscripts e and p represent eutectic and peritectic reactions respectively.

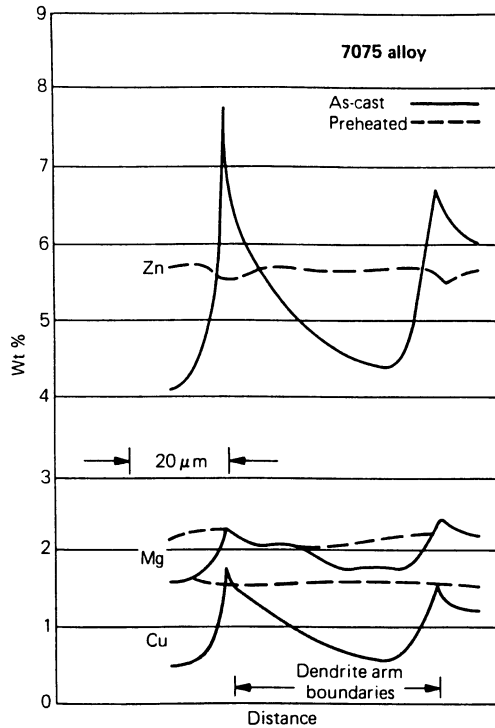
Other, different phases to those previously mentioned could also occur within the microstructure of the alloy [112]. For example, the element Cr could occur in such phases as  $\text{Al}_{18}\text{Mg}_3\text{Cr}_2$ ,  $\text{AlCrMgZn}$ ,  $\text{Al}_{13}(\text{Fe,Cr})_4\text{Si}_4$ ,  $\text{Al}_7(\text{Fe,Cr})$  and  $\text{Al}_{12}(\text{Cr,Mn})$ . The element Ti is also an addition found in AA7075, and when present is generally found in solution within  $\text{Al}_7\text{Cr}$ . The transition element Zr occurs as the phase  $\text{ZrAl}_3$  [114] when not held in solid solution in AA7X50 alloys. However, it must be noted that Conserva *et al.* in their analysis of the Cr distributions present within as-cast, commercial AA7075 found no trace of primary Cr precipitation [114]. For Zr-containing alloys, all the Zr present within the alloy has been reported to be held in solid solution only, when such alloys are in the as-cast state.

Thus, the as-cast microstructure can contain a wide variety of phases, some of which can be stable equilibrium phases, and some metastable non-equilibrium phases (in an equal, if not greater proportion), under commercial casting conditions.

### 3.3 HOMOGENIZATION

The initial thermal operation applied to ingots prior to hot working is referred to as 'ingot preheating' or 'homogenizing' and has one or more purposes depending on the alloy, product, and fabricating process involved. One of the principal objectives is improved workability. The microstructure of most alloys in the as-cast condition is quite heterogeneous. This is true for alloys that form solid solutions under equilibrium conditions and even for relatively dilute alloys. The cast microstructure is a cored dendritic structure with solute content increasing progressively from centre to edge with an interdendritic distribution of second-phase particles or eutectic.

Because of the relatively low ductility of the intergranular and interdendritic networks of these second-phase particles, as-cast structures generally have inferior workability. The thermal treatments used to homogenize cast structures for improved workability were developed chiefly by empirical methods, correlated with optical metallographic examinations, to determine the time and temperature required to minimize coring and dissolve particles of the second phase. More recently, methods have become available to determine quantitatively the degree of microsegregation existing in cast structures and the rates of solution and homogenisation. Figure 3.4 shows the microsegregation measured by an electron microprobe across the same dendrite cell in the as-cast condition and after the cell was homogenized by preheating. Rapid solidification, because it is quite different from equilibrium, produces maximum microsegregation across dendrite walls, and these cells are relatively small. The situation is complex, however, and in typical commercial ingots, large cells are more segregated than fine cells and, because diffusion distances are longer, large cells are more difficult to homogenize. For example, electron microprobe analyses of unidirectionally solidified castings of an Al-2.5%Mg alloy indicated that the degree of microsegregation



**Fig. 3.4** Effect of homogenization on ingot microsegregation. (Courtesy Alcoa)

was greater in the coarser, more slowly solidified structure, and that the approach to uniform solute distribution during heating at 425°C was more rapid for the finer structure, as shown in Fig. 3.5.

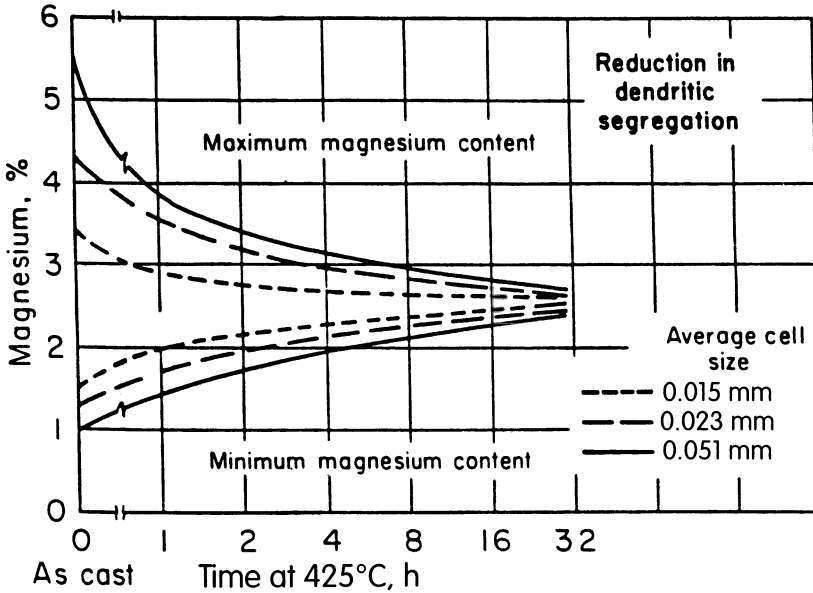
Solution of the intermetallic phases rejected interdendritically during solidification, effected by the homogenizing operation, is only one step toward providing maximum workability. Because most of the solute is in solid solution after this heating, further softening and improvement in workability can be obtained by slow cooling, to re-precipitate and coalesce the solute in an interdendritic distribution of fairly large particles.

Hence we see that in addition to the constitutional equalization, normally considered to be the principal aim of the homogenization process, a number of other diffusion related processes may be desirable or unavoidable:

- grain coarsening or recrystallization;
- precipitation of supersaturated elements;
- dissolution of unstable phases or precipitates;
- coarsening of stable intermetallic particulates;
- surface oxidation;

- hydrogen degassing;
- pore generation and agglomeration;
- localized melting.

Clearly, if we wish to quantify the homogenization process, some basic knowledge of the diffusion process is essential.



**Fig. 3.5** Effect of time at 425°C on maximum and minimum Mg content within dendrites of cast Al-2.5 Mg alloy. (Courtesy Alcoa)

### 3.3.1 Atomic movements and $D$

Up to this point our discussion has completely ignored the atomic nature of the metal and is therefore called a continuum analysis. This approach has advantages and shortcomings similar to those of a thermodynamical analysis. That is, since no assumptions were made concerning the atomic nature of the diffusion process, the conclusions are valid for all mechanisms. However, since the atomic nature of the solid is ignored, no detailed information about the atomic movements can be deduced from it.

Though the atoms in a lattice have well defined sites, the existence of diffusion proves that the atoms move from site to site. Each atom is continually oscillating about a site and occasionally the oscillation of it and its neighbours becomes violent enough to allow it to make a jump to a neighbouring site. A

detailed study of the atomic jump process shows that a large fluctuation in energy and a careful synchronization of the movement of several atoms is required even for a jump to a nearest neighbour site. A jump of a greater distance would be so difficult and so rare that we can ignore the possibility. Thus the problem is to relate the random jumping of an astronomical number of atoms from site to site, to Fick's first law. To illustrate this we may consider the flow of atoms in one direction  $x$ , by taking two atomic planes A and B of unit area separated by a distance  $b$ . If  $c_1$  and  $c_2$  are the concentrations of diffusing atoms in these two planes ( $c_1 < c_2$ ) the corresponding number of such atoms in the respective planes is  $n_1 = c_1 b$  and  $n_2 = c_2 b$ . If the probability that any one jump in the  $+x$  direction is  $p_x$ , then the number of jumps per unit time made by one atom is  $p v_v$ , where  $v_v$  is the mean frequency with which an atom leaves a site irrespective of direction. The number of diffusing atoms leaving A and arriving at B in unit time is  $(p_x v_j c_1 b)$  and the number making the reverse transition is  $(p_x v_j c_2 b)$  so that the net gain of atoms at B is:

$$p_x v_j b (c_1 - c_2) = J_x$$

with  $J_x$  the flux of diffusing atoms. Setting  $c_1 - c_2 = -b(dc/dx)$  this flux becomes:

$$J_x = -p_x v_j b^2 (dc/dx) = -D(dc/dx) \quad (3.2)$$

which is identical to Fick's first law.

In cubic lattices, diffusion is isotropic and hence all six orthogonal directions are equally likely so that  $p_x = 1/6$ . For simple cubic structures  $b = a$  and thus

$$D_x = D_y = D_z = \frac{1}{6} v_j a^2 = D$$

whereas in f.c.c. structures  $b = a/\sqrt{2}$  and  $D = \frac{1}{2} v_j a^2$ , and in b.c.c. structures  $D = \frac{1}{2} v_j a^2$ .

The transport of atoms through the lattice may conceivably occur in many ways. The term 'interstitial diffusion' describes the situation when the moving atom does not lie on the crystal lattice, but instead occupies an interstitial position. Such a process is likely in interstitial alloys where the migrating atom is very small, e.g. carbon, nitrogen or hydrogen in iron. In this case, the diffusion process for the atoms to move from one interstitial position to the next in a perfect lattice is not defect-controlled. A possible variant of this type of diffusion has been suggested for substitutional solutions in which the diffusing atoms are only temporarily interstitial and are in dynamic equilibrium with others in substitutional positions. However, the energy to form such an interstitial is many times that to produce a vacancy and, consequently, the most likely mechanism is that of the continual migration of vacancies. With vacancy diffusion, the probability that an atom may jump to the next site will depend on: (i) the probability that the site is vacant (which in turn is proportional to the fraction of vacancies in the crystal), and (ii) the probability that it has the required activation energy to make the transition. For self diffusion where no complications exist, the diffusion coefficient is therefore given by:

$$\begin{aligned}
 D &= a^2 f v \exp \left[ \frac{(S_f + S_m)}{k} \right] \exp \left[ \frac{-E_f}{kT} \right] \exp \left[ \frac{-E_m}{kT} \right] \\
 &= D_0 \exp \left[ -\frac{(E_f + E_m)}{kT} \right] = D_0 \exp \left( \frac{Q}{GT} \right) \quad (3.3)
 \end{aligned}$$

The factor  $f$  appearing in  $D_0$  is known as a correlation factor and arises from the fact that any particular diffusion jump is influenced by the direction of the previous jump. Thus when an atom and a vacancy exchange places in the lattice there is a greater probability of the atom returning to its original site than moving to another site, because of the presence there of a vacancy;  $f$  is 0.80 and 0.78 for f.c.c. and b.c.c. lattices, respectively.  $E_f$  and  $E_m$  are the energies required for the formation of a vacancy and the energy of migration respectively and their sum  $Q$  is the activation energy for self diffusion as described above.

### *Quick guide to dissolution times*

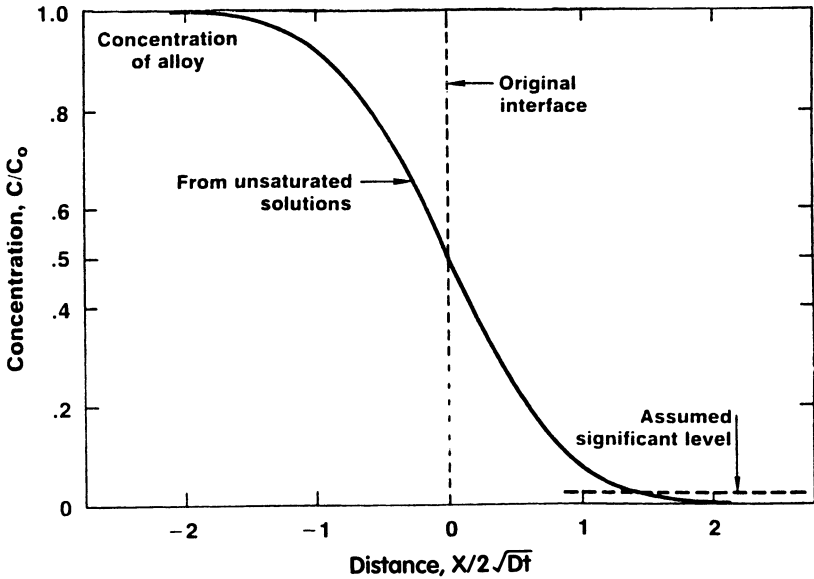
Heating an ingot for homogenization – indeed any thermal operation – is an attempt to control the diffusion which occurs within the metal [115]. Unfortunately, the equations which describe how rapidly diffusion occurs are, as we have seen, difficult to solve. The simple fact, however, is that elementary diffusion calculations, often read directly from graphs, can give straightforward results useful to practising metallurgists.

The traditional starting point for describing diffusion is the diffusion penetration curve of Fig. 3.6 which is identical to that given for the solution of the Boltzmann/Fick differential equation given in Chapter 2. This is often drawn to show that all of the diffusing element was present to the left of the vertical dashed line at the start of the heating operation, and, after diffusion, the concentration of this element was given by the S-shaped curve. The concentration scale at the left of the graph has been normalized by the concentration  $c_0$  originally to the left of the interface. The distance scale has also been normalized, this time by a factor  $2\sqrt{Dt}$ . The diffusion coefficient  $D$  (typical units are  $\text{cm}^2\text{s}^{-1}$ ) is an adjustable parameter which makes the experimentally determined concentration data fit on the curve. The curve of Fig. 3.6 is a universal curve fitting all diffusion conditions. The temperature is implicit in  $D$ .

### *Depth of penetration*

It is often necessary to know how far diffusion has proceeded away from the original supply. The answer must be indefinite because there is no sharp dividing line between the diffused and undiffused regions. If, however, one arbitrarily says that diffusion has reached a particular place when the concentration has risen to a certain level (say 2.5% of the amount in the original diffusion supply), the time at

which this occurs is readily calculable (from the value of the point marked by the arrow in Fig. 3.6).



**Fig. 3.6** Generic diffusion penetration curve with normalized concentration and distance scales. The arrow marks the distance at which significant diffusion has occurred.

For the calculation, it is necessary to know the rate of diffusion at various temperatures for various elements, but these are available. Figure 3.7, for example, shows depth of penetration as a function of diffusion coefficient for various heating times. To make the figure more useful, the coefficients for the common alloying elements of aluminium are given so temperatures and elements are available directly.

To determine, for example, how long it takes diffusion to penetrate through a 0.05 mm cladding on a copper-bearing alloy at 500°C, locate the intersection of a horizontal line at 0.05 mm with a vertical line at 500°C on the copper scale. The result shows that the overall diffusion front will be at the surface of the cladding in 2 h (somewhat sooner at grain boundaries).

#### *Homogenization of dendrite cells*

The initial distribution of an element due to coring in a dendrite cell is more complex than in the simple diffusion couple. But it is not much of an exaggeration to model the starting situation as if all of the solute were present after casting only at the edges of dendrite cells and none was present within the cells. This is certainly



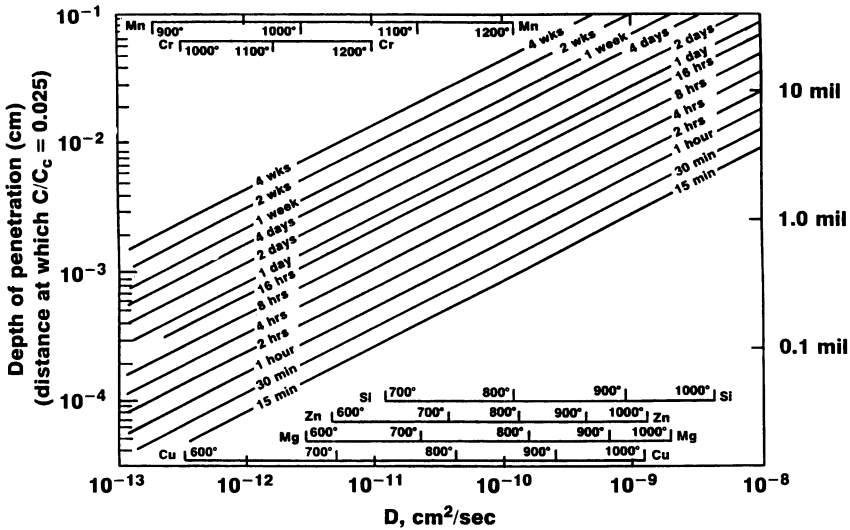


Fig.3.7 Penetration depth for combination of time and temperature for various elements. (After W.G. Fricke.)

more realistic than the cosine function presented in Chapter 2 and frequently used in mathematical texts.

Figure 3.5 shows examples of this where magnesium is the diffuser at 425°C. Consider the situation where the magnesium was initially present at two infinitely thin layers located at 0.0 and 0.5 mil (0.125 mm) on the distance scale. After only 102 s, diffusion proceeding towards the right from the 0.0 source and towards the left from the 0.5 source have met midway between, and the concentrations from the two sources have begun to be additive. The solute distribution at this time looks similar to that in a real dendrite on solidification.

After 103 s, the continued diffusion of solute into this region from two directions had produced an almost uniform distribution of solute. In other words, the material was almost homogenized. When the diffusion front from the left source has reached the distance of the right source and vice versa, the addition of the two concentration gradients produces a homogeneous material.

This means that the penetration curves of Fig. 3.7 can be used to estimate homogenization times. Using the previous figures, copper can be homogenized over a 0.05 mm dendrite cell in about 2 h at 500°C.

Obviously, the larger the dendrite cells in an ingot the greater the diffusion distances involved. The ratio  $x/2\sqrt{(Dt)}$  in the distance scale of Fig. 3.7 shows that if the distance to be travelled,  $x$ , is doubled, the time must be quadrupled to keep the ratio constant and give the same amount of diffusion. Figure 3.8 also shows thin film calculations for magnesium sources at 0.25 mm and 0.625 mm. Times of only  $10^3$  s (17 min) are inadequate to homogenize cells of these larger sizes. Obviously, if cell sizes become smaller the time for homogenization becomes less.

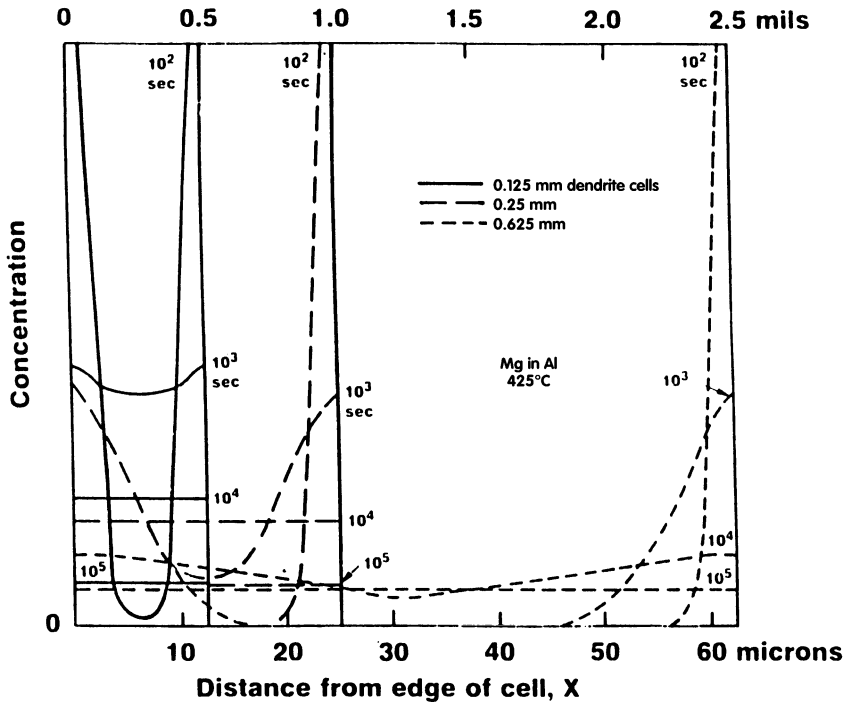


Fig. 3.8 Diffusion of Mg from film source. (After W.G. Fricke)

For comparison with the calculations, actual measurements of magnesium concentrations at the centre and edge of dendrites of the average sizes of Fig. 3.8 have been shown in Fig. 3.7. Whether the curves of Fig. 3.6 or 3.7 are used to predict homogenization times, the estimated times are 1/2, 2 and 12 hours for the three cell sizes. The actual curves of Fig. 3.5 suggest these times are somewhat short, probably because the actual material had some cells larger than the average on which the calculations are based. Doubling, or even tripling, the estimated times is a conservative measure, especially for small average cell sizes.

Nevertheless, knowing which element requires homogenization (usually slowest diffusing species) and the temperature involved, it is possible to make a first estimate of the times needed for homogenization (Fig. 3.9). These times do not include heat-up times or the times needed to dissolve particles.

Elements which diffuse slowly, such as manganese and chromium, have diffusion coefficients so much smaller than magnesium or copper that even when the cell size is small the time to homogenize is long and may be commercially prohibitive.

Once a heating practice is developed for a product, it is sometimes necessary to raise the temperature to speed things up or to lower the temperature to utilize a partial furnace load; it is then necessary to revise the time required under these new conditions.

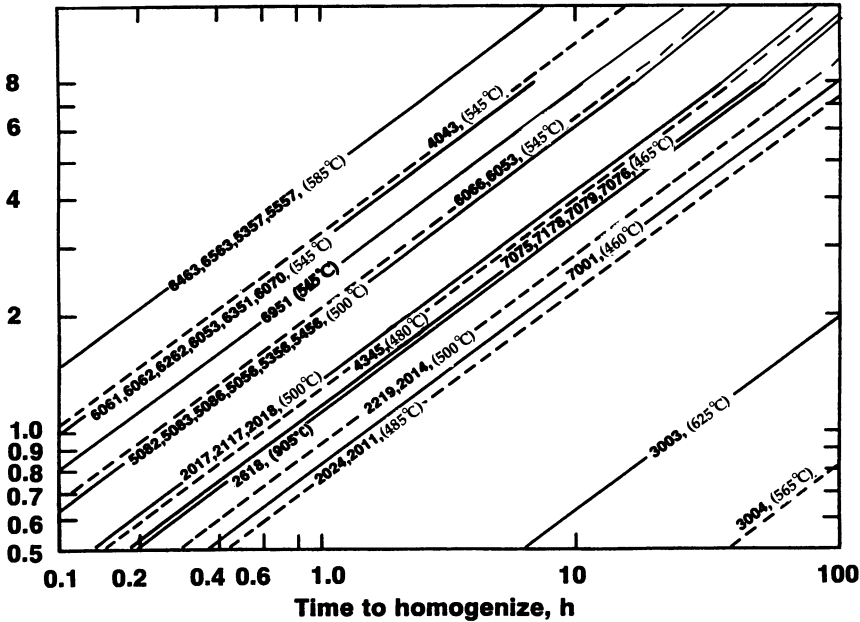


Fig. 3.9 Time to homogenize derived from penetration curves of changing heating conditions. (After W.G. Fricke.)

This is a straightforward calculation, provided certain metallurgical restrictions are met. Two different times,  $t_1$  or  $t_2$ , produce the same amount of diffusion at absolute temperatures  $T_1$  or  $T_2$  if:

$$\frac{t_1}{t_2} = \exp \left[ \frac{Q}{R} \left( \frac{1}{T_1} - \frac{1}{T_2} \right) \right] \quad (3.4)$$

In this equation,  $Q$  is the activation energy for diffusion for a particular element and  $R$  is the gas constant.

The above equation is solved most easily with a graph (Fig. 3.10). A point such as A is selected to represent the time and temperature for the initial condition (2 h at 500°C, in this case). A line is drawn through A parallel to the line on the slope scale for the activation energy of the element diffusing (Mg in the example). All combinations of time and temperature along this line produce the same amounts of diffusion provided one does not cross a solubility line or violate other metallurgical incompatibilities.

The activation energy for diffusing magnesium in aluminium is typical of all soluble elements. In the preheat temperature range, dropping the temperature 50°C requires the ingot to be in the furnace about three times as long. The same 50°C drop in the annealing temperature range increases the time tenfold (and, of course, has a profound effect on the driving force for recrystallization).

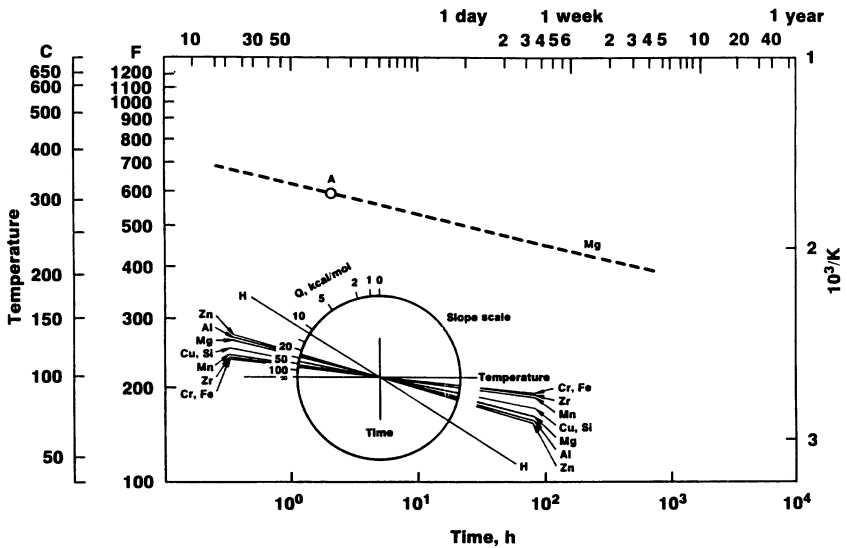


Fig. 3.10 Calculation of equivalent times and temperatures. Example shown is combinations equivalent to 2 h, at 315°C. (After W.G. Fricke)

There are factors we have neglected which affect the diffusion rate. Cold work (dislocations), grain boundaries, presence of other elements and concentration, do produce measurable effects. These occur primarily at temperatures of no interest to the heat treater or are minor effects. The practical metallurgist is interested in getting a first approximation to try for heating the product.

### 3.3.2 Metallurgical consideration of homogenization

#### *Diffusion*

The homogenization process causes the microstructure to move towards the equilibrium corresponding to the temperature employed. The alloying elements respond differently depending upon their solid solubility and their rate of diffusion in the aluminium matrix (see above). They may be grouped in three categories:

- moderate solubility, very low diffusion rate  $J$  – Cr, Mn, Ti, V, Zr;
- appreciable solubility, high diffusion rate  $J$  – Cu, Mg, Si, Zn;
- extremely low solubility, very low diffusion rate  $J$  – Fe.

The aim of homogenization is the equalization of concentration differences within the dendrite arms. Examples of electron probe microanalytic line traces for Al–0.21%Ti [116] and Al–5.5%Mg–0.19%Cr [117] permanent mould cast alloys have been presented. The titanium concentration inside the cored structure is about 3.6 times the nominal Ti content. To obtain Ti at equilibrium level would require 3 weeks for completion. The magnesium coring is eliminated readily by thermal

exposure at 430°C for 20 h, but the chromium segregation remains virtually untouched. As diffusion proceeds, the minimum Mg content increases and the maximum Ti concentration decreases with time. The Cr addition lowers the Mg at the centre of the dendrite arm and increases the precipitation of non – equilibrium compounds. The diffusion rate in the alloy containing Cr is slower at 450°C due to the precipitation of  $Al_{18}Mg_3Cr_2$  during the early stages of thermal exposure.

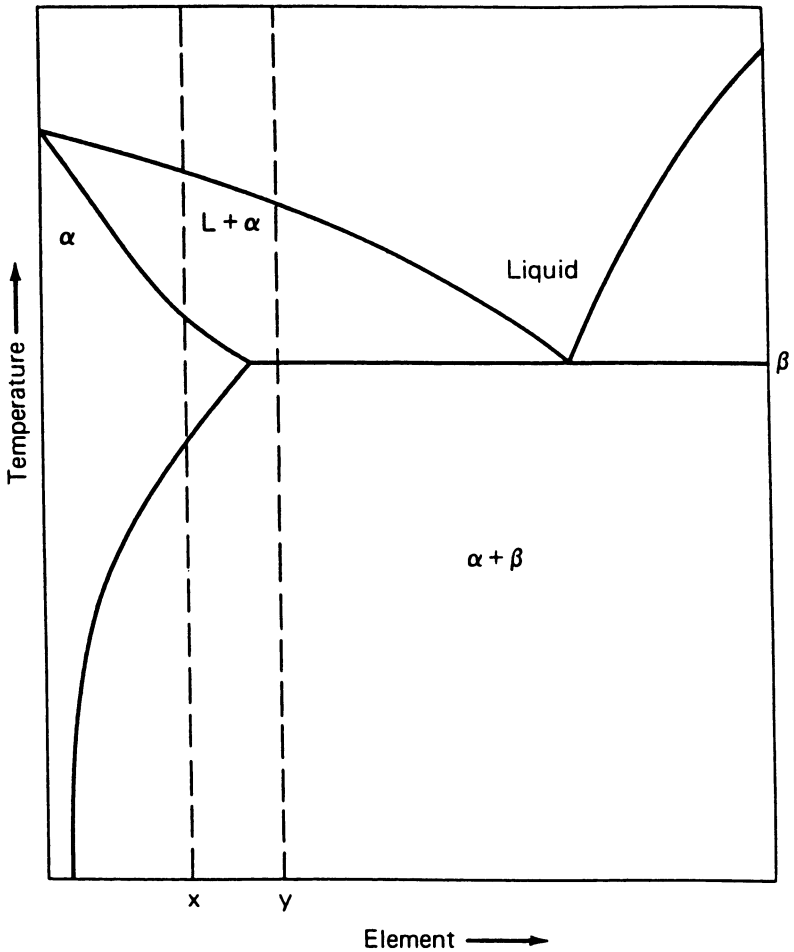
Generally, where two or more phases form after solidification, and at least one is soluble in the matrix, then the aim of the homogenization treatment is first to dissolve the non-equilibrium second phases followed by equalization of the residual concentration gradients. Al alloys containing Mg, Cu, Zn and Si in particular form non-equilibrium phases which require dissolution prior to concentration homogenization.

We have seen above that there are a number of solutions based on simplifying assumptions which can give reasonable estimates of homogenization practices. The equations above may also be solved numerically [118] and take into account the temperature and chemical dependence of  $D$  and describe the alloying element distribution in the cast structure.

For a given alloy system, if the constitution diagram and the solid state diffusion coefficients are known, along with the relationship of secondary dendrite arm spacing to time, it is possible to calculate the end temperature of solidification, concentration distribution in the secondary spacing during solidification and homogenization, and the quantity of non-equilibrium second phase at the end of solidification and during homogenization. This procedure will allow the simultaneous consideration of continuous heating, dissolution kinetics and concentration equalisation.

Figure 3.11 illustrates some of the restrictions that must apply to ingot pre-heating because of the phase diagram. The same principles apply to more complex systems, but the details differ because different phases have different solvus temperatures and the eutectic may be a trough instead of a point.

Different compositions on the diagram represent different types of commercial alloys. Alloy X represents an alloy in which the alloy content does not exceed the maximum solubility. This is typified by relatively dilute alloys such as 2117, 6063 and 7029, but it is also true of alloys 7075 and 6061. cursory examination of the phase diagram indicates that the ingot preheating range can be located anywhere between the solvus and solidus temperatures. However, to avoid the possibility of non-equilibrium melting, as explained below, either the upper limit should be below the eutectic temperature or the time below the eutectic temperature should be of sufficient duration to produce complete solution of the elements comprising the eutectic. Alloy Y represents an alloy in which an excess of soluble phase always remains undissolved. The upper end of the preheat temperature range must lie below the equilibrium eutectic temperature if melting is to be avoided. This case is typified by alloys 2219, 2011 and 7178. Alloys such as 2024 may respond like either alloy X or alloy Y, depending on the amounts and proportions of the alloying and impurity elements.



**Fig. 3.11** Schematic phase diagram. Alloy X melts at the eutectic temperature if B is not dissolved below this temperature. Alloy Y always melts at the eutectic temperature.

Incipient melting, or the beginnings of liquid phase formation, can occur under either equilibrium or non-equilibrium conditions. Alloy Y in Fig. 3.11 obviously produces melting whenever its temperature is at or above the eutectic temperature. However, it is not as obvious that the same reaction occurs for alloy X, which has a higher equilibrium solidus temperature than alloy Y. When alloy X is in the as-cast condition, it contains a non-equilibrium eutectic structure. If reheating to the eutectic temperature is done at a rapid enough rate so that the soluble intermetallic cannot dissolve, the eutectic melts. Holding alloys like alloy X for sufficient time between the eutectic temperature and the true solidus causes the liquid phase to disappear as the soluble element passes into solution. The solution of the elements in the liquid

phase leaves evidence in the form of microporosity at the previous sites of eutectic if the hydrogen content is above some critical level. The size of the micropores is smaller than the shrinkage porosity in good quality as-cast ingot. The principles expounded above apply to non-heat-treatable alloys as well as to heat treatable ones.

The real test of the harmfulness of overheating is whether there is microstructural damage of a type that cannot subsequently be repaired. Damage consists of excessive void formation, segregation, blistering, cracking or severe external oxidation. Rosettes, the spherical structural features that occur when eutectic liquid solidifies during cooling after overheating, are very hard and persistent. They have been detected in thin sheet fabricated from thick, overheated ingot, despite extensive thermomechanical treatments used during the fabrication.

### *Loss of supersaturation*

The low solubility elements in aluminium alloys become supersaturated in the aluminium matrix if (i) the nominal concentration of the supersaturating element is higher than its equilibrium concentration and (ii) the freezing rate is sufficiently high. Although electron probe point analysis can give an indication of the type and extent of the dissolved species, a more accurate measure of the matrix supersaturation is the electrical resistivity.

Among the alloy systems which have been examined carefully by this technique are Al–Mn [119], Al–Fe [120], Al–Mn–Fe [121], Al–Mn–Cu [122], Al–Mn–Si [123], Al–Mn–Fe–Si [124], 3003 [125], 3004 [126] and Al–Sc [127]. Mn, Fe and Sc are the supersaturating species, and the degree of as-cast supersaturation increases as the freezing rate increases.

The equilibrium solubility of a dissolving element is determined by the alloy composition as well as by its mechanical history and state. For example, the solid solubility of Mn in Al is reduced by Fe, Si, Mg and Cu. A complex alloy such as 3003 or 3004 has a lower equilibrium Mn solubility than an Al–Mn binary alloy. In the deformed condition, the equilibrium solubility decreases significantly, especially in extrusion where the high strains assist precipitation during the process, shifting the alloy to a greater state of metastability.

The extrusion of 3003 (1% Mn, 0.38% Fe, 0.14% Si) reduces the dissolved Mn throughout the process.

It has been proven that in the as-cast state about 94% of total Mn is present in solid solution. At 0.38% Fe and 0.14% Si, the equilibrium solubility, however, is significantly less than 0.94% Mn. The degree of supersaturation at 610°C is about 0.30% Mn and at room temperature about 0.55% Mn. Extrusion further reduces the equilibrium Mn concentration to about 0.15%. If not subjected to the homogenization and exposure, the extrude would be in a highly unstable condition with about 0.56% Mn in the supersaturated state.

To illustrate the effect of alternate elements on diffusion the work of Nagahama and Miki [120] considered the loss of iron supersaturation in an Al–0.043% Fe and Al–0.043% Fe–0.056% Si alloys after deformation and thermal

exposure. The loss of supersaturation increased with silicon addition, temperature and degree of cold reduction; the loss is particularly rapid during the early stages, concurrent with recrystallisation of the deformed matrix.

The effect of 0.06% Fe and 0.20% Cu on the loss of Mn supersaturation in Al–1%Mn alloy at 550°C was investigated by Theler and Furrer [121]. The impact of Fe on the Mn loss was found to be especially pronounced. An examination of the effect of iron contents between 0.0005 and 0.57% on the loss of Mn supersaturation at 530 and 550°C revealed that as little as 0.02% Fe was sufficient to stimulate high loss of Mn supersaturation. In the absence of Fe or Cu, up to 0.2% Si had a significant effect on the loss of Mn supersaturation but the Si effect was eliminated when both Fe and Si were present.

### *Precipitation*

With the loss of supersaturation during thermal exposure, the phase components are precipitated as globules, needles and platelets throughout the bulk of the dendrites. Usually, these dispersoids are not uniformly distributed but reflect the pre-existing dendritic microsegregation. Fine dispersoids, up to 0.2  $\mu\text{m}$ , are first precipitated in the peripheral areas and then in the bulk of the cells. In general, the dispersoid size increases towards the cell centre as cell size increases, concentration of precipitating component decreases, and cooling rate after thermal exposure decreases. The dispersoids are absent or sparse in that portion of the matrix which is formed by a eutectic reaction.

Let us again take as an example the Al–Fe alloys (representing the dilute 1XXX system). The concentration of Fe lies far above the limit of maximum solubility of Fe in Al and almost all of the Fe content is present in the as-cast intermetallics [120]. In the Al–Mn alloys, on the other hand, Mn partitions preferentially into the Al matrix and even becomes supersaturated. Hence in the Al–Mn–Fe alloy, because of the greater tendency of Fe atoms to segregate, the intermetallics formed during solidification contain more Fe than Mn [128]. The presence of Fe in the Al–Mn alloys affects the diffusion kinetics of Mn atoms and the free enthalpy of the Mn-containing phases. In effect, the Mn atoms diffuse more rapidly and the substitution of Mn by Fe atoms in the  $\text{Al}_6\text{Mn}$  phase reduces enthalpy of the  $\text{Al}_6(\text{Mn,Fe})$  phase.

Even a very small addition of Fe to the Al–Mn alloy greatly facilitates the Mn precipitation and prevents the formation of the metastable phases encountered in the Al–Mn alloys. No ternary precipitation phase appears, but Mn atoms are substituted in  $\text{Al}_6\text{Mn}$  by Fe atoms. During homogenization, Mn enters  $\text{Al}_6(\text{Mn,Fe})$  until the phase has achieved its maximum stability at  $\text{Al}_6(\text{Mn}_{0.5}, \text{Fe}_{0.5})$ .

During the early stages of thermal exposure, a high degree of precipitation is attained by the growth of existing Al(Mn,Fe) particles. In the regions where the  $\text{Al}_6(\text{Mn,Fe})$  particles are absent or are not favourably oriented, secondary particles are precipitated. The secondary precipitates are much finer (0.1–0.3  $\mu\text{m}$ ), are predominantly plate-like and contain little Fe. Further precipitation continues



during cooling and holding at lower temperatures, and corresponds to the receding solubility of Mn and Fe with decreasing temperature.

In more complex 1XXX, 3XXX and 5XXX series aluminium alloys, the precipitation effects are similar. Si enhances precipitation of Fe; Fe, Cu, Mg and Si enhance the precipitation of Mn; Fe, Si and Cr enter the  $Al_6Mn$  phase during thermal exposure; Mg, Si, Cr are present in the secondary precipitates. Cr may form  $AlCrMg$ , Si may form  $AlMnSi$  and Zr may form  $ZrAl_3$  or coherent metastable phases. Existing non-equilibrium phases may dissolve or transform to more stable phases; for example, the transformation of  $FeAl_3$  to  $AlFeSi$  or  $Al(Fe,Mn)Si$ .

### *Precipitate dissolution*

Precipitate dissolution takes place in three circumstances:

1. non-equilibrium phases generated near the dendrite cell boundaries during solidification dissolve upon thermal exposure before constitutional equalization can proceed;
2. fine precipitates in the immediate vicinity of a large primary particulate dissolve and redeposit on the particulate as a part of the coarsening process during thermal exposure;
3. fine precipitates formed at lower temperatures during cooling from the casting or from the homogenization temperature revert back to solid solution when the casting is reheated for homogenization or is preheated prior to hot rolling or extrusion.

The time for precipitate dissolution at a given temperature increases as the precipitate size or the precipitate volume fraction increases or as the diffusion rate of precipitate components decreases. With the decreasing freezing rate and increasing casting size, the time to complete solution at a given temperature increases because of the larger primary precipitate size. Rapid cooling of the casting after freezing or after homogenization generates finer secondary precipitates and facilitates dissolution during subsequent reheating and thermal exposure.

Dissolution kinetics may be characterized by differential scanning calorimetry (DSC) and quantitative metallography. The as-cast microstructure is shown to relate to the solvus temperature and the as-cast DSC measurements to relate to the chemistry and the casting conditions, thus correlating DSC measurements directly with the solvus temperature. By using DSC to follow the microstructural changes during preheating, as shown, for example by Lalli and Dauer [129] for 6XXX alloys, it is possible to monitor the dissolution kinetics. They showed that growth of  $Mg_2Si$  occurs during heat-up before the dissolution commences. In fact the morphology of the phase changes from  $\beta$  to  $\beta'$  to  $\beta''$  during this stage and the heat-up to extrusion temperature may therefore adopt a critical role. The DSC scan also gives the relevant information on the lowest melting point of the alloy. We shall return to this point later when considering more complex industrial alloys.

### *Particle coarsening*

During second-phase coarsening the number of phase particles, per unit volume of the system decreases with exposure time at the elevated temperatures, adopting a more compact morphology and larger size of the second phase. The interdendritic stringers undergo destabilization and shape change, the discrete precipitates undergo Ostwald ripening, and the mobile dispersed hydrogen and low melting phases undergo coalescence [130]. Diffusion rate, solubility and interface energy control the coarsening process, which would be aided by any prior or concurrent deformation, or by simultaneous recrystallization, during thermal exposure [131]. The stable phases containing Si, Cu, Mg and Ni (high diffusion rate and/or high solubility) coarsen rapidly whereas those containing Mn, Fe, Cr and Zr do so only at relatively high temperatures.

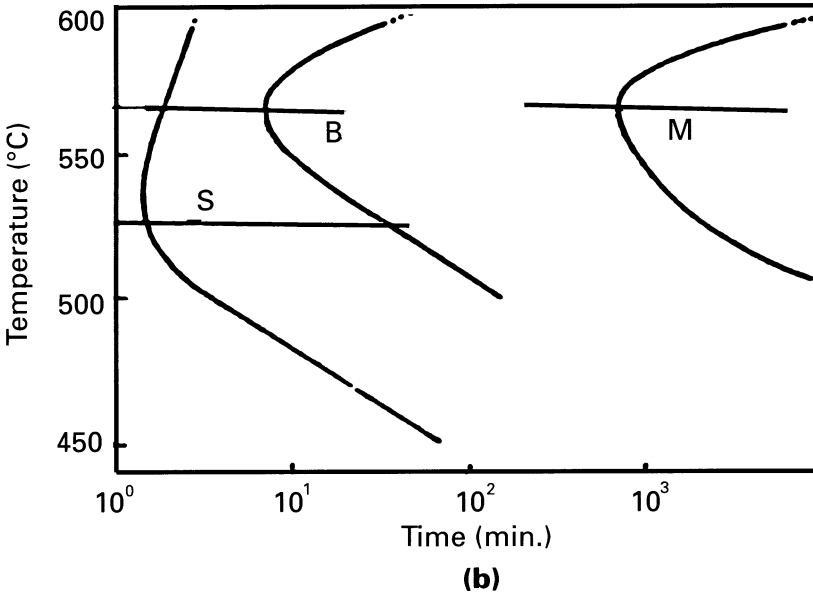
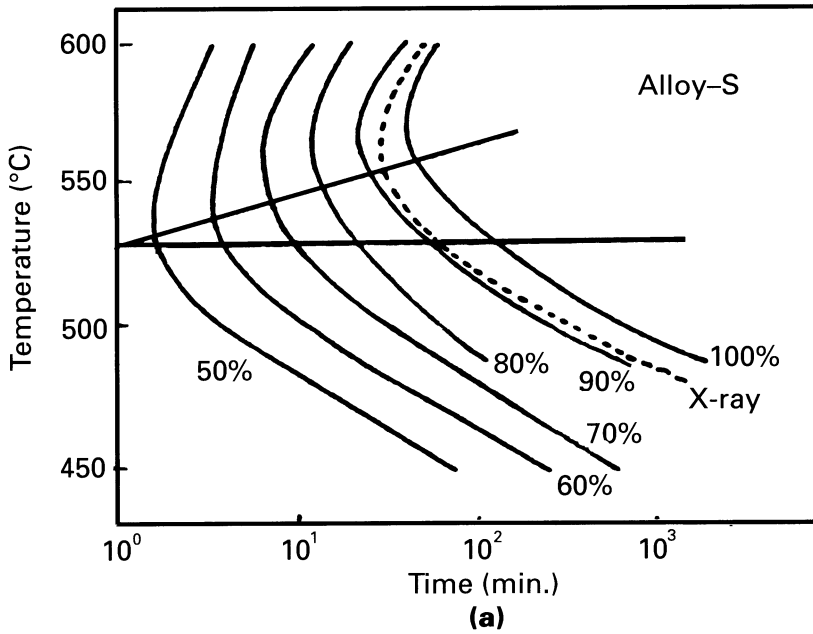
The freezing rate during casting has an important bearing on the achievable final particle size and hence can be expected to vary with billet size. As the freezing rate increases, the second phase volume fraction, the interdendritic stringer thickness and the eutectic phase lamella spacing decrease, and the degree of eutectic lamella branching increases. All these effects of increasing freezing rate contribute to a smaller homogenized particulate size. The addition of Fe to the Al–Mn alloys, likewise, increases the degree of branching of the eutectic phase and yields a larger number of smaller particulates.

An investigation of coarsening kinetics of the intermetallic phases  $\text{Al}_6\text{Mn}$  and  $\text{Al}_{20}\text{Cu}_2\text{Mn}_3$  indicated that the coarsening of  $\text{Al}_6\text{Mn}$  [134] in a solid matrix obeys the  $\bar{d} \approx t^{1/3}$  law, where  $\bar{d}$  is average particle size and  $t$  is the coarsening time, indicating lattice diffusion controlled coarsening. Similar kinetic observations have been made in 3004 [132] where the coarsening again occurs according to the  $\bar{d} \approx t^{1/3}$  law.

### *Phase changes*

Replacement of existing metastable phases by stable phases occurs during thermal exposure. The presence and proportion of metastable phases depends upon the alloy composition and upon the casting freezing rate. Examples of phase changes are  $\text{FeAl}_3 \rightarrow \alpha\text{AlFeSi} \rightarrow \alpha\text{Al}(\text{Fe},\text{Mn})\text{Si}$  in the 6XXX series [133,134],  $\text{Al}_6\text{Fe}$  (or  $\text{Al}_m\text{Fe}$ )  $\rightarrow \text{Al}_3\text{Fe}$  in the Al–Fe and Al–Fe–Mg alloys [135] and  $\text{Al}_6(\text{Fe},\text{Mn}) \rightarrow \sim \text{Al}_{12}(\text{Fe},\text{Mn})\text{Si}$  in the 3004 [136] base alloys. The equilibrium may permit several phases to coexist but a judicious heating and holding sequence should be utilized to arrive at the desired mix of phases.

X-ray diffraction and microscopy, have been used to investigate the transformation in the 3004 [136] type alloys. The as-cast structure in the standard 3004 alloy (1% Mg, 1% Mn, 0.45% Fe, 0.2% Si, 0.15% Cu) usually contains the  $\text{Al}_6(\text{Fe},\text{Mn})$  as well as the  $\alpha\text{-Al}-(\text{Fe},\text{Mn})\text{Si}$  phase. The major proportion of the  $\alpha$  phase is formed directly from the melt by the eutectic reaction, and the remainder by the peritectic reaction. Higher than normal Mg and lower than normal Si



**Fig. 3.12** TTT diagram for a transformation in 3004: (a) complete transformation for alloy S with excess Si (0.35%) and (b) 50% transformation C-curves for alloy B (basic 0.2% Si), alloy S, and alloy M (high 1.6% Mg) after Watanabe *et al.*

tend to suppress the formation of the  $\alpha$  phase in the casting. Conversely, low Mg and high Si tend to stimulate the formation of as-cast  $\alpha$  phase.

The  $\alpha$  transformation  $\text{Al}_6(\text{Fe,Mn}) \rightarrow \text{Al}_{12}(\text{Fe,Mn})\text{Si}$  occurs at high temperatures, initiating at the  $\text{Al}_6(\text{Fe,Mn})$ /matrix interface and growing toward the interior of the  $\text{Al}_6(\text{Fe,Mn})$  phase. The  $\alpha$  phase generates directly from the  $\text{Al}_6(\text{Fe,Mn})$  phase without passing through an intermediate phase. The diffusion of Mn and Si through the matrix must occur for the reaction to proceed, and the reaction is controlled by the diffusion of Mn. The  $\alpha$  transformation is accelerated when high Si is present and is suppressed in the presence of high Mg. In other words, if the Si is tied up as  $\text{Mg}_2\text{Si}$  due to high Mg or low Si or both, the activation energy for the  $\alpha$  reaction is higher and the reaction is controlled by the disassociation of  $\text{Mg}_2\text{Si}$ .

The effect of excess Mg is to shift the C-curve nose to longer time (Fig. 3.12), the  $\alpha$  transformation in this case is slow and a complete transformation would require an unduly long thermal exposure. Excess Si is a more effective means of ensuring a high proportion of  $\alpha$  phase in the 3004 alloy. The  $\alpha$ - $\text{Al}_{12}(\text{Fe,Mn})\text{Si}$  has a significantly higher hardness [137,138] than the  $\text{Al}_6\text{Mn}$ ,  $\text{Al}_6(\text{Fe,Mn})$  and  $\alpha$ - $(\text{AlMnSi})$  phases, and thus offers a distinct advantage in wear related tribological applications.

We should also note in this section the differing morphologies associated with Zr additions. Zr precipitates out as the intermetallic phase  $\text{Al}_3\text{Zr}$  during the homogenization process. If precipitated at low temperatures  $\text{Al}_3\text{Zr}$  forms a metastable superlattice in the aluminium matrix whilst at higher temperatures this metastable phase transforms to the tetragonal  $\text{Al}_3\text{Zr}$  equilibrium phase and coarsens. In effect this means that the alloy must be heated slowly between 380 and 420°C during the homogenization cycle.  $\text{Al}_3\text{Zr}$  is then obtained as a fine, near sub-micron, precipitate and will act both as a dispersion hardener will decrease the subgrain size and inhibit recrystallization. If precipitated at high temperatures in the tetragonal form it has little effect on the alloy structure.

### 3.4 THERMAL ACTIVATION

The equilibrium ratio of vacancies to atoms at a given temperature  $T$  is:

$$\frac{n_v}{n_0} = \exp\left(\frac{-Q_f}{GT}\right) \quad (3.5)$$

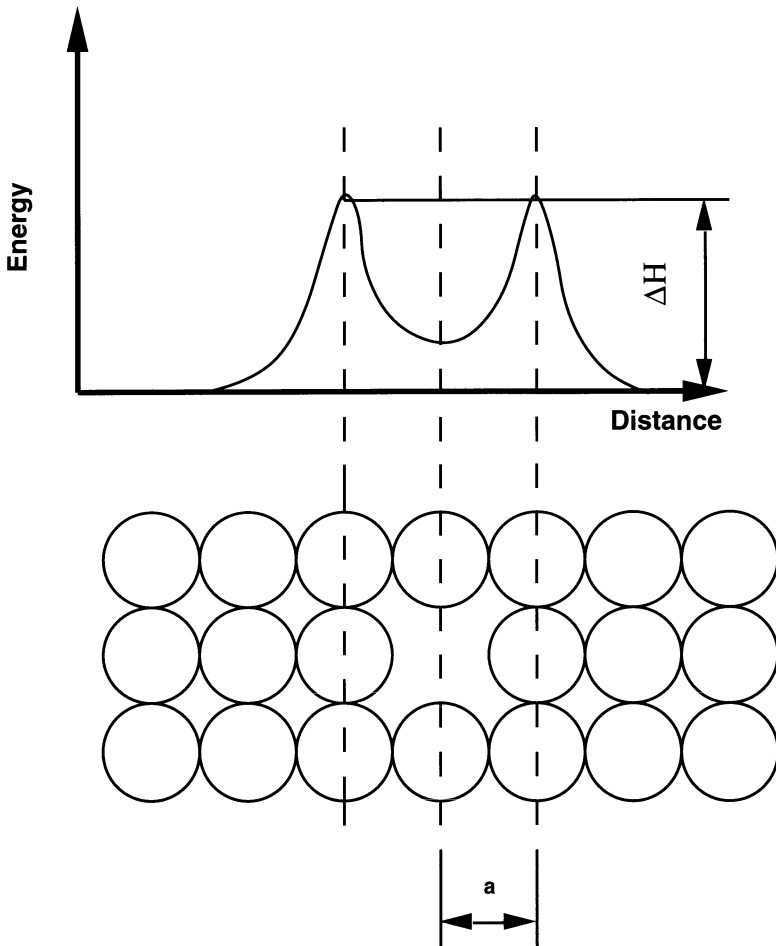
where  $n_v$  is the number of vacancies,  $n_0$  is the number of atoms,  $Q_f$  is the work required to form one mole of vacancies and  $G$  is the universal gas constant.

The time required to attain an equilibrium number of vacancies is important. Since the movement of vacancies is caused by successive jumps of atoms into vacancies then the fundamental law governing this jump is important. An energy barrier must be overcome whenever a jump is made, and the required energy is supplied by the thermal or heat vibrations of the individual crystal.

If  $q_0$  is the height of the energy barrier that an atom with spacing 'a', as in Fig. 3.13, must overcome in order to jump into a vacancy, then the jump can only occur if the atom possesses a vibration energy greater than  $q_0$ . Conversely, if the vibration energy is lower than  $q_0$ , the jump cannot occur. The chance that a given atom possesses an energy greater than  $q_0$  has been found to be proportional to the function  $\exp(-q_0/kT)$ , or:

$$p = j \exp\left(\frac{-q_0}{kT}\right) \quad (3.6)$$

where  $p$  is the probability that an atom possesses an energy equal to or greater than a given energy  $q_0$ ,  $j$  is a constant,  $k$  is Boltzmann's constant and  $T$  is the absolute temperature.



**Fig. 3.13** Thermal activation schematic of energy barriers and jumps (schematic).

The above equation was originally derived for the energy distribution of atoms in a perfect gas (Maxwell–Boltzmann distribution). However, this same function has also been found to predict quite accurately the vibration energy distribution of the atoms in a crystalline solid.

Since the above function is the probability that a given atom has an energy greater than that required for a jump, the probability of jumping must be proportional to this function. Therefore, we can write:

$$r_v = A \exp\left(\frac{-q_0}{kT}\right)$$

where  $r_v$  is the number of atom jumps per second into a vacancy,  $A$  is a constant,  $q_0$  is the activation energy per atom (height of the energy barrier), and  $k$  and  $T$  have the usual significance. If the numerator and denominator of the exponent in the above equation are both multiplied by  $N$ , Avogadro's number  $6.02 \times 10^{23}$ , we have:

$$r_v = A \exp\left(\frac{-Q_m}{GT}\right) \quad (3.7)$$

where  $Q_m$  is the activation energy for the movement of vacancies in calories per mole, and  $G$  the gas constant ( $8.314 \text{ J mol}^{-1} \text{ }^\circ\text{C}^{-1}$ ).

The constant  $A$  in the above equation depends on a number of factors. Among these is the number of atoms bordering the hole. The larger the number of atoms able to jump, the greater the frequency of jumping. A second factor is the vibration frequency of the atoms. The higher the rate of vibration, the more times per second an atom approaches the hole, and the greater is its chance of making a jump.

Let us consider the above equation with respect to the temperature of a metal. Consider the difference between room temperature and a typical forming temperature of  $500^\circ\text{C}$ . then the ratio of jumps is:

$$\frac{r_{v773}}{r_{v303}} = \frac{A \exp\left(\frac{-Q_m}{G \times 773}\right)}{A \exp\left(\frac{-Q_m}{G \times 303}\right)} \cong 5.2 \times 10^{15}$$

The tremendous difference in the rate with which vacancies move at deformation temperatures, compared with their rate at room temperature, is quite apparent.

In one second at  $500^\circ\text{C}$  the vacancy moves approximately 20 billion times, while at room temperature a time interval of about  $10^6$  s, or 11 days, occurs between jumps. This explains why metals deform more easily at elevated temperatures.

Extrusion is a deformation process in which atomic planes slip over each other (assisted by dislocations) and in which atomic bonds are individually broken and new bonds formed. Plastic flow is the consequence of this action and the

macroscopically observed change is the summation of individual atomic events. The two most important features of plastic flow are incorporated in the concept of dislocations which provide high-energy atomic configurations in association with lowered energy barriers and vacancies into which material may move. Plastic flow may thus be regarded as a mass-transfer problem. Interstitial diffusion and vacancy diffusion are also controlled by thermally activated bond-breaking processes and the combination of the point-line defect deformation system illustrates the complex kinetics controlling plastic deformation. Of the various mechanisms by which dislocations may move (cross-slip, climb, glide etc.), more than one may be operative at any one time. Where the operative mechanisms are dependent upon one another, the one that is slowest and requires the highest activation energy will govern the deformation and is rate controlling. In the high stacking fault energy (SFE) materials (such as Al-alloys), climb aided by cross-slip has been established as the rate-controlling mechanism, the explanation being that in these materials vacancies exist in large numbers at high temperatures and they diffuse to dislocations, causing them to climb. Hence, in these materials the activation energy will be more or less equal to that for self-diffusion depending upon the influence of cross-slip.

### 3.5 RECOVERY AND RECRYSTALLIZATION

The recovery and recrystallization of deformed structures is an integral part of the thermomechanical process. This annealing process may occur wholly or partially after the extrusion process and continue during a prolonged solution soak. The softening may be utilized simply to facilitate further processing such as drawing or forming of the engineering component after the extrusion operation, or may be undesirable because the properties of the 'press effect' are a necessary specification of the final product. In some of the stronger heat-treatable alloys an unrecrystallized structure may be specified because of damage tolerance, fatigue crack propagation or corrosion requirements. Clearly, a process which may affect all of these properties in the final component must be regarded as technologically important.

Although some softening can occur by static recovery events, complete softening can be achieved only by replacing the deformed structure with new strain-free recrystallized grains. Most of the existing literature concerns itself with the mechanism of nucleation and growth of such grains, usually from a cold deformed structure, and provides little or no quantitative data which could relate the softening processes to the conditions of deformation. Furthermore, it is, in general, model systems which have been analysed, utilizing pure metals or simple binary alloys to provide experimental data; results concerning commercial alloys have, in general, not been reported. However, some parametric studies, mostly concerning rolling of ferrous alloys, have been published [139–144] which indicate the important role of the deformation variables on the softening process.

In the previous work, direct metallographic techniques indicated that the recrystallization kinetics were dependent upon the total strain, the strain rate and temperature of deformation (a measure of the stored deformation energy), and the annealing temperature (the thermal energy supplied to assist the motion of high-angle boundaries) [139–144]. It has also been widely reported that nucleation occurs preferentially at grain boundaries [145–148], and hence it would be reasonable to expect that the initial grain size might influence the recrystallization kinetics (this is likely to be a much weaker effect in the extrusion process because of the large single deformation step). Further analysis of reference [139] reveals that the range of stress investigated has been limited and, in general, has not approached the strains encountered in industrial practice, primarily owing to the mode of deformation utilized in the experimental trials. Hence, the effect of hot strain does not appear to have been adequately established.

### 3.5.1 Dynamic recovery and dynamic recrystallization

Although recrystallization and recovery are normally considered to be static processes which occur in the absence of strain during annealing following cold working, the processes also take place during the application of stress and strain at high temperatures (i.e. under conditions obtained during the extrusion process). The events are then quite different from static recovery and recrystallization, and are termed dynamic recovery and dynamic recrystallization. These softening processes during deformation not only ensure the absence of work-hardening during extrusion but also influence the properties obtainable in the extrudate.

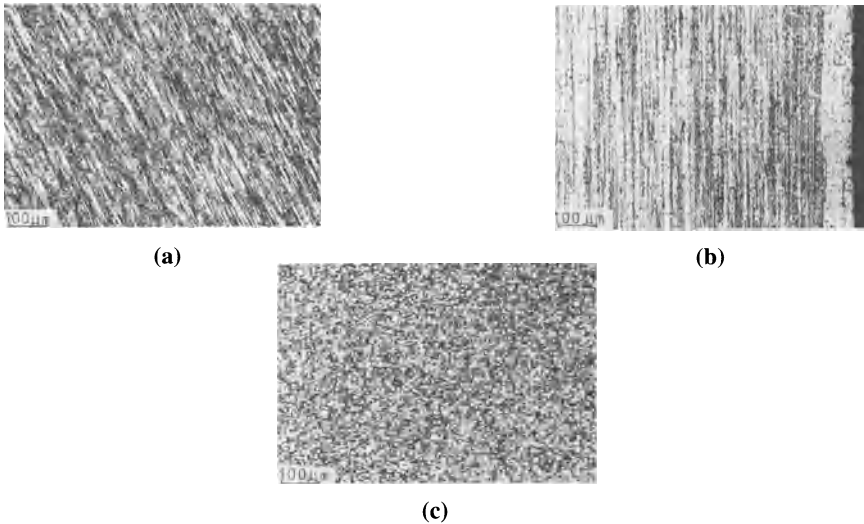
When dislocations exist or are generated, they can be either positive or negative in sign; unlike dislocations attract each other, and if they intersect, are mutually annihilated. On the other hand, like dislocations have stress fields which repel each other. In high SFE materials, dislocation movement is relatively easy and cross-slip and climb allow the intersecting like dislocations to move away from each other to a configuration of minimum energy. Hence, dislocations tend to arrange themselves in walls which are roughly equispaced, so forming subgrains. The subgrain size in high SFE materials is an important structural feature which determines not only the as-extruded conditions, but also the material reaction to subsequent processing. Since these features are related to the applied stress it is apparent that they may be controlled by suitable adjustment to the strain rate (speed) and the temperature.

After dynamic recovery in the quasi-static zone during extrusion there is generally a small amount of static recovery in the extrudate, which is governed by the process parameters (see below) and which can be followed by recrystallization. Recrystallization is, however, relatively slow and can be prevented by adjustment of the press processing and cooling conditions.



### 3.5.2 Microstructure

In Al materials which deform by dynamic recovery, the microstructure most usually appears 'fibrous' as shown in Fig. 3.14(a). The structure consists of the original cast grains elongated into the extrusion direction and having an aspect ratio roughly equal to the extrusion ratio. The fibrous effect is due to the high angles existing between the string-like grains. Although static recovery may have occurred after extrusion, static recrystallization has not. This is the structure which ideally should be produced, and the speed and temperature of extrusion should be controlled such that the fibrous structure is both obtained and stable. Incorrect extrusion conditions may lead to gross heterogeneity in the product in which the surface layer recrystallizes to produce large recrystallized grains, giving a product having very poor fracture toughness and corrosion properties. Such a structure is shown in Fig. 3.14(b). It is also possible to produce structures which completely recrystallize after extrusion, as shown in Fig. 3.14(c), where the structure consists of fine recrystallized grains. The least desirable structure is clearly that shown in Fig. 3.14(b), and in most aluminium and related alloys it is possible to produce the structure shown in Fig. 3.14(a). In heat-treatable alloys, however, not only must such a structure be produced, but it is also necessary to ensure that the substructure is sufficiently homogeneous and of low energy configuration such that gross heterogeneity is not produced after heat treatment. Ideally, the reaction of the substructure to solution soaking should be subgrain coalescence without recrystallization, but if static recrystallisation is to occur then the extrusion conditions must be controlled to ensure a uniform small recrystallized grain size.



**Fig. 3.14** Extrusion structure 7075 alloy; (a) fibrous; (b) coarse outer grain; (c) recrystallized.

### 3.6 RECRYSTALLIZATION AND LAYER THICKNESS AFTER SOLUTION SOAKING

Recrystallization kinetics are usually found to be represented quite well by the Avrami [149–151] equation:

$$X_v = 1 - \exp(-A t^n) \quad (3.8)$$

where  $X_v$  = volume fraction recrystallized,  $A$  represents nucleation and growth kinetics,  $t$  is the time to recrystallize fraction  $X_v$  and  $n$  is associated with the geometry of the growth sites activated.

In an attempt to write a more general rate law describing recrystallization Cahn [149], after analysing differing grain boundary nucleated reactions suggested that a more appropriate form of equation 3.8 could be written:

$$X_v = 1 - \exp\left[-A' \left(\frac{t}{t_f}\right)^n\right] \quad (3.9)$$

where  $t_f$  is the time to recrystallize the fixed volume fraction  $f$ ,  $t$  is the annealing time and the constant  $A'$  takes the form:  $A' = -\ln(1-f)$ .

It has been a common experimental feature that the fraction  $f$  is given the value 0.5; hence  $A'$  assumes the value 0.693.

The exponent  $n$  has taken only integral values depending on the recrystallization mode; thus Christian [152] has reported values of  $n$  from 0.5 where there is a saturation of nucleation sites at grain corners to 2.5 where random nucleation occurs.

The exponential forms of equations 3.8 and 3.9 result from the concept of extended volumes, where in the later stages of growth, the recrystallized grains impinge upon each other. Equation 3.8 can be differentiated and converted into the form of a rate equation by making the substitution  $\Psi = \ln[1/(1-X_v)]$  whence:

$$\frac{d\Psi}{dt} = n \left\{ \frac{A'}{\Psi} \right\}^{\frac{1}{n}} \quad (3.10)$$

$\Psi$  may be considered a state variable since it directly relates to the volume fraction of recrystallized grains. Thus equation 3.10 is in a form consistent with a state variable concept and may be integrated in time for arbitrary temperature–time histories. Such integration would assume path independence which would have to be tested by careful experimentation. We now wish to show that the rate equation depends on the same state variable  $s$  as does the flow stress. Recrystallization studies after hot working aluminium alloys have shown that the parameter  $A$  (usually defined as  $t_{0.5}$  in accordance with Cahn's interpretation) is related to several variables: initial grain size  $d_0$ , total strain  $\bar{\epsilon}$ , the strain rate  $\dot{\bar{\epsilon}}$ , temperature of deformation  $T_{\text{def}}$ , the annealing temperature  $T_{\text{ann}}$ , and the activation energy for recrystallisation  $\Delta H_{\text{rec}}$ . Based on empirical data, Raghunathan *et al.* [153] have shown that:

$$\begin{aligned} \text{For 5056: } t_{0.5} &= 2.31 \times 10^{-10} d_0^{1.58} \bar{\epsilon}^{-1.9} Z^{-0.35} \exp(212000/RT_{\text{ann}}) \\ \text{For 5083: } t_{0.5} &= 4.5 \times 10^{-10} d_0^{2.45} \bar{\epsilon}^{-1.97} Z^{-0.58} \exp(183000/RT_{\text{ann}}) \end{aligned}$$

where  $Z = \exp(\Delta H/GT_{\text{def}})$ .

Strictly speaking, the  $Z$  term must be non-dimensionalized by the introduction of a  $Z_0$  term or by using the value of  $A$  in the steady state constitutive equation:

$$Z = A (\sinh \alpha \sigma)^n$$

Thus, small initial grain sizes, high strains, high  $Z$ s and high annealing temperatures all decrease  $t_{0.5}$  and hence increase the kinetics. The constants in the equations are not dissimilar and it would appear to be possible, given sufficient data, to fix some values, at least for specific alloy systems. Sellars [154] has given similar data for a Al-1%Mg alloy but surprisingly the results contain  $d_0^{-4}$ , and  $\bar{\epsilon}^{-5.4}$  which are contrary to the above results and affect the kinetics in a manner which would not be expected.

However, for several reasons, these forms of equation are not fundamental nor consistent with the concept of internal state variables that evolve with time and are associated with microstructure as, for example, described by Ness *et al.* [155]. The strain term cannot be utilized as a state variable in constitutive theories of deformation, since the flow stress and structure cannot be uniquely defined by strain, strain rate and temperature. It is also not clear how to interpret the strain term which could represent grain boundary area, contribute to the stored energy, or relate to some other microstructural feature such as deformation bands or texture. The power exponents of the grain size and strain terms are, however, similar and it would thus appear that the grain boundary area per unit volume is actually the state variable being incorporated and affects recrystallization through enhanced nucleation. The theory proposed by Ness *et al.* [155] involves the dubious identification of several varying nucleation sites and, in effect, alloy dependent parameters as does the pseudo-internal variable equation 3.8. Moreover the expressions for  $t_{0.5}$  lead us to the conclusion that the internal variable involved in this definition is, in effect, the dislocation density  $\rho$  and hence the equation involves only the extended volume and the dislocation density. All the previous work has also considered only the rolling situation which with several interpasses is considerably more complex and differs in some important detail to deformation in the extrusion process. It is thus sensible to consider equation 3.8 in its more normal form:

$$\ln \ln \left( \frac{1}{1 - X_v} \right) = \ln B + \ln t_x \quad (3.11)$$

which when introducing the concept writing  $t_f$  as a temperature compensated time as described above yields:

$$\ln \ln \left( \frac{1}{1 - X_v} \right) = -\Omega_1 + n \ln(t) + \Omega_2 \ln(d_0) + \Omega_3 \ln(\bar{\epsilon}) + \Omega_4 \ln(Z) - n \left( \frac{\Delta H}{GT} \right) \quad (3.12a)$$

The values of the constants  $\Omega_r$ ,  $n$  and  $\Delta H$  can quite readily be determined by a suitable multiregression technique when the experimental data is available.  $\Delta H$  is the activation energy for the combined nucleation and growth process. Clearly when considering the extrusion process a problem occurs because equation 3.8 and subsequent equations are based on the concept of temperature compensated time and the term  $t_{0.5}$  is introduced. Now in most extrusion processes the extrude is either quenched or the fraction recrystallized  $X_v$  controlled to be less than 50%. Hence equation 3.12 must be modified to deal with this situation. We will therefore assume that we can replace  $t_{0.5}$  by any other  $t$  and select the  $t$  which will just give zero recrystallisation  $t_0$ . Now both of the constants  $n$  and  $\Delta H$  are average values based on nucleation and growth whilst our revised time  $t_0$  will be short and although containing the same terms as  $t_{0.5}$  the values of  $n$  and  $\Delta H$  will be expected to be quite different values; in particular the activation energy will be more closely related to that required for nucleation. Moreover, in the practical extrusion process the original grain size is not a variable and the  $\Omega_2$  term may be incorporated into the  $\Omega_1$  term. We must also allow for the inhomogeneity of flow which, in the extrusion process, is related to the relative speed between the deformation zone and the dead metal zone which is clearly related to the strain rate  $\dot{\epsilon}$ . It has been shown [148] that a shape factor

$$\lambda^2 \left( \frac{\text{periphery of shape}}{\text{periphery of rod}} \right)_{R = \text{constant}}$$

must be applied to the extrusion ratio and to the temperature compensated strain rate; we might therefore expect an identical adjustment to the terms in the equation describing the recrystallization kinetics. During anneal following rolling it is a common observation that the annealing temperature has an independent influence depending on the deformation temperature and in unpublished work by the author a term  $(T_{\text{ann}} - T_{\text{def}})$  has been shown to greatly increase the correlation if included in the  $t_{0.5}$  equation; this is consistent with the grain boundary mobility term in classical physical metallurgy. In the extrusion process we can clearly only assume that  $T_{\text{def}}$  will be the relevant term in the F-temper and  $(T_s - T_{\text{def}})$  in the solution soaked or T6 condition. Incorporating these observations the resultant equations should therefore read:

$$\begin{aligned} \ln \ln \left( \frac{1}{1 - X_v} \right) &= -\Omega_1 + n \ln t + \Omega_2 \lambda^2 \dot{\epsilon} + \Omega_3 \ln \lambda^2 R + \Omega_4 \ln \lambda^2 \frac{Z}{A} - n \frac{\Delta H}{GT} \\ \ln \ln \left( \frac{1}{1 - X_v} \right) &= -\Omega_1 + \Omega_2 \lambda^2 \dot{\epsilon} + \Omega_3 \ln \lambda^2 R + \Omega_4 \ln \lambda^2 \frac{Z}{A} + \Omega_5 \cdot \langle (T_s) - T_d \rangle \end{aligned} \quad (3.12b)$$

where  $\dot{\epsilon}$  is the strain rate given by:

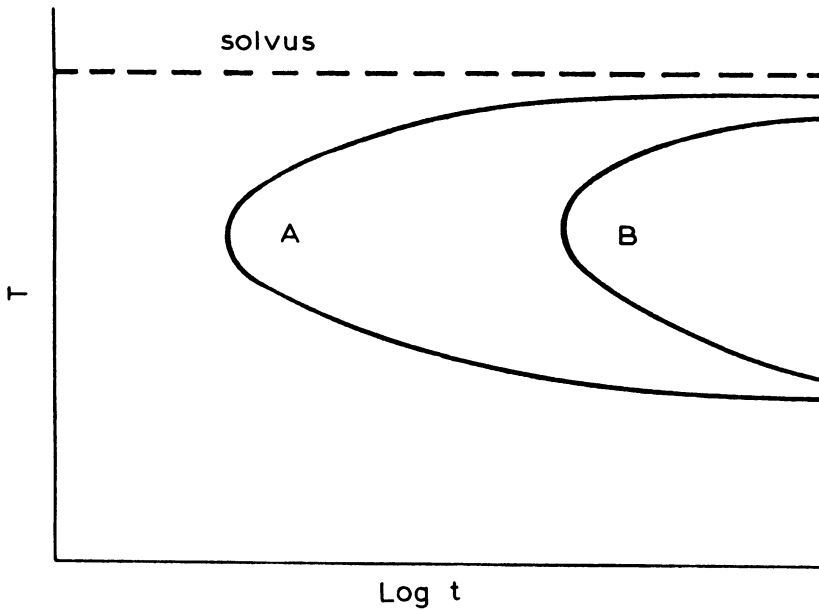
$$\dot{\epsilon} = \frac{6(0.171 + 1.86 \ln R) \tan [54.1 + 3.451] V_R}{D_B^3}$$

### 3.7 QUENCH SENSITIVITY

If a precipitation hardenable alloy is cooled from above the solvus temperature, the change in free energy increases as the difference between the temperature and the solvus increases. The change in free energy of the system with undercooling is the driving force for nucleation of a new phase. The nucleation rate  $\dot{N}$  as a function of temperature  $T$  can be expressed as:

$$\dot{N} = A_1 \exp\left[\frac{-\Delta H_m}{kT}\right] \exp\left[\frac{-\Delta H_n}{kT}\right] \quad (3.13)$$

where  $A_1$  is a rate constant.  $\Delta H_m$  is the activation energy for diffusion,  $\Delta H_n$  is the activation energy for nucleation, and  $k$  is Boltzmann's constant. Thus, the driving force for precipitation is the degree of supersaturation, which increases as the temperature decreases, but the process depends upon the diffusion of solute atoms to nucleation sites and the diffusion rate decreases with temperature. Therefore, the precipitation kinetics are described by the typical C curve which may be constructed for any convenient property (i.e. strength, toughness or hardness) and is illustrated in Fig. 3.15. It is commonly assumed that if the nose of this curve is encountered during slow cooling after deformation, heterogeneous nucleation occurs leading to large incoherent precipitates with attendant poor mechanical and corrosion properties.



**Fig. 3.15** Diagram of zero (A) and 100% (B) precipitation boundaries as a function of time  $t$  and temperature  $T$  (schematic).

In fact, the situation is more complex than this simple interpretation and is discussed below.

It is this quench sensitivity of aluminium alloys which dictates their suitability for press quenching. Time–temperature–property (TTP) curves have been presented by Marchive and Deschamps [156], Renouard [157], Fink and Willey [158], and Gulati *et al.* [37], for some aluminium alloys.

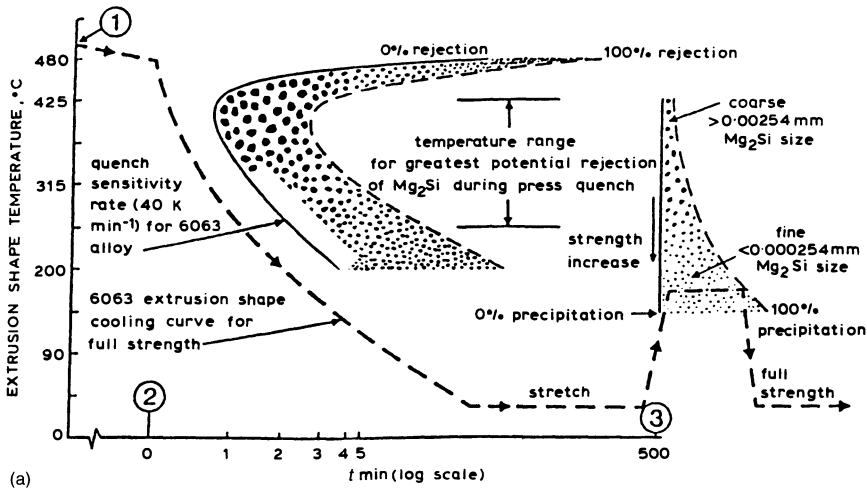
A schematic diagram of a press heat treatment cycle given by Lynch [159] but typical of many other publications is shown in Fig. 3.16.

It is erroneous because Cahn [160] has shown that reactions at different temperatures are additive whenever their transformation rates differ only by a time constant. For additive reactions Cahn showed that a measure of the amount transformed during continuous cooling is given by the integral:

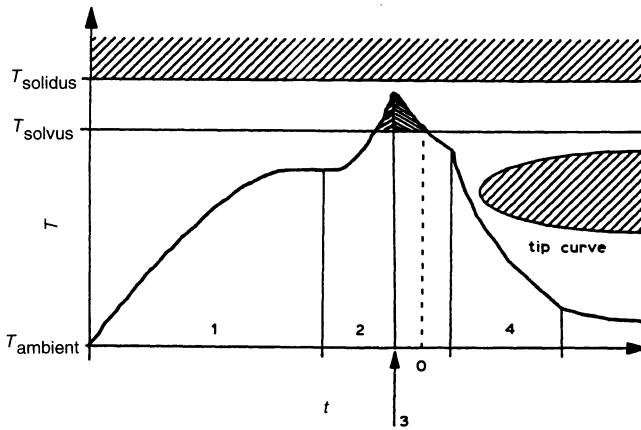
$$\tau = \int_{t_0}^{t_f} \frac{dt}{C_1} \quad (3.14)$$

where  $\tau$  is the amount transformed,  $t$  is the time from the cooling curve,  $t_0$  is the time at the start of quench,  $t_f$  is the time at the finish of quench, and  $C_1$  is the critical time from the time–temperature–transformation curve. When  $\tau = 1$ , then obviously the fraction transformed equals the fraction represented by the C curve.

A numerical technique to evaluate the value of  $\tau$  has been given by Evancho and Staley [161] which illustrates that it is not sufficient just to ensure that the cooling curve misses the nose of the C curve. It is important that the value of  $\tau$  should be kept sufficiently low to ensure that the ageing sequence following the quench can be satisfactorily performed. Nevertheless, Fig. 3.16 may be used to illustrate some of the metallurgical and equipment features required for successful press quenching.



(a)



(b)

**Fig. 3.16** Diagram of press heat treatment (schematic). (a) Press heat treatment cycle: (1) first stage, die exit temperature = 500°C; (2) second stage, start of intentional press quench (usually air quench); (3) third stage, start of intentional artificial ageing. (b) Temperature curve of metal (for one location on extrusion) from reheating to quenching: (1) reheating of billet; (2) extrusion; (3) exit from die; (4) quench.

## REFERENCES

1. Dix, E.H. and Richardson, H.H. (1926) *Trans. AIME*, **73**, 560.
2. Knock, J.A., Holt M. and Sprowls, D.O. (1961) *Metal Progress*, **80**(3), 87.
3. Wilm, A. (1911) *Metallurgie*, **8**, 225.
4. Mozely, P.P. (1943) *J. Aer. Sci.*, **10**(6), 180.
5. Dix, E.H. (1945) *Trans. AIME*, **35**, 130.
6. Horn, K.R. (1967) *Aluminium*, Vol. 1, A.S.M., Metals Park, Ohio.
7. Perrone, A. (1976) *Aluminio*, **45**, 512.
8. Mondolfo, L.F. (1976) *Aluminium Alloys*, Vol 1, Butterworth, London.
9. Ross, R.B. (1972) *Metallic Materials Specification Handbook*, Spon, London.
10. Hyatt, M.V. (1977) *Aluminio*, **46**(2), 81.
11. Thompson, D.S. (1975) *Met. Trans.*, **6A**, 671.
12. Westengen, H., *et al.* (1980) Proc. 1st Riso Intl. Symp. Met. and Mat. Sci, Riso Laboratories, Denmark.
13. Lancker, M.V. (1967) *Metallurgy of Aluminium Alloys*, Chapman & Hall, London.
14. Dix, E.H., Fink, W.L. and Willey, L.A. (1933) *Trans. AIME*, **104**(2), 335.
15. Hollinshead, P.A. (1986) Ph.D. Thesis, University of London.
16. Mondolfo, L.F. (1958) *Manganese in Aluminium Alloys*, Manganese Centre, London.
17. Sheppard, T., Flower, H.M. and Tutcher, M. (1979) *Mat. Sci. J.*, **6**, 473.
18. Sheppard, T., Parson, N.C. and Zaidi, M.A. (1983) *Met. Sci.*, **17**, 481–490.
19. Zaidi, M.A. (1980) Ph.D. Thesis, University of London.
20. Russell, K.C. and Aaronson, H.I. (1976) *Precipitation Process in Solids*, TMS-AISE, New York.
21. Hatch, J.E. (1984) *Properties and Physical Properties*, American Society for Metals, Warrendale, PA.
22. Mulherin, J.P. and Rosenthal, H. (1971) *Met. Trans.*, **2**, 427.
23. Humphreys, F.J. (1979) *Acta Metall.*, **27**, 1801.
24. Polmear, I.J. (1981) *Light Alloys*, Edward Arnold, London.
25. Theler, J.J. and Bichsel, H. (1967) *Metall.*, **21**, 195.
26. Sanders, T.H. (1981) *Metallography*, **14**, 177.
27. Marchand, G. (1958) *Trans. Am. Soc. Metals*, **50**, 612.
28. Zaidi, M.A. and Sheppard, T. (1984) *Met. Tech.*, **11**, 313.
29. Sheppard, T. and Paterson, S.J. (1982) *Met. Tech.*, **2**, 389.
30. Raghunathan, N. (1987) Ph.D. Thesis, University of London.
31. Reiso, O. (1984) Proc. 3rd International Extrusion Technology Seminar, Chicago, **1**, 31. Aluminum Association, Washington DC.
32. Walters, V.R. and Franz, E.C. (1984) Proc. 3rd International Extrusion Technology Seminar, Chicago, **1**, 75. Aluminum Association, Washington DC.
33. Evans, D.W. and Aucote, J. (1984) Proc. 3rd International Extrusion Technology Seminar, Chicago, **1**, 53. Aluminum Association, Washington DC.
34. Barry, W.G. and Harris, R.W. (1977) Proc. 2nd International Extrusion Technology Seminar, Atlanta, **1**, 271. Aluminum Association, Washington DC.
35. Annenkoff, A. and Marchive, D. (1984) Proc. 3rd International Extrusion Technology Seminar, Chicago, **1**, 69. Aluminum Association, Washington DC.
36. Lang, G. and Castle, A.F. (1978). *Met. Tech.*, **4**, 434.
37. Gulati, D.V., Crane, J. and Setzer, W.C. (1977) Proc. 2nd International Extrusion Technology Seminar, Atlanta, **1**, 9. Aluminum Association, Washington DC.
38. Traenkner, F.O. (1977) Proc. 2nd International Extrusion Technology Seminar, Atlanta, **1**, 339. Aluminum Association, Washington DC.



39. Langerweger, J. (1982) *Aluminium*, **58**(2), 107.
40. Langerweger, J. (1984) Proc. 3rd International Extrusion Technology Seminar, Chicago, **I**, 41.
41. Ashley, D.W.P., Jacobs, M.H. and Vietz, J.T. (1967) *Phil. Mag.*, **16**, 51.
42. Hains, R.W. (1984) Proc. 3rd International Extrusion Technology Seminar, Chicago, **I**, 81.
43. Baumgarten, J. (1984) Proc. 3rd International Extrusion Technology Seminar, Chicago, **I**, 45.
44. Hewitt, P. (1986) Ph.D. Thesis, University of London.
45. Bryant, A.J. (1971) *Z. Metallkd.*, **62**, 701.
46. Barry, W.G. and Hains, R.W. (1977) Proc. 2nd International Extrusion Technology Seminar, Atlanta, **I**, 271.
47. Lynch, C.V. (1971) *Z. Metallkd.*, **62**, 710.
48. Blade, J.C., Bryant, A.J. and Thomas, A.T. (1976) *Met. Tech.*, 380.
49. Barry, W.G. (1984) Proc. 3rd International Extrusion Technology Seminar, Chicago, **I**, 7.
50. Mondolfo, L.F. (1976) *Aluminium Alloys 1*, Butterworth, London.
51. Dunwoody, B.J., Moore, D.M. and Thomas, A.T. (1973) *J. Inst. Met.*, **101**, 172.
52. Beatty, E.C. (1969) Proc. 1st International Extrusion Technology Seminar, New Orleans, Paper No. 10. Aluminium Association, Washington DC.
53. Beatty, E.C. (1977) Proc. 2nd International Extrusion Technology Seminar, Atlanta, **I**, 225.
54. Bryant, A.J. (1969) *J. Inst. Met.*, **97**, 311.
55. Maitland, A. and Reid, A. (1977) Proc. 2nd International Extrusion Technology Seminar, Atlanta, **I**, 297.
56. Ohori, K., Takeuchi, Y. and Matsuyama, H. (1984) Proc. 3rd International Extrusion Technology Seminar, Chicago, **I**, 165.
57. Bichsel, H., Langerweger, J. and Reid, A. (1981) Proc. 7th International Light Metals Congress, Leoben-Vienna, 286. Aluminium Verlag, Dusseldorf.
58. Schwelling, P., Zoller, H. and Maitland, A. (1984) Proc. 3rd International Extrusion Technology Seminar, Chicago, **I**, 17.
59. Geisler, A.H. and Hill, J.K. (1948) *Acta. Cryst.*, **1**, 283.
60. Lutts, A. (1961) *Acta. Met.*, **9**, 577.
61. Lambot, H. (1950) *Rev. Met.*, **47**, 709.
62. Pashley, D.W., Rhodes, J. and Sendorek, A. (1966) *J. Inst. Met.*, **94**, 41.
63. Jacobs, M.H. (1972) *Phil. Mag.*, **26**, 1.
64. Kelly, A. and Nicholson, R.B. (1963) *Progress in Material Science*, Vol. 10, Pergamon, Oxford, 51.
65. Kelly, A. and Nicholson, R.B. (1963) *Progress in Material Science*, Vol. 10, Pergamon, Oxford, 3.
66. Schmalzried, H. and Gerold, W. (1958) *Z. Metallkd.*, **49**, 291.
67. Asano, K. and Hirano, K. (1968) *Trans. Japan Inst. Met.*, **9**, 24.
68. Shashkov, O.D. and Buinov, N.N. (1962) *Phys. Met. Metallogr.*, **14**(6), 43.
69. Harris, I.R. and Varley, P.C. (1953) *J. Inst. Met.*, **82**, 379.
70. Baba, Y. (1982) Ph.D. Thesis, Kyoto University.
71. Dowling, J.M. and Martin, J.W. (1973) Proc. 3rd International Conf. on the Strength of Metals and Alloys, Cambridge, 170, Cambridge University Press.
72. Fornerod, R.C. and Bichsel, H. (1973) *Aluminium*, **49**, 737.
73. Hatch, J.E. (ed.) (1984) *Aluminium: Properties and Physical Metallurgy*, American Society for Metals, Warrendale, PA.

74. Private communication, Alcan International Limited, Banbury, UK.
75. Gruhl, W. (1978) *Aluminium*, **54**, 323.
76. Hunsinker, H.Y., Staley, J.T. and Brown, R.H. (1972) *Met. Trans.*, **3**, 701.
77. Santner, J.S. (1978) *Metall. Trans.*, **9A**, 769.
78. Spiedel, M.O. and Hyatt, M.V. (1972) *Advances in Corrosion Science and Technology*, Vol.2, Plenum, New York, 115.
79. McAlister, A.J. (1982) *Bull. Alloy Phase Diagrams*, **3**, 177.
80. Silcock, J.M. (1959–60) *J. Inst. Met.*, **88**, 357.
81. Tamura, M., Mori, T. and Nakamura, T. (1970) *J. Japan Inst. Met.*, **34**, 919.
82. Yoshi-yama, T., Hasebe, K. and Mannami, M. (1968) *J. Phys. Soc. Japan*, **25**, 908.
83. Noble, B. and Thompson, G.E. (1971) *Mat. Sci. J.*, **5**, 114.
84. Costas, L.P. and Marshall, R.P. (1962) *Trans. Met. Soc. AIME*, **224**, 970.
85. Nozato, R. and Nakai, G. (1977) *Trans. Japan Inst. Met.*, **18**, 679.
86. Williams, D.B. and Edington, J.W. (1975) *Met. Sci.*, **9**, 529.
87. Ceresara, S., Cocco, G., Fagherazzi, G. and Schiffini, L. (1977) *Phil. Mag.*, **35**, 373.
88. Cocco, G., Fagherazzi, G. and Schiffini, L. (1977) *J. App. Cryst.*, **10**, 325.
89. Gayle, F.W. and Vandersande, J.B. (1986) *Aluminium-lithium Alloys III*, (ed. C. Baker, *et al.*), Institute of Metals, London, 376.
90. Gayle, F.W. and Vandersande, J.B. (1984) *Bull. Alloy Phase Diagrams*, **5**, 19.
91. Sigli, C. and Sanchez, J.M. (1986) *Acta Metall.*, **34**, 1021.
92. Papazian, J.M., Sigli, C. and Sanchez, J.M. (1986) *Scr. Metall.*, **20**, 201.
93. Balmuth, E.S. (1984) *Scr. Metall.*, **18**, 301.
94. Noble, B. and Thompson, G.E. (1972) *Mat. Sci. J.*, **6**, 167.
95. Baumann, S.F. and Williams, D.B. (1985) *Met. Trans.*, **16A**, 1203.
96. Jones, W.R.D. and Das, P.P. (1959–60) *J. Inst. Met.*, **88**, 435.
97. Levinson, D.W. and McPherson, D.J. (1956) *Trans. ASM*, **48**, 689.
98. Friedlander, I.N., Shamray, V.F. and Shiryayeva, N.V. (1965) *Izv. Akad. Nauk, SSSR, Metally*, **2**, 153.
99. Thompson, G.E. and Noble, B. (1973) *J. Inst. Met.*, **101**, 111.
100. Sanders, T.H. and Niskansen, P.W. (1981) *Res. Mech. Lett.*, **1**, 363.
101. Dinsdale, K., Harris, S.J. and Noble, B. (1981) in *Aluminium-lithium Alloys I*, (eds T.H. Sanders and E.A. Starke), The Metallurgical Society of AIME, Warrendale, PA, 101.
102. Baumann, S.F. and Williams, D.B. (1981) in Ref. 26, 17.
103. Friedlander, I.N., Ambertsumyan, S.M., Shiryayeva, N.V. and Gabidullin, R.M. (1968) *Met. Sci. Heat Treat. Met.*, **3**, 211.
104. Hardy, H.K. and Silcock, J.M. (1955–56) *J. Inst. Met.*, **84**, 423.
105. Tosten, M.H. and Howell, P.R. (1981) in Ref. 28, 727.
106. Huang, J.C. and Ardell, A.J. (1933) in Ref. 14, 329.
107. Gregson, P.J. (1983) Ph.D. Thesis, University of London.
108. Miller, W.S., Cornish, A.J., Titchener, A.O. and Bennett, D.A. (1981) in Ref. 26, 335.
109. Peel, C.J., Evans, B., Baker, C., Bennett, D.A., Gregson, P.J. and Flower, H.M. (1981) in Ref. 26, 363.
110. Kar, R.J., Bohlen, J.W. and Chanani, G.R. (1981) in Ref. 26, 255.
111. Sankaran, K.K. and Grant, N.J. (1980) *Mat. Sci. Eng.*, **44**, 213.
112. Strawbridge, D.J., Hume-Rothery, W. and Little, A.T. (1947–48) *J. Inst. Met.*, **74**, 191.
113. Sperry, P.R. (1956) *Trans. ASM*, **48**, 904.
114. Conserva, M., DiRusso, E., Giarda, A. and Waldman, J. (1973) *Metallography*, **6**, 367.
115. Fricke, W.G. (1988) Proc. International Conference on Homogenisation and

- Annealing of Aluminium and Copper Alloys, The Metallurgical Society, Warrendale, PA, 118.
116. Kamio, A., Tezuka, H., Choi, J., Fujii, M. and Takaheshi, T. (1985) *J. Japan. Soc. Light Met.*, **35**(6), 321.
117. Kamio, A., Tezuka, H., Choi, J. and Takaheshi, T. (1985) *J. Japan. Soc. Light Met.*, **35**(6), 255.
118. Waldman, J., Sulunski, H. and Markos, H. (1974) *Metall. Trans.*, **5**, 573.
119. Oelschlagel, D., Kawano, O. and Izumi, O. (1970) *J. Japan. Soc. Light Met.*, **20**(11), 531.
120. Nagahama, K. and Miki, I. (1970) *J. Japan. Soc. Light Met.*, **20**(3), 137.
121. Theler, J.J. and Furrer, P. (1974) *Aluminium*, **50**(7), 467.
122. Goel, D.B., Furrer, P. and Warlimont, H. (1974) *Aluminium*, **50**(8), 511.
123. Day, K.B. (1959) *Mem. Sci. Rev. Metall.*, **56**(2), 201.
124. Warlimont, H. (1977) *Aluminium*, **53**(3), 171.
125. Tilak, R.V. and Morris, J.G. (1985) *Mat. Sci. Eng.*, **73**, 139.
126. Elagin, V.I., Zakharov, V.V. and Rostova, T.D. (1983) *Met. Sci. Heat Tr.*, **25**(7/8), 546.
127. Lendvai, J., Honyek, G., Ungar, T., Kovacs, I. and Turmezey, T. (1986) *Aluminium*, **62**, 363.
128. Backerud, L. (1968) *Jerkont. Ann.*, **152**, 109.
129. Lalli, L.A. and Dauer, R.A. (1987) in *Aluminum Technology '86*, (ed. T. Sheppard), Institute of Metals, London.
130. McLean, M. (1978) *Met. Sci.*, **12**, 113.
131. Grishkovets, Y.G., Budaniva, L.V. and Morgacheva, D.A. (1983) *Met. Sci. Heat Tr.*, **25**(7/80), 604.
132. Skolianos, S., Rattamis, T.Z., Chung, Y.R. and Merchant, H.D. (1987) *Met. Trans A*, **18a**, 1179.
133. Ho, E. and Weatherly, G.C. (1977) *Met. Sci.*, **11**, 109.
134. Furrer, P. and Schwellingner, P. (1980) in Proc. Conf. Structure of Metals, Bad Neuheim, West Germany, 285. Springer-Verlag. Dusseldorf.
135. Kosuge, H. and Takada, H. (1979) *J. Japan. Inst. Light Met.*, **29**(2), 64.
136. Watanabe, H., Ohori, K. and Takeuchi, Y. (1983) *J. Japan. Soc. Light Metals*, **33**, 121.
137. Hanemann, H. and Schrader, A. (1952) *Teraere Legierungun des Aluminium Verlag Stahleisen*, NBH, Aluminium Verlag, Berlin.
138. Zogg, H., Timm, J. and Warlimont, H. (1979) *Aluminium*, **55**, 261.
139. Barraclough, D.R. and Sellars, C.M. (1979) *Met. Sci.*, **13**, 257.
140. Towle, D.J. and Gladman, T. (1979) *Met. Sci.*, **13**, 246.
141. Sellars, C.M. and Whiteman, J.A. (1979) *Met. Sci.*, **13**, 187.
142. Jonas, J.J., Sellars, C.M. and Tegart, W.M.McG. (1969) *Metall. Rev.*, **14**, 1.
143. Mcqueen, H.J. and Jonas, J.J. (1975) in *Plastic Deformation of Metals*, (ed. R.J. Arsenault), Academy Press, New York, 281.
144. Sellars, C.M. (1979) in *Hot Working and Hot Forming*, (ed. C. and W.J. Advise), The Metals Society, London, 3.
145. English, A.T. and Backofen, W.A. (1964) *Trans. AIME*, **230**, 369.
146. Speich, G.R. and Fisher, R.M. (1966) in *Recrystallisation, Grain Growth and Texture*, (ed. H. Margolin), The American Society for Metals, Metals Park, Ohio, 563.
147. Cahn, J.W. (1956) *Acta Metall.*, **4**, 449.
148. Sheppard, T. (1996) Proc. 6th International Al. Ext. Tech. Seminar, Chicago, May, **1**, 163–171.
149. Avrami, M. (1939) *J. Chem. Phys.*, **7**, 1103.
150. Avrami, M. (1940) *J. Chem. Phys.*, **8**, 8.

151. Avrami, M. (1941) *J. Chem. Phys.*, **9**, 117.
152. Christian, J.W. (1965) in *The Theory of Transformations in Metals and Alloys*, Pergamon, London, 710.
153. Raghunathan, N., Zaidi, M.A. and Sheppard, T. (1986) *Mat. Sci. Tech.*, **2**, 938.
154. Sellars, C.M. (1979) in *Hot Working and Hot Forming*, The Metals Society, London, 3.
155. Ness, E., Vatne, H.E. and Daaland, O. *et al.*, (1994) Proc. ICAA4., Atlanta, September.
156. Marchive, D. and Deschamps, R. (1979) *Rev. Alum.*, **489**, 37.
157. Renouard, M. (1979) *Mem. Sci. Rev. Metall.*, **776**, 18.
158. Fink, W.L. and Willey, L.A. (1948) *Trans. AIME*, **175**, 414.
159. Lynch, C.V. (1969) Proc. 1st. International Extrusion Technology Seminar, New Orleans, Paper 25, Aluminium Association, Washington DC.
160. Cahn, J.W. (1956) *Acta Metall.*, **4**, 449.
161. Evancho, J.W. and Staley, J.T. (1970) *Metall. Trans.*, **5**, 43.

# Extrusion processing

4

## 4.1 INTRODUCTION

The extrusion process is complex, involving interaction between the process variables and the material's high-temperature properties. Theoretically, the process variables which may be controlled are the extrusion ratio  $R$ , the ram speed  $V_R$ , and the extrusion temperature  $T$ . However, the extrusion ratio is generally fixed by customer specification so that the temperature and the speed become the only controllable factors.

## 4.2 THE ZENER–HOLLOMON PARAMETER AND FLOW STRESS

### 4.2.1 Flow stress

We have illustrated the important role of the high-temperature flow stress in determining structure. Since this quantity is a fixed function of the material and varies with the temperature-compensated strain rate, it will be instructive to review how this latter parameter may be calculated. It is most conveniently achieved using a simple testing method such as tension, compression or torsion. The torsion test is the most suitable of such methods [1], because high strains in excess of 20 are easily achieved in most materials including aluminium alloys although it should be noted that the test has, in general, been utilized using comparatively low strains for stress evaluation, the higher strains being used in an attempt to quantify ductility behaviour. The tension and compression testing methods have intrinsic limitations upon the maximum attainable strain. The necking phenomenon in tension limits the attainable strain to typically 0.3; the barrelling phenomenon in compression limits this method to strains up to 1.0 (however, with suitable platen lubricant, strains of 2.0 are achievable). Discrepancies in the flow stress derived from each method were first reported by Ludwik and Scheu [2], and since then numerous workers have reported the same, for example Canova *et al.* [3]. These discrepancies have been

thought to be due to two effects: yield criterion differences and differing work-hardening rates and texture developments. Hence it is useful to present experimental evidence using 7075 alloy tested in the same laboratory in both tension and compression, since by far the largest bank of data is available from the torsion test technique. The torsion test has complications because its data requires post-testing analysis to convert the measured torque and twist variables into their respective true stresses and strains. The torsion test is further complicated [4] by lengthening or shortening of the specimen during testing. A change in dimensions cannot be easily accommodated in the stress analysis, and so specimens should be axially restrained during testing. This restraint introduces an axial stress component to the system, but this is preferable to a specimen geometry change. At high homologous temperatures the axial stress developed is negligible and is often ignored [5]. As the testing temperature is reduced, the contribution of the axial stress component to the Von Mises effective stress becomes more important, and the rotation of the principal stress axes become more prominent. However even at the lowest testing temperatures, their contribution to the effective stress is never greater than 0.3%. It is clearly important to model the theoretical effective stress and temperature behaviour for torsion testing in an effort to establish whether the assumption that the two tests yield differing relationships is valid when the data is treated in the correct manner.

To describe the deformation of Al-alloys the most commonly used equation is that proposed by Zener and by Sellars and Tegart [4] and subsequently modified by Sheppard and Wright [6] to yield the steady state flow stress  $\bar{\sigma}$  from the equation:

$$Z = A [\sinh(\alpha\bar{\sigma})]^n = \dot{\bar{\epsilon}} \exp\left(\frac{\Delta H}{GT}\right)$$

from which:

$$\bar{\sigma} = \frac{1}{\alpha} \ln \left\{ \left( \frac{Z}{A} \right)^{\frac{1}{n}} + \sqrt{\left[ \left( \frac{Z}{A} \right)^{\frac{2}{n}} - 1 \right]} \right\} \quad (4.1)$$

in which  $Z$  is termed the temperature-compensated strain rate,  $\Delta H$  is the activation energy for deformation,  $\dot{\bar{\epsilon}}$  is the mean equivalent strain rate,  $G$  is the universal gas constant ( $8.314 \text{ J mol}^{-1} \text{ K}^{-1}$ ). The remaining terms in the equation require definition because  $\dot{\bar{\epsilon}}$  is specific to extrusion geometry and the temperature  $T$  varies throughout the extrusion ram stroke. The activation energy may be regarded as a material constant in the hot-deformation range.

Thus the flow stress is given as a function of the process parameters and several constants which must be experimentally established. The relationship is widely used both in extrusion and rolling [7–9] and has been used by the aluminium companies for on-line control in extrusion and tandem mill rolling. The criticism of the equation is that it says nothing concerning the structural events occurring and does not consider the evolution of structure which determines the current flow stress for subsequent operations.

During deformation, the microstructure evolves as dislocations are generated, annihilated and arranged into low energy configurations. Single internal state variable theories [10–14] attempt to represent the effect of microstructure on stress by the state variable  $s$ ; in many cases this variable could, for example, represent, the dislocation density and as such would evolve with continued straining. The evolution of kinetic laws for  $s$  will vary with the temperature and strain rate of deformation. Such equations are usually considerably more complex than the purely empirical equation above and although proposed as fundamental metallurgical relationships still require determination of arbitrary constants for each alloy considered. Moreover, in the case of extrusion the structure is developed from cast and homogenized to as-worked in a single operation and the process is less amenable to finite-difference or finite-element analysis in three dimensions. It would therefore appear that, because the area in which small strains occur should not significantly affect either the pressure or the properties, equations such as 4.1 would be adequate to describe the extrusion process.

#### 4.2.2 Theoretical considerations

We first assume that equation 4.1 above satisfactorily describes flow stress relationships. The procedure is then to obtain stress strain data from torsion testing following the method described by Barraclough [15] in which the measurement of stress is taken at 0.72 of the outer radius( $r_{\text{eff}}$ ) of the specimen where the value may be determined because at this point:

$$\bar{\sigma} = \sqrt{3} \left( \frac{3M}{2\pi r_0^2} \right), \quad \varepsilon = \left( \frac{r_{\text{eff}} \theta}{l\sqrt{3}} \right), \quad \dot{\varepsilon} = \left( \frac{r_{\text{eff}} \dot{\theta}}{e\sqrt{3}} \right)$$

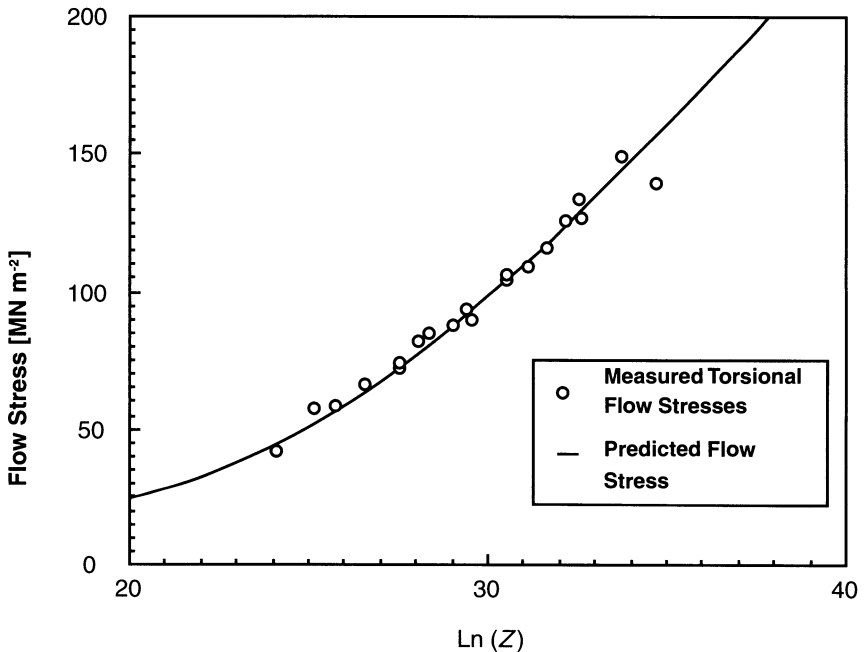
The constitutive equation cannot now be evaluated before the temperature rise obtaining in the torsion test has been established by a finite difference technique as described by Sheppard and Wright [16] and establishing a value for a following the method suggested by Garafalo [17]. The constitutive equation may then be obtained by multiple regression of the equation:

$$\ln [\sinh (\alpha \sigma)] = \frac{\ln (A)}{n} + \frac{\ln (\dot{\varepsilon})}{n} + \left( \frac{\Delta H}{GT} \right) \frac{1}{T}$$

Alternatively the constants may be obtained by straightforward integration for the torque values followed by multiregression as described by Sheppard and Wright [18]. Care must, however, be taken to ensure that the design of the torsion specimen is such that the temperature in the test section remains as homogenous as possible. Thus the test section should be kept as short as possible with the length:diameter ratio no greater than unity.

#### 4.2.3 Comparison of compression and torsion in material assessment

Sheppard and Jackson [19] investigated the results obtained from torsion and from compression of a number of 7XXX alloys. The raw data from these plots gave differing values of the flow stress. However when both sets of data were corrected for temperature rise [16] occurring in the process the two sets of data coincided as shown in Fig. 4.1.



**Fig. 4.1** Comparison of the temperature-corrected torsion flow stresses with those predicted by compression.

If the source of the flow stress discrepancies arose from crystallographic effects then the torsion flow stresses measured would be expected to be consistently lower than those predicted from compression at all  $Z$  values. In any case the torque values used to calculate the constitutive equations were always extracted from the data where the torque was greatest and hence at a point where substantial textural development could not have occurred. If, however, discrepancies only occur at the higher  $Z$  values (and this was the indication in the compression tests) then the conclusion that the effect of temperature rise during testing has the greatest significance upon the measured flow stress is reasonable. The material used in the experimental work under discussion was an AA7075 aluminium alloy containing predominantly M(AlZnCuMg) and T(AlZnCuMg) type dispersoids, together with  $Al_{18}Cr_2Mg$  type precipitates. These dispersoids provide



AA7XXX series alloys with their very high strengths. Therefore, the ease of deformation of an AA7XXX alloy is not governed predominantly by the number of slip systems available, but by the ability of the dislocations present in the material to overcome the pinning effects of these dispersoids. It is therefore obvious that modification of the flow stress equation due to crystallographic effects are not justified and that once torsion results are analysed in the correct manner then the resultant equation is valid.

From Fig. 4.1 it can be seen that a much greater correlation with compression can be achieved if temperature is taken into account. The torsion hot working relationship was recalculated using this temperature correction, and the resultant temperature modified equation is:

$$Z = \dot{\epsilon} \exp \left\{ \frac{155100}{GT} \right\} = 1.7 \times 10^{12} [\sinh(\alpha\sigma)]^{6.4}$$

This new equation has an improved correlation compared to the previous torsion equation, together with a closer similarity to that equation obtained by compression. Figure 4.1 shows clearly that flow stress data derived using either torsion or compression tests are equally acceptable and Table 4.2 shows these constitutive equations for a number of aluminium alloys. Figure 4.2 is a graphical representation of these equations for some of the easily extrudable alloys and for some of the so-called 'hard alloys'. It is clear that seemingly a difference in the exponent  $n$  describes the temperature compensated strain rate sensitivity. Figure 4.3 indicates that slightly differing flow stresses result from differing heat-up and cooling rates for the 7150 alloy.

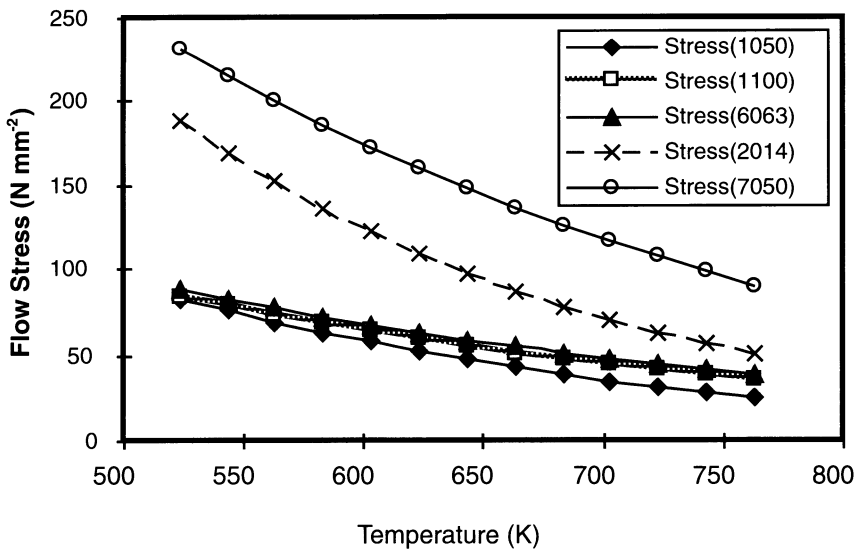


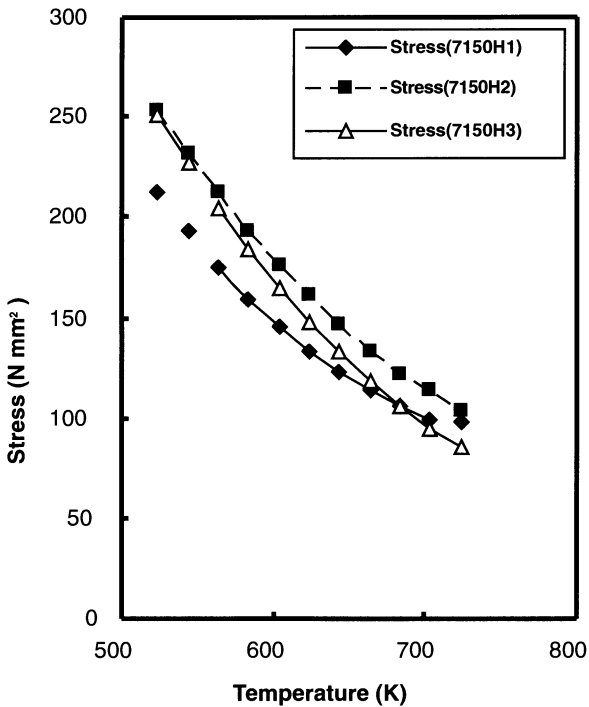
Fig. 4.2 Comparison of the temperature response of 'weak' and 'hard' alloys.

**Table 4.1** Constants in the constitutive equation for some Al-alloys

<i>Alloy</i>	$\alpha$	n	$\Delta H$	G	<i>ln A</i>	<i>Remarks</i>
1050	0.037	3.84	156 888	8.314	26.69	
1100	0.045	5.66	158 300	8.314	24.67	
2011	0.037	3.712	142 000	8.314	19.2	
2014*	0.0118	5.86	176 867	8.314	31.43	PH.–SS [32]
2014	0.0152	5.27	144 408	8.314	24.41	
2024	0.016	4.27	148 880	8.314	19.6	
3003	0.0316	4.45	164 800	8.314	26.9	
3004	0.0344	3.6	193 850	8.314	28.21	
3005	0.0323	4.96	183 100	8.314	29.87	
3105	0.0248	4.83	179 300	8.314	29.98	
4047	0.04	2.65	129 300	8.314	20.47	
5005	0.029	5.8	183 576	8.314	26.65	
5052	0.016	5.24	155 167	8.314	24.47	
5054	0.015	5.43	173 600	8.314	26.61	
5056	0.015	4.82	166 900	8.314	23.05	
5083	0.015	4.99	171 400	8.314	23.11	
5182	0.062	1.35	174 200	8.314	22.48	
5456	0.0191	3.2	161 177	8.314	23.5	
6061	0.045	3.55	145 000	8.314	19.3	
6082	0.045	2.976	153 000	8.314	19.29	
6063	0.04	5.385	141 550	8.314	22.5	
6105	0.045	3.502	145 000	8.314	20.51	
7004	0.035	1.28	153 000	8.314	20.12	
7050	0.0269	2.86	151 500	8.314	22.85	
7075H1	0.0141	5.41	129 400	8.314	20.75	24h. Soak
7075H2	0.01	6.14	158 432	8.314	26.32	Sl.Ht.-F.Cool [23]
7075H3	0.012	7.8	155 336	8.314	27.54	F.Ht-Sl.Cool
7075H4	0.01	8.5	156 325	8.314	27.14	F.Ht-F.Cool
7075H5	0.011	6.32	156 837	8.314	26.38	Sl.Ht-Sl.Cool
7150H1	0.01	5.7	161 402	8.314	29.8	F.Ht-F.Cool
7150H2	0.013	6.1	158 806	8.314	29.2	F.Ht-Sl.Cool
7150H3	0.01	5.5	159 832	8.314	30.7	Sl.Ht-F.Cool

A comparison of the flow stress values given from torsion testing on some 6XXX alloys is shown in Fig. 4.4. As expected, they show the same temperature dependence and the specific values are what would be expected. Table 4.1 indicates that the strain rate sensitivity and the activation energy are similar indicating that self diffusion is the operative mechanism. Table 4.1 does, however, also show that for these alloys and for others the activation energy may be slightly below or higher than that for self diffusion. In the case of highly alloyed material or those alloys containing high Mg contents this is clearly explainable but for the weaker alloys the discrepancies are most probably due to the regression analysis.

It would therefore be instructive at this point to examine the interpretation of the alloy constants derived from the hot working equation. Consider first, the constant value denoted as  $\alpha$ . The constant  $\alpha$  is a reciprocal flow stress, and its



**Fig. 4.3** Effect of differing heating and cooling rates on the flow stress of 7150 alloy as a function of temperature.

value gives the position where the dependence of flow stress upon strain rate changes from a power relationship to an exponential one. In general, the flow stress ( $\bar{\sigma}$ ) is considered [14] to obey a power relationship with strain rate in the region  $(\alpha\bar{\sigma}) < 0.8$ , and an exponential relationship in the region  $(\alpha\bar{\sigma}) > 1.2$ . The value of  $\alpha$  is determined from the two steady state deformation gradients,  $d \ln \dot{\epsilon} / d \ln \bar{\sigma}$  (termed  $b$ ) and  $d \ln \dot{\epsilon} / d \ln \bar{\sigma}$  (termed  $h$ ). For steady state creep, the greater these two gradients are, the greater will be the creep rate. Alloying produces either a solid solution, or, a second phase particle distribution. Both products increase strength by decreasing the mobility of dislocations within the material. At the lower creep temperatures, the creep mechanism is controlled by dislocation mobility. Thus, the more resistant a material is to dislocation motion, the lower will be its creep rate (i.e.  $b$  and  $h$  will be lower). The value of  $b$  is generally much more sensitive than that of  $h$ , and hence the  $b:h$  ratio falls with decreasing creep susceptibility. From the analogy of creep and hot working, it can thus be expected that the more resistant a material is to deformation, the lower will be its value for  $\alpha$  in both processes. The value for  $\alpha$  of  $0.011 \text{ m}^2 \text{ MN}^{-1}$  found for most of the hard 7XXX alloys is indicative of the material's intrinsic ability to resist deformation, and in the 7XXX alloys dislocation mobility is impeded to a large extent by the second-phase particles formed during homogenization.

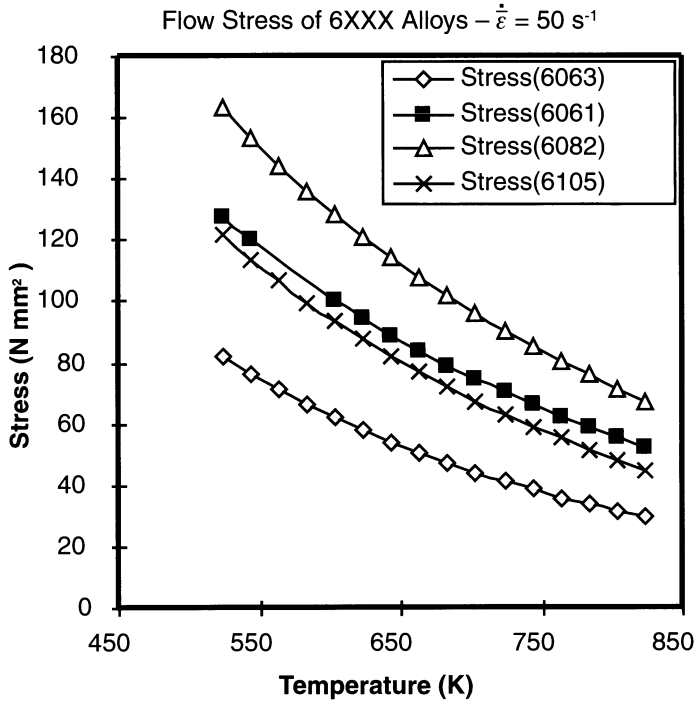


Fig. 4.4 Comparison of 6XXX alloys.

Compare the value of  $0.011 \text{ m}^2 \text{ MN}^{-1}$  found for  $\alpha$  with that of  $0.04 \text{ m}^2 \text{ MN}^{-1}$  found for alloy AA6063 by Clode [20]. Alloy AA6063 is an Al–Mg–Si group alloy, which exhibits a wide hot-workability range as a result of low deformation strength and high ductility. The AA6XXX group of alloys have generally the widest deformation ranges of all the aluminium alloys, and such alloys are often used as the optimum scale against which other alloys are judged. The loads required to extrude the AA7XXX alloys [19] are much greater under the same conditions than those required for AA6063 [21]. Thus it would be expected, and is indeed found, that the value for  $\alpha$  in alloy AA7075 is significantly lower than that for alloy AA6063.

The constant  $n$  can be termed the ‘inverse of the temperature compensated strain rate sensitivity’. The actual value of this constant is strongly dependant upon the value of  $\alpha$ . Consider conducting two tests upon the same material at a constant temperature, using two different strain rates,  $\dot{\epsilon}_1$  and  $\dot{\epsilon}_2$ , and let the flow stresses be denoted by  $\sigma_1$  and  $\sigma_2$  respectively. Under such testing conditions, the hot-working equation can be reduced to:

$$\frac{\ln \dot{\epsilon}_1}{\ln \dot{\epsilon}_2} = n \left[ \frac{\sinh(\alpha\sigma_1)}{\sinh(\alpha\sigma_2)} \right]$$

Hence lower  $\alpha$  values automatically generate higher  $n$  values. If a material in two different conditions exhibits hot working constants which are identical in all values except the value for  $n$ , the material with the lower  $n$  value is more sensitive to changes in temperature-compensated strain rate ( $Z$ ). Under such conditions, it may be reasonable to assume that the condition corresponding to the lower  $n$  value corresponds to a condition of greater work hardening during deformation. However, misinterpretations can result if the value of  $n$  is considered as indicative of the temperature-compensated strain rate response, without consideration of the other hot-working constants. This can be illustrated very simply by again contrasting the hot working constants for alloys AA7075 and AA6063. The response of alloy flow stresses to changes in temperature can be plotted as in Fig. 4.2 and it can be seen that, for the same change in temperature, alloys AA7075 and AA2014 have a greater flow stress response than the more dilute alloys, even though their individual  $n$  constants are greater. This is because, if the Zener–Hollomon equation is inspected in detail, it can be shown that the constants  $A$ ,  $\Delta H$  and  $n$  are interrelated since equation 4.1 indicates that if, for example, the activation energy  $\Delta H$  were considered to always have the value for the self diffusion of aluminium ( $153\,000\text{ J}^{-1}$ ) then the values of  $A$  and  $n$  could be altered without changing the value of the flow stress by writing:

$$\frac{1}{n_{\text{reg}}} \ln \left( \frac{Z_{\text{reg}}}{A_{\text{reg}}} \right) = \frac{1}{n'} \ln [Z_{153\,000}] + \frac{1}{n'} \ln (A')$$

where the subscript ‘reg’ refers to the results from regression analysis,  $Z_{153\,000}$  incorporates the new value of activation energy and  $A'$  and  $n'$  the corresponding revised values of these constants. In effect we are observing that the use of regression analysis cannot be avoided but will only give the best fit to the experimental data.

During steady state deformation, the work-hardening processes occurring in the material are in dynamic balance with the work-softening processes (e.g. dynamic recovery). To achieve this dynamic balance, an energy threshold must be overcome. The hot working constant,  $\Delta H$ , represents this threshold, and is often termed the activation energy for hot working. This activation energy is limited to the rate determining mechanism occurring in the dynamic softening processes. The softening mechanism operative in almost all Al-alloys during hot working is dynamic recovery. It is generally accepted that the rate determining mechanism in dynamic recovery is that of vacancy diffusion. A value of  $153\text{ kJ mol}^{-1}$  for lattice self diffusion in pure aluminium has been established and the values given in Table 4.1 compare reasonably well with this self diffusion value. Many reviews and studies on hot working in Al-alloys report activation energies  $\cong 150\text{ kJ mol}^{-1}$  for hot working (e.g. McQueen [21]) showed  $\Delta H = 152\text{ kJ mol}^{-1}$  for some Al–Mg alloys). When this value is not assumed then regression fits show a variation in  $\Delta H$ , but the value is always close enough for us to assume that the basic deformation mechanism is one of self diffusion. We may conclude that both compression and torsion testing give a good estimate for the activation energy for hot working in commercial Al-alloys.

The physical significance of the constant,  $A$ , in the hot working equation has not been specifically determined. At high stress levels, the constant  $A$  is termed a 'structure factor', and is considered to be a measure of the activateable sites in the material and the probability that a deformation event will occur at that site.

We may conclude that the hot working constants found in both compression and torsion testing (after consideration of temperature rises during testing) are suitable methods for their determination and the values of the constants given in Table 4.1 are adequate to describe the flow stress during extrusion of Al-alloys. Care must, however, be exercised if the values are to be utilized as a precision tool because it is clear that heating and cooling rates can produce variations in the flow stress. We may presume that there may be considerable variations if the homogenising practices are vastly different (i.e. when considering homogenized versus cast material).

### 4.3 MATERIAL FLOW IN EXTRUSION

Unlike rolling and wire-drawing, extrusion as usually carried out is not truly quasi-static because of the high friction forces involved. In the extrusion of aluminium, friction is extremely high; often so high that plastic shearing occurs in subcutaneous regions of the billet in preference to sliding at the interface. Under these conditions the deformation zone is not stationary but gradually extends inwards from the container wall by the progressive thickening of zones of heavy shear. On the other hand, under conditions of very good lubrication the deformation zone is more restricted and the process becomes more nearly quasi-static.

On this basis it would seem to be a helpful simplification to regard any particular instance of extrusion as operating under conditions that lie between the two extremes: (i) completely unlubricated with generation of sticking friction or (ii) lubricated with frictionless slipping at the billet container interface.

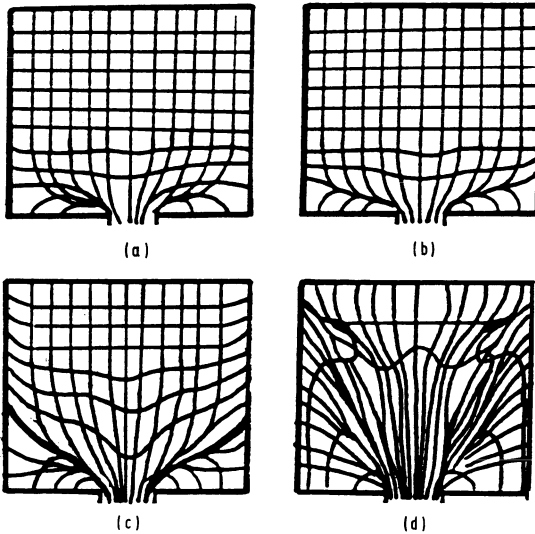
The true situation, however, is rather more complex than this and Pearson and Parkins [22] found it necessary to postulate three types of metal flow (i) unlubricated; (ii) lubricated and (iii) a type characterized by the presence at a fairly late stage in the process of a defect known as extrusion defect or back-end defect.

Hot extrusion of aluminium as carried out under normal industrial conditions is unlubricated, and may be considered to approach sticking conditions at the interface.

#### 4.3.1 The three types of flow

Flow during the process has been categorized (Fig. 4.5) by Pearson and Parkins as:

- S – indirect;
- A – unlubricated;
- B – lubricated;
- C – with extrusion defect.



**Fig. 4.5** Flow under differing conditions in the extrusion process (a) indirect; (b) lubricated; (c) direct; (d) with back end defect.

Before extrusion can proceed the billet must be inserted into the container and to facilitate entry there is generally appreciable clearance between the two.

The first effect of extrusion pressure is thus to compress or 'upset' the billet into firm contact with the cylinder wall. In indirect extrusion there is little friction between the billet and container and flow is streamlined as shown in Fig. 4.5(a). The surface of the billet becomes the surface of the extrude which is the reason why it is normal practice to scalp all billets when using the indirect process. This does of course involve an additional and expensive operation. Although it is assumed that there is no dead metal zone in indirect extrusion we shall see below that experimentally this can be shown to be untrue. In lubricated direct extrusion (Fig. 4.5(b)) a conical dead metal zone forms in front of the die but there is little shearing at the container/metal interface; there is thus a tendency to extrude part or all of the surface into the surface of the extrude and this is the reason why little or no lubrication is used in aluminium alloy extrusion. When the billet is unlubricated, as extrusion proceeds and the billet shortens, there is a tendency for relative motion between the container and the skin of the billet (Fig. 4.5(c)). Because of the intimate contact and lack of lubrication, high friction forces are generated at the interface and zones of heavy shearing occur just beneath the skin of the billet. Quite early in the process a dead metal zone is formed at the front of the billet and is usually assumed to extend over the die face to the orifice making an angle of  $45^\circ$  with the container. Both of these assumptions are only approximately correct. With progressive shortening of the billet the zones of shear thicken and begin to be forced through the die where they occupy the surface regions of the extruded bar. Because of friction at the container wall, there is not much tendency for the surface of the billet to move

forward through the die and the surface of the extruded bar is therefore made up of material having its origin in the zones of heavy shear within the billet – this being the reason for the good surface quality of extrusion produced in this way. The effect of the continued shearing of the billet past its peripheral length causes the latter to build up at the rear end of the billet in front of the pressure disc and when the billet has been reduced to about one-third of its original length, the accumulated material bulges inwards and begins to affect the deformation of the metal in the centre. Ultimately the bulges come right in and reduce the more lightly worked core to a narrow cone so that the last 10% of the extruded bar has a heavily deformed outer ring which extends almost to the middle of the bar.

The properties of extruded products are generally quite good and acceptable and it is important to remember this in the light of the following remarks.

#### *Type C flow – the extrusion defect*

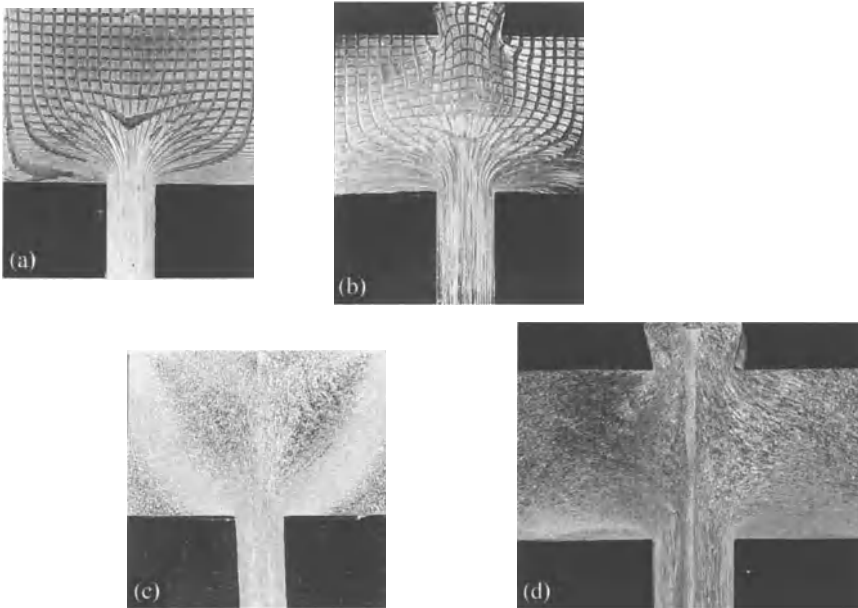
The well known extrusion defect occurs under unlubricated conditions. This defect occurs at a fairly late stage in the process where material from oxidized and contaminated surfaces of the billet flows round from the back of the billet to take the place of the core of the billet which has passed through the die. Because of the symmetry of the process the impure material eventually passes through the die in the form of an annulus which separates sound material in the outer part of the cross-section from equally sound material in the core. At times the discontinuity is so complete that part of the core can be withdrawn from the back end of the billet. The defect has been identified to be the result of high friction at the billet/container interface and is rarely a problem in Al-alloys.

Although the mechanism of formation of extrusion defect is still in doubt, its origin in the oxidized and contaminated skin of the billet fortunately is not, so that practical steps can be taken to avoid the worst of its consequences. Probably the best method is to scalp the billet and pre-heat it in an inert atmosphere; this is usually done for high grade and expensive materials. A cheaper and more commonly practised method is to employ a pressure pad having a diameter smaller than that of the billet. The pressure pad then shears through the billet leaving the impure skin behind as a shell or skull which is subsequently removed with the residual part of the billet or discard. These back-end extrusion defects cannot, of course, occur in indirect or inverted extrusion.

There are a number of experimental methods to determine the actual flow during the extrusion process involving either the insertion of grids on billets split longitudinally or the use of discs and/or pegs of a similar material to the billet which show a marked difference when etched. Similar observations may be made on suitably macroetched sections.

Both techniques are shown in Fig. 4.6 illustrating the difference in flow for the cases of direct and indirect extrusion. Figures 4.6(a) and (b) show gridded specimens which clarify the alterations to flow when, as in the indirect case, there is no die wall friction. These illustrations also show the presence of the typical

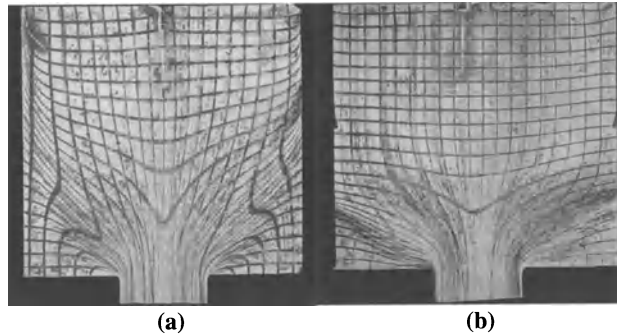




**Fig. 4.6** Metal flow during extrusion; (a) gridded billet – direct extrusion; (b) gridded billet – indirect extrusion; (c) macroetched section – indirect extrusion; (d) macroetched section – indirect extrusion.

dead metal zone in the direct case and the apparent absence of this morphology in indirect flow. The surfaces are also clearly generated from the interior of the billet in direct extrusion and the surface of the billet in indirect. Macroetched sections of direct indirectly extruded billets of AA1100 alloy are shown in Figs. 4.6(c) and (d) at commencement of extrusion and approaching the discard stage. Similar flow to that described above is clear but these billets indicate that there is indeed a dead metal zone formed on the flat die face prior to entry into the die orifice. Flow is relatively uniform across the extrude with little increased fibreing at the surface layers. This feature is a distinct advantage of the indirect process, reducing the tendency to recrystallize during the solution treatment common to all of the hard alloys. In these experiments [23] it was necessary to back extrude the visible tongue being the only method to extract the discard from the container; the flow is, however, still well defined.

Hinesly and Conrad [24] have reported the effects of both temperature and ram speed upon the flow pattern during the extrusion of alloy AA2024. Their results indicated that the commonly observed flow containing just a single maximum on the major axis of the billet was only observed at high  $Z$  (low temperature) extrusions and at higher values the flow was substantially different. Previous workers [25,26] had explained this in terms of lubrication differences whilst Conrad suggested this to be the result of differing plastic properties and hence temperature differences within the deformation zone. These workers had



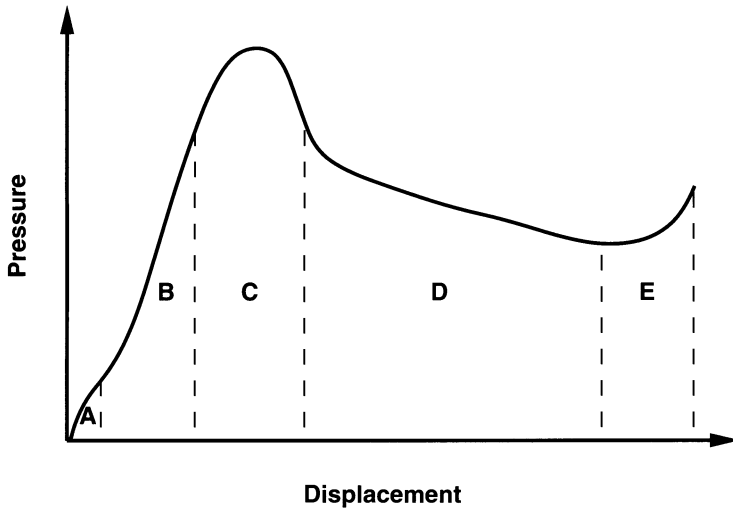
**Fig. 4.7** Deformation patterns for an extrusion ratio of 30:1; (a) high-temperature extrusion; (b) low-temperature extrusion.

based their experimental finding on extrusion through conical dies but Tatcher [23] was able to demonstrate the effect when extruding AA5456 alloy through normal flat-faced dies. His results for extrusions of 10:1 and at temperatures of 335 and 500°C are shown in Fig. 4.7 for AA5456 alloy.

#### 4.4 THE PRESSURE/DISPLACEMENT DIAGRAM

Most theoretical analyses of the extrusion process attempt to relate extrusion pressure to reduction ratios, and/or predict the flow of the material within the deformation zone. Moreover, the theories discuss steady-state flow and the steady-state pressure. Figure 4.8 is a smoothed pressure–displacement trace from a 2XXX alloy extrusion and is more or less typical of all aluminium alloys. It is clear that steady-state conditions do not exist. We can observe that the diagram consists of six principal and easily recognizable phases as identified by Sheppard [27]:

- A. The billet is upset to fill the container when localized deformation at the container wall and die entry may be observed. Dislocation walls will begin to form at isolated areas.
- B. The billet is further compressed. Dislocation walls become more prevalent and outcrops of subgrains begin to form. This heterogeneous structure with progressively increasing dislocation and subgrain density mainly concentrated in the die region, continues until the next phase is encountered. Roughly at the end of this phase, extrusion commences with a product of low dislocation density and essentially an as-cast structure.
- C. The ‘peak’ pressure region. The extent of this region is alloy dependent. At commencement of this phase a deformation zone is not evident and dead metal zones cannot be detected. The dead metal zone is, however, fully established by the time the peak pressure is reached but changes in shape from convex to slightly concave by the end of the phase. It is during this phase that cylinder



**Fig. 4.8** Pressure/displacement trace for 'hard' alloy.

wall shear becomes apparent and a full established deformation zone consisting of more or less equiaxed subgrains is formed. The reason for the peak appears to be that a greater dislocation density is required to reach 'steady-state' extrusion than is required to maintain it [28].

- D. The so-called 'steady-state' region in which the product maintains a fibrous structure. The region is not in fact steady state because the temperature rises during this period and friction gradually diminishes so that the pressure continually falls. The apparent increase in thickness of the fibrous band of material adjacent to the dead metal zone indicates that there is a differential flow of material: the surface of the billet is retarded by container wall friction and material actually flows towards the dead metal zone and then along it. We are in fact observing a deformation history. The important point is that significant macrostructural and microstructural changes occur after the peak pressure. The difficulty in obtaining steady state extrusion is alloy dependent, being more difficult in those alloys which are complex and contain second phases, precipitates, solutes etc., which hinder dislocation movement.
- E. The extrusion pressure rises sharply because the remaining portion of the billet becomes so short that flow is inhibited.

In practice, extrusion is terminated before phase E is reached.

#### 4.5 THE STRAIN RATE DURING EXTRUSION

The strain rate varies throughout the deformation zone and may be evaluated by the methods described in Chapter 2. Figure 4.9 shows the results from an upper-

bound model describing the strain rate at the dead metal zone boundary and along the axis of the billet. It is clear that such analyses cannot be used in this form; just one value of the averaged strain rate is required. This can be achieved by time averaging the individual strain rates throughout a deformation zone grid but this method would also require extensive computation for each extrusion. Tatcher [23] noted that in practice the deformation zone semiangle varied with the extrusion ratio and by extensive optimisation of the upper bound solution established that the Feltham formulae should be modified to read:

$$\dot{\epsilon} = \frac{6V_r D_B^3 (0.171 + 1.86 \ln R) \tan(38.7 + 6.9 \ln R)}{D_B^2 - D_E^2}$$

Figure 4.10 compares the value of this modified equation with the values calculated from a time averaged axisymmetric upper-bound solution. Since the upper bound, by definition, is greater than the actual value it would appear that the modified equation can be used for all practical purposes.

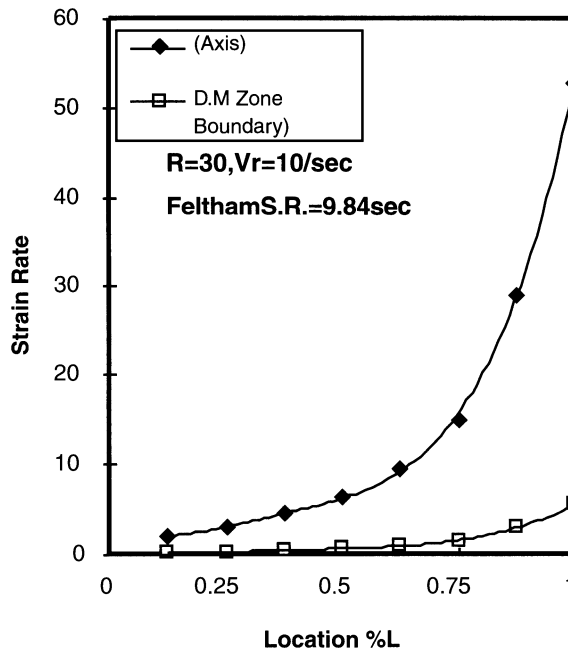
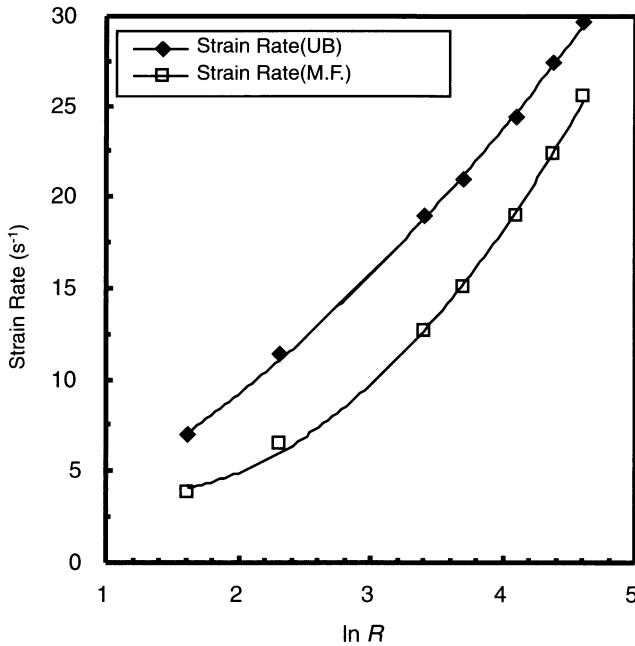


Fig. 4.9 Variation of strain rate along streamlines in the deformation zone.



**Fig. 4.10** The modified Feltham strain rate compared to a time averaged upper-bound solution.

#### 4.6 EXTRUSION PRESSURE – PRACTICAL CONSIDERATIONS

Traditionally, the pressure requirements necessary to ensure that breakthrough of an extrusion is facilitated, have been calculated using equations such as equation 2.7, calculated as shown above or using FEM or finite difference techniques. Each will predict the steady-state extrusion pressure for rod extrusion and produce an equation of the form:

$$p = \bar{\sigma} (a + b \ln R) \quad (4.2)$$

The effects of the initial billet temperature and extrusion ratio on the increment of peak pressures were as first reported by Castle and Sheppard [29] and could clearly be related to the temperature-compensated strain rate of the extrusion process. It is also noticeable that the total peak pressure is a strong function of the billet temperature and the extrusion ratio. Thus the peak pressure increases with an increase in the extrusion ratio for a constant temperature. It is also obvious that the peak pressure increases rapidly with decrease in the temperature. In general, the pressure required to extrude can be divided into four parts:

1. the pressure required to deform the metal homogeneously;
2. the pressure required to overcome the friction mainly at the container/billet interface;

3. the pressure required to compensate for losses due to redundant work (i.e. the force not directly contributing to the shape change);
4. the pressure required to ensure breakout (i.e. the incremental peak).

The force necessary to deform the metal homogeneously is a material property. Conventional theory indicates that this force is a strong function of temperature and strain rate. The process of plastic deformation at these temperatures and strain rates is controlled by one of the various mechanisms by which the dislocations migrate in a material (cross-slip, climb, glide, etc.). The upper-bound analysis developed in Chapter 2 yields the specific equation:

$$\frac{p}{\bar{\sigma}} = (0.171 + 1.8594 \ln R) \quad (4.3)$$

which may be regarded as a standard steady-state equation. We should note that this equation is the result of linear regression and is valid for rod extrusion up to a ratio of 100. It can be shown that the constant can assume a negative value for higher ratios and, hence, cannot be considered as a measure of the redundant work as is commonly assumed.

#### 4.6.1 The effect of friction

Friction is usually dealt with by assuming that the material/container interface is subjected to a velocity discontinuity which is proportional to the shear yield stress; thus modifying equation 4.3 to read:

$$p = \bar{\sigma} \left[ 171 + 1.86 \ln R + \frac{4mL}{\sqrt{3}D_B} \right] \quad (4.4)$$

where  $m$  has been observed, experimentally, to vary between 0.8 and 0.9 which is close to sticking conditions at the boundary. Discussion of the various methods of dealing with the friction problem have been dealt with in Chapter 2.

#### 4.6.2 The effect of the temperature-compensated strain rate

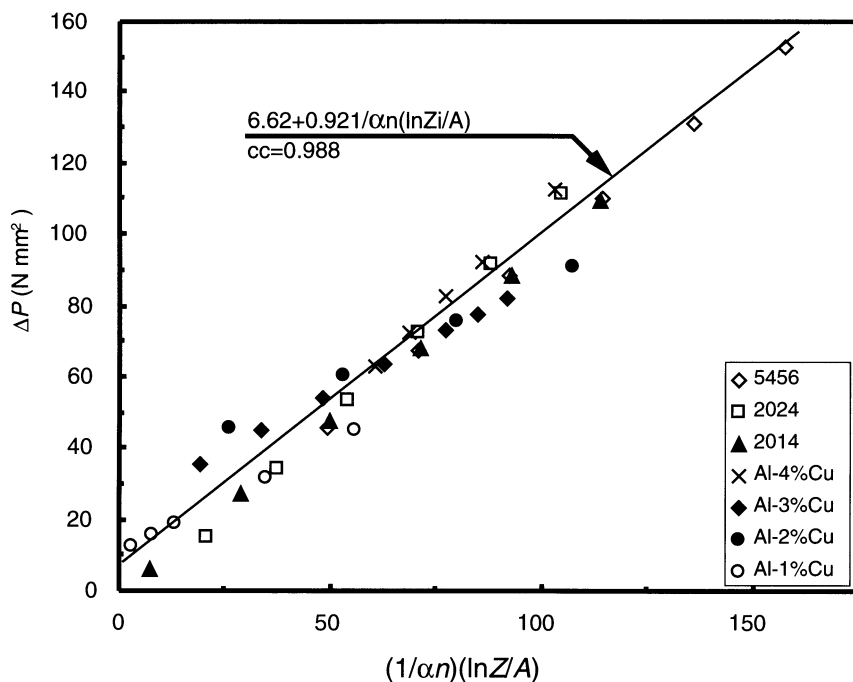
The increment of pressure required to ensure breakthrough takes the general form (Fig. 4.11):

$$\Delta p = 6.62 + 0.921 \frac{(\ln Z/A)}{\alpha n} \quad (4.5)$$

where the constants have been shown to be valid over a wide range of Al-alloys and, as above

$$Z = A[\sinh(\alpha\sigma)]^n = \dot{\epsilon} \exp\left(\frac{\Delta H}{GT}\right)$$

Figure 4.11 contains experimental data [29–38] from the extrusion of 2XXX, 5XXX, 6XXX and 7XXX alloys.



**Fig. 4.11** Variation of the incremental pressure required to effect breakthrough.

Straightforward consideration of equations 4.2 to 4.5 suggests that the total pressure requirement would be predicted by an equation of the form:

$$p = \bar{\sigma} \left[ A + B \ln R + C \left( \frac{L_B}{D_B} \right) \right] + \Delta p \tag{4.6}$$

which is not ideal for on-line control.

A similar conclusion may be reached by considering the flow stress given by the Zener–Hollomon parameter:

$$\bar{\sigma} = \left( \frac{1}{\alpha} \right) \ln \left\{ \left( \frac{Z}{A} \right)^{\frac{1}{n}} + \sqrt{ \left[ \left( \frac{Z}{A} \right)^{\frac{2}{n}} + 1 \right] } \right\} \cong \left( \frac{\ln 2}{\alpha n} \right) + \frac{1}{n} \ln \left( \frac{Z}{A} \right) \tag{4.7}$$

It is clear that substituting equation 4.7 into equation 4.4 will yield a similar equation to equation 4.6 but including the material constitutive constants:

$$p = \frac{1}{\alpha n} \left[ A + B \ln R + C \left( \ln \frac{Z}{A} \right) + D \left( \frac{L_B}{D_B} \right) \left( \ln \frac{Z}{A} \right) \right] \tag{4.8}$$

The term containing the product of  $\ln R$  and  $\ln (Z/A)$  may be omitted because it is statistically insignificant. Since the constants in the constitutive equation are

readily available for a number of alloys this is a convenient equation to represent the total pressure requirement. The constants  $A$ ,  $B$ ,  $C$  and  $D$  can be evaluated from actual extrusion runs of easily extrudable shapes and have been established in laboratory scale experiments for the alloys shown in Table 4.2.

**Table 4.2** Constants in the pressure equation

<i>Alloy</i>	<i>A</i>	<i>B</i>	<i>C</i>	<i>D</i>	$\alpha n$
5456	0.616	8.0503	3.124	1.156	0.059
5083	4.119	10.817	4.933	0.187	0.075
5056	23.677	8.171	3.910	0.706	0.035
5052	-3.644	7.721	4.053	0.700	0.072
2014(5%Cu)	7.8158	6.894	3.239	0.1081	0.065
2014(4%Cu)	2.6744	7.546	2.888	0.634	0.080
1100	-3.9056	3.849	1.728	0.0179	0.192
7049	17.785	10.90	1.141	2.084	0.093
7075	14.176	11.60	1.757	2.211	0.093
7150	9.818	13.89	2.613	2.084	0.079

#### 4.6.3 The effect of section shape

Practical experience indicates that very large increases in the extrusion load can be encountered as the section geometry diverges from simple rounds to complex shapes containing re-entrant corners or thin fin sections, depending on the complexity of the shapes. Apart from a very slight increase in the resistance to deformation, a portion of the increased pressure is required to overcome the increased frictional resistance associated with the increase in the contact area in the die land regions. Perhaps the major portion of the increased load is used for the redundant deformation associated with the bending of the flow lines in to the die (similar to the events occurring at the inlet and outlet regions of the deformation zone), when there are re-entrant corners. In these cases the metal must divide, forming regions of divergent flow. Further load is required to overcome the shear losses at the narrow sides of a flat section.

The effect of the die geometry on the peak pressure was investigated [36] for both direct and indirect mode of extrusion and for a number of sections (Fig. 4.12). The data was plotted as the peak pressure against  $\ln(Z)$  instead of plotting independently against the temperature and the ram speed and it was observed that for both modes the pressure increased with increase in the complexity of the section.

If we wish to go further than a mere collection of empirical factors for individual cases, the question arises as to the nature of the parameter that can represent the complexity of the die and hence the flow. In the extrusion literature several such parameters, which also assume a distinction between the effects of friction and the redundant deformation, have been quoted. In the present case, the peripheral ratio,  $\lambda$ , defined as the ratio of the periphery  $\Omega_s$  of the section to the periphery  $\Omega_r$  of a rod of equivalent cross-section, has been used. Since  $R$  is related



to  $(D_B/D_E)^2$  it is reasonable to assume that the degree of difficulty of extrusion will be given by  $\lambda^2$ . Sheppard and Wood [31] have shown that the temperature-compensated strain rate must be treated in a similar manner such that equation 4.8 should be modified to read:

$$p = \frac{1}{\alpha n} \left\{ A + B \ln \lambda R + C \left[ \ln \lambda^2 \left( \frac{Z}{A} \right) \right] + D \left( \frac{L_B}{D_B} \right) \left[ \ln \lambda^2 \left( \frac{Z}{A} \right) \right] \right\} \quad (4.9)$$

The constants may be evaluated using multiple regression techniques and the pressures recorded are shown in Figs. 4.13(a) and (b) for direct and indirect extrusion respectively. The resultant equation for direct extrusion of 2024 alloy [31] is:

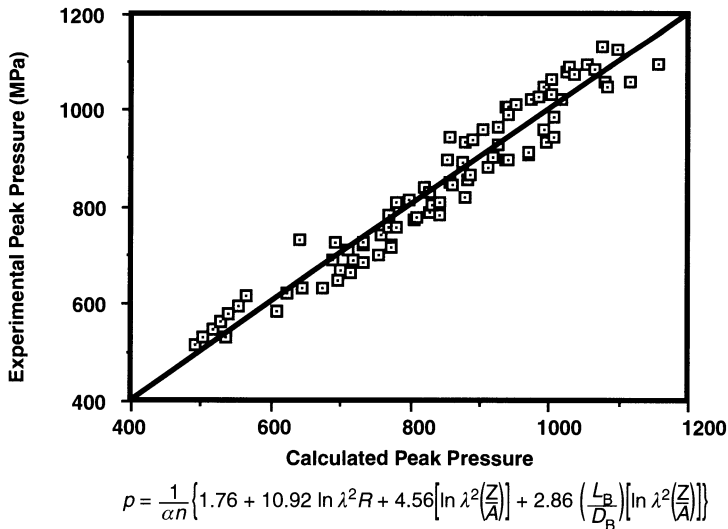
$$p = \frac{1}{\alpha n} \left\{ 1.76 + 10.92 \ln \lambda^2 R + 4.56 \left[ \ln \lambda^2 \left( \frac{Z}{A} \right) \right] + 2.86 \left( \frac{L_B}{D_B} \right) \left[ \ln \lambda^2 \left( \frac{Z}{A} \right) \right] \right\}$$

for which the correlation coefficient = 0.9752, and for indirect extrusion:

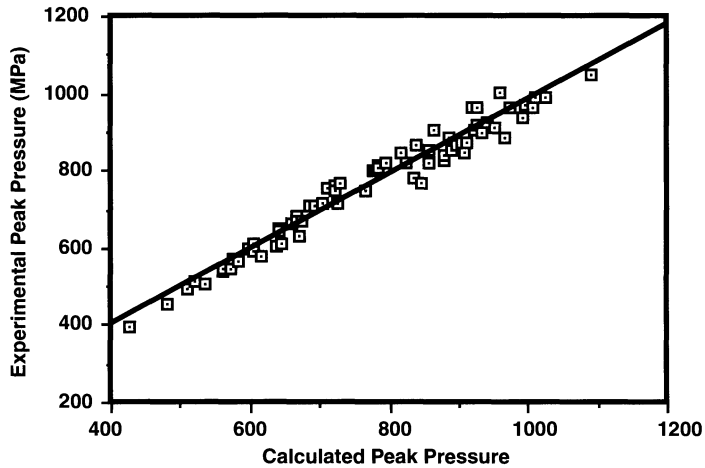
$$p = \frac{1}{\alpha n} \left\{ 0.61 + 3.86 \ln \lambda^2 R + 8.72 \left[ \ln \lambda^2 \left( \frac{Z}{A} \right) \right] \right\}$$

for which the correlation coefficient = 0.9819.

We should note that the constant associated with friction in the direct extrusion equation implies a flow stress at the container/billet interface of about twice the calculated average flow stress, assuming that sticking friction obtains (which must be the case). This indicates that the temperature at the interface is lower but calculations assuming that the temperature was that of the container still did not produce the required constant (i.e. 1.93). Clearly the classical methods of dealing



**Fig. 4.12(a)** Experimental pressure versus predicted pressure for direct extrusion of 2024 alloy.



$$p = \frac{1}{\alpha n} \left\{ 0.61 + 3.86 \ln \lambda^2 R + 8.72 \left[ \ln \lambda^2 \left( \frac{Z}{A} \right) \right] \right\}$$

**Fig. 4.12(b)** Experimental pressure versus predicted pressure for indirect extrusion of 2024 alloy.

with this phenomena must be incorrect. In fact, rough calculations (based on the assumption that the increase in flow stress must be due to strain-rate effects) indicate that shearing at the interface must occur over a distance of about 40–60  $\mu\text{m}$ . The difficulty of extrusion is thus defined by the  $\lambda^2$  parameter and is, for example, a useful method of judging the difficulty of extrusion of a new order. Moreover, there is considerable further evidence that this method can be justified [39–42]. We should note, however, that using a value of  $\lambda$  would not substantially alter the regression analysis since the effect of squaring the parameter only alters the regression constants and not the equation fit.

Thus far we have considered only the extrusion of rods and simple shapes; a small proportion of the output from aluminium alloys. There is little in the literature concerning the extrusion of multiholes or extrusion using bridge or porthole dies. Castle [38] reported experiments concerning the extrusion of shapes as well as extrusion through multihole dies. Unfortunately the work was performed some years ago and the treatment of the data can be improved. The author has used this data to show that for multihole extrusion the correction factor required may be expressed in terms of the peripheral ratio calculated using all the holes (i.e. for the extrusion of multiple rounds the ratio is simply  $\sqrt{N}$  where  $N$  is the number of holes) and the pitch circle diameter such that  $\lambda' = \lambda(D_B/D_B - D_p)$  where  $D_p$  is the pitch circle diameter and  $D_B$  is the billet diameter. Figure 4.13 shows the results of the analysis and Castle's experimental data.

An estimate of the pressure required to extrude through bridge or porthole dies may be approached by considering the operation as two separate extrusions. The pressure required to force the metal into the weld chamber is first calculated as if it were a multihole extrusion giving a shape factor  $\lambda_1$  for an extrusion ratio

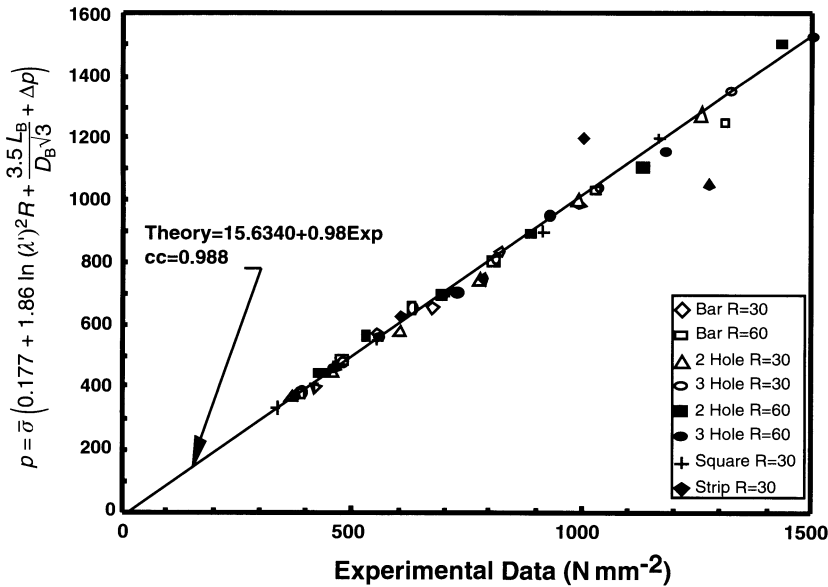


Fig. 4.13 Experimental results for multi-hole dies and comparison with single-hole and shaped extrusions.

$$R_1 = \left( \frac{\text{area between bridge arms}}{\text{area of billet}} \right)$$

followed by extrusion of the tube from the weld chamber giving a shape factor  $\lambda_2$  for an extrusion ratio  $R_2$

$$R_2 = \left( \frac{\text{cross sectional area of weld chamber}}{\text{area of extrude}} \right)$$

This gives a total equivalent extrusion ratio  $R_f$  of:

$$R_f = \lambda_1^2 \lambda_2^2 R_1 R_2$$

where:

$$\lambda_1 = \left( \frac{\text{periphery of arm area}}{\text{periphery of rod of identical extrusion ratio}} \right) \left( \frac{D_B}{D_B + D_p} \right)$$

$$\lambda_2 = \left( \frac{\text{periphery of tube}}{\text{periphery of rod of identical extrusion ratio}} \right)$$

where  $D_p$  is the pitch circle diameter and  $D_B$  is the billet diameter.

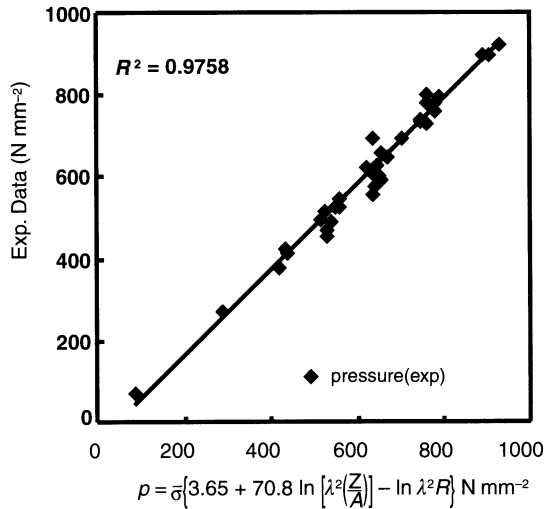
Therefore the modified extrusion ratio is:

$$R'_t = \lambda_1^2 R_1 \lambda_2^2 R_2$$

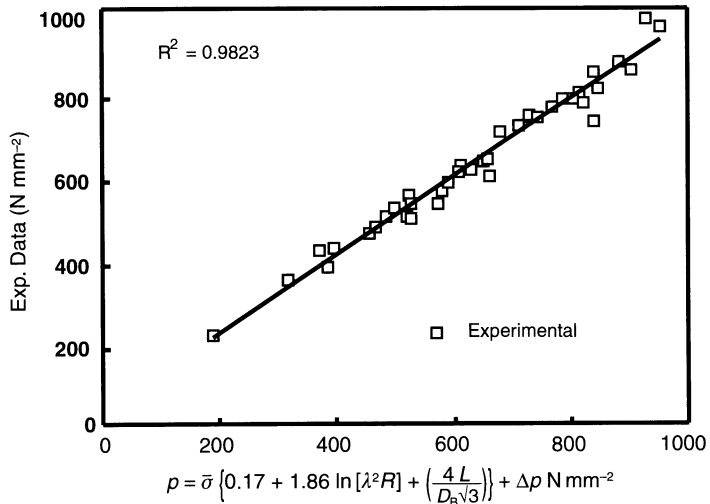
where  $R'_t$  = modified extrusion ratio in tube extrusion,  $R_1$  = extrusion ratio of the

metal passing the bridge and  $R_2$  = extrusion ratio of the metal leaving the chamber and passing through the mandrel die gap.

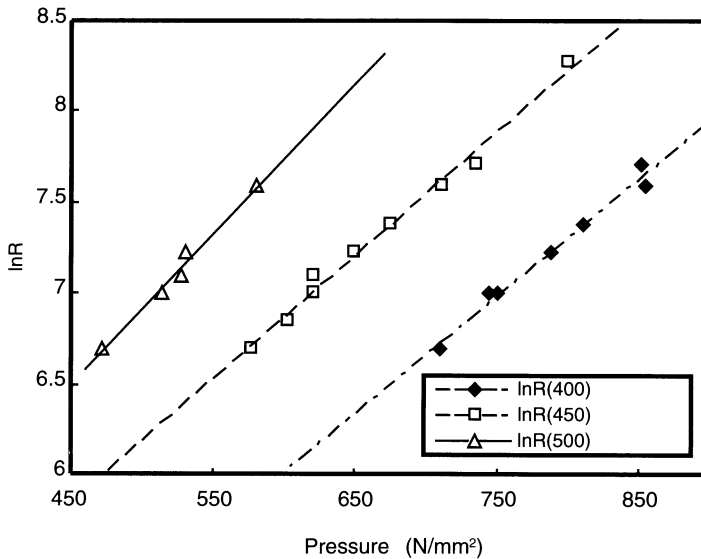
The application of this approach has been demonstrated by Sheppard, Nisarataporn and Mcshane for the extrusion over a bridge of both bars and circular tubes having a wall thickness of 2 mm. Their results are shown in Figs. 4.14(a), (b) and (c).



**Fig. 4.14(a)** Showing the correlation with Zener–Hollomon type equation for bridge die extrusion.



**Fig. 4.14(b)** Theoretical upper bound solution compared with experimental results for bridge die extrusion.



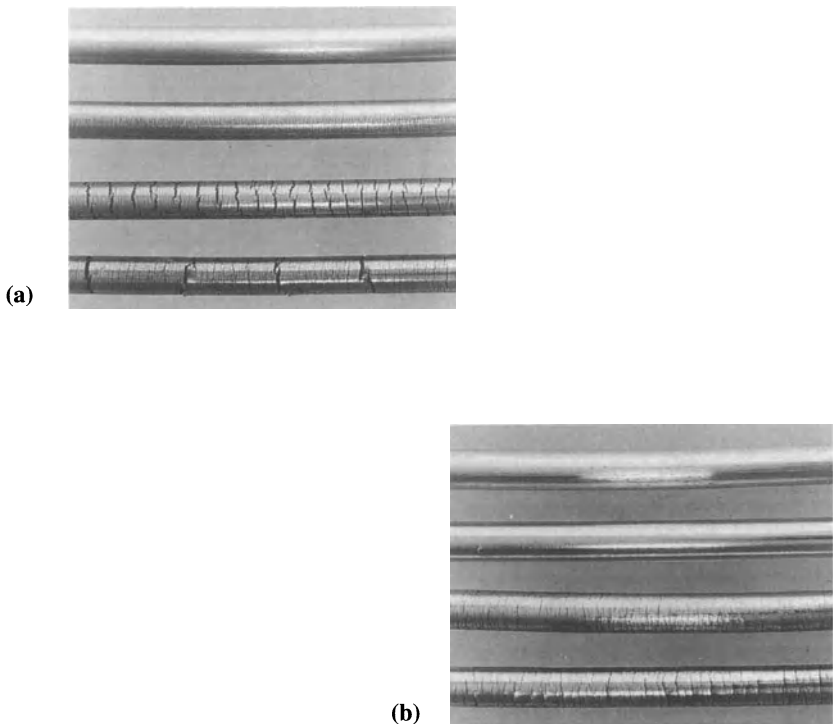
**Fig. 4.14(c)** Showing the relationship between temperature and pressure for varying bridge die extrusions (400°C, 450°C, 500°C).

## 4.7 SURFACE QUALITY CONSIDERATIONS

It is accepted that the process variables, temperature and speed (strain rate), determine the acceptability of surface quality in the extrudate. During extrusion of aluminium alloys the temperature term appears to be dominant while in the extrusion of metals at higher temperatures both speed and temperature effects are important. Essentially, Al extrusion is performed unlubricated. It should be noted that temperature and speed are not independent variables and hence correlation between surface quality and temperature-compensated strain rate should be the objective. The surface quality in most extrusions depends upon the stress conditions obtaining near the die land regions. If the tensile friction force exceeds the fracture stress of the materials, then some tearing is encountered. Additionally if the heat generation near the die land area increases the local temperature in excess of the solidus point, localized melting can occur, which can cause severe cracking of the surface. This temperature generation is a function of the alloy chemistry, extrusion speed, extrusion ratio, aspect ratio, container temperature and the initial billet temperature. Much of the heat generation to the surface occurs through the dead metal zone/deformation zone shear band which terminates on the face of the die immediately prior to the die land area, resulting in a steep rise in the temperature as the material approaches the die land. It is obvious that the heat generation increases with an increase in the extrusion ratio and the

ram velocity. It is also closely related to the initial billet temperature such that differences in billet heating tend to be equalized by the work generated. Heat generation is comparatively less in the indirect mode of extrusion compared to the direct mode. The major effect of this heat generation is to restrict the speed of operation at high temperatures. Another defect commonly found in aluminium extrusion is die lines and surface scoring. It is believed that the die lines are caused by the entrapment of coarse inclusions ( $3\text{--}4\ \mu\text{m}$ ) between the metal and the die bearing area. These defects and their origin will be dealt with in Chapter 6 which considers 6XXX alloys in which these defects are more important to product quality. In high-strength aluminium alloys where this defect has only a secondary importance to the mechanical property requirements (because the surface often has to be machined to remove recrystallized layers) the defect is tolerated provided the die lines are not so coarse that stress concentrations arise. The surface finish can thus be categorized into one of the three types:

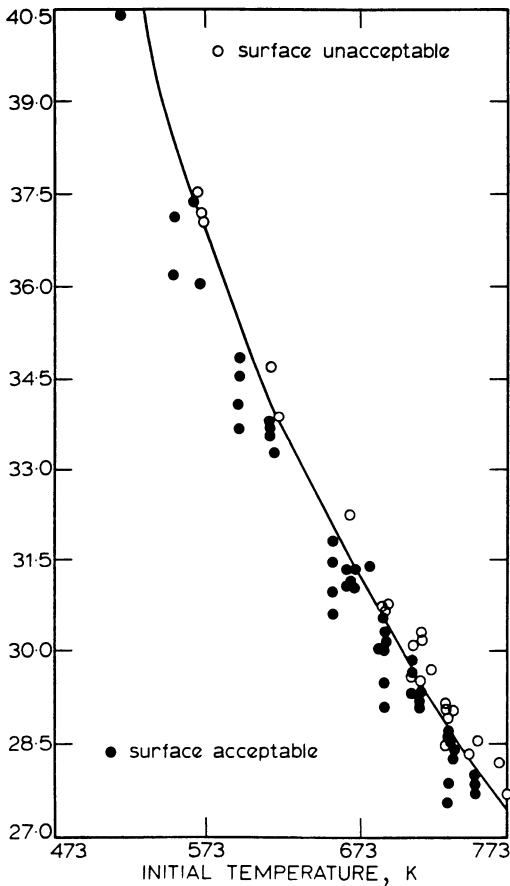
- no cracking;
- cracking commences at some distance along the extrudates;
- cracking commences from the beginning.



**Fig. 4.15** Typical examples of extrude surfaces; (a) direct extrusion,  $T = 350, 400, 440$  and  $480^\circ\text{C}$ ; (b) indirect extrusion,  $T = 350, 400, 440$  and  $480^\circ\text{C}$ .

Typical examples are shown in Fig. 4.15. The trend is similar for both modes of extrusion. However, the severity of cracking is less in the indirect mode than in the direct mode. The danger of cracking increases in shaped extrusions near the re-entrant corners. In sections containing ribs then, in an extreme case there is a danger of the rib disintegrating.

Sheppard and Tatcher previously investigated the incidence of speed cracking in the rod form of AA5456 alloy [30] and showed that the Z parameter may be used to correlate results over widely varying temperature and speed conditions. Figure 4.16 shows that there is a clear division between acceptable and unacceptable surface qualities and this division may be represented by a continuous function yielding the two inequalities:



**Fig. 4.16** Experimental evidence of division between acceptable and poor surfaces for AA5454 alloys.

for acceptable surface quality:

$$\ln\left(\frac{Z_i}{A}\right) \leq \frac{6.35 \times 10^{20}}{T^{7.06}}$$

for unacceptable surface quality:

$$\ln\left(\frac{Z_i}{A}\right) \geq \frac{6.35 \times 10^{20}}{T^{7.06}}$$

The variation in slope of the dividing function illustrates the obvious point that, at lower billet temperatures, higher reduction and greater ram speeds may be used before the onset of plastic instability or incipient melting at the surface. This figure also illustrates that the basic mechanism of surface damage is the balance between the friction forces imposed in the die land area and the resistance of the material to deformation represented by its high temperature flow stress. Such a mechanism explains the incidence of die lines in the aluminium industry where pick up on the die leads to high localized friction forces.

The discussion concerning the flow stress parameters in section 4.2 has indicated that the three parameters  $\alpha$ ,  $n$  and  $\Delta H$  are dependent. It is thus sensible to express the onset of unacceptable surfaces by formulae of the type:

$$\frac{1}{n} \ln\left(\frac{Z_i}{A}\right) \leq aT^{-b}$$

This type of analysis has also been applied to the observed surfaces of shaped extrusions in 2024 alloy [41] and introducing the  $\lambda^2$  modification for shaped extrusion acceptable surfaces were achieved when:

$$\frac{1}{n} \ln\left(\lambda^2 \frac{Z_i}{A}\right) \leq \frac{2.113 \times 10^9}{T^{2.866}}$$

for direct extrusion and

$$\frac{1}{n} \ln\left(\lambda^2 \frac{Z_i}{A}\right) \leq \frac{2.4 \times 10^{10}}{T^{3.57}}$$

for indirect extrusion.

These two criteria are shown in Fig. 4.17, and Fig. 4.18 shows the criteria plotted for a number of Al-alloys.

When interpreting this figure the reader should recall that, for any of the loci shown, surface defects will be encountered if the extrusion conditions are such that they are described by a point which lies above and to the right of the appropriate locus. Thus, for example, 7XXX alloys are clearly difficult to extrude, which is the case for all of the so-called hard alloys. It may also be observed that for alloy 6063 pick-up becomes a problem before the stage of incipient melting



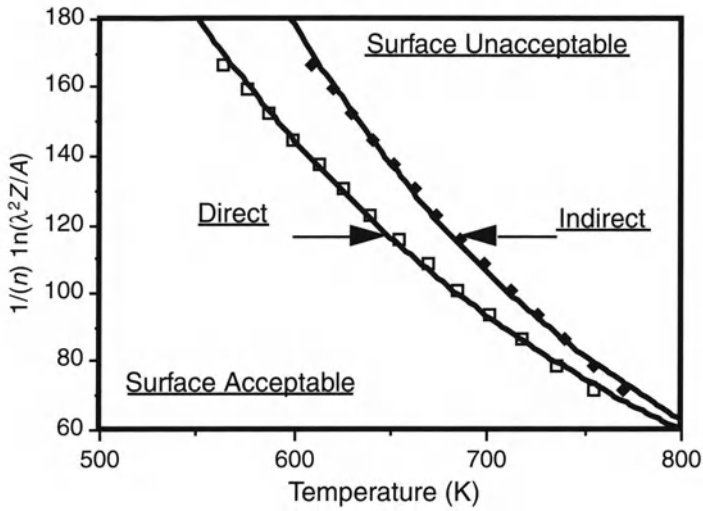


Fig. 4.17 Surface criteria for extrusion of 2024 alloy shapes.

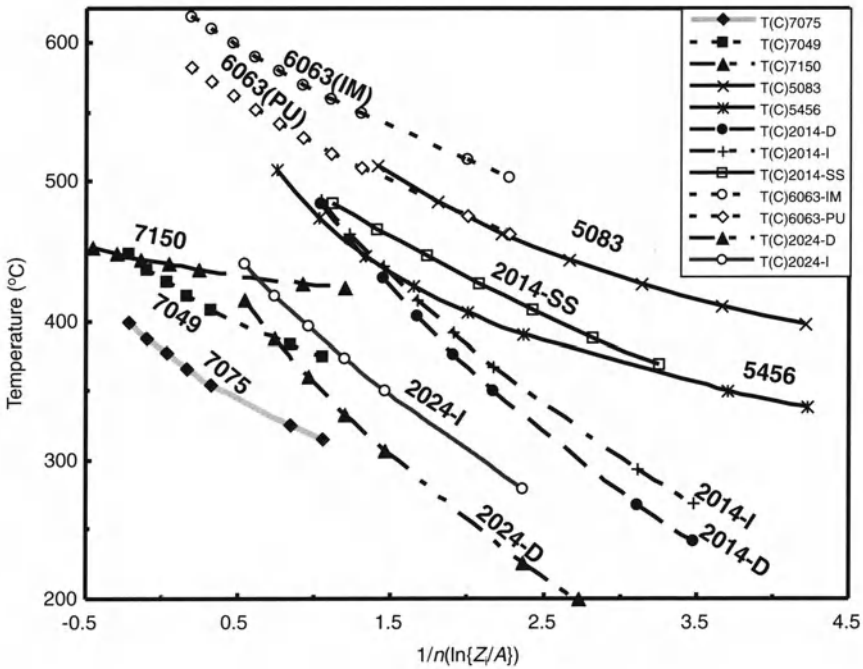


Fig. 4.18 Surface acceptability criteria for some aluminium alloys.

is reached. In this diagram the apparent anomaly is the 5XXX alloys but note that their loci lie to the left (or low temperature region) of the diagram such that their extrudability is limited because in the practical case there will be insufficient pressure to extrude.

#### 4.8 PROCESS-STRUCTURE RELATIONSHIPS

Most of the research reported using materials which dynamically recover has been related to the extrusion of aluminium and its alloys, although there are less thorough investigations reported on zinc and titanium. The extruded subgrain size has clearly been established to be a function of the temperature-compensated strain rate and a relationship of the form:

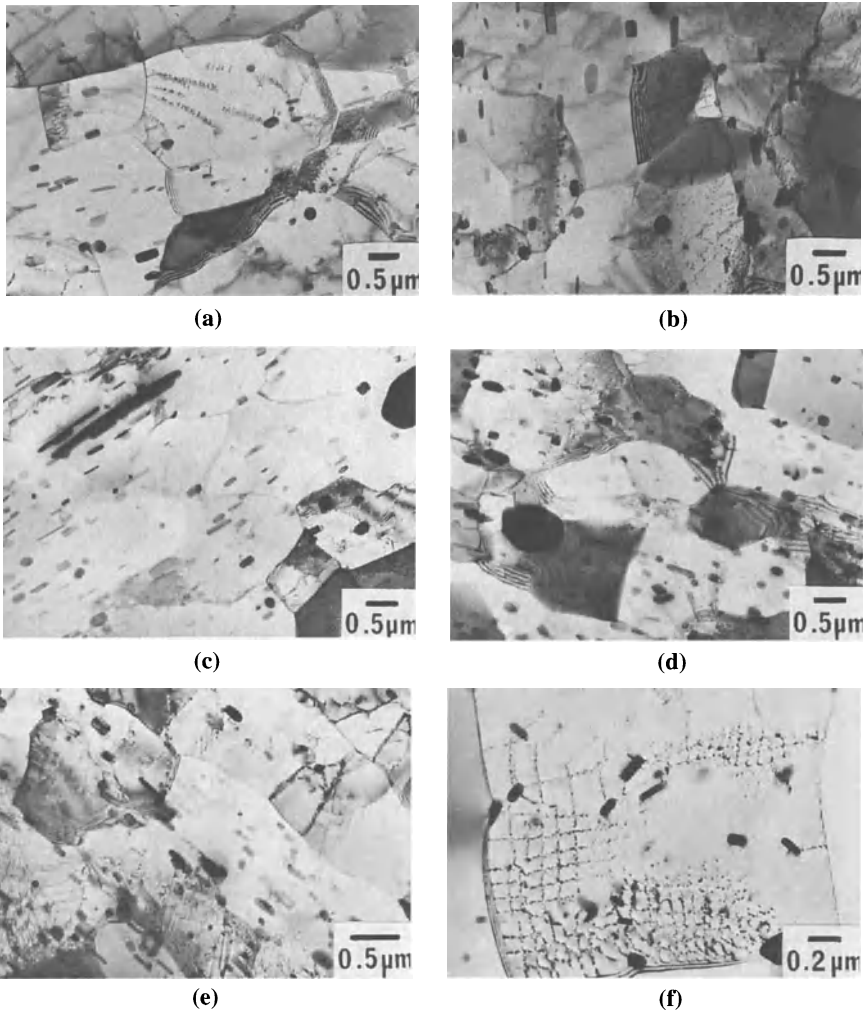
$$d^{-m} = x + y \ln Z \quad (4.10)$$

has been clearly established for most commercial alloys usually after the  $Z$  value has been calculated with the temperature rise being incorporated and written  $Z_c$ .  $Z_1$  then refers to the original conditions.

The substructure will thus vary considerably according to the control exercised during processing. The F-temper substructures produced in an Al-Cu-Si-Mn-Mg alloy (AA 2014) at varying  $Z_c$  values [43] are shown in Fig. 4.19 and a typical variation from centre to edge of an extrusion in Fig. 4.20. When extruding at a nominal mean equivalent strain rate of  $6.5 \text{ s}^{-1}$  and an initial billet temperature of 573 K the temperature at the end of the extrusion cycle has risen to 690 K resulting in a variation in  $\ln Z$  of 5.55. Transmission electron micrographs were obtained from extrudates quenched at the die and optical microscopy revealed a fibrous structure to be present over the complete extrudate cross-section. They clearly indicated a variation in subgrain size with varying temperature-compensated strain rate, and hence an increase in subgrain size from front to rear of the extrusion. In this work the variation in subgrain size throughout an extrusion cycle was investigated for three extrusion runs. The calculated variations in  $\ln Z_c$  for the three tests were: (a) 26.83–29.18, (b) 30.48–33.05, and (c) 31.17–34.57. These results clearly fit the same equation as those results obtained from differing individual extrusions. The regression fit to those results was:

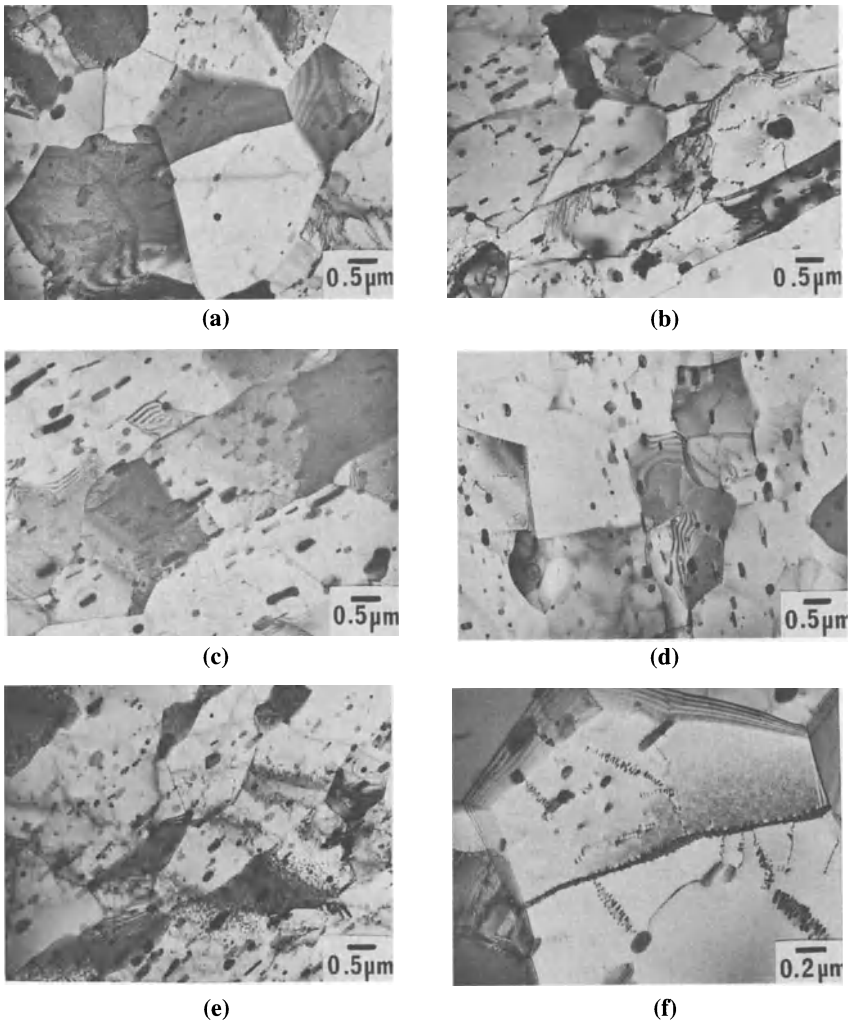
$$d^{-1} = 0.15 + \ln Z_1 - 3.5$$

Many of the alloys which soften by dynamic recovery are subjected to heat treatment after extrusion in order to obtain specific properties. The as-extruded structure might, therefore, appear to be a somewhat irrelevant parameter to investigate. However, reference to Figs. 4.19 and 4.20 indicates a large volume fraction of precipitate at subgrain boundaries and also subgrain boundaries pinned by larger precipitate particles. This is because some precipitation has occurred during homogenization and cooling to extrusion temperature whilst some has occurred during the extrusion. It might, therefore, be expected that the substructure



**Fig. 4.19** Substructures observed in longitudinal plane of direct extrudates of 2014 alloy; (a)  $T = 480^{\circ}\text{C}$ ,  $\ln Z = 22.9$ ; (b)  $T = 440^{\circ}\text{C}$ ,  $\ln Z = 23.8$ ; (c)  $T = 400^{\circ}\text{C}$ ,  $\ln Z = 24.9$ ; (d)  $T = 350^{\circ}\text{C}$ ,  $\ln Z = 26.4$ ; (e)  $T = 300^{\circ}\text{C}$ ,  $\ln Z = 27.5$ ; (f) screw dislocations forming distinctive network providing nucleation sites for the ageing process.

will affect both optimum solution soak and ageing times. This feature has been thoroughly investigated for both 2014 and 2024 alloys. In 2024 alloy [44], for example, the extrudates contained a well recovered subgrain structure whose sizes were modified by the presence of the inclusions and precipitates. Change in section shape was observed to produce little variation in the substructure. Figure 4.21(a) shows the variations in the subgrain sizes with the extrusion parameters in which the initial billet conditions have been used to calculate the temperature-compensated strain rate  $Z$ . A consistent variation in the subgrain size was



**Fig. 4.20** Variation of substructure from centre to edge; (a) direct extrusion  $\ln Z = 25.87$  centre; (b) direct extrusion  $\ln Z = 25.87$  edge; (c) indirect extrusion  $\ln Z = 26.81$  centre; (d) indirect extrusion  $\ln Z = 26.81$  edge; (e) direct extrusion  $\ln Z = 27.5$  centre; (f) direct extrusion  $\ln Z = 27.5$  edge showing advantageous helical dislocations.

observed between the indirect and direct modes of extrusion. This difference is inevitable because of the differences in heat generation between the two modes and the impossibility of predicting the temperature with sufficient accuracy at the point of sampling. Nevertheless the linear nature of the relationships gives some confidence that structural control could be effected.

All precipitation hardening aluminium alloys are normally given a solutionizing anneal in order to eliminate any process variations, prior to ageing treatment.

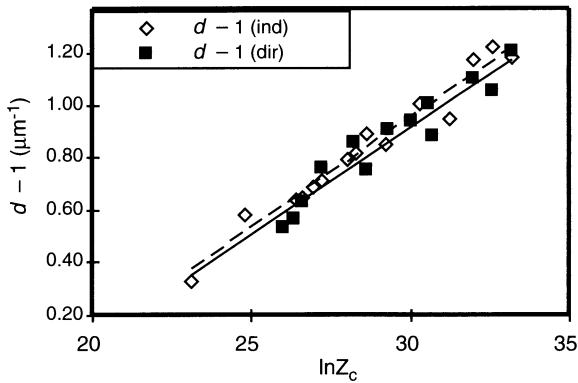


Fig. 4.21(a) Variation in subgrain size with Zener-Hollomon parameter.

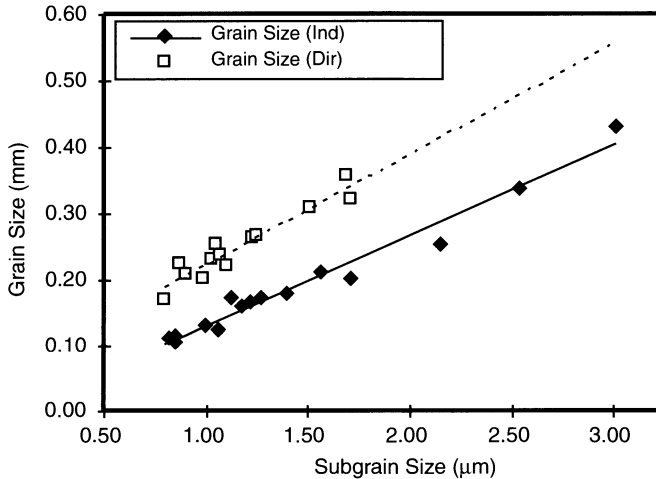


Fig. 4.21(b) Showing linear relationship between subgrain and recrystallized grain size.

This treatment generally varies between 20 min and 2 h at a temperature in excess of 470°C. This will necessarily introduce structural changes. Figure 4.21(b) illustrates the linear relationship between the as-extruded subgrain size and the recrystallized grain size in those areas where recrystallization has occurred. This is a strong indication that nucleation has been primarily by subgrain coalescence offering the possibility of grain size control by suitable attention to the processing parameters. In this alloy the desired structure after solution soak is usually one exhibiting as little recrystallization as possible, but in some applications a structure with as small a grain size as possible is preferred.

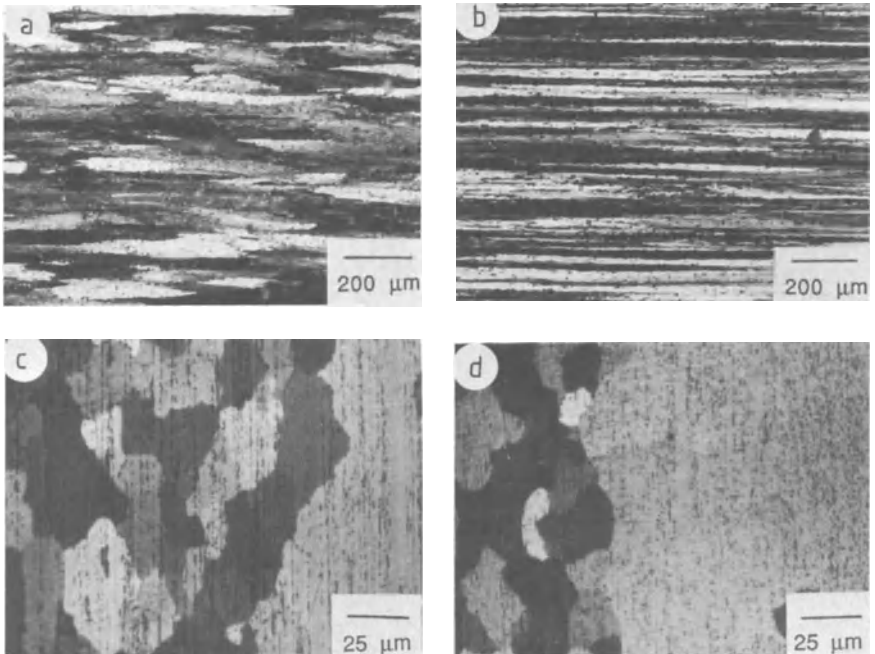
## 4.9 RECRYSTALLIZATION

The work described in reference [36] is concerned with the effects of hot extrusion parameters on the recrystallization kinetics of four commercial alloys (AA2024, AA5052, AA5056 and AA5083). This allowed the parameters described in equation 3.12 to be evaluated and to ascertain the effect of the process variables on the recrystallized structure.

### 4.9.1 Structure after extrusion

All aluminium alloys after extrusion and press quenching exhibit two types of structure. The first contains a fibrous core of extruded grains with heavily sheared grains along the periphery, normally observed in low-temperature extrusions. The second type consists of the fibrous core surrounded by a shell of recrystallized grains. Recrystallization is also observed in the indirect mode but to a much smaller extent than in direct extrusions.

The structure of typically extruded rods is shown in Fig. 4.22. At all temperatures, the structure along the centre of the rods is predominantly fibrous. The

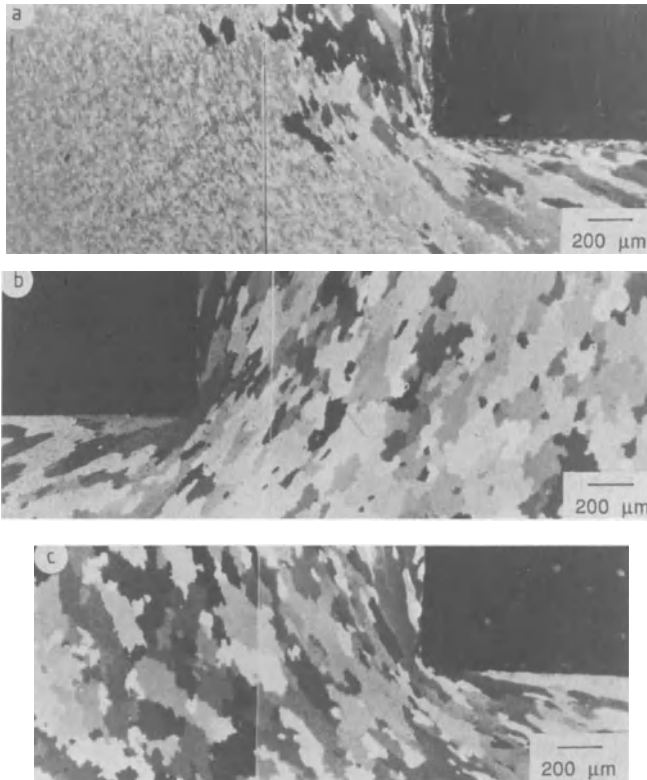


**Fig. 4.22** Microstructure of extrudates after press quench; (a) extrudate periphery,  $T = 300^{\circ}\text{C}$ ; (b) extrudate centre,  $T = 300^{\circ}\text{C}$ ; (c) extrudate periphery,  $T = 450^{\circ}\text{C}$ ; (d) extrudate periphery (indirect extrusion),  $T = 450^{\circ}\text{C}$ .

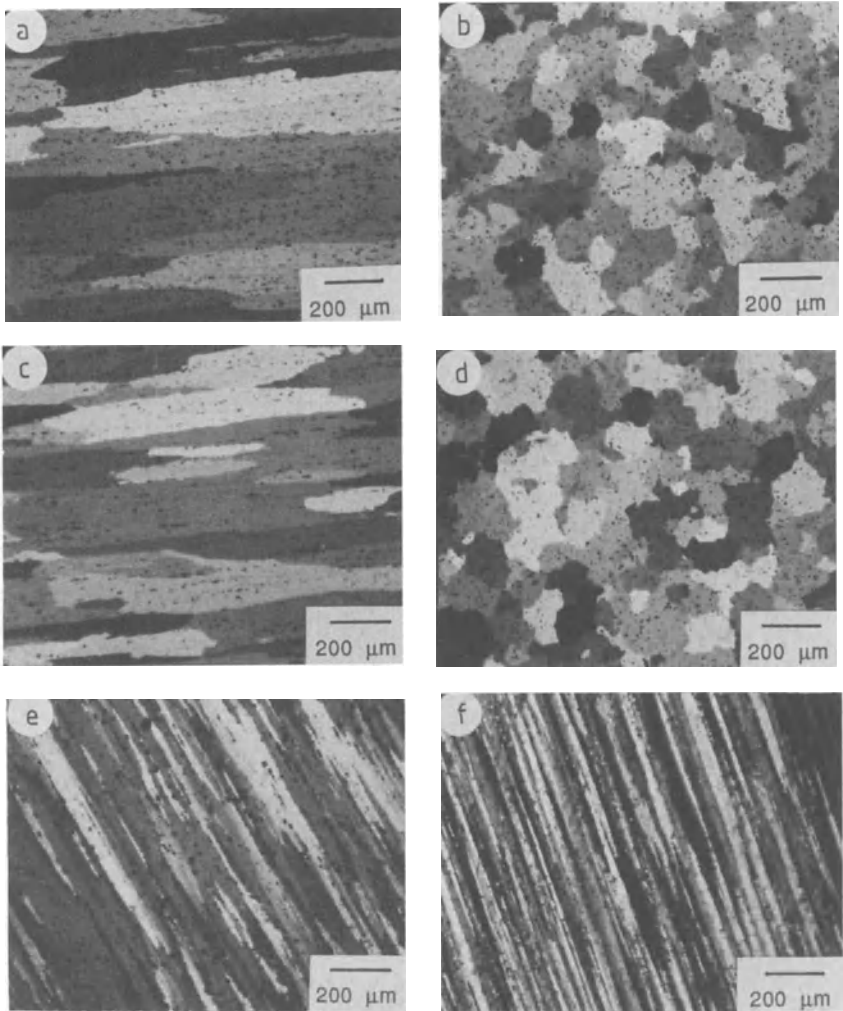
surface of the extrudates contained a predominantly recrystallized structure in the high-temperature extrudates. In the low-temperature (<350°C) extrudates there were some signs of recrystallization, but the grain structure was very fine and equiaxed compared with that of the high-temperature extrudates. The structures along the transverse plane were mainly equiaxed, which indicated that the grains could be considered equivalent to fibres.

Additionally, the extent of recrystallization varies along the periphery of shaped extrusions. Thus near the re-entrant corners the recrystallized shell has a higher thickness than the average elsewhere (Fig. 4.23) but is generally observed to be in correspondence with standard stress concentration factors used in mechanical design for the relevant geometries.

The structural modification after the solution heat treatment is shown in Fig. 4.24. Subsequent to the solution anneal the extrudates were heat treated at temperatures in the range 160–190°C for a period of 16–24 h. The optical micrographs of the low temperature extrudate centre and edge are shown in Figs. 4.24(a)–(d);



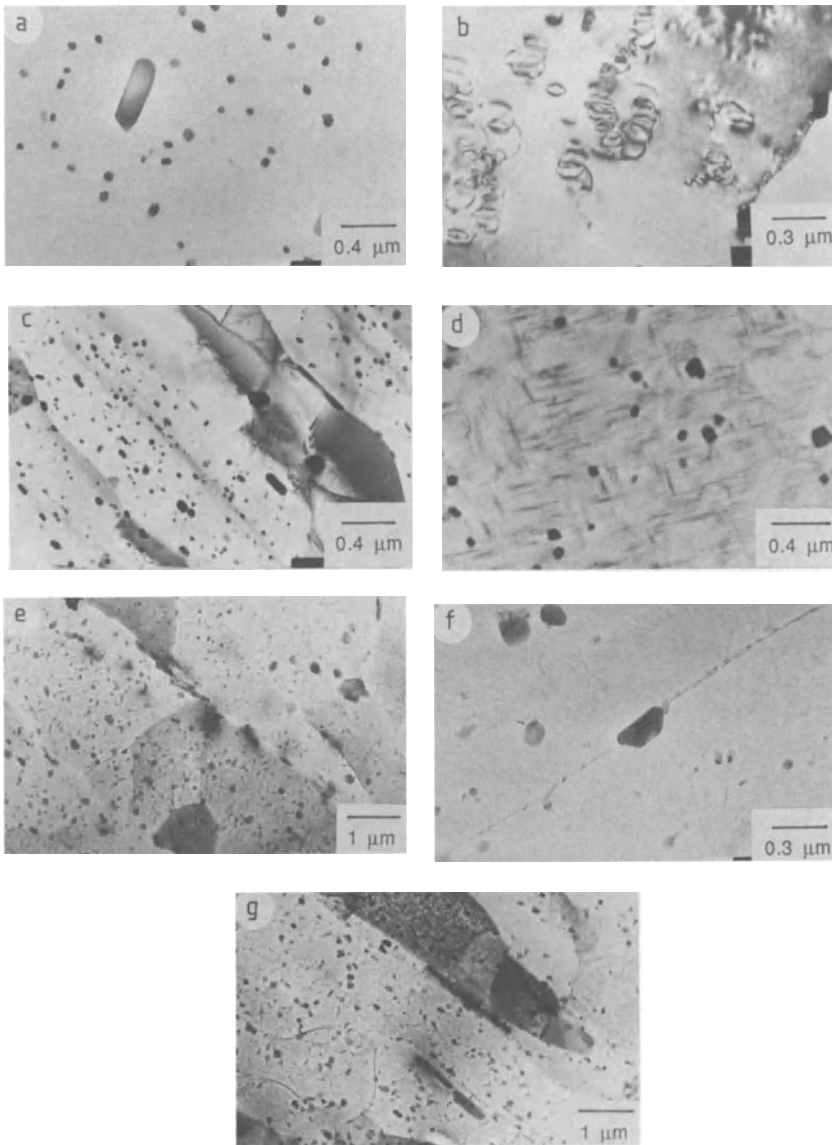
**Fig. 4.23** Microstructure of shaped extrudates after press quench and solution soak; (a) T-section, press quench,  $T = 450^{\circ}\text{C}$ ; (b) T-section, 0.5 h soak at  $500^{\circ}\text{C}$ , quench; (c) U-section, 0.5 h soak at  $500^{\circ}\text{C}$ , quench.



**Fig. 4.24** Microstructure of extrudates after 500°C solutionizing followed by water quench; (a) and (b) 350°C extrudate, 0.5 h soak, quench, longitudinal and transverse; (c) and (d) 350°C extrudate, 1.0 h soak, quench, longitudinal and transverse; (e) 450°C extrudate periphery, 1 h soak, quench; (f) 450°C extrudate core, 1 h soak, quench.

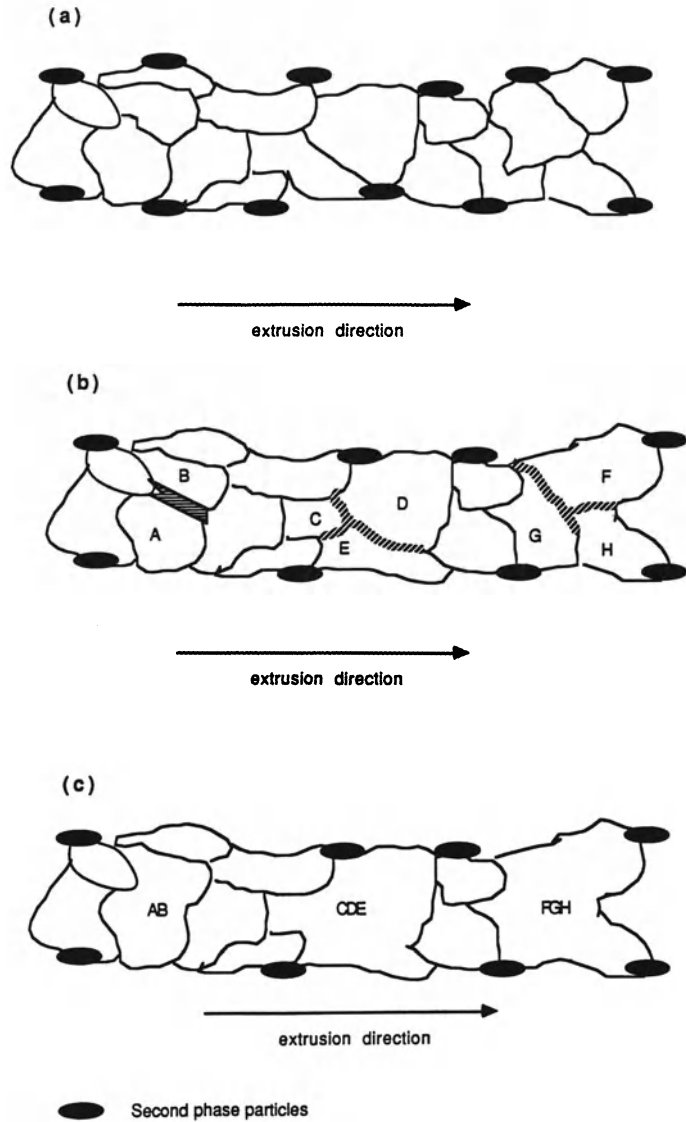
from these it is clear that recrystallization has occurred during solutionizing and has spread to the core of the extrude. Conversely the high-temperature extrudates show little further recrystallization at the periphery and the core remained predominantly unrecrystallized (Figs. 4.24(e) and (f)). This is confirmed by high resolution TEM observations (Fig. 4.25). Nevertheless, the subgrains have grown in size as part of the recovery process. The structure of the low-temperature extrudates shown indicates that recrystallization occurred extensively and progressed





**Fig. 4.25** Substructures of extrudates after 500°C solutionizing followed by water quench and after ageing at 160°C quench; (a) 300°C extrudate, 1 h soak, quench – showing lack of substructure; (b) 300°C extrudate, 1 h soak, quench – showing helical dislocations; (c) 450°C extrudate 1 h soak, quench – showing retention of substructure; (d) 350°C extrudate, peak aged 18 h at 160°C T6 – showing Widmanstätten type precipitation; (e) 450°C extrudate peak aged T6 – showing retention of substructure; (f) 450°C extrudate, peak aged T6 – showing narrow GP zone; (g) 450°C extrudate, peak aged T5 – note similarity to T6 structure.

almost to completion (Figs. 4.25(a) and (b)). Figure 4.25(b) also shows the importance of the quench in promoting helical dislocations which act as prime sites for precipitation during the extrusion process. The important feature of the retention of the subgrain structure in the high-temperature extrudates is illustrated in 4.25(c) and the similarity in T5 and T6 structures can be seen by comparing Figs. 4.25(c)

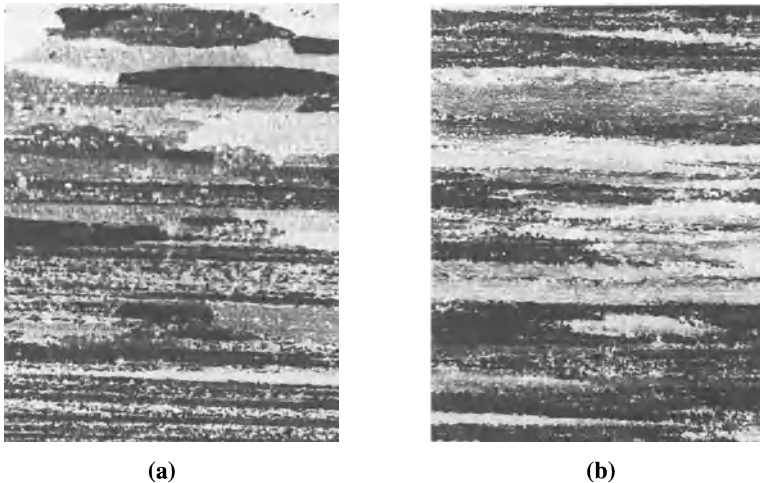


**Fig. 4.26** Mechanism of grain growth. Sequence is (a) → (b) → (c)

and (e). Figure 4.25(f) shows the existence of a very narrow precipitate-free zone at the subgrain boundary, another important feature in promoting excellent fracture and corrosion properties (see below). The structure in Figs. 4.24(a)–(d) shows the pinning effect of the  $\text{Al}_6\text{Mn}$  dispersoids on the advancing high-angle grain boundary. It can be seen that, even after recrystallization, the grains retain the elongated wrought structure, thus giving an impression that the growth rate during recrystallization may be higher along the extrusion direction than in the transverse direction. The dimension of the grain in the transverse direction is much finer than that in the longitudinal direction. This mechanism of grain growth was observed in both high- and low-temperature extrusions and is shown diagrammatically in Fig. 4.26.

It would appear that the size and volume fraction of precipitate will therefore depend not only on the solution soak and ageing times but also on the nature of the as-extruded structure. Thus an important conclusion must be that any optimum solution soak and age cycle must be associated with a given process condition.

Finally in this section, we turn our attention to the structures produced after extrusion of the non-heat-treatable alloys in the 5XXX series. Each of the alloys also exhibited an unrecrystallized core surrounded by recrystallized material, with the exception of 5052 which recrystallized completely between die exit and quench for all extrusion conditions. This illustrates the effect of drag forces caused mainly by the Mn precipitates in 5XXX alloys 5052 having no Mn alloying component. The alloys 5456 and 5083 showed similar structures; illustrations of the recrystallized surface and fibrous appearing core can be seen in Fig. 4.27. We should note, at this stage that 5456 has been reported to be the only commercial Al-alloy to exhibit dynamic recrystallization [44]. The apparent greater volume fraction of recrystallized grains is thus actually greater than 5083.



**Fig. 4.27** Alloy 5456,  $R = 10:1$ ,  $T = 460^\circ\text{C}$ ,  $V_f = 12.6 \text{ mm s}^{-1}$ ; (a) peripheral structure; (b) internal structure. Optical  $\times 64$ .

#### 4.9.2 Volume fraction recrystallization in the F-temper and after solution soaking

The volume fraction of material recrystallized may be established by image analysis and the results submitted to multiregression analysis based on equations 3.12. Figure 4.28 compares the theoretical and experimental results obtained for the various alloys and it is clear that the form of the equations must be correct.

Hence for materials in the F-temper, for example alloy 5456:

$$\ln \ln \left\{ \frac{1}{1 - X_v} \right\} = -0.18 + 3.14 \ln t + 1.25\lambda^2\dot{\epsilon} + 2.63 \ln \lambda^2 R + 0.5 \ln \lambda^2 \frac{Z}{A} - \frac{11580}{T}$$

and for materials in the solution soaked condition (2024):

$$\ln \ln \left\{ \frac{1}{1 - X_v} \right\} = -7.45 + 0.043\lambda^2\dot{\epsilon} + 1.16 \ln \lambda^2 R + 0.039 \ln \lambda^2 \frac{Z}{A} + 0.012 (T_s - T_b)$$

We may now use these equations to investigate the effect of variables on the volume fraction recrystallized. It is clear that the operator will not be interested in the form of the equations as presented above but will require the influence of parameters to be couched in terms of the volume fraction recrystallized  $X_v$ . This can clearly be achieved by taking the double exponential of each equation.

Considering first the effect of temperature on the extrusion of the 5XXX alloys, Figs. 4.28/29 indicates that the more highly alloyed 5456 is more sensitive to temperature and that for each alloy the volume fraction recrystallized decreases when the temperature exceeds some value which is in the region of 450°C. This is a direct result of the driving force diminishing because it is largely a function of the dislocation density whilst the drag force of the Mn particles remains sensibly constant. At higher strain rates (i.e. higher extrusion ratios and ram speeds)

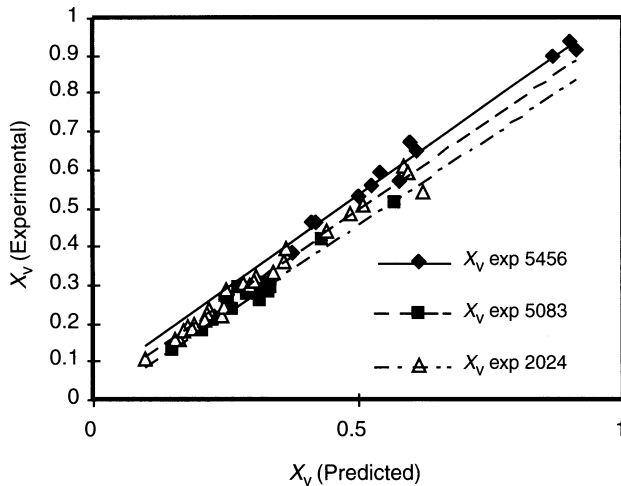
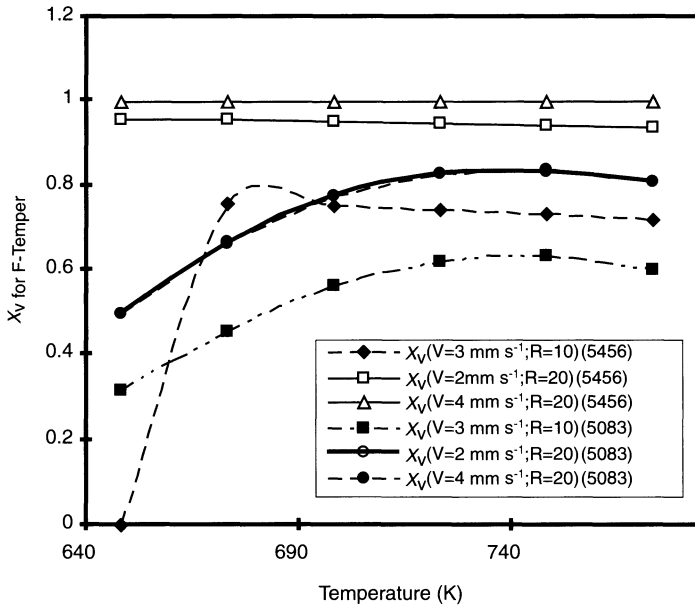


Fig. 4.28 Comparison of the theoretical form of equation with the experimental results.



**Fig. 4.29** Effect of extrusion temperature on recrystallization in 5XXX alloys.

the alloy 5456 almost completely recrystallizes at each test temperature whilst at lower strain rates it exhibits an unusual discontinuous behaviour. This is a direct result of the fact that this is the only alloy in the AA specifications which dynamically recrystallizes by a mechanism involving increased pinning forces due to the higher Mg content producing Mg–vacancy interactions which decrease the propensity for dislocation climb. Figure 4.30 illustrates the effect of extrusion ratio and also shows the more rapid kinetics in the 5XXX alloys compared to the 2024 alloy. This is caused by the increase particle count in the 2024 alloy and the higher Mg levels in 5456 and 5083. We also note that the form of the curves are different with the 5456 alloy again exhibiting two turning points. Recrystallization for the alloy 2024 when directly extruded is shown in Fig. 4.31 which shows that the volume fraction recrystallized in these alloys is much lower under all operating conditions and that parameters could be controlled such that zero recrystallization occurs. In general this would require high temperatures with the incumbent productivity problems associated with low ram speeds. The figure also shows the significant effect of the shape factor and hence the practical problems encountered when extruding the high-strength heat-treatable alloys. Such evidence as exists [45] would suggest that alloys in the 6XXX series exhibit recrystallization kinetics which are more similar to the 2024 than the 5XXX alloys, in which the volume fraction recrystallized is greater at lower temperature caused by the outer layers being more highly deformed and subsequently reheated by the interior of the extrude prior to the quench. Figure 4.32 illustrates the effect of the solution treatment in which some further recrystallization is

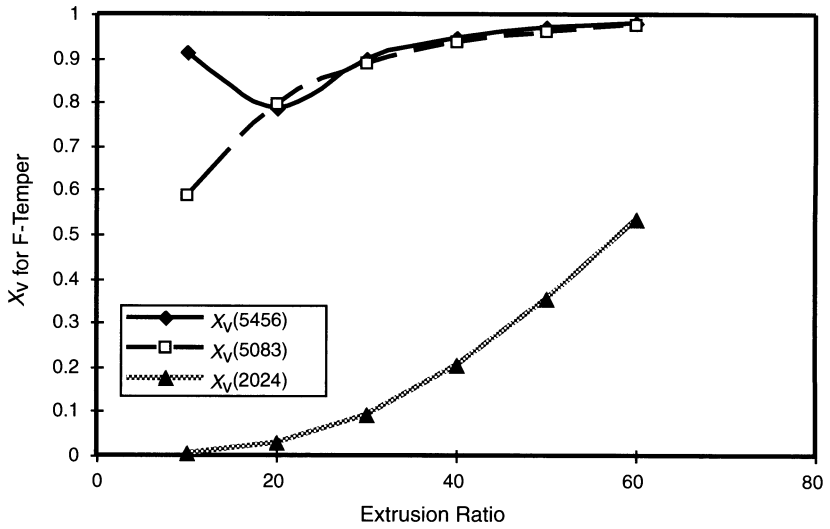


Fig. 4.30 Effect of extrusion ratio on volume percentage recrystallized.

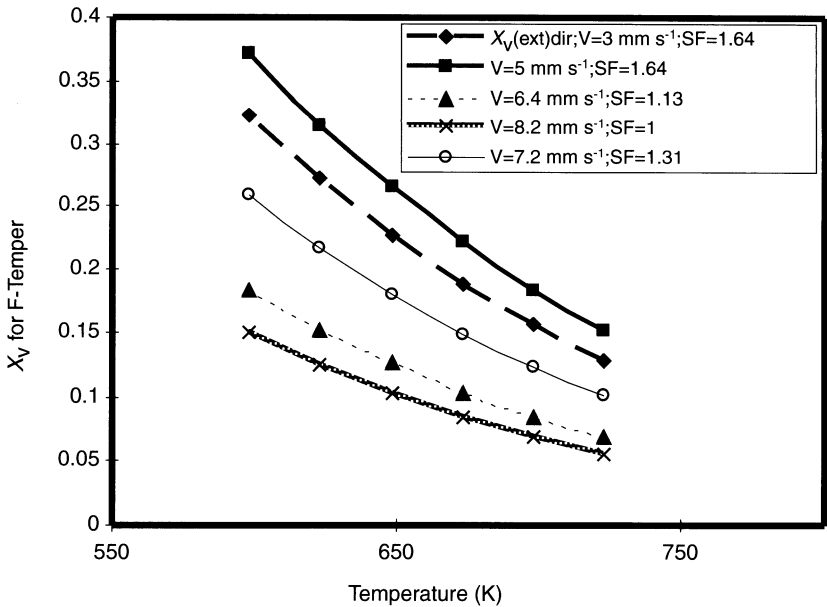


Fig. 4.31 Recrystallization in 2024 alloy, direct extrusion.

observed. However, if extrusion conditions ensure that the subgrain size is as large as possible there is little driving force for further activity (compare the lower curves in Figs. 4.33 and 4.34). Finally Fig. 4.33 shows the significant advantage

of indirectly extruding the 2024 alloy; the solution treated structure being far more acceptable especially at lower extrusion temperatures.

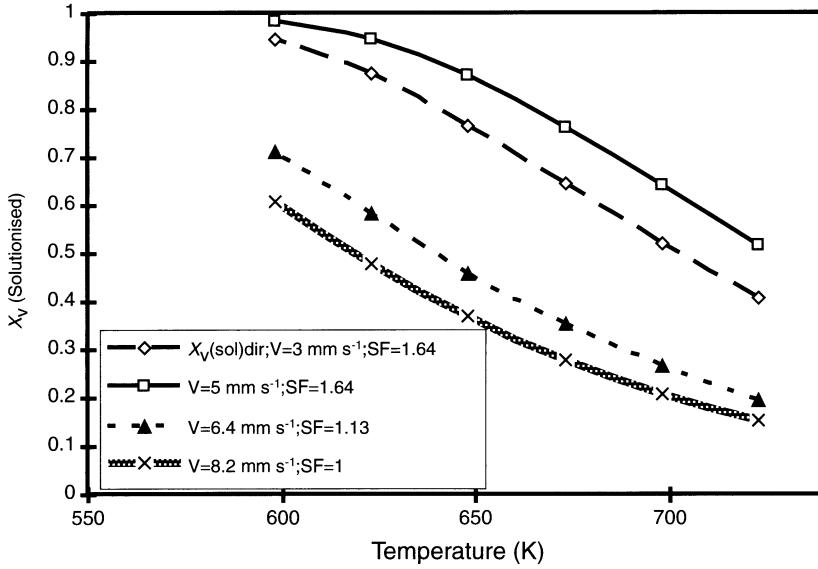


Fig. 4.32 The effect of solution treatment on  $X_v$ .

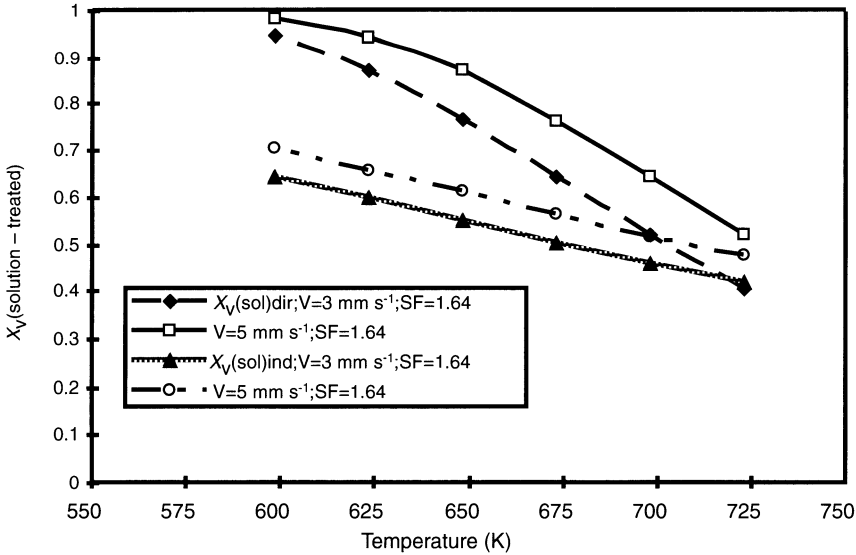


Fig. 4.33 Showing the significant advantage of indirectly extruding the 2024 alloy.

### Summary

The observations strongly suggest that recrystallization occurs by a subgrain coalescence mechanism, probably originating at grain boundaries. The 5052 alloy exhibited a fully recrystallized structure of equiaxed grains under all extrusion conditions. Each of the other alloys investigated showed only partial recrystallization which in general consisted of an unrecrystallized core surrounded by a recrystallized annulus. Equations developed from the basic Avrami type kinetics describe the behaviour of all of the alloys, both in the 'F' and the solution treated conditions with some precision and with good correlation coefficients being obtained. The equations have been formulated such that reasonably complex sections may be included in the analysis. The equations are in a form suitable for on-line control of the structure of extrusions.

## 4.10 THE RELATIONSHIP BETWEEN PROCESS PARAMETERS AND PROPERTIES

Although the structural behaviour of metals, discussed above, is clearly of fundamental importance, it is the properties arising from that structure which are of primary interest to the processor. Sheppard [42] has shown that for aluminium alloys in the F-temper, relationships can be expressed which clearly relate the properties to the temperature-compensated strain rate. Figure 4.34(a) shows relationships obtained for alloy AA5083 [46] involving the proof stress, the ultimate

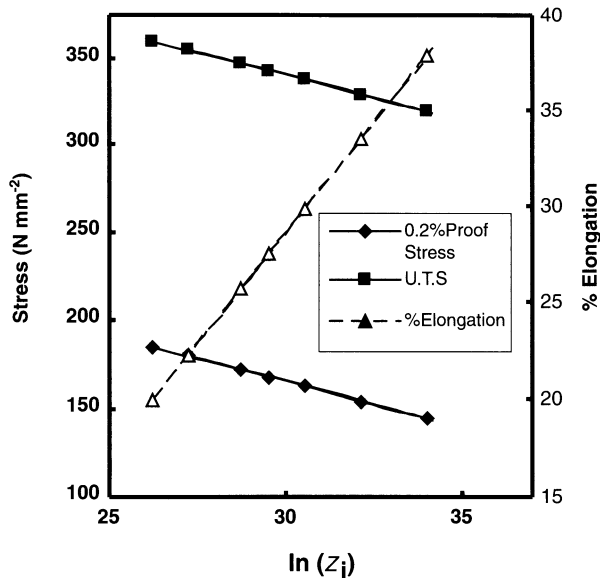


Fig. 4.34(a) Variation of properties with processing for 5083 alloy.



stress, and the total elongation. It is obvious that linear relationships exist and for this alloy may be written:

$$\sigma_{\text{proof}} = 323 - 5.25 \ln Z$$

$$\sigma_{\text{ult}} = 498 - 5.25 \ln Z$$

$$\% \text{ elongation} = -40 + 2.29 \ln Z \quad (4.11)$$

When scatter is reduced by extensive experimental work, the linear relationships may be approached with some confidence. The reader should note, however, that the results presented are for as-extruded material and are for an alloy which has been directly extruded and was observed to show negligible recrystallization. If recrystallization were to intervene then we would expect non-linear relationships but showing similar trends to the results presented since recrystallization has been shown to be lower at lower extrusion temperature (i.e. higher  $Z$  values). The relationships indicate substantial substructural strengthening which could not all be expected to be carried through the heat-treatment cycle. Hence this strengthening would be more important in 1XXX, 3XXX and 5XXX series alloys. Nevertheless, some substructural strengthening will remain after heat treatment and in the aerospace alloys a strengthening effect of  $7\text{--}8 \text{ N mm}^{-2}$  can be significant (Fig. 4.34(b)). Moreover the as-extruded structure determines the basic kinetics of the heat-treatment cycle. It is likely, therefore, that fatigue, fracture toughness and corrosion may each be improved by selecting optimum process conditions. This, of course, illustrates the basic requirement for adequate process control.

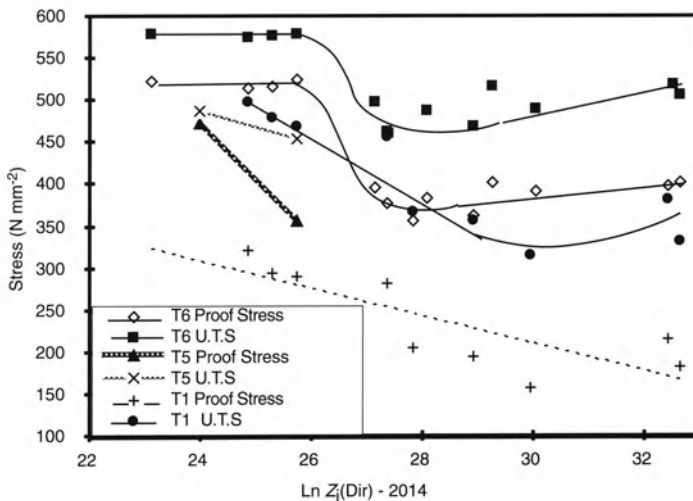


Fig. 4.34(b) Variation of properties with processing for 2014 alloy.

Figure 4.34(b) indicates that for the T5 temper (extrusion followed by ageing without a solutionizing treatment), the high-temperature extruded material had the better ageing response (similar to the T6 response) compared with the low-temperature extruded material. This confirms the suggestion that 2014 press quench aged material can develop properties at least equal to that of material heat treated traditionally. For low temperature extruded materials the T5 properties were poor. To understand this, it is necessary to understand the mechanisms of ageing. For a precipitation hardening system, two conditions must be obtained: a sufficient supersaturation of (i) the solute elements and (ii) the point defects such as vacancies. The decomposition of the supersaturated solid solution occurs by precipitation of the excess solute and this requires the migration of solute or solute clusters aided by counterdiffusion of vacancies in the aluminium lattice. In the low temper extrudates, the excess concentration of vacancies is sufficient in the press quenched state to allow precipitation of solutes in a very fine homogeneous distribution. Hence the decomposition reactions are slow and the precipitation must occur by heterogeneous means during ageing, leading to poor strength. It is also likely that a proportion of solute may have precipitated during the hot working aided by the pressure and temperature, since the operating temperature for extrusion in this case is well within the C curve for the precipitation of  $\theta$  phase. This would remove a certain amount of the solutes out of solution, leaving behind a reduced amount of solute to be precipitated in a useful form. The natural ageing in Al-Cu alloys depends primarily on the quaternary additions. Since natural ageing requires the formation of zones and metastable solute clusters at room temperature, the quaternary addition must be capable of promoting this behaviour. Traditionally, magnesium and silicon are added to improve the room-temperature ageing response. To obtain any appreciable, natural ageing response, the ratio of magnesium:silicon should be about 5:1. Since, in 2XXX alloys, the ratio is far below this required level, natural ageing is severely restricted.

Now, with regard to the influence of processing on mechanical properties, two trends may be observed, one due to mechanical working and the other due to heat treatment. The material worked at high temperature possessed high strength (PS and UTS) consistently in all tempers. Thus, in the T1 temper, the difference in PS and UTS are about 23 and 16%, respectively, between the high- and low-temperature extruded materials and in the T6 temper, the high-temperature extruded materials have a PS and UTS 16% higher than those of the low temperature extruded materials. Also the PS for high-temperature extrudates increases by about 23% on heat treatment, while for the low-temperature extrudates the increase is about 32%. The increase in the UTS is negligible for both extrusion temperatures. The work-hardening ability, measured by the work-hardening exponent in the function  $\sigma = k\varepsilon^n$  (where  $\sigma$  is low stress and  $\varepsilon$  is strain also decreases with heat treatment for both extrudate temperatures.

It is well known that, in aluminium alloys, especially the heat-treatable alloys, the main contribution to strength arises from the interaction of the precipitate formed during heat treatment with mobile dislocations. This contribution may be:

- by offering resistance to the motion of the dislocation because of the difference in the shear modulus between the precipitate and the matrix;
- due to the chemical differences of the precipitate from the matrix;
- due to the coherency strains between the precipitate and the matrix;
- due to Orowan looping of the dislocations, giving rise to pile-ups in front of incoherent precipitates.

However, there is a contribution to strength, albeit minor, from the residual substructure present in the material, especially when the material is deformed at high temperatures. On comparing the structures described above, it can be seen that in the high-temperature extrudates in the T6 temper, both contributions are evident, while in the low-temperature extrudates the contribution from the substructure vanishes due to complete recrystallization during solutionizing; this represents about 16%. However, comparing the T5 and T6 strength of the high-temperature material, it becomes clear that the contributions cannot be viewed simply as additive, since the dislocation substructure always interacts with ageing by offering heterogeneous nucleation sites for precipitation in which the substructure itself may be destroyed concurrently and, hence, reduce that contribution to the strength. It can also be discerned that for the 2014 alloy the absence of a separate solutionizing for the low Z extrudates does not reduce the strength drastically compared with the T6 strength levels, while also retaining other properties at acceptable levels. For the low-temperature extrudates, however, the absence of a solutionizing reduces the strength levels by about 30% in the T5 temper as compared with the T6 temper. These data, in conjunction with the ageing response indicate again that 2014 alloy can be press quenched and aged to the same mechanical property levels as can be achieved by conventional heat treatments, providing the deformation temperature is sufficiently high and the prior homogenization is such that all the precipitate-forming elements (copper, magnesium and silicon) are maintained in solution during deformation.

The damage tolerance of 2XXX [43,48] alloys have been investigated. The fracture surfaces obtained from short rod fracture toughness samples indicated the crack plane to be in the extrusion direction (the grain flow direction). The fracture of T1 temper material was predominantly transgranular, irrespective of the extrusion temperature, although occasionally some splitting along the boundary was observed. The surfaces obtained after ageing and solutionizing (T6 temper) showed that at the high extrusion temperature the fracture propagated along the high angle grain boundaries in many regions and, in some regions, across the grain, resulting in a mixed mode fracture, very fine dimples along the grain surfaces coexisting with larger dimples associated with coarse particles. In the low-temperature extrudate the fracture plane contains a number of ridges and valleys having a steplike appearance, which can be explained only if the main crack has been allowed to branch across the grain at an angle to the crack plane, possibly assisted by some coarse shear across the grains. In the T5 temper, fracture occurred once again as in that of T6 temper by the process of intergranular splitting.

Two important microstructural features of interest affecting the fracture properties are the second-phase particles and the grain structure. The microstructure can be classified into two groups, the first group containing fully deformed elongated grains with substructure (high-temperature extrusions) and the second group containing fully recrystallized elongated coarse grains (low-temperature extrusions after solutionizing). In both groups the material contains a certain amount of coarse intermetallic compounds, which are located either along the grain boundary predominantly in unrecrystallized structures or in the interior as in a recrystallized grain structure. The role of these coarse particles in controlling the fracture toughness has been the theme of many investigations [49,50]. It has been shown that, for the same type of grain structure, the reduction in the volume fraction of the coarse particles improves the fracture toughness in all directions for the same proof stress levels. The role of the intermediate size particles containing elements such as manganese, chromium etc. is still not clear. In fact, very little is known about the role of intermediate size particles acting independently. Perhaps their role is linked mainly to their effect in controlling the recrystallization grain size and shape. It is considered that the intermediate size particles help to homogenize slip and, hence, prevent the build up of dislocation pile-ups close to the grain boundaries. The effect of hardening precipitates which result from heat treatments depends on their sizes. The greatest size difference occurs between the naturally aged tempers and the artificially aged tempers. The mechanism by which these particles influence the toughness is somewhat complex. On the one hand, the precipitation of these particles decreases the work-hardening capacity of the materials. The loss of work-hardening capacity results in local plastic instabilities such as coarse slip band formation and large slip offsets around the boundaries. Such events occur also more commonly in materials with coarse grain size. It is known that in aluminium alloys very coarse grain size produces coarse grain scale shear bands along which the material fractures. The presence of intermediate size particles in these bands aids nucleation growth, and coalescence of voids resulting in a transgranular dimpled rupture. On the other hand, during precipitation of these particles, thin regions close to the grain or subgrain boundaries free from any precipitates are formed. Such regions are generally known as PFZs. This leads to a structure in which islands of grain interiors, which are hardened by the precipitates, are embedded in a continuum of relatively soft PFZs of constant thickness. For a material of grain size  $D$ , if the deformation is concentrated in the soft boundary in the above composite structure and if fracture occurs by intergranular rupture, then the fracture toughness  $K_{1c}$  can be given by the equation [50]:

$$K_{1c} \propto n_i \sqrt{\left( \frac{P \varepsilon_{ci}}{D} \right)} \quad (4.12)$$

where  $n_i$  and  $P$  are the work-hardening exponent and yield stress, respectively, of the grain boundary PFZ of thickness  $d$  and  $\varepsilon_{ci}$  is the critical failure strain for localized intergranular failure. This localized intergranular failure is enhanced by the

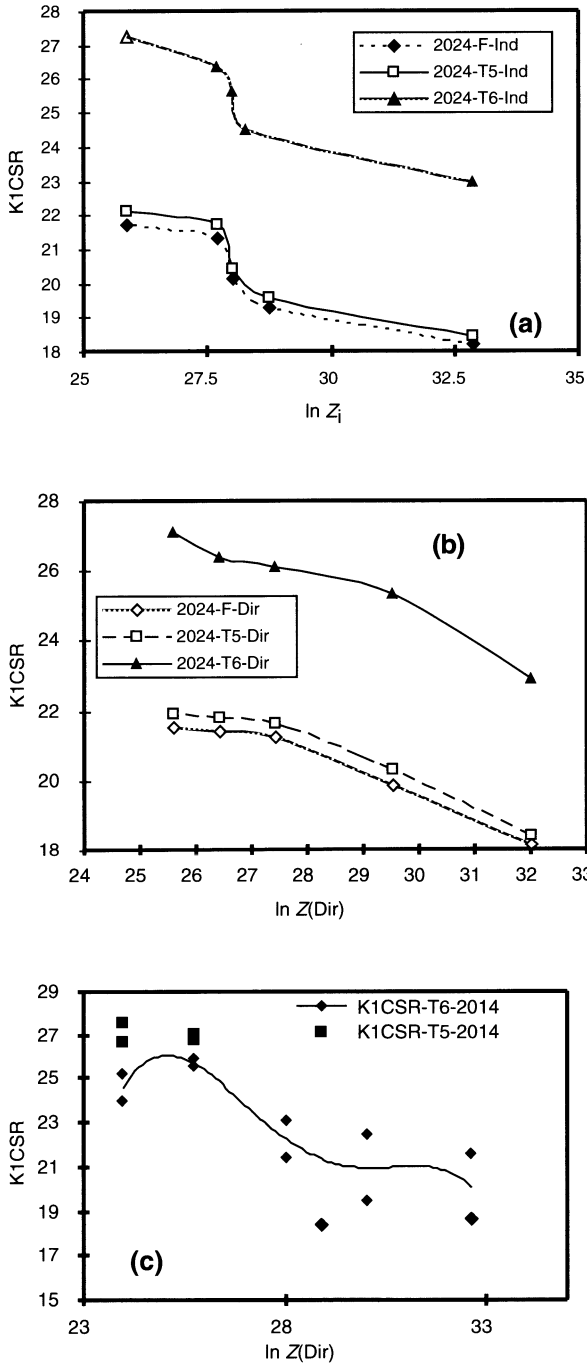


Fig. 4.35 Fracture toughness versus processing parameters 2XXX alloys.

precipitation along the boundary which also helps to nucleate voids along the boundaries and, thus, reduces the critical strain for fracture. The above analysis indicates clearly the influence of grain size on the fracture toughness. In Al–Zn–Mg alloys such intergranular failures had been observed in the peak aged and overaged conditions. In many alloys, the prior grain structure has a more equiaxed nature. When considering an elongated grain structure, it is only in certain isolated locations that such failures have been observed, generally resulting in mixed mode fractures.

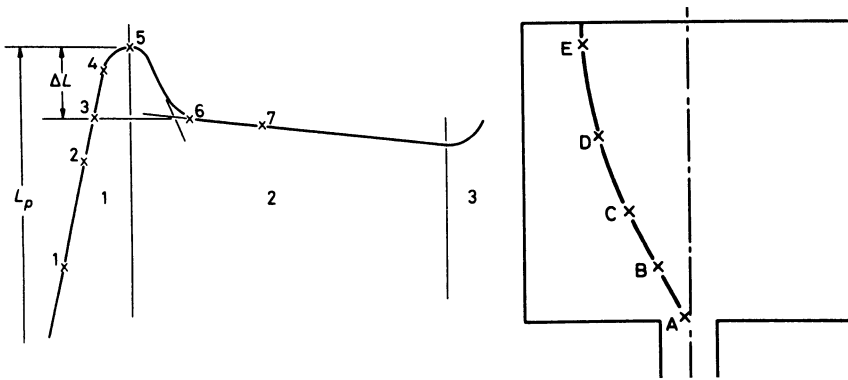
Figure 4.35 shows the variation in toughness with processing parameters for 2024 alloys; corresponding plots for 2014 alloy are very similar.

In 2014 alloy, the low temperature extrudates have lower toughness than the high-temperature extrudates in the T6 temper. Since the influence of coarse particles in both extrudates is the same, the difference can be attributed to the differences in the grain structure and the associated microstructure. It has been observed that recrystallized grain structures (low-temperature extrudates after solutionizing) are associated with thick PFZs and coarse precipitates along the grain boundaries which promotes shear fracture, and is responsible for the low fracture properties of the low-temperature extrudates. In the high-temperature extrudates, owing to the retention of subgrain structure, the PFZs along the subboundaries are thin and, hence, the associated subgrain boundary precipitation is also very fine. This is presumed to be the reason for the better fracture properties in the T6 temper and is directly the result of processing parameters.

## 4.11 MATERIAL FLOW AND INHOMOGENEITY – STRUCTURAL CONSIDERATIONS

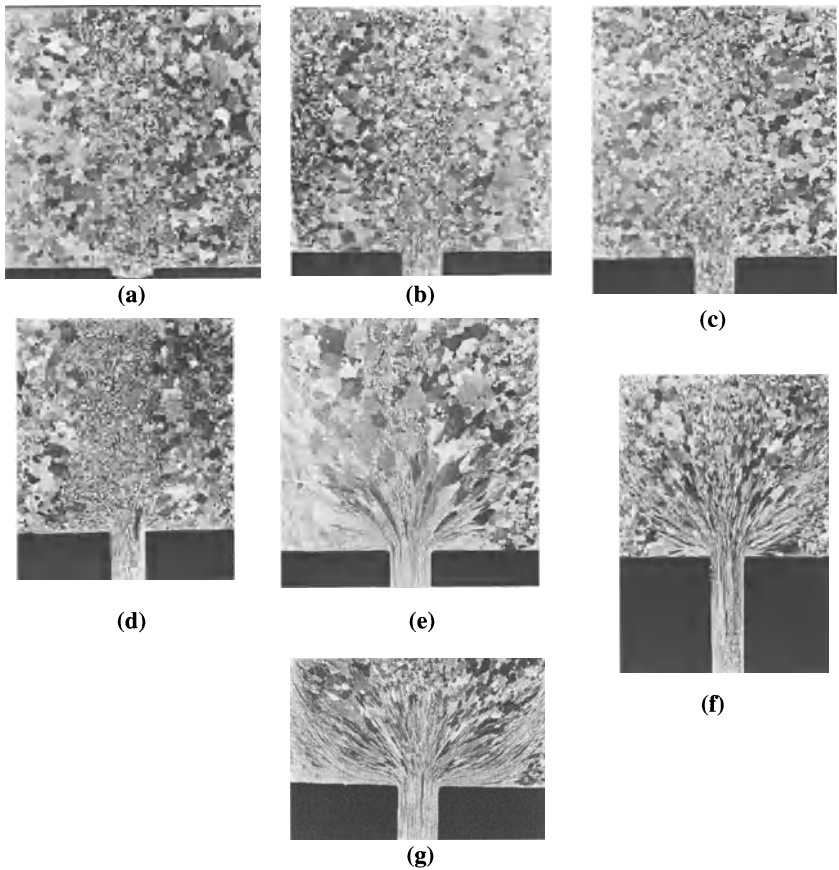
### 4.11.1 Development of structure in the extrusion container

An Al–5%Mg alloy was produced [51] without an efficient recrystallization inhibitor during casting such that the grains were relatively large in order to follow the macroscopic flow. The specimen locations selected for examination during the extrusion cycle are shown in Fig. 4.36. There was no significant volume fraction of precipitate in the alloy. Figure 4.37(a) depicts the billet during the upsetting stage. The macrostructure does not vary from that of the original billet with the exception of the region adjacent to the die entry where some deformation may be detected. There is no evidence of deformation elsewhere in the billet although container/billet shear is suggested by the grain structure at the periphery. Figure 4.37(b), illustrating the structure at a later stage in the upsetting process, does not exhibit radical changes, but an extension of the main deformation zone has occurred and the grains in this die entry region have become elongated. It is interesting to note that a small quantity of material has been forced through the orifice and that the extreme front end reveals quite clearly the original undeformed structure. Even at this stage, however, there is a variation in structure from front to rear of the extruded pip. Figure 4.37(c) shows the situation



**Fig. 4.36** Load/displacement curve showing peak geometry and sample locations.

after a further increase in pressure but with little ram travel and shows the deformation zone extending back into the billet. There is still little change in bulk structure and no identifiable dead metal zone but cylinder wall shear appears to have extended over the complete billet surface. Figure 4.37(d), corresponding to location 4 in Fig. 4.36, shows an almost identical macrostructure but the fibrous nature of the extruded structure suggests an increase in total deformation. The structure in Fig. 4.37(e) is located approximately at the point of peak pressure and shows very pronounced changes in morphology. The extrudate exhibits the typical fibrous or 'cold worked' structure and it should be noted that at this stage a considerable length of material has been extruded. Clearly the 'breakthrough' pressure does not correspond to the commencement of extrusion. The deformation zone has again extended backwards into the billet and dead metal zones are becoming apparent. Considerable cylinder wall shear is apparent and the billet peripheral layers are quite heavily deformed. The latter feature is less predominant in the surfaces adjacent to the die plane, supporting the observation that the dead-metal zone will be established in this area. In fact the deformation zone extends well back into the billet and grains can quite easily be identified which have been elongated within the central deformation zone. Figure 4.37(f) shows the structure when the pressure has fallen by an amount  $\Delta p$  after the peak pressure and considerable ram travel has occurred. The central deformation zone has now developed fully and intense shear is occurring at this location; cylinder wall shear also appears to be more intense but it should be recalled that it is a deformation history which is being observed since quasi-static conditions do not obtain at this location. It should also be noted that although the dead metal zones can be identified clearly it is the lessening of surface shear and gradation of grain deformation which allows this observation; there is definite evidence that the quasi-static deformation zone is about to be established. Figure 4.37(g) illustrates the macrostructure in the steady state region. The quasi-static deformation zone is fully developed and the dead metal zone can very easily be identified. Regions of significant shear can be seen extending from die entry and along the central



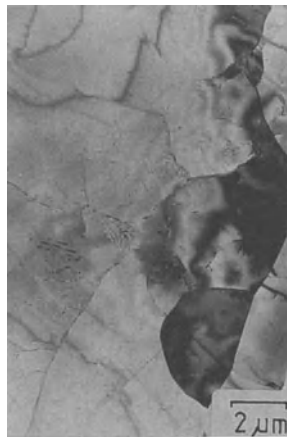
**Fig. 4.37** Development of microstructure during hot direct extrusion with specimens corresponding to locations shown in Fig. 4.36; (a) location 1; (b) location 2; (c) location 3; (d) location 4; (e) location 5; (f) location 6; (g) location 7.

axis and from die entry to the periphery of the billet bounded by the dead metal zone and the container/billet interface. The large initial grain size allows the recognition of grains passing through three regions of intense deformation. The identification of two regions of lesser deformation on either side of the central zone and sandwiched by it and the 'peripheral' zone suggests a buffer zone which serves primarily to supply material to the regions of high deformation in the billet. Material flowing from the peripheral region of the billet can be seen to occupy about 35% of the extrudate cross-section while material from the axial deformation zone occupies about 55%. This implies that the two zones of lesser deformation are feeding only about 10% in total of the material section shown in Fig. 4.37(g). Clearly, if these zones were not primarily feeding the intense shear zones, vortices would form within the deformation zone. This can, of course, occur when the dummy block destroys the mass balance of the various deformation zones.

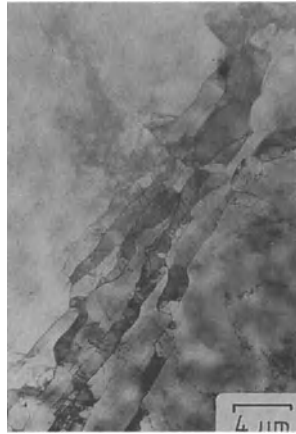


#### 4.11.2 Substructural considerations

The dislocation structure within the billet arrested at position 1 in Fig. 4.37 was heterogeneous. Specimens extracted from the rear of the billet (positions C, D and E) had similar structures having a uniform dislocation density. In isolated areas, however, walls of dislocations were beginning to form. Similar walls were observed in the other rear positions indicating that the upsetting operation causes deformation throughout the billet. There did not appear to be any special deformation associated with possible ram/billet interaction. Further forward, in position B, dislocation wall formation was more pronounced and outcrops of subgrains were observed at high-angle boundaries. In general subgrains were not observed consistently at any position in this billet, which is consistent with the thesis that strains imposed on the material during the upsetting process are absorbed by shear at the grain boundaries. This will involve the production of dislocations to produce the strain and additional dislocation generation for storage within grains to maintain the strain gradients imposed by grain boundary shear. Thus the dislocation density is necessarily increased and a driving force for subgrain formation created; Fig. 4.38 illustrates this feature. Although most grains were devoid of subgrains the specimen extracted from the die mouth (position A) showed a subgrain banding phenomenon. Bands of subgrains were observed bisecting the grains and being elongated quite severely in the potential extrusion direction (at this stage extrusion has not commenced). Misorientations were higher between these bands than between the subgrains along them which can be seen in Fig. 4.39 by noting the small contrast between the individual subgrains and the large difference in contrast between these and the remainder of the grain. The banding would seem to be the result of strains exerted upon abnormally large



**Fig. 4.38** Subgrain formation at high-angle grain boundary (running down the right-hand side) during initial upsetting of billet. Sample taken from position C in billet where general subgrain formation is not observed at this stage of deformation.



**Fig. 4.39** Bands of elongated subgrains formed in material at die mouth (position A) during initial upsetting of billet (location 1 in load/extension curve).

grains as they pass the velocity discontinuity associated with entry to the die mouth. These grains are preferentially elongated and the resulting localized regions of high strain require that areas of higher dislocation density also exist. Hence in this area there is sufficient dislocation mobility and density to effect the formation of subgrains. This observation may be even more significant in the industrial context where we would expect greater heterogeneity in the 'homogenized' billet by larger grain sizes, more diverse dendritic morphology and the presence of dissociated soluble constituents.

Specimens extracted at times 2 and 3 during the process exhibited similar structures. Banding was once more observed in the die entry region, in this case



**Fig. 4.40** Deformation bands containing subgrains formed in large grain. Sample taken from position A in billet, at location 2 on load/displacement curve. Selected area diffraction patterns from the three areas indicated that all have zone axis very close to  $\langle 112 \rangle$  but the central band is rotated by  $33^\circ$  about this axis with respect to its neighbours.

producing more equiaxed subgrains as shown in Fig. 4.40. It should also be noted that in these subgrains there is considerable internal dislocation density and, in general, the walls are more clearly defined than those observed earlier in the extrusion cycle. At locations towards the rear of the billet dislocation wall build-up is more pronounced and isolated outcrops of small subgrains emanating from high-angle boundaries can be identified. Dislocation wall formation was also observed to be aided by precipitates; these sites clearly act as locking points and extended walls can be observed which have their extremities at precipitates. The probability that subgrain wall formation will develop is thus enhanced at these sites. This could also be an important feature in the industrial alloy (AA5456) in which a greater volume fraction of precipitate will be present. The dislocation density within subgrains indicates incomplete recovery, and within completely unrecovered regions the dislocation density is much greater than earlier in the ram stroke.

Specimens taken from the billet corresponding to the point of peak pressure (location 5) show an equiaxed subgrain structure in positions A, B and C. These subgrains were slightly elongated in the die mouth (Fig. 4.41) and are heterogeneous in size, being smaller at high-angle boundaries. It is interesting to note that the dislocation density within subgrains is lower in specimens B and C (i.e. proceeding backwards into the deformation zone) which is consistent with lower strains and lower strain gradients in these regions than those which occur around the theoretical exit velocity discontinuity. Nevertheless it is clear that at this stage the deformation zone is not quasi-static and the dead metal zone has not been fully developed since areas can be identified within the deformation zone in which subgrain formation is incomplete and the macrographs indicate that the dead metal zone is not well defined.



**Fig. 4.41** Elongated subgrains containing very high dislocation density observed at mouth at peak pressure. Dynamic recovery is incomplete.

When the ram has advanced to location 6, an equiaxed subgrain structure can be observed in positions A, B, C and D. Some banding can still be detected at position A (Fig. 4.42) but, in general, subgrains are equiaxed, locally smaller at high-angle grain boundaries and having a high internal dislocation density (Fig. 4.43). The specimen from the back of the billet contains only small outcrops of subgrains located at high-angle grain boundaries and intergranular dislocation walls. These subgrains and dislocation wall formations are most probably remnants



**Fig. 4.42** Equiaxed subgrains within deformation bands in sample taken from the same position as that in Fig. 4.41 but at location 6 in the load/displacement curve when steady-state deformation is attained.



**Fig. 4.43** Sample containing high-angle grain boundary (arrowed) taken from the same location and position in the load/displacement curve as Fig. 4.42. Comparison of Figs. 4.42 and 4.43 shows that once steady-state deformation is achieved the microstructure becomes much more uniform.

from compression during the upsetting stage. Although this deformation is not detectable in the macrosections it is clear that compressive flow must occur throughout the billet during the initial ram contact. Proof that large strain gradients are associated with high-angle grain boundaries is shown in Fig. 4.44. This depicts a section of high-angle grain boundary involving a bend through 90°. Subgrains which are formed heterogeneously at high-angle grain boundaries can be seen to be much better defined along the boundary aligned parallel to the billet axis (and the vertical axis of the micrograph) and at the grain extremity than along the segment at right angles to it.



**Fig. 4.44** Specimen taken from the back of the billet at location 6 in the load/displacement curve. Deformation in this zone is still limited although steady-state deformation has essentially been attained.

Samples inspected from the steady-state position (location 7) revealed equiaxed subgrain structures. In locations A and B the subgrains were of uniform size but location C included smaller subgrains at high-angle boundaries. Presumably this phenomenon is associated with a less acute breakdown of original structure than has occurred at later stages in the deformation zone, i.e. locations A and B. Original high-angle grain boundaries were impossible to find in the deformation zone exit region because of the intense deformation history of the material in that location. Typical structures are illustrated in Fig. 4.45. The dislocation density within subgrains is higher at the deformation zone exit than at position C which is consistent with the very rapid increase in strain rate (and hence strain) which occurs in that region.

#### 4.11.3 Extrudate structure

The extruded structure exhibited a fibrous type core consisting of equiaxed subgrains surrounded by an annulus of recrystallized grains containing no substructure. The recrystallized grain boundaries could be seen to be pinned at some locations by precipitates at triple points. This duplex structure is produced because much higher strains are imposed upon the material fed to the surface layers



**Fig. 4.45** Typical subgrain and dislocation structure observed during steady-state extrusion. Sample taken from position B in billet at location 7 in load/displacement curve.

and these provide a driving force for recrystallization which is not present in the central regions of the extrudate. Nucleation probably originates at subgrain boundaries and must involve rapid subgrain coalescence and subgrain boundary migration. In the commercial alloy this process would be aided by additional sites available at second-phase particles but in this superpurity base system there is a very low volume fraction of precipitates.

#### 4.11.4 Subgrain size

Subgrain sizes were measured by an intercept method. Since average strain rates must increase greatly throughout the ram stroke and in addition must be very low at the rear of the billet (due to compression only) these observations are consistent with the concept that the subgrain size is dependent upon the temperature-compensated strain rate  $Z$ . However, there is no noticeable change in subgrain size when moving from position C to position A in any of the billets. This is somewhat surprising since we would expect the strain rate to vary by a factor of about two during this period. This will also produce a temperature rise and in general  $\ln Z$  would be expected to decrease, perhaps by an order of magnitude, between locations C and A. Some difference in subgrain size should therefore be detected. It is clear that the equation of state relating  $Z$  to subgrain size must therefore be violated in this region, and this perhaps explains why so many workers have obtained excellent substructural correlations using initial extrusion conditions or models based upon bulk temperature rise and average strain rates. It is clear that the substructure cannot change as rapidly as any equation of state would dictate and it is not sufficient to propose a model which does not include time as a variable. Moreover, there must therefore be a critical rate of

change of  $Z$  or  $\ln Z$  beyond which the equation of state cannot be observed. If, for example, at entry to the deformation zone the material contains larger subgrains with low density walls (as has been observed) and at exit contains smaller subgrains with high density walls and some internal dislocation density then rearrangement is necessary as an element passes through the deformation zone. The final subgrains are in general equiaxed and the number of subgrains at exit is unlikely to be a number which would integrally fit the subgrain size pertaining at entry to the deformation zone. Therefore, at each step during continuous deformation, considerable adjustment must be required. This clearly implies that any equation of state must be sensitive to the rate of change of strain and must include at least a limiting time factor.

#### 4.11.5 Development of dislocation structure related to peak pressure

The general reduction of pressure during the extrusion process has always been attributed to the reduction in friction as the billet length decreases. The pressure curves observed for this alloy indicate that the reduction in pressure is so non-linear that this explanation cannot be justified. Castle and Sheppard [28] showed that the peak increased as extrusion rates increased and was reduced by increasing initial temperature. The relationship between peak pressure and temperature was shown to be of an Arrhenius type with an activation energy of about  $160 \text{ kJ mol}^{-1}$  which is close to the activation energy for bulk self diffusion in aluminium. The results indicate strongly that the peak is controlled by thermally activated events involving the production, interaction and annihilation of dislocations.

It is clear that dislocation generation and motion commences and spreads from the die entry as the pressure is applied. Dislocation density increases rapidly as a consequence of the interaction of mobile dislocations with each other and with dislocations stored within grains. These latter dislocations are a necessary consequence of the strain gradients which exist both on a macroscopic scale (e.g. between the deformation zone and regions of undeformed material) and on a microscopic scale i.e. across grain boundaries at which multiple slip is required from the start of deformation in order for the grains to remain conterminous. Dislocation density increases most rapidly in these regions in which strain and strain gradients are highest. Grain boundaries, at which dislocations are generated, are necessarily such sites. Eventually the stored dislocation density achieves a magnitude such that recovery by cross-slip and climb occurs resulting in the formation of subgrains. This mechanism is consistent with the observation that subgrains are first observed at grain boundaries and at high strain regions near the die entry. As extrusion proceeds the deformation extends backwards to form the deformation zone and isolated subgrain outcrops are observed progressively further back in the billet. In the later stages of extrusion when steady-state conditions obtain, the generation and annihilation of dislocations are in balance so that recovery and subgrain formation ensure zero work-hardening effects. At this stage subgrains are equiaxed and constant in size and misorientation. It should be

recalled that in the earlier stages of deformation subgrain walls are ragged and elongated in the extrusion direction and the cells contain a high internal dislocation density.

At peak pressure the steady-state deformation zone is not fully established but this condition is achieved by the time the pressure has diminished by an amount equal to the additional increment required. Considering the necessary fact that changes in substructure require finite time intervals it is clear that the pressure peak is required to effect the establishment of the quasi-static deformation zone. A side effect is quite obviously that a quasi-static dead metal zone is also formed. Hence it is not surprising that the pressure peak is associated with an activation energy similar to that for bulk self diffusion and for creep since the climb of dislocations is the controlling process in each case.

### *Summary*

1. The quasi-static deformation zone is not fully established until a short time after the peak pressure is attained which implies that an additional increment of pressure is required to establish this zone. This suggests that the peak pressure is associated with the ease of dislocation mobility and should therefore be alloy dependent, varying with volume fraction precipitate size, second-phase particles etc.
2. There is no deformation of any consequence at the rear of the billet until steady state is achieved.
3. The softening process in this alloy system is dynamic recovery producing a stable equiaxed subgrain structure of approximately constant size and misorientation.
4. Subgrain banding occurs in the die entry region during upsetting and is a result of inhomogeneous deformation. This is probably aided by large grain sizes and heterogeneous grain size distribution.

## **4.12 PRESS QUENCHING AND PRESS SOLUTIONIZING**

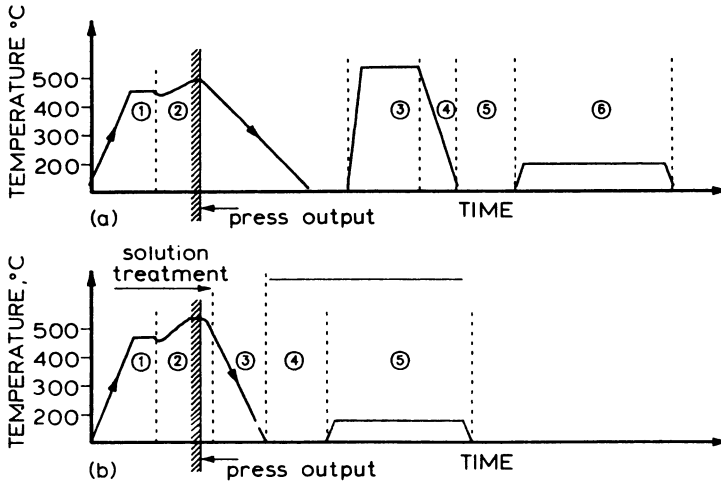
### **4.12.1 Introduction**

Most of the 6XXX alloys are quenched immediately after extrusion, followed by a natural or artificial ageing sequence. In general, alloys in the 7XXX series which contain copper are solution treated in a separate operation and artificially aged. Those alloys in the 7XXX series not containing copper are amenable to quenching and natural ageing and are more often given this treatment. The 2XXX alloys are always subjected to a separate solution and age, but it has been reported that these alloys were successfully press quenched during the Second World War [52].

Press quenching is a method of combining solution treatment and extrusion which offers potential economic savings, but requires control of a large number of parameters. It is possibly because of the control required that the process is



confined to the 6XXX and Al–Zn–Mg (7XXX) alloys. A comparison between separate quench and press quenching operations is shown in Fig. 4.46. The greater simplicity of the press quench operation and the elimination of separate operations is obvious.



**Fig. 4.46** Diagrams of two quenching operations (schematic); (a) separate quenching – 1 reheating; 2 extrusion; 3 solution treatment; 4 quenching; 5 waiting period; 6 annealing; (b) press quenching – 1 reheating; 2 extrusion; 3 quenching; 4 waiting period; 5 annealing.

From an economic standpoint, the process eliminates one solution treatment stage, saving perhaps  $1.6 \text{ J kg}^{-1}$ . Handling is reduced, resulting in both labour and energy savings. If correctly planned there are also large capital savings which can represent 25–30% of processing costs. In terms of extrudate quality, the process minimizes the possibility of coarse surface grains and in general produces a non-recrystallized oriented structure possessing superior properties to those obtained from a separate solute soak treatment.

Heat treatable alloys are typified by a marked increase in solubility of the major alloying element with increasing temperature as shown, for example, in Fig. 4.47 for an Al–Mg–Si alloy having a ratio of magnesium to available silicon of 1.73:1. The maximum solubility of  $\text{Mg}_2\text{Si}$  is 1.85% at  $595^\circ\text{C}$ , falling to 1.08% at  $500^\circ\text{C}$  and 0.097% at  $200^\circ\text{C}$ . Therefore, the first stage of any heat treatment must be to form a solid solution by soaking the material at a temperature above the solvus. For example, a 1.08%  $\text{Mg}_2\text{Si}$  alloy would be soaked at a temperature in excess of  $500^\circ\text{C}$  but below the solidus of  $595^\circ\text{C}$  to avoid incipient melting. In order to complete the solute treatment, the alloy must be cooled so rapidly that  $\text{Mg}_2\text{Si}$  precipitation will be avoided and the magnesium and silicon maintained in supersaturated solid solution.

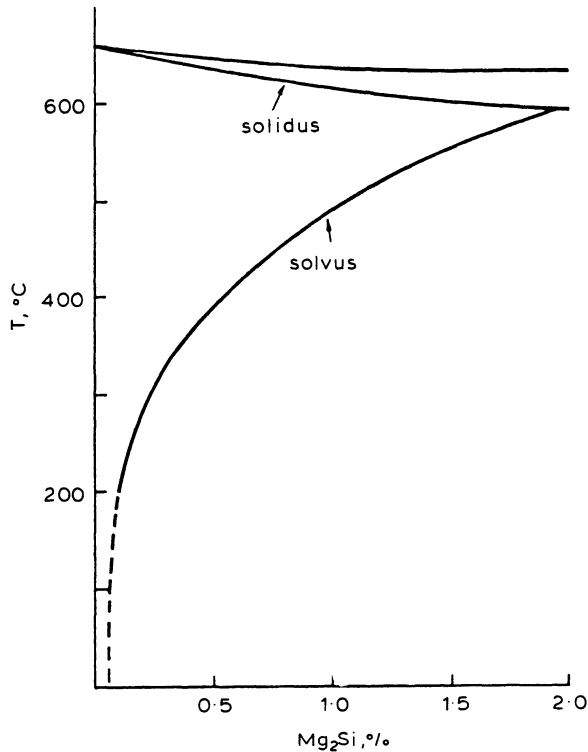


Fig. 4.47 Solubility of  $Mg_2Si$  as a function of temperature.

#### 4.12.2 Metallurgical aspects

##### *Homogenization*

The elements essential to the precipitation process must be in solution as the extruded section leaves the die and remain there until encountering the quench. Hence, billet homogenization must be adapted to the alloy composition. The cooling rate after homogenization is perhaps most critical because slow cooling, while aiding extrudability, increases the  $Mg_2Si$  size, hence making dissolution at a later stage more difficult. Iron, manganese, and chromium commonly found in most alloys (Table 4.3) present a difficulty, since they act as heterogeneous nucleation sites when present in fine form, hence increasing the critical quench rate. If present as large precipitates they promote recrystallization, thus destroying the 'press effect' which is discussed below. Beatty [53] pays particular attention to the iron constituent pointing out that  $\alpha$ -Al-Fe-Si is far better than the  $\beta$  form. He concludes that the billet should have been rapidly cooled from a high homogenization temperature to give small uniformly distributed  $Mg_2Si$  and a minimum volume of small rounded or disjoined  $\alpha$ -Al-Fe-Si constituents. Although paying more

**Table 4.3** Typical percentage compositions of 6000 series alloys

<i>Alloy</i>	<i>Si</i>	<i>Fe</i>	<i>Cu</i>	<i>Mn</i>	<i>Mg</i>	<i>Cr</i>	<i>Mg<sub>2</sub>Si</i>	
6063EE		0.35	0.16	0.01	0.02	0.50	0.01	0.79
6063E	0.43	0.16	0.01	0.01	0.50	0.01	0.79	
6063	0.48	0.24	0.01	0.02	0.50	0.01	0.79	
6763		0.39	0.06	0.08	0.01	0.50	0.01	0.79
6101		0.45	0.14	0.01	0.01	0.50	0.01	0.79
6061		0.60	0.25	0.02	0.05	0.95	0.06	1.50
6005		0.70	0.25	0.05	0.05	0.50	0.02	0.79

attention to extrudability, Beatty lists these qualities for press quenching 6061 alloy. Thus, time and temperature for homogenization are determined by iron phase transformation rather than  $Mg_2Si$  solution. Therefore, a typical commercial sequence for 6063 might involve a 6 h soak at 575°C followed by forced cooling between 480 and 250°C and rapid cooling to room temperature.

It is obvious that the requirements during homogenization are those which will produce good properties in an extrudate, whether press quenched or separately treated. Unfortunately they also reduce extrudability. Marchive and Deschamps [54] summarize the requirements as given in Table 4.4.

**Table 4.4** Factors aiding successful press quenching

<i>Mechanism</i>	<i>Advantage</i>
Reduction in size and density of hardening elements precipitated before extrusions	High temperature homogenization Rapid cooling after homogenization Rapid reheat
Increase in exit temperature of extruded section	High temperature reheat High extrusion ratio High billet temperature High strain rate

### *Reheating*

The dissolution of the precipitate remaining in the rapidly cooled homogenized billet must occur during the reheat to solution temperatures which must be rapid, during any holding time and during the extrusion process itself. This dissolution will depend upon:

- the size and distribution of the precipitates remaining after homogenization;
- the temperature and holding time above the solid solute limit;
- the temperature and extent of deformation.

The kinetics of dissolution in the absence of deformation are relatively slow and may require several minutes if the precipitates are relatively coarse and the temperature is only just above the solid solution limit.

However, Fornerod [55] points out that the solution heat treatment on the press is greatly assisted by the plastic deformation which increases the kinetics of dissolution in two ways: the larger of the precipitates are broken, thus reducing their size and spacing, and the deformation produces defects in the microstructure (i.e. vacancies and dislocations), which increases diffusion rates. The vacancy concentration in particular is increased and Underwood and Manning [56] have shown that dissolution under a tensile flow stress of only  $1 \text{ N mm}^{-2}$  was sufficient to reduce the activation energy of the process from 268 to  $153 \text{ kJ mol}^{-1}$  for an Al-Cu<sub>3</sub> alloy. Therefore, solution heat treatment on the press is rarely a problem.

In Al-Mg-Si alloys, for example, billets are usually heated to a temperature below the solid solution limit and the heat of deformation is used to ensure that the exit temperature exceeds that limit ( $500\text{--}540^\circ\text{C}$ ). The homogenization treatment described above with forced cooling from  $480$  to  $250^\circ\text{C}$  is important to achieve dissolution and also raises the resistance to deformation; hence, greater heat is generated in the process. Al-Zn-Mg alloys, which may find increasing use in those applications where greater strength and weldability than is possible with 5000 and 6000 alloys is required, present few problems in solution treatment on the press. The solid solution limit is about  $310^\circ\text{C}$  and the reheat is usually above this temperature. In these alloys it is more critical to avoid recrystallization since the fibre texture increases corrosion resistance. Finally, on reheating, Beatty mentions the possibility of reheating above the extrusion temperature and then quenching. Since deformation is such a critical factor in dissolution, it would appear that this should be used only when necessary.

### *Composition*

Given the characteristics of microstructure presented above in the discussion on homogenization and reheating, some general points relevant to the composition of 6000 alloys must be considered. The suitability for press quenching decreases with increase in supersaturation, excess of silicon and density of the dispersed phases. Supersaturation depends mainly on the Mg<sub>2</sub>Si content while chromium, manganese, and zirconium promote nucleation by providing Mg<sub>2</sub>Si heterogeneous nucleation sites during cooling. The critical quench rate is sensitive to the quantity and distribution of these phases. A fine distribution of these precipitates during cooling increases the critical quench rate, with chromium being the most deleterious. Marchive concludes that 6063 is easily press quenchable. The 6061 and 6082 alloys require water quenching, but yield good properties and, because of the homogenization treatment, are difficult to extrude. Alloy 6005A has been developed by Pechenet [57] specifically for press quenching giving properties close to 6061 and good extrudability. The properties of 6XXX alloys are closely related to the properties of Mg<sub>2</sub>Si and to the excess silicon present; both factors

lead to better properties. Increasing the silicon content decreases quenchability. Copper content up to 0.1% has no effect on quench rate, but increases properties and decreases extrudability. Chromium, manganese and zirconium are necessary to ensure good strength and fracture characteristics; the failure mode is intergranular in the absence of these precipitates and transgranular when present. However, all are unfavourable from the quenching viewpoint, chromium being the most critical element. Optimization of magnesium, silicon, copper, manganese and zirconium led to the development of alloy 6005A, the applications of which are similar to 6061. Devaley [58] shows how extrusion conditions, minor compositional changes, and quench rate change the fracture mode and Charpy values from 28 to 8 J m<sup>2</sup>. Details are given in Table 4.5. From the viewpoint of composition, it may be concluded that elements which strengthen 6XXX alloys generally increase quench sensitivity, raise the flow stress, and decrease extrudability. Hence, as in 6005A alloy, the composition is inevitably a compromise.

**Table 4.5** Variations in properties of Al–0.5%Mg–0.65%Si alloy

<i>Conditions</i>	<i>Type of fracture</i>	<i>Elongation (%)</i>	<i>Notch impact (J m<sup>-1</sup>)</i>
Mn = 0%	I	10	8
Mn = 0.5%	I/T	17	19
Mn = 0.8%	T	20	28
Cooling rate = 45°C s <sup>-1</sup>	I	14	18
Cooling rate = 200°C s <sup>-1</sup>	T	15	27

T = transgranular, I = intergranular

### 4.12.3 Technological problems

#### *Thermal considerations*

The metal temperature must be kept between the solid solution limit and the solidus during the extrusion process and this is obviously dependent upon the heat balance during the extrusion process. The temperature distribution in the billet during extrusion depends upon the initial and boundary conditions. The initial conditions are the temperature of the billet and any variation in temperature: for example, it is common practice to taper heat the billet such that the front end is hotter than the rear. The problem of combined heat transfer can be solved numerically, but a qualitative approach is still of some use.

The various heat flows  $Q_1-Q_8$  occurring in the process when it is assumed that all deformation occurs in the deformation region in front of the die have been discussed in Chapter 2 and have indicated the complexity of the thermal equilibrium during the extrusion process. There is heat conduction to the container and dies, through the dead metal zone and in the billet itself, depending upon the initial heating cycle. Moreover, the conduction to the container may vary along the

cylinder wall since the temperature of the billet will not be uniform. In practice, there is greater deformation at the dead metal zone boundary and at the container wall interface, leading to greater temperature increases in these areas which usually form the surface of the extruded shape in direct extrusion. The integral profile approach has been shown to yield results similar to numerical analysis and has the advantage that it can be used on-line. Clearly this approach to temperature prediction will be useful especially when coupled to a pyrometer at the press installation. Certainly for high conductivity aluminium alloys, this form of temperature increase may be sufficiently accurate for practical use.

The extrusion ram speed may be incorporated in the Peclet number  $Pe = V_B(D/\alpha)$ , where  $D$  is the container diameter and  $\alpha$  is the thermal diffusivity. At high values of this number the ram speed determines the exit temperature; at low values, the temperature of the tools is the decisive factor. If the parameter is correctly chosen, the average temperature of the emergent extrude can be kept to  $\pm 10^\circ\text{C}$ .

Of equal importance is the variation in temperature of the extrudate from surface to centre which of course cannot be measured. Using the Avitzur flow model it can be shown [59] that, for the adiabatic case, the temperature differential between surface and core, when assuming, as Akeret does, that half the force acting on the die is utilized to shear metal in an annular zone one-tenth the diameter of the cone, could be calculated as:

$$\Delta T_{sc} = 140^\circ\text{C}$$

a quantity which obviously could be reduced if the extrusion speed were lower. This analysis shows a greater  $\Delta T$  than either the integral profile method or Stuwe's analysis.

This temperature difference decreases a very short time after exit from the die (of the order of  $0.5l^2/\alpha$ ), where  $l$  is the diffusion distance. These problems are encountered only when thick sections or sections containing both thick and thin arms are encountered. Under these latter conditions the cross-section of the extrusion becomes a limiting factor in press quenching. This is particularly so in the more complex 2000 and 7000 alloys where the temperature limit between the solid solution and solidus of the alloy is narrow. Then, it becomes impossible to maintain temperature homogeneity without exceeding the solidus at the surface.

### *Quenching*

The cooling process can be considered in three phases: die to quench medium; quench period (generally in water or forced air); and air cooling to ambient temperature.

In still or forced air, cooling is governed by the equation:

$$\frac{T - T_{\text{air}}}{T_i - T_{\text{air}}} = \exp \left\{ \frac{-t}{\tau_a} \right\} \quad (4.13)$$

where  $T$  is the temperature at time  $t$ ,  $T_i$  is the initial temperature and  $\tau_a = (\rho C v)/A_s h$ ,  $\rho$  being the density,  $C$  the specific heat,  $v$  the extruded volume,  $A_s$  the surface area and  $h$  the heat transfer coefficient. It is possible to redefine  $\tau_a$ , by  $\tau'$  which would be the time taken for the dimensionless temperature to achieve a value of  $1/2$ :

$$\frac{T - T_{\text{air}}}{T_i - T_{\text{air}}} = \frac{1}{2} = \exp\left\{\frac{-t}{\tau_a}\right\}$$

$$\frac{-\tau'}{\tau_a} = \ln\left(\frac{T - T_{\text{air}}}{T_i - T_{\text{air}}}\right) = -\ln 2$$

giving  $\tau'$  or  $\tau_a \ln 2$  or  $\tau_a \tau'/\ln 2$ , thus it can be evaluated that:

$$\frac{T - T_{\text{air}}}{T_i - T_{\text{air}}} = \exp\left\{\frac{-t \ln 2}{\tau'}\right\}$$

When press quenching an alloy, one must know its ability to tolerate:

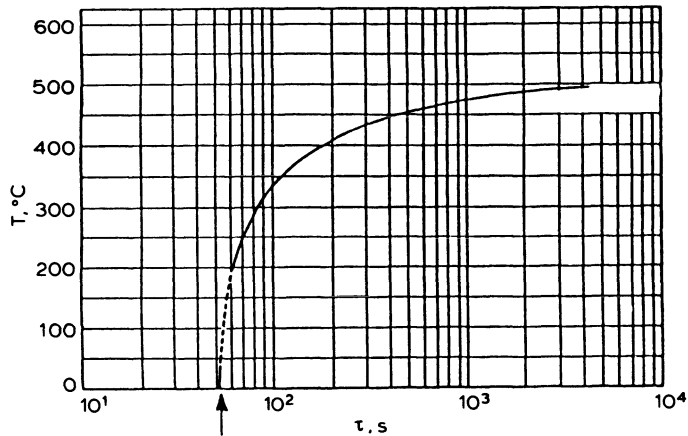
- the transfer time from die to quench;
- a low cooling rate or a long period of semi-cooling;
- a slow conclusion of the quench in still air.

All this information can be gained from the C curves presented in Chapter 3. Most diagrams exhibit a critical quench region between 450 and 250°C with a tip at about 350°C. Below 250°C, cooling in air can usually be tolerated, but should still be included in the integral given in equation 3.14. Utilizing the horizontal ordinate of the tip, the suitability of any particular alloy for air quenching can be established. The critical transfer conditions (i.e. the minimum quench temperature as a function of  $\tau'$  or the critical time constant for air quenching) cannot easily be established. Numerous TTP diagrams have been published from which it can be noted that the most important feature is that the critical quench region does not vary from alloy to alloy.

Another type of diagram is extensively used; the  $\tau'$ TP. Instead of step quenching, the material is cooled from the solid solution limit exponentially for varying values of  $\tau'$  and cold water quenched from various temperatures. The curves then present the line of a property as a function of  $\tau'$  and quench temperature. Such a curve for an Al-1Si-0.8Mg-0.3Mn alloy is shown in Fig. 4.48. From such a curve it is possible to obtain directly the period of cooling before quench, the quench temperature acceptable, and the critical  $\tau'$  values  $\tau'_{\text{crit}}$  for quench in air.

The  $\tau'_{\text{crit}}$  value varies considerably for each alloy since it is dependent upon the type of alloy, concentration of alloying elements, and minor additions such as chromium, manganese, and zirconium. The role of these differing factors has been discussed above in terms of the C curve. Therefore, it is sufficient to note:

- that increased alloying elements lower the  $\tau'_{\text{crit}}$  value because the alloy supersaturation is higher;



**Fig. 4.48**  $\tau'$ TP diagram of Al-1%Si-0.8%Mg-0.3%Mn alloy, UTS = 310 N mm<sup>-2</sup>. Arrow indicates critical  $\tau'$  values ( $\tau'_{\text{crit}}$ ) for quench in air.

- that the  $\tau'_{\text{crit}}$  value is highly dependent on each hardening element;
- the higher the proportion of minor additions (chromium, manganese, zirconium), the lower is the  $\tau'_{\text{crit}}$  value.

### *Extrudability*

In terms of press quenching, extrudability means the compatibility of an alloy to withstand high speed extrusion. Obviously, this is not a well defined property and, as has been noted above, the factors producing acceptable quenchability in general increase the flow stress of an alloy. This increase in flow stress leads to higher temperature increases and more rapid surface deterioration. Thus, extrudability depends upon the same factors as quenchability but can be modified by attention to heat transfer characteristics and to the mode of deformation. Increased speed is possible by utilizing the indirect process.

### *Thermal aspects of quenching*

The  $\tau'_{\text{crit}}$  value of the alloy and the wall thickness of the extrusion determine the minimum value of the heat transfer coefficient between the quench medium and the metal. If  $S$  is the cross-section of the product and  $P$  is the periphery in contact with the coolant, the period of cooling is:

$$\tau' = \frac{\rho C}{h} \frac{S}{P} \ln 2$$

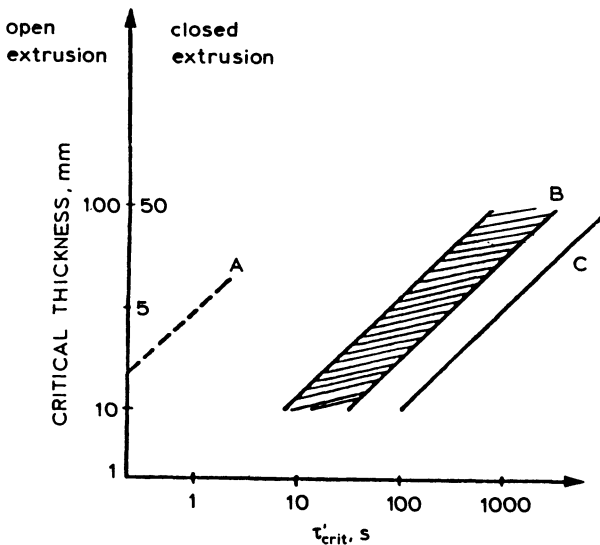


for constant cross-section temperature. Thus, the minimum heat transfer coefficient is given by:

$$h_{\min} = \rho C \frac{S}{P} \frac{1}{\tau'_{\text{crit}}} \ln 2$$

The value of  $S/P$  is approximately equal to half the wall thickness of an open profile extrusion and to the wall thickness of a cellular extrusion. Values of  $h$  for common quenching media are  $h = 10 \text{ W m}^{-2} \text{ }^{\circ}\text{C}^{-1}$  for still air,  $30\text{--}120 \text{ W m}^{-2} \text{ }^{\circ}\text{C}^{-1}$  for forced air and  $2000\text{--}40\,000 \text{ W m}^{-2} \text{ }^{\circ}\text{C}^{-1}$  for water. Therefore, there is a critical thickness of extrusion which varies with  $\tau'_{\text{crit}}$  as shown in Fig. 4.49 which is based on results for various quenching media obtained from laboratory tests and shown in Fig. 4.50.

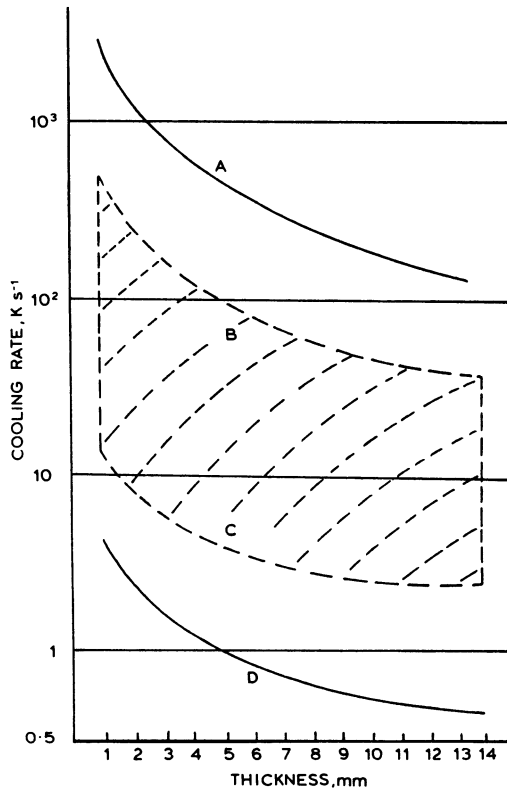
The spread observable in Fig. 4.50 for water quenching is a result of the variation of  $h$  for water. It is low if a stable vapour film forms, increases from about 2000 to  $40\,000 \text{ W m}^{-2} \text{ }^{\circ}\text{C}^{-1}$  at intermediate temperatures when the vapour film becomes unstable, and diminishes when isolated bubbles form or when cooling becomes convective only.



**Fig. 4.49** Critical thickness as function of  $\tau'_{\text{crit}}$  for various quench media ( $h$  is heat transfer coefficient); A, water,  $h = 2000 \text{ W m}^{-2}$ ; B, forced air; C, still air.

### Distortion

The temperature of the extrudate can vary from section to section and through the thickness of the extrudate. Under these conditions distortion of the extrudate can



**Fig. 4.50** Influence of quench medium on cooling rate; A, water; B, mist; C, blown air; D, still air.

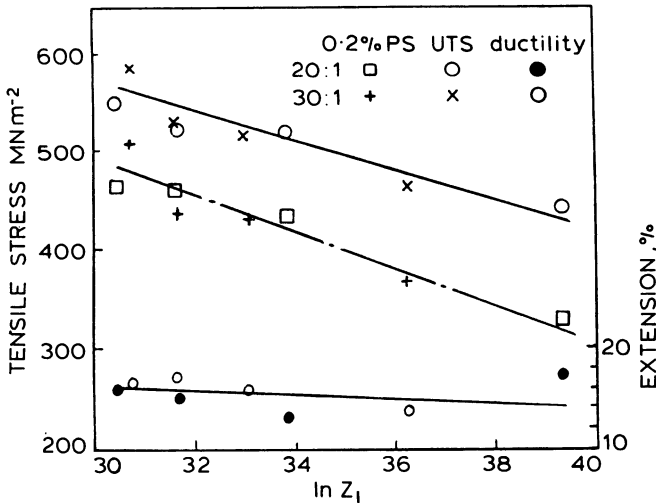
occur. Then a compromise must be achieved, balancing distortion and  $\tau'_{crit}$ . It may not be possible to quench using water but water mist designed sprays have proved to be successful.

#### *Press effect*

Aluminium alloys do not in general recrystallize during extrusion but static recrystallization, either partial or complete, may occur after leaving the die. Recrystallization can be impeded by manganese, chromium and zirconium, which are particularly effective in the form of finely distributed precipitate. Considerable strengthening, improved toughness, and improved corrosion resistance are obtained when a fibre structure is pronounced: crystallographic anisotropy results in a considerable difference in tensile strength parallel and perpendicular to the direction of extrusion. This effect is reported to be greater in thicker sections than thin sections although the reasoning presented by many authors is incorrect. They assume that the substructure is more perfect in

thin sections and this aids the ageing mechanism. In the author's experience there is little or no difference in substructure and it seems probable that for thin sections the method of testing is likely to be the reason for the observed increase in homogeneity. Thus, the so called press effect is fairly well understood and it has been shown that even when alloys are not press quenched then a retained substructure after heat treatment is advantageous.

Obviously, it could be an advantage to retain all the substructure in the aerospace 2XXX and 7XXX alloys. However, the C curves given in Chapter 3 do not promise particularly satisfying results if 2000 series alloys were press quenched. The only reference to such a procedure is that describing very briefly the press quenching of 2XXX alloys in the period 1942–1944. Some work on 2014 alloy involved a presolution soak preceding the extrusion step [60]. The mechanical properties of the extrudate were measured after an artificial ageing treatment and are shown in Fig. 4.51. There were two features worthy of consideration: the maximum strength obtainable ( $550\text{--}590\text{ MN m}^{-2}$ ) is as good as can be obtained from conventional extrusion with slightly better elongation values, and the values of tensile strength vary in a linear manner with the value of temperature-compensated strain rate. However, an increase in strength with increasing  $\ln Z$ , would usually be expected, which suggests that, since the lowest temperatures ( $275^\circ\text{C}$ ) were below the C curve knee and the highest temperatures ( $475^\circ\text{C}$ ) above it, then copious heterogeneous nucleation has occurred. These extrusion billets were air cooled to extrusion temperature (from  $500^\circ\text{C}$ ) and this could certainly be improved by using a water mist or forced air cooling. Although it is the corrosion



**Fig. 4.51** Tensile properties as a function of  $\ln Z_1$  for 2014 alloy subject to prolonged reheat soak at  $500^\circ\text{C}$ ;  $Z_1$  is the temperature-compensated strain rate calculated using the initial billet temperature.

resistance which is critical in these alloys, the results warrant further investigation. It should be borne in mind that these extrudates show no surface recrystallization, promising the ability to extrude to net shape which would offer a considerable economic advantage. Obviously, however, extrusion must be performed at low  $\ln Z$  values (i.e. high temperatures).

Finally, it is perhaps pertinent to note that all data for quench rate sensitivity and C curve determination have been obtained from fully recrystallized structures which are not typical of the as-extruded structure. It might be expected that the data available might not be accurate for press quench analysis in which a substructure will most certainly be a feature of the morphology.

Press quenching is an economic method to produce extrudates having the required properties in most of the 6XXX alloys and the 7XXX Al-Zn-Mg alloys. The theory exists to predict the precipitation events occurring during the sequence but it appears to be misused in many cases. Nevertheless it must be recognized that material of adequate quality is produced in this way.

Some results suggest that at least some of the 2XXX alloys should be press quenchable and research in this area might be productive. It is not clear that the C curves produced using usual experimental procedures are directly applicable to the process, since they have been derived from varying structural morphologies.

### 4.13 LIMIT DIAGRAMS

The extrusion process must usually produce an engineered product satisfying strict geometric, cosmetic and property specifications. This complex process involves interaction between the process variables and material high-temperature characteristics. Process variables available for control are the extrusion ratio  $R$ , the ram speed  $V$  and the extrusion temperature  $T$ . Material variables include homogeneity, ease of dislocation interaction, alloying elements and billet condition, all of which may be affected by preheat conditions.

One limiting factor lies in the inherent stiffness of alloys even at elevated temperatures. It may make the required load higher than the extrusion press capacity. Another major factor limiting the process parameters is the maximum temperature that can be tolerated during the process. This latter factor has always been associated with incipient melting, but in practice a press operator will in general observe other undesirable features before incipient melting occurs. The representation of these two factors upon one diagram was first proposed by Hirst and Ursell [61] who suggested that the load limitation could be represented by a specific pressure line and the temperature limitation by an incipient melting line calculated assuming adiabatic conditions and relating temperature rise to extrusion reduction ratio. Such diagrams were termed limit diagrams and are schematically shown in Fig. 4.52. After this initial research, limit diagrams underwent various modifications in the variables used for abscissa and ordinate [62–64]. However, probably the most useful form of such diagrams is in the format

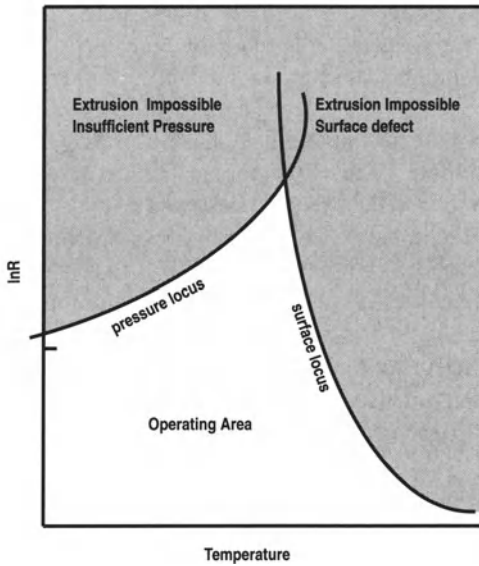


Fig. 4.52(a) Limit diagram (schematic) [68].

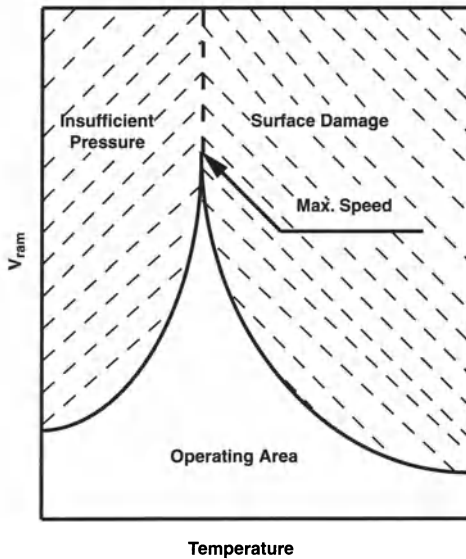


Fig. 4.52(b) Limit diagram (schematic) [64].

developed by Sheppard and Raybould [65]. The format utilized constant strain rate curves and also showed that limit diagrams could provide specific metallurgical data upon the structure of the final extrude, thus providing the press operator with the capacity for metallurgical process control [66–68]. They also indicated that equations used in previous works to determine temperature could lead to

quite serious errors. Stenger [64] at a much later date depicted diagrams using velocity and temperature as the axes, keeping the extrusion ratio  $R$  as a constant. We shall see in Chapter 5 that such diagrams pose some problems in interpretation.

To construct the pressure-limiting line, the flow stress [15] must be determined in terms of the strain rate  $\dot{\bar{\epsilon}}$  and extrusion temperature  $T$ . In most published work, this stress has been established by camplastometer, by torsion or by straightforward back calculation from extrusion formulae without consideration of temperature rises occurring in the process. The author is of the opinion that the torsion test, if coupled with a satisfactory estimate of temperature rises, provides a suitable evaluation of flow stress for the extrusion process. An important observation is that interpretation of friction conditions is eliminated. The pressure-limiting line has also been in error, because maximum pressure has been calculated by adding the friction component to the calculated load occurring at the 'discard' stage of extrusion. Many workers have observed that in addition to this load an additional pressure is required to initiate friction. This additional load is a function of dislocation dynamics, and so produces a peak or breakthrough pressure.

Temperature rises occurring during extrusion should be referred back to initial billet conditions; otherwise the diagrams would be of little practical use. As previously noted, flow stress is likely to be erroneous, and this parameter must appear in all temperature-rise calculations, since the work of deformation produces the energy input.

The impediments to the use of extrusion limit diagrams by industrial units no longer exists. The pressure line is accurate, because peak pressure is now represented and because diagrams now incorporate flow stress data which is known to be accurate. The assumption that a temperature-limiting line is the curve at which incipient melting occurs is false. The actual limiting curve will depend upon cosmetic and structural considerations. The temperature rise occurring during the extrusion process must be accurately predicted in order to construct an adequate billet heating schedule. This is most conveniently accomplished using the integral profile technique.

We shall deal with practical limit diagrams in Chapter 5, using this discussion to derive the necessary equations. Equations require setting up both for the original Hirst-Ursell type diagram (ram speed constant) and for the Stenger alternative (extrusion ratio constant). We need to recall that the extrusion pressure is given by:

$$p = \bar{\sigma} \left[ 0.171 + 1.86 \ln R + \frac{4mL}{\sqrt{3}(D)} \right] + \Delta p$$

$$\frac{\dot{\bar{\epsilon}}}{\dot{\bar{\epsilon}}} = \frac{6V_B(0.171 + 1.86 \ln R) \tan(38.7 + 6.9 \ln R)}{D_B}$$

Hence:

$$p - \Delta p = \frac{1}{\alpha} \ln \left[ \left( \frac{Z}{A} \right)^{\frac{1}{n}} + \sqrt{\left\{ \left( \frac{Z}{A} \right)^{\frac{2}{n}} + 1 \right\}} \right] \left[ 0.171 + 1.86 \ln R + \frac{4mL}{\sqrt{3}(D)} \right]$$

and:

$$\frac{(p - \Delta p) \alpha n}{\left[ 0.171 + 1.86 \ln R + \frac{4mL}{\sqrt{3}(D)} \right]} - n \ln 2 + \ln A - \frac{\Delta H}{GT} = \ln \dot{\epsilon} = \ln \frac{6K_{\epsilon} V_R}{D_B}$$

from which:

$$\exp \left\{ \frac{(p - \Delta p) \alpha n}{\left[ 0.171 + 1.86 \ln R + \frac{4mL}{\sqrt{3}(D)} \right]} - n \ln 2 + \ln A - \frac{\Delta H}{GT} \right\} \frac{D_B}{6K_{\epsilon}} = V_R \quad (4.14a)$$

where  $K_{\epsilon} = (0.171 + 1.86 \ln R) \tan (38.7 + 6.9 \ln R)$  and

$$\left\{ \frac{(p - \Delta p) \alpha n}{\left[ 0.171 + 1.86 \ln R + \frac{4mL}{\sqrt{3}(D)} \right]} - n \ln 2 - \ln \frac{6K_{\epsilon}}{V_R} + \ln A \right\}^{-1} \frac{\Delta H}{G} \cong T \quad (4.14b)$$

Thus the pressure limitation may be expressed in terms of either temperature or ram velocity depending upon which is required to be the dependent variable.

The equation governing the breakdown of the surface (i.e. incipient melting, die lines etc.) can be described by equations of the form [28]:

$$\ln \left( \frac{Z_i}{A} \right) = aT^{-b}$$

$$\ln \frac{6K_{\epsilon} V_B}{D_B} + \frac{\Delta H}{GT} = aT^{-b} + \ln A$$

from which

$$V_B = \frac{D_B}{6K_{\epsilon}} \exp \left( aT^{-b} - \frac{\Delta H}{GT} + \ln A \right) \quad (4.15a)$$

and

$$\left[ \ln \left( \frac{6K_{\epsilon} V_B}{AD_B a} \right) + \frac{\Delta H}{aGT} \right]^b = T$$

which is non-linear in  $T$ . However the surface limitation locus may also be plotted as a value of  $\ln R$ . Hence:

$$\ln K_{\dot{\epsilon}} = aT^{-b} - \frac{\Delta H}{GT} + \ln \left( \frac{AD_B}{6V_B} \right) = \ln (0.171 + 1.86 \ln R) \tan (38.7 + 6.9 \ln R)$$

$K_{\dot{\epsilon}}$  may be reduced by regression to  $5.62(\ln R) - 5.6$  with a regression coefficient of 0.998 which aids in computation.

$$\frac{\exp \left( aT^{-b} - \frac{\Delta H}{GT} - \ln A \right) \frac{AD_B}{6V_B} + 5.6}{5.62} = \ln R \quad (4.15b)$$

Schematics of the two types of limit diagram are given in Fig. 4.52.

In each case areas are depicted on the diagrams where extrusion is not possible, either because of damage to the surface or insufficient press pressure. The operating area is thus defined and within this area will lie the ideal operating point which will depend upon structural as well as productivity considerations.

## REFERENCES

1. Patterson, S.J. (1981) Ph.D. Thesis, University of London.
2. Ludwik, P. and Scheu, R. (1925) *Stahl und Eisen*, **45**, 373.
3. Canova, G., Shrivastava, S.C., Jonas, J.J. and G'Sell, C. (1982) The use of torsion testing to assess material formability, in *Formability of Metallic Materials-2000AD*, ASTM STP 753 (eds J.R. Newbury and B.A. Niemeier), ASTM, Philadelphia, PA, USA, 189-210.
4. Sellars, C.M. and Tegart, W.J.McG. (1972) *Intl. Met. Rev.*, **17**, 1.
5. Hodiernne, F.A. (1962) *J. Inst. Met.*, **91**, 267.
6. Sheppard, T. and Wright, D. (1979) *Met. Tech.*, 215-223.
7. Sheppard, T. (1987) Proc. 8th Int. Light Metals Congress, Leoben-Vienna, 301-311.
8. Sheppard, T. and Raghunathan, N. (1989) *Mat. Sci. Tech.*, **5**, 194-201.
9. Sheppard, T. (1993) *Mats. Sci. Tech.*, **9**, 430-440.
10. Mecking, H. and Kocks, U.F. (1981) *Acta Met.*, **29**, 1865.
11. Estrin, Y. and Mecking, H. (1984) *Acta Met.*, **32**, 57.
12. Anand, L. (1982) *J. Eng. Mat. Tech.*, **104**, 32.
13. Sample, V.M. and Lalli, L.A. (1986) *Aluminium Technology '86*, (ed. T. Sheppard), Metals Society of London, 175-185.
14. Ness, E., Vatne, H.E., Daaland, O., Furu, T., Orsund, R. and Marthinsen, K. (1994) Proc. International Conference on Aluminium Alloys 4, September, Atlanta.
15. Barraclough, D.R. (1973) *J. Testing and Evaluation*, **1**(3), 220-226.
16. Sheppard, T. and Wright, D.S. (1979) *Mat. Tech.*, **6**, 224-229.
17. Garafalo, F. (1973) *Trans. Met. Soc. AIME*, **227**, 351.
18. Sheppard, T. and Jackson, A. (1996) Proc. 6th Int. Al. Ext. Techn. Seminar, Chicago, May, 223-229. Aluminium Association, Washington DC.
19. Tunnicliffe, P.A. (1979) Ph.D. Thesis, University of London.
20. Clode, M.P. (1987) Ph.D. Thesis, University of London.
21. McQueen, H.J. (1977) *Met. Trans.*, **8A**, 807-824.



22. Pearson, C.E. and Parkins, R.N. (1961) *The Extrusion of Metals*, Chapman & Hall, London.
23. Tutcher, M.G. (1979) Ph.D. Thesis, University of London.
24. Hinesly, P. and Conrad, H. (1973) *Mat. Sci. Eng.*, **12**, 47.
25. Zimmerman, Z. and Avitzur, B. (1970) *J. Eng. Ind.*, **92**, 119.
26. Sohrabapour, S., Shabaik, R.H. and Thomsen, E.G. (1970) *J. Eng. Ind.*, **92**, 461.
27. Sheppard, T. (1982) Proc. Int. Symposium Extrusion, Garmisch Partenkirchen. DGM, Dusseldorf and The Metals Society, London.
28. Castle, A.F. and Sheppard, T. (1976) *Met. Tech.*, **2**, 465–475.
29. Raybould, D. and Sheppard, T. (1973) *J. Inst. Met.*, **101**, 73–78.
30. Sheppard, T. and Tutcher, M.G. (1980) *Met. Tech.*, **7**, 488–493.
31. Sheppard, T. and Wood, E.P. (1980) *Met. Tech.*, **7**, 56.
32. Sheppard, T. and Vierod, R.P. (1985) *Mat. Sci. Tech.*, **1**, 321–324.
33. Sheppard, T., Patterson, S.J. and Tutcher, M.G. Proc. Symposium at the Annual Meeting of TMS, NY, 1985, in *Microstructural Control in Aluminium Alloys*, (eds E.H.Chia and H.J. McQueen), (1986) AIME, PA, 123–154.
34. Vierod, R.P. and Sheppard, T. (1987) *Mat. Sci. Tech.*, **3**, 285–290.
35. Clode, M.P. and Sheppard, T. (1990) *Mat. Sci. Tech.*, **6**, 755–763.
36. Sheppard, T. (1993) *Mat. Sci. Tech.*, **9**, 430–440.
37. Jackson, A. and Sheppard, T. (1997) *Mat. Sci. Tech.*, **13**, 23.
38. Castle, A.F. (1974) Ph.D. Thesis, University of London.
39. Wood, E.P. (1978) Ph.D. Thesis, University of London.
40. Sheppard, T. (1996) Proc. 6th Int. Al. Ext. Tech. Sem., Chicago, **1**, 163.
41. Sheppard, T., Nisaratanaporn, E. and McShane, H.B. (1998) *Z. Metallkd.*, **89**.
42. Sheppard, T. (1982) Proc. Int. Symposium Extrusion, Garmisch Partenkirchen. DGM, Dusseldorf and The Metals Society, London.
43. Sheppard, T., McShane, H.B., Raghunathan, N. and Subramaniyan, J. (1990) Proc. International Conference on Aluminium Alloys 2, Beijing, 325–337. International Academic Publishers, Beijing.
44. Tutcher, M.G. and Sheppard, T. (1980) *Mat. Sci. J.*, **7**, 579–589.
45. Clode, M.P. (1987) Ph.D. Thesis, University of London.
46. Cooper, P.S. (1985) Ph.D. Thesis, University of London.
47. Sheppard, T., Yin, X. and Raghunathan, N. (1991) *Mat. Sci. Tech.*, **7**, 341–352.
48. Barker, L.M. (1977) *Eng. Fract. Mech.*, **9**, 361.
49. Kirman, I. (1971) *Metall. Trans.*, **2**, 1761.
50. Hornbogen, E. (1975) *Z. Metallkd.*, **66**, 571.
51. Tutcher, M., Flower, H.M. and Sheppard, T. (1979) *Mat. Sci. J.*, **6**, 473.
52. Smith, C.S. (1951) *The Extrusion of Aluminium Alloys*, The Institute of Metals, London.
53. Beatty, E.C. (1977) Proc. 2nd International Extrusion Technology Seminar, Atlanta, **1**, 31. Aluminum Association, Washington DC.
54. Marchive, D. and Deschamps, R.D. (1979) *Rev. Alum.*, **489**, 37.
55. Fornerod, R.C. (1981) *Rev. Metall.*, **2**, 27.
56. Underwood, E. and Manning, G.R. (1963) *Mem. Sci. Rev. Metall.*, **60**, 637.
57. Belgian Patent No.869353 (1979) *Process for extruding high strength Al alloys*. Cegedur Pechenet.
58. Devaley, R. (1980) *Rev. Alum.*, **477**, 39.
59. Akeret, R. (1972) *Mem. Sci. Rev. Metall.*, **69**(9), 633.
60. Vierod, R.P. and Sheppard, T. (1985) *Mat. Sci. Tech.*, **1**, 321.
61. Hirst, S. and Ursell, D.H. (1958) *Metal Treatment*, **25**, 409.
62. Ashcroft, K.A. and Lawson, G.S. (1960/61) *J. Inst. Met.*, **89**, 369.

63. Meadows, B.J. and Cutler, M.J. (1969) *J. Inst. Met.*, **97**, 321.
64. Stenger, H. (1975) *Wire World Int.*, **17**, 54.
65. Sheppard, T. and Raybould, D. (1973) *J. Inst. Met.*, **101**, 73.
66. Sheppard, T., Tunncliffe, P.A. and Patterson, S.J. (1982) *J. Mech. Work. Tech.*, **6**, 313–331.
67. Sheppard, T. (1993) *Mat. Sci. Tech.*, **9**, 30–440.
68. Sheppard, T. (1977) Proc. 2nd International Extrusion Technology Seminar, Atlanta, 331–337. Aluminium Association, Washington DC.

# Homogenization and extrusion conditions for specific alloys

## 5.1 INTRODUCTION

The object of this chapter is to consider the conditions required for practical homogenization and its effect on extrusion processing parameters and, where appropriate, investigate how property development is influenced by homogenization. The examples are drawn from more recent work for aluminium alloys in each of the alloy series. In sections 5.1–5.8 we shall, in the main, discuss metallurgy and the homogenization requirements leaving the extrusion considerations for discussion under the heading of ‘limit diagrams’. It is normal to relate alloy extrusion to maximum extrudate speeds but the reader will be aware from the discussion on shape considerations in Chapter 4 that it is, in general, meaningless to suggest a maximum speed without taking into account the extrusion ratio, the shape factor, metallurgical factors (i.e. the retention of the press effect in 6XXX alloys or the structural factors required to produce acceptable fracture toughness in 2XXX or 7XXX alloys) and geometrical specifications of the product. Therefore we shall show these effects by means of limit diagrams and, at the conclusion of that consideration, will be able to grade the alloys in terms of extrudability.

In all process–property relationships the process variables are linked to the properties because the structure and substructure of the material at the exit of the extrusion press is directly related to the homogenization, reheat and extrusion practices. This structure, of course, determines the alloy morphology at commencement of the solution soak and ageing sequence in the case of heat-treatable alloys and is the final structure of the 1XXX, 3XXX and 5XXX alloys.

Homogenization temperatures for the commercial aluminium alloys are typically about 20–50°C below the solidus and as near as possible to the initial hot working temperature. Table 5.1 shows these temperatures.

**Table 5.1** Solidus, homogenization and extrusion temperatures for aluminium alloys

<i>Alloy</i>	<i>Solidus (°C)</i>	<i>Homogenization temperature (°C)</i>	<i>Extrusion temperature (°C)</i>
1XXX	640–650	560–605	450–550
2XXX	500–650	480–530	400–480
3XXX	630–645	530–620	480–520
5XXX	570–630	380–550	400–480
6XXX	580–620	560–600	430–500
7XXX	>500	400–500	390–450

## 5.2 1XXX ALLOYS

All grades of commercially pure aluminium contain insoluble elements albeit in very small amounts and these decorate the grain boundaries in cast material. The network is formed almost entirely by the Fe and Si constituents, the nature and size being determined by the Fe:Si ratio. In the Al–Fe–Si system two ternary compounds are formed,  $\text{Fe}_2\text{SiAl}_8$  and  $\text{FeSiAl}_5$ . In addition  $\text{FeAl}_3$  and silicon may be present. The metastable  $\text{FeAl}_6$  can also be formed on the outer regions of thick DC cast billets. The presence of trace amounts of Cu, Mn and Cr together with the rapid cooling rates of the DC process facilitate the formation of the cubic  $\text{Fe}_3\text{Si}_2\text{Al}_{15}$  in place of the  $\text{Fe}_2\text{SiAl}_8$ . During homogenization equilibrium is reached and  $\text{Fe}_2\text{SiAl}_8$  and  $\text{FeAl}_3$  are usually the compounds observed in commercial material.

1XXX alloys are by definition at least 99%Al and require a homogenization treatment because of the decoration of the grain boundaries by the small amount of usually unintended alloy additions. If not homogenized the product will be more brittle but processing is almost unaffected. For these reasons there is little literature on the homogenization of alloys corresponding to AA specification.

In a slowly cooled Al–0.30%Fe–0.15%Si alloy [1], the effect of increasing the homogenization temperature is to increase the subsequent recrystallization temperature. The effect is especially noticeable between 400°C and 500°C. The fine precipitates formed during casting were reported to redissolve during thermal exposure, thus retarding softening during anneal and favouring the formation of coarse imperfect grains. As shown above the precipitates will be, in the main, Fe compounds and their size and morphology are unlikely to be affected unless the homogenization temperatures exceed 560–570°C. If this is the case then the precipitate will spheroidize and disperse thus acting as pinning sites for dislocations. If, however, the precipitate retains its as-cast morphology then nucleation at those precipitates can occur and recrystallization will be enhanced leading to some quite coarse grains along with the smaller grains nucleated by a subgrain coalescence mechanism.

Eliminating the homogenization step altogether [2] for the 1000 series alloys yields higher strength and lower ductility for DC cast billet in all of the as-extruded tempers.

The influence of homogenization temperature on hot deformation in a series of Al-Fe, Al-Si and Al-Fe-Si alloys has been investigated [3]. High-temperature (550°C) exposure was reported to promote dynamic recovery and substructure development during hot deformation, whilst low-temperature (350°C) exposure led to more spasmodic dynamic recovery. This behaviour again illustrates the effect of homogenization temperature on the precipitate size and number, and the tendency of fine precipitates in turn to control dynamic recovery; the effect of precipitates smaller than 0.2  $\mu\text{m}$  on workability during hot deformation is that, as the number of fine precipitates increases, that is the homogenization cooling rate increases, the workability decreases. We should note that this is a general behaviour pattern for all aluminium alloys since the extent of dynamic recovery is very strongly influenced by dislocation density and by vacancy concentration, both of which are strongly temperature dependent.

The influence of Mn, Fe, Si and Mg in the Al-Mg, Al-Si, Al-Fe, Al-Mn, Al-Fe-Si and Al-Mn-Mg alloys on the dynamic recovery and restoration has been systematically studied [4,5]. The homogenization generated fine precipitates in the alloys containing Fe and Mn tending to restrain dynamic recovery, whereas those containing Si and Mn have little effect. Furthermore, the number of fine precipitates smaller than 0.2  $\mu\text{m}$  is greater in the Al-Fe and Al-Fe-Si alloys than in the Al-Mn-Mg alloys. The Mn-containing precipitates are larger and fewer than the Fe-containing precipitates. Hence the effect of homogenization on dynamic recovery is greater in the iron- than in the manganese-containing alloys. This is mainly the result of having to accept that it is extremely difficult to redissolve the Mn compounds at any reasonable homogenization temperature.

The degree of dynamic restoration (related to recovery recrystallization and grain growth) defined as  $(C_v - H_d)/(C_v - R_v)$ , where  $C_v$  is the yield strength of the extruded material,  $R_v$  the yield strength of annealed material after extrusion and  $H_d$  the deformation stress after extrusion, is plotted against homogenization temperature in Fig. 5.1. The dynamic restoration rate is high in the 99.99% Al, Al-Si, Al-Fe and Al-Fe-Si alloys with low matrix solute content and is low in the Al-Mg, Al-Mn and Al-Mn-Mg alloys with considerable matrix solute content. Subgrains are more easily formed in the Al-Mg than in the Al-Fe alloy due to the lower solubility of Fe in Al. Increasing the homogenization temperature to a high level increases the dynamic restoration rate; the dynamic recovery is accelerated, the subgrain size increases and the hot working tends to change from 'pure metal type' to 'alloy type'. This modification to the texture of the material is important and the implication is that if homogenous texture is required (and it usually is) then a high-temperature homogenization is required and should probably exceed 600°C.

It would appear that for the 1XXX grades of aluminium an exposure at 600°C for at least 6 h would be recommended followed by furnace cooling (air cooling might be acceptable on economic grounds).

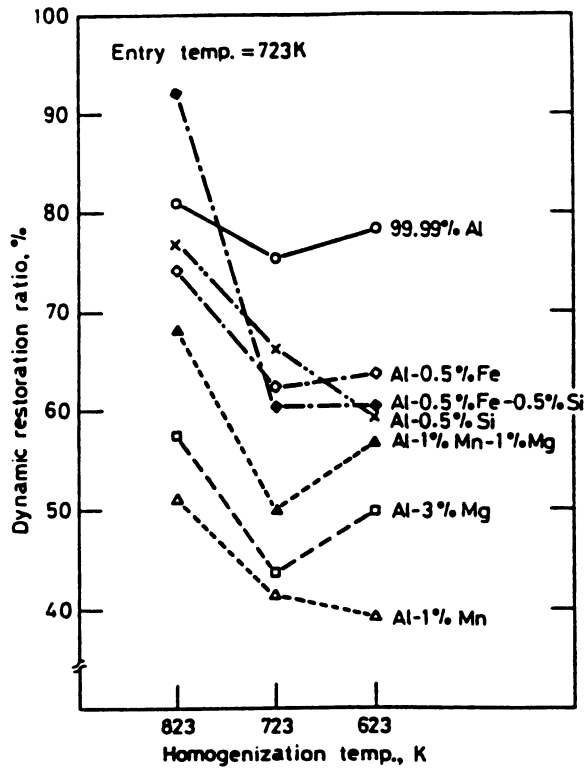


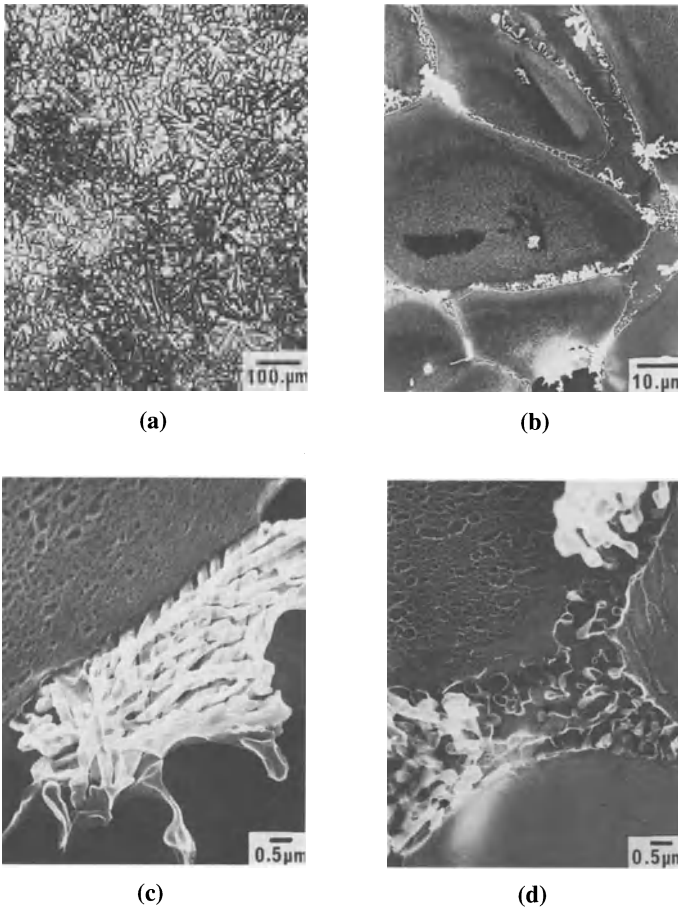
Fig. 5.1 The effect of homogenization temperature on dynamic restoration index.

### 5.3 2XXX ALLOYS

In experiments conducted using 2014 alloy [6] the structure of the as-cast material was generally as shown in Fig. 5.2(a); an optical micrograph taken of the centre of a direct-chilled ingot, but typical of the structure observed throughout the material. The micrograph indicates a strong dendritic structure with a considerable fraction of dark interdendritic eutectics. The structure was further examined at higher magnification using the scanning mode of a TEMSCAN and the structure at relatively low magnification was as shown in Fig. 5.2(b). The dominant feature of the micrograph is the dendritic structure, but this magnification reveals the interdendritic region to be composed of both bright and dark constituents. Segregation, both within the dendrite arms and in the eutectic, can easily be identified. The two differing eutectics are shown at higher magnification in Figs. 5.2(c) and (d). The bright fibrous eutectic can be clearly shown to be brittle in nature (Fig. 5.2(b)) and EPMA analysis revealed this to be an aluminium–silicon compound. The darker, more spherical, eutectic (Fig. 5.2(c)) was found to be copper rich. The presence of these eutectics can be deduced from the quaternary phase diagram shown in

Fig. 5.3 which strictly is only valid for the 460°C isothermal. It does, however, indicate the possible reactions during cooling. The approximate composition of the alloy is marked X on the diagram but, under the conditions of non-equilibrium cooling obtaining during casting, copper and magnesium will be retained in solid solution and the composition of the eutectic displaced towards the bottom left-hand corner of the diagram. The eutectics present and identified in Fig. 5.3 are therefore, quite clearly  $\alpha + \text{Si}$  and  $\alpha + \theta + \text{Q}(\alpha + \text{CuAl}_2 + \text{Cu}_2\text{Mg}_8\text{Si}_6\text{Al}_5)$ .

The structure is clearly not suitable for forming in the as-cast condition because of the brittle nature of the  $\alpha + \text{Si}$  eutectic and the detrimental effect on the age-hardening properties of the alloy which will result from the segregation of copper in the copper-rich eutectic.



**Fig. 5.2** Microstructure of as-cast DC logs; (a) optical; (b) TEM showing dendritic structure and nature of interdendritic; (c) TEM showing Si-rich interdendritic; (d) TEM showing Cu-rich interdendritic.

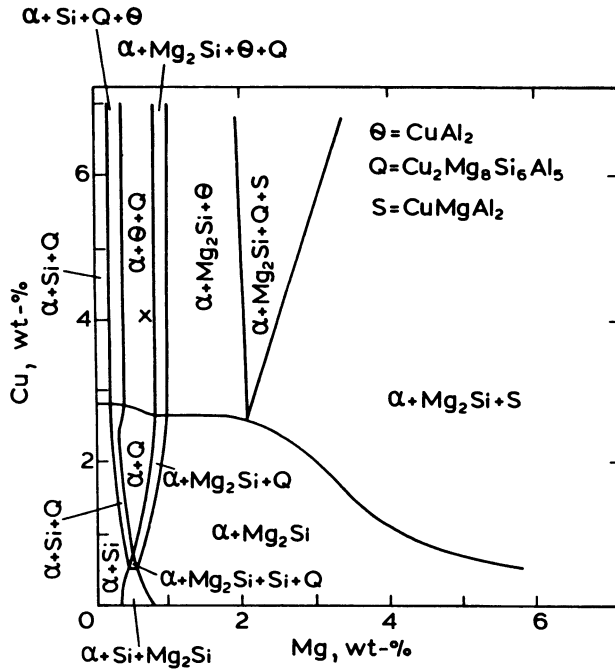
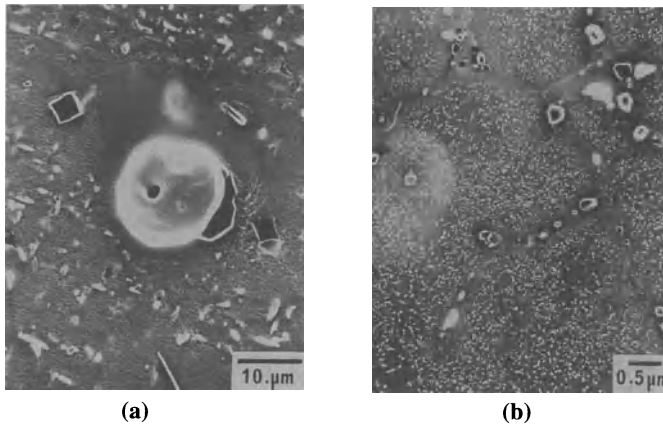


Fig. 5.3 Quaternary phase diagram. 'x' marks the location of the alloy used.

Inspection of the material by optical microscopy after soaking at 500°C for 8, 16, and 24 h, respectively and air cooling showed that there is considerable modification to structure after 8 h soaking, but the dendrite arms are still clearly visible within the recrystallized grains. Further soaking results in the diffusion removal of most of the cast structure but even after 24 h some evidence of the dendritic structure still remains. It is also clear that, as expected, there is no substantial grain growth during homogenization. The structures were also examined at higher magnification in the scanning mode of a TEMSCAN. The structure after exposure at 500°C for 8 h (Fig. 5.4(a)) showed that segregation had been very considerably reduced and the soluble components redistributed throughout the structure by diffusion. That part of the original structure which has been retained has left a residue of large particles in the intergranular regions. In one of these areas observed, the micrographs depicted a relatively large particle located in a precipitate-denuded area surrounded by much smaller precipitates. The composition of the large particle was found to be the complex copper–magnesium–silicon phase  $\text{Cu}_2\text{Mg}_8\text{Si}_6\text{Al}_5$ . The adjacent precipitate-free zone was mainly aluminium, with some dissolved copper, whilst smaller particles of needle type morphology were  $(\text{Fe}, \text{Mn})\text{Al}_6$  and  $\text{MnAl}_6$ ; diffraction pattern analysis showed that, in general, these particles lay on the cubic planes of the matrix. The particles almost certainly formed during cooling from the homogenization temperature.





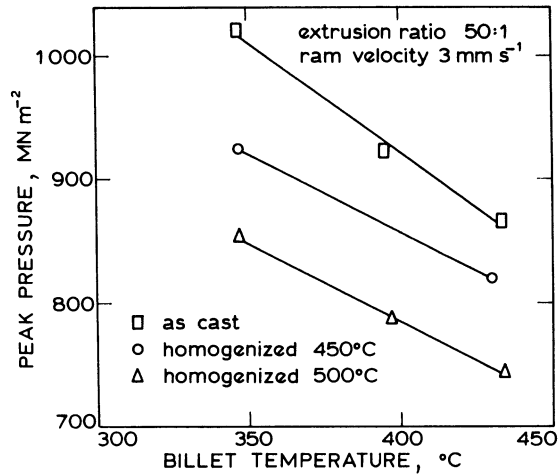
**Fig. 5.4** Homogenized structures; (a) 500°C for 8 h; (b) 500°C for 24 h.

The effect of soaking at 500°C for 24 h is shown at higher magnification in Fig. 5.4(b). Comparison with Fig. 5.4(a) demonstrates the advantages of prolonged exposure at high temperature. The structure consists of a uniform distribution of small precipitates with only a few isolated large particles. One of these large particles was examined in the transmission mode and was identified as an  $\text{Mg}_2\text{Si}$  particle in a precipitate-free area. This would suggest that the increase in copper taken into solution during homogenization forces the silicon to combine preferentially with the magnesium to form  $\text{Mg}_2\text{Si}$ . The size of the  $\text{Mg}_2\text{Si}$  particles was typically 0.06 µm, compared to the 1.5 µm particles found in the material soaked for only 8 h. Thus the extended soak enabled further diffusion to reduce the size of the larger particles. The smaller particles evident in the structure were once more identified as  $(\text{Fe},\text{Mn})\text{Al}_6$  and  $\text{MnAl}_6$ , having a size of about 0.05–0.075 µm.

It is thus obvious that homogenization time and temperature are important variables in the thermomechanical process. For this particular alloy it would appear to be desirable to utilize an extended soak (at least 12 h) at 500°C. The same metallurgical result could, however, presumably also be achieved at some other time in the cycle. Hence, it will be instructive to investigate the effect of homogenization on the extrusion process.

The preceding section has indicated that the time and temperature involved in the homogenization cycle have a pronounced effect on the structure of the material which enters the extrusion container. The effect of these structures on the extrusion pressure and the resultant structure of the extrudate will now be considered.

Billets have been extruded in the as-cast condition, after homogenization for 24 h at 450°C, and after homogenization for 24 h at 500°C [7]. The effect of the initial billet structure on extrusion pressure is shown in Fig. 5.5, it is evident that the initial structure quite drastically affects the extrudability of alloy 2014. The as-cast material requires about 20% more pressure than that required to extrude a



**Fig. 5.5** Extrusion pressure dependence on initial billet temperature and homogenized condition.

billet given a thorough homogenization treatment, owing to internal stresses and segregation in the cast material. The result of gross segregation is that hard brittle eutectics and large volume fractions of precipitate are present during the extrusion process; these raise the flow stress of the material consequently raising the required extrusion pressure. The billets homogenized for 24 h at 450°C required about 10% additional pressure, confirming that the continued presence of partial segregation is deleterious. The excess pressure also implies that the temperature rise during the extrusion process will be greater in the as-cast material, leading to more difficulty in controlling surface defects especially those due to incipient melting. The extrusion limits are thus generally reduced when extruding incorrectly homogenized material.

The structure resulting from the extrusion of an as-cast billet was one in which the dominant feature of the morphology were stringers of large particles aligned in the extrusion direction. These particles had the as-cast eutectic as their origin and had been fragmented by shear during the extrusion process. EPMA analysis identified them as the  $Mg_2Si$  and  $CuAl_2$  phases. Thus the segregation observed in the as-cast structure is retained through the extrusion process, so becoming detrimental to the normal age-hardening process. It might also be expected that these stringers and large particles would be detrimental to the extrudate fracture properties. The substructure is also affected by these stringers taking on a 'brick-like' morphology, rather than the usual, more equiaxed, subgrain structure.

The above sections have indicated that, even at 500°C, the possibility of effecting structural variations by adjusting the homogenization conditions does not seem promising. Hence, preheating for prolonged times at extrusion temperatures of less than 440°C is unlikely to affect either the extrusion-process flexibility or

the extrudate structure. However, if the billet was preheated to 500°C and rapidly cooled to the extrusion temperature, then some additional solubility must occur and some of the soluble elements should be retained in solution; this increase in solubility should be greater at the surface, which should result in an increased resistance to deformation at the surface of a directly extruded billet. Surface cracking during extrusion occurs because the tensile stresses in the die land area are sufficient to fracture the material: thus, any preferential flow stress increase in the surface region would prove advantageous.

To test this hypothesis, fully homogenized billets were heated to 500°C, soaked for 30 min [8], and rapidly cooled to 400°C, before being extruded. The billets were extruded at a ratio of 50:1 over a wide range of ram speeds. The use of such a two step preheat (SS) results in improved surface condition of the extrudate (Fig. 5.6). It was also observed that the extrusion pressure was increased by about 3–5% but, providing that the resultant pressure is within the press capacity, the method offers the possibility of increased production without the usual incidence of surface cracking.

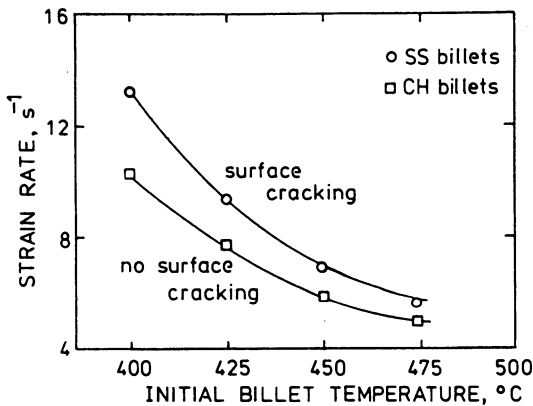
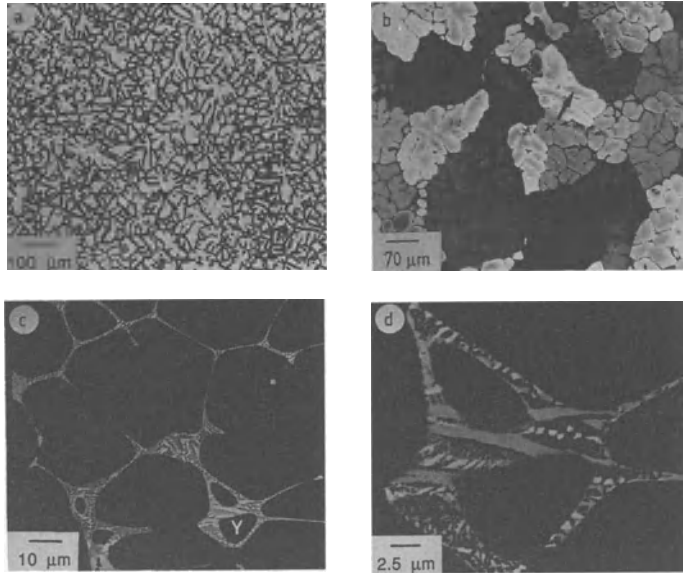


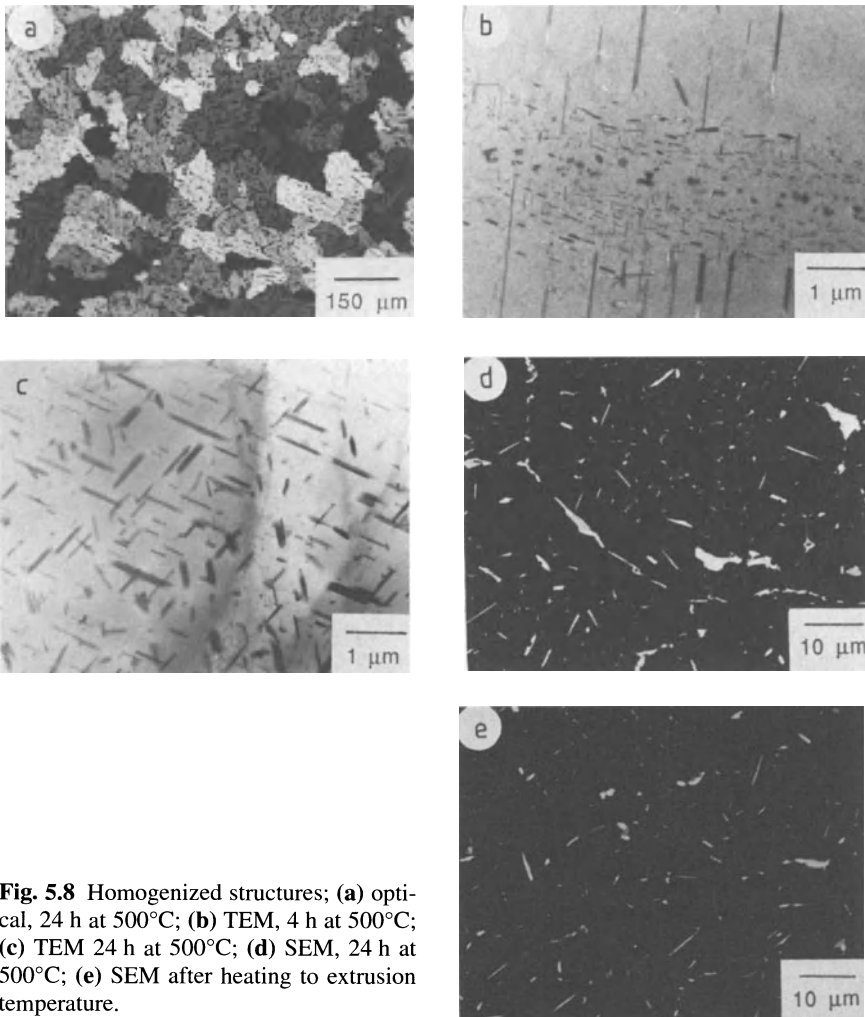
Fig. 5.6 Dependence of surface cracking on preheat cycle during extrusion.

Structural modifications occurring throughout homogenization of 2024 alloy have also been investigated in detail [9]. The starting microstructure of a DC cast billet is shown in Fig. 5.7. The structure, Figs. 5.7(a) and 5.7(b), clearly indicate the dendritic nature of the solidified billet. The structure reveals clearly the cored dendrites (labelled X in Fig. 5.7(b)) surrounded by the interdendritic eutectic, which appear darker in the optical micrographs. The grain structure is also revealed in Fig. 5.7(b) with the average grain size obtained in the cast metal being 90  $\mu\text{m}$ . Scanning electron microscopy analysis revealed (Figs. 5.7(c) and 5.7(d)) the darker interdendritic eutectic to consist of either  $\alpha + (\text{FeMnSiCu})\text{Al}$  or  $\alpha + \theta + (\text{Cu}_2\text{Mg}_8\text{Si}_6\text{Al}_3)$  whilst the lighter eutectic was  $\text{CuAl}_2$ ,  $\text{CuMgAl}_2$  or  $\text{CuFeMnAl}_6$ .



**Fig. 5.7** As-cast structures of alloy AA2024; (a) and (b) optical; (c) and (d) SEMs.

Clearly the cast structure with its low melting interdendritic eutectic, large concentration gradients, and intermetallic interdendritics is unsuitable for direct processing since it is indicative of poor workability. In addition the hardening constituent is partially tied up in interdendritic eutectics and heterogeneously distributed and is therefore not in a form which will be suitable to produce the required properties in the product. Differential scanning calorimetry tests on the as-cast material revealed a dissolution peak at about  $511^{\circ}\text{C}$ . Hence a homogenization treatment was given which included holding the billets for 24 h at  $500^{\circ}\text{C}$  followed by furnace cooling at  $80^{\circ}\text{C h}^{-1}$ . Homogenized structures of the alloy are shown in Figs. 5.8(a) and (b). The heavy coring and the dendritic structure present in the as-cast alloy is completely eliminated. It should also be noted that there was no substantial grain growth during the homogenization treatment; the approximate grain size was found to be  $95\ \mu\text{m}$ . The micrograph (Fig. 5.8(a)) indicates that most of the copper and magnesium from the interdendritic eutectic phases has been dissolved and taken back into solution. These structural changes occurring in the interdendritic areas is shown in Figs. 5.8(b) and (c) which indicate that segregation is largely eliminated and that the soluble components have been distributed throughout the original cells by diffusion. The structure is one of a uniform distribution of small particles with only isolated large particles. Homogenization dissolves much of the copper and magnesium but leaves some  $\text{CuMgAl}_2$  and possibly some  $\text{CuAl}_2$  out of solution. All the iron-containing phases undergo transformation to  $\text{Al}_7\text{Cu}_2\text{Fe}$  and  $\text{FeMnAl}_6$  suffering a change in morphology in the process, possibly accompanied by other minor phases, and remain in the dendrite



**Fig. 5.8** Homogenized structures; (a) optical, 24 h at 500°C; (b) TEM, 4 h at 500°C; (c) TEM 24 h at 500°C; (d) SEM, 24 h at 500°C; (e) SEM after heating to extrusion temperature.

core. Simultaneously, manganese is precipitated from solid solution as  $\text{Cu}_2\text{Mn}_3\text{Al}_{20}$ . A typical example of this is shown in Fig. 5.8(d). The needle like structure shown in high magnification was identified as  $\text{CuAl}_2$  or  $\text{CuMgAl}_2$  and adopts a Widmanstatten structure primarily due to slow cooling as shown in Fig. 5.8(c). The smaller lighter particles were difficult to analyse but found to be generally  $\text{FeMnAl}_6$  and  $\text{MnAl}_6$  while the darker particles were found to be  $\text{Mg}_2\text{Si}$ . The presence of  $\text{Mg}_2\text{Si}$  implies that the increase in copper taken into solution during homogenization results in silicon combining preferentially with magnesium. The same structure in the SEM mode, Fig. 5.8(d), reveals the transition metal particles along the grain boundaries and prior dendrite boundaries. The structure obtaining after heating to the extrusion temperature is shown in Fig. 5.8(e), indicating the

continued presence of the intermetallics, as expected, which represent potentially active nucleation sites in the recrystallization process and an indication that a significant proportion of the precipitates have been solutionized during the preheat. Nevertheless there are sufficient small particles, which act as growth inhibitors, remaining to prevent widespread growth at those nuclei stimulated at the large particles.

The dissolution peak revealed in the studies on 2014 and 2024 alloys will most certainly be present in the higher strength alloys (e.g. 2618) and we may conclude that 500°C must be the highest soak temperature for the complete range of the 2XXX alloys. This will automatically set the billet temperature at 430–470°C. Clearly the free cutting lead-containing alloys must be homogenized at a lower temperature.

#### 5.4 3XXX ALLOYS

Until recently the alloys 3003 and 3004 were exclusively rolling alloys finding their main application in can making. Consequently the existing literature and homogenization recommendations refer to those properties required for that application and are mainly connected with the attainment of suitable texture. However these alloys are now finding application in the extruded state, mainly in the automotive industry, and hence it will be instructive to review their homogenization.

The search for optimum processing conditions to develop cube textures and 0/90 earing in both 1100 and 3004 alloys [10] has been the major objective of research in the 3XXX alloys. In the referenced study the 1100 alloy was cast as 2.5 cm thick slab, homogenized, cold rolled to 0.1 cm thickness and annealed. The 3004 alloy was cast as 50 cm thick ingot, homogenized, hot rolled at 460°C entry and 260°C exit temperatures to 0.42 cm thickness, cold rolled to 0.10 cm and annealed. The heating rate during homogenization treatment was 40°C s<sup>-1</sup> and the cooling rate 20°C s<sup>-1</sup>. Two alternate anneal sequences were used: (i) box type with 25°C h heat rate and 350°C, 2 h hold and (ii) continuous anneal with 25°C s<sup>-1</sup> heat rate and a few seconds hold at 500°C.

For the 1100 alloy, 0/90° earing is achievable only after continuous annealing and the window for homogenization hold temperature is 400–450°C. For the 3004 alloy, the optimum homogenization hold is about 530°C for batch-type anneal and about 610°C for the continuous anneal. (Note that these optimum temperatures correspond approximately to the C curve nose for the 1100 and 3004 alloys, that is the temperatures for most rapid precipitation of Fe and Mn from the cold rolled supersaturated matrix.) It was found that for temperatures above the optimum decreasing the homogenization temperature, and for temperatures below the optimum increasing the homogenization temperature, resulted in a decrease in dispersoid density and an increase in precipitate-free zones, hence an increase in after-anneal cube textures. The behaviour of 3004 after continuous anneal, where recrystallization occurs without dispersoid interaction, is an

exception: the cube textures increase monotonically with temperature and 0/90 earing is achievable at the highest homogenization temperatures.

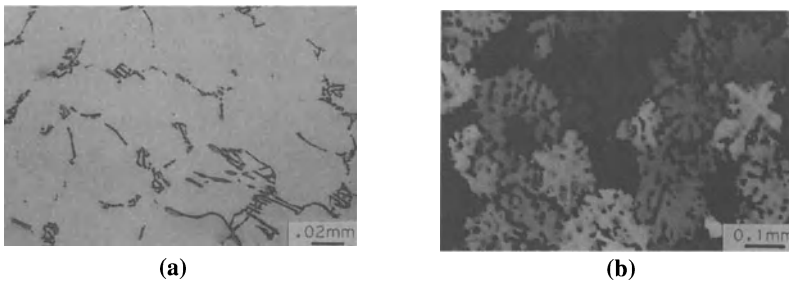
The enhanced 0/90° earing in ingot cast 3004 after low-temperature homogenization and batch-type anneal has been independently confirmed [11,12]. The effect, however, is dependent on the iron content, being specially pronounced at the low Fe levels. Although for continuous anneal, Fe content has little effect on 0/90 earing, at over 0.5% Fe and for high temperature homogenization, the continuous anneal yields somewhat higher 0/90 earing than the batch-type anneal.

If the annealing cube textures are relatively stable during subsequent deformation, the effect of the homogenization window can be discerned also in the cold rolled sheet for both ingot cast 3004 and batch-type anneal [13]. The largest proportion of cube textures, that is the lowest 45 earing, is obtained after 535°C 4 h homogenization treatment, a temperature which also corresponds to the minimum cold rolled earing. Sharpness of the minimum, however, is dependent upon the annealing temperature. At lower anneal temperatures, the recrystallization is incomplete, the strength of cube textures smaller and the as-rolled earing higher – especially at temperatures below the optimum homogenization temperature.

All of this work concerning 0/90° does not address the major problem in the 3004 alloys; that of securing low 45° earing in the H19 condition. The literature concerning this alloy is thus of only minimal use.

The as-cast structure contains about 5% of second-phase particles: mainly  $\text{Al}_6(\text{Fe},\text{Mn})$  and  $\alpha'\text{-Al}(\text{Fe},\text{Mn})\text{Si}$ . Microscopy reveals a cored dendritic structure, the coring being due to Mn segregation (Fig. 5.9). The Mn content of the dendrite cores are of a fairly uniform Mn content ; marginally below the average Mn content of the alloy whilst the dendrite arm peripheries exhibit an Mn concentration roughly half that of the nominal composition. The peripheries also contain the majority of the constituent particles. Fe levels are low in the matrix being concentrated in the constituent particles whilst Mg appeared to be evenly distributed throughout the matrix. The Mn is held in supersaturated solid solution.

The homogenization sequence for 3004 is well established involving a critical soak which must be above 605–610°C to ensure the precipitation of the Fe phases to assist scouring in the can-making process (this is also essential for earing



**Fig. 5.9** As-cast microstructure of AA 3004; (a) etched to show constituent particles; (b) etched to show grain boundaries.

properties because large iron-bearing particles result in preferential particle stimulated nucleation) followed by cooling at rates between 5 and 30°C h<sup>-1</sup> to ensure acceptable earing quality. The soak at above 605°C is thus mandatory; below this temperature earing quality cannot be maintained.

During soak at 605°C a very fine dispersoid forms which is confined to the dendrite cores, is the result of the rejection of Mn from supersaturated solid solution, and takes the form Al<sub>12</sub>(Fe,Mn)<sub>3</sub>Si. The large constituent particles break up and spheroidize and the macrosegregation becomes more apparent because of the fine dispersoid. As time at soak is increased Figs. 5.10(a) and (b) show that there is a gradual increase in conductivity and this certainly cannot be attributed to the formation of further dispersoids since the Mn has been first rejected and then redissolved during the heat-up sequence. The increase could be due to coarsening and spheroidization of particles or phase changes occurring in particles. However the most likely cause is the thermal stability of the Al<sub>12</sub>(Mn,Fe)<sub>3</sub>Si phase which varies with the Mn:Fe ratio. At commencement of the homogenization cycle the cores are supersaturated with Fe–Mn in particles. The first phase to form would be Mn rich because the solvus of the high Mn-bearing phase is lower than it's Fe equivalent. Above 500°C the solvus is exceeded and the phase is dissolved. The Fe phase remains stable and can precipitate at 605°C thus increasing conductivity. Redistribution of Mn and Fe within the phase stabilizes it as Fe rich. As cooling proceeds, conductivity increases due to the rejection of Fe and Mn to form Al<sub>12</sub>(Mn,Fe)<sub>3</sub>Si as their solubilities decrease.

Optical microscopy revealed that, in the homogenized material a very fine dispersoid had formed and was confined to the dendrite cores. This was due to the rejection of Mn from the supersaturated solid solution, in the form of Al<sub>12</sub>(Mn,Fe)<sub>3</sub>Si. Figure 5.11(a) shows these features very clearly and also illustrates

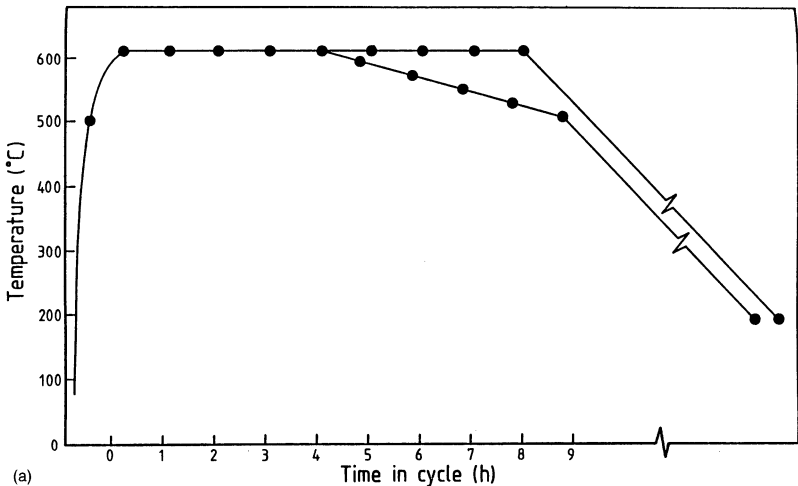
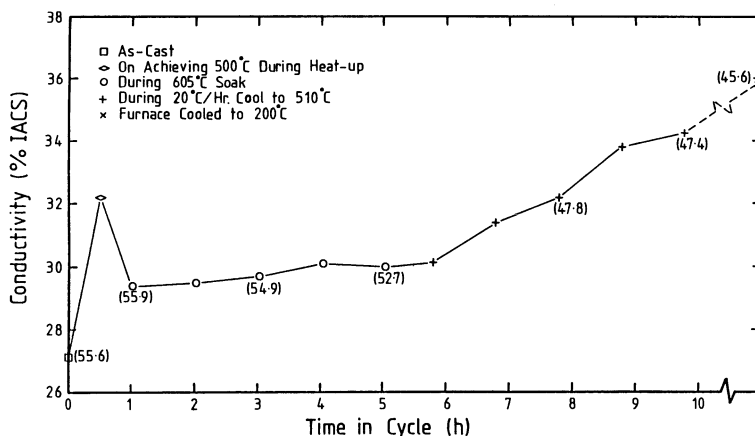


Fig. 5.10(a) Sampling points for conductivity measurements.





**Fig. 5.10(b)** Increase of conductivity during the homogenization cycle.

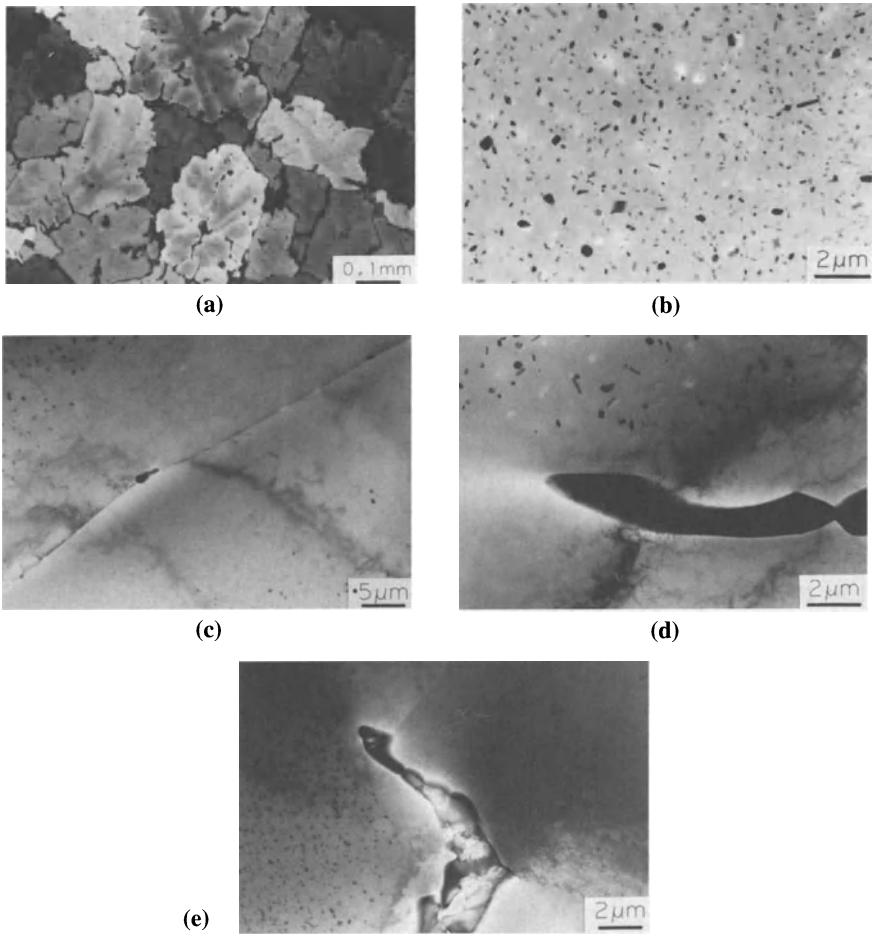
how the larger constituent particles break up and spheroidize during the homogenization cycle. Figures 5.11(b) and (c) show how the microsegregation becomes more apparent with the formation of the fine dispersoid; the electron micrograph in Fig. 5.11(d) reinforces these points.

Thus the literature reveals the changes occurring during a typical 3003 or 3004 soak intended to promote satisfactory earing in rolled sheet. It becomes obvious that the very high temperature soak is not necessary for the normal product in extrusion. However the coring observed in Fig. 5.9 is not acceptable and a homogenization procedure will be necessary. From the evidence it would appear that a soak at 575°C for about 5 h followed by a slow cool (furnace or air) would be satisfactory.

## 5.5 4XXX ALLOYS

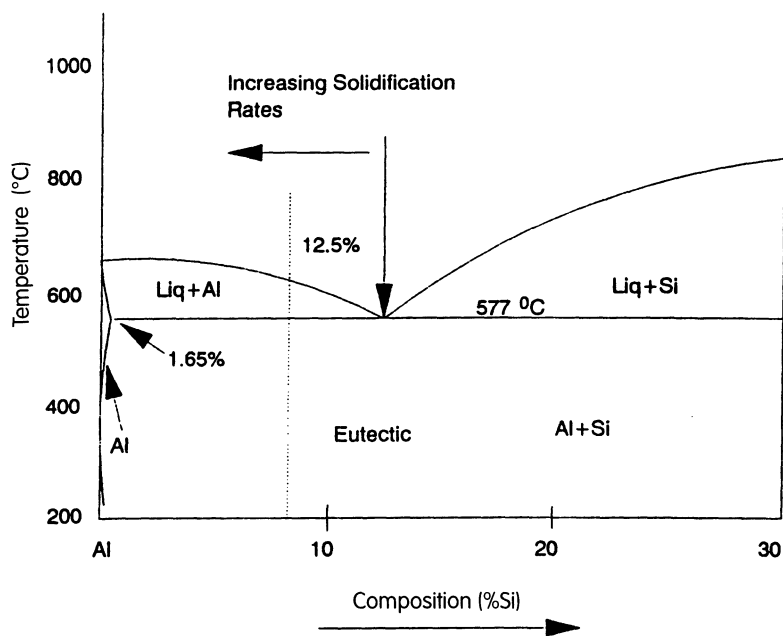
The 4XXX alloys are close to binary Al-Si and find their main application as casting alloys. A recent application has, however, involved the development of these alloys in the extruded form in the automotive industry for those applications requiring good wear properties. In general the alloys are of higher Si content together with enhanced levels of Cu and Mn.

When used as foundry alloys the structure will be either hypoeutectic, hyper-eutectic or eutectic; with a hypoeutectic composition large amounts of primary Al dendrites will be present in the structure. This will reduce the machinability of the alloy and also its wear resistance. A hypereutectic alloy will contain primary silicon particles instead of primary Al- $\alpha$  dendrites. These particles will reduce machinability quite dramatically, but improve the wear resistance of the alloy.



**Fig. 5.11** Homogenized material; (a) optical showing spheroidization of larger constituents; (b) TEM, fine dispersoid at dendrite core; (c) TEM illustrating precipitate free zone (PFZ) formation at grain boundary; (d) PFZ around constituent particle; (e) PFZ around constituent particle at grain boundary.

The microstructure of extruded 4XXX alloys is quite different; the solidification rate in billet casting is much higher and results in a significant difference in structure even for the same composition; this is shown schematically in Fig. 5.12. The higher solidification rates have the effect of pushing the structure towards the left on the phase diagram producing a hypoeutectic structure with a higher level of Al- $\alpha$  dendrite formation for an essentially eutectic structure. The DC cast form would therefore be inferior with respect to machinability and wear. Hence this inhomogeneity must be removed by the homogenization and extrusion process. When used in the extruded form, elements may be added to form either solid solutions, precipitates, eutectic or primary particles.



**Fig. 5.12** Phase diagram (schematic) showing a shift in the solidification line of a eutectic towards a hypoeutectic structure.

The most common additions to impart precipitation hardening are Mg and Cu which raise the hardness significantly. These elements will enter solid solution during heating to extrusion temperature and can raise the flow stress thus lowering the extrusion speed. The most common elements forming eutectic particles are Ni, Mn, Fe and of course Si. These elements form complex but stable phases enabling properties to be maintained at temperatures up to about 150°C. Celliers *et al.* [14] has shown that high silicon alloys have flow stresses at extrusion temperature (~450°C) of the same magnitude as some of the hard alloys (7XXX) such that, for example, the billet length extrudable is about 1.25 times that of a 7075 billet. Billets must be homogenized as close to the solidus as possible (from 560–570°C) with high-temperature soak extending to at least 8 h to allow spheroidization of the Si, Ni, Fe, Mn and the inherent complex intermetallic compounds.

## 5.6 5XXX ALLOYS

The homogenization process in the high Mg aluminium alloys has been examined by many investigators [15–22]. Differential scanning calorimetry (DSC) analysis of as-cast 5083 ingot [15] has shown that the DSC thermogram, indicating a sharp

endothermic reaction, vanishes at  $5^{\circ}\text{C min}^{-1}$  scan rate or if the specimen is held at  $427^{\circ}\text{C}$  for 20 min prior to the DSC analysis. A progressive melting in the solid solution matrix occurs from  $525^{\circ}\text{C}$  with  $20^{\circ}\text{C min}^{-1}$  heating rate to  $557^{\circ}\text{C}$  with  $5^{\circ}\text{C min}^{-1}$ ; indicating significant incipient melting of highly segregated regions of the casting when rapid heating is used.

Although both Mn and Mg should be depleted in the dendrite centre, an inverse segregation pattern develops because of large eutectic temperature differences ( $210^{\circ}\text{C}$ ) between the Al–Mg and Al–Mn systems. While Mg becomes redistributed during homogenization, diffusing toward the dendrite centre, Mn in supersaturated state begins precipitating. However, Mg affects the Mn solubility which, along with the Mg and Mn concentration gradients across the dendrites, result in the characteristic ring of Mn dispersoids near (but not at) the dendrite arm boundaries. Well within the dendrites, Mg content is low and Mn precipitation is not favoured despite high Mn concentration because the Mn solubility is high. Likewise, at the boundaries themselves Mg content is high and Mn low so no precipitation occurs despite the low Mn solubility. Slightly inside the dendrite arm edge Mg content is still high, Mn solubility low and Mn concentration high enough to induce precipitation.

The Al–Mg alloys containing high Mg (5083 and 5456 in particular) are not easy to hot work. A two stage homogenization treatment,  $375\text{--}425^{\circ}\text{C}$  for 1 to 2 h followed by  $500\text{--}530^{\circ}\text{C}$  for about 8 h, has been found to aid subsequent hot working that is to relatively lower the deformation stress and increase ductility (strain to fracture). The submicron dispersoids formed during casting exert major influence on hot ductility. As little as 0.05% Si is substantially harmful to hot ductility due to its effect on the microsegregation of Mn and the distribution of the dispersoids [16]. The influence of homogenization on ductility is due to reduction in Mg and Mn microsegregation and through coarsening of dispersoids. The Fe-bearing primary interdendritic intermetallic or the  $\text{Mg}_2\text{Si}$  precipitates do not seem to affect the hot ductility.

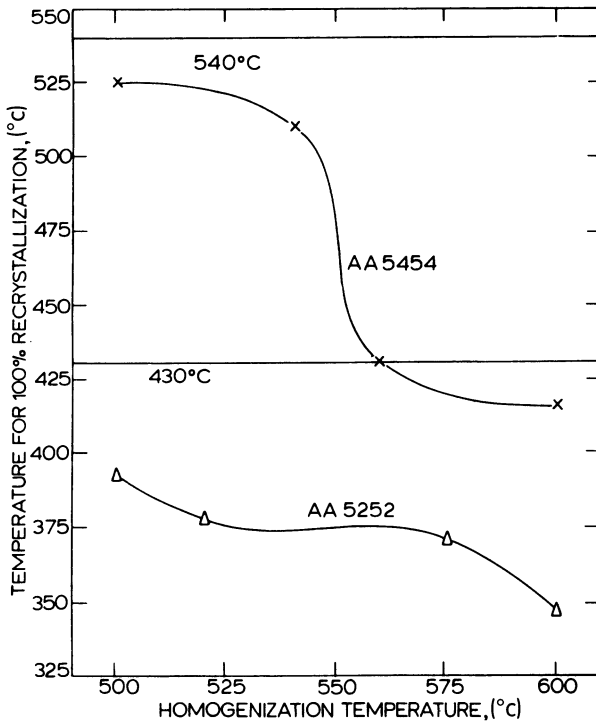
The dispersoids important to hot ductility in the Al–4.6%Mg alloys containing Mn, Fe and Cr have been identified as  $\text{Al}_4\text{Mn}$  containing minor components of Fe and Cr [17]. The  $\text{Al}_4\text{Mn}$  dispersoids have a rod shape with a hexagonal cross-section, the lengthwise direction along the C-axis and the aspect ratio ranging from one to several tens. Although the dispersoids formed in the Al–Mn system are mainly  $\text{Al}_6\text{Mn}$ , about 4.5% Mg renders the  $\text{Al}_4\text{Mn}$  more stable than the  $\text{Al}_6\text{Mn}$  at about  $500^{\circ}\text{C}$ . The presence of up to 0.13% Fe and 0.05% Si does not affect the stability of  $\text{Al}_4\text{Mn}$  or its precipitation mode.

The homogenization treatment affects not only the hot forming (rolling or extrusion) of the casting but also the subsequent recrystallization [19]. Generally, the higher the extrusion temperature, the larger the subgrain size and the higher the recrystallization temperature. The unhomogenized material requires a substantially higher temperature for recrystallization than does the homogenized material. Figure 5.13 illustrates the effect of homogenization temperature on the

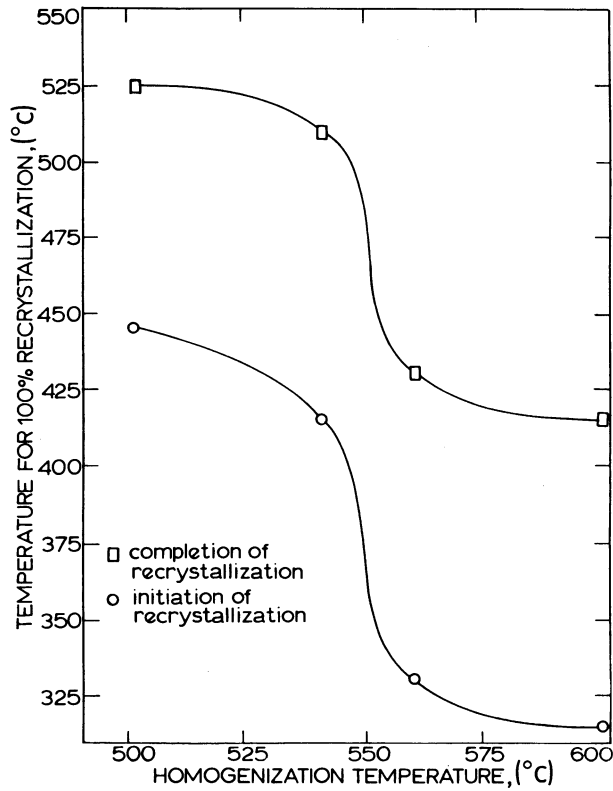
temperature for 100% recrystallization for the Al–Mg alloys 5252 and 5454 after hot rolling 50% at 400°C. The horizontal lines indicate recrystallization temperatures of similarly deformed as-cast unhomogenized material: 430°C for AA5252 and 540°C for 5454. During extrusion where the strains are substantially higher we might expect the effect to be more pronounced. If the homogenization soak is at 600°C rather than 500°C, a significant drop in the recrystallization temperature is possible: 40°C for AA5252 and 100°C for AA5454.

It is apparent that the homogenization treatment can be designed such that subsequent recrystallization may be enhanced or retarded.

Work at Imperial College [21,22] revealed that the as-cast structure examined optically contains predominantly equiaxed grains with serrated boundaries typical of a cast structure. Coring (dendrites of Al solid solution) may be observed under polarized light; the average grain size measured was 163  $\mu\text{m}$ . The structure consists of coarse intermetallics aligned along the grain boundaries of the Al matrix. The micrographs reveal two phases; one appearing dark, the other light grey (Fig. 5.14(a)). These are also shown at a grain boundary (Fig. 5.14(b)) and illustrate that

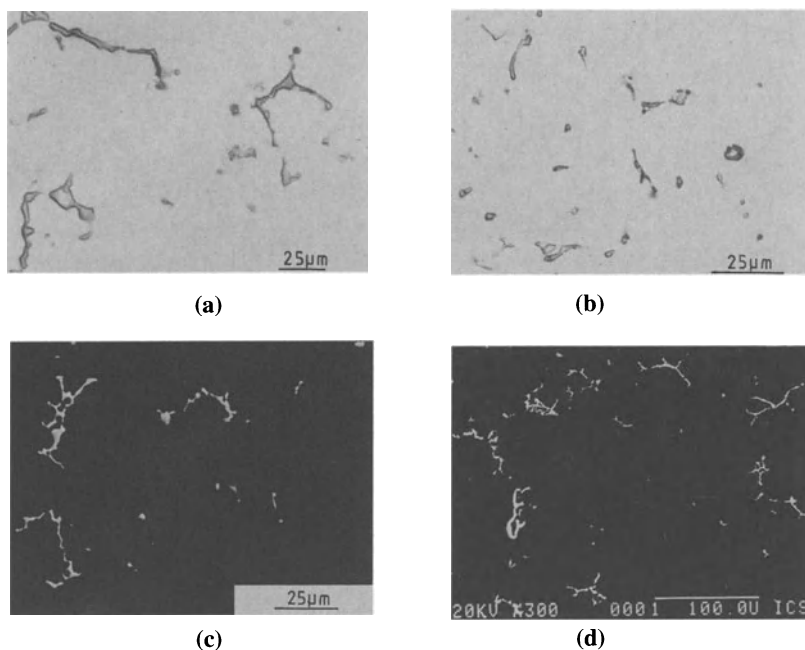


**Fig. 5.13(a)** Effect of homogenization temperature on temperature for 100% recrystallization for alloys 5252 and 5454.



**Fig. 5.13(b)** Effect of homogenization temperature on initiation and completion of recrystallization for alloy 5454.

the size (2.5 mm) and acicular morphology make the structure unsuitable for immediate processing. They were identified as  $(\text{Cr,Fe})\text{Al}_6$  and  $(\text{Mn,Fe})\text{Al}_6$ ; they occupied an area of 4.5% on a polished plane section. It can be seen that they are of irregular morphology and considerable size variations may be observed. Further examination in the TEM illustrates the heterogeneity of the cast product. PFZs (Fig. 5.15(a)) can be seen at the grain boundaries and are frequently associated with coarse (1.5 mm) segregated globular particles identified as  $\text{Mg}_5\text{Al}_8$  (which would melt at extrusion temperatures if not completely dissolved). These zones are caused by a depletion of vacancies during rapid cooling due to vacancy migration and any associated coarse precipitate/matrix interface. This results in regions in which dislocation motion and boundary segregation will be considerably easier than in regions in which the morphology is one exhibiting a large volume fraction of fine precipitates. Areas in which dense distributions of fine second-phase particles associated with grain boundaries can also be observed, not necessarily associated with PFZs. The fine particles marked 'A' are too small to identify using

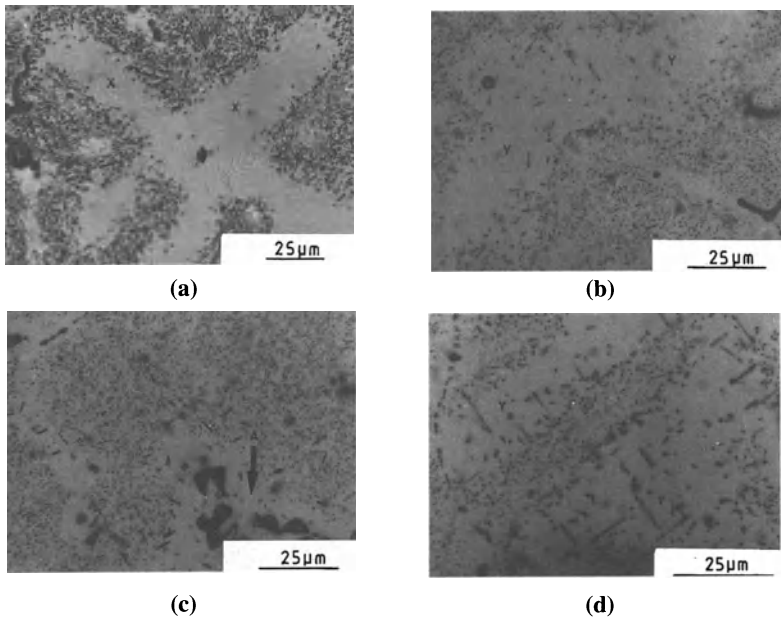


**Fig. 5.14** Intermetallics in 5XXX alloys; (a) 5083, optical; (b) 5056, optical; (c) 5083 SEM; (d) 5056 SEM.

normal techniques but appear to be  $\beta(\text{Mg}_5\text{Al}_8)$ . The platelike precipitates are  $\text{Al}_{18}\text{Mn}_2\text{Mg}_3$  and  $\text{Al}_{10}(\text{Mg},\text{Mn})_3$  in which Cr may replace Mn.

The material was subjected to various homogenization schedules and the modification to the structure, as homogenization proceeded, was examined.

As the temperature increased the fine precipitates in the interdendritic regions ( $\text{Mg}_5\text{Al}_8$ ) began to dissolve at temperatures as low as  $300^\circ\text{C}$ . However there was no visible modification to the dendrite core. On reaching  $450^\circ\text{C}$  further dissolution was observed in the interdendritic regions, whilst in the dendrites adjacent to the boundaries some precipitation was observed (marked 'X' in the micrograph Fig. 5.15(a)). These processes continued and at  $550^\circ\text{C}$  it was more difficult to delineate the original dendrite boundaries because of large scale precipitation in the boundary regions (marked 'Y' in Fig. 5.15(b)). EDX analysis showed these particles to be the same transition metal compounds as those found in the cast alloy. After 10 h at  $550^\circ\text{C}$  some platelike particles 8–12  $\mu\text{m}$  in length had formed in the dendrite core in addition to the coarse particles present in the dendrite boundary regions. At the same time most of the precipitates had dissolved leaving the transition compounds of the type Al–Mg–(Mn,Cr). The non-uniform precipitate distribution persisted even after 24 h at  $550^\circ\text{C}$ . Copious precipitation along the grain boundaries is evident. The original grain boundary intermetallic phase required 24 h at  $550^\circ\text{C}$  for spheroidization to occur, whilst soaking at  $450^\circ\text{C}$  produced considerably more retention of the original dendritic structure



**Fig. 5.15** Microstructural evolution during homogenization; (a) during heating to 450°C; (b) heating to 550°C; (c) after 24 h at 550°C, water quenched; (d) after 24 h at 550°C, FC.

and the dissolution of the interdendritic  $Mg_5Al_8$  was not substantially affected. Such a structure if extruded before dissolution, could cause localized melting whilst the unmodified intermetallics would lead to stress concentration, voiding and possible fracture.

The non-uniform distribution of Mn-bearing particles thus persisted even after prolonged soaking at 550°C. This was reduced by introducing a prolonged soak at 570°C followed by a second step at 480°C.

The effect of homogenization indicated that the single step procedure was not acceptable in terms of producing consistent properties. Similar experiments conducted using an alloy with less Mn content (0.13%) indicated that such is the critical role of this element that a single stage treatment was sufficient; the high temperature soak was, however, still required.

Excessively high homogenization temperature or very long exposure times, however, have drawbacks due to incipient melting at such high temperatures. The melting starts with the liquation of second phases and is then followed by the liquation of grain boundaries as the temperature or time further increases. A serious drop off in the ductility of as-cast and homogenized alloys 5052, 5056 and 5083 has been observed when extruded or homogenized at too high a temperature; the cause for ductility shortfall is the localized melting which produces large intergranular non-ductile phases. For these alloys, an improvement in ductility due to homogenization is possible for exposure up to about 500°C. A two step heating sequence is a further deterrent to incipient melting and property deterioration.



## 5.7 6XXX ALLOYS

This alloy system represents about 85% of all Al-alloy extrusions. As such the system is dealt with separately in Chapter 6.

## 5.8 7XXX ALLOYS

### 5.8.1 Al–Zn–Mg alloys

Over the past 20 years Al–Zn–Mg alloys have gained an important place in Europe as an age-hardenable and weldable construction material. The most widely used version is Al–4.5%Zn–1.3%Mg (AA7020). This alloy has a Cu content of up to 0.15% and a UTS ranging from 360 to 420 MPa. It has achieved special significance because of high strength levels that can be obtained in weld joints as a result of natural age hardening. Another characteristic of this alloy type is the slow decomposition reaction after solution treatment, which allows simple air cooling at the exit of the extrusion press.

Weldable AA7008/7108 extrusion alloys have been applied extensively to transport and construction applications. More dilute versions, similar to 7004, for a lower strength level (UTS = 310–350 MPa) offers several processing advantages over the high-alloyed 6XXX series normally representing this strength range.

Of particular advantage is the slow decomposition rate below the Zn/Mg solvus temp. (~370°C), which permits air cooling of complex hollow sections at the press.

Improved toughness and weld properties make such alloys very suitable for modern construction purposes.

Homogenization of billets at 480–530°C has produces acceptable results in the production of extruded sections of the alloy AA7020. With heat treatments in this temperature range, not only can the required mechanical properties be attained within an economically acceptable ageing time but also a structural condition insensitive to stress corrosion cracking can be obtained. An essential reason for this is the structural formation brought about in the billet by this thermal treatment. Most important is the dense arrangement of secondary precipitates along the cell and grain boundaries, especially after homogenization at 480°C. With rising temperatures of homogenization the particles are redissolved such that after a homogenization at 580°C, the density of the precipitates is severely reduced. This is why one observes differences in volume fraction recrystallized in the extruded sections with varying homogenization temperatures. Billet homogenizing in the middle temperate range, particularly at 480°C, produces very fine but numerous precipitates: (MnFeSi), Cr and Zr respectively. At both the lower and the higher extrusion temperature these exert a restraining influence on recrystallization since the precipitate structure is not fundamentally altered in the short-period warming up to 450 or 550°C.

For billets which are unhomogenized and those homogenized at a high temperature, the restraining influence is not effective because of the small degree of dispersion, and this leads to a very considerable amount of recrystallized structure in the extruded sections. It is of course well known that the state of the microstructure has a considerable effect both on the mechanical properties and also on the resistance to stress corrosion cracking [23,24]. Gruhl and co-workers [25] have attributed, in the case of Al–Zn–Mg alloy, the differing life endurences of specimens made from billets homogenized at high temperatures or at low temperatures to the different elongation of the grain structure as being the principal cause. The concentration of solid solution or the form in which the stress corrosion restraining elements, preferably Cr, Zr and Fe, are precipitated – dictated by the thermal treatment of the as-cast billets – also exercises an important influence on the life endurance. The effect of the concentration of solid solution or of the structure of the precipitate has been clearly shown by Scharf [26], since the size and elongation of the grains produced in his experimental work differed only slightly in the recrystallized sections whilst considerable differences in endurance life were observed.

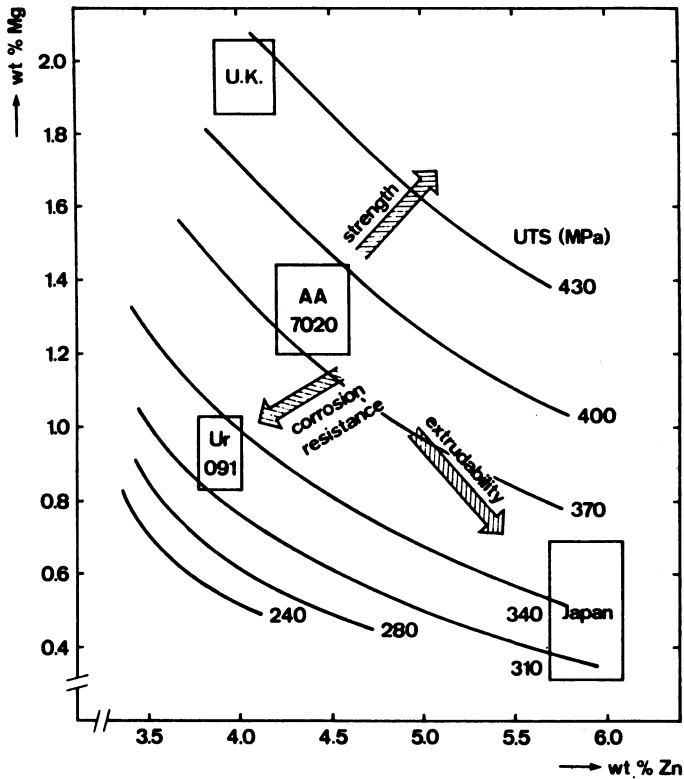
Al–Mg–Si alloys are normally used as construction alloys whenever lower weld strength is required. Examples are large hollow sections for the new Alusuisse design of railway carriages, welded together over the whole length. For this purpose the alloy AA6005A was chosen with a strength level of 260–280 MPa. In order to extend the strength of Al–Mg–Si alloys to 310–340 MPa, alloys of the type AA6061 and AA6082 have to be used, but this is only achieved at the expense of extrudability. Furthermore high alloyed Al–Mg–Si alloys have to be water quenched at the press so that they can meet the strength and toughness requirements.

Water quenching often causes severe distortion on profiles, which might either be a serious limitation in profile design or introduce an extra cost penalty as a straightening operation is required. This can be avoided whenever air cooled profiles are used (i.e. Al–Zn–Mg alloys).

The objective of achieving excellent extrudability led especially in Japan to alloy modifications characterized by an extremely high Zn:Mg ratio. Alloys with 5.5–6.2% Zn and low Mg contents, around 0.3–0.6%, were produced by various Japanese aluminium firms. However, in order to minimize the risk of corrosion, the Zn content should not be higher than 4.5% (Fig. 5.16). Numerous corrosion studies [27–30] and investigations into the influence of solute profiles on grain boundaries have shown that the stress corrosion susceptibility of Al–Zn–Mg alloys is related to an increased Zn concentration in the precipitate free zones [31,32].

This accumulated knowledge has been consequently applied during the development of technical Al–Zn–Mg alloys (alloy composition and processing), e.g. by limiting the (Zn + Mg) content below 6%, by applying a slow cooling rate from solution temperature or by step ageing treatments.

However, as far as welded joints are concerned, an optimum structure cannot be obtained for both weld and parent metal. Especially in the heat affected zone,



**Fig. 5.16** Composition range and strength level (in T6 condition) of weldable Al-Zn-Mg alloys.

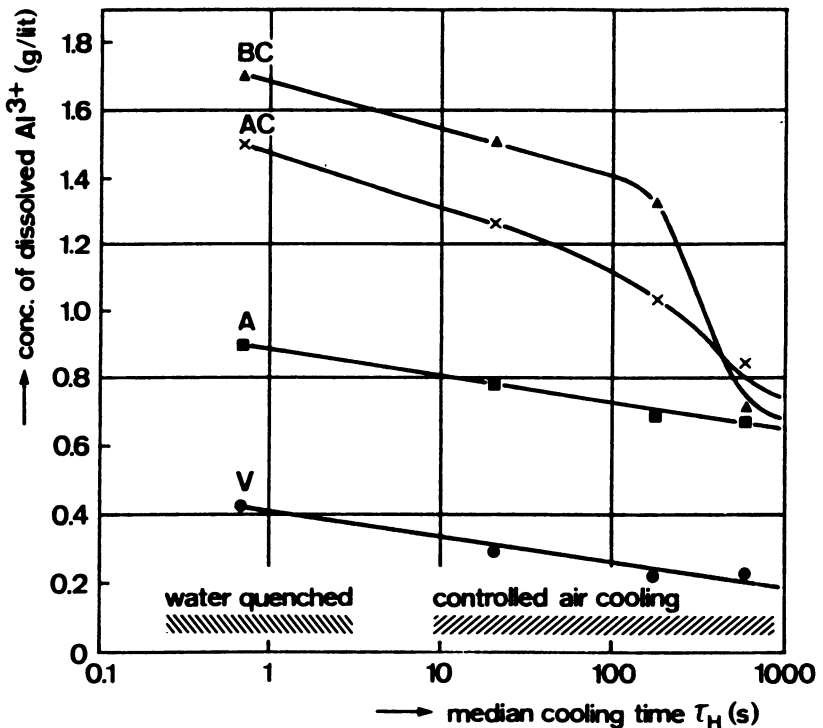
corrosion problems can arise because of the different electrochemical potentials for condition T6 (parent metal) and T4 (heat affected zone).

The effect of individual elements when considering more dilute alloys is given in Table 5.2. It follows that the negative influence on corrosion processes has essentially determined the individual changes in element concentrations of the new alloy when compared with the standard M 7020. Results of quantitative corrosion studies [33] shown in Fig. 5.17 confirm that exfoliation corrosion drops with decreasing (Zn + Mg) content. From the fact that corrosion rates become in general lower with decreasing cooling rate, it can be concluded, that the (Zn + Mg) content in solid solution is the controlling factor. This behaviour is a consequence of precipitation of Zn and Mg during slow cooling from solution temperature [33]. Alloys containing chromium are, as expected, more cooling rate dependent, but exhibit in general higher corrosion rates than Cr-free alloys.

Figure 5.18 gives data from a plant trial [34] in which 7020, 7004 and 6083 alloys were extruded under identical conditions, showing the change of extrusion force with extruded billet length. The 7020 and 7004 alloys were both homogenized

**Table 5.2** Effect of alloying elements

<i>Alloying elements</i>	<i>Effect on properties</i>
Zn-content below 4%	Improvement of general corrosion behaviour, e.g. intercrystalline and exfoliation corrosion
Zn-content below 4%	Compromise between good extrudability and required strength
Fe, Mn, Si: reduced to their lower composition limits	Fewer stringers of primary particles, increased toughness and decreased exfoliation corrosion, no Mg <sub>2</sub> Si re-precipitation
Cu: increased to tolerable limit for weldability	Shifts corrosion potential of matrix in cathodic direction, strength increase of 20 MPa
Zr: increased	Fine grain size, stabilizes hot working structure, Al <sub>3</sub> Zr precipitates provide nuclei for $\eta'$ phase
Cr: omitted	Less exfoliation corrosion, Zr replaces Cr completely



**Fig. 5.17** Influence of cooling rate ( $\tau_H$ ) from solution temperature on the corrosion intensity of four Al–Zn–Mg alloys in the T4 condition; BC, 5.3%Zn+2.8%Mg+0.15%Cr; AC, 4.5%Zn+1.3%Mg+0.15%Cr; A, 4.5%Zn+1.3%Mg, 0%Cr; V, 3.7%Zn+0.8%Mg, 0%Cr, lower Fe, Mn, Si concentrations. (After Yoshida and Baba [33].)

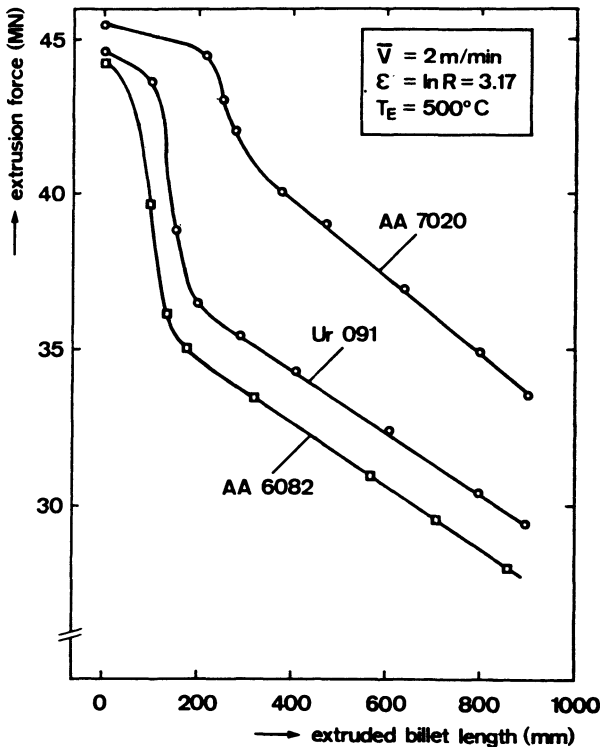


Fig. 5.18 Comparison of extrudability of 7020, 7004 and 6083 alloys [34].

at  $470^\circ\text{C}$  for 8 h with the high Zr alloy being slowly heated during the temperature range  $380\text{--}420^\circ\text{C}$ . It is clear that the 7XXX alloys can approach the extrudability of the harder 6XXX alloys. It should be mentioned that for both Al–Zn–Mg alloys a moderate fan cooling was applied, which provides a cooling time  $\tau_h \sim 4$  min. However, the Al–Mg–Si material had to be water quenched to achieve the required strength values.

Versions of 7004 containing no Cr, and limited Mn content (0.2%) could be disadvantageous because both elements are known for their ability to produce fibrous grain structures due to a fine dispersion of aluminide phases which prevents recrystallization. A similar effect can be achieved with Zr, which precipitates out as the intermetallic phase  $\text{Al}_3\text{Zr}$  during ingot homogenization.

$\text{Al}_3\text{Zr}$  forms a metastable superlattice of the type L12 ( $\text{Cu}_3\text{Au}$ ) in the aluminium matrix. The optimum temperature range for forming this phase is said to be  $380\text{--}420^\circ\text{C}$ . At higher temperatures, e.g. above  $500^\circ\text{C}$  this metastable  $\text{Al}_3\text{Zr}$  is precipitated as the tetragonal  $\text{Al}_3\text{Zr}$  equilibrium phase and coarsens. A homogeneous and fine dispersion of  $\text{Al}_3\text{Zr}$  precipitates is desirable to stabilize the hot worked structure during extrusion. This can be achieved during ingot homogenization by adopting a slow heating rate of about  $40^\circ\text{C h}^{-1}$  over the temperature

interval 380–400°C. During the hot working process this fine, dense precipitation of  $\text{Al}_3\text{Zr}$  interacts with dislocation and subgrain boundaries by pinning them, thus preventing the formation of coarse recrystallized grain at the extrusion surface.

### 5.8.2 Al–Zn–Mg–Cu alloys

The alloys 7075, 7049 and 7050 have recently [35] been investigated in some detail; the as-cast microstructures of the three alloys were found to be similar. These microstructures consisted of mainly large aluminium dendrites, (approximately 20  $\mu\text{m}$  secondary dendrite arm spacing), surrounded by interdendritic, low melting point eutectic compounds and phases. These dendrites would be expected to exhibit coring due to the relatively quick cooling rates employed in chill casting. The predominant eutectic structures in these three alloys consist of the quasi-binary reaction product; the coupled network of  $\alpha\text{-Al}$  and  $[\text{AlMgZnCu}]$ . This eutectic evolves from the parallel solidification of two quasi-binary eutectic reactions, forming the  $[\alpha\text{-Al/T}(\text{AlMgZnCu})]$  and the  $[\alpha\text{-Al/M}(\text{AlMgZnCu})]$  coupled networks respectively. Other intergranular phases are also present in these alloys, formed from the minor alloying element additions/impurities. Such phases were found to be mainly of the  $\text{Al}(\text{Fe, Mn})\text{Si}$  and  $\text{Mg}_2\text{Si}$  type.

The general homogenization practice used for AA7XXX alloys is to hold them at a temperature between 450°C and 480°C for up to 24 h. The homogenization temperature must clearly not exceed the lowest melting point phase temperature in

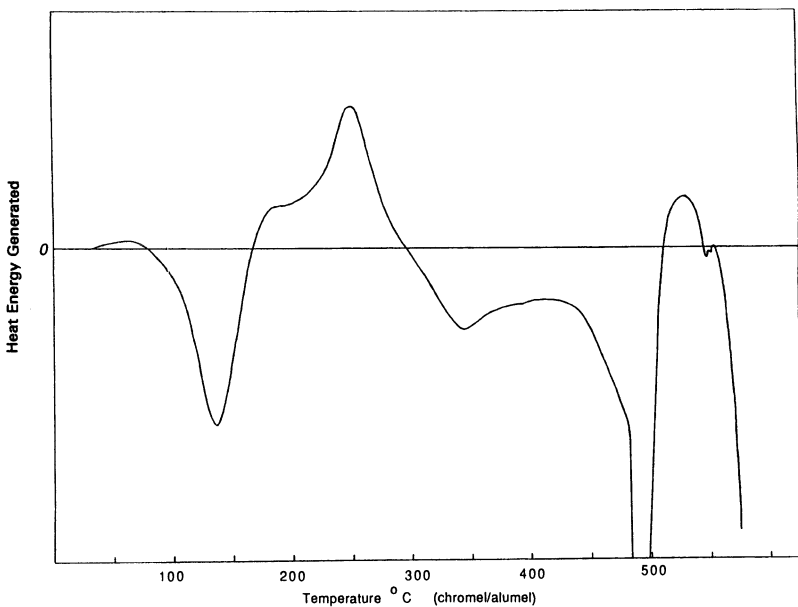


Fig. 5.19 DSC trace for as-cast 7075 alloy.

the alloy, resulting in localized melting, as this could in severe cases cause microstructural damage of a type that cannot subsequently be repaired. Damage consists of excessive void formation, segregation, blistering and cracking. Initially, all three alloys in the as-cast state were examined by means of differential scanning calorimetry (DSC) to establish the lowest melting point in the AA7XXX system. All three alloys showed the presence of a low melting point phase between 480°C and 485°C. One of the DSC traces obtained, that for alloy AA7075, is shown in Fig. 5.19. This low melting point phase was identified as being the [AlMgZnCu] eutectic component. The presence of this phase thus limits the maximum safe homogenization temperature for these alloys to approximately 475°C.

Samples from each of the three alloys were taken and held at a soak temperature of 475°C for 1, 2, 4, 8, 16 and 24 h periods, prior to water quenching. The samples were subsequently examined using microscopy and X-ray analysis techniques to determine the structural phase changes occurring in the samples. The results of this study are summarized as Table 5.3.

The coarse [AlMgZnCu] type eutectic phases in all three AA7XXX alloys are shown to dissolve during homogenization. This dissolution becomes increasingly advanced as homogenization time proceeds, and almost complete removal of these phases is achieved after 16 h at 475°C. At the homogenization temperature, Cu, Mg and Zn start to diffuse out of the [AlMgZnCu] complex, but, simultaneously, Al<sub>2</sub>CuMg (S) forms very rapidly from residual M[AlMgZnCu] by a solid state reaction analogous to a peritectoid transformation. Local concentrations of this S phase can cause incipient melting at temperatures below 480°C in subsequent hot working. Therefore the almost complete removal of S phase during homogenization should be considered a necessity. Table 5.3 shows that although Al<sub>2</sub>CuMg forms very rapidly, this phase is very slow to redissolve, and at 475°C a soak time of 24 h is necessary to remove it.

Homogenization causes a number of significant changes in the microstructures of AA7XXX alloys, which can be summarized as the dissolution of the coarse [AlMgZnCu] grain boundary phases, the precipitation of Cr-, Mn- and Zr-rich dispersoids, and the spheroidization of the insoluble, impurity-rich grain boundary phases. At a temperature of 475°C, homogenization is virtually complete after 16 h, but an extended soak time of 24 h is recommended to ensure the complete removal of the low melting point phase Al<sub>2</sub>CuMg (S), prior to hot working.

A commercially used AA7XXX homogenization treatment normally consists of three stages, and is shown schematically as Fig. 5.20.

The first stage in this treatment (stage I), a hold at 200°C for 2 h, is a stress relieving stage. In the large commercial ingots, stresses can build up as a result of variations in cooling rate during casting, and cracking can result if the billet is subsequently reheated to a very high temperature very quickly. The second stage of this treatment (stage II) is a hold for 4 h at 460°C. As shown in Table 5.3 and Fig. 5.19, the as-cast AA7XXX alloys contain an incipient melting point around 480°C. This second stage in the homogenization cycle is intended to remove most of these low melting point grain boundary phases, such that the risk of incipient

**Table 5.3** Structural phase changes during the homogenization of AA7XXX

<i>Time at 475°C (h)</i>	<i>AA7075</i>	<i>AA7049</i>	<i>AA7150</i>
(as-cast)	M; T; S; $\beta'$ ; Mg <sub>2</sub> Si; Al(Fe, Mn)Si; Al <sub>3</sub> Fe present	M; T; S; $\beta'$ ; Mg <sub>2</sub> Si; Al(Fe, Mn)Si; Al <sub>3</sub> Fe; MnAl <sub>6</sub> present	M; T; S; $\beta'$ ; Mg <sub>2</sub> Si; Al(Fe, Mn)Si; Al <sub>3</sub> Fe present
1	M; T; more S; $\beta'$ ; Mg <sub>2</sub> Si; Al(Fe, Mn)Si; Al <sub>3</sub> Fe; CrAl <sub>7</sub> ; E present	M; T; $\beta'$ ; Mg <sub>2</sub> Si; Al(Fe, Mn)Si; Al <sub>3</sub> Fe; CrAl <sub>7</sub> ; E; more S and MnAl <sub>6</sub> present	M; T; more S; $\beta'$ ; Mg <sub>2</sub> Si; Al(Fe, Mn)Si; Al <sub>3</sub> Fe present
2	Less M and T; $\beta'$ ; Mg <sub>2</sub> Si; Al(Fe, Mn)Si; Al <sub>3</sub> Fe; more S, CrAl <sub>7</sub> and E present	Less M and T; $\beta'$ ; Mg <sub>2</sub> Si; Al <sub>3</sub> Fe; Al(Fe, Mn)Si; more S, CrAl <sub>7</sub> , E and MnAl <sub>6</sub> present	Less M and T; more S; $\beta'$ ; Mg <sub>2</sub> Si; Al(Fe, Mn)Si; Al <sub>3</sub> Fe present
4	Less M, T and $\beta'$ ; same S; Mg <sub>2</sub> Si; Al(Fe, Mn)Si; Al <sub>3</sub> Fe; more CrAl <sub>7</sub> and E present	Less M, T and $\beta'$ ; same S; Mg <sub>2</sub> Si; Al <sub>3</sub> Fe; Al(Fe, Mn)Si; more CrAl <sub>7</sub> , E and MnAl <sub>6</sub> present	Less M, T and $\beta'$ ; same S; less $\beta'$ ; Mg <sub>2</sub> Si; Al(Fe, Mn)Si; Al <sub>3</sub> Fe present
8	Less M, T, S and $\beta'$ ; Mg <sub>2</sub> Si; Al(Fe, Mn)Si; Al <sub>3</sub> Fe; more CrAl <sub>7</sub> and E present	Less M, T, S and $\beta'$ ; Mg <sub>2</sub> Si; Al(Fe, Mn)Si; Al <sub>3</sub> Fe; more CrAl <sub>7</sub> and E; coarser MnAl <sub>6</sub> present	Less M, T, S and $\beta'$ Mg <sub>2</sub> Si; Al(Fe, Mn)Si; Al <sub>3</sub> Fe present
16	Very little M and T; less S; coarser CrAl <sub>7</sub> and E; spheroidized Mg <sub>2</sub> Si, Al(Fe, Mn)Si and Al <sub>3</sub> Fe present	Very little M and T; less S; coarser CrAl <sub>7</sub> , E and MnAl <sub>6</sub> ; spheroidized Mg <sub>2</sub> Si, Al(Fe, Mn)Si and Al <sub>3</sub> Fe present	ZrAl <sub>3</sub> identified; less S; very little M and T; spheroidized Mg <sub>2</sub> Si, Al(Fe, Mn)Si and Al <sub>3</sub> Fe present
24	Coarser CrAl <sub>7</sub> and E; spheroidized Mg <sub>2</sub> Si, Al(Fe, Mn)Si and Al <sub>3</sub> Fe present	Coarser CrAl <sub>7</sub> , E and MnAl <sub>6</sub> ; spheroidized Mg <sub>2</sub> Si, Al(Fe, Mn)Si and Al <sub>3</sub> Fe present	ZrAl <sub>3</sub> ; spheroidized Mg <sub>2</sub> Si, Al(Fe, Mn)Si and Al <sub>3</sub> Fe present

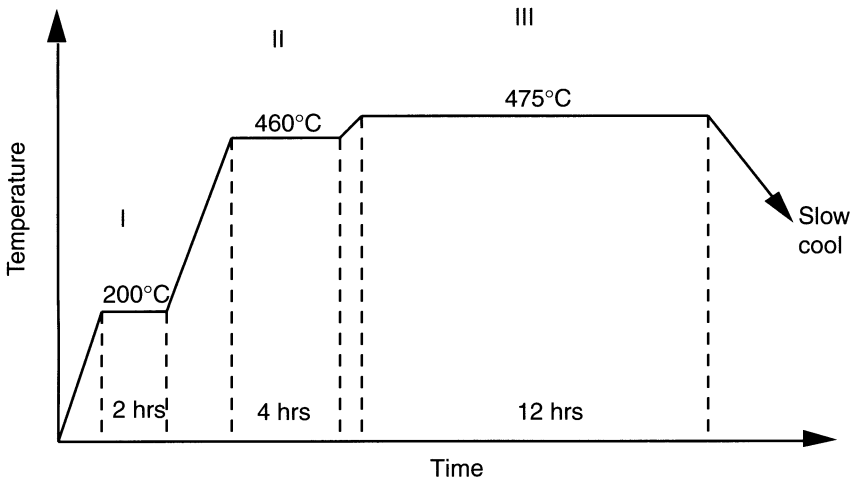
M = M[AlMgCuZn], S = Al<sub>2</sub>CuMg,  $\beta'$  =  $\beta$ -Al<sub>3</sub>Mg<sub>2</sub>, T = T[AlMgCuZn], E = Al<sub>18</sub>Cr<sub>2</sub>Mg

melting arising from any slight overheating during stage III is minimized. Figure 5.21 shows the DSC analysis of this structure after stage II. It can be seen that this stage is sufficient to remove the incipient melting point of 480–485°C.

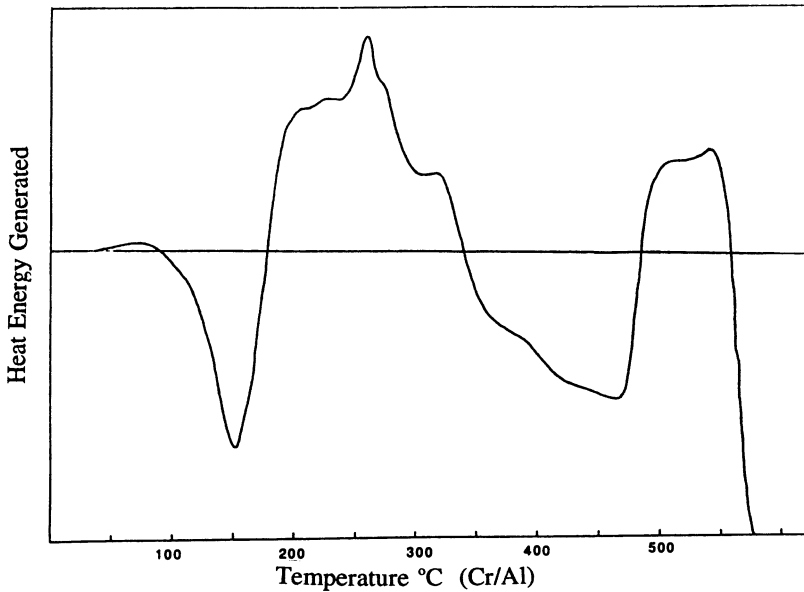
The third stage in this commercial treatment (stage III) is intended to produce the greatest structural changes, and as such is the most important stage. The homogenized structure after this stage reveals that the insoluble grain boundary phases have spheroidized, and the Cr-rich dispersoids have precipitated out in a heterogeneous fashion. The EPMA results indicated that Zn, Mg and Cu are held in solid solution with the absence of any major concentration gradients.

After stage III, the homogenized alloys are allowed to air cool, precipitating out the M[AlMgZnCu] phase. The final structure obtained after such cooling is





**Fig. 5.20** Diagram showing the commercial treatment for homogenization of AA7XXX alloy (schematic).



**Fig. 5.21** DSC trace after stage 2 of the 3-stage commercial homogenization of 7075 alloy.

very similar to the structure obtained by homogenising AA7075 for 24 h at 475°C (heating rate 15°C min<sup>-1</sup>) and subsequently furnace cooling.

The homogenization heating rate was found to have an effect upon the homogeneity of the Cr- and Mn-rich dispersoids found in the AA7075 and AA7049 alloys. A slower heating rate results in a more homogeneous dispersoid distribution.

This was explained in terms of a longer dwell time spent in the zone of maximum nucleation rate, when the heating rate was lower, thus allowing nucleation to occur in zones of lower Cr and Mn concentrations. For the Zr-bearing AA7150 alloy, the homogenization heating rate was found to have no effect upon the Zr-rich dispersoid distributions (note that in this work a slow heat from 380–420°C was not applied).

For all three alloys investigated the transition elements Cr, Mn and Zr formed dispersoids which precipitated during homogenization. Precipitates of  $\text{Al}_{18}\text{Cr}_2\text{Mg}$  and  $\text{CrAl}_7$  are present in the AA7075 and AA7049 microstructures after about one hour at 475°C. In alloy AA7049, dispersoids of  $\text{MnAl}_6$  are also observed. With extended times at the homogenization temperature, the Cr- and Mn-rich precipitates coarsen, with the Mn-rich precipitates coarsening at a greater rate. The coarse, insoluble grain boundary phases such as  $\text{FeAl}_3$  and  $\text{Al}(\text{Fe},\text{Mn})\text{Si}$  are spheroidized during homogenization in all three AA7XXX alloys. The coarse  $[\text{AlMgZnCu}]$  type eutectic phases in all three AA7XXX alloys are shown to dissolve during homogenization. Almost complete removal of these phases is achieved after 16 h at 475°C. As these phases dissolve,  $\text{Al}_2\text{CuMg}$  (S phase) forms very rapidly from residual  $[\text{AlMgZnCu}]$ .

The homogenization cooling rate was examined. For all three AA7XXX alloys examined, it was found that a fast cooling rate ( $1000^\circ\text{C min}^{-1}$ ) retains Mg, Cu and Zn in solid solution, resulting in a microstructure containing only the transition element dispersoids. Slow cooling ( $10^\circ\text{C min}^{-1}$ ) allows the  $\text{M}[\text{AlMgZnCu}]$  and  $\text{T}[\text{AlMgZnCu}]$  phases to precipitate in a coarse morphology throughout the microstructure. Such phases exhibit incipient melting temperatures between 480 and 485°C.

## 5.9 ALUMINIUM–LITHIUM ALLOYS

All commercial Al–Li based alloys contain >1% Cu. The improvement in the mechanical properties as a result of Cu in these alloys is attributed to the coprecipitation of  $\text{Al}_2\text{CuLi}$  (T1) or  $\text{Al}_2\text{CuMg}$  ( $S'$ ) precipitates in addition to  $\text{Al}_3\text{Li}$  ( $\delta'$ ) precipitates, as in 8090 and 8091 alloys. Cui *et al.* [36] have systematically studied the effect of Cu on the mechanical properties by adding 1–6% Cu to an Al–2.5%Li–0.17%Zr alloy. They found that increasing the Cu content increased the 0.2% proof stress and decreased the percentage elongation. They attributed the increase in the strength to the increasing amount of coprecipitation of T1 precipitates and the decrease in ductility to the increase in the number of coarse precipitates containing Al, Li and Cu, with increasing Cu content. However, there had been no systematic investigation of the effect of low additions of Cu, i.e. < 1% Cu, in Al–Li alloys, except a very brief study by Parson [37]. They found that even small additions of Cu increased the strength significantly and decreased the percentage elongation in the 170°C peak aged condition. It has been shown [38] that small additions of Cu increase the strength and decrease the fracture

toughness of the Al–Li–Mg–Zr alloys. The optimum combination of mechanical properties (values comparable to AA 8090) is obtained for the addition of 0.1% Cu in the underaged condition. Small additions of Cu do not influence the mechanical properties by coprecipitation. It is suggested that the small additions of Cu affect the nucleation of  $\delta'$  precipitates and ultimately their precipitate size distribution and/or volume fraction in the aged conditions.

Zirconium is added to all the commercial Al–Li based alloys as an effective grain refiner and recrystallization inhibitor [39]; it also influences the ageing behaviour of Al–Li based alloys [40].

A stepped heating procedure during homogenization has been proposed for the Al–Li–Mg, Al–Li–Cu and Al–Li–Cu–Mg alloys. The accepted homogenization treatment calls for exposure at 500°C or for stepped heating to 455°C (to allow  $Zr_3Al$  precipitation) followed by exposure at 515°C; however, some residual Cu-bearing phases remain undissolved and prevent a full development of mechanical properties during the subsequent thermomechanical treatment. This is especially true for the products which do not undergo heavy reductions from the cast state. The fracture toughness properties are often inadequate. It is essential to homogenize these alloys at 530°C or above to take into solution the as-cast intermetallic phases which are not fully dissolved at conventional homogenization temperatures. Such high-temperature exposure in the industrial environment is difficult to sustain without considerable incipient melting.

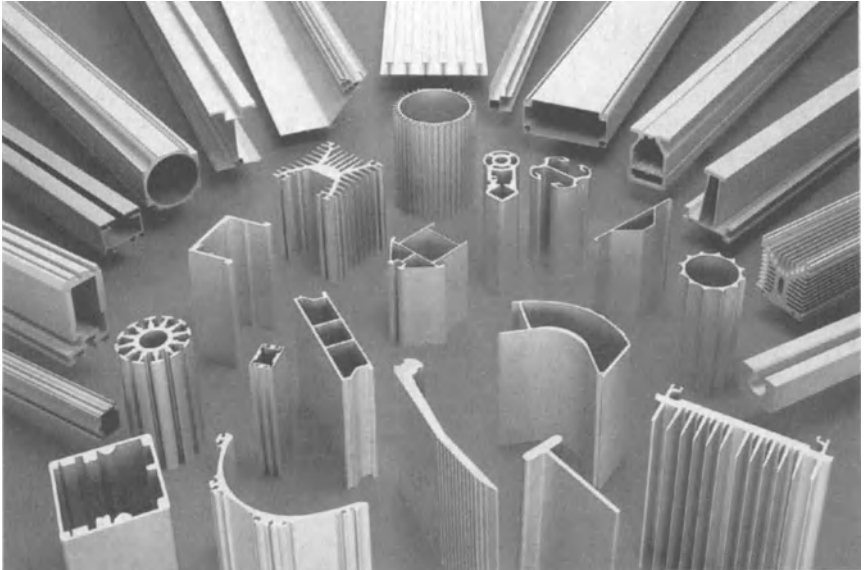
Limiting Mg to 2% and slow heating at less than 50°C h<sup>-1</sup> allows a final homogenization temperature in the 520–560°C range. Furthermore, a minimum hold time allows rapid homogenization without permitting the dispersed intermetallic particles to be transferred into liquid phases. Specifically, slow heating from about 400°C at 35°C h<sup>-1</sup> and holding at 530°C for 5 h below the 539°C melting temperature of the Cu-bearing phases, allows the coarse phases to dissolve. Further dissolution of the higher melting phases can be ensured by slow heating at 20°C h<sup>-1</sup> in the 540–560°C range and by removal from the furnace after minimum exposure time at the high temperature. The ingot homogenized in this fashion is rendered less temperature sensitive during subsequent working stages, and can be subject to greater reductions, due to elimination of the low melting phases.

The strength of the extrudates decreases and the ductility increases in the as-extruded condition with increases in the extrusion temperature and the extrusion ratio. The solution treatment decreases the strength and increases the ductility. The fracture toughness remains almost unaffected either by variation of the extrusion temperature and ratio or with solution treatment. However, in the solution-treated condition, although the effect of the extrusion ratio on the mechanical properties is found to be the same as in the as-extruded condition, the trend changes with the extrusion temperature, and the extrusion temperature does not exhibit a simple trend in its influence on the mechanical properties. The reason for this change in the trend is not very clear. In the aged conditions, the recovered and recrystallized microstructures, as well as the effect of the extrusion temperature and ratio on the mechanical properties, remains roughly the same as in the solution-treated condition.

## 5.10 EXTRUDABILITY, LIMIT AND PRODUCTIVITY DIAGRAMS

### 5.10.1 Extrudability

Most aluminium sections are produced from the Al-Mg<sub>2</sub>Si 6XXX alloys with a further substantial portion from the Al-Zn-Mg alloy. There is virtually no section which could not be produced in these alloys, which are easily extruded. Typical examples of complex shapes are shown in Fig. 5.22. These sections are, in the main, produced using the 6XXX alloys which are marginally easier to extrude than the Al-Zn-Mg alloys.



**Fig. 5.22** Examples of extruded shapes. (Courtesy of Hoogovens Aluminium.)

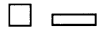
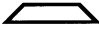

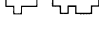
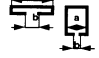




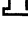


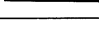
The harder alloys of the 2XXX, 5XXX (>3%Mg), and 7XXX series are more difficult to extrude and consequently are used for more stringent applications such as aerospace applications. We should, of course, note that the value added during the extrusion process is much greater; the fabricator is no philanthropist! and considerably more skill and control is necessary in the production of components from these materials.

One measure of extrudability is the flow stress of the alloy since this parameter, for any given section, determines the pressure locus on the extrusion limit diagram. Reference to Table 4.2 and Figs. 4.2–4.5 allows us to determine, for this criterion, the relative extrudability of Al-alloys. These are shown in Table 5.4 where all alloys are compared with 6063 whose extrudability index is 100 and increasing number indicates greater difficulty. In general the difficulty agrees with Fig. 4.18 showing the limits for acceptable surfaces.

**Table 5.4** Comparison of the relative extrudability of Al-alloys

<i>Alloy</i>	<i>Difficulty</i>	<i>Alloy</i>	<i>Difficulty</i>
1000	77	3004	180
1100	86	6082	197
6063	100	2014	202
3005	106	5052	229
3003	112	5056	232
6105	134	2024	247
4047	128	5054	265
3105	126	7150	269
6061	151	7050	280
5005	154	5083	281
7004	157	5182	293
2011	171	5456	300
		7075	316

**Table 5.5** Comparison of Laue's 'difficulty of extrusion' with modified shape factor

<i>Category</i>	<i>Section type</i>	<i>Example</i>	<i>Shape factor</i>
A	Simple bar		2.8
B	Shaped bar		
C	Standard sections		4.8
D	Simple solid sections		6.76
E	Semi-hollow sections		21.16
F	Sections with abrupt changes; thin walls; wide sections		54
G	Sections with difficult tongues, narrow inlets		46
H	Tubes		40
J	Simple hollow sections		82
K	Difficult hollows		90
L	Tubes with projections		120
M	Tubes with internal projections		130
N	Large or wide hollow sections		N/A

The section shape is quite clearly the most important factor in the extrudability considerations and as observed previously the most complex shapes are extruded either from 6XXX or Al-Zn-Mg alloys. Laue [41] has attempted classification based on experience; we shall investigate whether the use of section

factors obtains the same gradation. Laue ranks the degree of extrudability from A to N and such is the complexity that it is clear that the experiments reported in Chapter 4 cover only a small fraction of the permutations. One of the complications is solid sections with section inlets as shown for example in Table 5.5 and Köblitz [42] has suggested a form factor for such shapes;  $\lambda^* = \sqrt[3]{(ab)}$  and it would appear sensible to multiply the factor defined in Chapter 4 by this factor to achieve at least a measure of the degree of difficulty. Clearly the experimental evidence will not exist in each case to claim that the factor may be used to predict pressures and surface defects. However, as can be seen from Table 5.5, there is sufficient experimental evidence to suggest that these modified shape sections can be used with some confidence.

We should observe that the shape factor does not agree in all cases and that Laue's observations are based upon practical observations. Also, we have calculated the shape factor for categories F and G for particularly difficult sections. There is also the observation that using the shape factor defined as  $\lambda^2$  will fit data as well as if it were defined as  $\lambda$  since the term is always used within logarithmic definition. Nevertheless the use of  $\lambda^2$  has been proven to predict the pressures, surface defect and recrystallization from theoretical concepts (but not for categories F and G).

### 5.10.2 Limit diagrams

The equations and the general form of limit diagrams have been developed in Chapter 4. Here we shall concentrate on diagrams for specific alloys and their extension to productivity predictions. We should note that, in general, the limit diagrams published in the literature and references in Chapter 4 have been constructed directly from experimental data and consequently the curvature of the pressure line varies from the theoretical.

A simple practical diagram is shown in Fig. 5.23 for AA2014 aluminium alloy and for two ram speeds. The best possible extrusion ratio consistent with the maintenance of product integrity indicates that the operating conditions at the ram speeds shown would be at points A and A' ( $R \cong 120$ ,  $T \cong 350^\circ\text{C}$  and  $R \cong 60$ ,  $T \cong 637^\circ\text{C}$  respectively). However, it will not be possible to operate at these points because, under industrial conditions, the control of billet temperatures to better than  $20^\circ\text{C}$  would be considered excellent. Thus, the peaks on the diagram must be severed by horizontal lines passing through A and A'. This lack of control in the industrial process is often much worse, some operators claiming  $50^\circ\text{C}$  to be a more representative figure. Even the imposition of a  $\pm 20^\circ\text{C}$  limit reduces the extrusion ratios obtainable to approximately 60 and 45, respectively. It is an obvious conclusion that better control of the extrusion process is mandatory if productivity is to be significantly increased. A more typical plant problem is to determine the optimum speed for some fixed extrusion ratio and it is possible to construct limit diagrams giving this information. Figure 5.24 shows such a diagram which now plots speed on the vertical axis and is considered for a reduction ratio of 30. It is this type of

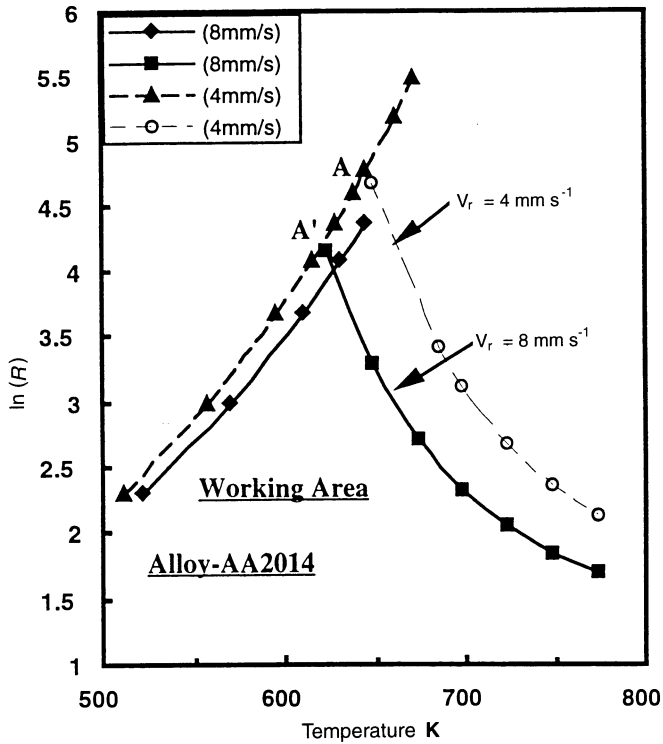
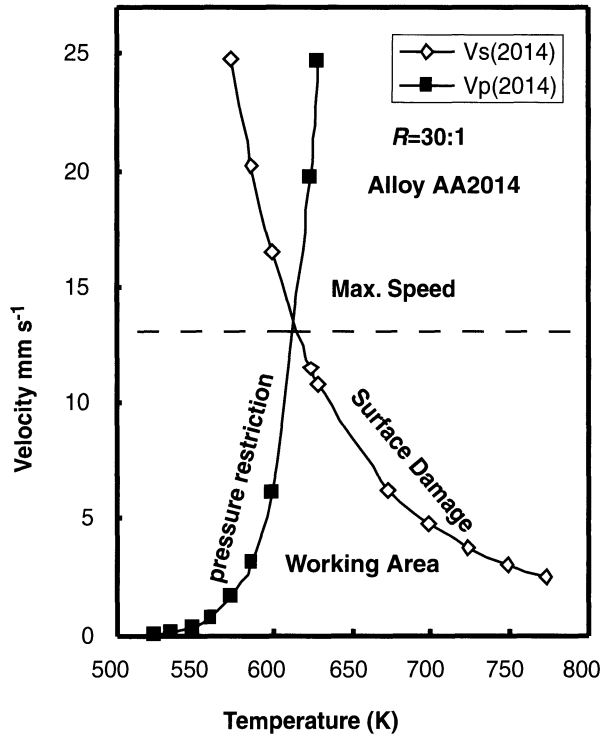


Fig. 5.23 Limit diagram for AA2014 constructed from theory.

diagram first proposed by Stenger [43]. To move from Fig. 5.24 to Fig. 5.25 it is only necessary to realize that, at some specified flow stress, the term  $Z/A$  imposes a load limit at a specified speed (i.e. the flow stress is strain rate sensitive). Thus  $\bar{\epsilon} \exp(\Delta H/GT)$  is constant and the pressure-limiting line may be constructed. The importance of temperature control is more clearly illustrated by this type of diagram. Control to  $\pm 20^\circ\text{C}$  means that the optimum constant press speed is reduced by about 10% and if control is no better than  $\pm 50^\circ\text{C}$  the relevant figure is a speed reduction of 50%. The implication of these temperature-control requirements is that the ram speed must be controlled within fine limits and must be variable so that it is possible to 'move' along the temperature locus during extrusion. There are now presses currently equipped to monitor speed and temperature and certainly control of these parameters should now be mandatory. However, the only process variable which is certainly adequately monitored is the extrusion ratio, and this only because it is a prerequisite for sales. The working area indicated in Figs. 5.23 and 5.24 indicate the operating area which should be the production goal. We should, however, have some caution because considerations of product properties and of product tolerance may dictate that some other point within the working area should be



**Fig. 5.24** Alternative limit diagram for AA 2014 showing permitted velocities and temperature.

selected. Consider, for example, Fig. 5.25 in which the subgrain size of the extruded product has been plotted. This is relatively simple since we have seen that  $d^{-1} = a + b \ln(Z/A)$  and hence

$$\left\{ \left[ \exp\left(\frac{d^{-1} - a}{b}\right) \right] A - \ln \frac{6V_r K_{\dot{\epsilon}}}{D_B} \right\} \frac{G}{\Delta H} = \frac{1}{T}$$

So for each subgrain size there is a variation of  $T$  with extrusion ratio and with speed such that constant subgrain size could be achieved. We have seen that in the case of non-heat-treatable alloys there is a direct relationship between properties and subgrain size and in heat-treatable alloys the subgrain size at exit of the press may influence recrystallization and fracture toughness, proof stress and corrosion properties. In many cases these properties may be directly shown on the limit diagram, for example by showing the optimum subgrain size for fracture toughness as a fracture toughness line (e.g.  $d = 2 \mu\text{m}$  in Fig. 5.25). Figure 5.26 shows clearly the significance of allowing for breakthrough pressure. The line a–b is the pressure line predicted from considerations of steady state conditions. The net effect is to reduce, by almost 40%, the maximum extrusion ratios possible at the specific pressure and ram speeds specified. Figures 5.25 and 5.26 show clearly



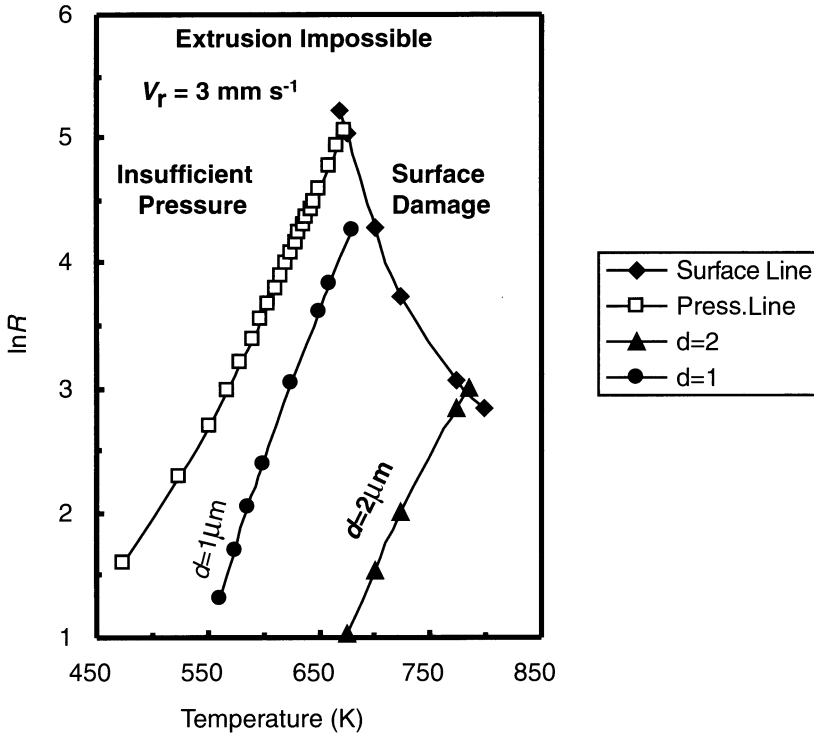


Fig. 5.25 Limit diagram showing structural information.

how the total working area is much reduced compared with the original diagrams proposed by Hirst and Ursell.

From the discussion of structural considerations and the relationships presented in section 4.7 it is clear that both desired structure and property parameters may be presented on an extrusion limit diagram. Figure 5.27 [43] is constructed from experimental data and shows such a diagram indicating loci for various sub-structural and structural conditions in AA2024 alloy. The temperature limit shown represents the onset of tearing and the diagram shows quite clearly the advantage of indirect extrusion.

When processing architectural alloys such as 6063 the limit diagram approach can be misleading. Stenger [43], for example, shows a diagram such as Fig. 5.28 in which the implication is, that for the softer alloys (e.g. 6063) the only limit on speed is the press capacity, which clearly cannot be correct. There are several factors which contribute to this anomaly. It is normal that the extrusion will be of complex design, perhaps extruded through a bridge or porthole die which, as shown in Table 5.5, has a considerable difficulty factor. This will modify the diagram to take the form illustrated in Fig. 5.29 indicating a much reduced working area. If we also consider that in these alloys it is necessary to extrude at a temperature such that all

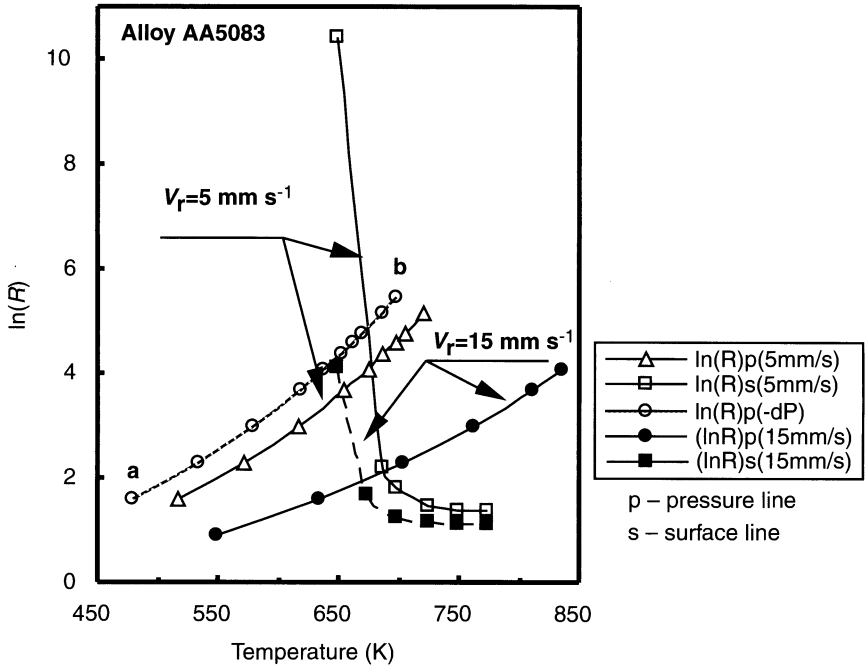


Fig. 5.26 Showing the importance of allowing for the 'peak' increment.

$Mg_2Si$  is taken into solution in the process (extrude between 450 and 475°C) then the press limitation does not exist, certainly when the temperature rise during the process is also considered. We will return to consideration of alternative representation of limit diagrams for the 6XXX alloys in Chapter 6.

#### *Effect of homogenization on extrudability*

Sheppard and Jackson [44] have shown that for the case of Al–Mg–Zn–Cu (7XXX) alloys the homogenization process can effect the extrudability. They investigated the alloys 7075, 7049 and 7150 which had been subjected to differing heating and cooling rates. The extrusion limit diagrams for 7075 in the four homogenized conditions are illustrated by Fig. 5.30. The loci on the left describe the pressure conditions beyond which extrusion is not possible, and those on the right show the processing conditions which produce an unacceptable surface. The variations in each respective locus have been discussed [45] and as such need not be repeated here. From examination of Fig. 5.30, the homogenization condition using a ramp rate of 15°C min<sup>-1</sup> and a cooling rate of 10°C min<sup>-1</sup> appears to offer the greatest flexibility for extrusion.

For alloy AA7150 the homogenization cooling rate had a minimal effect on the range of extrusion conditions permissible, compared to that of the homogenization

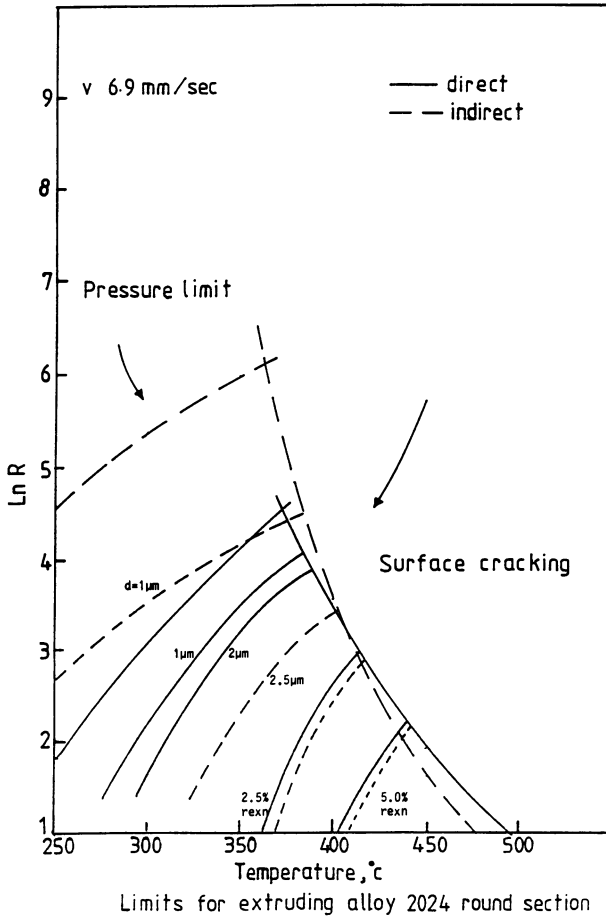


Fig. 5.27 Limit diagram showing structural features.

heating rate. A slow heating rate yielded material able to utilize a greater range of extrusion ratios during extrusion under a fixed production rate. The range in extrusion conditions permissible to produce a sound product was observed to be greater for AA7049. This illustrated the importance of cooling rate upon the range of permissible extrusion conditions; slow cooling from the homogenization temperature increased this range. The effect of heating rate is minimal compared to that of cooling rate in this alloy.

### 5.10.3 Productivity diagrams

Any point within the limit diagrams of Fig. 4.52 represents a constant production rate  $\bar{F}$  kg s<sup>-1</sup> ( $\rho$  is the alloy density).

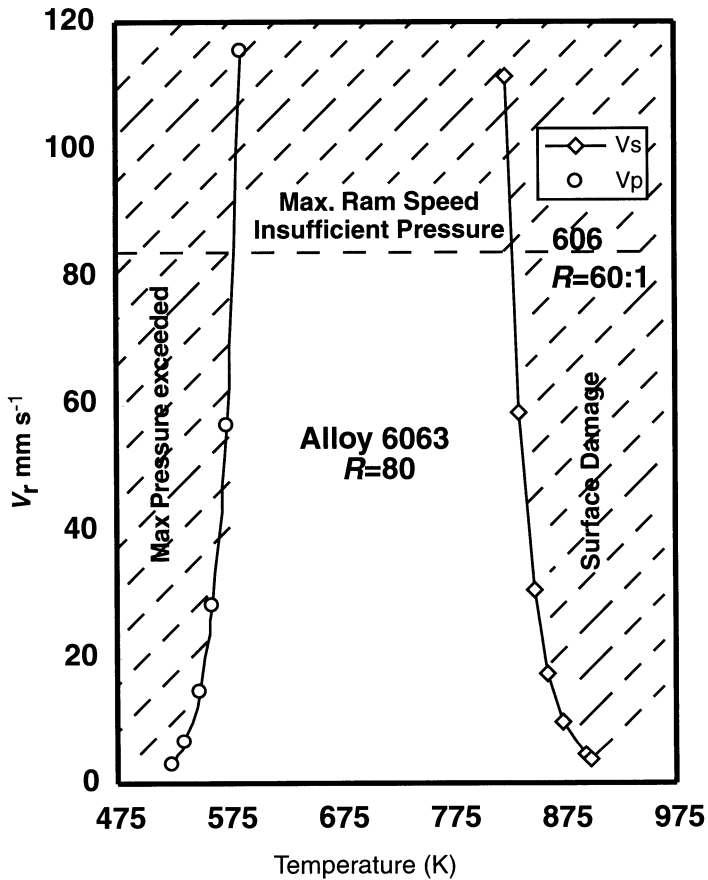


Fig. 5.28 Limit diagram for AA6063 constructed according to Stenger.

$$\bar{F} = \rho \frac{\pi(D_c)^2}{4} V_R$$

To ascertain the production rate variations of say four homogenization treatments, various limit diagrams would need to be constructed at different ram speeds. Such a practice would be very time consuming and material intensive, and as such would not be practical. It is immediately obvious that we can illustrate the extrusion working window at various production rates by constructing the limit diagrams using an abscissa of logarithmic extrusion speed. However this approach has the drawback that such a diagram would represent fixed product dimensions (i.e. to draw such a diagram the extrusion ratio would need to be kept constant). Thus, the diagram could provide information on the production rate flexibility each homogenization treatment allows, but gives no indication of how these rates change with product dimension. Jackson used the type of equation 4.8

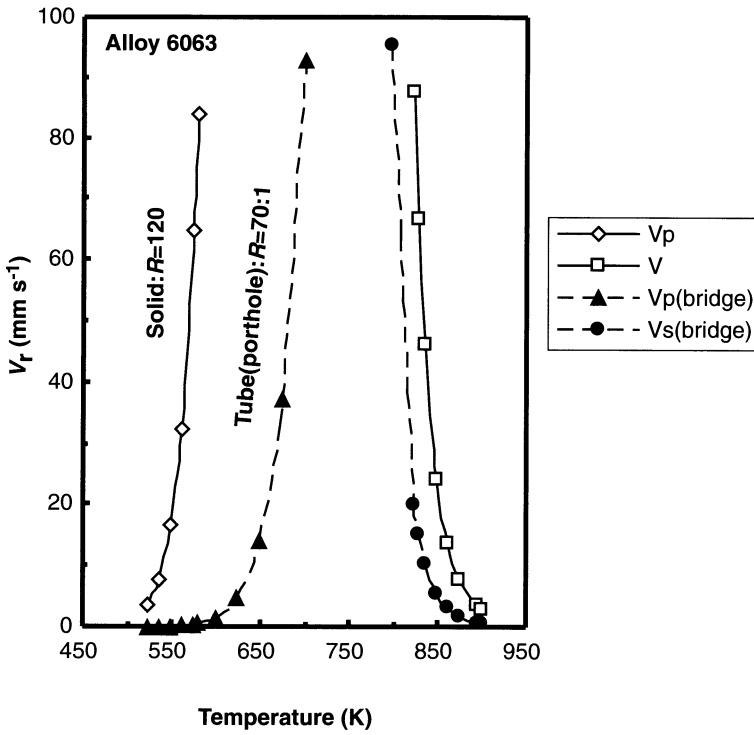


Fig. 5.29 Illustrating the limited area for a practical extrusion in AA6063.

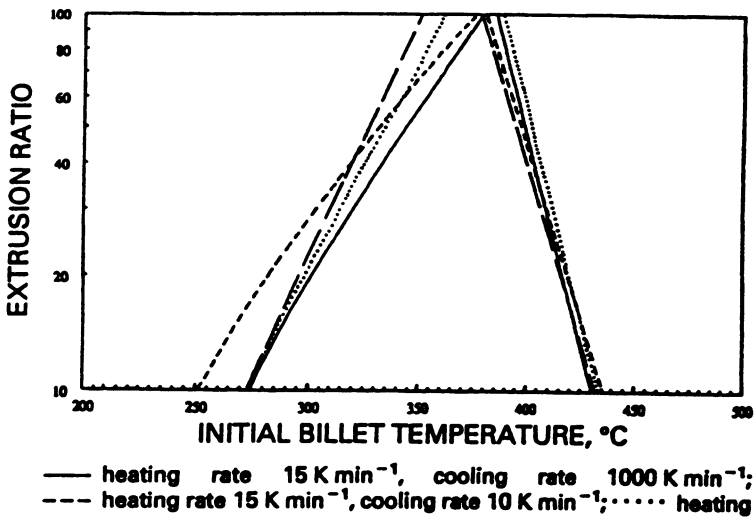


Fig. 5.30 Limit diagram for AA7075 in four different homogenized conditions.

to predict the pressure requirements; hence in the limit diagrams the pressure line has a different curvature. The point of maximum productivity is the point where the pressure and surface quality lines intersect. Hence, recalling equations 4.14(a) and 4.15(a) we arrive at:

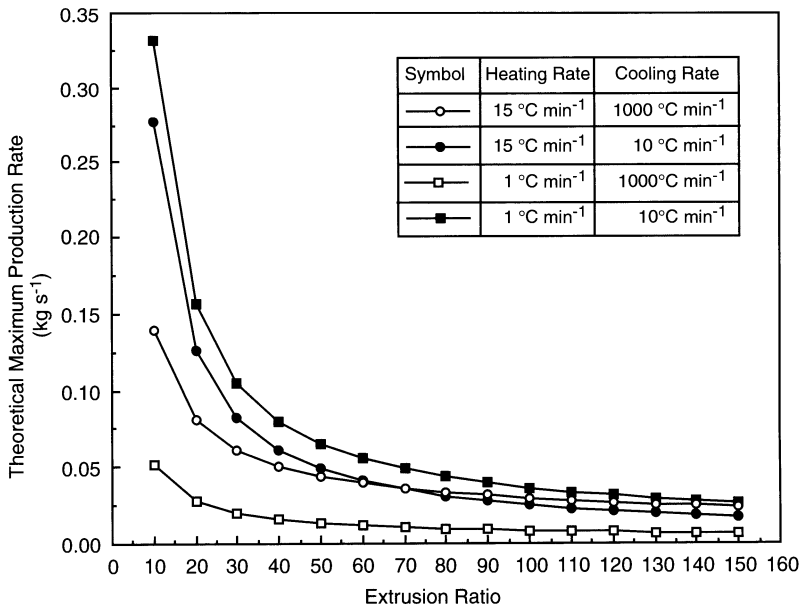
$$aT^{-b} = (p_{\max} \alpha n - n \ln 2) \quad \text{or} \quad T_{\max} = \left( \frac{p_{\max} \alpha n - n \ln 2}{a} \right)^b \quad (5.1)$$

It can therefore be concluded, that the maximum production rate ( $\bar{\Phi}_p$ ) for any one extrusion ratio is limited to an initial billet temperature  $T_{\max}$  such that equation 5.1 is satisfied. The extrusion ram velocity can then be found from back substitution of the initial temperature (and consequent peak and steady-state temperatures) into either of equations 4.14a or 4.15a. The maximum production rate can then be obtained from equation 5.2.

$$\bar{\Phi}_p = \frac{\rho \pi D_B^2}{4} V_{\max} \quad (5.2)$$

Using this analysis, it is possible to chart the theoretical maximum production rates for the four homogenized conditions as a function of extrusion ratio. The curves are illustrated in Fig. 5.31.

In plotting the apex of the limiting extrusion envelope, we are examining extrusion carried out at the limit of the process with no flexibility for error or change in the processing variables. In practice, the analysis could work to a fixed



**Fig. 5.31** Theoretical AA7075 productivity in four homogenized conditions as a function of extrusion ratio.

percentage of this maximum, thereby in effect working within a selected region of the limiting window.

Figure 5.31 shows the theoretical productivities calculated for the four homogenized AA7075 alloys. The maximum productivity of an alloy is limited by both the maximum working pressure of the press being used, and by the maximum temperatures and strain rates allowable to maintain product integrity. Due to the abundance of controlling factors on these productivity values, a complete explanation of each curve's variation is not possible. However, some reasons for the general appearance of the curves may be suggested. The maximum production rate decreases as extrusion ratio increases. Such an observation would be expected because an increase in ratio increases both the peak extrusion pressure and the susceptibility to hot cracking (due to greater temperature rises and deformation strains and strain rates). To counter such effects a reduced ram speed is required, leading to a decrease in production rate. Those billets cooled slowly show greater productivities compared to those rapidly cooled. This arises due to the lower flow stresses of these materials due to their homogenization treatment, and their lower flow stress sensitivities to changes in strain rate and temperature. Such responses would lead to reduced pressure requirements for extrusion and hence allow greater rates of deformation (i.e. ram speeds). The homogenization employing a slow ramp rate coupled with a rapid cooling exhibits the lowest productivity. The reason for this is because this homogenization has the greatest peak pressure sensitivity to strain coupled with the lowest hot ductilities. Figure 5.31 clearly illustrates the necessity to present extrusion limit diagrams in alternate forms if their usefulness to the extrusion press operator is to be optimized. If we define extrudability as 'the range in product cross-sectional variation that can be achieved for a given production throughput', then limit diagrams constructed for that production rate (i.e. ram speed) would clearly illustrate the extrudability. However, most extrusion plants will generally be mass producing a specific product of fixed dimensions (not necessarily the 7XXX alloys), and could not use such extrudability information in process optimization. Such an industry would require extrudability defined as 'the maximum extrusion throughput admissible for a given product cross-section to produce a sound product'. Thus, the analysis created in this study should be of extreme interest to the extrusion industry because the information produced expresses extrudability in productivity terms. The reader should note, however, that there are structural features which may be critical and are not represented in this analysis. Thus the retention of a substructure, volume% recrystallized or specific properties may dominate production considerations. In this case it would be necessary to use alternate equations to 5.2 to construct a useful diagram.

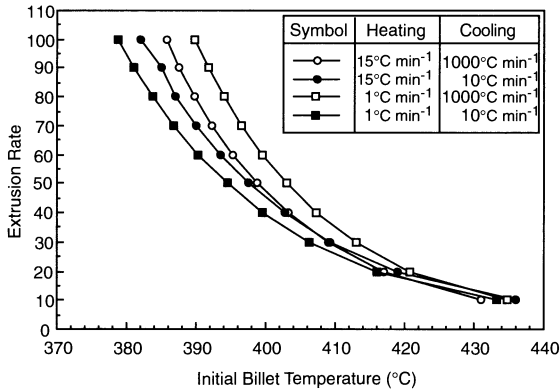
The equations for peak pressure generation relate to a very complex, non-steady state deformation schedule which at present is poorly understood. Although the equations are semi-empirical they are based upon careful experimental work. Figure 5.32 represents the hot cracking behaviour of alloy AA7150. Points to the left of the loci represent conditions which produce a satisfactory

surface; those to the right do not.. The schematic representation (Fig. 5.33) illustrates this figure in a form more easily interpreted. Curves (a) and (b) in Fig. 5.33 illustrate the susceptibility to hot cracking for AA7150 alloys employing a rapid heating rate during homogenization. Condition (b) has a greater hot ductility and a lower incipient melting temperature than that of (a). Over much of the cracking range displayed, condition (b) is more susceptible to hot cracking, and this is attributed to incipient melting. In the low ratio and high temperature region, condition (a) becomes more susceptible than that of (b). In this region, the steady state temperatures are greater in condition (a) material, whereas in the region of high ratios and lower temperatures, condition (b) material exhibits the greater steady state temperature rises: such a fact is easily proved through use of the relationships previously documented. The ductilities of both conditions are also lower in the high-temperature region. The increased susceptibility of (a) in this region is attributed to a lower ductility and a higher temperature rise, hence inducing failure (via a tensile mode) at lower initial billet temperatures than those required to initiate failure in (b). The decreased susceptibility of condition (c) material compared to that of (d), is attributed to the lower incipient melting temperature present in (d) material [30]. Contrasting curves (a) and (c) illustrates how, for rapidly cooled homogenized AA7150 material, an increase in ramp rate increases the cracking susceptibility. During torsion testing the ductility of condition (a) was found to be marginally less than that of (c). The increased cracking susceptibility displayed by condition (a) with respect to condition (c) can thus be attributed to such reduced ductility. Condition (d) material can be seen to exhibit a greater susceptibility to cracking compared with that of (b). Both conditions (b) and (d) exhibit the same incipient melting point, and hence this increased susceptibility of (d) must arise from some other factor such as reduced ductility.

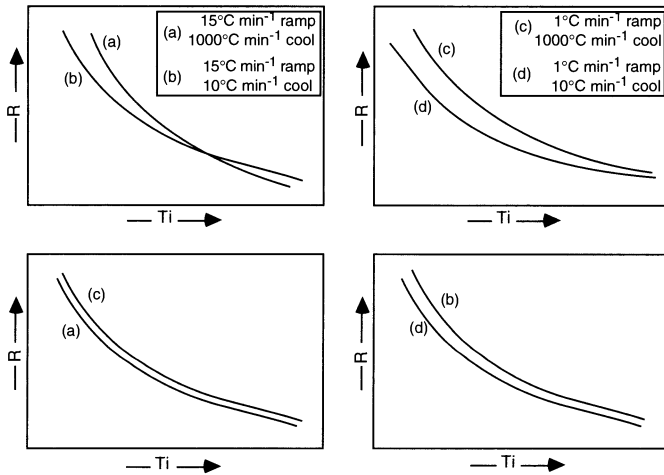
In alloy AA7075, a transition between a melting failure mode and a tensile failure mode was introduced. Such a transition in AA7150 was not observed. This is because the hot cracking of AA7150 may always involve tensile failure associated with reduced hot ductility, even when an incipient melting defect is generated through excessive temperature rises during extrusion. Thus, a transition between the two distinct modes of hot cracking would not be observed. Hot cracking in AA7150 is apparently never purely associated with failure due to incipient melting, and the mode of hot cracking varies from one of pure tensile failure to one of combined tensile and melting failure. Thus, AA7150 in its various homogenized conditions would be expected to display very similar hot cracking susceptibilities when compared with the much larger variations of AA7075.

Productivity diagrams will clearly be useful when considering the extrusion of alloys in which the final structure is acceptable in a fully recrystallized condition or, for example when manufacturing forging feedstock. If the structure required is one exhibiting a definite substructure then 'limit diagrams' should be the analysis most suitable. In either case the analyses are readily transferable to a controlling PC.





**Fig. 5.32** Hot cracking susceptibility for homogenized AA7150 as a function of initial processing conditions.



**Fig. 5.33** Representation of the susceptibility of AA7150 to hot cracking (schematic).

## REFERENCES

1. Richards, T.L. (1959/60) *J. Inst. Met.*, **88**, 141.
2. Thorley, R.T. and Tucker, G.E.C. (1957/8) *J. Inst. Met.*, **86**, 353.
3. Usui, E., Inaba, T. and Shinano, N. (1985) *Z. Metallkd.*, **76**(2), 786.
4. Usai, E., Inaba, T. and Shinano, N. (1986). *Z. Metallkd.*, **77**, 179.
5. Usai, E., Inaba, T. and Shinano, N. (1986) *Z. Metallkd.*, **77**, 684.
6. Sheppard, T. and Paterson, S.J. (1982) *Met. Tech.*, **9**, 389–398.
7. Paterson, S.J. and Sheppard, T. (1982) *Met. Tech.*, **9**, 274–281.
8. Vierod, R.P. and Sheppard, T. (1985) *Mat. Sci. Tech.*, **1**, 321.
9. Sheppard, T. (1996) Proc. 6th Int. Al. Ext. Techn. Seminar, Chicago, May, 163–171. Aluminium Association, Washington DC.

10. Fukada, K., Mizouchi, M. and Kajiyama, T. (1986) in *Aluminum Physical and Mechanical*, EMAS 483. Japan Light Metal Society.
11. Oscarsson, A., Hutchinson, B. and Karlsson, A. (1987) Proc. 8th Light Metals Congress, Leoben–Vienna. Aluminium Verlag, Dusseldorf.
12. Karlsson, A., Oscarsson, A., Lehtinen B. and Hutchinson, W.B. (1988) *Homogenisation and Annealing of Aluminium and Copper Alloys*, The Metallurgical Society, AIME, Warrendale, PA, 245.
13. Kitao, Y., Usai, E. and Inaba, T. (1982) *Kobe Res. Dev.*, **32**(2), 27.
14. Celliers, O.C., Musulin, I. and Rogers, S.J. (1991) Proc. 5th International Extrusion Technology Seminar, Chicago, May, 551. Aluminium Association, Washington DC.
15. Sanders, T.H. Jr. (1981) *Metallography*, **14**, 177.
16. Ueki, M., Horie, S. and Nakamura, T. (1979) *J. Mech. Work. Tech.*, **3**, 51.
17. Lee, S.L. and Wu, S.T. (1986) *Met. Trans. A*, **17A**, 8.
18. Lee, S.L. and Wu, S.T. (1987) *Met. Trans. A*, **18A**, 1353.
19. Zaidi, M.A. and Sheppard, T. (1984) *Met. Tech.*, **11**, 313.
20. Sultan, M.M. (1985) Proc. Conf. 4th International Congr. on Heat Treatment Mats., 1458. The Metallurgical Society, AIME, Warrendale, PA.
21. Raghunathan, N. and Sheppard, T. (1989) *Mat. Sci. Tech.*, **5**, 542–547.
22. Sheppard, T. and Raghunathan, N. (1989) *Mat. Sci. Tech.*, **5**, 268.
23. Gruhl, W. and Cordier, H. (1968) *Aluminium*, **44**, 403.
24. Scharf, G., Achenbauch, D. and Gruhl, W. (1969) *Z. Metallkd.*, **60**, 515.
25. Gruhl, W., Cordier, H. and Brungs, D. (1972) *Metall.*, **26**, 207.
26. Scharf, G. and Eulitz, J. (1973) *Aluminium*, **49**(8), 549.
27. Taylor, I.T. and Edgar, R.L. (1971) *Met. Trans. A.*, **2**, 833.
28. Bichsel, H. (1971) *Metall.*, **25**, 229–235.
29. Maitra, S. and English, G.C. (1981) *Met. Trans. A.*, **12**, 535–541.
30. Ward, D.E. and Lorimer, G.W. (1973) Proc. 3rd Int. Conf. on Strength of Metals and Alloys, Cambridge, **1**, 488. Cambridge University Press, Cambridge.
31. Doig, P. and Edington, J.W. (1975) *Met. Trans. A.*, **6**, 943.
32. Hollrigl, G. (1981) Proc. 7th International Light Metal Congress, Leoben–Vienna.
33. Yoshida, H. and Baba, Y. (1982) *Trans. Jap. Inst. Met.*, **23**(10), 620–630.
34. Hollrigl, G., Bichsel, H. and Zoller, H. (1986) Proc. 4th International Extrusion Technology Seminar, Atlanta, May, 163–171. Aluminium Association, Washington DC.
35. Jackson, A. and Sheppard, T. (1996) Proc. 6th International Extrusion Technology Seminar, Chicago, May, 541. Aluminium Association, Washington DC.
36. Cui, J., Liu, Q., Lu, L. and Ma, L. (1990) *J. Northeast Univ. Tech. (China)*, **4**, 367.
37. Parson, N.C. (1985) Ph.D. Thesis, University of London.
38. Kumar, S., Ozbilen, S., Sheppard, T. and McShane, H.B. (1992) Proc. International Extrusion Technology Seminar, 439–446. The Aluminum Association/Aluminium Extruders Council, Washington DC.
39. Starke, E.A.Jr., Sanders, T.H.Jr., and Palmer, I.G. (1981) *J. Met.*, **8**(33), 24.
40. Makin, P.L. and Stobbs, W.M. (1984) in *Aluminium Lithium Alloys 2*, (ed. T.H. Sanders Jr. and F.A. Starke Jr.), The Metallurgical Society of AIME, Warrendale, PA, 392.
41. Laue, K. (1963) *Z. Metallkd.*, **54**, 667.
42. Köblitz, H. (1971) *Al-Handbuch*, VEB Verlag Technik, Berlin.
43. Stenger, H. (1975) *Wire World Int.*, **17**, 54.
44. Sheppard, T. and Jackson, A. (1997) *Mat. Sci. Tech.*, **13**, 15.
45. Sheppard, T. (1984) Proc. 3rd International Extrusion Technology Seminar, Atlanta, **1**, 107. Aluminium Association, Washington DC.

## 6.1 HOMOGENIZATION

This section presents only the major considerations of the metallurgy of 6XXX alloys. Following sections investigate some of the principal specific alloys.

Magnesium and silicon will combine in the presence of aluminium to form magnesium silicide,  $Mg_2Si$ . All 6XXX alloys contain magnesium silicide as their principal strengthening agent. This phase must be properly distributed throughout the microstructure to obtain the strengthening required in the aluminium extrusion.

The magnesium silicide needs to be in solid solution during the extrusion operation. This will require homogenizing of the ingot or billet and correct preheating of the billet immediately prior to extrusion. Finally, artificial ageing causes precipitation of the magnesium silicide to occur in the final extrusion to give the desired strength characteristics for the customer's application.

### 6.1.1 General principles of heat treatment

All 6XXX alloys contain a quantity of soluble magnesium silicide which exceeds the equilibrium solid solubility limit at room temperature; however, it does not exceed the maximum solubility limit. It is schematically represented by line x-x in Fig. 6.1(a).

Fig. 6.1(a) indicates that as the temperature is increased from room temperature into the  $\alpha$  region and held for sufficient time, equilibrium is attained and the magnesium silicide goes completely into solid solution. If the temperature is subsequently reduced below the solvus line (curved line which separates the  $\alpha$ -region from the  $\alpha + \beta$  region), there is a tendency for the excess magnesium silicide over the amount actually soluble at the lower temperature to precipitate. This same relationship is shown in Fig. 6.1(b) for magnesium silicide [1].

The driving force for precipitation increases with the degree of supersaturation and, consequently, with decreasing temperature; the rate also depends on atom mobility, which is reduced as temperature decreases. Fortunately, the precipitation reaction for low alloyed 6XXX materials is relatively slow. For this reason,

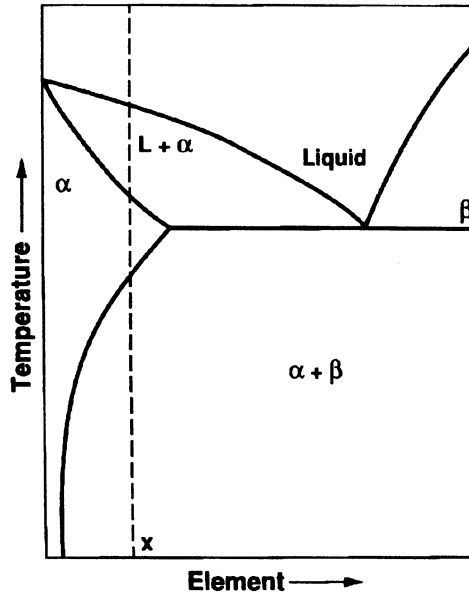


Fig. 6.1(a) Phase diagram (schematic).

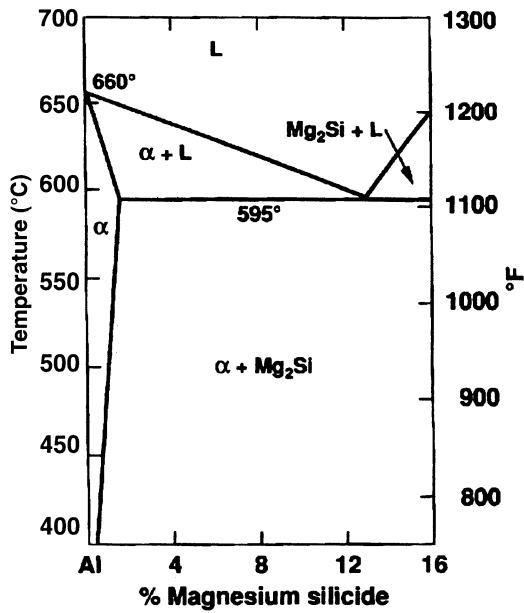


Fig. 6.1(b) Pseudo-phase diagram.

it is not mandatory to introduce a separate step of solution heat treating in the fabricating sequence; magnesium silicide stays in solution by quenching (usually by air) immediately after extrusion. This unstable state is maintained until the extrusion is ready for artificial ageing at a suitable temperature, typically around 200°C.

The mechanism for strengthening has been studied at great length. It was found that:

1. Appreciable strengthening occurs at room temperature over an extended period of time.
2. Zones are formed; short ageing times at around 200°C produce fine needle shaped zones approximately 6 nm (60 Å) in diameter and 20–100 nm (200–1000 Å) in length.
3. Further ageing causes 3-dimensional growth to rod shaped particles with a structure corresponding to a highly ordered Mg<sub>2</sub>Si.
4. At higher temperatures, this transition phase, designated β', undergoes diffusionless transformation to the equilibrium Mg<sub>2</sub>Si.
5. The normal precipitation sequence may be designated:



### *Microstructure*

Many of the problems found in an extruded shape are known to be caused by lack of uniform microstructures present at various steps in the production cycle. For example, composition needs to be uniform with limits on both wanted and unwanted elements. A fast and uniform freezing pattern during casting would both minimize shell depth (chill or border zone), cell size, cell size variations, constituent size and cold shuts, and also create a finer dendritic arm spacing (DAS).

### *Composition*

Since it is the amount of magnesium silicide and any excess Si that is of interest, it is useful to indicate the calculation necessary to obtain these values given the weight percentages of magnesium and silicon.

The chemical reaction is clearly the combination of 2 molecules of Mg with 1 of Si thus giving Mg<sub>2</sub>Si. The atomic weights are Mg = 24.305, Si = 28.085, Mg<sub>2</sub>Si = 76.695. Thus for an alloy containing 0.4% Mg and 0.38% Si the % Si required for the reaction is

$$\frac{0.4 \times 28.805}{2 \times 24.305} = 0.23$$

giving 0.4 + 0.23 = 0.63% Mg<sub>2</sub>Si and 0.15% excess Si. It will be clear that the %Mg/1.7038 gives the Si content for a balanced alloy.

The influence of the various elements normally found in 6XXX alloys are:

1. Magnesium lowers extrudability by significantly increasing maximum extrusion pressure regardless of silicon content, increases quench sensitivity for strength, increases strength and lowers both ductility and toughness.
2. Silicon lowers extrudability if in excess although it is not as influential as magnesium. It has a minor influence on quench sensitivity for strength. It is a good strengthener, especially up to about 0.4%. With a high ratio of Si/Mg<sub>2</sub>Si, the alloy extrudes well, has lower quench sensitivity and higher strength compared to low excess silicon combinations. Silicon will diminish both ductility and toughness, by precipitating elemental silicon on grain boundaries.
3. Iron has negligible effect on extrudability, quench sensitivity for strength and strength itself. Ductility and toughness will improve at low concentrations; at higher concentrations, toughness diminishes. It is in general detrimental to surface finish and care must be taken during homogenization to minimize this factor,
4. Copper is normally kept in concentrations less than 0.1% and treated as a minor (tramp) element. As such, it has very little effect on extrudability or other properties including quench sensitivity for strength, inherent strength, ductility or toughness.

#### *Influence on strength*

A number of factors influence the final strength of the finished extrusion. The strengthening due to both Mg and Si has been well documented. Figure 6.2 [2] gives the response of extrusions produced with conditions held constant at extrusion temperature = 540°C; exit velocity = 30 m min<sup>-1</sup>; quench rate = 4°C s<sup>-1</sup>; ageing = 8 h at 175°C. It is very important to know that strength variations within a given composition are due to two causes; some result from compositional differences and others result from Mg<sub>2</sub>Si transformation conditions. Of these two causes, approximately 25% of the mechanical property variation observed in final extrusion form is due to compositional variations existing within the alloy. The remainder is due to all the other variations in processing conditions.

The effect of thermal exposure in the 500–600°C range is to dissolve the precipitate formed during casting, as can be seen by microscopic, electron probe and electrical resistivity data. The hold temperature is a critical factor in determining extrudability and surface appearance of the extrudate by converting β(Al,Fe,Si) to the less detrimental α-phase. The β to α transformation involves loss of Si from β to the matrix which renders the α-iron phase less brittle and also provides a greater amount of Mg<sub>2</sub>Si for subsequent precipitation. The iron phase transformation is complete after 6 h at 565°C. The introduction of small amounts of Mn moves the α(Al,Fe,Si) phase field in the direction of a lower Fe:Si ratio thus accelerating the β to α transformation. The initial transformation occurs with no shape change but continued exposure produces a gradual spheroidization of the dispersoid which is

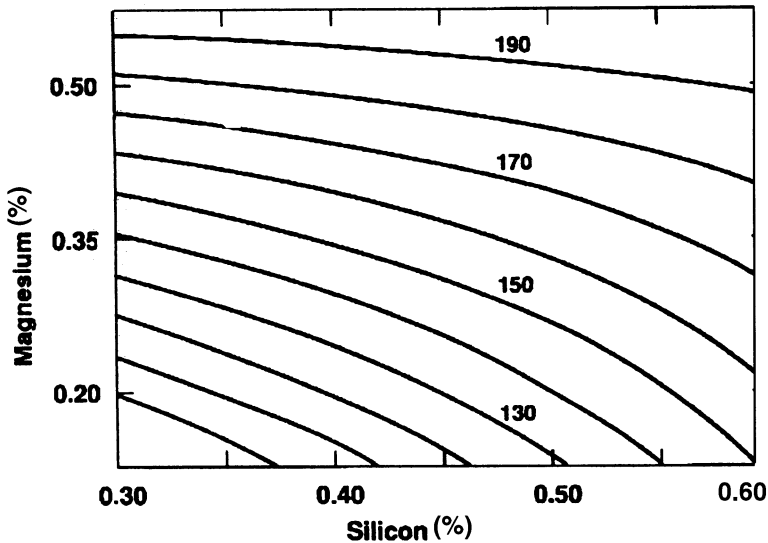


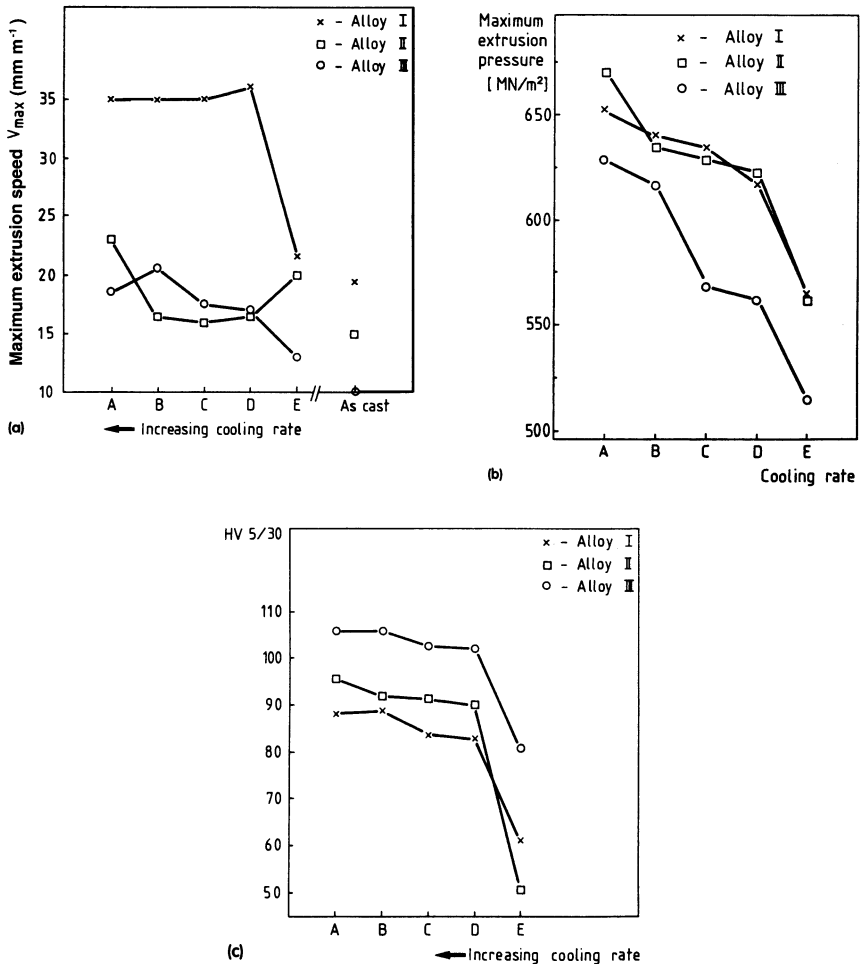
Fig. 6.2 Iso-0.2% proof stress (MPa) depending upon Mg and Si concentrations.

also desirable for workability.  $Mg_2Si$  enters solid solution rapidly at temperatures in excess of  $465^\circ C$ ; requiring about 2 h at this temperature for complete dissolution. Thus the temperature and hold time for homogenization are determined solely by the iron phase consideration. The cooling rate after homogenization is also critical. Slow cooling after homogenization results in nucleation and growth of  $Mg_2Si$  precipitates in the grain, along the grain boundaries and on the iron-rich particle surfaces. It is specially desirable to restrain precipitate growth if induction reheating is to be used; large  $Mg_2Si$  precipitates require more time to redissolve upon reheating for extrusion or during the extrusion process and may cause an unacceptable reduction in strength properties if the material is to be aged in the as-quenched state. A cooling rate of  $38^\circ C h^{-1}$ , for example, has been shown to yield precipitates of  $2 \mu m$  in size which is quite unacceptable in the industrial context producing excessive pick-up and poor properties.

Depending upon the cooling rate from the hold temperature, differing quantities of Mg and Si remain in solid solution, from virtually 100% dissolved up to 100% as  $Mg_2Si$ . A fast cooling rate after homogenization will retain most of the Mg and Si in solution and produce small uniformly distributed precipitates; at  $315^\circ C h^{-1}$  the precipitate size is  $0.25 \mu m$ . In practice it is usual to use a shortened treatment and exposure at  $575^\circ C$  for 6 h followed by cooling at  $150^\circ C h^{-1}$  down to  $250^\circ C$  and air cooling is considered satisfactory. The surface quality of the extruded section, the extrusion and frictional loads, the maximum extrusion rate achieved and the mechanical properties of the extrusion after ageing all depend upon size and distribution of the  $\alpha-AlFeSi$  phase and the morphology of the  $Mg_2Si$  precipitation. The effect of cooling rate on the maximum extrusion pressure and

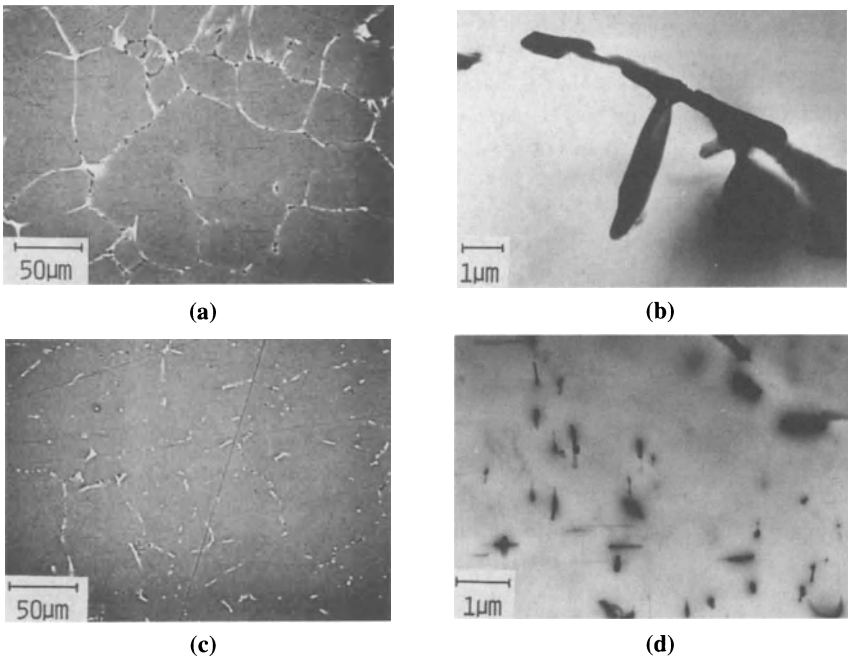
the hardness of the extrusion after ageing is shown in Fig. 6.3(a) for three Al–Mg–Si alloys [5]. The controlled high-temperature soak and suitable cooling after homogenization give a structure which offers optimum surface quality, extrusion speed and mechanical properties (Fig. 6.3(b)).

Two important factors which affect extrudability are Mg and Si in solid solution and coarse  $Mg_2Si$  phases in the structure. The extrudability is reduced by increasing amounts of Mg and Si in solid solution, either by increasing alloy content or by increasing cooling rate after homogenization. Equally, when coarse



**Fig. 6.3(a)** Effect of cooling rate on (a) maximum speed; (b) maximum pressure; (c) hardness after ageing at 185°C for 6 h Al–Mg–Si alloys: I, 0.45% Mg + 0.78% Si; II, 0.66% Mg + 0.45% Si; III, 0.45% Mg + 0.79% Si. Cooling rate: A, water quenched; B, 350–540; C, 205–210; D, 115–120; E, 20°C h<sup>-1</sup>.





**Fig. 6.3(b)** Structures produced during commercial homogenization (a) optical as-cast cored structure; (b) TEM showing the as-cast acicular  $\beta\text{AlFeSi}$  phase; (c) coring reduced by homogenization; (d) TEM showing fine  $\text{Mg}_2\text{Si}$  distribution together with spheroidized  $\alpha\text{AlFeSi}$ .

$\text{Mg}_2\text{Si}$  phases are present in the structure, due to high Mg and Si content or a slow cooling rate after homogenization, a sharp reduction of extrudability results.

The most serious aspect of the 6XXX series alloys is that in service a sudden fracture often occurs at an unspecified stress level below the ultimate tensile stress. The effect of Mn, Cr, Zr and Cu on the notch toughness of the pseudobinary Al– $\text{Mg}_2\text{Si}$  alloy has been investigated [3]. Small additions of Mn or Cr, optimal homogenization and fast cooling from the hold temperature permit maximization of toughness. Although the homogenization temperature has no influence on the notch toughness of the balanced Al–Mg–Si alloy (1% Mg, 0.5% Si), the Cr- and Mn-bearing dispersoids show an evident influence: higher toughness values after higher homogenization temperatures. The toughness is also increased by the utilization of the so-called press effect: the retention of a substructure in the material [4].

Increasing the homogenization temperature in the Al–Mg–Si alloy also shifts the  $\text{Mg}_2\text{Si}$  precipitation curve to the right, which increases the incubation period for precipitate nucleation, especially in the presence of about 0.2% Mn or 0.2% Cr. The Mn and Cr also increase the dispersoids which act as preferential nucleating sites for  $\text{Mg}_2\text{Si}$  precipitation, hence increasing the quench sensitivity of the alloy and requiring fast cooling after homogenization to effectively increase the notch toughness. The improvement in toughness depends upon the ability of transition

elements (Mn, Cr, Fe, Zr) to form stable, uniformly distributed, incoherent dispersoids during homogenization. There is also some evidence that these transition element precipitates contain Si; that is they have the ability to bind the excess Si which otherwise would cause intergranular fracture and brittleness.

The combined effect of cooling rate after homogenization and billet preheating practice before extrusion has been studied for an AlMgSi alloy through full-scale industrial experiments [5].

The results show that air cooling after homogenization caused the material to fail by a mechanism involving eutectic melting of  $Mg_2Si$  phase particles for low preheating temperatures. This low melting point reaction is associated with low maximum extrusion speeds. As the billet temperature is increased the  $Mg_2Si$  phase particles will dissolve. Thus eutectic melting is avoided, and the material may withstand a higher critical temperature before tearing occurs. This results in higher maximum extrusion speeds, and a sharp increase in extrudability is recorded at a specific transition billet temperature where the change in tearing mechanism occurs. This transition temperature may serve as a measure for the extrudability; the lower the transition temperature, the better the extrudability. As this temperature is related to the microstructure, it was found to decrease by increasing cooling rates after homogenization.

The mechanical properties of the extruded sections were also found to depend on both the cooling rate after homogenization and the billet preheating practice. The higher the cooling rate, the higher the strength of the extruded sections and the less variation in the strength by the billet preheating temperature.

No eutectic melting reactions occurred during extrusion of billets which had been water quenched after homogenization and therefore no change of tearing mechanism was observed. Thus, at billet temperatures below the transition temperature for the air cooled billets the water quenched billets could be extruded at a much higher rate (approximately 60–90%) as compared to the air cooled ones.

The extrusion pressure was found to increase by water quenching the billets. However, if the press capacity becomes a limiting factor for productivity this increased pressure can be compensated for by increasing the billet temperature and significant improvements in the extrusion speed for these billets is still obtained.

Very surprisingly, however, these promising results in extrudability for the water quenched billets was counteracted by a loss in the mechanical properties after ageing. The ultimate tensile strength in the extrusions from these billets was found to be very dependent on the billet preheating temperature, due to an increased quench sensitivity of the material. Thus, water quenching after homogenization can be recommended only if the cooling rate of the extrusions is high enough to prevent loss in mechanical properties. (Very often this means water quenching of the extrusions, with its associated inconveniences.)

The results showed that overheating is a possible practice to increase both the extrudability and the section properties. Overheating of the billets is also a way of negating the effects of different cooling rates after homogenization, thus making the billets less sensitive to variations in this process parameter.

On the basis of his results, Reiso concluded that, in order to maximize both extrudability and section properties for AlMgSi alloys of the types AA6060 and AA6063, the billet preheating temperature should be kept as low as the available extrusion pressure allows, but at a temperature just above the transition temperature. At the same time it appears that the billets should be cooled from the homogenization temperature at the highest possible rate (but avoiding water quenching) in order to avoid a reduction of the maximum extrusion speed, as well as a loss in the mechanical properties at these low preheating temperatures.

If precipitation of  $Mg_2Si$  phase particles cannot be avoided (for example, due to high alloy compositions or slow heating rates to the extrusion temperature), overheating the billets prior to extrusion appears to be the most promising way of optimizing the extrudability and section properties.

In practice the industrial treatment is often short, comprising exposure for about 6 h at 575°C, cooling at 150°C h<sup>-1</sup> to 250°C and then air cooling.

## 6.2 ALLOYS FOR SPECIFIC APPLICATIONS

The 6XXX series alloy range is by far the most commonly used in extrusion. Within this series there are a number of alloys which range widely in composition, extrudability and properties. There are in excess of fifty 6XXX series alloys (AA registered). However, there is a great deal of overlap between a number of these alloys [6] such that we need only discuss the most commonly extruded products:

- 6060, 6063 and 6106 – low to low-medium strength alloys;
- 6061/6261 – medium strength alloys (high  $Mg_2Si$  levels);
- 6005A/6351/6082 – medium strength alloys (moderate-to-high excess Si levels).

Small additions to fairly common alloys or control of impurities can produce extrusions with quite specific properties and applications. These include 6262 for screw machine stock, 6463A (and similar alloys) for chemical brightening and alloys such as 6101 for electrical conductor applications.

### 6.2.1 High extrudability, general purpose alloys

The most common of the 6XXX alloys are 6060 and 6063 (Fig. 6.4), which have very high extrudability and can be used for many applications. The uses are quite varied due to the alloys' good surface finish, corrosion resistance, and excellent response to anodizing. Typical applications for dilute 6060 have been for profiles where shape is more important than strength. Both 6060 and 6063 can be used for light wall architectural sections as well as general purpose extrusions. For medium-weight architectural sections and tube and solid general purpose geometric shapes, both 6060 and 6063 can be used, depending on the specific chemical composition.

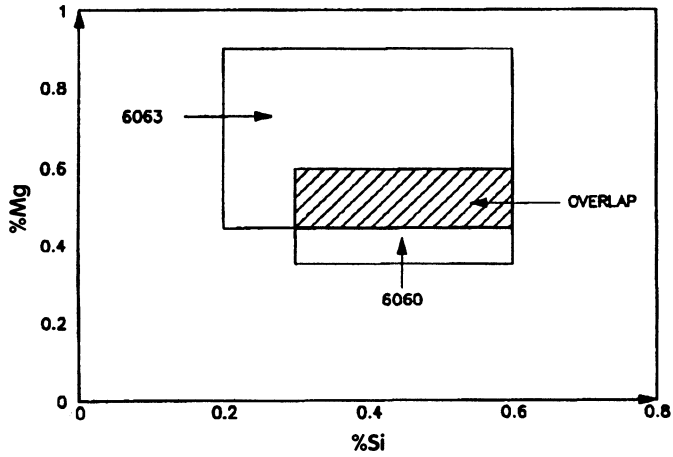


Fig. 6.4 Overlap of composition for alloys 6060 and 6063.

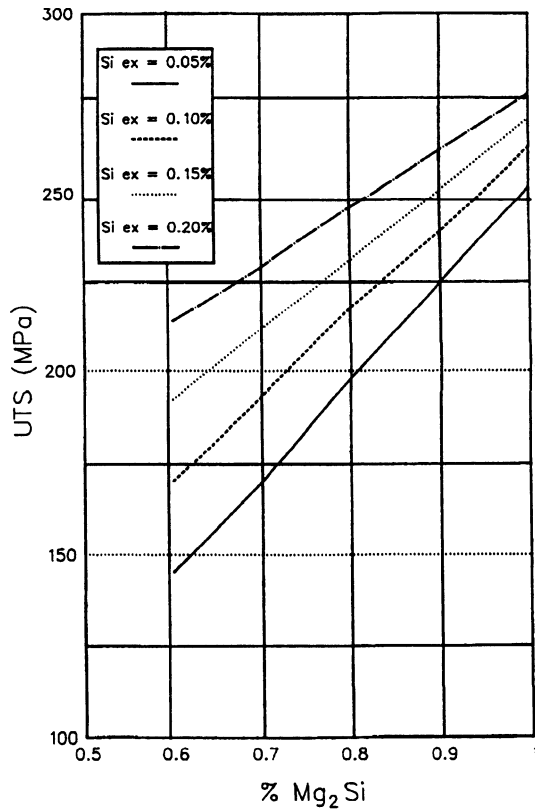


Fig. 6.5 The effect of excess Si and Mg<sub>2</sub>Si on mechanical properties. (After Marchive.)

Marchive and Deschamps [3] (Fig. 6.5) demonstrated quite clearly the relationship between Mg and Si and mechanical properties. It is obvious that those 6063 compositions approaching a minimum Mg level (0.45%), will easily meet the minimum mechanical properties.

The advantage of 6060 is that lower levels of Mg can be used which improves extrudability, but at the expense of mechanical properties. By increasing the level of excess Si, the mechanical properties are increased. The extrudability is not reduced as significantly as with increases in  $Mg_2Si$  [7–11]. Typical applications for 6106 include solid and hollow sections applications not requiring severe cold work, but for which strength in excess of 6063 T6 is required. Additional applications include ladder sections and tubular handrails.

### 6.2.2 Medium-strength alloys

There are a number of medium-strength alloys available with different compositions and based on different alloy design philosophies. Those most commonly used are 6061, 6351, 6082 and 6005A.

The medium-strength alloys can be classed into balanced alloys (little or no silicon excess) and those with a high Si excess. The latter alloys normally contain greater levels of toughening elements. The level of these additions, subsequent homogenization treatment and press quenching can significantly affect the extrudability.

#### *Balanced alloys*

One of the more commonly used 6XXX series alloys is 6061. It is used in many applications, e.g. yacht masts and structural sections, angles and T sections often used in boat building and in the transport industry. Alloy 6061 is commonly used for medium to heavy sections for heavy duty applications which require good strength combined with good corrosion resistance and which may be anodized.

The compositional limits for 6061 allow Mg levels as low as 0.80% with a predominantly balanced alloy (zero excess Si or slight excess Si above that required for  $Mg_2Si$  formation) and a moderate Cu addition. The minimum T6 mechanical properties can easily be realized under normal extrusion conditions. In fact, the alloy (in terms of meeting minimum T6 properties) is still overdesigned. By using  $Mg_2Si$  levels at the bottom of the compositional range and limiting Mn and Cr to relatively low levels, extrusions can be produced to meet minimum properties and benefit from lower quench sensitivity and higher extrusion speeds. This also allows slower cooling rates to be applied without significant losses in mechanical properties.

Using a low level of Mn and Cr, high homogenization temperatures (which coarsen Mn/Cr dispersoids) and slow press quench rates can result in a coarse surface grain structure. Additionally, slow press quench rates may cause precipitate-free zones to form, reducing toughness. Depending on the final application, these points may have limited importance.

There is always the option to replace 6061 with 6261. Although these two alloys would appear quite similar in many ways, there is some scope to differentiate between the two. One of the differences between the two alloys is the significantly higher Mn content of 6261 compared to 6061. Alloy 6061 has the potential for a much greater Cr addition; however, Cr is reported [12] to have a much greater (negative) impact on extrudability than Mn. Therefore, the level of Cr is normally kept at the bottom end of the compositional range. It is not unusual for the Mn content of 6061 to exceed that of Cr.

Plant trials using hollow sections (with a wall thickness of 1.8 mm) were conducted by Musulin and Dietz [6] and demonstrated that 6061 was slightly less sensitive to press quench rates. This can be attributed to the higher Mn content of 6261.

### *High excess Si alloys*

There are a number of high excess Si alloys available, but they differ in the balance between  $Mg_2Si$ , excess Si, toughening elements and Cu additions. Additionally, the homogenization practice will contribute to the effectiveness of dispersoids.

The applications for 6351 and 6082 are quite similar to 6061 in heavy-duty structural sections. These alloys are also more suitable for forging applications as they have lower (surface) grain coarsening susceptibility than 6061. The applications for which 6005A are suited include profiles such as flag poles, ladder parts and as a medium strength alternative to 6061 for light sections (for example, some light yacht mast sections). The extrusion speeds for 6005A are superior to 6061 and the alloy is more suited to thin wall sections due to its lower flow stress.

### *Alloys 6351/6082*

The composition of 6351 and 6082 alloys contain a Mn level far in excess of other medium strength alloys such as 6061, 6261 and even 6005A. The two alloys are essentially the same in terms of major alloying additions (Mg/Si/Mn), the only differences being a higher minimum for Mg in 6082 and a greater potential for Cr additions. Additionally, the minimum T6 mechanical properties of these alloy are quite similar. The mechanical properties of alloys 6351/6082 are quite similar to the more balanced alloys such as 6061 (and 6261). The major differences between these alloys and balanced alloys are lower  $Mg_2Si$  levels, higher excess Si levels, very high level of Mn and a lower Cu level. The overlap in Mg and Si levels for alloys 6061 and 6082 emphasizes these significant compositional differences (Fig. 6.6).

The strengthening mechanism of these alloys could be further enhanced by Cu additions (such as the levels added to 6061). However, additions of Cu to alloys with high Si excesses is reported to reduce corrosion resistance [10] and this limits the Cu addition to 0.10%.

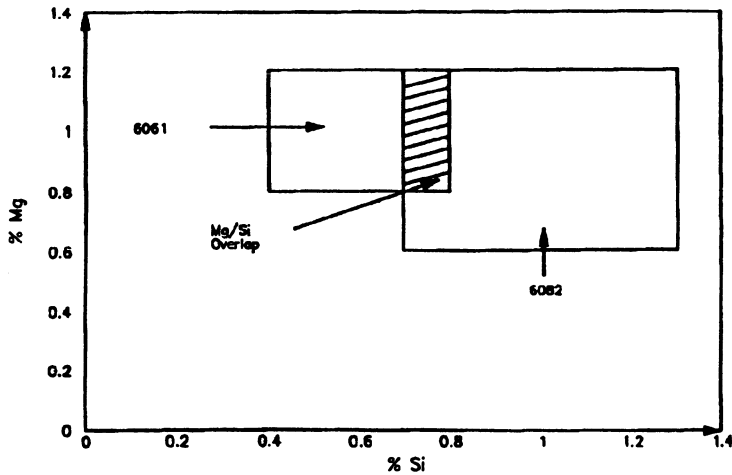


Fig. 6.6 Overlap of Mg and Si in alloys 6061 and 6082.

#### *Effect of dispersoids in 6351/6082*

The level of Mn (and Cr) as well as the homogenization practice greatly influences the extrudability, quench sensitivity and grain structure of AlMgSi alloys. As pointed out by Lohne and Dors [13] the homogenization temperature will affect the dispersoid density. The level of dispersoid additions cannot be taken into account without considering the homogenization treatment.

Low-temperature treatments can produce a very fine density of dispersoids. This will increase the material flow stress, and reduce the chance of recrystallization. These treatments are quite useful in reducing coarse grain formation from the T6 heat treatment of forging stock. Alloys such as 6061, which contain little Mn by comparison, are more prone to coarse grain formation during heat treatments and are therefore less suitable for these applications.

Apart from reducing extrusion speed, a dense precipitation of Mn dispersoids will also greatly increase quench sensitivity. The Mn dispersoids act as heterogeneous nucleation sites, increasing the chance for precipitation of  $\beta'$ Mg<sub>2</sub>Si rods. As dispersoid density increases, so should the required press quench rate. It is obvious that a lower homogenization temperature results in increased quench sensitivity.

#### *Alloy 6005A*

Alloy 6005A is similar in alloy design to 6351 and 6082; however lower Mn and higher Cu give the alloy a good balance of properties. The effect of this is to improve tensile properties with the Cu addition, as well as improving extrudability and reducing quench sensitivity with the lower manganese levels. The level of recrystallization and grain size can be expected to increase with the lower Mn levels.

Compared to alloys such as 6061 there is a greater effect on inhibiting recrystallization due to the generally higher Mn levels. Although Mn and Cr increase quench sensitivity this can be offset by a lower  $Mg_2Si$  level. The combination of these alloying elements will therefore determine quench sensitivity. Tests on the quench sensitivity of 6005A alloys showed that a greater Mn/Cr addition led to higher quench sensitivities [13]. The balance between toughness and quench sensitivity is therefore a critical factor depending upon application.

### *Speciality alloys*

A number of 6XXX alloys have been designed to meet specific requirements. This includes alloys for chemical brightening, among the most common being alloys 6463 (and 6463A) which have a 0.15% limit on Fe, free machining alloys such as 6262, which has better corrosion properties than the more commonly used alloys and even electrical conductor applications where the  $Mg_2Si$  addition gives much greater strength than the higher conductivity pure aluminium.

### *Summary*

The 6XXX series of alloys provides a wide range of properties and therefore applications. The leaner alloys such as 6060, with proper alloy design, can be extruded faster than 6063. These leaner alloys are particularly useful for more complex shapes or thinner wall sections as well as those requiring excellent surface finish.

There are a number of medium strength alloys. The alloy design of 6261 allows for higher extrudability without detriment to the mechanical properties. This has been achieved by slight compositional alterations, with lower  $Mg_2Si$  levels, higher Si levels and increased Mn to maintain toughness.

Alloys such as 6351 and 6082 have a significantly different design philosophy to 6061 and 6261, the main differences being a lower  $Mg_2Si$  level, high level of excess Si, with a large level of Mn for toughness. The homogenization treatment is critical when considering the effect of dispersoids. Lower homogenization temperatures have the same effect as increasing Mn content, as there is a denser precipitation at these lower temperatures. This effect can be quite beneficial when control is required for surface grain size, particularly important for forgings made from extruded stock. Alloy 6005A is, again, a compromise between 6351/6082 and 6061/6261 in terms of Mg/Si/Mn. The Cu addition to 6005A (as for 6061/6261) enables it to reach higher mechanical properties with little impact on extrudability.

The 6XXX range of alloys offers an endless number of alloys with many different properties and applications. Controlling  $Mg_2Si$ /excess Si levels; the additions of dispersoid forming elements such as Mn and Cr; control of impurities as well as the addition of specific alloy elements enables a wide range of applications to be met by 6XXX series alloys.



### 6.3 FACTORS AFFECTING QUENCH SENSITIVITY

Quench sensitivity is an expression of the instability of the supersaturated solid solution during cooling from above the solvus. The following factors increase this instability:

- slow cooling rate (large wall thickness, hollow sections, interior struts, sections containing abnormally thin fins etc.);
- high diffusivity of certain solute elements (magnesium and silicon);
- high solute concentrations (instability at higher temperature and therefore higher diffusion rates);
- high number of nucleation sites (grain boundaries, intermetallic particles).

Since the main interest is in the strength attainable through artificial ageing, any secondary effects that affect precipitation behaviour must also be considered. They include the effect of cooling rate on the response to holding at room temperature, precipitate-free zone formation, and any other factor affecting clustering behaviour.

#### 6.3.1 Cooling rate

The solid solutions of AlMgSi compositions that can be considered for air cooling are generally most unstable in the temperature range from 300 to 375°C. Extrusions should therefore be cooled fastest through this critical temperature range.

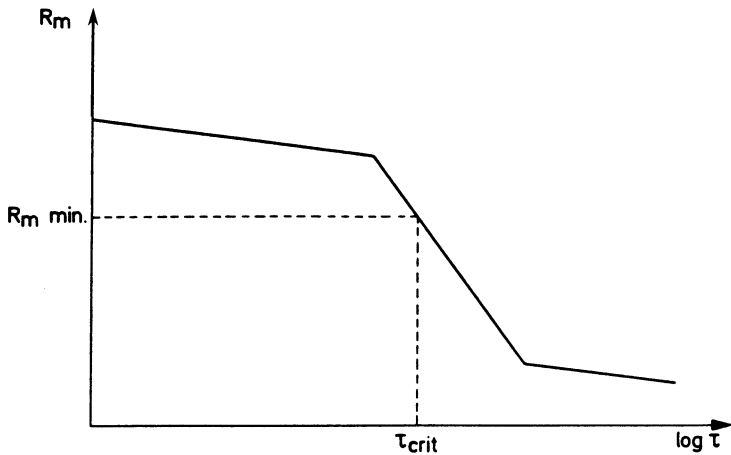
As a rule, it is difficult to speak of a single cooling rate for the whole temperature range. To compare quench sensitivities, we resort to the concept of a median cooling time,  $t$ , defined as the time required to cool the material to a temperature midway between its temperature at the start of cooling and the temperature of the cooling medium. The body is assumed to cool according to the exponential relationship developed in Chapter 4:

$$\frac{T - T_{\text{air}}}{T_i - T_{\text{air}}} = \exp \left\{ \frac{-t \ln 2}{\tau'} \right\}$$

$\tau'$  is, therefore, equivalent to the inverse of a specific cooling rate on a specific cooling curve. By plotting  $\log \tau'$  versus the strength after subsequent artificial ageing the quench sensitivities of different alloys can be properly compared.

This type of presentation (Fig. 6.7) shows that there are, theoretically, three stages of quench sensitivity. At low  $\tau'$  values there is a slight loss of strength due mainly to homogeneous precipitation at temperatures below the critical temperature range. The steep part of the curve represents the conditions under which extensive heterogeneous precipitation occurs.

At very slow cooling rates there is another slight loss in strength. The quench sensitivity of an alloy is given therefore by the  $\tau'$  value at which the curve begins to fall steeply, and by the slope of the steep part of the curve. Moreover, for any



**Fig. 6.7** Typical plot of tensile strength as a function of the median cooling time  $\tau$ . For any given strength there is a critical time,  $\tau_c$ , which should not be exceeded.

given strength level there is a critical  $\tau'$  value that cannot be exceeded if the properties are to be reached.

The maximum attainable strength depends mainly on the  $Mg_2Si$  level. Though the quench sensitivity increases as a function of the  $Mg_2Si$  content, the alloying range of these elements is largely fixed by the minimum amount required for strength and the maximum amount permissible before extrusion becomes too difficult. (If compelled to raise the extrusion temperature to enable certain sections to be extruded, there will be an increased tendency for recrystallization.) Magnesium, in particular, increases the required extrusion force, and does so, in fact, by at least twice as much as the same concentration of silicon. Moreover, an excess of silicon over the stoichiometric amount required to form  $Mg_2Si$  provides considerable additional strength.

#### *Influence of copper*

Since a basic alloy can be expected to reach a specified tensile strength only under the most favourable cooling conditions, by counting on a slight gain from stretching prior to artificial ageing, additional means may be required of increasing strength. Copper is known to be useful, especially in small amounts that apparently participate in the formation of the GP zones that precede  $Mg_2Si$  precipitation. Additions of up to 0.4% Cu have been found to raise the strength at all cooling rates without increasing the quench sensitivity achieving an additional 20–30 N mm<sup>-2</sup> in ultimate tensile strength.

Copper additions to AlMgSi alloys are not so readily accepted, because of anxiety over reduced corrosion resistance. It is known, however, that if the copper

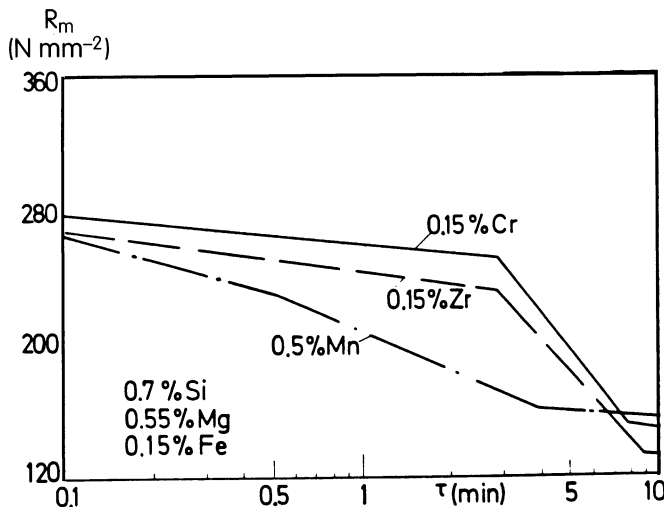
addition is small there is no danger that mechanical properties will be impaired, provided an element such as Mn or Cr is present. This is attributed to the reduced amount of grain-boundary precipitation in the presence of Cr and Mn [18].

### 6.3.2 Recrystallization inhibitors

Since toughness requires preservation of the fibrous structure produced by extrusion, manganese, chromium and zirconium are often added, either singly or in combination. These elements also increase quench sensitivity, by providing the nuclei for precipitation of Mg and Si during cooling. Thus low quench sensitivity and improved toughness are conflicting requirements.

Additions of Cr, Mn and Zr are compared in Fig. 6.8 for their effect on quench sensitivity (where the Mn level is raised to take into account its lower efficiency in reducing grain-boundary precipitation [19]).

The results clearly show the advantage of Cr. Even at the same level of alloying as Cr, Mn additions have been found [18] to make such alloys more quench sensitive than other recrystallization inhibitors. Larger Cr additions increase the quench sensitivity significantly, although the positive effect of holding at room temperature begins to compensate somewhat for the strength loss. At 0.15% Cr, the critical  $\tau$  value is about three minutes, within the range of many production facilities. The material is also relatively insensitive to holding time at room temperature, a further advantage in practice.



**Fig. 6.8** Tensile strength as a function of the median cooling time, showing the influence of Cr, Mn and Zr on quench sensitivity. Heat treatment, 24 h at room temperature + 160°C for 116 h.

### 6.3.3 Toughness

Without recrystallization inhibitors, AlMgSi alloys would be too brittle for construction uses. The intermetallic particles formed by these elements (principally Mn, Cr, Zr and to a lesser extent Fe) affect the toughness in various ways:

1. by ensuring the presence of a substructure thus preserving the fibrous grain morphology;
2. by reducing the amount of  $Mg_2Si$  precipitating at the grain boundaries;
3. by promoting multiple slip within the grains [19].

Fast cooling rates also improve toughness, presumably via mechanisms 2 and 3, since the width of the precipitate-free zone at the grain boundary decreases with increasing cooling rate.

If the cooling rate and amount of recrystallization inhibitors are already matched to permit air cooling, improved toughness can still be obtained by underaging during subsequent artificial age-hardening. With this approach, it is possible to get improved toughness without the sacrifice of increased quench sensitivity. Maximum strength is the usual goal, but greater toughness may sometimes be more desirable. With the alloy 6061, for example, a drop of  $30 \text{ N mm}^{-2}$  (10%) in ultimate tensile strength allows an increase of 30–40% in toughness.

### 6.3.4 Structural sensitivity

Another aspect of quench sensitivity can be misleading: the role of structure. The distribution of intermetallic particles prior to extrusion is determined by the homogenization treatment and by the heating cycle just before extrusion. In employing the minimum of recrystallization inhibiting elements, care must be taken not to make the particles unduly coarse and not to take too many of these elements into solution. For this reason, rapid heating to temperature and low extrusion temperatures are preferred together with a homogenization soak temperature not exceeding  $570^\circ\text{C}$ . In practice such a homogenization is the norm but we have seen that ideally a higher temperature would be required to optimize surface defects.

Fast extrusion rates, poor die design and thin regions in the section can also lead to recrystallization. Where recrystallization has been inhibited but finally occurs, the resultant grains can be very large. Quench sensitivity then varies from area to area, and a wide range of properties occurs in a single extrusion.

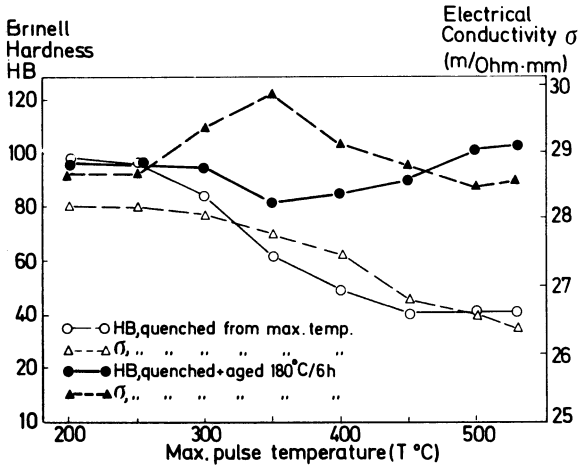
This is especially disadvantageous when recrystallized morphologies co-exist with the required fibrous grains.

### 6.3.5 Quench sensitivity in welding

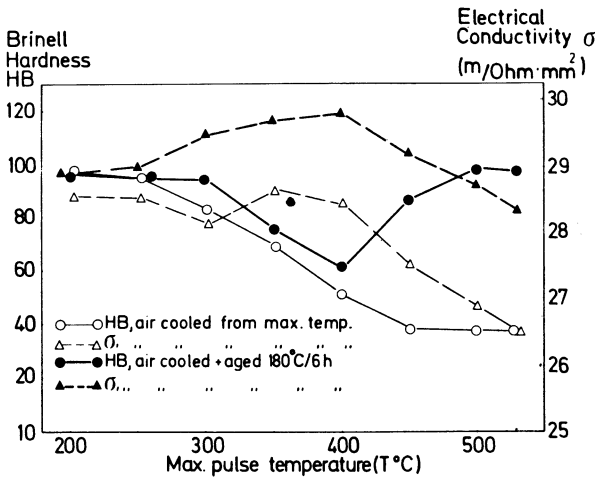
The most pronounced form of quench sensitivity suffered by AlMgSi alloys occurs during welding.

A series of 2 mm thick samples of fully age hardened (180°C for 6 h) 6061 sheet were subjected to the heating cycle undergone by various regions adjacent to the weld junction [17]. At each stage the conductivity ( $\sigma$  test) and the hardness were measured. The results are shown in Fig. 6.9.

It can be seen from the electrical conductivity of the water quenched samples that the heating cycle is one of re-solution of solute. On air cooling from temperatures above 350°C, reprecipitation occurs. The hardness plots for water cooled



(a) Water-quenched from maximum pulse temperature



(b) Air-cooled ( $\tau = 30$  sec) from maximum pulse temperature

**Fig. 6.9** Hardness and electrical conductivity ( $\sigma$ ) as a function of the maximum temperature reached in a series of samples of 6062 alloy (thickness 1 mm) subjected to a thermal pulse simulating a weldpass. Initial condition: heat treated 180°C for 6 h. (After Maitland and Reid.)

and air cooled samples immediately after cooling are approximately the same. On ageing again at 180°C, the strength of the water quenched material is substantially restored, whereas the air cooled material exhibits a pronounced minimum. In this case, quench sensitivity has been induced by the Mg<sub>2</sub>Si precipitates, which survived the dynamic resolution process during the heating part of the cycle.

Several alloys including 6061 can be readily welded using MIG and TIG techniques and after welding exhibit ultimate tensile strength values of 170 N mm<sup>-2</sup> and a 0.2% proof stress of 120 N mm<sup>-2</sup>. Yield strength of the welded section increases by 10 N mm<sup>-2</sup> over a period of three weeks after welding. This is attributed to the reconstitution of partially dissolved precipitates and/or the formation of GP zones promoted by the presence of copper atoms.

Quench sensitivity is evidently a problem encountered at all stages from the extrusion billet to the final construction. The complex roles of the elements that affect this sensitivity make it necessary to compromise in a way acceptable to both the alloy producer and the user.

## 6.4 SURFACE PROBLEMS AND SURFACE GENERATION

### 6.4.1 Introduction

Surface appearance in the mill-finish condition or after anodizing or painting is one of the most important characteristics of high quality 6XXX extrusion. Die lines, scoring, pick-up and tearing all detract from the appearance of the as-extruded profile. Subsequent processing, such as painting, can mask defective surfaces if the paint film is thicker than the defect height, but often the defects are actually exaggerated. For example, painting without vigorous cleaning in the pre-treatment stage, sometimes only covers pick-up particles, not necessarily visible at the press, leaving blemishes on the painted surface. In addition, during electrostatic processes, localized charging can occur at the site of any defects, again causing blemishes on the final finish. A rough surface, i.e. one with heavy die-lines or scores, is not always improved by painting and these defects are sometimes exaggerated by a thin layer of gloss paint. Etching and anodizing can usually remove pick-up particles but cannot always remove all surface defects produced at the press, depending on how much metal is removed in the etch tank.

Those who have spent time near the press will know that the die can play a significant part, sometimes an overriding one, in determining the quality of the surface. Extruded profiles that require multiple copies often illustrate this, with dies that appear to be identical, behaving very differently. The end result of this is that extrusion trials carried out to identify the critical metallurgical conditions for improved surface finish are difficult to design and are often inconclusive due to the complex interaction of all these factors.

Furthermore, extruded surfaces are difficult to quantify and assessment of what is good and bad is often subjective. As a result, the problem of surface finish

is still far from falling off the list of extrusion problems. Quality requirements continue to improve; shapes continue to get thinner and the drive for increasing extrusion productivity all make the understanding of surface generation important.

The prime objective of some work reported by Clode and Sheppard [20] was to study the effect of the shape of the die bearing on surface finish and to develop a 'test' die. Using this die, the role played by the main extrusion process variables, billet temperature and extrusion speed, on the surface finish were established.

The extrusion process is a convenient route for producing lengths of complex section which meet strict geometric, mechanical property and cosmetic goals. The relative importance of these goals is governed by the product application. By far the largest volume is produced for the building and construction industries in the form of frames and decorative trim. It is in these products that the incidence of surface defects is of particular concern.

There are numerous defects which occur during the production of aluminium alloy extrusions [21–24] and, of these, it is surface cracking, pick-up and die lines which presents the largest problem for the extruder. Surface cracking is most commonly associated with high strength aerospace aluminium alloys [25,26] but it is also observed in the more dilute architectural alloys of the AA6XXX series. Reiso [27] reported that the extrudability of Al–Mg–Si alloys, on an industrial scale extrusion plant, was strongly influenced by the Mg and Si content and the homogenization practice. He found that the extrudability reduced with increased amounts of Mg and Si in solid solution, resulting from either increasing the cooling rate from the homogenization temperature or increasing the alloy content. The surface cracks were reported to be caused by tearing in the aluminium matrix.

However, it was also suggested that a second type of crack initiation mechanism occurred when slow cooling rates from the homogenization temperature were employed. In this case the presence of coarse  $Mg_2Si$  precipitates in the subcutaneous layer represented a region of local weakness in the structure which was unable to withstand the stresses at the die. The weakened structure subsequently sheared, leaving a pore in the structure to act as a crack initiation point. This work emphasized the importance of the thermal history and the choice of alloy composition.

'Pick-up' and 'die lines' are the most serious defects observed in the common alloys such as AA6063. Despite the commercial significance of such defects, there is surprisingly little documented research in the technical literature on the origins of their formation, especially in the case of die lines. Present evidence suggests that during extrusion a thin film of extrudate material adheres to the die land surface, and it is this interaction that results in the formation of these defects. The exact mechanism of this adhesion has not been formulated.

The pick-up defect is usually thought to be enhanced by inclusions in the cast billet, inadequate homogenization treatment [28] and die deflection [29]. The defect is also temperature sensitive. Apart from improved casting procedures [30] and homogenization practices, attempts at eliminating the defect have focused on modifications to tooling and improved extrusion practices. These include die

modifications by nitriding or the use of die materials less prone to aluminium build-up (i.e. non-wetting), such as  $Zr_2O_3$  [31] and Syalon [32].

Employment of an inert atmosphere [35] to prevent oxidation of the extrudate and the use of die cooling [36] have also been shown to reduce the incidence of pick-up. A novel method [37] of using a thin leader pad 1–2 mm thick with an addition of 0.01–0.5% boron to the billet composition, was also seen to reduce pick-up by maintaining a clean (or minimum build up) die land.

Die lines are also believed to be caused by the interaction of the die land area, although this must involve a different area of the die land to that causing pick-up. Die lines also occur when highly polished die lands are used and when the die operates in the optimum ‘choked’ condition. When operating at these optimum conditions for surface generation the die lines are finer and more shallow and are termed ‘micro-die lines’. These may be a particular inconvenience when the extrudate is to be anodized following extrusion.

#### 6.4.2 Surface features

An inherent feature of the extrusion process is that the nature of the shear involved produces a continuous ‘virgin’ surface which, in the case of aluminium extrusion, is in intimate contact with the die steel. Moreover, this clean surface is absolutely critical from a commercial consideration. The extrudate–die land interaction involves the development of an aluminium coating on the die land area during the extrusion process, thus producing score lines on the product known as pick-up or die lines. Die lines may also be observed which are not associated with the die land coating. In such cases, the lines are finer and more shallow and are termed micro-die lines. In order that the formation mechanisms of the three surface defects might be studied – pick-up, die lines and micro-die lines – specially designed split-die tooling has been used [20]. The effect of die land length on the surface formation has also been studied using a series of dies with varying lengths from 8 mm to knife-edge.

##### *Pick-up*

This defect is observed as intermittent score lines of varying lengths between 3 mm and 12 mm and often terminates in a fleck of aluminium debris which is referred to as ‘pick-up deposit’. As indicated above, the severity of pick-up is governed by numerous factors but these may be grouped into the three main categories:

1. alloy, condition, heat treatment;
2. tooling and equipment;
3. extrusion process parameters.

In one study [20] the alloy and heat treatment were kept constant at conditions typical of industrial practice and the object was to determine the effect of extrusion processing.



The alloy under investigation, 6063, was supplied in the form of semi-continuous, direct chill (DC) cast logs based on commercial purity aluminium. The alloy's structural cleanliness was similar to that produced for normal industrial processing.

The alloy received a short homogenization treatment prior to the extrusion trials, which effected an iron phase transformation from acicular to spherical and produced a fine distribution of  $Mg_2Si$  in the  $\beta'$  form (Fig. 6.3(b)), the iron phase transformation being aided by a small amount of Mn in the alloy [34]. Because of the short industrial type homogenization treatment, complete spheroidization of the iron phase was not always achieved and some of the coarser  $Mg_2Si$  remained.

This enhanced pick-up formation when extrusion conditions were favourable to aluminium build-up on the die land.

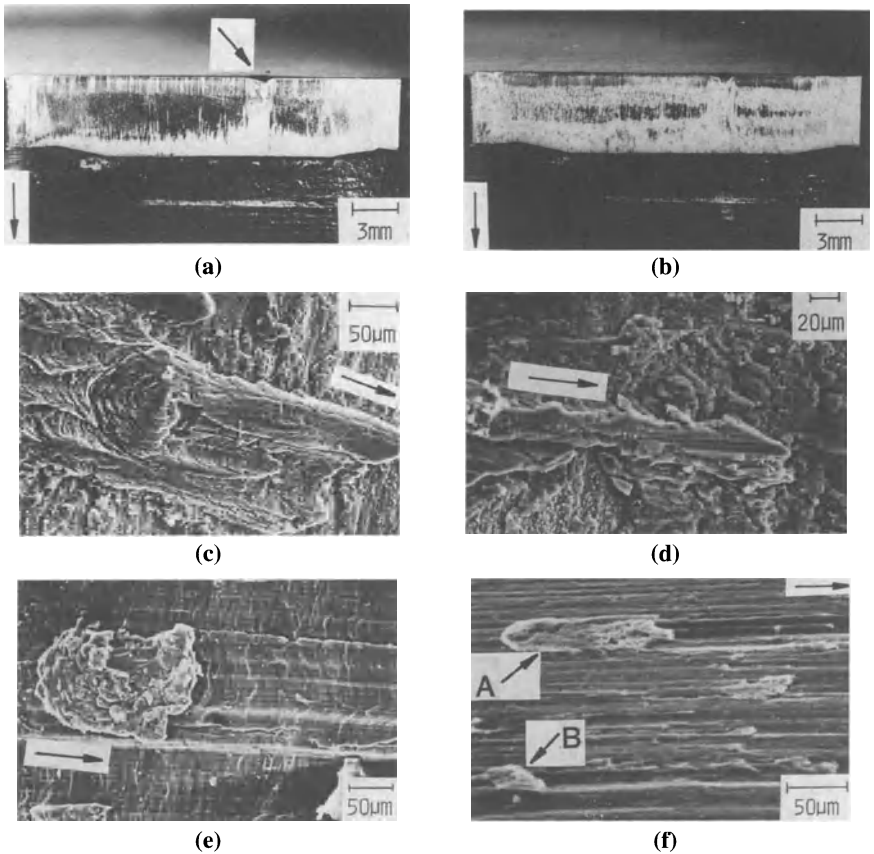
#### *Pick-up formation*

Keeping the factors governing pick-up in categories 1 and 2 constant, the effects of the extrusion temperature and strain rate could be established. These process parameters were observed to have significant effects on aluminium build up in the die land area and, as a consequence, pick-up formation.

Before the start of extrusion, the surface layers of both extrusion billet and die land consist of reaction products composed mostly of oxides. Due to the shear involved in the extrusion process both at the container and dead metal zone interfaces, these protective layers are subjected to shear and indentation resulting in direct metal to metal contact and therefore adhesion at the die location. The extrudate material is thus locally deformed, and fragments may be sheared and removed from the matrix and subsequently deposited onto the harder die land surface. Concurrently these deposits are further elongated in the extrusion direction. This appears to be continuous throughout the extrusion cycle, producing large areas of transferred material. Eventually, the end zones of the ironed layers on the rear portion of die land begin to spall and a 'pick-up deposit' detaches and becomes embedded in the extrusion product.

Figures 6.10(a) and (b) show the die land area of a die for the extrusion of a  $25 \times 5$  mm rectangular cross-section bar. The long edge of the die land area is depicted and has experienced three extrusions at  $500^\circ\text{C}$  and  $575^\circ\text{C}$  in (a) and (b), respectively. The choked area at entry to the die can be seen to have collected a uniform adhered layer of aluminium which was observed to remain stable throughout future extrusion runs. This area is thus responsible for the development of extrudate surface and determines the incidence of the die line phenomenon discussed below and plays little part in the development of pick-up.

Following this choked area, the aluminium surface is exposed to the atmosphere and consequently oxidizes. It is in the wake of the choked area that flakes of aluminium can be observed to be deposited in the mid-section of the die land. Most of these flakes are carried forward by the emerging extrudate and accumulate at the die land exit. Considerable pick-up can be observed on the die at exit, the 'flaked' area of the die being considerably less for the  $575^\circ\text{C}$  extrusion which



**Fig. 6.10**(a) Die land area after extrusion at 500°C; (b) die land area after extrusion at 575°C; (c) aluminium build-up at exit to die land (500°C); (d) aluminium build-up at exit to die land (575°C); (e) pick-up formed by stick-slip mechanism; (f) pick-up formed by debris removal from the aluminium coating on the die land 'A'. Arrows indicate extrusion direction.

is clearly subjected to greater exit pick-up. The 'pick-up' area in both cases is shown in greater detail by the scanning electron micrographs in Figs. 6.10(c) and (d). Figure 6.10(c) indicates that for the case of the 500°C extrusion the exit area consists of a background deposit of aluminium which probably remains stable, but some of the flakes have agglomerated and been ironed as they progress through the die, producing a large pick-up deposit, smeared at the tail end, which will dissociate from the die and become embedded in the extrusion product. In this case the process is a series of isolated events in which separate agglomerates are successively transferred to the extrudate.

In the 575°C extrusion (6.10(d)) far more ironing of the particles has occurred and agglomerates have been extended quite substantially in the extrusion direction, largely because of the lower flow stress of the material. Spalling has

occurred on either side of the elongated agglomerate, which when deposited on the exit side of the die land hardens because of the lower die temperature. Pick-up occurs by dispersion of the material on either side of the elongated agglomerate, which will continue to score the extrudate until it is also transferred to the extrusion product. The pick-up damage is thus much greater at 575°C than at 500°C.

In Fig. 6.10(a) there is evidence (arrowed) that the throat area of the die has suffered severe damage and, as a result, a considerable increase in the aluminium film in the wake of the damage. Such damage would lead to immediate withdrawal of the die from service.

#### *Dual pick-up mechanisms*

We can thus accept that the formation of the pick-up defect is quite clearly due to extrudate/die interaction. The precise mechanism by which this occurs is, however, not so obvious. There are at least two possibilities.

The pick-up deposit could simply consist of debris from the coating at exit to the die land, or alternatively a mechanism involving transient sticking between the extrudate and the die may be responsible for accumulation of extruding material, and this could cause the pick-up deposit. This latter mechanism would be analogous to the formation of transfer elements in the wear process. EDX analysis of the pick-up could not distinguish between these two possibilities when only single-alloy extrusions were performed.

Accordingly an AA5456 billet was extruded at 500°C through a clean die prior to a series of 6063 trials, thus producing an initial deposit of different composition to that of the extrusion billet. The 6063 billet was then extruded at 600°C at an exit speed of 0.9 m s<sup>-1</sup> resulting in both pick-up and surface tearing. The major pick-up deposited, indicated as A in the SEM (Fig. 6.10(f)), was analysed by EDX and found to contain higher magnesium and manganese peaks that would be expected from the parent material, indicating that their origin was from the 5456 material. However, pick-up deposits with the same element intensities as the parent material (marked B in Fig. 6.10(f)) were also observed, suggesting that the transient stick-slip mechanism was also operating. After the processing of six billets there was no further trace of pick-up originating from the 5456 material, a large proportion of deposits having a high percentage of AlFe(Mn)Si phase.

The results therefore indicated that dual mechanisms were operating. When the propensity for extrudate–die interaction is strong, there is a rapid build up of aluminium at exit of the die land resulting from severe frictional forces on the aluminium coating causing agglomeration, work-hardening, elongation in the extrusion direction and finally spalling, which is the ultimate cause of the pick-up on the extrudate. When adhesion between the die and extrudate is approximately equal to the cohesive strength of the metal forming the extrudate surface, then the pick-up flakes are continuously transferred between die and extrudate in the die land area, eventually agglomerating as a pick-up deposit. This mechanism is most commonly observed when commissioning new dies, where

the pick-up deposit consists of metal originating from both the extrudate and the die land coating. An extrusion involving super-purity aluminium produced an excellent sample of this mechanism (Fig. 6.10(e)). EDX analysis indicated the debris, clearly formed by a stick-slip mechanism, to be identical to the parent material.

The stick-slip mechanism is less common and results in less severe extrusion damage than occurs when the deposit is produced by continuous accumulation at the die exit. In the latter case the damage is generally observed as a deep score line with the pick-up deposited at its termination as shown in Fig. 6.10(f), labelled A.

#### *Quantifying excessive pick-up*

The occurrence of excessive pick-up is a matter of prime concern especially where cosmetic features are commercially important. It is therefore necessary to attempt to quantify the phenomenon, perhaps in a similar manner to that derived for acceptable surface in the high-strength aluminium alloys [27]. The severity of pick-up increased with temperature and strain rate which coincided with a greater degree of aluminium build up on the die land. The process conditions at which excessive pick-up occurred (i.e. gross product damage) should thus be related to the temperature-compensated strain rate which is defined as:

$$Z = \dot{\epsilon} \exp\left(\frac{\Delta H}{GT}\right)$$

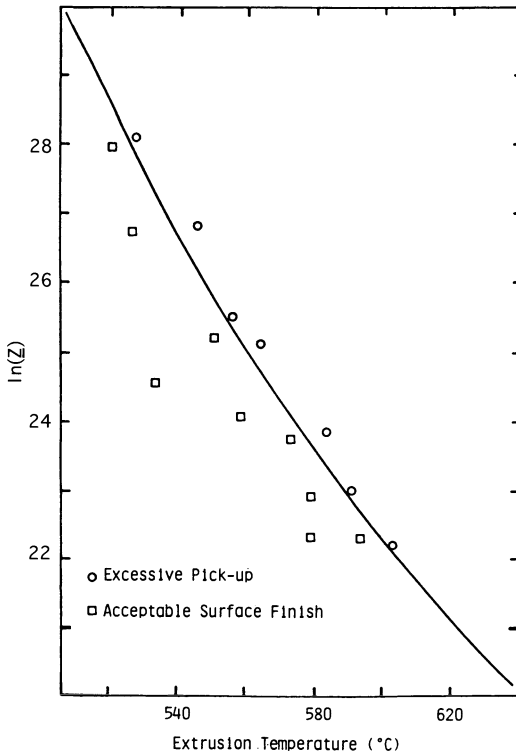
where  $\dot{\epsilon}$  is the strain rate,  $T$  the extrusion temperature,  $\Delta H$  an activation energy and  $G$  is the universal gas constant. Moreover, the flow stress of the material is a function of  $\ln Z$ . Hence Fig. 6.11 shows the function  $\ln Z$  plotted against the initial billet temperature  $T$ . The locus dividing the experimental results exhibiting an acceptable surface and those showing excessive pick-up is clearly divided by the inequality:

$$\ln Z \leq aT^{-b}$$

The reader should note that the values of  $a$  and  $b$  in this equation may be unique to the conditions utilized in these experiments, for example, alloy, cast condition, homogenization treatment, tooling design and tooling temperature. However, it is likely that the functional form would be applicable to most extrusion conditions and provides a useful relationship which, when used in conjunction with a microcomputer, could rapidly be utilized as an industrial tool.

#### *Die lines*

The Aluminium Association has defined die lines as 'longitudinal depressions or protrusions formed on the surface of the drawn or extruded material due to imperfections on the die surface'. Although extrudate-die interaction is clearly a major cause of die line formation, an alternative mechanism of generation has been observed giving rise to micro-die lines.



**Fig. 6.11** Prediction of excessive pick-up.  $\ln Z < aT^{-b}$ .

The two types of die line generation operate simultaneously during extrusion, resulting in a surface with combined features. For the moment we will consider only die line formation but bear in mind that the complete surface topology determining brightness, reaction to anodization etc. consists of at least two components.

### *Surface finish*

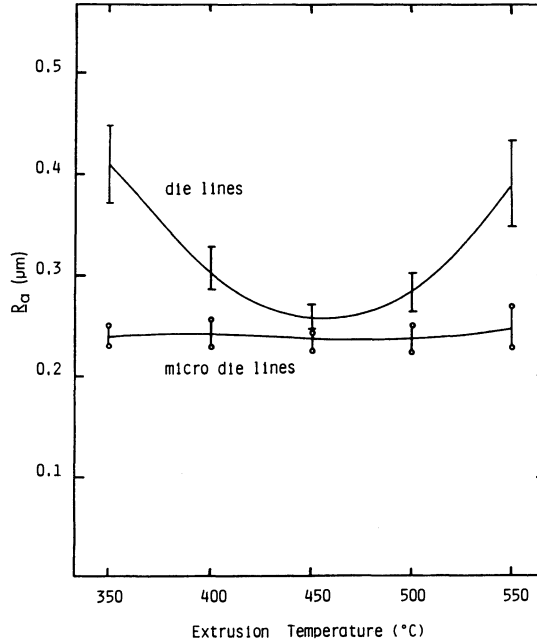
Before differentiating between the two types of die lines it is useful to study the global features of the extrudate surface finish. In order to achieve this, trials performed at temperatures of between 350°C and 550°C and at an exit speed of 1 m s<sup>-1</sup> will serve as illustration. Three billets were processed at each temperature. The die lands were cleaned prior to the first extrusion at each temperature and the surface finish measured using a stylus type instrument. Measurements were made directly in the case of the split die tooling and using replica resins when conventional dies were used. The surface finish in each case was approximately 0.5 μm Ra.

### *Die line mechanisms; generation and modification*

The extrudate surface roughness was sampled at 0.5 μm intervals along the product using the replica resin. Because of the variation in the Ra values at each test

temperature, they are presented as scatter bands in Fig. 6.12. The plot indicates that there is an optimum operating temperature range from 425°C to 475°C in which the smoothest surface finish is obtained. Also shown in Fig. 6.12 is the micro-die line roughness which is discussed below.

The variation in the surface roughness can be directly related to the morphology of the aluminium film on the die land area. This film has two characteristic features. At the front portion of the die land the newly formed extrudate chokes



**Fig. 6.12** The effects of temperature on the as-extruded surface finish.

the die throat. The extrudate surface and the die land are in intimate contact, preventing exposure to the atmosphere. After leaving the choked area of the die land, the small amount of die deflection causes the extrudate to dissociate from intimate contact, permitting oxide formation on the surface. The interaction between extrudate surface and die land then creates the flaking and aluminium film development to which pick-up can be attributed.

Therefore, the final surface formation mechanism may be regarded as one of generation and modification. The surface is generated at the forward position of the die throat in the absence of oxygen. Once generated, the rear portion of the die land serves only to deteriorate the surface by the imposed ironing and galling of the extrusion product. It is the relative contribution of the two areas on the die land that governs the surface finish at each temperature condition.

At the high-temperature condition, 550°C, the choked aluminium at the entrance to the die throat adheres and produces a bandlike formation flowing into the valleys of the ground surface (Fig. 6.13(a)). The banded aluminium film becomes harder than the adjacent extrudate material, due to die quenching and work-hardening. Because of the low flow stress of the material, the die valleys overflow and ridges of hard aluminium are present in the choked area. The surface layers of the extrudate are therefore formed by the ridges of the aluminium film at this location. As the extrudate leaves the choked position, the surface possesses the topographical features of the aluminium film. The continued interaction with the remainder of the die land creates an unstable aluminium film, accumulating at the exit side of the die, which scores the surface and could also cause pick-up. The aluminium coating at the front of the die land is more stable and does not appear to alter significantly with extrusion runs.

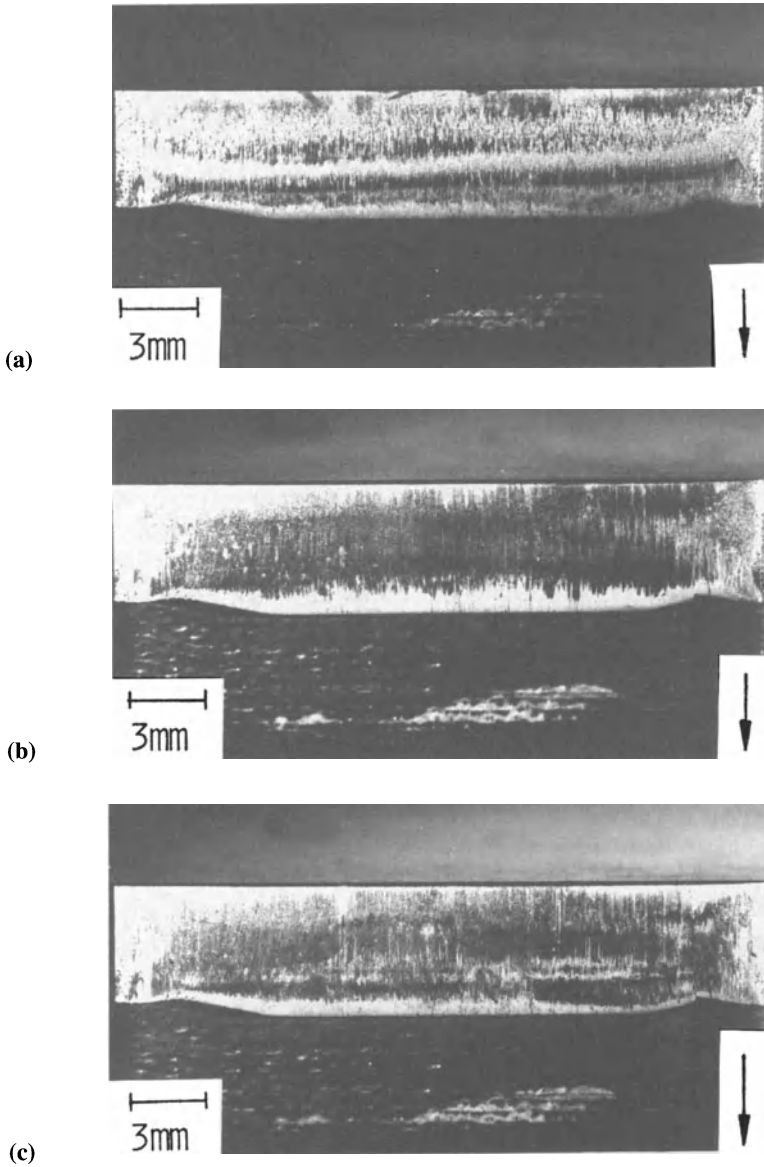
In the mid-temperature range (425°C to 475°C) the aluminium film appears more speckled at the choked portion of the die land. This can be seen in Fig. 6.13(b). In this range, the aluminium in immediate contact with the die land resides in the ground surface topography but, unlike the high-temperature condition, does not protrude above the original ground surface. This effectively reduces the surface roughness of the die land. The die is now effectively perfectly smooth and permits sliding of the surface without deleterious high friction conditions, thus producing a smoother product. The reduced aluminium film on the leading portion of the die land is probably due to the scouring effect of the harder (Fe,Mn)Al<sub>3</sub> and small Mg<sub>2</sub>Si particles, finely distributed throughout the matrix.

There is also a build up of aluminium on the exit side of the die land which must increase the extrudate's surface roughness. However, the film in this case is more stable than in the high-temperature condition and does not appear to cause pick-up.

At the lowest temperature condition (350°C) an increase in the surface roughness is observed and accompanied with a greater scatter of results. At this temperature the rejection of Mg<sub>2</sub>Si is high, forming coarse precipitates and hence largely eliminating any scouring effect. Indeed the possibility of such acicular precipitates lodging in the valleys of the die surface cannot be rejected. The reduced temperature also causes an increase in the flow stress of the metal, producing higher extrusion pressures and increased die deflection, which is known to enhance build up of aluminium on the die land [30]. This feature is clearly illustrated in Fig. 6.13(c). The aluminium coating in the choked area has increased slightly and coarse bands of aluminium have accumulated, aligned in the extrusion direction. This film is formed in the absence of oxygen and, unlike the higher extrusion temperatures, there is less resultant build up of aluminium on the exit side of the die. Therefore, the product surface is produced by further extrusion through the choked aluminium film, thus adopting its coarser topographical features.

It is evident from the results presented in Fig. 6.11 and the observations made on the aluminium coating on the die land areas, that the die land-extrudate interaction plays an important role in determining the surface finish of the extrudate.

We may also observe that the surface is generated in the choked area and the remaining die land deleteriously modifies the product finish. The effect of die land length on product quality is thus very clearly important.

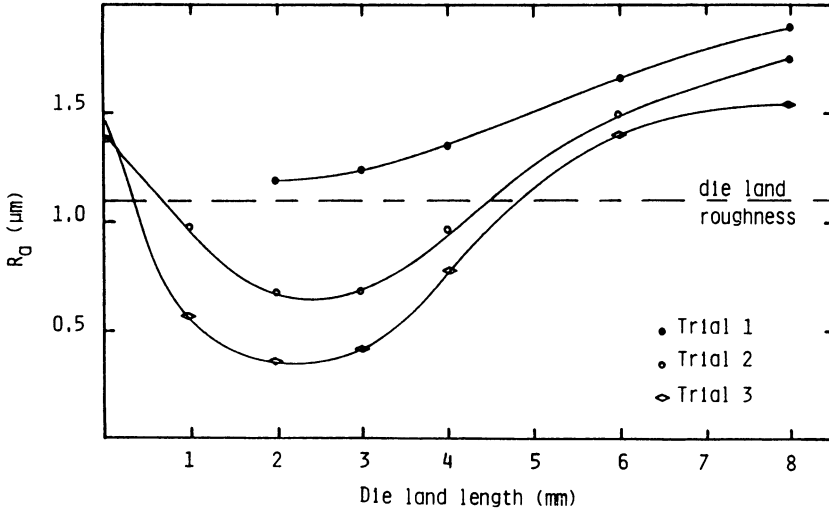


**Fig. 6.13** Morphology of aluminium build-up on the die land area; (a) 550°C; (b) 450°C; (c) 350°C.



*Die land length*

From the experiments described above there is an apparent optimum operating temperature in the vicinity of 450°C, which is consistent with industrial practices for AA6063 extrusion. Tests were therefore conducted utilizing land lengths varying from 8 mm to knife edge (0 mm). The dies were ground perpendicular to the extrusion direction with a surface finish of 1.1  $\mu\text{m Ra}$ . Three billets were processed through each die in turn and the results are shown in Fig. 6.14.



**Fig. 6.14** The influence of die land length and number of extrusion trials on the extrudate surface finish.

The initial billets processed through the dies exhibited a rough topography and displayed a high percentage of tearing; the roughness and tearing increasing with the die land length. This feature is commonly observed when commissioning new dies because the adhesion between the newly generated extrudate surface and the clean, ground die land is intermittent both across and along the die land area. This leads to areas of the extrudate material being torn from the adjacent flowing surface, then ironed into the extrudate surface, as it continues to traverse the die land. An illustration of the severe tearing observed is shown in Fig. 6.15.

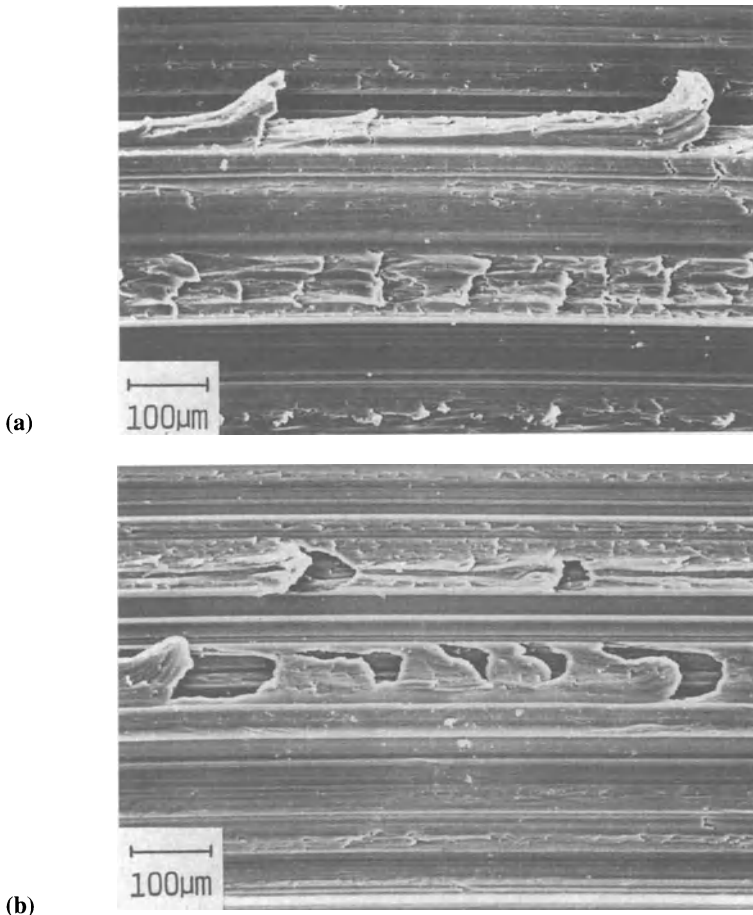
The third and final extrusion run of the series produced a slightly smoother surface than the second, the effects of the die land length being similar. The coating of aluminium on the die land in this case was more fully established, residing in the grooves of the die land surface.

An interesting feature observed after the trials was that the build up on the working area of the die land (i.e. the front portion) was about 2 mm in length for each of the bearing die land lengths. This provides further evidence that the surface is generated at the entrance to the die throat and that the remainder of the die

land towards the exit side serves only to increase friction and provide greater surface area for material transfer and hence a rougher product and increased likelihood of pick-up.

Figure 6.15 shows that the surfaces produced with land lengths less than 1 mm were rougher than those of 2 mm and 3 mm die land lengths; this is primarily due to the instability of a knife edge under extrusion loading, causing a chattered surface appearance.

It becomes evident that there is a minimum die land length (in this case about 2 mm) for successful surface operation. At this optimum condition the entire land length is choked, preventing the introduction of oxygen to the virgin surface; the resultant prevention of an aluminium oxide film having the propensity to score the extrudate surface is most clearly a critical observation.

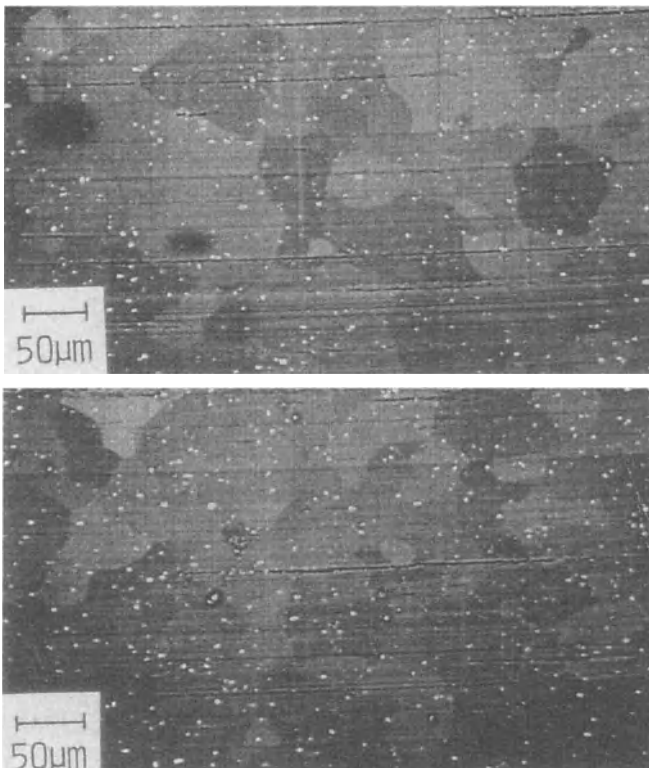


**Fig. 6.15** Surface tearing from extrudate–die land interaction; (a) land length 0.75 mm; (b) land length 2 mm.

*Micro-die lines*

The discussion above has indicated that to achieve the best possible surface finish, extrusion must be performed at about 450°C with the die in the choked condition. However even at these optimum conditions, die lines are still observed to occur. Polishing the die lands has some effect, reducing die line occurrence and improving the surface quality. However, it does not eliminate the defect. Closer examination of the lines reveal that they are both finer and less deep than die lines produced by the mechanism discussed above. Clearly their origins lie in some other mechanism.

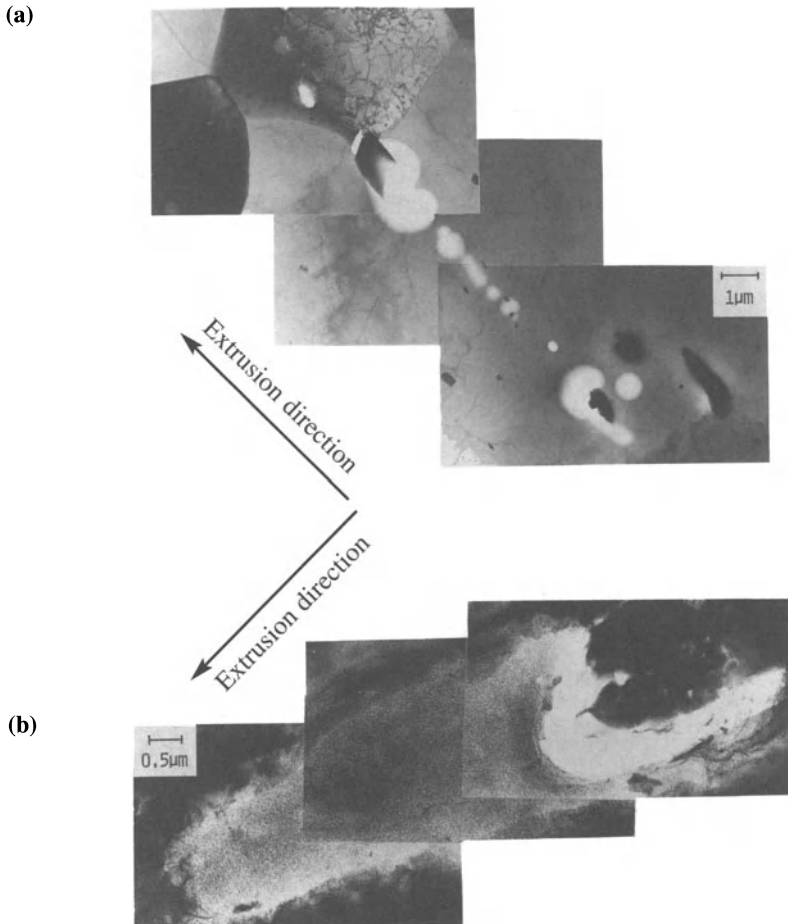
When the extrudate surface produced under these conditions was observed under the SEM, in the BEI mode, elongated iron phase precipitates could be identified in the subcutaneous layers and were clearly associated with surface scoring. Figures 6.16(a) and (b) are examples of the as-extruded surface viewed by back scattered imaging. The iron phase which appears white in the micrographs can be identified in the subsurface layers, aligned in the extrusion direction. It is these precipitates that appear to be associated with the fine score lines on the extrudate surface, which we will henceforth term micro-die lines. One other interesting feature of the back scattered imaging is that the recrystallized grain structure may be discerned.



**Fig. 6.16** As-extruded surface viewed in BEI mode.

Observation of the electropolished foils polished on one side only in the TEM made it quite clear that the iron phase precipitates identified earlier were in fact fragments of larger precipitates interspersed with considerable cavitation. The cavitation links each fragment linearly and it is these strings of voids which appear as micro-die lines on the extrudate surface. One example of this mechanism is illustrated by Fig. 6.17(a) which also clearly shows the 'press quench' effect with subgrains clearly visible in the top left-hand corner of the micrograph.

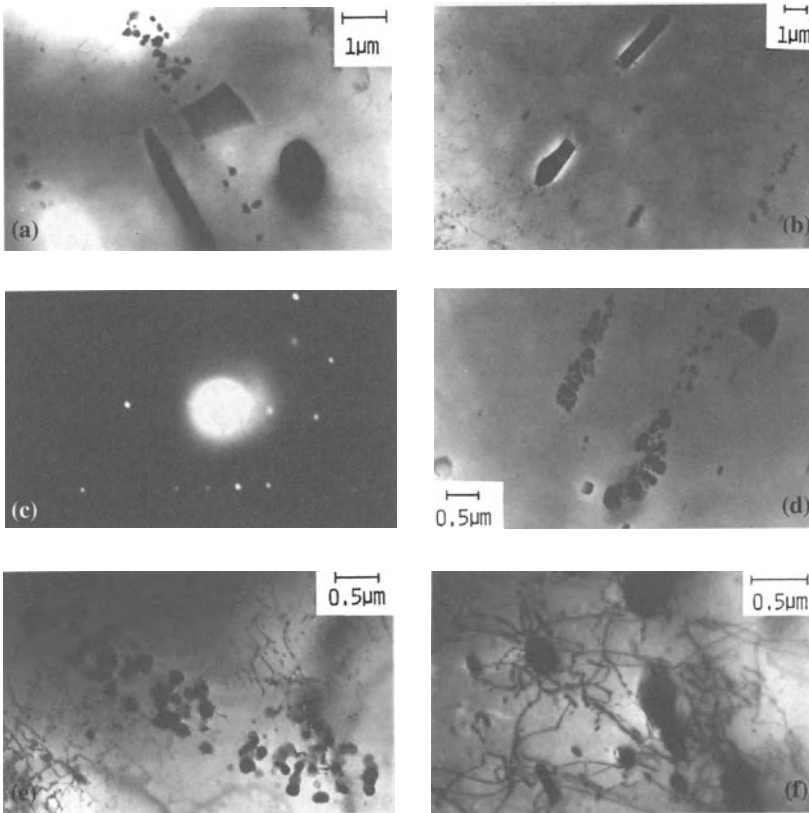
In addition to the micro-die lines some die lines are also observed originating from the interaction of the extrudate and die land area. Fig. 6.17(b) shows one example of a die line termination point. The cause of this surface score was a build up of fragmented iron phase particles in the aluminium film on the die land. As extrusion proceeds, the iron phase cluster spalls, detaches from the die land, and transfers to the extrudate's surface layers.



**Fig. 6.17(a)** Cavitation between AlFeSi fragments in the subcutaneous layers of the extrudate; **(b)** die line termination point.

Figure 6.18 provides further proof [43] of the role of the fractured iron phase in surface generation. It is clear that, in addition to the fragmented coarser AlFeSi precipitates, bands of small spherical precipitates are also present (Figs. 6.18(a) and (b)). The SADP shown in Fig. 6.18(c) identifies these precipitates as AlFe(X)Si whose morphology was not observed elsewhere in the extrudate, being quite specific to the subcutaneous layers. These particles, as indicated in Fig. 6.18(d), originate from the disintegration of the coarser precipitates and are observed predominantly at entry to the die throat area where the extrudate experiences very severe shear deformation.

The morphology observed in Fig. 6.18(e) suggests that the particles originate from that part of the material which is located near to the flat face of the die, on the edge of the dead metal zone and traversing more slowly into the extrudate surface. Pressure-assisted capillarity-driven diffusion processes [37] would quite rapidly transform fragmented precipitates into a spheroidized form at such locations.



**Fig. 6.18** Morphology of precipitates residing in the subcutaneous layers. (a) and (b) residual fragmented coarse AlFeSi and bands of spheroidized material; (c) SADP showing particles of AlFe(x)Si; (d) disintegration of coarse particles; (e) particles located close to the die face; (f) particles at edge of the deformation zone and on the die face.

Moreover such spheroidized fragmented particles could not be identified in any other location in the deformation zone.

The small precipitates proceed to the die throat–extrudate interface and are released into the subsurface layers. The considerable dislocation activity at these precipitates (Figs. 6.18(e) and (f)) affects the surface topology by rearranging into an equilibrium array and eventually coalescing to form recrystallization nuclei. It appears that these small precipitates are almost completely released into the subsurface layers, forming the dispersion shown in Fig. 6.18(b) presumably due to the retarded flow of material close to the flat face and into the radiused choke area of the die.

#### *Micro-die line origin area*

This evidence clearly suggests that the internal shear/dead metal zone boundary is effectively the origin of all micro-die lines. Fig. 6.19 shows the micrographs observed and their precise location in the deformation zone. At entry to the shear zone (location A) the iron phase precipitates start to align themselves into the direction of flow, concomitantly pinning subgrain boundaries: the apparently spherical precipitates shown in Fig. 6.18(b) are of course the needle type precipitates, observed in cross-section. At this position there is little evidence of fragmentation of the precipitates although the volume fraction might suggest that some of the precipitates originate from even larger particles residual from the homogenization process.

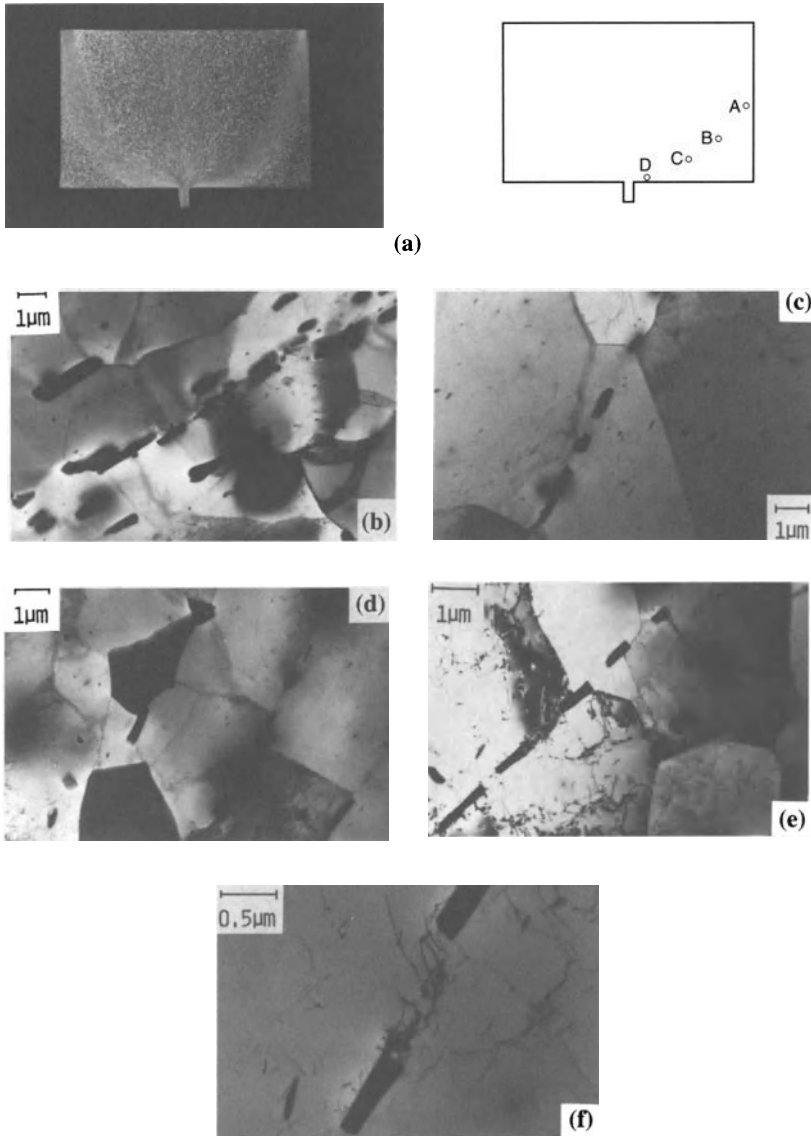
As the particles approach the die throat, however, it is clear that they are elongated, sheared and become aligned into the high shear direction (Figs. 6.19(c) and (d)). Fig. 6.19(e) shows the fracture of this iron phase with the associated stress field generating dislocations between the individual remnants of the original particles. This is shown at higher magnification in Fig. 6.19(f). This stress field between the fragments eventually leads to cavitation which is the direct cause of the observed micro-die lines.

#### *Origin of spheroidal particles*

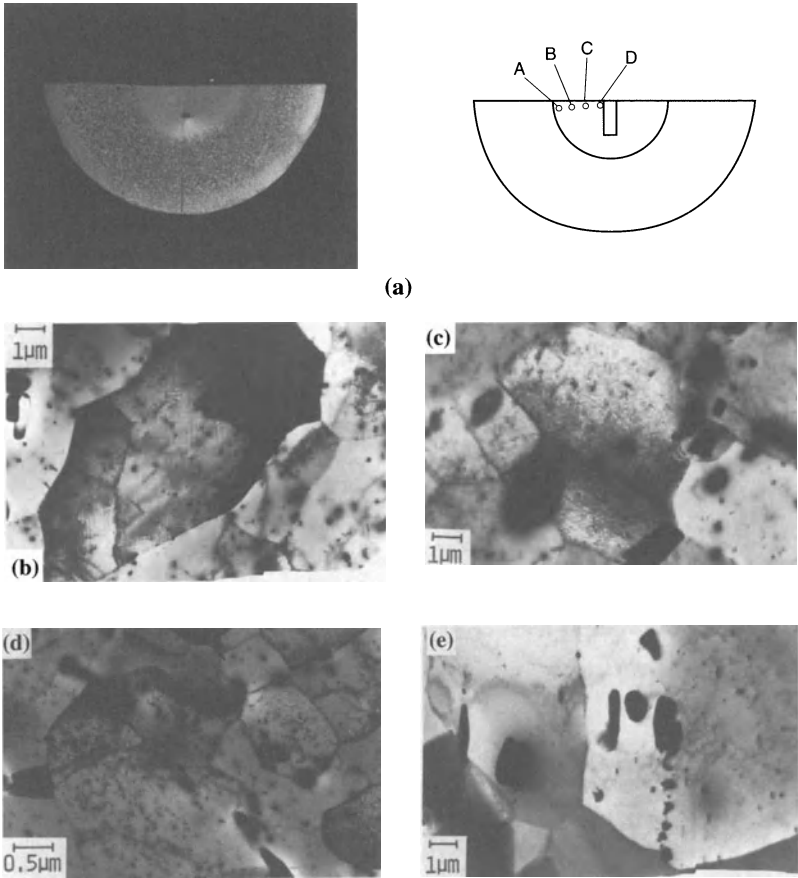
We have discussed above and shown in Fig. 6.19 that bands of spheroidized iron-rich particles may be detected concomitant with the fragments of broken acicular phase in the subcutaneous layers of the extrudate. When the die throat was examined in more detail (by TEM) the prime origin of these spheroidal particles became clear. The macrograph Fig. 6.20(a) indicates that the periphery of the face is composed of coarse recrystallized grains and is truly quasi-static, as is the region spreading in from the outer edges to about 1/3 of the billet diameter composed of much smaller recrystallized grains. The core of the material appears to be heavily deformed with material flowing into the die throat.

We should note that the material along the face is feeding the die throat much slower than the material in the shear zone adjacent to the dead metal zone. It is in this volume at the die face that coarse fragmented particles congregate, awaiting

release into the extrudate surface. Clearly the volume fraction of dispersoid is much higher, as indicated in Figs. 6.20(b) and (c), which show a well formed sub-structure, the boundaries being pinned by small  $Mg_2Si$  particles with quite large precipitates being observed elsewhere. It is likely that, at this stage, the precipitates



**Fig. 6.19** (a) Extrusion billet macrograph with specimen locations indicated; (b) alignment of  $AlFeSi$  particles at 'A'; (c); (d); (e) further alignment and subsequent fracturing of  $AlFeSi$  particles at 'B', 'C' and 'D'; (f) dislocation activity between  $AlFeSi$  fragments at 'D'.



**Fig. 6.20** (a) Macrograph of front billet face and locations of specimen extraction; (b) high volume fraction of precipitates at 'A'; (c) increase in coarse precipitation at 'B'; (d) alignment and fracturing of AlFeSi and coarse  $Mg_2Si$  precipitates; (e) initial stages of precipitate disintegration and spheroidization.

are not aligned into the flow direction and hence the micrograph is showing most of the particles in cross-section. The reader should also note the considerable dislocation activity within subgrains; suggesting that flow is still developing in this region. The precipitates observed are mainly  $Mg_2Si$  caused by the billet reaction with the cooler die interface ( $350^\circ C$ ) [39–41].

In regions closer to the die throat entry, there is an increase of the iron phase fragments which become more aligned as the material moves from location B to location C (i.e. Figs. 6.20(c) and (d)). These fragments are clearly deposited by the intense shear zone moving along the dead metal zone boundary. In addition to the alignment occurring between B and C some spheroidization also occurs



due to the shear-assisted capillarity processes discussed above and similar to that described by Sheppard and Zaidi [41]. The fragmentation of the residual large particles just before entry to the die is clearly illustrated in Fig. 6.20(e) from the specimens extracted from location D.

It is thus clear that the surface of the extrudate originates from two distinct regions of the material. The major contribution is from the deformation zone of intense shear, decorating the dead metal zone. The smaller volume moving more slowly along the die face collects the mainly fragmented iron phase, assists in spheroidization of this phase and is also responsible for the introduction of small  $Mg_2Si$  precipitates into the surface. Thus the origin of the micro-die lines can be attributed to the major region of intense shear but probably would not operate efficiently without the aid of the die face deformation zone. Thus there is clearly scope for revision of die designs in an attempt to solve this problem.

### 6.4.3 Extrusion topology (limit) diagrams

Extrusion limit diagrams have been reported [42–45] which are able to indicate operating conditions to predict strength, toughness, elongation, acceptable surface etc. When processing architectural alloys such as 6063, the production requirements and quality of extrudates are dictated mainly by cosmetic considerations. For such alloys it would be helpful to present the surface generated features within the limit diagram framework.

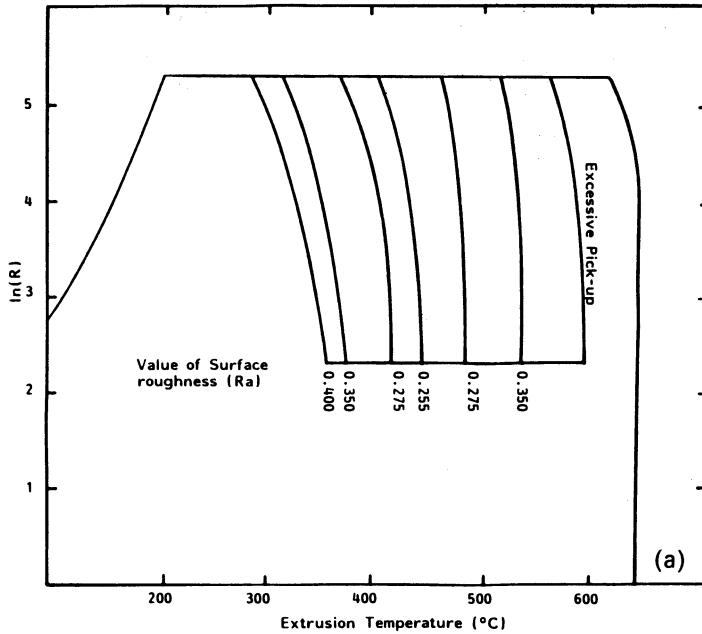
The limiting criterion for an acceptable/unacceptable surface condition on the original limit diagram [42] was when incipient melting occurred. Alternatively, the onset of hot shortness, due to insufficient tensile strength at the extrudate surface, can be used to represent this limit. When cosmetic features are the prime requisite of extrusion, it is the incidence of excessive pick-up that defines the extrusion limit. The conditions for excessive pick-up can be presented in the form:

$$\ln Z \leq 1.236 \times 10^6 T^{-1.7}$$

Thus it is possible to represent the results on the extrusion limit diagram. Fig. 6.21 shows such a diagram for 6063. The pick-up line appears in the operating area of the diagram adjacent to the incipient melting line. It is clear that it is this limit that governs the operating area for architectural alloys. The limit conditions for the onset of excessive pick-up are additionally dependent upon the process non-variables such as cast cleanliness, homogenization treatments and extrusion tooling and practices.

Therefore, the limit line may vary from one extruder to the next and between batches of the cast alloy. However, it is clear that the form of the representation will be consistent.

The most common surface defect in aluminium extrusion is die lines which appear at all processing conditions. Although die lines are termed a surface defect, they are tolerated in many high strength alloy extrusions as they do not appear to affect mechanical properties. However, die lines prove to be most deleterious in architectural alloys especially where anodizing treatments are to be



**Fig. 6.21** Extrusion topology (limit) diagram with contours representing surface roughness and the limit for the onset of excessive pick-up.

used. It was shown above that the average die line value (Ra) varied with temperature and temperature-compensated strain rate. This allowed conditions for constant surface roughness to be formulated. As these results were presented in a quantitative form it is possible to include them on the extrusion limit diagram. A useful form of the diagram is one displaying operating areas in which an extrudate surface roughness within a given Ra band might be obtained. This form of diagram is shown in Fig. 6.21 which could clearly guide the operator into the appropriate processing area. The diagram also explains the apparent incongruity of the Stenger-type diagram. Surface topology and structure must be considered.

These results were obtained under laboratory conditions where control of die conditions and process parameters was relatively simple. Consequently, it is expected that industrially there will be some variation in results when extruding varying sections. However, the general form of the equation should enable the extrusion press operator to generate sufficient data to correlate with his industrial results. Almost certainly, the information would be held in a microcomputer and the data used directly rather than by construction of diagrams.

#### *Limit diagrams; inclusion of structural data*

It is accepted that the subgrain size is dependent on processing conditions, increasing in size with temperature and, to a lesser extent, with decreasing strain

rate. Therefore, it would appear reasonable that a relationship between subgrain diameter  $d$  and temperature-compensated strain rate should exist. It has been shown, for a number of aluminium alloys, that a relationship of the form:

$$d^m = a + b \ln Z$$

results in good correlation. In this equation,  $a$ ,  $b$  and  $m$  are constants, with  $m$  taking the value of 1.

Subgrain measurements were obtained from extruded 6063 and the value of the temperature-compensated strain rate was corrected for the temperature increase produced during deformation, using the integral profile method. The best fit equation obtained was:

$$d^{-1} = 0.025 \ln Z - 0.455 \quad \text{for direct extrusion and}$$

$$d^{-1} = 0.019 \ln Z - 0.391 \quad \text{for indirect extrusion.}$$

These equations are consistent with those of other workers [45–47] except that the subgrain size is less sensitive to processing conditions because of the high rate of recovery operative during deformation of AA 6063.

Another important feature is the non-coincidence of the best fit lines through the data from direct and indirect extrusion. It is not obvious why such a departure exists, other than possible inaccuracies in defining strain rates and in calculating the temperatures from two different heat balance systems. It was also shown by Sheppard and Paterson [48] that a rapid increase of strain rate close to the die entry during indirect extrusion affects the structure significantly; they concluded that the use of a mean strain rate was inadmissible.

The quantification of the relationship between subgrain size and temperature-compensated strain rate allows these results to be represented on the extrusion limit diagram. In Fig. 6.22 lines of constant subgrain size are plotted, demonstrating that a particular subgrain size may be obtained at numerous temperature–extrusion ratio pairs. Sheppard [49] has shown that these substructure lines have the added advantage of representing room temperature mechanical properties, since they are related to the subgrain size (and, hence,  $Z$ ). However, the results indicated that, for heat treatable alloys such as AA 6063, the relationship between process conditions (and subsequent structure) and mechanical properties is more complex, unless the material is utilized in the press quenched condition. Nevertheless there is an increase in both strength and fracture toughness from a retained substructure and it is the subgrain size which plays an important role in any recrystallization events.

#### 6.4.4 Summary

The surface formation mechanism in extrusion is one of generation and modification; the surface is generated at the choked portion of the die land and is subsequently modified by interacting with the remainder of the die surface. The homogenization treatment is essential to reduce excessive pick-up by transforming

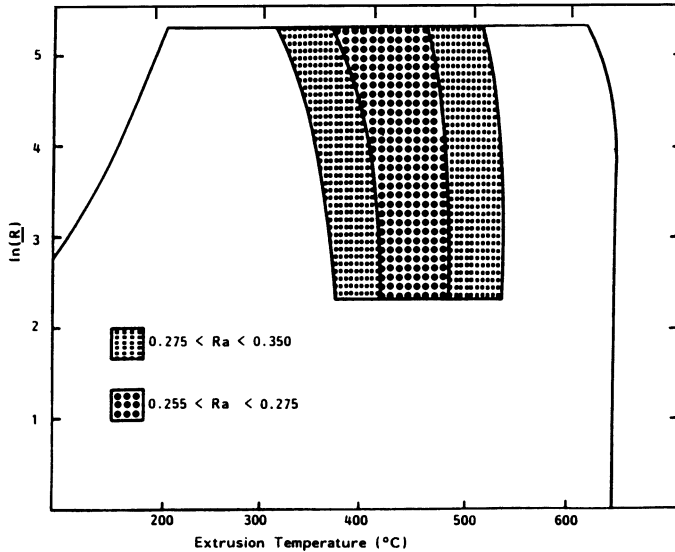


Fig. 6.22 Extrusion topology (limit) diagram (operation area represented).

the intermetallic iron phase from  $\beta$  to  $\alpha$  and in redistributing the Mg and Si. The generation of the pick-up defect occurs by two mechanisms: (i) transient sticking between extrudate and die land resulting in accumulation of extrudate material (analogous to the formation of transfer elements in the wear process) and (ii) debris removal from the aluminium coating on the die land area. The latter mechanism is the most common in AA6063 extrusion. Die lines are largely the result of interaction between the extrudate and the choked portion of the die land.

Optimum process conditions can be established, together with a minimum die land length. The optimum die land length is that which gives sufficient stability together with a land length which is totally choked. However, operating at optimum conditions, and with highly polished dies, continues to generate die lines. In this event they are less deep and are termed micro-die lines.

The origin of micro-die lines lies in the fracture and subsequent cavitation between fragments of coarse iron-bearing precipitates when traversing the deformation zone, adjacent to the dead metal zone and on the die face. The cavitation appears as shallow score lines on the extrudate surface.

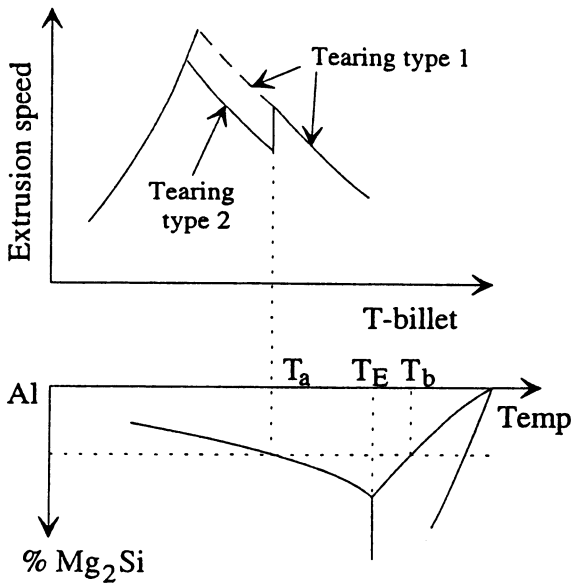
The surface is generated from two deformation zones: (i) the front of the main deformation zone, outlining the dead metal zone and (ii) a small deformation volume on the die face, adjacent to the die throat. The latter deformation volume traps coarse precipitates which are subsequently released into the extrudate surface and along the die land area.

Topological and structural features can be incorporated in the limit diagram framework.

## 6.5 ALTERNATIVE METALLURGICAL DIAGRAMS

Reiso [50] proposed somewhat different limiting diagrams than those discussed based primarily on the nature of the  $Mg_2Si$  precipitates. The results from extrusion tests performed with a specially designed extrusion die indicated that extrudability may be significantly improved by using billet preheating practices other than 'normal' production practices. At high billet temperatures a sharp increase in extrudability was recorded (~30% and ~60% for the two alloys investigated) and a further gain in extrudability was obtained by a solutionizing of the billets followed by cooling into the 'normal' temperature range, prior to extrusion. The increase in extrusion speed is alloy dependent. Furthermore, the extrusions from these billets which gave the highest extrusion speeds, were also found to have better mechanical properties and better surface quality as compared to the ones from billets heated directly into the 'normal' preheating temperature range. The results were explained by the influence of the process parameters upon the structure development in the material, causing the material to fail by different mechanisms: incipient melting (type 2) and tearing initiated at the die-extrusion interface (type 1).

Temperature measurements by a thermocouple mounted as part of the die bearing indicated two different but constant critical temperatures for tearing of type 1 and 2, and temperature measurement in the die is suggested as a future method for process control during extrusion.



**Fig. 6.23** A limiting diagram for 6XXX alloys proposed in reference 50 combined with a phase diagram.

A modified extrusion limit diagram was presented in which the temperature limit was discontinuous with type 2 tearing at lower temperatures and type 1 at high temperatures as shown in Fig. 6.23.

Subsequently Lefstad and Rieso [51] suggested that the limiting diagram could be combined with a phase diagram to explain the discontinuity, based on the microstructure of the material at different billet temperatures. At billet temperatures below  $T_a$  (the solvus temperature), 6XXX series alloys are assumed to contain  $Mg_2Si$  particles precipitated during cooling from the homogenization temperature and/or during preheating before extrusion (when the material is heated directly from room temperature).

At billet temperatures above  $T_a$  the material contains no  $Mg_2Si$  particles. It was found as indicated in the limiting diagram, that there was a sudden increase in maximum speed (and profile temperature) at billet temperatures above  $T_a$  (tearing type 1).

Temperature measurements in the die showed that the profile surface temperatures seemed to be constant along the limiting lines, and were linked to the solidus temperature  $T_b$  (or another limitation below the solidus temperature) for both the dashed line and the solid line above a billet temperature of  $T_a$ . For the solid line below  $T_a$  the limitation was coupled to the eutectic temperature  $T_E$ .

The lower (and left) part of the solid line (tearing type 2 in Fig. 6.23) was therefore assumed to represent the limitation when the material contains  $Mg_2Si$  particles. The upper and right parts of the solid line together with the dashed line (tearing type 1) illustrated the speed limitation when all Mg and Si are in solid solution.

### 6.5.1 Possible phase transformations

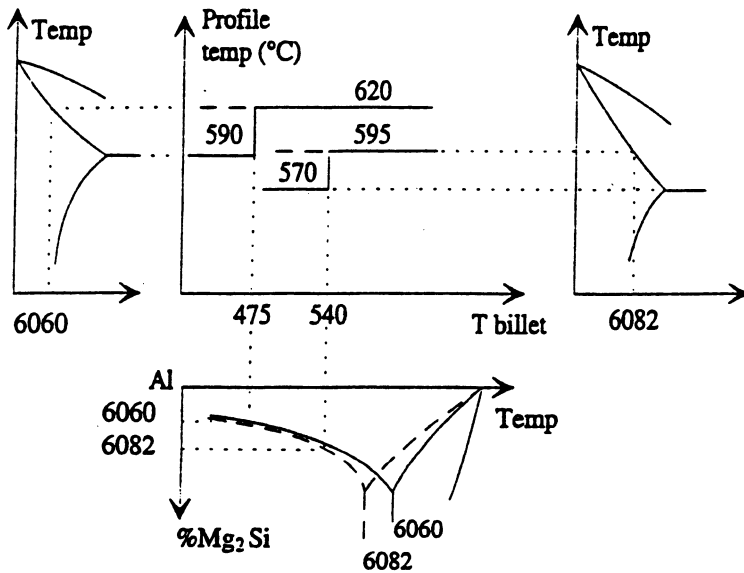
The solvus, eutectic, and solidus temperatures are different for the various alloys in the AlMgSi system. Table 6.1 shows those temperatures for some 6XXX alloys. While extruding 6060, one should therefore expect maximum profile surface temperatures before incipient melting occurs, at 590°C (the eutectic temperature) when the billet contains  $Mg_2Si$  particles (if the billet is heated directly to temperatures below 475°C, the solvus temperature). The incipient melting will occur at 620°C, the solidus temperature, when all the Mg and Si is in solid solution. This applies for billets heated directly to temperatures above 475°C, or for overheated billets below 475°C.

**Table 6.1** The solvus, eutectic and solidus temperatures (°C) for the same 6XXX alloys, as given by Phillips [52]

<i>Alloy</i>	<i>Solvus temperature</i>	<i>Eutectic temperature</i>	<i>Solidus temperature</i>
6060	475	590	620
6063	500	591	612
6082	540	570	595

The corresponding profile temperature limitations for 6063 are 591 and 612°C, and for 6082 they are 570 and 595°C, respectively. The maximum allowable temperatures in all alloys therefore increase by 20–30°C before incipient melting occurs when all the Mg and Si is in solid solution when the material enters the die exit, compared to the conditions when there are  $Mg_2Si$  particles precipitated in the material. A good surface can therefore be maintained at higher surface temperatures if all Mg and Si is in solution

Figure 6.24 combines the limiting diagram with phase diagrams for both the billet temperature and the profile temperature for 6060 and 6082, to illustrate the conditions referred to above.



**Fig. 6.24** A limiting diagram concerning profile temperatures as a function of billet temperature for both 6060 and 6062, together with the corresponding phase diagrams.

When extruding 6060 while heating the material directly to billet temperatures below 475°C, incipient melting of the  $Mg_2Si$  particles will occur at the profile temperature of 590°C. If the billet material is heated to temperatures above 475°C, or overheated and cooled rather quickly to a billet temperature below 475°C, the maximum allowable profile surface temperature is now 620°C. This is seen while combining the limiting diagram with the phase diagram to the left (Fig. 6.24).

The conditions and arguments for 6082 are the same as those for 6060, except for different billet and profile surface temperatures. For 6082, below billet temperatures of 540°C, the maximum allowable profile temperature is 570°C when

the billet is directly heated to the extrusion temperature. At billet temperatures above 540°C, and for overheated billets below 540°C, the maximum profile temperature is 595°C. This is illustrated in Fig. 6.24 by combining the limiting diagram with the phase diagrams to the right. Lefstad and Reiso do not discuss the observation that there are other imperative reasons why all of the Mg<sub>2</sub>Si should be in solution at the die exit.

In their work, limiting diagrams were produced while extruding a 10 mm diameter rod, a strip of 60 × 1.4 mm and a tube of outer diameter 25 mm with a wall thickness of 1.08 mm. The profiles were extruded in dies with different bearing lengths and different degrees of choked die bearings. The purpose of doing this was to investigate whether it was possible to find other limiting lines than the metallurgical ones described in Figs. 6.23 and 6.24. The limitation was expected to be the maximum speed before tearing was observed in the profile surface. The experimental results showed that for some dies another surface defect, referred to as spalling, had to be taken into account when producing the limiting diagrams. Billet material both with and without Mg<sub>2</sub>Si particles was investigated.

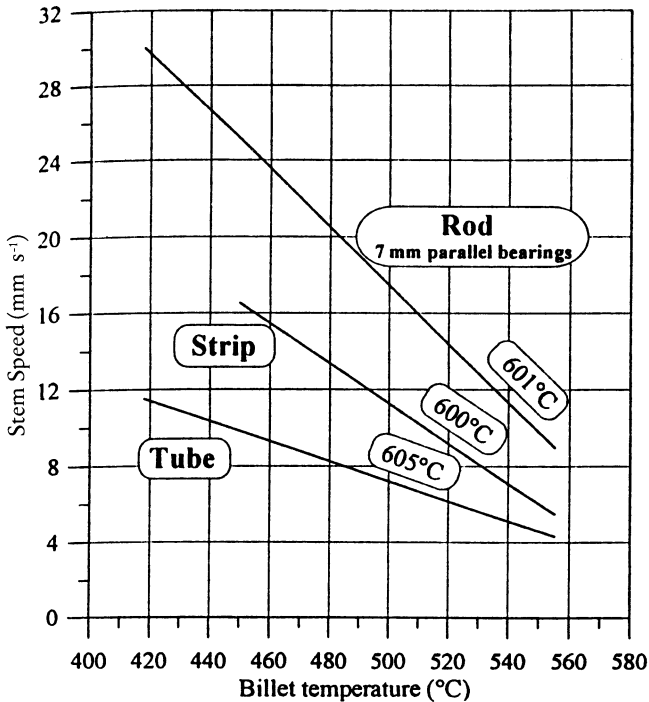
When increasing the bearing length while extruding a rod in parallel bearing dies, it was found that the maximum extrusion speed was raised with increasing bearing length. When taking the spalling into account, the maximum allowable speed in the choked dies was the same as that found for the corresponding parallel bearing die. The latter was true for both the rod and the strip extrusions.

The speed limiting factors for the rod extrusions were found to be tearing for the parallel bearing dies and spalling (reduced rod diameter) while extruding in the choked die. In the strip extrusions, tearing was most distinctive at low billet temperatures, and spalling (reduced strip thickness) was the dominating speed limitation at high billet temperatures for the parallel bearing die. In the choked die extruding the strip, spalling was the most distinctive at all billet temperatures. In the tube extrusion the tearing of the inner profile surface and the spalling (reduced tube thickness) were the criteria for the construction of the limiting diagrams.

The limiting lines for the differing profiles varied as suggested by Clode and Sheppard [20] as shown in Fig. 6.24 for alloy 6082. In Fig. 6.25 all limiting lines are directly comparable because the same alloy (6082) was extruded for all profile shapes. The variation of maximum allowable extrusion speed therefore reflects the differences in extrusion force and heat generation necessary to produce profiles of different geometrical shapes. Figure 6.24 shows that the speed is reduced by 50% when changing from rod extrusion to the extrusion of a tube in the billet temperature range of 460–500°C. While extruding a strip the speed limit is half way between the rod and the tube for the whole billet temperature range investigated. The profile surface temperatures along all lines were found to be 600–605°C.

Rieso's measurements showed that the temperature along a limiting line is constant for a given alloy and microstructure. This means that when the surface material exceeds a certain temperature the surface defect occurs, independently





**Fig. 6.25** The limiting lines determined for all dies when extruding AA6082 (for material with no  $Mg_2Si$  particles). The temperatures determined along the limiting lines are also indicated. [51]

of the billet temperature and extrusion speed. Although the surface defects have different appearances (tearing and/or spalling), they can be regarded as different modifications of the surface defects that appear when some material melts at the profile surface when encountering the bearing.

The temperatures recorded at the tearing/spalling limitations, were compared to the eutectic and solidus temperatures for the different alloys. It was found that the lower line in the limiting diagrams could be linked to the eutectic temperature (when the billet contained  $Mg_2Si$  particles), while the upper line in the limiting diagrams was coupled to the solidus temperature (when the material contained no  $Mg_2Si$  particles).

The temperatures at all speed limitations (for all alloys and dies investigated) could thus be linked to the eutectic or the solidus temperatures of the materials. This showed that no other limitations than the metallurgical ones were found.

Reiso and his colleagues concluded that large variations in profile shapes and die designs used indicated that the maximum allowable extrusion speed may be expected to be related to metallurgical reactions for most of (or a very high portion of) industrial extrusion dies. Although this clearly must be true the authors

did not include the morphology of the Fe-phase in their investigations. Significantly, in this later work, the authors were unable to detect any discontinuity in the surface line. It is also somewhat curious that the surface limiting line appears above the solidus line in the final diagrams.

Lefstad and Rieso's work also indicated a linear relationship between initial billet temperature and maximum allowable speed. This is at variance with the results of other workers where exponential relationships are presented [20,45–49,53,54].

Parsons *et al.* [54] have also reported comprehensive studies concerning the surface of 6XXX extrusions. They presented methods to numerically assess pick-up, surface roughness and grey scale and conclude that:

- The quality of the surface finish, as measured by any of the parameters used, deteriorates to a minimum at a critical exit speed that is dependent on the billet temperature.
- The critical exit speed decreases with increasing billet temperature.
- All the measurement parameters showed good agreement.

There are a number of ways to improve surface quality. A low exit speed will always give a good surface but productivity is sacrificed. However, this is the solution most often adopted in practice. Using the lowest billet temperature possible will generally give a good surface but there are implications in terms of specific pressure requirements, and achievement of mechanical properties. Another approach, used by some press operators is to increase the billet temperature, for example from 450°C to 500°C in order to reduce pick-up. Similarly increasing the speed past the pick-up peak can have the same effect and while this has been observed many times in production, it is seldom used as a solution.

Regarding a mechanism for pick-up formation, one factor known to influence the finish is the temperature of the aluminium passing over the die bearing [55]. This is determined by the billet temperature plus the temperature rise due to deformation.

Other experimental work [56] has derived relationships between section and die parameters, billet temperature and speed on the surface temperature at the bearing. From these empirical relationships, it is possible to make an estimate of the surface temperature one might expect under varying conditions. Figure 6.26 shows the combination of billet temperature and speed that will result in the surface temperature attaining 600, 610, 620 and 630°C.

While this prediction takes data gathered from 175 mm and 200 mm presses and extrapolates to a 100 mm press, and therefore one might question its predictive accuracy, it nonetheless demonstrates the logic that the combination of a low billet temperature and high speed can be the same as a high billet temperature and low speed. It is also interesting to note that these workers show a non-linear relationship between billet temperature and speed.

One could postulate that pick-up and surface roughness are worst at some critical temperature (for example 610°C), and then improve above this temperature

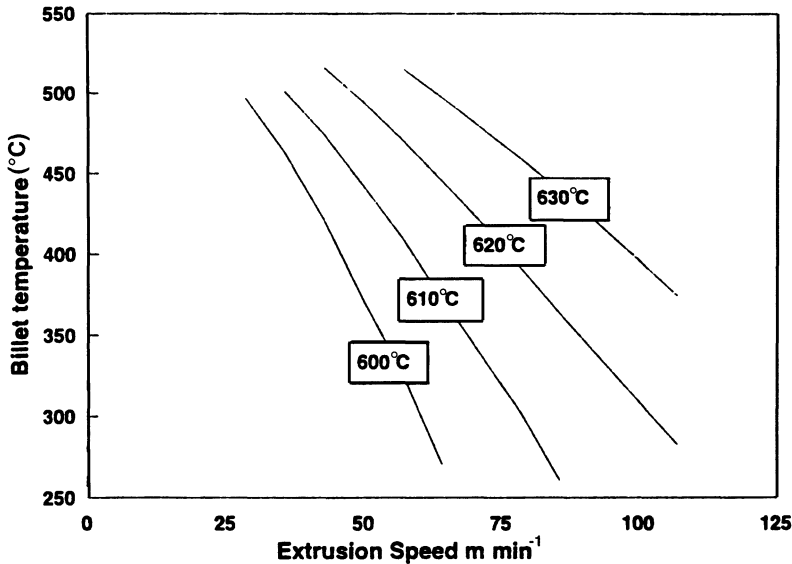


Fig. 6.26 Prediction of the die bearing surface temperature for different billet temperatures and speeds.

until the alloy solidus (which lies between 620 and 630°C) is reached when tearing and surface liquation occurs. In this light the experimental results appeared very reasonable. Work by Imai and Rabonowicz [57] and by Cocks [58] illustrates how friction and metal transfer can reach a maximum at some temperature below the melting point of an alloy and then decrease as a regime of near-liquid metal lubrication is approached.

Parsons [54] warns that the relationship between surface finish and press parameters illustrated relates to a specific die and billet and one would expect the relationship to change with both alloy and billet type. Therefore, when comparing billet or alloy types in terms of extrudability, it is unsatisfactory to simply conduct the test at an arbitrary speed and temperature.

Another interesting feature of their results was the fact that, as shown by the results at 350°C, die line severity does not necessarily increase with extrusion speed, which is a commonly held belief.

## 6.6 TEXTURE

Another of the governing factors for the surface appearance of 6XXX extrusions, i.e., the light-reflecting properties of as-extruded sections, is the crystal orientation (the texture). This has been considered in an elementary way by Aukrust *et al.* [59]. Upon anodizing, the etching response of the extrusions can depend on

microstructural factors such as the crystal orientation and the grain structure as well as the particle distribution. These factors depend on the condition of thermo-mechanical processing, i.e. of the total temperature history and deformation path. Local variations in these parameters caused by the complex shape of dies can therefore lead to differences in surface appearance.

In the building industry, extrusions in the AA6060 alloy are frequently used due to their excellent surface properties. Aukrust and co-workers [59], however, used the alloy AA6082 since it exhibits only a small degree of recrystallization. In other words, this alloy was used as a model material to study how the deformation texture and grain structure are created.

The extrusion experiment is simulated with a Eulerian finite element model FIDAP(4) where isotropic material properties are assumed. The velocity gradient along selected particle paths is extracted from the results of finite element simulations. The velocity gradient data is converted to a strain history and subsequently transferred to the polycrystalline Taylor model (S). The texture evolution can then be easily simulated even for very complex forming operations, without being excessively demanding on computing power. The predicted texture is compared with the experimental measurements.

In their work, the texture and the grain structure in the surface boundary layer of an extruded section was studied. The grain structure in the extrudate showed that there was a transition from where the grains were lamella shaped to where the lamella structure is broken up; taking place around 200  $\mu\text{m}$  below the surface. This was consistent with the results which showed that there was also a transition from a bulk region with a rolling type of texture to a surface boundary layer with shear type of texture taking place between 400  $\mu\text{m}$  and 165  $\mu\text{m}$ . The main component of the shear texture in the surface was close to (113) [332]. This corresponds to the idealized shear texture, the skew cube (001) [110], rotated about 25° about the transverse axis. However the authors demonstrated that the local texture in thin surface layers can change from one type of shear texture to another which is symmetric about the extrusion direction which would produce apparent differences in brightness after anodization.

The simulated texture for the centre of the section, where there is plane strain compression, corresponds to the well known behaviour of rolling type of texture for both the full constraint and the relaxed constraint Taylor model when (111)<110> slip systems are used for f.c.c. materials [60]. The Taylor model has been successfully applied in a number of cases for simulation of shear and torsion texture [61–63]. In the reported work, the simulated texture for the surface had qualitatively the same features as the experimental texture, with the same amount of rotation of the skew cube.

Thus, the simulated texture was found to reproduce the qualitative feature of the experimental data in the bulk of the profile and for the surface. The shear zone was found to be broader in the simulation than in the experiment.

## 6.7 EXTRUSION DEFECTS

When process parameters have been optimized and the press is running at high exit speeds then the onset of metallurgical defects affecting surface quality often becomes the limiting factor.

The recovery figure obtained from an extrusion press is also limited by the onset of metallurgical defects. Although factors such as planning of cut lengths, stretcher scrap and reduction of in-house damage significantly affect recovery and are clearly important, the avoidance of metallurgical defects such as transverse weld and back-end defect is equally important, since these defects can account for a significant amount of scrap on every billet extruded. In addition the demands on the performance of 6XXX alloys are becoming greater: for example, formability in ladder manufacture, product integrity in transportation and off-shore applications, and anodized colour matching for architectural sections. As a result 6XXX extruders will have to attend to both the mechanical properties and the microstructure of their products in order to tailor these metallurgically for a particular customer's requirements. This has not hitherto been the case and is certainly not the norm amongst the majority of extruders.

### 6.7.1 Metallurgical factors affecting press productivity

In the production of the vast majority of 6XXX extrusions there are three sets of restrictions that define the press conditions that can be used and the resulting productivity:

1. avoidance of surface defects;
2. specific pressure requirements;
3. attainment of mechanical properties.

Parson *et al.* [65] shows how these process/property factors can be introduced into a limit diagram as previously shown for various structural factors [66–70] as shown in Fig. 6.27 where the three sets of restrictions define a working window. Clearly for maximum productivity one should aim to control press conditions in order to operate as near as possible to the apex of this area. Experimentally determined limit diagrams have been produced showing surface defect lines. However, the working area is not fixed and will vary for a given alloy between different presses and sections; hence Fig. 6.27 is drawn schematically. The effects of press variables are best discussed separately for each set of restrictions.

#### *Avoidance of surface defect*

The onset of mill finish surface defects is related to the temperature rise generated at the surface of the product as it is deformed.

The level of temperature rise increases rapidly with exit speed due to the greater rate of work input and reduced heat loss to the tooling. This is demonstrated in

Fig. 6.28 which shows die bearing temperature measurements made on a commercial press as a function of exit speed. The surface temperature of the product is roughly proportional to the log of the extrusion speed. Clearly at a high enough

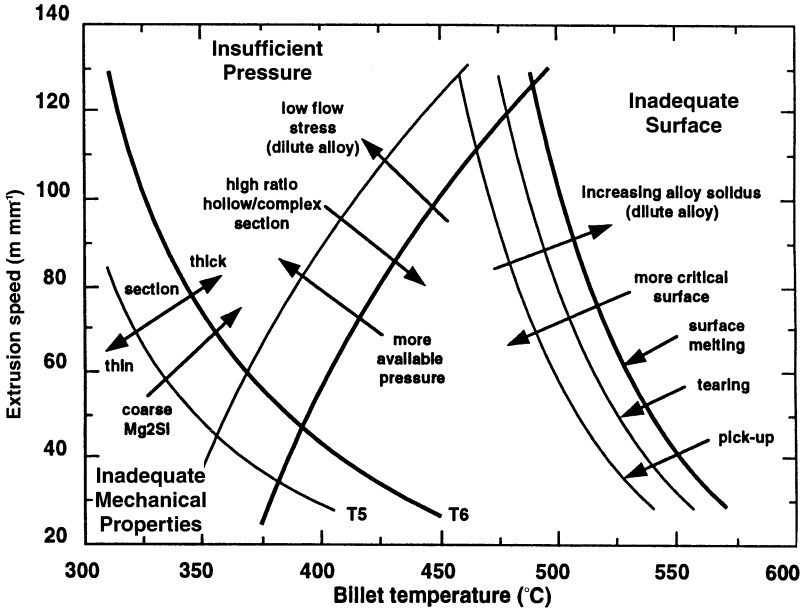


Fig. 6.27 Limit diagram (schematic) for 6063 alloy showing the effect of common press variables. (Courtesy of Alcan International.)

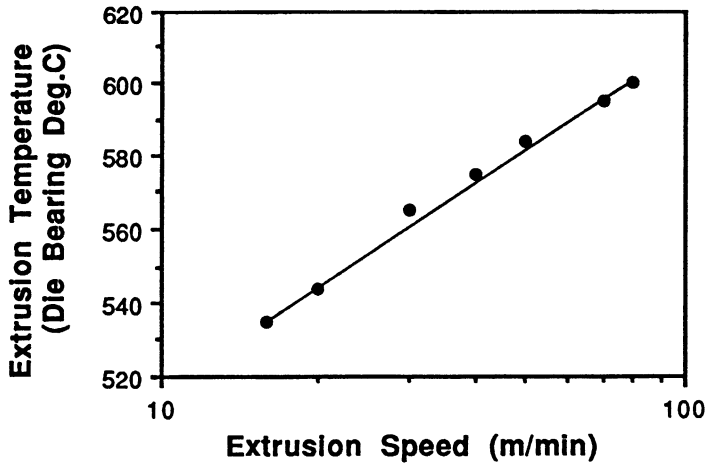
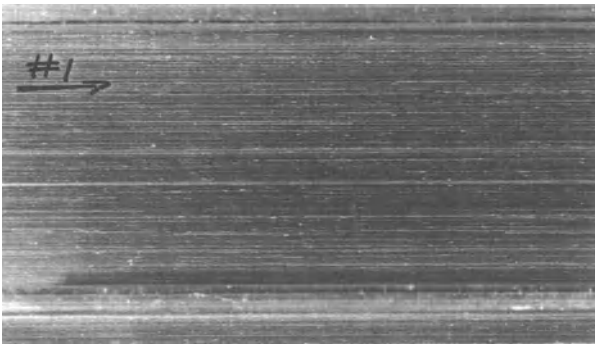


Fig. 6.28 Die bearing temperature as a function of exit speed. Extrusion ratio = 120:1, round bar, billet temperature 480°C. (Courtesy of Alcan International.)

exit speed the solidus temperature of the alloy is attained and local melting will occur. This condition gives rise to the classic ‘hot shortness’ or ‘U-speed cracking’ defect. This is more frequently encountered with the medium strength alloys (identical surface topology to Fig. 4.15) due to their lower solidus temperature [71] but can be encountered in more dilute alloys such as 6063 when extruded at very high speeds. The cracking occurs by local tensile failure at areas of melting due to the tensile stress state present at the edge of the die bearing.

However, in most cases the surface finish becomes unacceptable for decorative or architectural applications before this situation is reached, due to the onset of pick-up or, in more extreme cases, tearing. Fig. 6.29 shows an extreme case of pick-up on a 6063 extrusion which would be unacceptable for most applications. The formation of pick-up and tears has been studied in detail and discussed at length above.



**Fig. 6.29** Severe pick-up on a 6063 section. (Courtesy of Alcan International.)

The speed at which the surface becomes unacceptable can be increased by reducing the billet temperature and moving towards the apex of Fig. 6.27 by effectively offsetting the exit temperature. Dilution of the alloy composition, for example to less concentrated 6063 or even 6060 variants, also increases the speed at which pick-up forms by simultaneously raising the solidus temperature and decreasing the work done during extrusion.

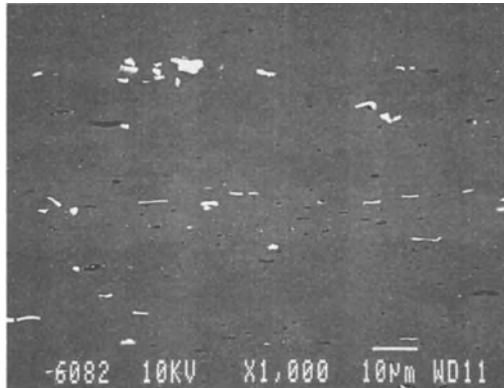
### *Specific pressure requirements*

The lines forming the left hand side of the apex in Fig. 6.27 are loci of billet temperature and ram speed combinations that require the same breakthrough pressure. Extrusion pressure is relatively insensitive to extrusion speed at low speeds but begins to increase as higher exit speeds are attained. Billet temperature has a stronger effect on pressure due to its powerful effect on flow stress. The series of lines drawn in Fig. 6.27 show the consequence of having lower specific pressure available, for example as a result of changing container sizes or switching a particular section to a different press. The working area is severely reduced along with the maximum speed

attainable because of the need to extrude at higher billet temperatures. It is possible to operate beyond the maximum pressure limit but breakthrough and ram acceleration times become excessive and, although the theoretical maximum extrusion speed is higher, the overall contact time can be increased [65].

#### *Attainment of mechanical properties*

Apart from very large specialized extrusions, which are generally given a separate solution treatment, all 6XXX extrusions rely on the process heat associated with the billet preheat and temperature rise during deformation to dissolve sufficient of the available magnesium silicide and allow mechanical properties to be attained by artificial ageing. In order for this to take place the metal must be taken to a temperature sufficiently above the solvus temperature to allow dissolution to occur in the extremely short time spent in the deformation zone. If this condition is not met, some magnesium silicide will remain undissolved, as shown in Fig. 6.30, which can result in poor ageing response. In practice, exit temperature is used as an indicator of whether sufficient heat has been generated. A minimum exit temperature of 495°C, as measured by a probe thermocouple at the end of the die tunnel, is normally regarded as being acceptable for 6063.



**Fig. 6.30** Undissolved  $Mg_2Si$  in a 6082 extrusion (BEI) longitudinal. (Courtesy of Alcan International.)

The third limit on the bottom left of Fig. 6.27 represents combinations of billet temperature and speed necessary to achieve an adequate exit temperature for a given alloy. Clearly the strength level required by the customer dictates the position of this line and a T5 specification allows lower billet temperatures than a T6 requirement. As they are drawn in Fig. 6.27, these lines do not seriously interfere with press productivity since, providing the section is extruded sufficiently rapidly, magnesium silicide dissolution will take place. Clearly the magnesium



silicide distribution presented to the press in the homogenized and preheated billet strongly influences the position of this part of the limit diagram.

A common cause of coarse  $Mg_2Si$  is poor temperature profiles or metal holdups during reheating, particularly in gas-fired furnaces. Holding metal in the temperature range 330–360°C is particularly deleterious and should be avoided. The trend of using a hot log shear equipped with a continuous gas-fired furnace appears to be particularly prone to this type of problem. Strictly, any metal involved in a press delay within this temperature range should either be rehomogenized or resolutionized at 530°C prior to extrusion.

### 6.7.2 Recovery related defects

Most of the defects associated with recovery loss occur either at the start or end of an extruded length. There are four main types of defect in this category:

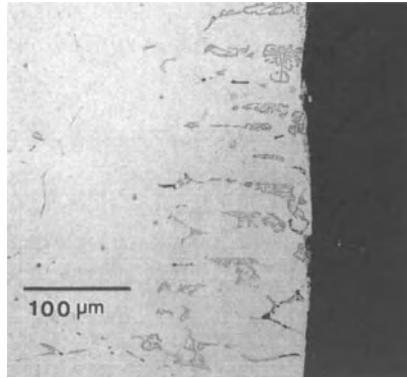
1. extrusion/back-end defect;
2. transverse weld;
3. defective longitudinal welds;
4. blistering.

These will be considered in the following sections.

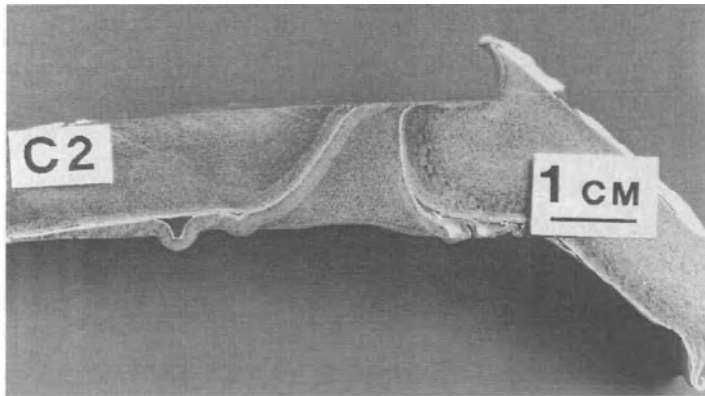
#### *Extrusion/back-end defect*

This is the most common defect encountered during 6XXX extrusion. Avoidance of it in the shipped product typically requires 5–20% of metal put onto the press being scrapped as discard. The origin of the defect lies in the nature of flow during hot, unlubricated aluminium extrusion. Billet–container friction results in the billet surface layers remaining stationary at the container wall whilst the billet core is sheared past. These layers then build up in front of the advancing pad. The material accumulated in this way contains the oxidized billet skin formed during casting, homogenization and reheat. It also contains any surface contaminants that were present on the billet surface, together with any inverse segregate. The layer is present at the surface of practically all extrusion ingots to some degree and a typical example is shown in Fig. 6.31. This region, nominally 100–200  $\mu m$  in depth, contains coarse iron-rich intermetallics and can be solute-rich in magnesium and silicon. After approximately 70% of the billet has been extruded the accumulated material begins to flow inwards across the face of the pad as a result of depletion of the billet core.

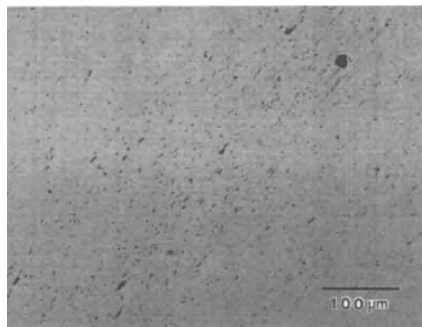
The region of dead metal that exists on the centre of the pad face directs this flow forwards giving rise to a cone shaped defect as shown in Fig. 6.32. In this case the discard length taken was insufficient to prevent the defect entering the section. Figure 6.33 shows the defect in more detail; the accumulated debris from the billet surface is now strung out as dense bands of oxide and coarse intermetallics. There is also some voiding which can result from trapped air or



**Fig. 6.31** Inverse segregate layer at the surface of a 171 mm 6063 ingot. (Courtesy of Alcan International.)

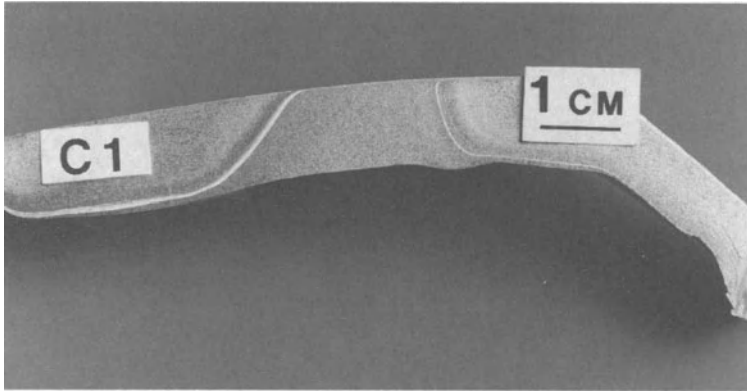


**Fig. 6.32** Section through 3% discard from a 171 mm diameter, 760 mm length 6060 billet exhibiting severe back-end formation. (Courtesy of Alcan International.)



**Fig. 6.33** Detail of back-end defect in Fig. 6.32 showing oxide films, porosity and coarse intermetallics. (Courtesy of Alcan International.)

volatilized lubricant. The defect is often found to contain carbon originating from the pad parting agent. Figure 6.34 shows the appearance of the defect in the cross-section of a solid 6082 extrusion.



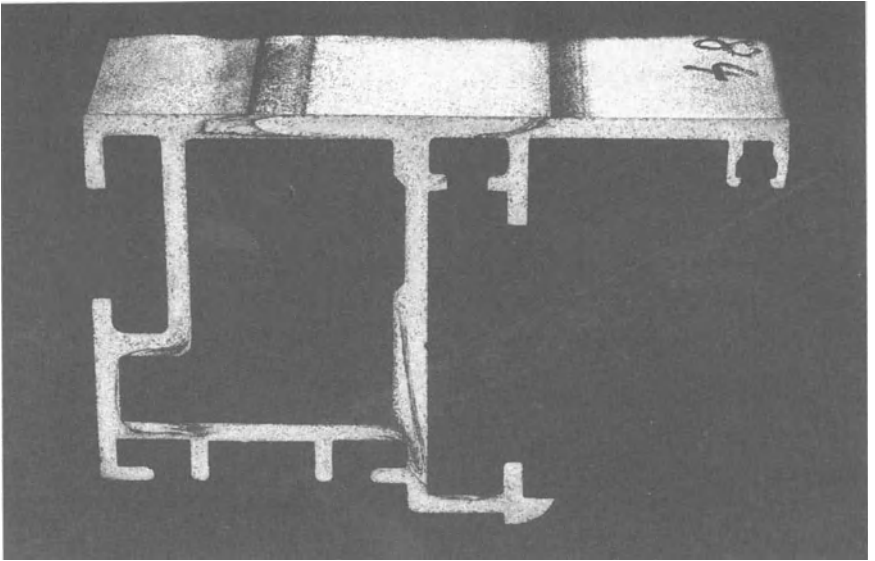
**Fig. 6.34** Back-end defect in a solid 6082 section. (Courtesy of Alcan International.)

In small architectural sections extruded at high ratio the defective material near the back end is generally broken up to such an extent that product homogeneity and surface quality are not seriously impaired. In these cases a discard of 5% or less can often be taken without any deleterious effect.

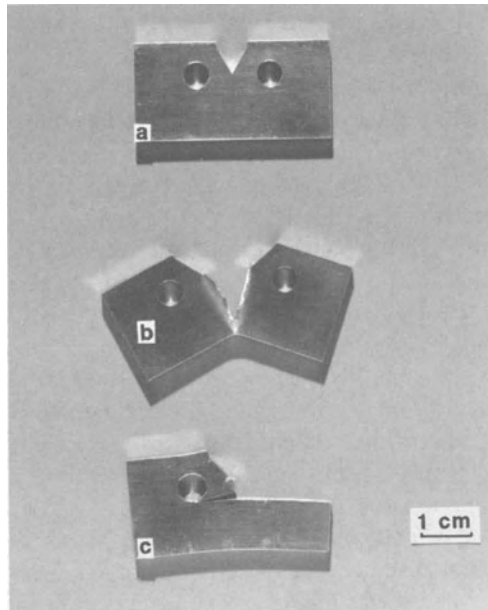
The requirements for material to be anodized are slightly more demanding. Fig. 6.35 demonstrates the form which back-end defect can take in thin-walled architectural section. Although the integrity and surface finish are not seriously impaired, as discussed above, the emergence of the defect at the surface, in this case at the weldline (see later section), alters the etching response giving a streaked appearance after anodizing.

The implications of making a product containing a back end defect are much more serious in the case of medium-strength alloys such as 6351/6061 produced for structural applications. Fig. 6.36 shows the effect of a back end defect on the failure mode during Kahn tear testing of a 6082 extrusion. Sample (a) is an untested specimen and sample (b) is typical of the normal failure mode in this type of test. Sample (c) contained a back end defect and in this case the test piece failed in a brittle manner with crack growth occurring parallel to the applied stress direction. Clearly the presence of such a defect in a structure would be unacceptable. For this reason, discards of 10–20% are generally taken on critical sections with etch tests being carried out to ensure the defect has not entered the section.

Although the extrusion defect occurs as a result of the metal flow during extrusion, it can be promoted or made more severe by certain factors. Overlubrication of the pad can assist the transverse flow as well as causing lubricant entrapment in the defect. Badly fitting pads or worn container liners can increase metal build up on the container wall which can add to the defect. There is also evidence [70]



**Fig. 6.35** Streaking after anodizing associated with transverse weld defect contaminated by back-end defect. (Courtesy of Alcan International.)



**Fig. 6.36** Kahn tear specimens; (a) untested specimen; (b) normal failure; (c) brittle failure in presence of back-end defect. (Courtesy of Alcan International.)

to suggest that the initial inward flow of the billet skin occurs during upsetting and the extent of folding is proportional to the amount of upset that takes place which is a function of billet container size mismatch and billet length.

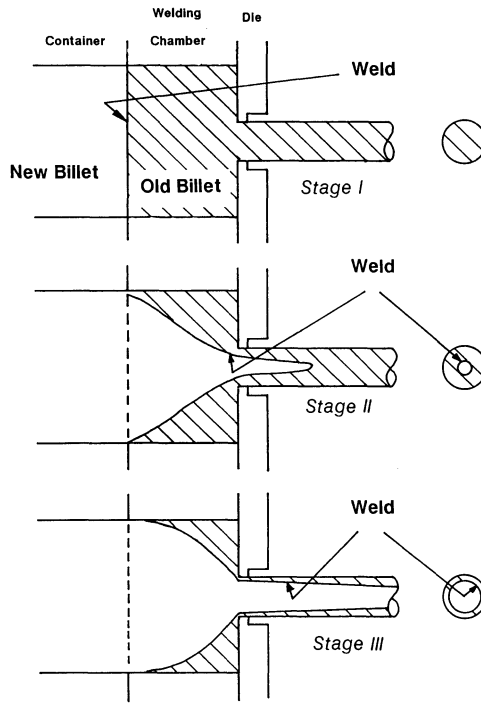
Having described the detrimental features of the extrusion defect, it is important to recognize that collection of the surface layers in the discard is actually desirable when compared to the alternative, which is detachment of this material from the container wall and its incorporation in the product surface as occurs, for example in copper extrusion. It is typically manifested as delamination or blistering. To prevent this defect, and encourage skin accumulation in the discard, a temperature differential of 25–50°C is normally maintained between the billet and the container.

Both types of defect are sensitive to billet quality. Ingots containing deep cold shuts or inverse segregate will either give rise to an increased volume of coarse intermetallics available to form the back-end defect or, in very severe cases, the segregation or shuts will extend beyond the layers of material held at the container wall and will pass into the extrusion at any point in the length. As a rough guide, surface defects deeper than 200 μm raise the possibility of this occurring.

### *Transverse weld*

It is now common practice to extrude billet on billet using a welding chamber or feeder ring to hold the back of the previous billet in the die and provide a surface for the next billet to weld on to. For solid sections, this is done primarily to reduce delay times associated with start up and pulling the extruded length away from the die if the section is run as a pullaway. On hollow and semi-hollow dies, where the back of the previous billet cannot be removed from the die, there is no alternative but to extrude billet on billet. If the mating surfaces were perfectly clean there would be no problem with this arrangement but, in practice, the billet ends are always oxidized, and the sheared face is often contaminated by stray lubricant and oxidized metal from the shear blade. As a result the billet-to-billet or transverse weld is usually defective and represents a discontinuity in the extruded product. The development of a transverse weld in a simple section is shown schematically in Fig. 6.37. In stage I, the discard from the previous billet has been sheared off across the back of the welding chamber and the container and ram have been advanced presenting the new billet to the sheared face. In stage II extrusion has recommenced. Metal flow takes place irrespective of the weld interface such that material from the billet core flows faster than that nearer the container/welding chamber wall. In this way metal from the second billet penetrates the disc of old metal left in the welding chamber and the transverse weld is extended as a conical interface. At this stage the weld line appears in cross-section as a circle of small diameter on the section axis.

As the ram advances the old metal is released, effectively cladding the section until stage III is reached where most of the previous billet has been cleared and the transverse weld line appears as a subsurface line in the cross-section. Soon after this point the transverse weld merges into the section surface. The final area



**Fig. 6.37** The development of transverse weld defect in a simple section with a welding chamber. (Courtesy of Alcan International.)

of the weld interface is considerably greater than the original billet area and it is this creation of new interface that allows the weld to be made. The extent to which the weld line is extended was shown by Akeret *et al.* [73] to increase with the ratio of the welding chamber area to the section area. At low extrusion ratios, the apex of the weld is actually compressed on a macroscopic scale giving a thick wavy weld line that is associated with low strength.

In 6063 architectural sections, where extrusion ratios are normally high and service loading is low, the transverse weld does not seriously impair the integrity of solid sections. The weld can sometimes give rise to streaks after anodizing and this may necessitate a scrap allowance. However, generally this is not the case and normally only stop mark scrap is taken. The situation is somewhat different for 6082 and 6061 structural sections. Here product integrity is clearly more important and the discontinuity associated with a line of contaminants on the transverse weld is not acceptable. In this type of product the length of extrusion containing the weld line should be scrapped. Various rules based on the extrusion length corresponding to the volume of the welding chamber are often used but, as shown in Fig. 6.37, the flow of metal in the welding chamber is not homogeneous and weld lines can persist longer than this.

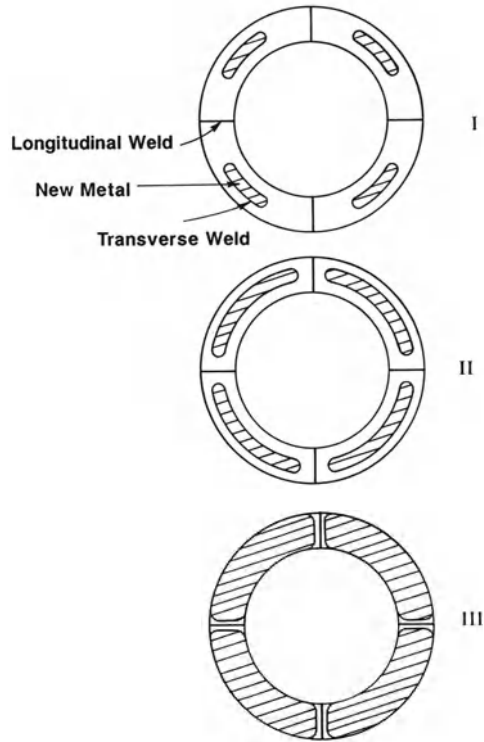
Another form of transverse weld is produced by the practice of two-piece billet extrusions. This is generally carried out to utilize the last cut length from an ingot when a hot shear or log saw is used. Each extruded length then contains two transverse welds. This is common practice for 6063 where the defect can be tolerated, but should not be carried out on structural sections.

### *Longitudinal welds*

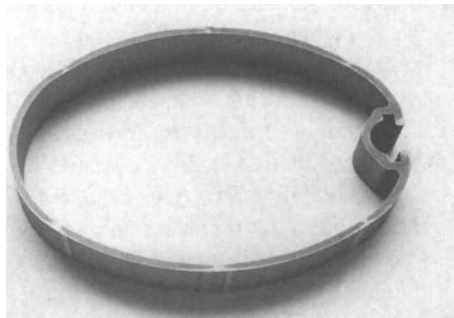
Defects on longitudinal welds take the form of either low weld strengths or streaking on anodizing. The latter have their origins in the differences in microstructure that can be produced along the weld line and these will be discussed in more detail below. Low weld strength can arise along the entire extrusion length in situations where the die design and extrusion conditions are inadequate for forming a pressure weld. This is not strictly an extrusion defect and will not be discussed further.

The main cause of poor longitudinal weld strength is contamination by the transverse weld which necessitates the taking of front-end scrap in virtually all hollow extrusions. In the previous section, the development of a transverse weld in a simple solid section was described. The situation is somewhat more complex in a hollow die, as a separate transverse weld is carried through each port of the die. This is shown schematically in Fig. 6.38 for a simple tube. In stage I the new metal emerges between the weld lines where the flow is least restricted. By stage II the new metal occupies most of the section apart from the weld lines. This situation is demonstrated in Fig. 6.39 where the different etching response of old and new metal has produced an anodizing streak. Further ram motion clears virtually all of the previous billet apart from a narrow region on the weld line (stage III).

Whereas in a solid section the transverse weld merges into the section surface, in a hollow it also merges into the longitudinal weld line. Fig. 6.40(a) shows this situation in a 6082 extrusion where close examination reveals three parallel lines present at the weld. The presence of the transverse weld and its associated contamination in close proximity to the seam weld constitutes a line of weakness. The weld in Fig. 6.40(a) failed routine drift testing for this reason. The fracture surface (Fig. 6.40(b)) was planar in nature and consisted of rafts of oxide films surrounded by areas of local ductility (Fig. 6.40(c)). Clearly such defects cannot be tolerated in most applications and, to prevent them going into service, a transverse weld scrap allowance is normally made from the stop mark. For critical samples, e.g. scaffolding, ladders, inspection towers and off-shore structures, it is normal practice to carry out quality control tests after the scrap allowance has been made. Weld quality can be checked on simple symmetrical hollows by drift testing and noting whether fracture occurs on the weld line or away from it. Figure 6.41 demonstrates examples of good and bad welds subjected to the test. Drift testing can be difficult to apply to some non-circular hollows and in these cases flattening or etching tests may be used.

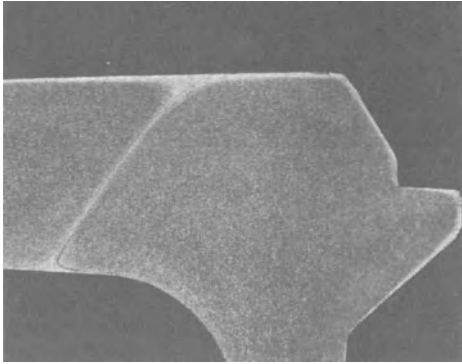


**Fig. 6.38** Development of transverse weld in the cross-section of a simple hollow section. (Courtesy of Alcan International.)

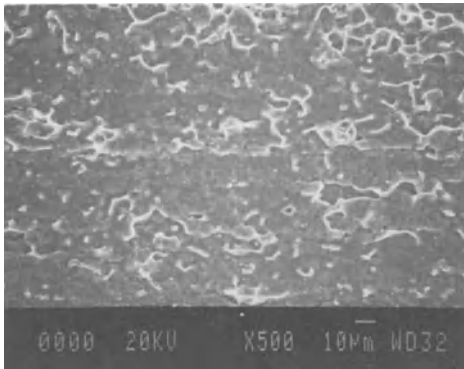


**Fig. 6.39** Anodized ship mast extrusion section containing transverse weld and exhibiting weld streaking. (Courtesy of Alcan International.)

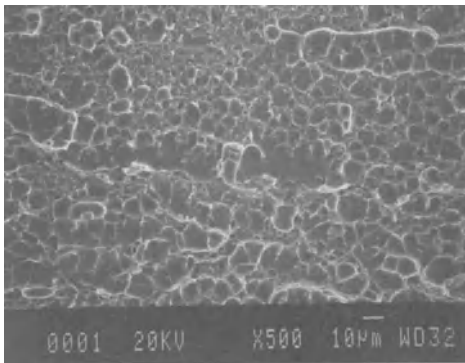




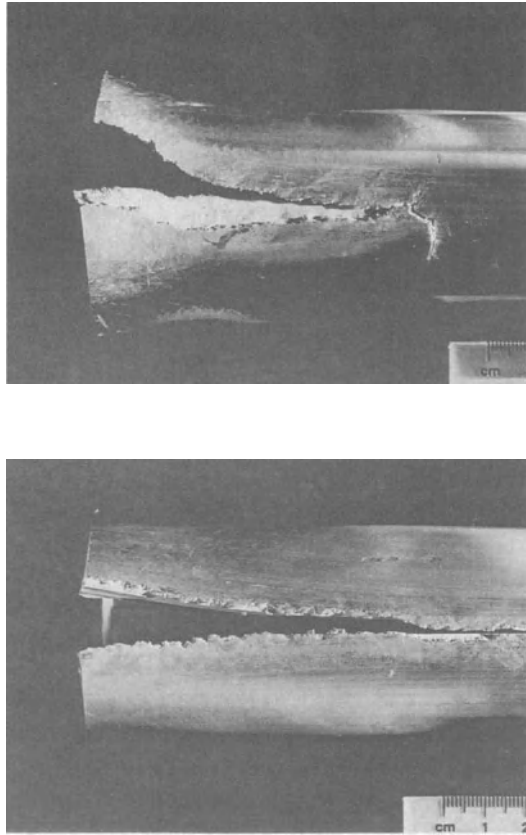
**Fig. 6.40(a)** Appearance of transverse weld in a 6082 hollow that failed drift testing. (Courtesy of Alcan International.)



**Fig. 6.40(b)** Appearance of failure at transverse weld after drift testing showing bands of oxide films. (Courtesy of Alcan International.)



**Fig. 6.40(c)** Appearance of failure at transverse weld after drift testing, showing ductile region. (Courtesy of Alcan International.)

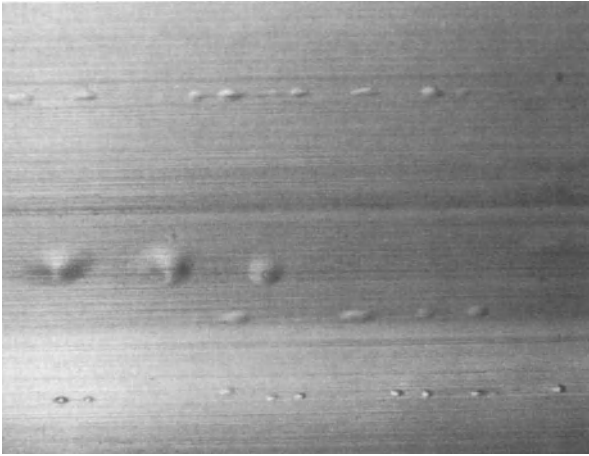


**Fig. 6.41** Drift test samples; (a) good weld; (b) defective weld. (Courtesy of Alcan International.)

### *Blistering*

Blistering (Fig. 6.42), can occur at virtually any position along the extrusion length as it can be associated with all of the defects described in the previous section, due to entrapped air or volatile lubricants. However, front end blistering is probably the most common form of the type of defect and can necessitate a scrap allowance being taken. Its cause is mainly due to air entrapment during loading and upsetting the billet. This can be exaggerated by factors such as a rough sheared surface on the back of the die or the shear pulling metal out of the welding chamber.

A certain amount of air is automatically trapped in the container during upsetting due to the billet–container size differential required for easy loading of the billet. This is compressed during upsetting and, if carried through the die, will expand on exiting the die, deforming the soft hot aluminium to form blisters. The



**Fig. 6.42** Front end blistering in a 6082 extrusion. (Courtesy of Alcan International.)

'burp cycle' is often used to prevent this occurring by removing the ram pressure momentarily after upset to allow the air to escape.

Measures to reduce blistering include reducing the billet-container mismatch as far as possible and maintaining a temperature taper along the billet length. A hot billet front end, as well as offsetting the temperature rise along the length, promotes upsetting from the front of the billet, forcing any trapped air to the back end where it can be accommodated in the back end defect. High billet hydrogen gas contents are often quoted as a source of blistering. However, there is little information to support this and the formation of blisters in this way would require extremely high rates of hydrogen diffusion.

### 6.7.3 Metallurgical defects visible after anodizing

Most of the defects dealt with here are met within 6063 or 6463 type alloys. Metallurgical defects becoming visible on the extrudate surface after anodizing may be classified according to their appearance under two main headings:

1. streaking-type defects;
2. non-uniform appearance.

Corrosion defects and those originating in the anodizing process will not be discussed here but these have been extensively reviewed [73].

#### *Streaking type defects*

Streak defects on the surfaces of anodized extrusions consist of bands or lines appearing darker or lighter, brighter or duller, in colour and tone than the remainder of the surface. The streaks may or may not be associated with changes in

section. These defects may have a variety of origins, from the material to post-extrusion treatments. The anodizing process itself is rarely the origin of such defects although almost all of them are revealed only by etching and anodizing. The most important origins of streak defects can be classified under the following headings:

1. ingot structure;
2. extrusion process, including die factors and section shape.

In all of these cases the basic cause of the streak lies in a difference in microstructure between the 'streaked' portion of the extrudate surface and the remainder. Specifically, the difference usually lies in the distribution of second phases, principally the iron-bearing insoluble phases, which leads to a difference in response to etching and anodizing owing to the difference in reaction rates between the iron phase and the matrix [72]. In turn, this brings about a change in surface topography of the anodic film interface and hence the change in apparent colour or tone of the anodized surface.

#### *Ingot structure streaking*

Streaks originating in ingot structure occur as a result of either surface segregation or a shell zone present in the ingot. Both of these features of the ingot microstructure are produced during the early stages of solidification during DC casting and therefore are situated in its peripheral zones. The depth of the surface segregation zone amounts to a maximum of 100  $\mu\text{m}$  in a good quality 180 mm diameter extrusion ingot, but may increase to around 1 mm in poor quality ingot and locally more where gross ingot defects such as cold shuts or 'blebs' are present. Therefore, segregation streak defects are normally absent on extrusion from good quality ingot since the normal extrusion flow process excludes the surface segregate zone from the extrudate surface unless the width of the section, or of the die layout in a multi-hole die, exceeds the critical circumscribing circle diameter (CCD) of the extrusion press container.

On the other hand, the shell zone extends much deeper into the ingot, up to 15 mm, and consequently may flow preferentially into regions of the section surface depending on the extrudate geometry. The increased rate of flow of metal into wider regions of the section surfaces intensifies the feeding of the shell zone material to these regions and so promotes the differences in etching and anodizing response which are the direct causes of the streaking visible on the flat surface.

Shell zone streaking cannot be avoided by measures taken to alleviate that caused by surface segregation owing to its much greater depth, but can be reduced by controlling the DC casting process to minimize shell zone depth.

#### *Extrusion process streaking*

This has a somewhat wider variety of sources than that originating in ingot structure, but the basic cause remains a difference in microstructure between the 'streaked' portion of the extrudate surface and the remainder. Most of the identified

sources of extrusion process streaking can be placed in the following three categories:

- die design streaks (sometimes called ‘pressure streaks’);
- weld streaks, mainly in hollow sections;
- extrusion defect streaks.

The appearance of die design streaks on the anodized section surface is similar to and sometimes almost identical with that of shell zone streaking, but sometimes, particularly in complex or hollow sections, may exhibit a difference in grain size as well as precipitate microstructure in colour or tone. Although the cause of such a change is not known with certainty, it is believed to lie in localized differences in strain or strain rate, owing to the complex flows occurring in the extrusion of some shapes which bring about a temperature profile change in the region of the streak. Streaks from this source cannot be removed by mechanical treatment of the section.

Weld streaking occurs mainly in hollow sections but can also be encountered in non-hollows extruded through feederplate dies. The metal flow processes involved in the formation of welds have been described above, and it will be appreciated that these cause microstructural changes similar to, but in many cases more marked than, those associated with die design.

Extrusion defect streaks are due to the ram approaching the extrudate too closely at the end of the stroke when the surface of the original billet forms a core to the extrusion stretching to the surface of the extrudate. This is normally eliminated by a discard of appropriate dimensions.

#### *Non-uniform appearance*

Many kinds of defect exhibiting a non-uniform surface aspect appear in anodized sections from time to time which originate from occasional irregularities of the etching, anodizing and/or colouring processes. Of the more frequently occurring defects, two types having a metallurgical background are of considerable importance: ‘hot spots’ (‘soft spots’) and ‘spangle’.

#### *Hot spots*

The characteristic appearance of this defect is as dark (grey or black) rough patches, at regular or random intervals along the extruded length. Usually such patches are considerably softer than the typical T5/T6 hardness of the bulk material. They are not visible on the as-extruded surface but appear readily after caustic etching as a heavy black smut, completely removed by the nitric acid desmut but reappearing on anodizing sometimes in paler shades if softening is less marked.

The cause of such defects is preferential etching and anodizing of localized coarse precipitation which results from different cooling rates of adjacent parts of the section. Usually this is met within an extrusion from presses where a section

has been in localized contact with a carbon support block on the run-out table and is momentarily cooled very rapidly in this localized region before being reheated from the adjacent mass of uncooled metal into a critical  $Mg_2Si$  precipitation temperature range (around 400°C).

This defect cannot be eliminated after it has formed. The only possible solution is to avoid contact between the hot extrusions and the run-out table for more than the shortest time necessary to carry out their removal to the lateral transfer table, where cooling to below the critical temperature range should be effected as fast as possible with fan assisted air cooling. It is also helpful to use material other than carbon blocks, e.g. slats of material having a lower thermal conductivity than carbon, in construction of the run-out conveyor.

### *Spangle*

This defect appears as a pronounced 'grainy' surface varying between a 'galvanized' effect, if the surface grain size is exceptionally fine, to a more obvious preferential grain attack on material of a relatively coarse grain size. The cause of this defect is a preferential grain attack, visually emphasized by a 'stepwise' appearance of adjacent grains owing to the dependence of the rate of attack on the orientation of the crystallographic planes of individual grains.

The preferential grain attack is enhanced by the presence of zinc, either as an impurity in the alloy, particularly if from a remelt source, or dissolved in the caustic etch solution. The effect becomes noticeable if the zinc content of the alloy exceeds 0.03% and increases in intensity with increasing zinc up to at least 0.1%, or roughly equivalent proportions in the etch solution. It can also be intensified by higher etch temperatures or the use of a new caustic etch solution.

## REFERENCES

1. Lyman, T. (ed.) (1948) *Metals Handbook*, ASM International, Materials Park, Ohio, 1246.
2. Annenkoff, A. and Marchive, D. (1984) Proc. 3rd International Extrusion Technology Seminar, Atlanta, **1**, 69.
3. Marchive, D. and Deschamps, R.D. (1979) *Rev. Alum.*, **76**, 489.
4. Sheppard, T. (1988) *Mat. Sci. Tech.*, **4**, 635–643.
5. Reiso, O. (1992) Proc. 5th International Extrusion Technology Seminar, Chicago, **1**, 31. Aluminium Association, Washington DC.
6. Musulin, I. and Dietz, D. (1988) Proc. 3rd International Extrusion Technology Seminar, Atlanta, **1**, 25. Aluminium Association, Washington DC.
7. Langerweger, J. (1980) Proc. Symp. on the Aluminium Industry of Egypt, (ed. M. Farag), University of Cairo, 167.
8. Parson, N.C. and Yiu, H.L. (1989) *Light Metals, 1989* (ed. P.G. Campbell), The Minerals, Metals and Materials Society, 719.
9. Heathcock, C.J., Cooke, J.D. and Nugent, S.A. (1988) Proc. 4th International Extrusion Technology Seminar, Chicago, **2**, 85. Aluminium Association, Washington DC.

10. Berry, W.G. (1984) *Rationalization of Structural Aluminium Magnesium-Silicide Extrusion Alloys*, Proc. 3rd International Extrusion Technology Seminar, Atlanta, **1**, 8. Aluminium Association, Washington DC.
11. Langerweger, J. (1984) Proc. 3rd International Aluminium Extrusion Technology Seminar, Atlanta, **1**, 41–42. Aluminium Association, Washington DC.
12. Lang, G. and Castle, A.F. (1978) *Met. Tech.*, **5**, 434.
13. Lohne, O. and Dors, A.L. (1983) *Scand. J. Metall.*, **15**, 34–36.
14. Laue, K. and Stenger, H. (1976) *Extrusion Processes, Machinery, Tooling*, **13**, 136–138.
15. Satee, R. (1972) *Products Finishing*, **5**, 52–53.
16. Sperry, P.R. (1984) Proc. 3rd International Aluminium Extrusion Technology Seminar, Atlanta, **1**, 26–27. Aluminium Association, Washington DC.
17. Maitland, A. and Reid, A. (1977) Proc. 2nd International Extrusion Technology Seminar, Atlanta, **1**, 297. Aluminium Association, Washington DC.
18. Harris, I.R. and Varley, P.C. (1953/54) *J. Inst. Met.*, **82**, 379.
19. Dowling, J.M. and Martin, J.W. (1975) Proc. 3rd. International Conf. on Strength of Metals and Alloys, Cambridge, 170. Cambridge University Press, Cambridge.
20. Clode, M.P. and Sheppard, T. (1990) *Mat. Sci. Tech.*, **6**, 755–763.
21. Bryant, A.J. (1971) *Z. Metallkd.*, **62**, 701.
22. Bauser, M. and Fees, G. (1971) *Z. Metallkd.*, **62**, 705.
23. Lynch, C.V. (1971) *Z. Metallkd.*, **62**, 710.
24. Clode, M.P. and Sheppard, T. (1986) *Aluminium Technology '86*, (ed. T. Sheppard), Institute of Metals, London, 230.
25. Tunnicliffe, P.A. (1979) Ph.D. Thesis, University of London.
26. Vierod, R.P. (1983) Ph.D. Thesis, University of London.
27. Reiso, O. (1984) 3rd International Extrusion Technology Seminar, Atlanta, **1**, 31. Aluminium Association, Washington DC.
28. Langerweger, J. (1982) *Aluminium*, **58**(2) 107.
29. Williams, T.R.G. (1954) M.Sc. Thesis, University College of Swansea.
30. Faunce, J.P. and Watts, J.M. (1984) Proc. 3rd International Extrusion Technology Seminar, Atlanta, **1**, 165. Aluminium Association, Washington DC.
31. Gulaki, S.T. (1984) *Met. Prog.*, **15**, 21.
32. Cother, N.E. and Hodgson, P. (1982) *Trans. J. Br. Ceram. Soc.*, **81**, 141.
33. Altwicker, M.J. (1963) British Patent No. 943530.
34. Scharf, G. (1979) *Aluminium*, **55**(3) 197.
35. Kobayashi, Y. and Okoniwa, S. (1977) Proc. 2nd International Extrusion Technology Seminar, Atlanta, **1**, 129. Aluminium Association, Washington DC.
36. Bichsel, M., Reid, A. and Langerweger, J. (1981) *Aluminium*, **57**, 878.
37. Sheppard, T., Tunnicliffe, P.A. and Paterson, S.J. (1982) *J. Mech. Work. Tech.*, **6**, 313.
38. Sheppard, T. and Zaidi, M.A. (1986) *Mat. Sci. Tech.*, **2**, 69.
39. Sheppard, T. (1977) Proc. 2nd International Extrusion Technology Seminar, Atlanta, **1**, 331. Aluminium Association, Washington DC.
40. Sheppard, T. (1987) Proc. 8th Light Metals Congress, Leoben–Vienna, Aluminium Verlag, Dusseldorf.
41. Sheppard, T. and Zaidi, M.A. (1987) *Mat. Sci. Tech.*, **3**, 146–148.
42. Hirst, J. and Ursell, D.H. (1958) *Metal Treatment*, **25**, 409.
43. Clode, M.P. and Sheppard, T. (1993) *Mat. Sci. Tech.*, **9**, 313–318.
44. Clode, M.P. (1987) Ph.D. Thesis, University of London.
45. Tutchter, M.G. and Sheppard, T. (1980) *Met. Tech.*, **7**, 488–493.
46. Vierod, R.P. (1983) Ph.D. Thesis, University of London.

47. Cooper, P.S. (1985) Ph.D. Thesis, University of London.
48. Sheppard, T. and Paterson, S.J. (1982) *J. Mech. Work. Tech.*, **7**, 39–56.
49. Sheppard, T. (1977) Proc. 2nd International Extrusion Technology Seminar, Atlanta, 1. Aluminium Association, Washington DC.
50. Reiso, O. (1988) Proc. 4th. International Aluminium Extrusion Technology Seminar, **1**, 287. Aluminium Association, Washington DC.
51. Lefstad, M. and Reiso, O. (1996) Proc. 6th International Extrusion Technology Seminar, Chicago, **1**, 11. Aluminium Association, Washington DC.
52. Phillips, H.W.L. (1959) *Annotated Equilibrium Diagrams of Some Aluminium Alloy Systems*, Institute of Metals, London.
53. Laue, K. and Stenger, H. (1981) in *Extrusion*, (ed. R.T. Shield), ASM, Metals Park, Ohio, 36.
54. Parson, N.C., Jarret, C.W., Pelow, C.V. and Fraser, W.C. (1996) Proc. 6th International Extrusion Technology Seminar, Chicago, **2**, 57. Aluminium Association, Washington DC.
55. Kempinen, A.V. (1968) *Metal Progress*, **20**, 147.
56. Jowett, C.W. and Johannes, I.V. (1992) Proc. 5th. International Aluminium Extrusion Technology Seminar, Chicago, **2**, 523. Aluminium Association, Washington DC.
57. Imai, M. and Rabinowicz, E. (1963) *ASLE Trans.*, **6**, 286.
58. Cocks, M. (1962) *J. App. Phys.*, **33**(7), 2152.
59. Aukrust, T., Lohne, O., Vatne, H.E., *et al.* (1996) Proc. 6th International Extrusion Technology Seminar, Chicago, **2**, 171.
60. Van Houtte, P. (1981) *ICOTOM 6*, (ed. S. Nagashima), (J.I.S.I), Tokyo, 428.
61. Sekine, K., Van Houtte, P., Sevilani, J.Gil. and Aernoudt, E. (1981) Proc. 6th International Conference on Textures of Materials, (J.I.S.I), 396.
62. Canova, G.R., Kocks, U.F. and Jonas, J.J. (1984) *Acta Metall.*, **32**, 211.
63. Leffers, T. and Hansen, N. (1992) Proc. 13th Riso International Symposium on Materials Science, (ed. S.I. Andersen, *et al.*), Riso National Laboratory, 57.
64. Bacroix, B. and Jonas, J.J. (1988) *Textures and Microstructures*, **8–9**, 267.
65. Parson, N.C., Hankin, J.D. and Bryant, A.J. (1992) Proc. 5th International Extrusion Technology Seminar, Chicago, **2**, 13.
66. Sheppard, T. and Clode, M.P. (1988) Proc. 4th International Extrusion Technology Seminar, Chicago, **2**, 329.
67. Parson, N.C. and Yiu, H.L. (1989) *Light Metals*, **47**, 713.
68. Ricks, R.A., Parson, N.C., Yiu, H.L. and Court, S.A. (1996) Proc. 6th International Extrusion Technology Seminar, Chicago, 214.
69. Oki, Y., Kumai, S. and Nunomura, S. (1990) *J. Japan. Inst. Light Met.*, **40**(7), 495–500.
70. Akeret, J. (1972) *Inst. Met.*, **100**, 202.
71. Short, E.P. and Sheasby, P.G. (1974) *Trans. Inst. Metal Finishing*, **52**, 66–70.
72. Cote, J., Howlett, E.E., Wheeler, M.J. and Lamb, H.J. (1969) *Plating*, **356**, 11.
73. Akeret, R., Bichsel, H., Schwall, E., Simon, E. and Textor, M. (1990) *Trans. Inst. Metal Finishing*, **68**(1), 20.



## 7.1 INTRODUCTION

In the preceding discussion we have investigated the physics and mechanics of the extrusion process and we will consider what is required in die design to ensure a product of the correct dimensions. Meeting these criteria should produce the correct product at the correct cost.

The computer has had considerable impact on the extrusion process. Many computer applications in the extrusion operation will be obvious, for example, comprehensive data acquisition of extrusion parameters, production monitoring and reporting, downtime logging, and extrusion optimization.

Of much greater importance, however, is that the degree of extrusion automation can relieve the press operator of much decision making; if all operators could be persuaded to take advantage of this fact then more general improvement in consistency would occur.

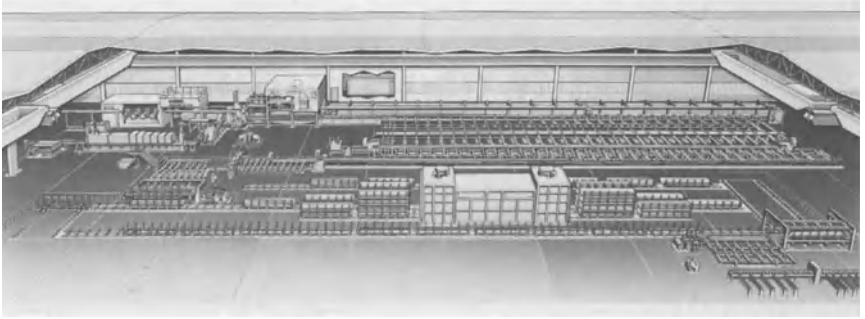
Billet lengths, upset rates, extrusion speeds, extrusion speed ramp rates, number of billets per order and even requests for sample cuts can all be controlled from a computer system. This presumes that the necessary thermomechanical information is available to the programming system, taking advantage of the technology outlined in previous chapters.

Until quite recently there was little control and automation of extrusion plants and the principles laid down were not, and in many cases could not be, utilized. In this chapter we will look at the requirements to produce any given section at a minimum cost, which will usually imply some degree of automation and computer plant control.

## 7.2 THE MODERN EXTRUSION PLANT

A typical modern plant layout is shown in Fig. 7.1.

Fully automated presses are now relatively common and are capable of running with a three-man crew:



**Fig. 7.1** Layout of a modern extrusion plant. (Courtesy of SMS Schloemann.)

- one man as press supervisor and operator;
- a second man for operating, die preparation at the press and support of stretcher head stock;
- a third man for supervising the saw and the stacking and ageing unit.

This requires working with the support of microcomputers to optimize extrusion parameters and the use of semi-automated packing to reduce manual work. The manual demands on the operating crew are thus decreased by utilizing the advantages of PLC-control. Such implementations have opened new opportunities in the extrusion market through greater productivity and increased consistency of product structure and properties.

In comparison with non-automated performance, production can be increased by up to 30% together with other specific advantages. Modifications to the plant layout may, however, be necessary. Some features which are mandatory will now be discussed.

### 7.2.1 The extrusion press

The extrusion press still takes the basic form of Dick's original press but has been somewhat refined [1]. Manual handling of the dummy blocks and the discards is no longer necessary. Fixed dummy blocks [1] and discard handling devices are in common use and have proven successful. The potential sticking of the discard can be alleviated by slight lubrication to the shear knife. Die changing can be done by the press operator by positioning the die changing device with the die shuffle on the operator's side only.

The fixed dummy block which screws onto the stem has now replaced the recycled dummy block on most presses. It is a far more complex tool and the design must allow it to perform several important functions:

- It must transmit the force of the press, under high temperature.
- It must maintain a secure seal with the container wall.

- It must allow easy separation from the aluminium billet discard left at the end of extrusion is clearly essential.
- It must return through the container without backward cleaning or stripping.

To perform all these functions, the design and construction of a fixed dummy block must take account of the block's deformation under pressure, the intensity of tensile stresses on withdrawal and the bonding of steel and aluminium under pressure.

During extrusion, the fixed dummy block must permit an aluminium alloy film about 0.4 mm deep to be left in the container.

To allow the return of the dummy block through a 200 mm diameter container without cleaning or reverse stripping of the container film and without developing high tensile stresses, a 1.5 mm clearance must be provided.

Hence, a fixed dummy block must have an elasticity under pressure which allows it to vary in diameter by 1.1 mm during extrusion, expanding under pressure to a 0.4 mm clearance and then contracting when the pressure is relieved to a 1.5 mm clearance for withdrawal. To achieve effective sealing, this increase in diameter must occur throughout the range of press forces that may be used for extruding, even when this press force is low.

The solution normally adopted to achieve the necessary deformation values are based on the principle illustrated in Fig. 7.2; the application of pressure on a movable taper or cone such that some of that pressure resolves to a radial force hence expanding the block.

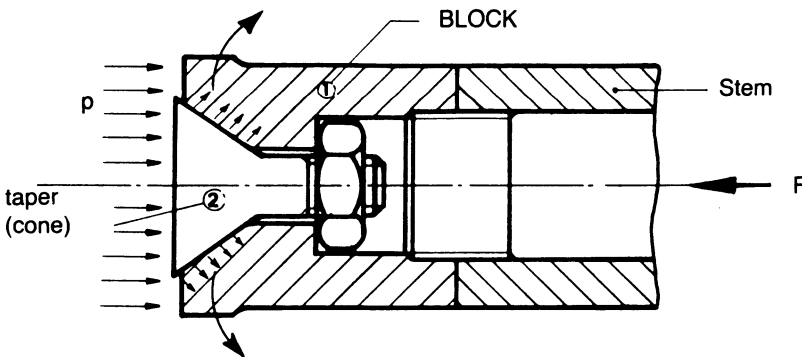
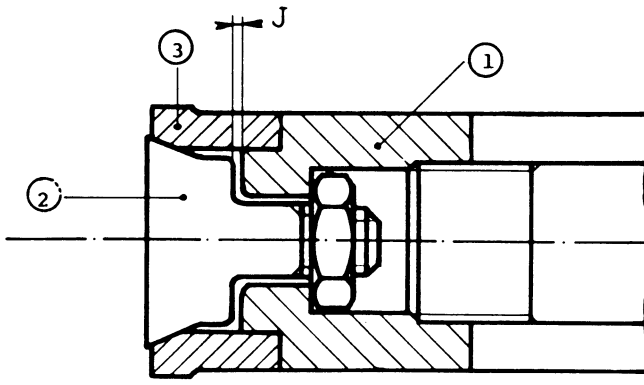


Fig. 7.2 Dummy block with free-moving taper. (Courtesy of Clecim.)

The three-part dummy block [2] is also now in common use and is shown in Fig. 7.3. The design of the taper (2 in Fig. 7.3) is similar to the limited penetration taper described above. The block, however, is redesigned and constructed in two parts; an essentially rigid main body (1 in Fig. 7.3), and a separate, flexible outer ring (3 in Fig. 7.3).



**Fig. 7.3** Three-part fixed dummy block (1, rigid main body; 2, taper; 3, flexible outer ring). (Courtesy of Clecim.)

The main body works only in compression and receives most of the force. Since the ring is separate from the main body, it is more easily expanded to ensure adequate sealing.

The simple shape of the ring also reduces its replacement cost. This is a significant advantage, since this is the main wearing part of the fixed dummy block.

At the conclusion of each extrusion cycle the dummy block must be separated from the discard without removing the profile from the die, and without damaging the block. Since sticking can be very significant (about 1 MN for a 200 mm dummy block), it is absolutely necessary to lubricate the fixed dummy block or the billet to make separation easier.

High stresses cause creep; hence regular inspections can be expected to show:

- permanent increase of the external diameter of the ring;
- reduction of the clearance;
- permanent deformation (caulking) of the supporting surface between the taper and block.

The most frequent maintenance operation consists of machining the dummy block to restore its original dimensions and, in some cases, nitriding it.

At each reassembly, the dummy block is lubricated between the taper and the block with a high-temperature grease.

Breakage of fixed dummy blocks is now very rare. However, since steels progressively lose their mechanical properties, the ring must be changed after 30 000 or 40 000 cycles, otherwise permanent deformation becomes increasingly likely.

## 7.2.2 Ancillary equipment

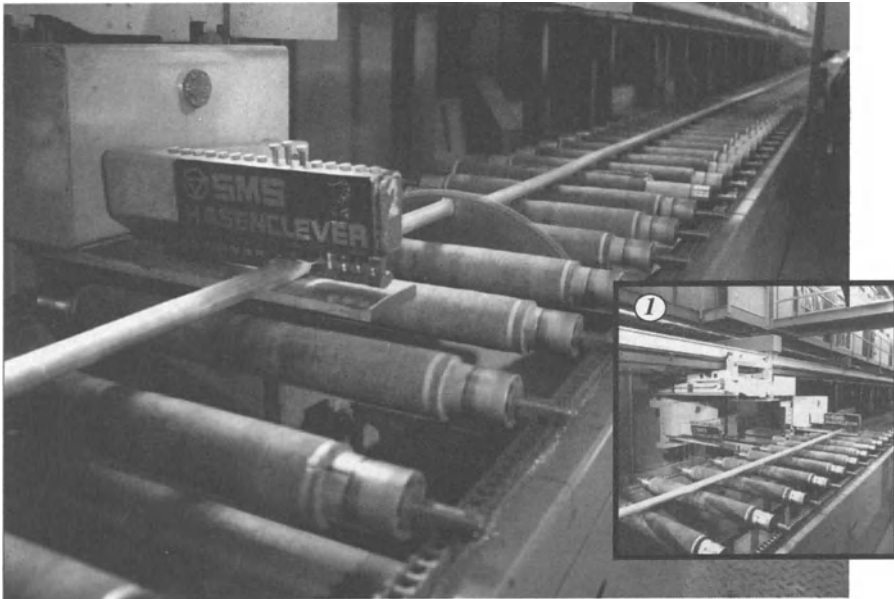
### *Log heater*

The unit has the task of minimizing charging work, and accurately controlling the temperature and taper required for high productivity and the shear-off of billets. One method of achieving this is by installing:

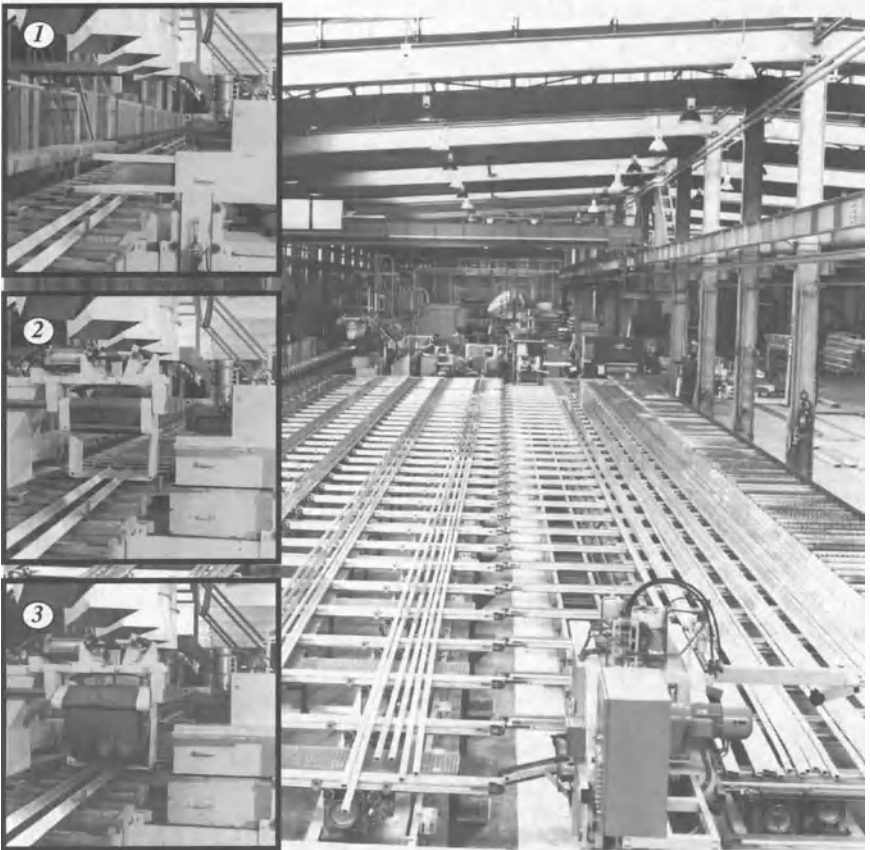
- a large log magazine consisting of four levels, each one able to take multiple logs of the required length;
- an induction heater with a multi-layer coil allowing accurate temperature control as well as the capability of adjusting the taper;
- a hot shear using a PLC-calculation program enabling it to avoid long lengths of waste product below 200 mm.

### *Run-out system*

A main puller is used for guidance of the profiles. Accurate positioning to meet the stretcher, after cutting off the extrusion with a shear, is done by a 'double puller' [3] (Fig. 7.4). The shear, adjustable in position, is a very good solution. It leads to an improvement of working conditions by avoiding chips and reducing noise. To minimize bending while cooling, a special cooling channel for compressed air may be utilized.



**Fig. 7.4** Double puller system. The flying saw can also be seen. (Courtesy of SMS Schloemann.)



**Fig. 7.5** Run out equipment for 40 MN press. (Inset: 1, hot shaping saw; 2, puller-blades open; 3, puller – section are gripped.) (Courtesy of SMS Schloemann.)

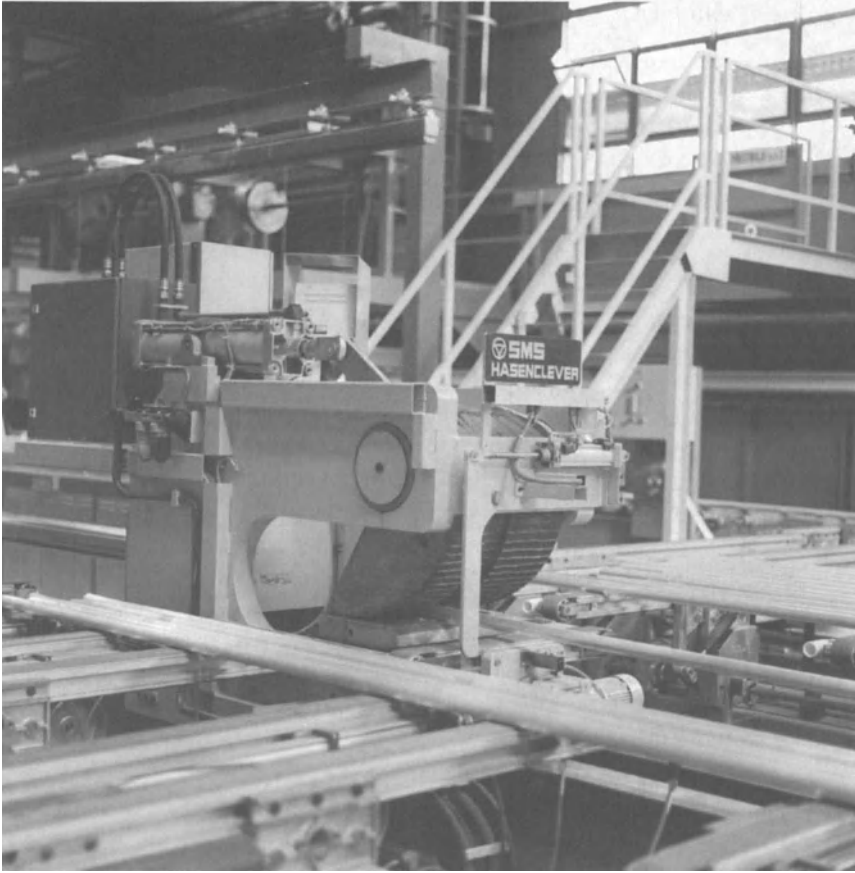
#### *Cooling table*

The cooling table is needed for positioning of profiles and profile cooling. For this purpose, a double chain cooling table with undertable cooling is recommended. Careful replacement of single plates of the chain is critical because their height has to be adjusted to any others, which may show wear.

#### *Stretcher and stretcher feeder*

The profiles to be stretched must be separated and guided into the stretcher head. This can be done with an independently driven belt system and by the guiding of profile ends by a chain on the stretcher head.

The stretching operation should be completely automated. Because of any given product mix, high productivity and deviations from straightness, it may not always be possible to work without manual support at the stretcher head stock (Fig. 7.6).



**Fig. 7.6** Stretcher headstock. (Courtesy of SMS Schloemann.)

Completely automated stretching is therefore not yet common and remains a goal for most operators.

#### *Saw conveyor, saw and stacking unit*

The requirements are automated scrap handling and an automated cycle to saw complete profile packs and to stack them into skips. This enables great manpower savings. The solutions, in successful operation, are:

1. a tilting table after the saw and belt transport within the saw gauge table to the scrap box;
2. a saw gauge stop with deflecting flaps and pre-selection of the number of cuts;
3. an overhead stacking system.

### *Ageing and skip transports*

Chain and roller transport systems from stacker to the ageing oven and back from packing to the stacker are used for automated skip handling.

The continuous ageing oven with internal skip transport shows very high flexibility. It allows profiles to be packed and ready for shipment within 24h after extruding.

### *Packing line*

To increase the packing productivity and reduce manual work, packing handling equipment is essential.

The equipment could consist of a destacker, belt transport, paper feeder, spacer feeder and a wrapping machine. The destacker could also be based on the overhead principle. It should place the profile packs onto a conveyor belt which guides them at human working height to the liftable packing station. Paper which is needed for packing is prepared in correct lengths by the paper feeder.

Only two people are required for packing. From there the pack is sent through a wrapping machine, put on a wooden pallet and stored for shipping. The spacers are also placed on a conveyor belt and fed into the spacer box by the spacer feeder. Finally, the empty skip and the full spacer box are transported on the roller and chain system to the stacker area.

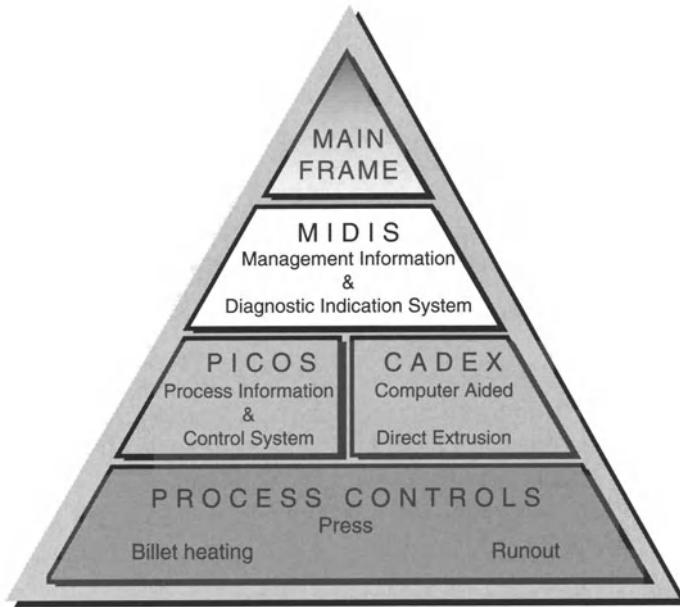
With the achieved reduction of heavy manual work, packing productivity can increase by more than 100%.

## **7.2.3 The extrusion process and parameter optimizing**

We have seen that extrusion productivity is determined by the extrusion speed and the billet taper and temperature (the Z parameter), and clearly is also determined by the acceleration and press time and the dead cycle time. To support decisions and demonstrate the consequences of changing parameters, microcomputers must be installed. The main task of the microcomputers is the optimizing of extrusion parameters within metallurgical and technical limits in order to reach highest productivity.

For this purpose, one computer prepares a process data file and a second one takes this file and optimizes parameters in a simulation model. Optimized parameters are shown on the screen at the press or directly transferred to the PLCs which are changing parameters directly (Fig. 7.7). All these registered data from the data file can also be used for production reports, price calculations and quality assurance. Productivity is increased with such an 'intelligent press'. The press computers must then be integrated with the commercial computers to form a fully integrated plant.





**Fig. 7.7** Hierarchical structure of control systems.

### *Planning*

There must be a limit to the minimum size of orders accepted and to the number of die changes permitted per shift. This will be a function of the press size and capacity. Norsk-Hydro [4] have recommended that for their Nenzing plant equipped with a 22 MN press the minimum order should be 500 kg, maximum die changes 8–12 per shift with a maximum die trial of between 5 and 7 per section.

### *Engineering*

The standards of engineering and maintenance crew generally increase with the implementation of advanced technology. Predictions and warnings that an especially educated crew would be required have proven to be completely false.

## **7.3 PRESS REQUIREMENTS**

The requisite specifications for the extrusion press in the automated plant must include sufficient sensors to prevent those potential disasters which were previously the domain of the operator, such as those caused by missing dummy blocks, discard/die sticking etc. Reliability, consistency and accountability must now be built into the press system.

The automated plant puts special demands on an extrusion press. 'Uptime' is the reward for a carefully planned system and press design. It is therefore useful to examine the factors which determine uptime, downtime and productivity.

We should note at this point that it is the digital nature of modern electronic controls that makes all this possible. 'Digital' means numbers, and numbers can be stored, retrieved, transferred and, most of all, repeated. When a press is running at peak performance the set-up parameters can be stored and then retrieved upon command for future set-ups. Additionally, the actual running conditions can also be stored for future reference and comparison purposes. This digital set-up also ensures that modelling of the process can be readily implemented.

### 7.3.1 Reliability

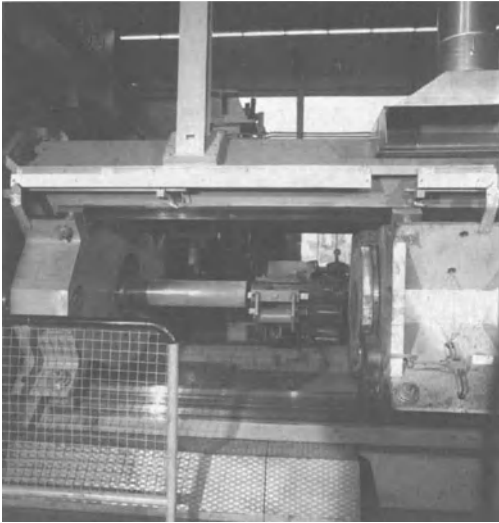
This is the area that really differentiates between uptime and downtime. The press design philosophy must be one with an eye towards longevity. This is as much a function of the press frame (i.e. platen, tie rods, main cylinder, etc.) as it is of the hydraulic system. The modern press will feature:

- self monitoring – through the use of the supervisory computer as well as a comprehensive diagnostic system;
- reliability – as a function of the press frame, i.e. platen, tie rod, main cylinder and hydraulic system;
- repeatability – acquired through the supervisory computer which stores the optimal extrusion parameters and downloads this information to the plant for successive runs;
- intelligence – gathered through the use of numerous high technology sensors which detect pressure, temperature and proximity, as well as other less discernible activities.

### 7.3.2 Mechanics

There seem to be few things on the extrusion press as simple to define and as elusive to measure as press alignment [2]. Countless discussions have been dedicated to the subject of how to align an extrusion press. Still more time has been spent by press manufacturers trying to convince prospective customers of the relative merits of a given press guiding system. There are, however, at least a few definitive statements which can be made on the subject.

A prestressed press frame will have only 50% to 60% of the tie rod elongation (and hence platen movement) of the corresponding conventional press. A prestressed press frame typically has only eight points of adjustment for platen and main cylinder housing parallelism compared to sixteen for the conventional press. (There are only half the number of places for something to go wrong.) A prestressed press frame more readily accommodates container and/or moving crosshead 'X' guiding. 'X' guiding is of particular benefit (Fig. 7.8). The distances from the container centreline to the load bearing or guiding surfaces tend to be more nearly



**Fig. 7.8** 'X' guide system for moving crosshead. (Courtesy of SMS Schloemann.)

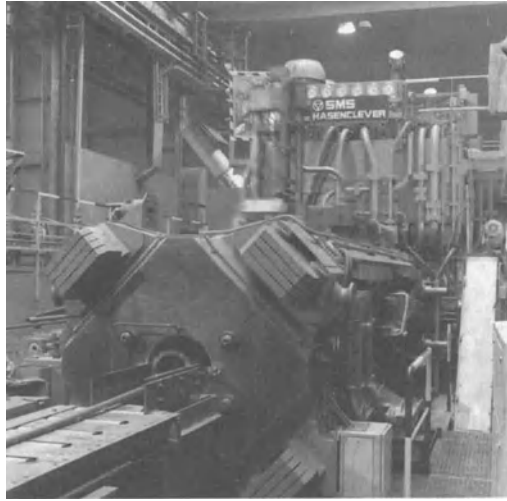
symmetrical about the press axis, no matter the point of reference. The container will still tilt, but has a greater tendency to seal squarely and move towards the press centreline. The centroid of the applied loads and the sealed position will always be the centre of the press. Additionally, the use of four container sealing cylinders allows higher container sealing forces to be designed into the press more easily. The cylinders can be made slightly smaller and mounted closer to the centreline of the press. This way, the bending experienced by the container housing is less, the stripping load is more uniform, and there is a greater tendency for the whole container assembly to stay in alignment.

Prestressed press frames, (Fig. 7.9) reduce the possibility of fatigue failure. While uniaxial stress states are not generally a fatigue concern for tie rods, conventional nut arrangements do cause some bending of the tie rod at the end.

A more likely cause of tie rod failure is loss of prestress leading to loss of press alignment. This leads to uneven loading. Conventional presses have sixteen possible places for adjustment. The prestressed frames have only eight.

Platen deflection must be kept to a minimum. While adequate die support is essential for achieving profiles within tolerance, good die support reduces die breakage. Automated systems should include some diagnostic means of recognizing a broken die although design should ensure that the incidence is rare; continuing to extrude once a die has broken may allow the metal to flow radially through the tool stack. The large surfaces then available to the aluminium under high pressure can destroy tool stacks, tear discard shear housings away from the platen and cause extreme damage to the lower die slide track.

While presses have for many years been built with cast steel main cylinders, these castings can be unreliable and designs utilizing an inserted forged steel



**Fig. 7.9** Prestressed laminated tie rods. (Courtesy of SMS Schloemann.)

cylinder into either a cast or fabricated housing, or alternatively a completely fabricated integral cylinder and housing, are becoming the norm.

The feeder plate dies necessary with automated systems require much higher discard shear forces, as the sheared section is generally equal to the billet diameter. Additionally, rigid guiding is necessary to minimize the amount of aluminium 'smeared' onto the lower die surface. Aluminium build up in this area can have far-reaching consequences but can usually be avoided by minimal lubrication as indicated above.

The higher production rates possible with automated systems allow faster extrusion speeds. These speeds can generally only be achieved through lower extrusion temperatures which necessitate higher specific pressures. This trend towards higher specific pressures requires higher and more uniform container sealing forces.

The interface area between container liner and die is critical. Aluminium build up caused by smearing from the discard shear blade, inadequate or incorrect die support or worn tooling is highly detrimental to this interface. The damage may be limited to an unusually high incidence of flashing, particularly on hollow dies. It may also cause container misalignment of sufficient magnitude to accelerate liner wear, shorten fixed dummy block life or even cause substantial amounts of stem breakage.

Simple yet effective mechanisms for billet transport and scrap handling are imperative. Billet shears incorporating 'topping and tailing' and 'no scrap' routines generate a high number of 'two piece' billets. Rolling of these billets over distances more than two billet diameters should not be considered a viable method of transport. The separate billet pieces tend to behave independently and unpredictably.

Material flow must always be a prime consideration. Areas often overlooked are the transition between the furnace and shear, the transfer from the billet shear to the press loader and the removal of discards from the press area.

### 7.3.3 Hydraulics

There are as many variations of extrusion press hydraulic systems [5,6] as there are manufacturers of hydraulic equipment. There are a number of important criteria, though, which all good extrusion press hydraulic systems should meet.

The biggest simple abuse to hydraulic power systems is the discharge of high-pressure oil over relief valves. Motors convert electrical energy into mechanical energy to drive the pumps, which then convert this energy into the potential energy of high-pressure oil. This energy is available to do work. The only work which should be performed is that to extrude the profile together with that required to strip the discard and reload the press.

High-pressure oil discharged over a relief valve does no useful work. Instead, that energy is released in the form of heat. Heat shortens pump life by reducing the pump's ability to release its own heat, built up by the friction of turning and by internal leakage. The viscosity of the hydraulic oil is reduced at elevated temperatures and this loss of lubricant further increases the heat due to friction.

The solution for a press hydraulic system is simple. The electronic servo controls of modern press systems must automatically 'short stroke' (reduce) the pump output as the pressure required for extrusion closely approaches the set discharge point of the relief valves.

### 7.3.4 Control and monitoring

#### *Closed loop speed control*

It has long been known that the single variable which has the greatest effect on the ability to hold surface finish and dimensional accuracy is the speed of the main ram. The closer it is possible to hold speed to a given setpoint or ramp, the higher the quality of extrusions produced. Focusing on extrusion quality, the analysis can not address the potential for improved productivity through closed loop ram speed control. It is understood that during the extrusion process the speed of the ram can vary due to changing conditions i.e. container friction and die temperature, and it is well known that these changing conditions affect the productivity of an extrusion press. In general, most extrusions can be run at some theoretical maximum speed before tearing or blistering occurs. Although this speed can be increased by controlling certain operating conditions, such as the die temperature, alloy etc., for a given set of circumstances if the operator tries to run too fast defects will occur. This would not be a problem if the operator could set the extrusion speed and vary it throughout the length of extrusion. In fact, however,

in most cases, there is decreasing resistance during extrusion. This reduced force causes the hydraulic pressure to decrease, and with lower hydraulic pressure the internal leakage in the hydraulic components (slip) proportionately decreases. The end result is that since more hydraulic fluid goes into doing useful work and less to making heat, the press speed increases. Closed loop control is therefore essential and is discussed in more detail below.

If we assign some realistic numbers to the variables, a typical press might increase in speed approximately  $5\text{--}10\text{ mm s}^{-1}$  from the beginning of extrusion to the end. If the maximum operating speed is  $70\text{ mm s}^{-1}$ , and the operator sets his initial speed at  $65\text{ mm s}^{-1}$ , it will take him approximately 2 s longer to extrude a 900 mm billet than if he had run it at a continuous speed of  $70\text{ mm s}^{-1}$ . This may not seem like a lot, but extruders are always looking for ways to decrease the dead cycle and 2 s normally represents approximately 10% of the total cycle.

The influence of this phenomenon becomes even more pronounced when running at slower speeds. It is easy to see that the slower the extrusion, the greater the impact closed loop speed control will have on productivity. It provides the flexibility to vary the ram velocity in any predetermined pattern when it is required to isothermally extrude to obtain consistent properties from front to back of the extrusion.

Modern analogue or proportional relief valves are designed to accept a signal from the press computer and so provide for an electrically variable press rating. This is extremely useful for protecting fragile dies which must be 'broken out' carefully to avoid breakage. It is important for the press control system to adjust the 'short stroking' setpoint to coincide with the variable analogue relief valve setpoint.

There are many physical design considerations for a press hydraulic system as well. Long radius piping bends, as opposed to welded fittings, promote smooth oil flow, reduce hydraulic shock, and allow fewer possible leakage points. The generous, redundant, sometimes obsessive use of pipe supports should be encouraged. Straight thread 'O' ring connections should be used wherever possible over conventional pipe thread connections. These taps generally require special tooling to manufacture but their ability to reduce leakage fully warrants the expense. 'Butt weld' flanges, again more expensive than the common socket weld type, are far superior in their ability to reduce leakage. Manifolding of hydraulic components is essential. This method so greatly reduces the number of leakage points and so consolidates and simplifies the piping system, that all modern hydraulic systems should be designed in this manner. Proportional valve technology should be employed, wherever practical, to provide for smooth acceleration of auxiliary components. Provisions must also be made for the deceleration of high inertial loads, a particular problem for long stroke swing type billet loaders.

#### *Electronic programmable limit switch*

Another way to take seconds off the extrusion cycle which is a little more straightforward is to minimize the time spent extruding material which will eventually

find its way to the scrap bin. The extruded product has to be a certain length and if the operator has no way to program billet lengths nor an easy way to adjust the discard length limit switch, he will be spending time extruding high quality scrap.

If we refer to the extrusion of a 900 mm billet at a slower ram speed of  $40 \text{ mm s}^{-1}$ , it is easy to calculate that it takes about 6 s to extrude 4 mm of billet. If the discard length switch is set even 20 mm longer than required, 2 s of production time is lost every cycle. Typically, this may represent approximately 15% of the dead cycle on a well running extrusion press.

One way to address this problem is to add an automatic billet shear, and cut the billets to the exact length required. This would be extremely efficient but somewhat costly.

A less expensive way would be to give the operator the ability to adjust easily the discard length limit switch. He would be able to set it so that the extrusions are to the exact length required. Now the scrap would be in the discard rather than the extrusion, and since the discard represents less expensive scrap than an equivalent weight of extrusion, it is wiser to scrap it.

#### *Electronic pump unloading*

Although not as recognizable, a third opportunity to gain some savings may be realized by destroking the hydraulic pump when the maximum preset pressure has been reached. Specifically, this control scheme will save energy as well as extending the life of the hydraulic equipment.

Typically, when a hard pushing die or cold billet is encountered, the hydraulic pressure reaches the maximum, which is limited by the system relief valve. Rarely will the operator reduce the speed setting when this happens and, in some cases, he will actually increase the pump volume setting, thinking this will increase the force.

The intelligent solution is to monitor the pressure electronically and, as it approaches the relief valve setting, gradually reduce the volume output (stroke) of the pumps. The idea is to have the pumps delivering just enough volume to make up hydraulic slip while maintaining maximum pressure. In this way, not only is the amount of heat generated minimized, but also since the pumps are at short stroke, the loading on the bearings in the pumps is also minimized. This extends pump life.

#### *Repeatability*

All of the above listed requirements apply to any modern extrusion press and, while decidedly important to the automated plant, they do not demonstrate the design philosophy necessary for such a plant to run successfully.

While an automated plant can be run (quite successfully) without a supervisory or host computer, the long term goal for any such installation is maximum production efficiency. As production of each profile is optimized in terms of billet

temperature, billet length, discard length, extrusion speeds etc., the operational goal is to repeat this performance on each successive run.

The supervisory computer, via the data acquisition capabilities of the automated plant, stores the optimal extrusion parameters and downloads this information to the plant for successive runs. If the extrusion equipment is unable to reproduce these operating parameters with a relatively high degree of accuracy, most of the information is then of limited value.

#### *Automated press set-up*

Once the ability to control the press accurately has been established, the next aim should be to give the operator the ability to duplicate set-up parameters precisely for any given die. This ensures that the press will be set up consistently for a particular die regardless of operator experience. These 'ideal' set-ups can be achieved in two ways: through a low level expert system, or by theoretical analysis. In either case the set-up routines are stored in the memory of the control system and the operator can retrieve them on command.

Those variables that might be included in a typical set-up are: extrusion speed, discard length, burp cycle (on/off), billet on billet cycle, bridge die (yes/no), container temperature, billet temperature, maximum tonnage, any controllable variable.

It should be noted that although the operator has the ability to retrieve set-up parameters, it is very important that he also has the ability to change them, since conditions outside of his control, e.g. alloy, may change and affect the operation.

#### *Diagnostics*

The purpose of diagnostics on any machine is to minimize downtime [7]. This can be accomplished in two ways: (i) by pinpointing existing problems, and (ii) by predicting potential problems. Today's diagnostic routines vary through a wide range of sophistication, from the very simple electrically activated alarms and displays to the very sophisticated software routines which analyse the actual machine cycle.

Diagnostic systems may in fact be the key to the future of the automated plant. Since we cannot rely on the operator to monitor the press at all times, the controls system must be able to perform this task. Diagnostic systems can be divided into two categories: passive and active. Each type is essential and easily supported by the computer.

Passive systems are used by maintenance personnel to quickly isolate a failed component and get the system back on line. The passive system is not utilized in an 'interlocking' capacity. It is used to report specific problems such as dirty filters, high oil temperature, low oil level etc. It can also be used to report 'illogical' conditions. An example might be that a failed limit switch tells the press that the discard shear is down. At the same time, a correctly functioning limit switch



senses that the discard shear is up. The system 'knows' the shear cannot be both up and down and reports that one of the two limit switches is faulty.

An active diagnostic system on the other hand 'gets involved' with the press operation. It can function as an 'early warning system', indicating deterioration of individual press functions. If the withdrawal time of the loader becomes longer and longer, the system can warn operating personnel in time to fix the loader before the main ram has a chance to destroy it. Erratic or improperly sequenced press operation can be detected and reported. For instance, a billet loader may begin to move towards the press centre during extrusion. This may be because of a faulty valve, a glitch in the control logic, or failed limit switches or other transducers. The diagnostic system can identify which of the three possibilities is in fact correct. In the case of a malfunctioning valve, the diagnostic system senses the movement of the loader off its home limit switch. It also 'knows' the programmable controller did not turn on the solenoid corresponding to 'loader in'. This allows us to eliminate the other two possibilities. A similar logical exercise can be used in each case to determine why the loader moved.

Photoelectric eyes can be used to scan the die face and to examine for a missing fixed dummy block. These signals are interlocked into the press logic control. As active diagnostics, these devices prevent destructive press operation.

'Maintenance memory' can be kept on file. When maintenance personnel fix a problem, the solution can be filed in the diagnostic system. When a similar problem arises in the future, other personnel will have easy access to this information.

### *Data acquisition*

In addition to improving the operation of an extrusion press through better control and diagnostics, gains in productivity can also be achieved through the proper handling and manipulation of production data. This data can be used to generate daily production reports, die histories or equipment efficiency logs. More importantly, it can be combined with a statistical process control program which should help to predict when the extrusion process is getting out of control.

Most modern presses have transducers monitoring hydraulic pressure, main ram position and velocity, container temperature, billet temperature, extrude temperature etc. Information from these transducers can be recorded at specific times during the cycle. This information may include the following: press position at crush (or fully upset), press position at peak pressure, time at peak pressure, press speed, pressure prior to decompression, press position at decompression, time at decompression, billet temperature, extrude exit temperature, container temperature, oil temperature, container seal pressure and pilot pressure.

This information can then be manipulated to generate such information as: date, time, die number, number of billets, production, discard scrap, average speed, pressure (average, high, low), pressure at end of cycle (average, high, low), dead cycle time (average, high, low), burp cycle time (average, high, low), billet temperature (average, high, low), oil temperature (average, high, low).

This information alone can give insight into some possible production problems. The performance of any one die or any press can be analysed. However, the analysis can take a giant leap forward if the data is analysed together with a statistical process control program.

#### *Statistical process control (SPC)*

This is a method of mathematically manipulating inspection data to determine not only if a particular process is operating within the specified control limits, but also if it is going out of control. This is a very important concept since the aim is to prevent defects rather than reject them.

SPC indicates when the average of the population starts to move towards the tolerance limits during any given production run. Then, by analysing the press operating characteristics, corrective action can be taken before scrap material is produced. The objective is zero defects by ensuring that remedial action is taken before the product moves out of the tolerance band.

#### *Quality*

The best way to ensure that a good, consistent uniform quality product is extruded is to determine first the proper production and handling requirements, then put them into a set of procedures and see that those procedures are followed every time the product is processed.

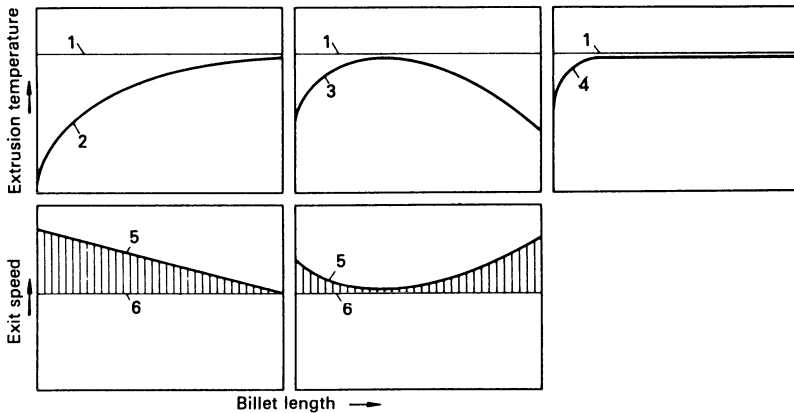
With SPC, it is a simple matter to convey those procedures relating to the extrusion process to production, by the electronic media, and then have that same press information system monitor the process.

By displaying the run speed, cycle times, billet lengths and temperature of the previous runs and the current run, along with the requirements, the operator can very closely match a previous production rate, maintain correct temperature settings and continuously produce a high quality extruded product, with the confidence of knowing that the correct production requirements were followed.

### **7.4 ISOTHERMAL EXTRUSION**

As discussed in previous sections, the exit temperature can increase or decrease during extrusion with a constant ram speed, depending on whether the predominating factor is the development of heat by friction and deformation in the container or heat losses to the tooling, especially the ram and container. A temperature increase towards the end of extrusion is generally observed, in agreement with the theoretical calculation, if either the exit speed is high or the container temperature is only slightly below or equal to that of the billet. Extrusion with a constant exit temperature is of practical interest for achieving a uniform product quality or for making the most efficient use of the maximum speed that the alloy can withstand without poor surface developing. The basic idea of so-called

isothermal extrusion (the temperature will still vary across the section) developed from a knowledge of the relationship between the exit temperature and the ram speed. The exit speed is varied via the press control system to give a constant exit temperature (Fig. 7.10).



**Fig. 7.10** Relationship between temperature profile and usable extrusion speed in isothermal extrusion (schematic). (1) maximum permitted extrusion temperature (start of cracking); (2) exit temperature increases; (3) exit temperature reaches a maximum, then decreases; (4) exit temperature profile for 'isothermal' extrusion; (5) possible extrusion speed in 'isothermal' extrusion; (6) actual extrusion speed. Shaded area = unused speed reserve.

The practical, that is the economic, value of isothermal extrusion is that, except at the very beginning, it allows the use of the optimum extrusion speed over the complete extrusion cycle. On the other hand, if the exit temperature varies during the cycle by an unknown amount, the press speed is usually adjusted with the maximum prevailing temperature. This sets the speed for the complete cycle and there is a wasted surplus speed capacity in the region of low exit temperature. This is shown schematically in Fig. 7.10. The temperature profile at a constant speed must first be determined by measurement in each case in order to decide whether isothermal extrusion is feasible and how the press control system could be modified. In the first example in the Fig. with a continuously increasing exit temperature typical of aluminium alloy extrusion, isothermal extrusion is possible in several ways:

- reducing the extrusion speed during the cycle according to the measured temperature. Continuous temperature measurement is required and the method is illustrated in the figure as occurring in the fifth extrusion;
- reducing the extrusion speed according to a preset speed program;
- non-uniform heating of the billet to give a lower temperature at the back of the billet. This is known as taper heating [8] and can be achieved most easily by the

use of an induction heater. It can also be achieved in gas heaters by varying the burner capacity such that the front of the billet is raised to a higher temperature. Alternatively all of a uniformly heated billet can be quenched by water spray [9]. Of these alternatives the most accurate is the use of an induction heater.

Of these three methods the first coupled with some taper heating is probably the best solution [10].

Only the first two methods can be used in the second example in Fig. 7.11, which is characterized by a maximum exit temperature followed by a decrease. A profile of this type can occur in aluminium extrusion if the container or, more importantly, the dummy block is relatively cold.

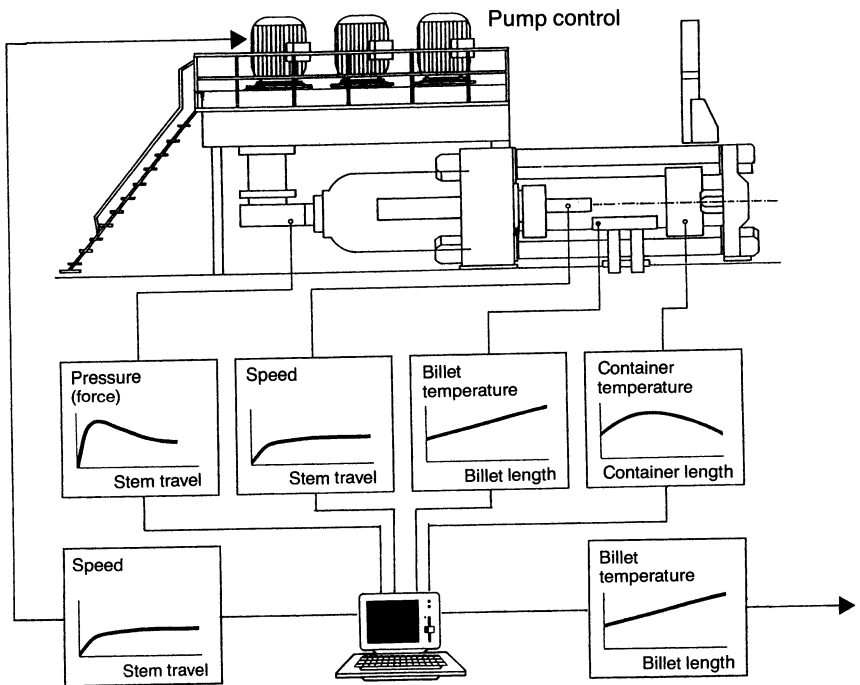


Fig. 7.11 Data exchange with CADEX. (Courtesy of SMS Schloemann.)

### 7.4.1 Process optimization

The productivity of a modern extrusion line is influenced by many different factors. Among these, determination of the optimum process parameters, such as extrusion speed and billet temperature, takes a particularly important part in process optimization. The aim of process optimization is to increase the output while meeting the section quality requirements. Priorities can vary distinctly. Depending on the customer's specific needs, there are strict or less exacting demands on the quality criteria of surface quality, strength properties and

dimensional accuracy of the section. Process optimization must take into account any changing requirements to enable a maximum output while achieving the selected quality.

The process is optimized by means of checking and controlling the influencing thermomechanical variables. The heat balance in the case of direct extrusion is essentially determined by the two contributing elements, container wall friction and heat generation in the deformation area.

The physics necessary to predict the temperature, load and temperature strain rate have been described in previous chapters. We have seen that presently the physics does not exist to predict all of the complex shapes encountered and hence software development must include the empirical relations included in the text and also some form of expert system to allow for the most difficult sections, including those which are both hollow and thin walled. Many software programs have been developed including those using the integral profile, modified upper bound techniques and Lange's analysis described in Chapter 2. Thermomechanical simulation of the extrusion parameters is thus possible for determining the optimized parameters.

#### **7.4.2 Features required in a comprehensive process optimization**

A system for perfect process optimization would need to be able to supervise all process variables affecting the output and quality of the section. These would include section temperature, deformation force and speed. Combining the speed and temperature gives the Zener–Hollomon parameter ( $Z$ ) allowing, to some extent, the control of properties.

The quality of the section surface is influenced by the section temperature which must be within a defined range in order to produce the specified final material properties.

A change in deformation force within an extrusion cycle may, in the case of critical tools, cause a modified expansion and in this way produce non-uniform section dimensions along the extrusion length. A change in speed may equally affect the dimensional accuracy of the section.

The first essential ingredient of process optimization must be isothermal extrusion. Constant temperature of the material entering the zone of deformation and a constant rate of deformation will result in a constant deformation force and uniform load on the die ensuring constant deformation of the die and stack and, perhaps just as important, the dimensional constancy which this produces.

An alternative way to accomplish isothermal conditions for the section would be extrusion of a homogeneously heated billet and setting of a speed profile. This characteristic line is selected in such a way that, on reaching the maximum permissible section temperature, the speed will be decreased by such an amount that the maximum temperature of the section is maintained at this level.

When this method is applied, it is important to consider another influence – the die load. The front end of the billet is usually colder than the back end in a

taper solution. This causes a higher flow stress of the material. Especially during the acceleration of the press, the die load may exceed the permissible value and cause deviation from the section's dimensional accuracy or – worse – die damage. The speed curve, therefore, has to be defined according to the maximum permissible section temperature and die load.

Another aspect of process optimization has taken on increasing significance during recent years. The billet temperature, for example, frequently differs from the optimized reference value. A modern process optimization system will, in such an instance, be required to react immediately and enter a new speed profile. Under these new conditions, section temperature and die load must equally be within their permissible limits in order to guarantee the desired quality.

Apart from quality improvement, a comprehensive process optimization ensures the maximum output for a section. This means that the maximum extrusion force available will be applied and the maximum section temperature will be run to the fullest extent tolerable with regard to the section quality. The demands on a comprehensive process optimization can be met by using a number of software-based control systems. The system enters a billet temperature and an extrusion speed that enables isothermal and isopressure conditions (as far as feasible) within a minimum extrusion time.

Most software can be run on a standard PC, which is directly connected to the PLC of the press. So optimization of the parameters is performed fully in the background. An optimization cycle is designed commencing with the extrusion of a section using standard process parameters for billet temperature and speed normal to the pressline. During this cycle, the system automatically acquires all data necessary for the mathematical model or modification of the proven model. On completion of the extrusion cycle, referred to as 'sample extrusion', the software computes the optimum parameters and sends a new billet temperature and speed profile to the PLC. For example, the assumed 'active extrusion ratio' may require adjustment, the theoretical flow stress may vary slightly or the tooling temperature may not be as assumed in the theoretical model. Corrections must be made by varying the ingoing temperature profile or the speed profile for the extrusion process. The press operator no longer adjusts these values manually, but concentrates on his most important task, i.e., supervision of the overall process. It is possible at any time to modify variables relative to quality, such as section temperature, speed, and deformation force. The system will immediately respond by changing the speed for the cycle in progress and, for the subsequent extrusions, request billets with re-optimized temperature matching the new conditions.

Visual display of the essential process parameters gives the press operator a quick survey on the actual process data. Since the control system specifies a section temperature determined by computation, it is not necessary to adjust and handle measuring devices, such as, for example, infrared pyrometers, although these devices give a feedback that the computed conditions are correct and play an important role in the setting up of the material parameters.

### 7.4.3 Results of process optimization

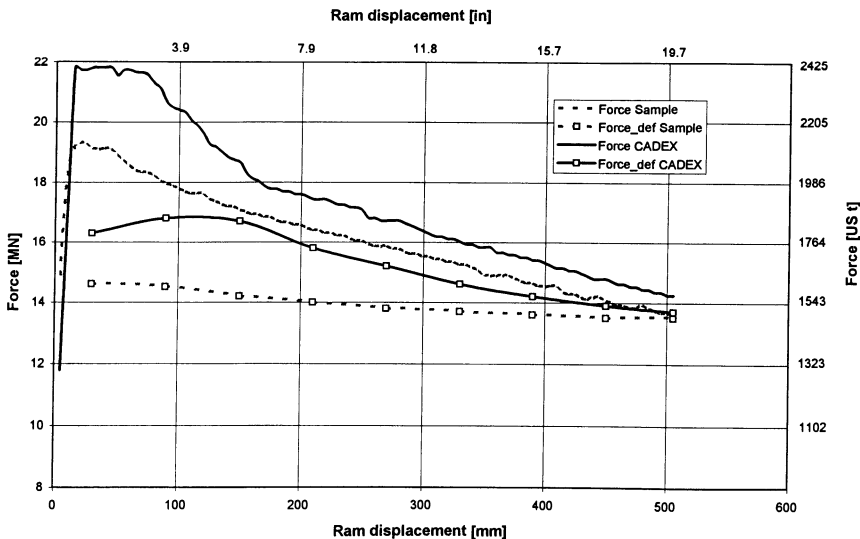
Some results of process optimization have been presented by SMS Schloemann [11]. The precise details of their deformation model are not clear but the temperature model is certainly not as precise as those discussed previously. The implication is that setting up and adjusting speed profiles could be more exact.

Evaluations are presented for two distinct plants, illustrating both taper and homogeneous temperatures. The conditions under evaluation are given in Table 7.1.

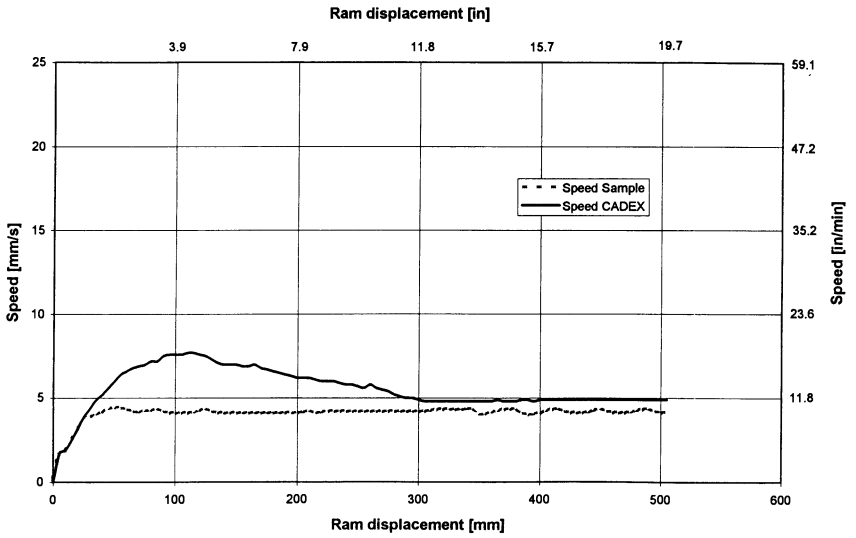
**Table 7.1** Plant details

Details	Plant No1	Plant No2
Press size	22 MN	32.5 MN
Billet length	995 mm	1350 mm
Billet diameter	204 mm	229 mm
Container diameter	214 mm	235 mm
Furnace	Gas, homogenous temperature	Induction, taper

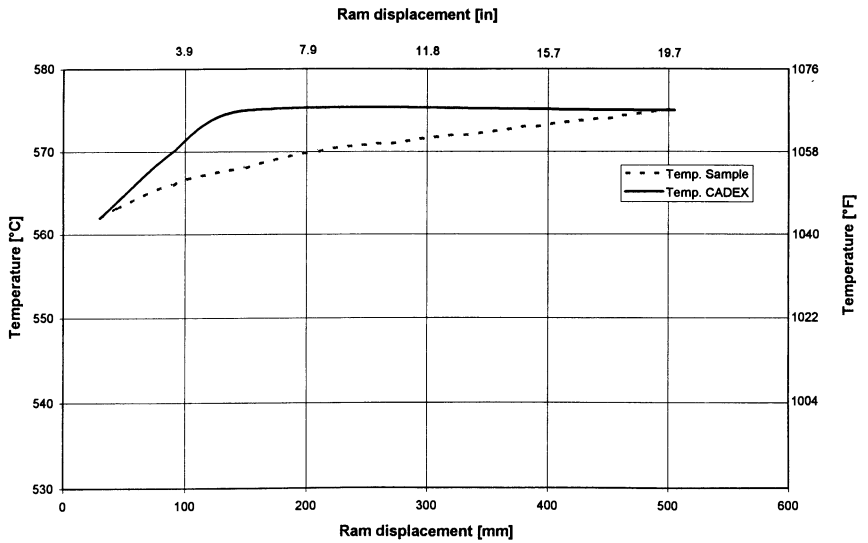
The benefit of the control system on Plant 1 lies in the possibility of extrusion time reduction by selection of a speed profile. When defining the speed profile, particular attention must be given to obtaining the desired properties of the product as well as the section temperature, speed, and die load. Figures 7.12, 7.13 and 7.14 show the parameters optimized with the help of the SMS system for a section that was extruded under the parameters indicated in Table 7.2.



**Fig. 7.12** Force versus ram displacement. Extrusion parameters according to Table 7.2. (Courtesy of SMS Schloemann.)



**Fig. 7.13** Speed versus ram displacement extrusion parameters according to Table 7.2. (Courtesy of SMS Schloemann.)



**Fig. 7.14** Section temperature versus ram displacement extrusion parameters according to Table 7.2. (Courtesy of SMS Schloemann.)



**Table 7.2** Section and process data – plant 1

Cross-section	hollow		
Wall thickness	2 mm.		
Section weight	1.03 kg m <sup>-1</sup>		
No of holes	1		
		<i>Sample cycle</i>	<i>Optimal cycle</i>
Billet temperature	°C	482	470
Maximum speed	mm s <sup>-1</sup>	4.5	7.5
Extrusion time	s	127	92

As a comparison, the sample extrusion traces are shown against the optimized values. Figure 7.12 shows the force characteristic line as a function of the ram displacement. It can be observed that the magnitude of the force used rises by about 14% when compared with the value established in the course of sample extrusion. The maximum force of the press is applied at the start of extrusion in order to obtain the highest acceleration rate possible. The values for ram speed and section temperature are shown in Figures 7.13 and 7.14. The speed rises to a maximum of 7.5 mm s<sup>-1</sup> compared to a value of 4.5 mm s<sup>-1</sup> during sample extrusion. With this speed profile, the extrusion time can be reduced from 127 to 92 seconds (27%).

A look at the development of the section temperature shows that, with setpoint entry by the SMS model, it remains constant at 575°C after extrusion of approximately one-third of the billet. So for most of the section isothermal conditions are available. The new setting of the section temperature is the maximum value reached by sample extrusion since a product of satisfying quality was extruded at this temperature.

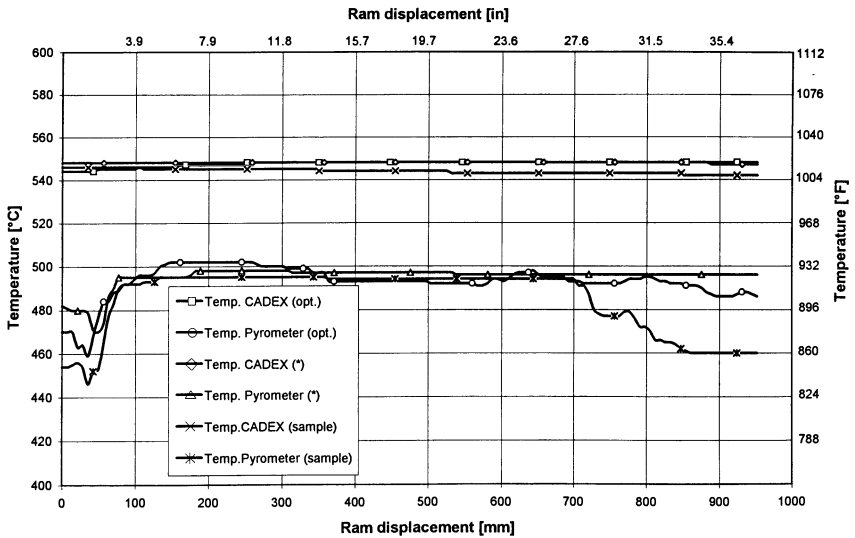
In the second example, process optimization was demonstrated for Plant 2, in which a temperature gradient could be set for the billet. On this pressline, an additional radiation pyrometer was available to measure the section temperature. The pyrometer was attached to the counterplaten and vertically directed at the section. The target area for this instrument had to be a minimum of 10 mm<sup>2</sup>. The purpose of the pyrometer is to compare the temperature calculated by the model with a measured value. The section extruded and the process parameters employed are given in Table 7.3. The parameters of the sample extrusion (normal practice) are: billet temperature is 490°C at the front end and 438°C at the rear. When extrusion is effected at a constant stem speed of 11 mm s<sup>-1</sup>, a section temperature of 495°C that is constant over almost the entire length was measured (Fig. 7.14). For these conditions a value of 542°C was calculated. The measured value shows a strong temperature drop (35°C) in the last third of the billet. This sudden drop cannot be explained physically; it probably shows the problem involved in pyrometry with the measuring spot deviating from that set. This shows that temperature measurement with infrared pyrometers can be suspect, especially if small sections with a multi-hole die are extruded.

**Table 7.3** Section and process data – plant 2

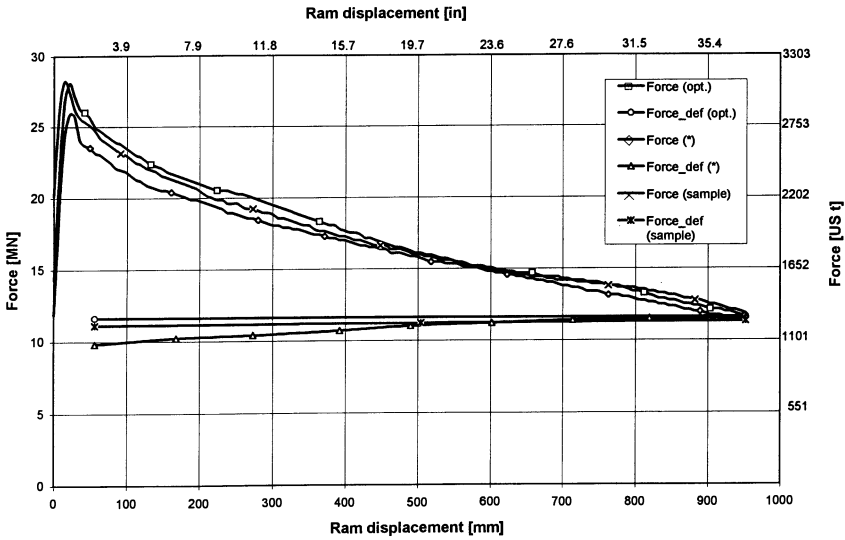
Cross-section	solid			
Wall thickness	2.5 mm.			
Section weight	0.5 kg m <sup>-1</sup>			
No of holes	6			
		<i>Sample cycle</i>	<i>Optimal cycle</i>	
Billet temperature	°C	490–438	495–423	510–436
Maximum speed	mm s <sup>-1</sup>	11	12.8	12.8
Extrusion time	s	99	85	101

The force versus ram displacement chart (Fig. 7.16) gives the actual measured total force in the sample run together with the force predicted by the SMS model and the optimized force. The total force is 28 MN at start of extrusion and drops to a value of 11 MN at the discard end.

On the basis of this extrusion the process parameters were optimized. For this purpose an increase of the deformation force by 3% as compared to the maximum sample extrusion value can be permitted (Fig. 7.16). The section temperature should not exceed the maximum value reached during the sample extrusion by more than 1°C. The SMS system calculates a new billet temperature of 495°C at the front and 423°C at the rear of the billet. If the billet is heated in this way, a constant ram speed of 12.8 mm s<sup>-1</sup> can be tolerated. The section temperature measured by the radiation pyrometer shows a slightly oscillating measurement for this extrusion with an average value of 495°C.



**Fig. 7.15** Section temperature versus ram displacement. Extrusion parameters according to Table 7.3. (Courtesy of SMS Schloemann.)



**Fig. 7.16** Force versus ram displacement. Extrusion parameters according to Table 7.3. (Courtesy of SMS Schloemann.)

The improvements expected from process optimization could then be assessed. By setting the new speed, extrusion time could be reduced from 99 to 85 s (14%).

This example shows that, when using a temperature gradient for the billet, the section temperature and extrusion force can be kept constant. In this way, isothermal and isopressure extrusion have been attained. The advantage offered by such models is that, while taking into account the limits imposed by quality, a billet temperature gradient can be determined, which will enable the minimum extrusion time. Extrusion plants that have been using temperature gradients for the billet can obtain a further reduction of extrusion time of about 5% by careful modelling and application of such systems.

Generally, any optimization system must be capable of generating speed profiles in response to signals of altered temperature conditions. It is not generally recognized that consistency is as important as quality and the well designed system provides the extruder with both. This can be seen by referring to Table 7.3 and Figs. 7.15 and 7.16.

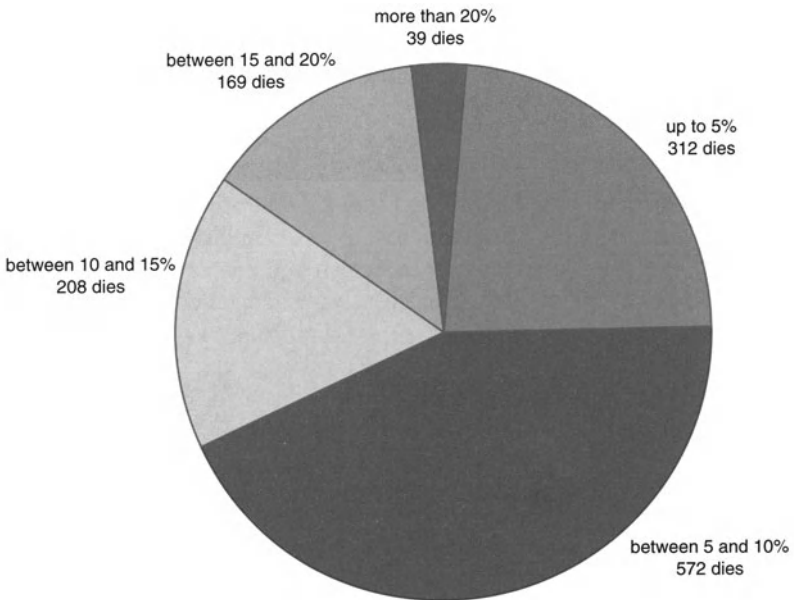
The furnace supplies a billet with a temperature gradient from 510°C to 436°C. For this billet temperature, the SMS system calculates a new speed profile while the billet is being loaded into the container and sends it to the press. As the billet is loaded with too high a temperature over its entire length, the first third of the billet is extruded at 9.9 mm s<sup>-1</sup>, which is much slower than the sample cycle. Towards the end of the billet, the speed can be increased up to 12.8 mm s<sup>-1</sup>. The measured value of the section temperature shows a constant line at 495°C and confirms the modelled temperature. This example shows that thermal calculation

of the extrusion process as a function of speed, billet temperature, and container temperature can be computed from quite simple models.

The aspect of extrusion time reduction as an objective of process optimization has been evaluated on the basis of production figures at various extrusion works. For determination of the extrusion time reduction, the extrusion time of the sample extrusion was compared to the average extrusion time of subsequent SMS-optimized extrusions. 1300 dies were tested at 10 different plants. The press sizes in this comparison were between 22 MN and 35.5 MN; in three plants, it was possible to select a temperature gradient for the billet. The results (Fig. 7.17) show that for 60% of the dies an extrusion time reduction between 5 and 15% can be achieved.

Thanks to the on-line connection of the system to the process, overall process supervision is ensured. The required quality can be repeated. In addition, the control system captures the real process parameters of all extrusions and stores them. This provides a full history of all extrusions for analysis and evidence.

There are other systems available such as those using 'fuzzy logic' [12] which appear to be equally proficient and require about the same modelling expertise and are available.



Basis: 1300 dies, 10 extrusion plants

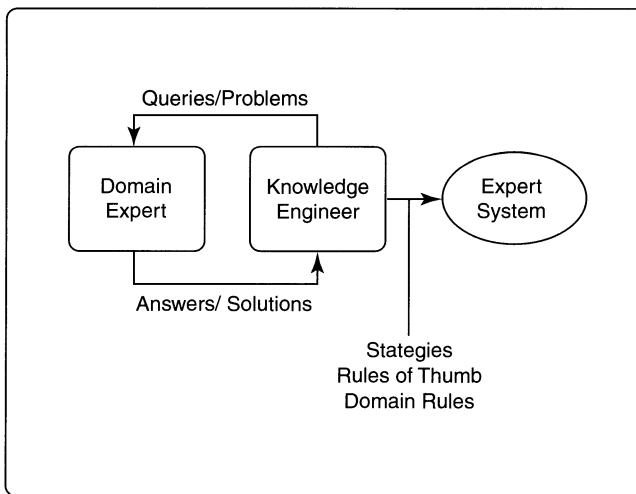
**Fig. 7.17** Extrusion time reduction due to installation of CADEX. (Courtesy of SMS Schloemann.)

## 7.5 EXPERT SYSTEMS

To help maintain complex machinery, systems known as expert systems have been developed and installed in many manufacturing plants [13]. Although by many these are associated with considerable expenditure this certainly is not true. With nothing more than a programmable controller, an alphanumeric smart display and a little programming, an expert can attend to an extrusion press 24 hours a day, ready instantly to offer expert advice and help solve problems. In fact, any piece of equipment controlled by a programmable controller can be equipped to provide valuable information to minimize downtime and lost production.

Expert systems are part of a broader field of artificial intelligence. Generally, artificial intelligence deals with programming computers to ‘think’ like human beings and often to be ‘creative’. Expert systems, though, narrow the application, programming computers to respond or mimic an expert’s reasoning process to play back how the expert would go about solving a particular problem.

To be able to do this, the expert system needs a knowledge base. This base is supplied by human experts. To transfer an expert’s knowledge to the computer’s knowledge base, an engineer interviews the expert by asking questions and posing problems for the expert to answer (Fig. 7.18). The engineer then transposes the expert’s knowledge into rules that have the following form: IF (this) THEN (that will follow). These IF–THEN rules form the foundation of the knowledge base.



**Fig. 7.18** Flow diagram for programming the knowledge base.

The knowledge base does not have to be static once programmed. It may be dynamic. The knowledge base can be linked to data bases or to spreadsheet programs (like Excel). However, when this information is used, it is still organized to follow the same IF–THEN rules.

These rules do not have to be total statements of fact. They can be assigned confidence levels. An expert may say that IF this happens THEN that will have a certain chance of happening. For example, IF billet temperature is low and there is hydraulic leakage, THEN billet will stick, confidence 30%. This statement would be programmed in the following format: IF temperature =  $T - \Delta T$  AND Oil to main ram =  $Y - \Delta Y$  THEN billet  $< >$  stick, CNF 30.

The second part of the expert system is called the 'inference engine'. This is part of the program that is the heart of the expert system. It uses the knowledge base to solve problems and draw conclusions during a consultation. The inference engine is the 'intelligence' that allows the expert system to understand and make conclusions based on the 'expertise' or 'knowledge' stored in the knowledge base (Fig. 7.19).

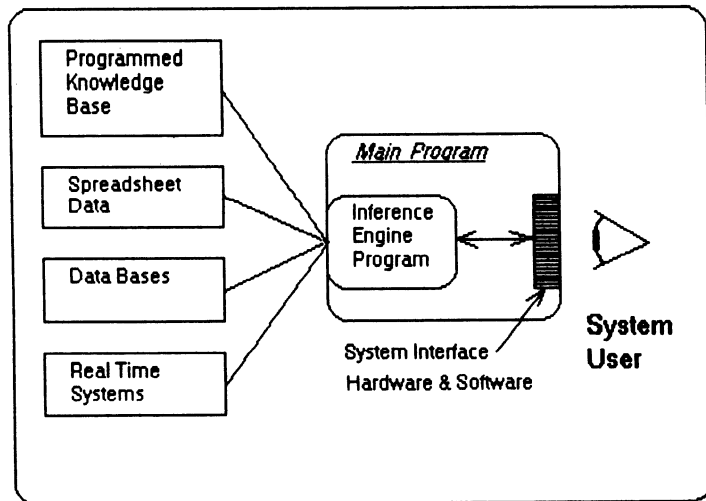


Fig. 7.19 Expert system (schematic).

There are two logical procedures an expert system uses to solve problems and give advice [12]. These procedures are known as forward chaining and backward chaining. Basically, it depends upon the question being asked as to which method is used to solve a problem. The easiest way to compare these two methods is to think of forward chaining as looking forward in time, answering the question: 'What will be the outcome of these circumstances?' Backward chaining, on the other hand, looks back in time and answers the question: 'What caused the situation?'

Mainly, forward chaining deals with predicting the outcome of a set of circumstances. The set of circumstances is given by the IF part of our knowledge base, and we are looking for the THEN parts that will tell us the outcome. An example of a forward chaining question asked of an expert press system would be: 'Given these press conditions today, when will service be due?'

Backward chaining, conversely, deals with finding the circumstances that led to a certain outcome. Here, the THEN part of the knowledge base is given and we are looking for the IF parts that satisfy this outcome. Using backward chaining, we would state a press question in the following way: ‘What press circumstances yesterday led to service being due?’

Expert systems are designed to program an expert’s knowledge in a specific area so that others, with less knowledge in this area, can get expert advice. Overall, expert systems are best suited to codifying very specific knowledge areas.

In the extrusion industry, the complicated machinery which has to be operated and maintained provides greater challenges as technology advances. For example, twenty years ago, we were talking about programmable controllers. Ten years ago, we were implementing them and, today, they are the standard control system on our equipment. The same is becoming true of expert systems [14–18] depending on the theoretical solutions available.

As the complexity of production equipment increases, it is becoming more difficult to troubleshoot and maintain. The programmable controllers opened many doors but have closed others. On the one hand, they have given programming and control flexibility. On the other hand, the control programs have become increasingly more complicated as the programming changes and enhancements become easier to make.

There are other problems. The number of expert people who diagnose and maintain equipment is decreasing. Either they are retiring or they are leaving for other careers. As they leave, there are knowledge voids in organizations. Replacing them is difficult, for quality individuals do not rush to heavy industry for careers.

Even when qualified individuals stay, they may forget important information about the equipment and how it operates if they do not work with the equipment regularly. Expert systems [18–21], then, give an alternative. In specific areas, they can codify knowledge so that the impact can be minimized when the 20-year veteran expert decides to leave.

### **7.5.1 An expert system applied to an extrusion press**

The initial premise is that the expert system must reside in the PLC and hence be more convenient and easy to use.

The main question seems to be knowing when the equipment has a problem. First of all, there are obvious situations where the equipment is in trouble; for example, when the oil temperature gets too high or the ram-rod safety switch is activated. These situations are relatively straightforward and easily programmed. But what about a situation where the main ram is not coming forward because the billet loader is not yet in position? Is this an equipment problem or not? Well, it may or may not be a problem. It depends: Is the load on its way up? Or, is it up and not closing the limit switch? The first situation is, of course, not a problem

and the second one is a problem. How is it possible to differentiate between these two situations?

There must be some way to differentiate a problem from a normal operational situation. Ultimately, an expert troubleshooting system must automatically answer all problems. But it is a complicated task trying to distinguish every possible situation that is an operational problem from a normal occurrence. Therefore, other possibilities must be considered that are less complex. A simpler solution is required so that it is easy to program and to maintain as changes are made to the press cycle. The expert system must be told when there is a problem. Then, the system can determine what the problem is. This eliminates the extra programming required for deciding if there is or is not a problem.

But this is still fairly complicated. From all the possibilities of what could be wrong, would the system have to determine the specific problem? In other words, if a 'trouble' push button is activated, the system must determine where the press is in its cycle, and its next operation. From this, it has to deduce the current problem. So, finding the problem again appears about ten times more complicated than diagnosing what the cause of the problem is in the first place.

Therefore, to achieve the simplest system possible, two things are important: first, the system must know when there is a problem, and, second, it has to be informed what the problem is. Once the system knows the problem, it can use backward chaining to check the associated controller logic and report any situations that cause the problem. For example, when the ram will not move forward, the system could report the following messages: 'Load up limit switch not closed' or 'Loader not up' or 'Loader not in position'. Any one of these messages will let the operator or the mechanic know instantly what the problem is.

The solution is to let the push button for the particular actuation tell the expert system when there is a problem and what it is. The operator would then simply push the 'ram forward' push button indicating (i) that he has a problem, and (ii) it is the ram not coming forward. The expert system can instantly check all the associated logic and determine why the ram is not coming forward.

### **7.5.2 A typical system description**

The knowledge base and inference engine can both be programmed in a PLC. The expert system identifies the causes of the problem and associates each one with a number. These numbers are sequentially sent to a smart display where the associated message is displayed. A smart display is preprogrammed with these messages and displayed on demand. Also, the smart display has the capability to send the message to a printer for a permanent record of the displayed messages.

The PLC's job as far as the expert system is concerned is to look for the possible causes of problems each time a control push button is pressed. Pressing a push button, the operator is telling the PLC that a specific action is requested and to check for any problems. Normally, no problems are found, no messages are sent to the display and the desired actuation takes place normally. However, when



there is a problem, it is not uncommon to have more than one message displayed. For more than one message, the PLC must store all the message numbers and sequentially send them to the display.

While the PLC is sending message numbers to the display unit, it does not search for any other problems until the stored message numbers have all been sent. The reason for this is to avoid re-queuing the same problem numbers over and over again or queuing other unrelated problem numbers as different push buttons are pressed repeatedly by the operator or mechanic.

A constant delay is used when sending numbers to the display. Usually, about four or five seconds between message numbers is sufficient to display the message. After the last message is sent, a null display number is transmitted to clear the display.

There are display units that will store and sequentially display the messages, but it is preferable to let the PLC perform this task. In this way, the display is always in synchronization with the PLC.

There are many ways to consult the 'extrusion expert'. Figure 7.20 shows a typical functional flow chart for an expert based module for a PC.

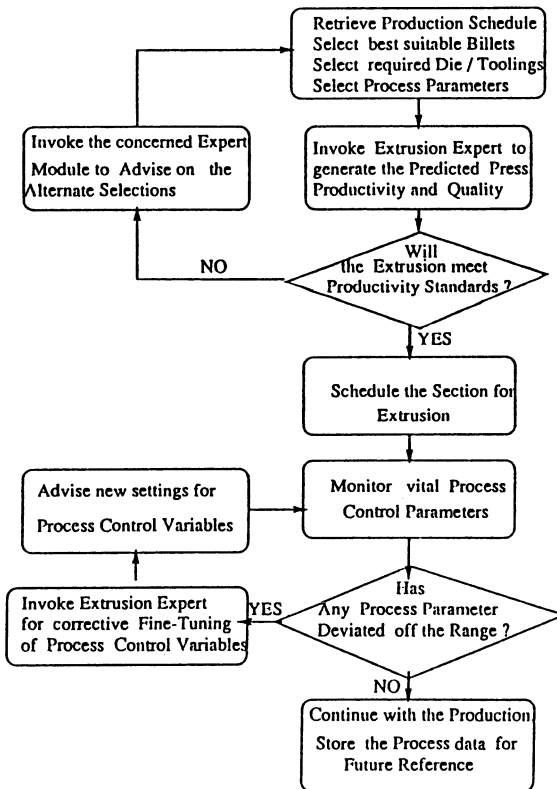


Fig. 7.20 Functional flow chart for expert-based module.

Progressing to more detail we can expect our expert to check during the processing of the product. Figure 7.21 shows a simplified rung of PLC logic. This rung is for the ram forward setup. In order for the ram to move forward, internal coil (CR 56) has to be energized. There are two constants that have to close to do this: Loader Up LS and Discard Shear Up LS. If either one of these limit switches is not closed, the ram will not move forward. These are two of the many possible conditions that must be checked when the ram forward push button is pressed.

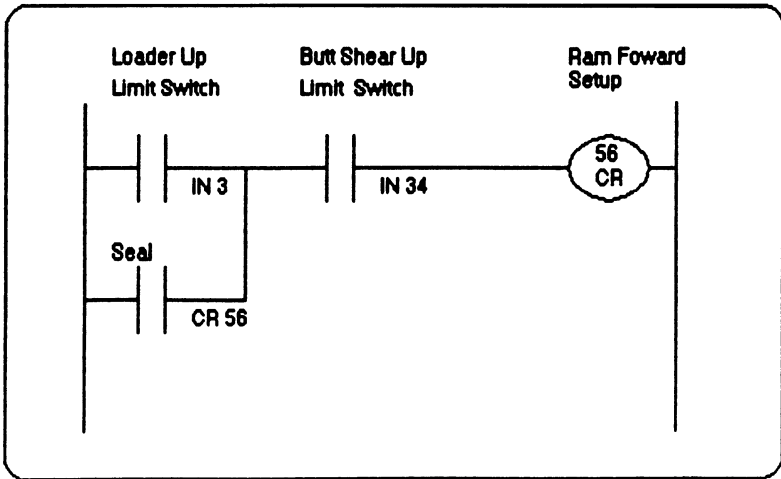


Fig. 7.21 Simplified rung: 'ram forward'.

Figure 7.22 shows the logic for checking for one of these conditions, the loader up limit switch. The object is to set the bit in the holding register that corresponds to this particular problem. Since there are 'n' bits in a register, 'n' errors can be assigned to each holding register.

On each scan of the controller program, the PLC checks all of the bit-follow coils and sets the bits in the holding registers where the coils are energized (where there is a problem). Once all the conditions have been checked, the PLC then codes these registers to a second set of registers that are used to relay the messages to the display panel.

As long as there are messages stored in this second set of registers, the PLC will not scan for any more problems until all message numbers have been sent to the display.

The PLC expert system has become a valuable tool for press operators and mechanics. It has given them instant access to information about the condition of the press. Probably, the real test for success is whether or not the system is really used. It is not uncommon to see the operator glance at the display for a possible message from time to time. The mechanics use the display as their first resource to troubleshoot the press. The PLC program loader with the electrical drawings to troubleshoot the press is rarely used.

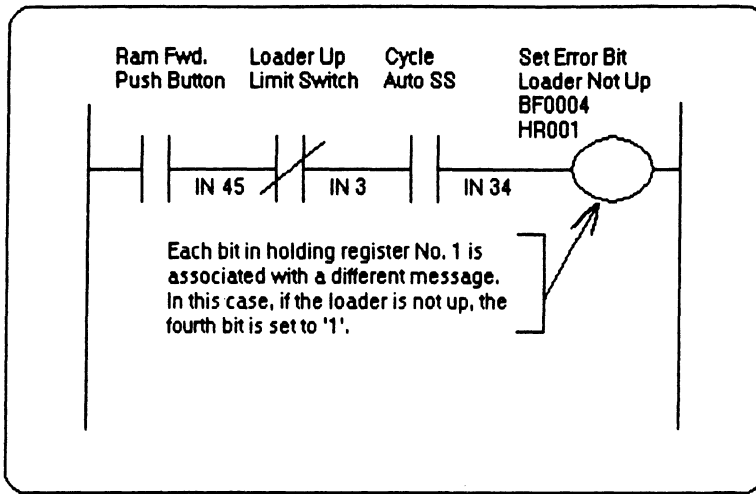


Fig. 7.22 Checking logic for 'ram forward'.

Overall, the potential for expert systems is exciting. With the cost of PC family computers decreasing while their computing power increases, and the growing availability of expert system software, anyone can develop a system for a modest investment in hardware and software.

## 7.6 ASPECTS OF DIE DESIGN AND CORRECTION

Extrusion plants range from the very basic to the most sophisticated with log furnace, billet shear, automatic handling gear etc. However they all have one thing in common: the ultimate success of the plant depends on a relatively small and inexpensive component: the extrusion die. A single press operation in Europe will typically purchase 750–1000 dies a year and a large number of these will be new sections. Very few plants now manufacture their own dies; most prefer to purchase from specialist die manufacturers.

Die making technology has changed dramatically over the past decades and most die makers have invested in CAD/CAM systems [22], CNC machines and wire spark machines to improve quality, delivery and repeatability. The success of a die depends not only on the method of manufacture but also on the skill and experience of the die designer. An extrusion die is a relatively cheap component and it is surprising that many extruders judge a die only on the price of the die and do not take into account the number of die trials needed to get a die into production. Good die design will reduce the overall number of die trials required.

Successful die design depends on close co-operation between the die maker and the extruder, as feedback on the performance of a die is essential. This ensures that a repeat die has a greater chance of being a first time runner.

The die designer has to have an intuitive feel of metal flow and die deflection under load. Unfortunately there has been virtually no work published on flow through commercial dies and a better theoretical knowledge of the factors that control flow through a die is clearly necessary to meet the industry's demand for faster running dies, tighter tolerances, thinner walls and reduced extrusion loads. Die design has evolved over the years to meet the increasing demands of customers, but experience is still the most important factor in good die design.

Die design consists of the following stages:

1. Determine layout, die type and dimensions.
2. Calculate shrinkage allowances on section dimensions.
3. Determine additional dimensional allowances for die dishing and tongue deflection.
4. Calculate bearing lengths to control flow of aluminium through the die.
5. Check that there is adequate support for critical sections.

The basic die configurations in common use at the present time are for solids or hollows and these are shown [23] in Figs. 7.23 and 7.24. Figure 7.23 shows the basic flat die arrangement for solid sections, consisting of the die plate, the backer and the bolster. The die plate contains the cavities that actually form the section. The backer provides the immediate support to the die to reduce die deflection and to minimize the die stresses.

Simple flat sections where deflection is not critical (i.e. no long tongues) are usually extruded using one of a standard range of backers. If the section contains critical sections that need good support then a custom backer with an aperture

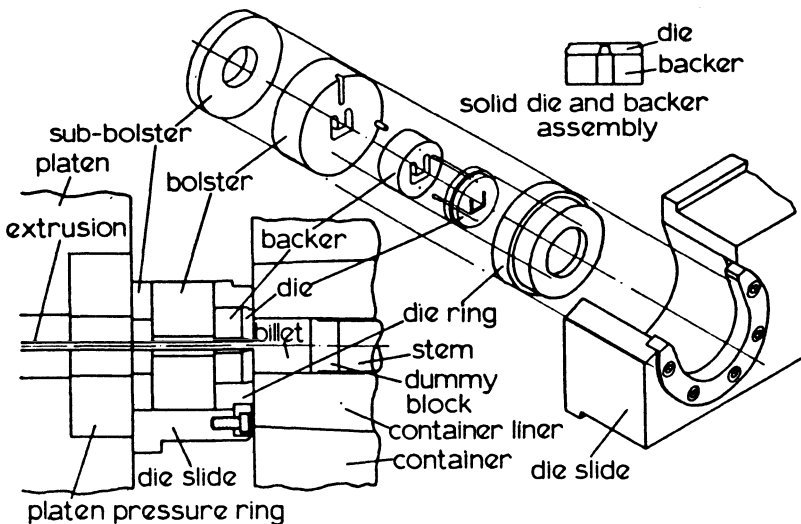
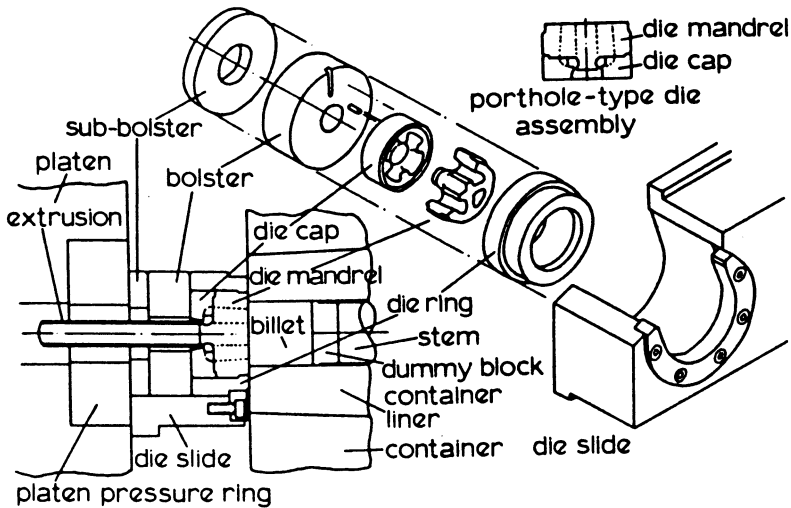


Fig. 7.23 Typical tooling arrangement for aluminium solid sections. (After Glicken.)



**Fig. 7.24** Typical porthole tooling arrangement for aluminium hollow sections. (After Glicken.)

almost identical to that of the die is necessary. This is a factor often ignored by the extruder and frequently leads to out-of-tolerance sections.

The bolster supports the backer and usually sufficient support can be achieved using a standard bolster. If the section is very critical and the designer feels that additional support of the die backer is needed then the usual practice is not to make a special full size bolster but to use an insert bolster designed to match closely the aperture in the die backer. This is held in an insert bolster holder.

A variant of the flat die arrangement is to use an additional feeder plate in front of the die. This is used for a variety of reasons, including:

- to enable successive billets to weld together;
- to enable wider sections to be extruded than is normally possible from any given container size.

Another option used by very many extruders is to sink the face of the die immediately around the cavity in the die plate. Again successive billets can be welded but there are additional advantages in that long thin tongues can be given additional support to minimize tongue deflection.

Hollow extrusions are primarily produced using porthole dies; Fig. 7.24 shows the usual arrangement. Other die arrangements used are: solid porthole, stepover die and shut-off die. These are used for solid sections with excessive tongue ratios; i.e. long thin tongues which if unprotected would lead to excessive die deflection under the action of the full die pressure, the same condition applying to combined solid and hollow sections.

Spider dies and bridge dies are rarely used today because of their limitations.

### 7.6.1 Die stack considerations

The designer has to work within the confines of the overall die stack [24], i.e. die ring bolster and shim, and this is determined by the press supplier. It is sometimes possible to increase the size of the die stack but this is usually expensive. Unfortunately there is no standard for tool dimensions although one was proposed in the mid-1980s; the dimensions in Table 7.4 are based on that proposal and give a good idea of the basic sizes in use today.

**Table 7.4** Typical tool dimensions

<i>Press Size</i>	<i>Total depth of die stack</i>	<i>Die and backer thickness</i>	<i>Die plate thickness</i>
16 MN	400 mm	115 mm*	25, 30, 40 and 50 mm
20 MN	450 mm	135 mm	25, 30, 40 and 50 mm

\*In practice typically between 100 and 128 mm

In practice the total depth of die and backer may have to be increased, e.g. if large hollows are produced on porthole dies where the leg lengths are excessive. A typical range of die and backer depths used in practice on a 20 MN press is:

- solid sections – 100, 160, 190 mm;
- porthole dies – 120, 160, 190 mm.

The die must be an accurate fit in the die ring and the entire die stack assembly must be a good fit inside the horseshoe in the die slide. Consequently certain tolerances are critical. However, it must be remembered that the die, die ring and backer are heated prior to loading into the press and that the dimensions will increase accordingly. Also the temperature of the die stack will vary during the shift and thus the overall stack dimensions will vary. It is therefore necessary to compromise between tight tolerances for accurate location and allowance for the variations in thermal expansion.

### 7.6.2 Die design steps

In the case of hollow sections the procedure also has to include the design of the mandrel including the number of legs and the leg length.

Extrusion tools are subjected to very high loads (although typical die stresses are often a secondary consideration because the major forces are taken by the back-up tooling) and great care must be taken to ensure that the tooling is both strong enough to withstand these loads and rigid enough to minimize deflection. Detailed stress analysis would be very involved and would require 3-dimensional sophisticated FEM programs probably combined with an expert systems approach; this would be impractical for most die designs. Instead the designer has to rely on experience and rules of thumb as well as the simple stress analyses described below. An important point to remember is that the stiffness of a section

is proportional to the width of the section and to the cube of the depth. Consequently depth of support is most important.

### *Die layout*

This is dictated by the availability of support tooling, and by production requirements in terms of handling after extrusion and the need to avoid contact between exposed surfaces and the run-out table. The number of cavities may be specified by the customer or left to the specialist designer and involves consideration of:

- extrusion ratio;
- available runout length;
- cut length required by customer;
- available billet sizes.

The layout used to be arranged to give the optimum flow through the die with all the sections placed symmetrically around the centre. This layout is no longer in use because of the constraints of handling the sections after the press.

Before a die can be designed, the container size and number of die openings for extruding a proposed section must first be established [25]. Die plans are next computed, indicating shrink (shrinkage upon cooling exhibited by the extruded metal), stretch reduction (shrinkage resulting from the stretching or straightening of the extrusions) and bearings. The maximum section that can be produced on a given die must fit within a circumscribing circle having a diameter no greater than 80% of the inner diameter of the container.

### *Bearing treatment*

Fine adjustments to the die, for correcting or changing rates of metal flow, are made by varying the amount of die metal at the aperture, known as bearing width, height or length. This alters the bearing friction. By decreasing the length of the bearing at a particular location the rate of flow is increased, by increasing the length the flow is reduced.

Treatment of bearing surfaces at the front and back of the die aperture is known as 'choke' or 'relief', respectively [25]. If the designer expects to encounter difficulty in filling sharp corners or completing thin sections, the bearing can be choked at an angle up to approximately  $3.5^\circ$ . This slows metal flow and consequently fills out the die aperture. Increasing the angle at the back or exit side of the bearing to as high as  $7^\circ$  to increase the velocity of metal flow, is to relieve, or 'speed' (Fig. 7.25). The effect of bearings on flow is discussed more fully below.

### *Establishing bearing lengths*

Long or short bearing lengths are used as one means of regulating metal flow. Varying bearing lengths are generally found in each die [26]. For instance, if

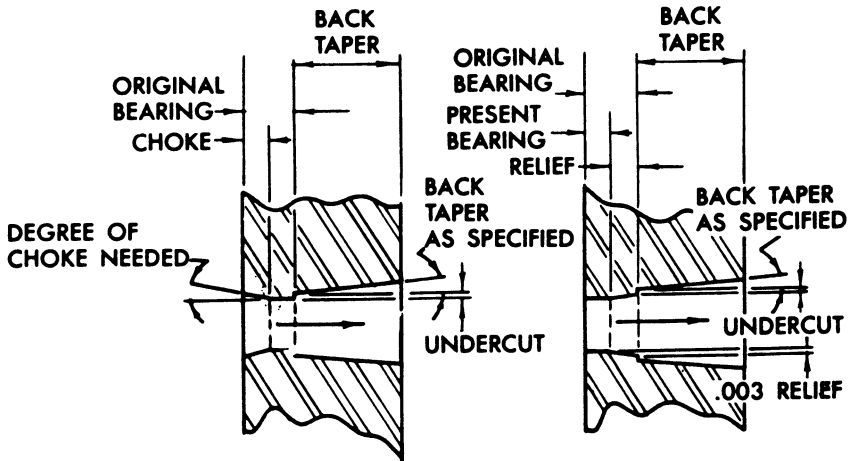


Fig. 7.25 Methods to adjust speed of extrudate using the extrusion die; (a) die opening choked to slow metal flow; (b) relieved die opening to speed metal flow.

adjacent legs of a section have different thicknesses, a bearing length approximately equal to or less than the thickness of each leg will cause a more even flow across the section and reduce twist tendencies.

For determining the dimensions of a second bearing, where an adjacent one is already established, various formulae have been computed. However, they are seldom employed outside the particular plant where used. Most formulae, however, are similar and results are essentially the same. Usually, for computing a bearing length, the designer starts with the smallest practical figure to control more adequately the accompanying section variations.

The European practice, with small sections, is to use a bearing approximately four times the section thickness. In the USA a bearing about equal to the section thickness is employed. Many designers attempt to keep about 2 mm as a minimum length in order to avoid chatter and adjust adjacent bearings to control flow.

An exception to the general rules concerns sections that 'toe' or 'wing in' (Fig. 7.26). The tips of the re-entrant legs need the shortest bearings. This is due to the deflection resulting from cantilevering, which causes a pinching or choking tendency at the bearings.

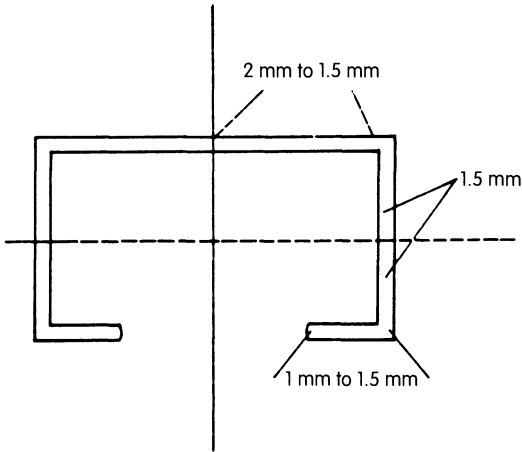
### *Bearing blends*

In addition to the calculations of bearing blends [26] discussed for Fig. 7.27, die designers have adopted variations for efficient production of extrusions.

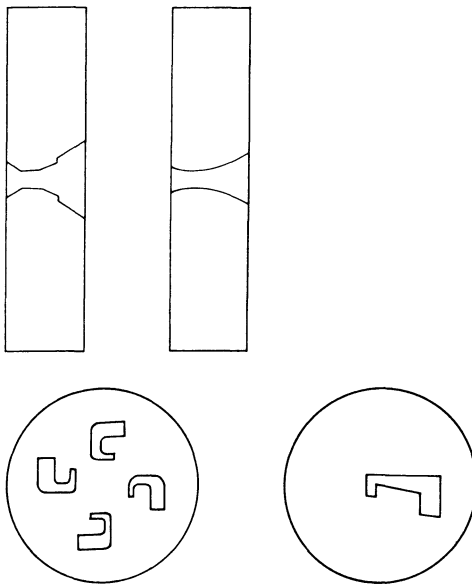
When a section is being run in a soft alloy, exposed surfaces adjacent to bearings having a variation more than 0.75 mm are generally blended at 45° (4.5 mm



$\times 45^\circ$  is sufficient). This is also the case for adjacent bearings on dies used for alloy 7075, having a difference of 3 mm or more. Those having a difference less than 12.5 mm require a single break line. A single break line is also required for designating the beginning or termination of a tapered bearing.



**Fig. 7.26** Example of bearing lengths on a section that 'wings in'; after Lotzenhiser.



**Fig. 7.27** Flow is greater at the centre of the die; hence thinner parts of the sections are placed in that position.

### *Apertures*

It is desirable to use the maximum number of holes in a die when using heat treatable alloys as these extrude relatively slowly. If shapes are complicated, four holes is generally the maximum, but when sections are small and simple, six have proven practical, although slight sacrifice in finish may result in some instances. Greater numbers of extrusions tend to scratch each other as they emerge at different speeds. When a larger production of small rods is undertaken, and special tools are warranted, a series of power-driven blockers can be utilized to keep the rods separated through tension. Little advantage can be gained by using multi-hole dies on alloys such as 1100 and 3003, which extrude easily.

### *Laying out sections*

Laying out a single hole is relatively simple. The normal practice is to place the opening so that its centre of gravity corresponds to the centre of the die. If there are considerable thickness variations, placement enabling the thinnest parts to be at the centre will improve the extruding operation. Typical examples are shown in Fig. 7.27.

If a section is thin and covers a large part of the die, the bearing will have to be increased toward the centre and relieved at its extremities.

Opinions vary as to the best section arrangement for multi-hole dies. These can be laid out radially or flat. The former is usually preferred. In 'radial' layout, the major axis of each shape lies along a radius, giving each portion of bearing surface the same relationship to the centre of the die as similar portions on other shapes.

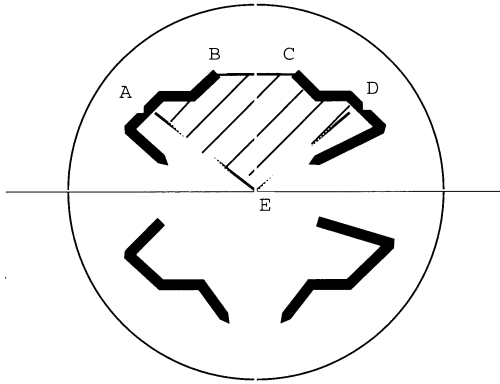
The major axis of each shape is at right angles, or parallel to a radius in 'flat' layout. One advantage in this type of layout is that all strands being extruded can lie on the run-out table with minimum twisting.

It is usually considered good practice to establish for each die size a standard circle (about  $\frac{2}{3}$  the die diameter), upon which all openings are centred. This assures 'backup' interchangeability which we have seen can, on occasions, be a disadvantage. Sections laid out symmetrically, relative to the centre of the die will simplify die correction and minimize twist at the die.

A layout that will assure adequate support on the runout table is to locate sections similar to that shown in Fig. 7.28. By restraining a tendency to twist on the runout table, twisting at the die is also lessened.

### *Bridge widths*

The distance between adjacent shapes of a multi-hole die is called the bridge. The minimum bridge distance is determined by several factors, such as die thickness and support tooling design. The layout also has to take into account the support tooling available. If the layout incorporating the section does not need additional



**Fig. 7.28** Symmetrically laid sections.

support then standard backers and bolsters are used. Custom backers and insert bolsters are used only if the die needs additional support. The designer also has to ensure that the layout follows some basic rules.

#### *Strength formula (bridge shear)*

Figure 7.28 illustrates symmetrically laid sections in a multi-hole die. In this case:

$A_s$  = area ABCDE; bridge width  $l_w = BC$ ; die depth =  $d_t$ ;  
die pressure ( $p$ ) = extrusion load/total die area.

The shear stress ( $\tau$ ) is given by:

$$\tau = \frac{p \times A_s}{l_w \times d_t}$$

Since the layout is symmetrical there is, in this case, no bending stress.

This will also apply to the solid shaped section shown in Fig. 7.29 where the section centre of gravity lies at the centre of the die.

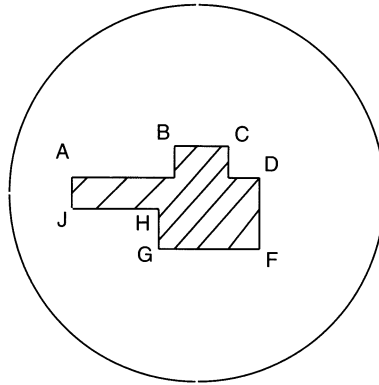
Here the shear stress is given by:

$$\tau = \frac{p \times (A_d - A_s)}{l_p \times d_t}$$

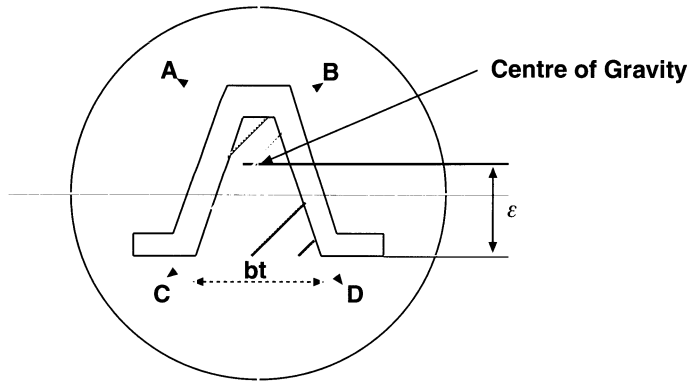
where  $A_d$  is the area of the die,  $A_s$  is the area of the extruded shape,  $l_p$  is the length of the extrude perimeter and  $d_t$  is the die thickness.

In the case of a die with unsupported tongue, as shown in Fig. 7.30, there are both bending and shear stresses.

If  $P$  is the load on the tongue and is equal to  $p \times A_s$  (where  $A_s$  = area ABCD) then the bending moment  $M_b = P \times \varepsilon$  where  $\varepsilon$  is the eccentricity of the section.



**Fig. 7.29** Solid section calculation; note the centre of gravity lies on the die centreline.



**Fig. 7.30** Die with unsupported tongue.

The bending stress is given by:

$$\sigma_b = \frac{6M_b}{b_t d_t^2}$$

The shear stress is given by:

$$\tau = \frac{P}{b_t d_t}$$

and using the Von Mises yield criterion the principal stress is:

$$\sigma_p = \sqrt{(\sigma_b + 3\tau^2)}$$

The stresses on the die backer and bolster must be calculated in a similar manner. It is clearly then important that the stresses are well within the high temperature yield stress of the tool steel material.

### *Dimensional allowances*

Having determined the layout of the sections in the die plate we must concentrate on determining the correct size of die aperture to ensure that the section falls within the tolerances specified. The dimensions of the aperture are increased to allow for the contraction of the aluminium on cooling. There is also the problem of incomplete filling of very thin sections and the increase in shrinkage as the extrusion speed increases.

### *Deflection*

Because of the high pressures and temperatures employed in the extruding process, the die face tends to dish or become concave. The terms 'dishing', 'caving' and 'sagging' are often used synonymously. Such deflection or 'dishing' of the die tends to close the opening, causing the section to extrude undersize. Providing the die is sufficiently supported, any given amount of deflection is proportionate to the circle size of the shape. Deflection [27] is greatest at the centre of the die face and diminishes toward the periphery.

The correction for dishing is usually small and can be ignored except where there is a wide thin part of the section. In this case if no allowance were made for dishing, the centre of the section would extrude thinner than the edges. The correction factor applied depends on the aspect ratio of the section, the overall size of the tool stack and the support under the die.

Tongue deflection has to be allowed for in many sections. The correction that has to be applied to the dimensions of the aperture will depend on the support that can be given to the tongue and whether the die has a sunken face or not. Practical experience has shown that tongue deflection with sunken face dies is less than with flat face dies. Sunken face dies have the additional advantage that the stiffness of the tongue can be increased by including a web running back to the die surface. If tongue ratios are excessive, then more complex designs, e.g. solid porthole or stepover dies, may have to be used.

In a single-hole die, the most severe effect a given amount of die deflection has on the extruded section occurs on those surfaces closest to the centre of the die. Similarly, the effects of deflection in multi-hole dies are generally greatest on those surfaces in each die opening which are closest to the centre of the die face.

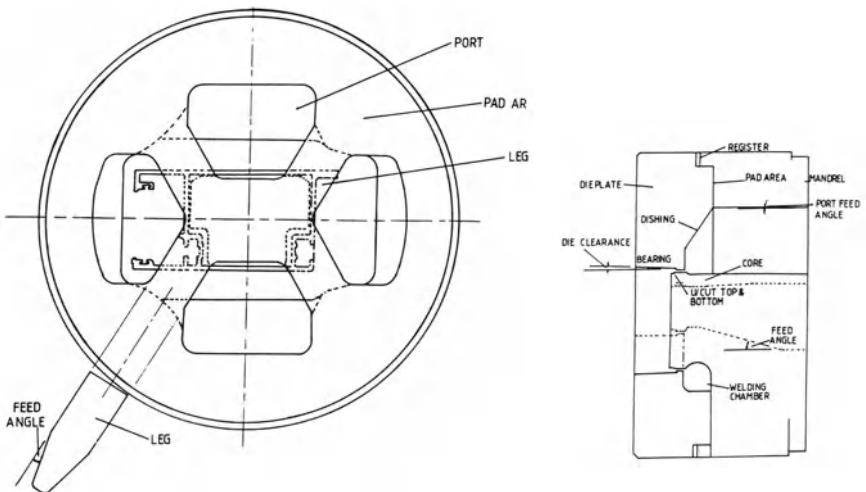
Variations in section thickness, due to deflection, are often difficult to predict. This is especially true where most of the contributing causes are not known or anticipated during the layout period, when probable final dimensions (often loosely referred to as 'shrinkage') must be figured and allowances made. However, experienced die men can usually come close to estimating deformation and make appropriate allowances, when ample data is available.

### *Hollow sections*

The design procedure for hollow dies is obviously more complex [28,29]. The initial stages are identical to those described for flat dies, i.e. determination of layout and dimensional allowances.

Having obtained the layout, the designer then has to determine the number of legs that he can use to support the core (Fig. 7.31). Each leg will result in a weld and these should be positioned as far as possible away from the exposed surfaces. The core is supported entirely by the legs of the mandrel and consequently they must be strong enough to resist the pressure applied by the billet. In this case there is no backer support and the stresses involved are directly related to the extrusion pressure. The stiffness of the core supporting legs is also important as core movement will result in dimensional changes in the finished section. The width of the leg is determined by experience and can range from less than 12 mm on multi-hole dies where four or more legs can be used to over 45 mm for large single-hole dies where the customer requirements permit only a single-leg die. The leg width must not be excessive, otherwise, it will reduce the area of the ports. This, in turn, will increase the extrusion pressure, hindering the maintenance of dimensional accuracy in the product and the efficiency of the weld chamber [30].

All the metal that forms the extrusion must flow through the ports. The mandrel can to some extent be considered to be a multi-cavity die and the designer has to try and ensure equal flow through each port. To achieve uniform flow, variation in the flow of the aluminium from the centre of the billet to the edge has to be considered. The outside edge of the ports should fall within the normal draw



**Fig. 7.31** Basic hollow die arrangement. (After Castle.)

area of  $0.80\text{--}0.90 \times$  the container diameter. The areas are then adjusted to take into account the difference in flow from the centre of the billet to the edge, trying to ensure uniformity of flow.

With the size of the ports fixed, the leg length, the distance from the die face to the bottom of the leg over the welding chamber, can be calculated. The leg length determines the overall stiffness of the core support and a good general rule is to use  $0.7 \times$  the overall leg span. The factor 0.7 may vary from 0.5 to as high as 1.1 depending on the die. The higher values are used on single leg designs where core movement is a problem and a very stiff design is needed.

The flow of the aluminium towards the weld zone is controlled by the feed angle on the legs and this usually falls in the range of  $10\text{--}18^\circ$  and need not be symmetrical. It is good practice to try to ensure that the projected surfaces of the legs meet above the die plate aperture at the point where the weld should be located.

The welding chamber immediately under the leg can be machined into the mandrel or into the die plate (dished die plate). The latter approach is now very common. The size of the welding chamber is governed by the overall leg width. The metal has to flow around the leg and weld behind it before passing through the die aperture. If the weld chamber is not deep enough then unsatisfactory or incomplete welding will occur. On the other hand excessively deep welding chambers also have to be avoided because this adds to the overall length of the core and the die depth. Locating the welding chamber in the die plate also has the advantage that the sides of the chamber can be tapered as a further means of control. Sometimes, particularly on small section multi-cavity dies, it is easier to machine the welding chambers in the die plate rather than in the mandrel.

The overall depth of the die is obtained from the sum of the leg length, the welding chamber depth and the depth of the die plate. This has to be matched to the depth of the support tooling to give the correct tool stack depth.

After completion of the basic die design the final stage is to determine the bearing lengths. The procedure is very similar to that used for flat dies but allowance must be made for the fact that the parts of the sections covered by the legs will not 'see' the aluminium to the same extent as the exposed regions and thus will flow more slowly. Particular care must be given to the selection of bearing lengths for screw bosses and other small details, as these often flow more slowly than expected and thus shorter bearings are needed. The bearings on the core are usually machined 1–2 mm longer than those on the die plate to allow deflection of the core under load and to compensate for any machining errors in the overall core length.

Again it must be emphasized that the design of hollow dies is a very individual process and varies from designer to designer. It will be appreciated by now that there is no single correct method of designing dies. Basic rules have to be followed but the designer has considerable freedom in applying these rules to the basic concepts.

### 7.6.3 Process factors to consider before modifying the die

#### *Press alignment*

Press elements and the die tool assembly must be in proper alignment. Platen, pressure ring (gate lock), die slide (tool carrier), container, liner and stem must be flat and 90° to each component part and also on exact centres. Any misalignment will influence die performance. Misalignment may cause uneven pressures on the die assembly which will influence the flow of aluminium through the orifice of the die, especially on multi-hole, porthole and spider dies. Evidence of press misalignment usually evolves in a definite pattern during running of successive dies. However the latest laser devices can be adopted, giving at least a one monthly check.

#### *Pressure ring or gate lock inspection*

Extrusion pressure rings or gate locks should be inspected periodically for flatness, wear and nicks (monthly is recommended) to ensure good die performance. If the pressure ring or gate lock is permanently deformed, this will cause excess caving or dishing of extrusion tools, creating a problem in holding the contour of complex solid and hollow shapes.

When it is necessary to counteract faulty alignment by adjusting the die, the latter should always be placed in the press in the same position, otherwise the die will have to be readjusted for any new misalignment in subsequent runs. Such practice not only causes excessive press time loss, but can greatly shorten die life. This is also a principal reason for not using the screw index for horizontal die adjustment, except in extreme cases, or for orientation of a die about a fixed mandrel to overcome eccentricities in wall thicknesses of hollow sections.

#### *Extrusion rate*

Excessive speed can accentuate distortion in a shape which may not have been noticeable at a slower extruding rate; fast areas flow faster and slow areas slower (proportionately) as speed is increased. Higher speeds demand better dies and greater skills in die correction.

The use of a homogenized billet is essential for maximum extrusion rates and where extremely thin sections are required. Flow in the last part of a push is often controlled by size of the discard. A high tongue ratio for a deep channel shape is more likely to generate distortion in the last few feet, especially if run fast. This can sometimes be helped by (i) slowing extrusion speed for the last few inches of billet, (ii) increasing discard size, and/or (iii) using a taper-heated billet.



### *Die and press as a unit*

It is important to remember that a die which has been corrected for use in a particular press will not necessarily operate satisfactorily in another [31]. Each press may have its own characteristics, extruding faster or slower in certain segments. When tendencies are known for a press, extruding faults can very often be corrected by a simple step such as a rotation of a die.

### *Container size*

The necessity for adjusting dies for shapes of maximum circle size, in order to eliminate 'roll correction', results in a tendency to depend upon die adjustment to correct all problems. This can be costly. Container size and number of die openings are of major importance, especially for those using self-contained presses. In the latter, maximum ram speed is a fixed value determined by the output of the press pump into the hydraulic cylinder. Thus, productivity is essentially predetermined, except for container size and number of apertures.

More scrap must be anticipated on shapes where container limitations are approached. If attempts to correct this in the die result in distortion of the front end of the extrusion, possibly even plugging the backer, the correction technician has to find a balance between distortion on the front and that on the back of the extrusion. In doing this, he will 'open the die up' and the metal will run toward the high side of tolerance. To correct this, it may be necessary to 'peen' the die. However, this is a last resort action, and in difficult dies usually means that unsatisfactory results will be obtained. Eventually the die must be replaced, and then the situation is the same as before, unless considerable care is exercised in the running of the shape.

### *Aperture location*

Apertures must be carefully placed. For example, when a multi-hole die has one hole higher than the other and the container is accurately centred with the die, the lower hole should run slower. This may be due to the slight cooling of the lower side of the billet after it has contacted the cooler machine components. When the bottom hole is faster it might indicate the container centreline is below the die centre, throwing the bottom hole closer to the centre of pressure. If such is the case, the die can sometimes be turned upside down, putting the top hole on the bottom. If the hole formerly at the top also runs fast in the bottom position, the press may be misaligned. The quickest method of checking for alignment is measuring the die imprint on the butt in relation to the outer diameter of the latter. However a monthly check using economic laser technology is by far the most efficient guarantee for section geometric consistency.

### *Die assembly*

One of the cardinal rules in successful extruding is to make sure that the die assembly is correct. Foreign material such as scrap metal, scale, filings or dirt can cause tool distortion or breakage, even if only fractions of an inch thick, especially when lodged between the die plate and backer.

Before any correction is attempted, it must be certain that no aluminium remains in the area to be filed. All pieces should be shaken or pulled out at the press. Hollow dies should be cleared of aluminium.

### *Improper seating of the die ring*

Improper seating of the die ring in the die slide can lead to misalignment. Dirt accumulation in the bottom of the die ring holder or an upset pin on the backer can hold the die ring out of the normal position. This brings the bottom hole nearer the container centreline, causing faster extrusion. All press tooling should be inspected and cleaned as normal operating procedure.

### *Rotating the die*

When it is possible to rotate the die 90° and have the die openings on either side of the vertical centreline, the die slide can be used to adjust the run-out to a slight degree. However, due to the shape of the die openings, in many cases rotating the die will not be practical.

### *Supporting run-out*

Obtaining consistent results for the full length of the run-out is one of the main problems requiring die correction. A run-out problem may often be solved by the simplest procedures. Light shapes that have little rigidity are aided by graphite canisters. These contact the back of the die and do not allow the soft extrusions to fuse. When fusing does occur and only one string runs faster than the other, a plugged die and stoppage may result.

Distortion can be held to a minimum, where the metal is still soft, by using graphite separators or guides for multiple extrusions. Power-driven conveyors lessen drag on the runout table. However, the conveyor and table top should be at about the same level, or distortion may be caused rather than corrected. The use of carbon blocks or canisters to 'bridge up' the extrusion as it runs out from the press can do much to control the snake-like undulations that sometimes occur. These are caused by the tendency of the extrusion to maintain a straight line relationship with the die opening. It is more pronounced on some of the heavier sections. The extrusion supports itself as a cantilever beam until its own weight pulls it down. Then it immediately starts to cantilever again. This goes on throughout the length of the extrusion in a series of bows. A block of carbon used

to prevent the 'falling' of the shape can very often eliminate the situation by supporting the hot metal until it is sufficiently cool to carry its own weight. Such support is also necessary in many cases to give satisfactory contour results. As the metal is subject to distortion as it leaves the die in a hot state, this can be used to advantage in correcting initial distortion. Experiments with various shapes will show which action is necessary in each instance for best results. However, sufficient support in line with the die opening may be required in addition to any corrective measures.

There will be considerable dishing in the extruding of some shapes if there is no contoured bolster provided for sufficient support. This is caused by extrusion pressure on the face of the die and varies with the temperature and direction of the metal flow entering the die. The metal temperature varies as the billet is extruded, changing the flow pattern, which, in turn, causes change in the die pressure and dish. Control of the die dish, to some extent, is possible by changing metal temperature or flow pattern with taper heating, fast or slow heating, water quench or varying ram speeds. Because these are not constant, the contour of a shape can be different from the lead-out end of an extrusion to the butt end. Isothermal extrusion as described above can ameliorate most of these problems.

#### *Temperature factor in extrusion*

Excessive wear, deflection, springing, poor tolerance and similar problems can be the result of extruding at unsuitable container, billet and/or die temperatures. Heat adjustment, on the other hand, can often eliminate the need for die correction due to those factors, if caught in time. The thickness and contour of the shape being extruded affect billet temperature. Trial runs will determine whether a hotter or colder billet is more satisfactory. Containers should normally be 25 to 75°C cooler than the billet.

When extruding alloy 6063, billet temperatures are determined by the exit temperature of the extrusion from the die. To start the die when extruding 6063, it is normal practice to use a billet of slightly elevated temperature (say, 25°C above normal operating temperature). This will ensure that the die will not 'plug' or 'hang up' due to a cold billet. After stabilizing the die by running two or three billets, the temperature may be reduced to a point that will ensure that the exit temperature of the shape is 500°C or higher. This will produce the best mechanical properties for 6063 alloy extrusions. Exit temperature requirements vary, depending upon alloy, die, section, subsequent heat treatment, other process factors and end-use specifications.

Tube sections may require higher billet temperatures due to the higher extrusion ratios and increased hot work. The ideal operating temperature for each die and alloy may be developed in the above manner.

Billet temperature control can often be employed to offset tongue deflection; a colder billet tends to close and a hotter one to open a 'U' channel, for example. Taper billet heating can also help control contour or size of the shape.

## 7.7 TOOL FAILURE

### 7.7.1 Characteristics

Although aluminium extrusion dies or component tools seldom fail in service, when the correct grades of steels are used, there may be occasional difficulties encountered before an extrusion has run its course.

The most probable types of tool failure include:

- dies – cracking, caving, tongue breakage;
- backers – caving, tongue breakage;
- bolsters – cracking, caving, tongue breakage.

Other failures in tools include splitting, wash (wear or erosion of bearing surfaces resulting in opening of the die orifice), loss of size, heat checking, upsetting, closing in (closure caused by a flow of die material decreasing the opening size), bending or pulling.

### 7.7.2 Preventative measures

Wear, closure, breakage and other conditions influencing tool life are influenced by tool hardness, tool support, alignment, extrusion shape, billet temperature, metal composition of the extrusion, extrusion ratio, extrusion speed, surface conditions and lubrication.

#### *Support*

Most dies fail because proper support is lacking when their elastic limit is reached. It is very important to support a die properly for anticipated operating conditions. Misalignment of extrusion tooling is a common mechanical factor that results in premature failure, ending in poor tolerance, worn, sprung or broken dies.

#### *Extrusion temperature*

This factor in the life of a die is partially determined by the resistance to deformation of an alloy and the extrusion ratio or percentage of reduction for a particular shape. Consistent temperature at the face of the die is necessary for optimum results, as well as maximum die life. For most alloys, tools are preheated from about 200 to about 450°C. For alloys in the higher temperature extruding ranges, tooling should be heated proportionately higher.

When the exit speed is excessive, die life is lowered by the higher frictional temperatures, and their effect on die hardness. This condition, when present, may cause lateral cracks or checks on extrusion finish. The same type extrusion defects can result when extruding speeds are too low, which permit longer die contact with the hot billet.

### *Stress relief*

Stress relieving of stems periodically, as well as of other high-hardness tools when used without preheating, will add to tool life. Frequent inspection of stems will decrease downtime; ultrasonic and magnetic particle methods are often employed. Stems are sometimes stored at about 75°C to maintain their properties.

### *Carburization or decarburization*

These are two of the most common surface conditions contributing to a decrease of the service life of tools. Nitriding of hot work steels to prolong their life is sometimes practised but this makes die correction or salvage more difficult.

### *Die lubrication*

Aluminium extrusion dies are lubricated to improve surface finish of the extruded section, to reduce die wear and to reduce pressure. The lubricant also lessens the tendency of aluminium to adhere to the steel bearing surfaces. Among the lubricants used are: colloidal graphite and water mix; colloidal graphite and oil mix; graphite and grease mix; various mixtures of these and mixtures of low flash point oils or greases which leave a deposit of graphite or carbon on the die.

There are specific reasons for the lubrication of different types of dies, usually due to an operator's preference; indeed it is difficult to predict theoretically that any lubricant will remain very long after experiencing breakthrough.

### *Die cleaning*

The use of sodium hydroxide rather than emery paper for die cleaning can result in a decrease in extrusion pressure and permit lower temperatures, higher speeds and less metal pick-up, partly because of the superior finish on bearing surfaces. Solutions of 10% to 25% are customary. When tanks are employed, 'standard' solutions are the rule, but a higher concentration is necessary if the solution is wiped on. Tank solutions are heated to about 75°C. Thorough rinsing is necessary following cleaning to guard against caustic effects on the aluminium.

## **7.8 SCRAP LOSSES**

When we consider a complete extrusion line from reheating furnace to product stacker; from the end to the beginning of the line there are a host of locations in which scrap occurs [32]:

- stretcher scrap;
- overlengths of extruded profiles;
- hot shear or saw scrap;

- raw material scrap due to die changing;
- billet scrap on the press (extrusion discards);
- billet scrap between foundry and press.

Each of these affect yield and their magnitude is controllable by the extruder. There are other sources of scrap which are more difficult for the extruder to control and which should only occur spasmodically. Examples of this type of defect are:

- die defects or tolerance defects;
- streak marks on profiles and other damage.

This scrap represents about 8–12% of the aluminium weight loaded in the furnace at the beginning of the line and is dealt with in section 7.6.

### 7.8.1 Extrusion losses

#### *Sawing scrap*

The stretching carried out through tension on a 2-head stretcher creates deformation which has to be eliminated by removing both ends. The length varies from 1 to 3 m and clearly does not depend on the length of the extruded profile.

Thus, the percentage scrap which they represent reduces if the length increases. For example 0.5 m scrap on a 50 m profile represents 2% of the total length but only 1% on a 100 m profile. The lengthening created by the stretcher during the stretching operation must be added to the previous scrap although most operators would be able to calculate and allow for this.

Therefore, yield can be improved through the increase of run-out table length. The percentage elongation employed by the stretcher should be automatically preset with the length of the extruded profiles so that it is reproducible and the final length can be more closely controlled.

A device which would ensure a controlled clamping force on the profile in the stretcher jaws would reduce the deformation zone, especially in the case of tubular profiles with a small section and large circumscribed diameter. The principle consists of detecting the contact point between jaw and profile through a pressure signal and carrying out a controlled clamping stroke which results in the deformation of the product being the minimum required without slipping from the jaws. The jaws should have pointed and high teeth, making clamping more effective.

The longitudinal position of the profile in the stretcher also has to be very precise. The positioning of the profile following hot shearing is made much more precise by the use of a puller instead of a conveyor, whose stopping is always linked with the distance between support plates. The precision is 100 mm instead of 400 mm.

The puller also registers the exact extruded length. This allows an automatic and very precise positioning of the mobile head of the stretcher and avoids possible shearing of profiles on the mobile head.

### *Overlengths of extruded profiles*

These arise from the imprecision of the extruded length and from length differences of extruded profiles in multi-hole dies. This indicates the care with which a multi-hole die should be designed

### *Imprecision of extruded length*

This results from variations in the weight of billets introduced into the press when the completion of extrusion is controlled by the press. This imprecision can be eliminated if the stopping is controlled by a puller measuring precisely the extruded length. The length variation is less than 100 mm and the corresponding percentage of scrap is nearly zero.

Extrusion with too short a billet also creates a significant loss since the extruded length is not a multiple of the commercial length.

For installations using precut billets of varying lengths with a 50 mm step, the extruded overlength generally corresponds to a billet section of 25 mm, for a 700 mm average length billet, that is to say 3.6%. In addition to this defect, there is also a tolerance allowed on the billet diameter. A 200 mm diameter with +1.5 mm tolerance creates an average 1.5% overlength.

### *Differences in extruded lengths*

During a multi-hole die operation, differences in length can reach 5% between the longest profile and the shortest one. The average loss represents 2.5%. It can be eliminated through the use of a puller and the improvement of die quality through better total length control.

### *Scrap from hot cut profiles*

The cutting of profiles at the press exit after extrusion is now necessary because of the use of weld plate dies and of automatic pullers. It creates a material loss when the cutting device is too close to the press. The scrap then has a length equal to the distance between the die and the cutting device, that is to say about 1.8 m added to about 0.8 m which will have to be discarded since it is the zone where profiles are welded with those of the following billet (the 'transverse weld').

To avoid this loss, a mobile saw or a mobile shear must be located at a distance from the die at least equal to the commercial length required. In this case, the scrap is limited to 0.8 m which corresponds to the defect zone caused by profile welding (the 'transverse weld'). Figure 7.32 illustrates both cases and shows that the saving is 900 mm or 2.2% of a 40 m length. The 500 mm extreme zones of defects are the overlengths for clamping and profile deformation by the stretcher.

Solution b in Fig. 7.32 requires profile welding ('transverse welds') to be able to resist tensile strains. That is the case with modern prechamber ('pocket' or 'weld-plate') dies.

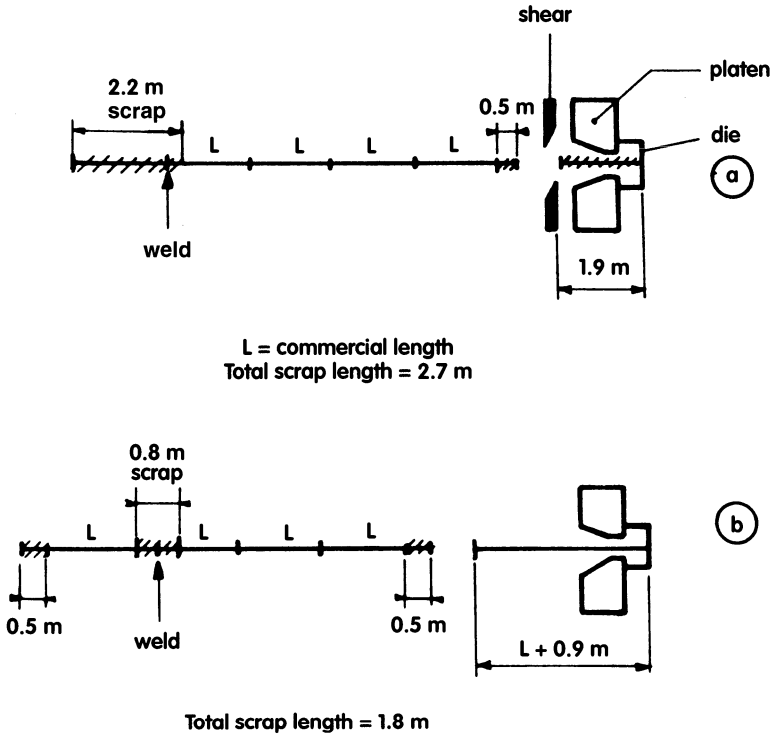


Fig. 7.32 Location of mobile saw.

### Material scrap during die changes

The percentage of scrap due to the change of tooling varies according to the tooling design and the number of changes carried out. It is about 0.7%.

Some presses are fitted with a special ('last billet') cycle used before every tool change, in order to eliminate completely (prechamber die) or almost completely (other die) aluminium left in the tooling. This helps minimize the amount of aluminium to be dissolved in the die cleaning caustic soda bath.

The cycle is called an extracting cycle. At the end of extrusion, due to aluminium shrinking in the container, aluminium can be extracted from the die. Thus, the die is emptied through the return stroke of the container, then the butt is freed and sheared. Therefore, die cleaning is greatly simplified.

## 7.8.2 Billet scrap

### Billet scrap in the press

At the end of extrusion, it is necessary to shear the discard (extrusion scrap). The use of a wide prechamber allows, in presses fitted with knife blade shear, minimum



discards (10–16 mm), retaining at the same time the impurities of the external layer of the billet.

If extrusion is stopped by the puller when the required length is reached, the weight of the billets introduced into the press has to be precisely calculated. The saving is due to discard reduction. Compared with a standard discard of 30 mm, an average discard of 12 mm allows a saving of 2.6% on yield.

Weight control of the billet put into the press can be obtained through shearing or sawing installations at constant weight, with a tolerance of about +0.5%.

This control works at the beginning of each batch where the billet must be allowed to fill the prechamber and the die. It also works at the end of the batch when the billet has to be shorter since there is no profile shearing at the end of extrusion and the whole length between the puller and the die is to be used.

The use of hollow dummy blocks whose expansion is generated by the aluminium pressure applied on a cavity in the front face of the dummy block must be avoided because it greatly increases the butt's weight.

#### *Billet scraps between foundry and press*

Generally, logs obtained through a semi-continuous casting of 6 m length are initially cropped at each end. Then they are either sawed into precut billets, or loaded into the extrusion line if it is fitted with a log shear between furnace and press.

The use of precut billets for extrusion creates a considerable volume of scrap at the foundry level first. When a log of 6 m is cut into billets of 900 mm, for instance, the scrap is 600 mm long, that is 10% of each log. This scrap, except in particular cases, automatically returns to the foundry.

More scrap is produced at the press level if the billet length is not perfectly fitted to the exact length necessary to extrude profiles of different weights, cut into different commercial lengths. Generally, precut billets are stored in fixed lengths with a step of 50 mm. The average loss is about 4%.

The use of a hot billet shear allows the maximum use of logs which have only to be cropped in the foundry. The control of extruded weight is complete and perfectly adjusted according to what is needed, even at the beginning and at the end of each batch. All the material loaded into the furnace can be used when the shears are able to carry out the management of scrap, the shearing at a constant weight, or the correction of sheared length in response to the thickness of the discard measured on the billet previously extruded in the same batch.

#### *Definition of yield*

It is necessary to be absolutely clear on the definition of the yield coefficient  $K$

$$K = \frac{\text{weight of billets introduced into the container}}{\text{weight of profile sold}}$$

This ratio, always higher than 1, varies according to the improvement level of the installation. For instance, for an installation with  $K = 1.3$ , it means that for 1000 kg of profiles sold, 300 kg return to the scrap foundry.

## 7.9 EXTRUSION CONTROL IN MANUFACTURING PROFILES OF COMPLEX SHAPES

There are just three principles which should be maintained in those plants producing particularly difficult complex shapes such as those discussed below:

1. no correction of extruded shapes;
2. complete die correction;
3. no restriction in circumscribing circle, plate thickness and tolerance.

### 7.9.1 Classification of complex shapes

The shape correction factor introduced in section 4.6.3 gives the initial measure of the degree of difficulty of extruding a complex shape:

$$\lambda^2 = \frac{\Omega_s^2}{\Omega_r^2}$$

As this coefficient increases, production becomes increasingly difficult, and dimensional and surface defects are prone to occur.

Apart from this, there are various features that affect the degree of difficulty and which the die designer must consider. These can conveniently be classified as dimensional accuracy of the extrusion cross section, accuracy in the longitudinal direction and surface properties.

It is also useful to distinguish between the intrinsic difficulties of individual section shapes and those variables which cannot easily be described by the simple shape factor. Such features of the shape might, for example, include:

- sections of large circumscribing diameter – divide shape factor by  $D_c/D_b$ ;
- sections with one very thin fin (say 0.5 mm) – introduced as a percentage of cross-section which is thin;
- sections which are offset from the die centreline – multiply the factor by the eccentricity;
- the tongue ratio height – increase  $\lambda$  accordingly;
- the number of holes in a hollow section – treat as two sections;
- sections with tight flatness tolerances;
- sections with a tight angularity tolerance at a right angle;
- sections with tight twist tolerances.

### 7.9.2 Improvement of billet quality

Billet quality is of prime importance to the improvement of productivity in the extrusion process. For those companies having casting and extrusion departments in-house, improvement of billet quality is a matter of prime concern.

One approach to improvement is to observe the surface properties in the extrusion process, for extruded shapes with large circumscribing circles and thin profiles.

#### *Composition control in the melting furnace*

The best approach is to add 50% to 60% scrap to the virgin ingot in the casting process. The use of a melt agitator is essential to make the composition uniform. By using such an agitator, it is possible to control the melt temperature within  $+5^{\circ}\text{C}$ .

#### *Reduction in inverse segregation layer*

It is imperative to reduce the segregation layer by using the hot top process. Billets cast by the conventional DC process can obtain an inverse segregation layer as deep as 120–150  $\mu\text{m}$  whilst billet cast by the hot top process has an inverse segregation layer of only 50  $\mu\text{m}$  or less.

#### *Reduction in oxide inclusions*

Oxide inclusions are eliminated by the use of radiant tube type ceramic filters.

#### *Reduction in gas content*

The gas content in the trough and distributor before or after melt treatment can be measured by the Telegas analyser and the gas content kept below  $0.12\text{ cm}^3$  per 100 litres Al.

The properties of extruded shapes can be remarkably improved with such modifications. Extrusion speed and the production of extruded shapes as well as quality increase substantially.

### 7.9.3 Extrusion press alignment

The centrelines of the stem, container and die slide all move during extrusion even though we might wish them to be coincident. Alignment of press stem, container bore and die slide is critical and greatly affects fixed dummy block life and the stability of the section during complex shape extrusion. An off-centre condition can result in twist, kinks and similar conditions in the extruded section. Many extrusion presses have substantial service and show signs of wear.

### 7.9.4 Extrusion condition

There are tolerances of cross-section and of length in users' specifications. The die factor plays an important role in maintenance of the tolerances in the cross section. Cooling after extrusion greatly affects tolerances in the longitudinal direction.

#### *Billet and die heating*

Correct billet and die heating are crucial. The desired billet temperature settings for each section extruded must be included as part of the set-up condition for the product. Billet temperatures are controlled within 10°C and the billet should be taper heated or the temperature controlled by the methods described above.

#### *Cooling*

The objective must be to cool uniformly from the elevated temperatures to at least some fixed temperature level at a specified cooling rate, to reduce distortion and damage to the product. The extruded shapes must be cooled to 200°C before they are transferred to the cooling table and this must be achieved whilst maintaining all of the Mg<sub>2</sub>Si in solution.

## 7.10 PRODUCT TOLERANCE

The production quantity of profiles for architecture and other critical tolerance uses has greatly increased over the years [33], and a further and a much larger increase in demand for precise tolerance thin-walled section is likely to come from the automotive industry [34]. With this increased production, customers have placed increased demands on the manufacturer in terms of: reduction of thickness of the extruded materials (down to 1 mm wall thickness), improvement in precision of the product dimensions, improvement in quality of the product surface, reduction of the average lot size and significant reduction in the product cost. All the comments made in this chapter will be useful when discussing how these customer demands may be met [35]. Each of the the constituent parts of the process must be considered to investigate the necessary care and modifications.

### 7.10.1 Die section

#### *Modernization of die preparation and maintenance*

Dissolution of Al in the die, and preparation previously done by manual labour must be automated. Equipment to be developed and/or introduced might include:

- automatic cleaning equipment for caustic cleaning of Al in the die;
- a customized die preparation and maintenance line to remove the need for hoisting;

- automatic die polishing machines in the PM line;
- automatic die loading/discard machines;
- computerized control of replacement of the die from the depository shelves, and modification of the working schedule.

These modifications and optimization of die maintenance will ensure the production of the optimum die presented to the press, together with a reduction in die maintenance personnel.

#### *Modifications to die design*

Die designs must be optimized. It has been shown in earlier sections that the pressure exerted on the die can be significantly affected by the layout of the die and the arrangement of portholes etc. It follows that:

- Computer analysis of die stress will allow substantial changes to be made to the die structure. Hollow dies, in particular may be greatly improved.
- The port diameter can be increased specifically by improvements to billet and extruding equipment.

These modifications allow the reduction of extrusion pressure. Thus, shortening the extrusion cycle and increasing extrusion speed such that increases in efficiency can be achieved.

The lead time, which occupies most of production time, may be reduced by introducing:

- standardized port die design (emphasizing port profile and thickness);
- a preprocessing system which includes heat treatment of the preprocessed dies;
- an automatic store for the preprocessed dies.

#### *Modifications to die temperature control*

Superior extrusion is not achieved if the die temperature fluctuates during operation. Recall that the die must be manufactured for a specific die and billet operating temperature. Hence:

1. A computer-controlled die heating system must be installed. Superior control of die heating duration and temperature improves the die temperature stability before extrusion and improves the die surface, thus improving product quality. Die temperature should be controlled in the range of 420–440°C and heating duration controlled in the range of 4–10 h.
2. Temperature control of the die oven and introduction of an induction heater will simplify the computer system.

These modifications will reduce problems caused by the die, and improve the yield and productivity. They also help to increase sales figures by reducing the lead time.

### 7.10.2 Extrusion section

#### *Minimization of die replacement*

Die replacement time can occupy a large part of non-operation time. Minimizing the lot size produces a lower operation rate and this can become an expensive problem. To improve the operation rate it is possible to introduce a system consisting of an automatic die loading/unloading device that automatically supplies a die to the die slide, and discards the used dies. With such modifications, the replacement time can be decreased by 20 s from the 100 s needed with manual labour.

#### *Minimization of idle time*

Minimization of idle time is an important factor in improving extrusion productivity. This implies:

- minimization of time to reach the standard speed by developing and introducing extrusion speed control equipment;
- thorough prevention of obstructive factors to maintain automated synchronization from the first billet;
- development and introduction of precise control measures governing the positions of container, main ram and main shear.

With such modifications, the idle time per billet can typically be reduced by 2.8 s from 22.5 s to 19.7 s. In this case, the idle time is measured from 'stop extrusion' to 'start extrusion', including discarding all residue from the die, inserting an Al billet to the container, carrying out a burp cycle and raising the press pressure to  $100 \text{ N mm}^{-2}$ .

#### *Improving the reliability of the press*

Without improvements in the reliability of the extrusion press, the various modifications would not work efficiently. To improve the efficiency of these modifications, an equipment maintenance schedule must be introduced and rigorously followed. Features might include:

- thorough prevention of oil leakage from both the press and the post-press equipment;
- improvement of extrusion press precision (alignment and its preservation);
- special improvement of the dieslide;
- a continual high standard of maintenance of the equipment after the extrusion press;
- special maintenance on the cooling table;
- improvement of the cutting precision and counter measures for scattered chips.

With these modifications, the idle time of the extrusion press will decrease and the net working rate increase.

### 7.10.3 Billet section

The modifications suggested thus far are mainly to the equipment. An examination of the billet materials and the extrusion conditions must also be evaluated.

#### *Examination of the billet materials*

One of the important factors that improve the extrusion rate is reduction of extruding pressure. As an example, for the 6063 alloy, which is a fairly weakly alloyed material, Mg, the main solute element, controls the deformation resistance during hot working. Therefore, a reduction in the quantity of Mg in the material and an examination of the heat treatment efficiency both at a high temperature and for a shorter time in the continuous heating furnaces may offer opportunities for greater efficiency.

### 7.10.4 Extrusion conditions

Various extrusion faults will occur if the extrusion rate is raised to improve the productivity under conventional conditions. Heat generated during extrusion may cause problems between the die and the extruded material. Extrusion conditions must be examined to prevent extrusion defects and to raise the extrusion rate.

To prevent the occurrence of pick-up, a high strain rate is advisable to enable the product temperature to be lower. Typically for a 1.2 mm wall thickness material a billet temperature of 480°C will allow an extrusion speed of 43 m min<sup>-1</sup> on a complex architectural section.

### 7.10.5 Improvements in yield

Improvements in both yield and productivity are important to manufacturers. Typically the following modifications would tend to produce better quality and yield:

1. development and introduction of an automatic welding machine for longer billets;
2. extension of the cooling table following the extrusion press;
3. lengthening of billets by modification to the press equipment;
4. flexibility in billet size to match extrusion orders;
5. minimization of discard by improvement of billet and modifications of equipment.

Such modifications could improve the yield rate by 5% and, perhaps more importantly, produce material to better tolerance and thinner wall thicknesses than are presently possible.

## REFERENCES

1. Shibamoto, J. and Ohno, M. (1992) Proc. 5th International Extrusion Technology Seminar, Chicago, **2**, 235. Aluminium Association, Washington DC.
2. Bessey, G. (1988) Proc. 4th International Extrusion Technology Seminar, Chicago, **2**, 131. Aluminium Association, Washington DC.
3. Gentry, C.B. (1992) Proc. 5th International Extrusion Technology Seminar, Chicago, **2**, 283. Aluminium Association, Washington DC.
4. Brandal, S.A. (1988) Proc. 4th International Extrusion Technology Seminar, Chicago, **1**, 239. Aluminium Association, Washington DC.
5. Hayes, J. (1992) Proc. 5th International Extrusion Technology Seminar, Chicago, **2**, 293. Aluminium Association, Washington DC.
6. Hayes, J. (1988) Proc. 4th International Extrusion Technology Seminar, Chicago, **1**, 261. Aluminium Association, Washington DC.
7. Schmitz, F. (1996) Proc. 6th International Extrusion Technology Seminar, Chicago, **1**, 281. Aluminium Association, Washington DC.
8. Lange, G. (1972) *Z. Metallkd.*, **62**, 571.
9. Jenista, D. (1996) Proc. 6th International Extrusion Technology Seminar, Chicago, **1**, 131. Aluminium Association, Washington DC.
10. Laue, K. (1960) *Z. Metallkd.*, **51**, 491.
11. Biswas, A.K. and Repgen, B. (1996) Proc. 6th International Extrusion Technology Seminar, **1**, 37. Aluminium Association, Washington DC.
12. Gers, H. (1996) Proc. 6th International Extrusion Technology Seminar, Chicago, **51**. Aluminium Association, Washington DC.
13. Wirtz, R. (1988) Proc. 4th International Extrusion Technology Seminar, Chicago, **1**, 387. Aluminium Association, Washington DC.
14. Raval, S. (1992) Proc. 5th International Extrusion Technology Seminar, Chicago, **1**, 171. Aluminium Association, Washington DC.
15. Bauser, M. and Tuschy, E. (1991) *Control Engineering*, **36**, 237.
16. Bugai, J.C. (1988) Proc. 5th International Extrusion Technology Seminar, Chicago, **1**, 571. Aluminium Association, Washington DC.
17. Gentry, C.B. (1988) Proc. 4th International Extrusion Technology Seminar, Chicago, **1**, 229. Aluminium Association, Washington DC.
18. Raval, S.C. (1992) Proc. 5th International Extrusion Technology Seminar, Chicago, **1**, 171. Aluminium Association, Washington DC.
19. Woodburn, W.A. (1985) *Control Engineering*, **32**, 114.
20. Anonymous (1985) AI to help mechanics at Renault do a better job. *Electronics*, **58**, 27.
21. Nelson, W.R. and Jenkins, J.P. (1992) Proc. 5th International Extrusion Technology Seminar, Chicago, **1**, 231. Aluminium Association, Washington DC.
22. Stockdale, C.O. (1992) Proc. 5th International Extrusion Technology Seminar, Chicago, **1**, 391. Aluminium Association, Washington DC.
23. Glicken, H. (1984) Proc. 2nd International Extrusion Technology Seminar, Atlanta, **2**, 127. Aluminium Association, Washington DC.
24. Castle, A., Flory, R. and Gagg, J. (1988) Proc. 4th International Extrusion Technology Seminar, Chicago, **2**, 25. Aluminium Association, Washington DC.
25. Lotzenhiser, C. (1984) Proc. 2nd International Extrusion Technology Seminar, Atlanta, **2**, 57. Aluminium Association, Washington DC.
26. Thomma, M., Reissner, J. and Lombardi, Z. (1996) Proc. 6th International Extrusion Technology Seminar, Chicago, **2**, 215. Aluminium Association, Washington DC.



27. Rodriguez, R. and Rodriguez, M. (1996) Proc. 6th International Extrusion Technology Seminar, Chicago, **2**, 179. Aluminium Association, Washington DC.
28. Duplancic, I. and Mioc, M. (1996) Proc. 6th International Extrusion Technology Seminar, Chicago, **2**, 169. Aluminium Association, Washington DC.
29. Castle, A.F., Flory, R. and Gagg, J. (1996) Proc. 6th International Extrusion Technology Seminar, Chicago, **2**, 25. Aluminium Association, Washington DC.
30. Valberg, H. (1996) Proc. 6th International Extrusion Technology Seminar, Chicago, **2**, 213. Aluminium Association, Washington DC.
31. Ingraldi, L., Giacomelli, V. and Pedersoli, M. (1992) Proc. 5th International Extrusion Technology Seminar, Chicago, **1**, 369. Aluminium Association, Washington DC.
32. Bessey, G. (1988) Proc. 4th International Extrusion Technology Seminar, Chicago, **1**, 175. Aluminium Association, Washington DC.
33. Takemura, K. (1988) Proc. 4th International Extrusion Technology Seminar, Chicago, **1**, 381. Aluminium Association, Washington DC.
34. Parkinson, R.D. and Logan, R. (1996) Proc. 6th International Extrusion Technology Seminar, Chicago, **2**, 283. Aluminium Association, Washington DC.
35. Hiroysu, N., Masaaki, K. and Kazuo, T. (1996) Proc. 6th International Extrusion Technology Seminar, Chicago, **1**, 45. Aluminium Association, Washington DC.

# **Appendix 1**

## **International alloy designations and chemical composition limits for wrought aluminium and wrought aluminium alloys**

(Courtesy of the Aluminium Association, Washington, DC, and  
the American Extruders Council, Pa)

**CHEMICAL COMPOSITION LIMITS**  
 Only composition limits which are identical to those listed herein for a registered designation (AA No.) are applicable to that designation.

**NATURAL IMPURITY LIMITS FOR WROUGHT UNALLOYED ALUMINIUM**

AA No.	Si	Fe	Cu	Mn	Mg	Cr	Ni	Zn	Ti	Ga	V	Others		Aluminium Minimum
												Each	Total	
1035	0.35	0.6	0.10	0.05	0.05	...	...	0.10	0.03	...	0.05	0.03	...	99.35
1040	0.30	0.50	0.10	0.05	0.05	...	...	0.10	0.03	...	0.05	0.03	...	99.40
1045	0.30	0.45	0.10	0.05	0.05	...	...	0.05	0.03	...	0.05	0.03	...	99.45
1050	0.25	0.40	0.05	0.05	0.05	...	...	0.05	0.03	...	0.05	0.03	...	99.50
1050A	0.25	0.40	0.05	0.05	0.05	...	...	0.07	0.05	...	...	0.03	...	99.50
1060	0.25	0.35	0.05	0.03	0.03	...	...	0.05	0.03	...	0.05	0.03	...	99.60
1065	0.25	0.30	0.05	0.03	0.03	...	...	0.05	0.03	...	0.05	0.03	...	99.65
1070	0.20	0.25	0.04	0.03	0.03	...	...	0.04	0.03	...	0.05	0.03	...	99.70
1070A	0.20	0.25	0.03	0.03	0.03	...	...	0.07	0.03	...	...	0.03	...	99.70
1080	0.15	0.15	0.03	0.02	0.02	...	...	0.03	0.03	0.03	0.05	0.02	...	99.80
1080A	0.15	0.15	0.03	0.02	0.02	...	...	0.06	0.02	0.03	...	0.02	...	99.80
1085	0.10	0.12	0.03	0.02	0.02	...	...	0.03	0.02	0.03	0.05	0.01	...	99.85
1090	0.07	0.07	0.02	0.01	0.01	...	...	0.03	0.01	0.02	0.05	0.01	...	99.90
1098	0.010	0.006	0.003	...	...	...	...	0.015	0.003	...	...	0.003	...	99.98

**REGISTERED COMPOSITIONS**

AA No.	Si	Fe	Cu	Mn	Mg	Cr	Ni	Zn	Ti	Ga	V	Others		Aluminium Minimum
												Each	Total	
1100	...	0.95 Si + Fe	0.05-0.20	0.05	...	...	...	0.10	...	...	...	0.05	0.15	99.00
1200	...	1.00 Si + Fe	0.05	0.05	...	...	...	0.10	0.05	...	...	0.05	0.15	99.00
1200A	...	1.00 Si + Fe	0.10	0.30	0.10	0.10	...	0.10	...	...	...	0.05	0.15	99.00
1110	0.30	0.8	0.04	0.01	0.25	0.01	...	...	...	...	0.02 B, 0.03 V + Ti	0.03	...	99.10
1120	0.10	0.40	0.05-0.35	0.01	0.20	0.01	...	...	...	0.03	0.05 B, 0.02 V + Ti	0.03	0.10	99.20
1230	...	0.70 Si + Fe	0.10	0.05	0.05	...	...	0.10	0.03	...	0.05	0.03	...	99.30
1135	...	0.60 Si + Fe	0.05-0.20	0.04	0.05	...	...	0.10	0.03	...	0.05	0.03	...	99.35
1235	...	0.65 Si + Fe	0.05	0.05	0.05	...	...	0.10	0.06	...	0.05	0.03	...	99.35
1435	0.15	0.30-0.50	0.02	0.05	0.05	...	...	0.10	0.03	...	0.05	0.03	...	99.35
1145	...	0.55 Si + Fe	0.05	0.05	0.05	...	...	0.05	0.03	...	0.05	0.03	...	99.45
1345	0.30	0.40	0.10	0.05	0.05	...	...	0.05	0.03	...	0.05	0.03	...	99.45
1445	...	0.50 Si + Fe	0.04	...	...	...	...	...	...	...	...	...	0.05	99.45
1150	...	0.45 Si + Fe	0.05-0.20	0.05	0.05	...	...	0.05	0.03	...	...	0.03	...	99.50
1350	0.10	0.40	0.05	0.01	...	0.01	...	0.05	...	0.03	...	0.03	0.10	99.50
1350A	0.25	0.40	0.02	...	0.05	...	...	0.05	0.03	...	0.05	0.03	...	99.50
1450	0.25	0.40	0.05	0.05	0.05	...	...	0.07	0.10-20	...	...	0.03	...	99.50
1260	...	0.40 Si + Fe	0.04	0.01	0.03	...	...	0.05	0.03	...	0.05	0.03	...	99.60

REGISTERED COMPOSITIONS continued

AA No.	Si	Fe	Cu	Mn	Mg	Cr	Ni	Zn	Ti	Ga	V	Others		Aluminium Minimum
												Each	Total	
1170	...	0.30 Si + Fe	0.02	0.03	0.02	0.03	...	0.04	0.03	...	0.05	...	0.03	99.70
1370	0.10	0.25	0.02	0.01	0.02	0.01	...	0.04	...	0.03	...	0.02 B, 0.02 V + Ti	0.02	99.70
1175	...	0.15 Si + Fe	0.10	0.02	0.02	...	...	0.04	0.02	0.03	0.05	...	0.02	99.75
1275	0.8	0.12	0.05-0.10	0.02	0.02	...	...	0.03	0.02	0.03	0.03	...	0.01	99.75
1180	0.09	0.09	0.01	0.02	0.02	...	...	0.03	0.02	0.03	0.05	...	0.02	99.80
1185	0.08	0.15 Si + Fe	0.01	0.02	0.02	...	...	0.03	0.02	0.03	0.05	...	0.01	99.85
1285	0.05	0.08	0.02	0.01	0.01	...	...	0.03	0.02	0.03	0.05	...	0.01	99.85
1188	0.06	0.12	0.02	0.01	0.02	0.01	...	0.03	...	0.03	...	0.03 V + Ti	0.01	99.85
1190	0.05	0.06	0.005	0.01	0.01	...	...	0.03	0.01	0.03	0.05	...	0.01	99.88
1193	0.04	0.07	0.01	0.01	0.01	0.01	...	0.02	...	0.02	...	0.01 V + Ti	0.01	99.90
1198	0.010	0.006	0.006	0.006	...	...	...	0.03	0.01	0.03	0.05	...	0.01	99.93
1199	0.006	0.006	0.006	0.002	0.006	...	...	0.010	0.006	0.006	...	...	0.003	99.98
2001	0.20	0.20	5.2-6.0	0.15-0.50	0.20-0.45	0.10	0.05	0.10	0.20	...	0.05 Zr	...	0.05	Remainder
2002	0.35-0.8	0.30	1.5-2.5	0.20	0.50-1.0	0.20	...	0.20	0.20	...	...	...	0.05	Remainder
2003	0.30	0.30	4.0-5.0	0.30-0.8	0.02	...	...	0.10	0.15	...	0.05-0.20	0.10-0.25 Zr	0.05	Remainder
2004	0.20	0.20	5.5-6.5	0.10	0.50	...	...	0.10	0.05	...	0.30-0.50 Zr	...	0.05	Remainder
2005	0.8	0.7	3.5-5.0	1.0	0.20-1.0	0.10	0.20	0.50	0.20	...	...	0.20 Bi, 1.0-2.0 Pb	0.05	Remainder
2006	0.8-1.3	0.7	1.0-2.0	0.6-1.0	0.50-1.4	...	0.20	0.20	0.30	...	...	...	0.05	Remainder
2007	0.8	0.8	3.3-4.6	0.50-1.0	0.40-1.8	0.10	0.20	0.8	0.20	...	...	...	0.10	Remainder
2008	0.50-0.8	0.40	0.7-1.1	0.30	0.25-0.50	0.10	...	0.25	0.10	...	0.05	...	0.05	Remainder
2009	0.25	0.05	3.2-4.4	...	1.0-1.6	...	...	0.10	...	...	...	...	0.05	Remainder
2010	0.50	0.50	0.7-1.3	0.10-0.40	0.40-1.0	0.15	...	0.30	...	...	...	...	0.05	Remainder
2011	0.40	0.7	5.0-6.0	...	...	...	...	0.30	...	...	...	...	0.05	Remainder
2011A	0.40	0.50	4.5-6.0	...	...	...	...	0.30	...	...	...	...	0.05	Remainder
2111	0.40	0.7	5.0-6.0	...	...	...	...	0.30	...	...	...	...	0.05	Remainder
2012	0.40	0.7	4.0-5.5	...	...	...	...	0.30	...	...	...	...	0.05	Remainder
2014	0.50-1.2	0.7	3.9-5.0	0.40-1.2	0.20-0.8	0.10	...	0.30	0.15	...	...	...	0.05	Remainder
2014A	0.50-0.9	0.50	3.9-5.0	0.40-1.2	0.20-0.8	0.10	0.10	0.25	0.15	...	...	0.20 Zr + Ti	0.05	Remainder
2014	0.50-1.2	0.30	3.9-5.0	0.40-1.2	0.20-0.8	0.10	...	0.25	0.15	...	...	...	0.05	Remainder
2217	0.20-0.8	0.7	3.5-4.5	0.40-1.0	0.40-0.8	0.10	...	0.25	0.15	...	...	...	0.05	Remainder
2017A	0.20-0.8	0.7	3.5-4.5	0.40-1.0	0.40-1.0	0.10	...	0.25	0.15	...	...	0.25 Zr + Ti	0.05	Remainder
2117	0.8	0.7	2.2-3.0	0.20	0.20-0.50	0.10	...	0.25	...	...	...	...	0.05	Remainder
2018	0.9	1.0	3.5-4.5	0.20	0.45-0.9	0.10	1.7-2.3	0.25	...	...	...	...	0.05	Remainder
2218	0.9	1.0	3.5-4.5	0.20	1.2-1.8	0.10	1.7-2.3	0.25	...	...	...	...	0.05	Remainder
2618	0.10-0.25	0.9-1.3	1.9-2.7	...	1.3-1.8	...	0.9-1.2	0.10	0.04-0.10	...	...	...	0.05	Remainder
2618A	0.15-0.25	0.9-1.4	1.8-2.7	0.25	1.2-1.8	...	0.8-1.4	0.15	0.20	...	...	0.25 Zr + Ti	0.05	Remainder
2219	0.20	0.30	5.8-6.8	0.20-0.40	0.02	...	...	0.10	0.02-0.10	...	0.05-0.15	0.10-0.25 Zr	0.05	Remainder

REGISTERED COMPOSITIONS continued

AA No.	Si	Fe	Cu	Mn	Mg	Cr	Ni	Zn	Ti	Ga	V	Others		Aluminum Minimum
												Each	Total	
2319	0.20	0.30	5.8-6.8	0.20-0.40	0.02	...	...	0.10	0.10-0.20	...	0.05-0.15	0.10-0.25 Zr	0.05	Remainder
2419	0.15	0.18	5.8-6.8	0.20-0.40	0.02	...	...	0.10	0.02-0.10	...	0.05-0.15	0.10-0.25 Zr	0.05	Remainder
2519	0.25	0.30	5.3-6.4	0.10-0.50	0.05-0.40	...	...	0.10	0.02-0.10	...	0.05-0.15	0.10-0.25 Zr	0.05	Remainder
2021	0.20	0.30	5.8-6.8	0.20-0.40	0.02	...	...	0.10	0.02-0.10	...	0.05-0.15	0.10-0.25 Zr	0.05	Remainder
2024	0.50	0.50	3.8-4.9	0.30-0.9	1.2-1.8	0.10	...	0.25	0.15	...	...	...	0.05	Remainder
2024A	0.15	0.20	3.7-4.5	0.15-0.8	1.2-1.5	0.10	...	0.25	0.15	...	...	...	0.05	Remainder
2124	0.20	0.30	3.8-4.9	0.30-0.9	1.2-1.8	0.10	...	0.25	0.15	...	...	...	0.05	Remainder
2224	0.12	0.15	3.8-4.4	0.30-0.9	1.2-1.8	0.10	...	0.25	0.15	...	...	...	0.05	Remainder
2324	0.10	0.12	3.8-4.4	0.30-0.9	1.2-1.8	0.10	...	0.25	0.15	...	...	...	0.05	Remainder
2424	0.10	0.12	3.8-4.4	0.30-0.6	1.2-1.6	...	...	0.20	0.10	...	...	...	0.05	Remainder
2524	0.06	0.12	4.0-4.5	0.45-0.7	1.2-1.6	0.05	...	0.15	0.10	...	...	...	0.05	Remainder
2025	0.50-1.2	1.0	3.9-5.0	0.40-1.2	0.05	0.10	...	0.25	0.15	...	...	...	0.05	Remainder
2030	0.8	0.7	3.3-4.5	0.20-1.0	0.50-1.3	0.10	...	0.50	0.20	...	0.20 Bi, 0.8-1.5 Pb	...	0.10	Remainder
2031	0.50-1.3	0.6-1.2	1.8-2.8	0.50	0.6-1.2	...	0.6-1.4	0.20	0.20	...	...	...	0.05	Remainder
2034	0.10	0.12	4.2-4.8	0.8-1.3	1.3-1.9	0.05	...	0.20	0.15	...	0.08-0.15 Zr	...	0.05	Remainder
2036	0.50	0.50	2.2-4.0	0.10-0.40	0.30-0.6	0.10	...	0.25	0.15	...	...	...	0.05	Remainder
2037	0.50	0.50	1.4-2.2	0.10-0.40	0.30-0.8	0.10	...	0.25	0.15	...	0.05	...	0.05	Remainder
2038	0.50-1.3	0.6	0.8-1.8	0.10-0.40	0.40-1.0	0.20	...	0.50	0.15	0.05	0.05	...	0.05	Remainder
2048	0.15	0.20	2.8-3.8	0.20-0.6	1.2-1.8	...	...	0.25	0.10	...	...	...	0.05	Remainder
2080	0.10	0.20	3.3-4.1	0.25	1.5-2.2	...	...	0.10	0.10	...	...	...	0.05	Remainder
2090	0.10	0.12	2.4-3.0	0.05	0.25	0.05	...	0.10	0.15	...	...	0.08-0.25 Zr	0.05	Remainder
2091	0.20	0.30	1.8-2.5	0.10	1.1-1.9	0.10	...	0.25	0.10	...	...	0.08-0.15 Zr	0.05	Remainder
2094	0.12	0.15	4.4-5.2	0.25	0.25-0.8	...	...	0.25	0.10	...	...	0.04-0.16 Zr	0.05	Remainder
2095	0.12	0.15	3.9-4.6	0.25	0.25-0.8	...	...	0.25	0.10	...	...	0.04-0.18 Zr	0.05	Remainder
2195	0.12	0.15	3.7-4.3	0.25	0.25-0.8	...	...	0.25	0.10	...	...	0.04-0.16 Zr	0.05	Remainder
X2096	0.12	0.15	2.3-3.0	0.25	0.25-0.89	...	...	0.25	0.10	...	...	0.04-0.18 Zr	0.05	Remainder
2097	0.12	0.15	2.5-3.1	0.10-0.6	0.35	...	...	0.35	0.15	...	...	0.08-0.16 Zr	0.05	Remainder
2197	0.10	0.10	2.5-3.1	0.10-0.50	0.25	...	...	0.05	0.12	...	...	0.08-0.15 Zr	0.05	Remainder
3002	0.08	0.10	0.15	0.05-0.25	0.05-0.20	...	...	0.05	0.03	...	0.05	...	0.03	Remainder
3102	0.40	0.7	0.10	0.05-0.40	...	...	...	0.30	0.10	...	...	...	0.05	Remainder
3003	0.6	0.7	0.05-0.20	1.0-1.5	...	...	...	0.10	...	...	...	...	0.05	Remainder
3103	0.50	0.7	0.10	0.9-1.5	0.30	0.10	...	0.20	...	...	0.10 Zr + Ti	...	0.05	Remainder
3103A	0.50	0.7	0.10	0.7-1.4	0.30	0.10	...	0.20	0.10	...	0.10 Zr + Ti	...	0.05	Remainder
3203	0.6	0.7	0.05	1.0-1.5	...	...	...	0.10	...	...	...	...	0.05	Remainder
3303	0.6	0.7	0.05-0.20	1.0-1.5	...	...	...	0.30	...	...	...	...	0.05	Remainder
3004	0.30	0.7	0.25	1.0-1.5	0.8-1.3	...	...	0.25	...	...	...	...	0.05	Remainder
3004A	0.40	0.7	0.25	0.8-1.5	0.8-1.5	0.10	...	0.25	0.05	...	0.03 Pb	...	0.05	Remainder
3104	0.6	0.8	0.05-0.25	0.8-1.4	0.8-1.3	...	...	0.25	0.10	0.05	0.05	...	0.05	Remainder

REGISTERED COMPOSITIONS continued

AA No.	Si	Fe	Cu	Mn	Mg	Cr	Ni	Zn	Ti	Ga	V	Others		Aluminium
												Each	Total	
3204	0.30	0.7	0.10-0.25	0.8-1.5	0.8-1.5	...	...	0.25	...	...	...	0.05	0.15	Remainder
3005	0.6	0.7	0.30	1.0-1.5	0.20-0.6	0.10	...	0.25	0.10	...	...	0.05	0.15	Remainder
3105	0.6	0.7	0.30	0.30-0.8	0.20-0.8	0.20	...	0.40	0.10	...	...	0.05	0.15	Remainder
3105A	0.6	0.7	0.30	0.30-0.8	0.20-0.8	0.20	...	0.25	0.10	...	...	0.05	0.15	Remainder
3006	0.50	0.7	0.10-0.30	0.50-0.8	0.30-0.6	0.20	...	0.15-0.40	0.10	...	...	0.05	0.15	Remainder
3007	0.50	0.7	0.05-0.30	0.30-0.8	0.6	0.20	...	0.40	0.10	...	...	0.05	0.15	Remainder
3107	0.6	0.7	0.05-0.15	0.40-0.9	...	...	...	0.20	0.10	...	...	0.05	0.15	Remainder
3207	0.30	0.45	0.10	0.40-0.8	0.10	...	...	0.10	0.10	...	...	0.05	0.10	Remainder
3207A	0.35	0.6	0.25	0.30-0.8	0.40	0.20	...	0.25	...	...	...	0.05	0.15	Remainder
3307	0.6	0.8	0.30	0.50-0.9	0.30	0.20	...	0.40	0.10	...	...	0.05	0.15	Remainder
3009	1.0-1.8	0.7	0.10	1.2-1.8	0.10	0.05	0.05	0.05	0.10	...	0.10 Zr	0.05	0.15	Remainder
3010	0.10	0.20	0.03	0.20-0.9	...	0.05-0.40	...	0.05	0.05	...	...	0.03	0.10	Remainder
3011	0.40	0.7	0.05-0.20	0.8-1.2	...	0.10-0.40	...	0.10	0.10	...	0.10-0.30 Zr	0.05	0.15	Remainder
3012	0.6	0.7	0.10	0.50-1.1	0.10	0.20	...	0.10	0.10	...	...	0.05	0.15	Remainder
3013	0.6	1.0	0.50	0.9-1.4	0.20-0.6	...	...	0.50-1.0	...	...	...	0.05	0.15	Remainder
3014	0.6	1.0	0.50	1.0-1.5	0.10	...	...	0.50-1.0	0.10	...	...	0.05	0.15	Remainder
3015	0.6	0.8	0.30	0.50-0.9	0.20-0.7	0.10	...	0.25	0.10	...	...	0.05	0.15	Remainder
3016	0.6	0.8	0.30	0.50-0.9	0.50-0.8	0.10	...	0.25	0.10	...	...	0.05	0.15	Remainder
3017	0.25	0.25-0.45	0.25-0.40	0.8-1.2	0.10	0.15	...	0.10	0.05	...	...	0.05	0.15	Remainder
3018	0.30	0.15-0.25	0.10-0.30	1.1-1.4	0.8-1.4	0.10	...	0.25	0.10	...	0.01 Pb	0.05	0.15	Remainder
X3030	0.15	0.35	0.10	0.10-0.7	0.05	0.05	...	0.05-0.50	0.50-0.35	...	...	0.05	0.15	Remainder
4004	9.0-10.5	0.8	0.25	0.10	1.0-2.0	...	...	0.20	...	...	...	0.05	0.15	Remainder
4104	9.0-10.5	0.8	0.25	0.10	1.0-2.0	...	...	0.20	...	...	0.02-0.20 Bi	0.05	0.15	Remainder
4006	0.8-1.2	0.50-0.8	0.10	0.05	0.01	0.20	...	0.05	...	...	...	0.05	0.15	Remainder
4007	1.0-1.7	0.40-1.0	0.20	0.8-1.5	0.20	0.05-0.25	0.15-0.7	0.10	0.10	...	0.05 Co	0.05	0.15	Remainder
4008	6.5-7.5	0.09	0.05	0.05	0.30-0.45	...	...	0.05	0.04-0.15	...	...	0.05	0.15	Remainder
4009	4.5-5.5	0.20	1.0-1.5	0.10	0.45-0.6	...	...	0.10	0.20	...	...	0.05	0.15	Remainder
4010	6.5-7.5	0.20	0.20	0.10	0.30-0.45	...	...	0.10	0.20	...	...	0.05	0.15	Remainder
4011	6.5-7.5	0.20	0.20	0.10	0.45-0.7	...	...	0.10	0.04-0.20	...	0.04-0.07 Be	0.05	0.15	Remainder
4013	3.5-4.5	0.35	0.05-0.20	0.03	0.05-0.20	...	...	0.05	0.02	...	...	0.05	0.15	Remainder
4014	1.4-2.2	0.7	0.20	0.35	0.30-0.8	...	...	0.20	...	...	...	0.05	0.15	Remainder
4015	1.4-2.2	0.7	0.20	0.6-1.2	0.10-0.50	...	...	0.50-1.3	...	...	...	0.05	0.15	Remainder
4016	1.4-2.2	0.7	0.20	0.6-1.2	0.10	...	...	0.20	...	...	...	0.05	0.15	Remainder
4017	0.6-1.6	0.7	0.10-0.50	0.6-1.2	0.10-0.50	...	...	0.20	...	...	...	0.05	0.15	Remainder
4018	6.5-7.5	0.20	0.05	0.10	0.50-0.8	...	...	0.25	0.10	0.20	...	0.05	0.15	Remainder
4032	11.0-13.5	1.0	0.50-1.3	...	0.8-1.3	0.10	0.50-1.3	0.25	...	...	...	0.05	0.15	Remainder
4043	4.5-6.0	0.8	0.30	0.05	0.05	...	...	0.10	0.20	...	...	0.05	0.15	Remainder
4043A	4.5-6.0	0.6	0.30	0.15	0.20	...	...	0.10	0.15	...	...	0.05	0.15	Remainder

## REGISTERED COMPOSITIONS continued

AA No.	Si	Fe	Cu	Mn	Mg	Cr	Ni	Zn	Ti	Ga	V	Others		Aluminum Minimum
												Each	Total	
4343	6.8-8.2	0.8	0.25	0.10	...	...	...	0.20	...	...	...	0.05	0.15	Remainder
4543	5.0-7.0	0.50	0.10	0.05	0.10-0.40	0.05	...	0.10	0.10	...	...	0.05	0.15	Remainder
4643	3.6-4.6	0.8	0.10	0.05	0.10-0.30	...	...	0.10	0.15	...	...	0.05	0.15	Remainder
4044	7.8-9.2	0.8	0.25	0.10	...	...	...	0.20	...	...	...	0.05	0.15	Remainder
4045	9.0-11.0	0.8	0.30	0.05	0.05	...	...	0.10	0.20	...	...	0.05	0.15	Remainder
4145	9.3-10.7	0.8	3.3-4.7	0.15	0.15	0.15	...	0.20	0.15	...	...	0.05	0.15	Remainder
4145A	9.0-11.0	0.6	3.0-5.0	0.15	0.10	...	...	0.20	0.15	...	...	0.05	0.15	Remainder
4046	9.0-11.0	0.50	0.03	0.40	0.20-0.50	...	...	0.10	0.15	...	...	0.05	0.15	Remainder
4047	11.0-13.0	0.8	0.30	0.15	0.10	...	...	0.20	0.15	...	...	0.05	0.15	Remainder
4047A	11.0-13.0	0.6	0.30	0.15	0.10	...	...	0.20	0.15	...	...	0.05	0.15	Remainder
4147	11.0-13.0	0.8	0.25	0.10	0.10-0.50	...	...	0.20	0.15	...	...	0.05	0.15	Remainder
4048	9.3-10.7	0.8	3.3-4.7	0.07	0.07	0.07	...	9.3-10.7	...	...	...	0.05	0.15	Remainder
5005	0.30	0.7	0.20	0.20	0.50-1.1	0.10	...	0.25	...	...	...	0.05	0.15	Remainder
5005A	0.30	0.45	0.05	0.15	0.7-1.1	0.10	...	0.20	0.20	...	...	0.05	0.15	Remainder
5205	0.15	0.7	0.03-0.10	0.10	0.6-1.0	0.10	...	0.05	0.05	...	...	0.05	0.15	Remainder
5305	0.08	0.08	...	0.03	0.7-1.1	...	...	0.05	0.02	...	...	0.02	...	Remainder
5505	0.06	0.04	...	0.03	0.8-1.1	...	...	0.04	0.01	...	...	0.01	...	Remainder
5605	0.01	0.008	...	...	0.8-1.1	...	...	0.01	0.008	0.008 Fe + Ti	...	0.003	...	Remainder
5006	0.40	0.8	0.10	0.40-0.8	0.8-1.3	0.10	...	0.25	0.10	...	...	0.05	0.15	Remainder
5010	0.40	0.7	0.25	0.10-0.30	0.20-0.6	0.15	...	0.30	0.10	...	...	0.05	0.15	Remainder
5110	0.08	0.08	...	0.03	0.30-0.6	...	...	0.05	0.02	...	...	0.02	...	Remainder
5210	0.06	0.04	...	0.03	0.35-0.6	...	...	0.04	0.01	...	...	0.01	...	Remainder
5310	0.01	0.008	...	...	0.35-0.6	...	...	0.01	0.008	0.008 Fe + Ti	...	0.003	...	Remainder
5014	0.40	0.40	0.20	0.20-0.9	4.0-5.5	0.20	...	0.7-1.5	0.20	...	...	0.05	0.15	Remainder
5016	0.25	0.6	0.20	0.40-0.7	1.4-1.9	0.10	...	0.15	0.05	...	...	0.05	0.15	Remainder
5017	0.40	0.7	0.18-0.28	0.6-0.8	1.9-2.2	...	...	...	0.09	...	...	0.05	0.15	Remainder
5018	0.25	0.40	0.05	0.20-0.6	2.6-3.6	0.30	...	0.20	0.15	...	...	0.05	0.15	Remainder
5019	0.40	0.50	0.10	0.10-0.6	4.5-5.6	0.20	...	0.20	0.20	0.20-0.6 Mn + Cr	...	0.05	0.15	Remainder
5119	0.25	0.40	0.05	0.20-0.6	4.5-5.6	0.30	...	0.20	0.15	0.10-0.6 Mn + Cr	...	0.05	0.15	Remainder
5021	0.40	0.50	0.10	0.10-0.50	2.2-2.8	0.15	...	0.15	...	0.20-0.6 Mn + Cr	...	0.05	0.15	Remainder
5022	0.25	0.40	0.20-0.50	0.20	3.5-4.9	0.10	...	0.25	0.10	...	...	0.05	0.15	Remainder
5023	0.25	0.40	0.20-0.50	0.20	5.0-6.2	0.10	...	0.25	0.10	...	...	0.05	0.15	Remainder
5040	0.25	0.7	0.25	0.9-1.4	1.0-1.5	0.10-0.30	...	0.25	0.15	...	...	0.05	0.15	Remainder
5042	0.20	0.35	0.15	0.20-0.50	30-4.0	0.10	...	0.25	0.10	...	...	0.05	0.15	Remainder
5043	0.40	0.7	0.05-0.35	0.7-1.2	0.7-1.3	0.05	...	0.25	0.10	0.05	0.05	0.05	0.15	Remainder
5049	0.40	0.50	0.10	0.50-1.1	1.6-2.5	0.30	...	0.20	0.10	...	...	0.05	0.15	Remainder
5149	0.25	0.40	0.05	0.50-1.1	1.6-2.5	0.30	...	0.20	0.15	...	...	0.05	0.15	Remainder
5249	0.25	0.40	0.05	0.50-1.1	1.6-2.5	0.30	...	0.20	0.15	0.10-0.20 Zr	...	0.05	0.15	Remainder

REGISTERED COMPOSITIONS continued

AA No.	Si	Fe	Cu	Mn	Mg	Cr	Ni	Zn	Ti	Ga	V	Others		Aluminium
												Each	Total	
5349	0.40	0.7	0.18-0.28	0.6-1.2	1.7-2.6	...	...	...	0.09	...	...	0.05	0.15	Remainder
5449	0.40	0.7	0.30	0.6-1.1	1.6-2.6	0.30	...	0.30	0.10	...	...	0.05	0.15	Remainder
5050	0.40	0.7	0.20	0.10	1.1-1.8	0.10	...	0.25	...	...	...	0.05	0.15	Remainder
5050A	0.40	0.7	0.20	0.30	1.1-1.8	0.10	...	0.25	...	...	...	0.05	0.15	Remainder
5150	0.08	0.10	0.10	0.03	1.3-1.7	...	...	0.10	0.06	...	...	0.03	0.10	Remainder
5250	0.08	0.10	0.10	0.04-0.15	1.3-1.8	...	...	0.05	...	0.03	0.05	0.03	0.10	Remainder
5051	0.40	0.7	0.25	0.20	1.7-2.2	0.30	...	0.25	0.10	...	...	0.05	0.15	Remainder
5051A	0.30	0.45	0.05	0.25	1.4-2.1	0.30	...	0.20	0.10	...	...	0.05	0.15	Remainder
5151	0.20	0.35	0.15	0.10	1.5-2.1	0.10	...	0.15	0.10	...	...	0.05	0.15	Remainder
5251	0.40	0.50	0.15	0.10-0.50	1.7-2.4	0.15	...	0.15	0.15	...	...	0.05	0.15	Remainder
5251A	0.50	0.7	0.25	0.20-0.7	1.6-2.2	0.10	...	0.25	0.10	...	...	0.05	0.15	Remainder
5351	0.08	0.10	0.10	0.10	1.6-2.2	...	...	0.05	...	...	0.05	0.03	0.10	Remainder
5451	0.25	0.40	0.10	0.10	1.8-2.4	0.15-0.35	0.05	0.10	0.05	...	...	0.05	0.15	Remainder
5052	0.25	0.40	0.10	0.10	2.2-2.8	0.15-0.35	...	0.10	...	...	...	0.05	0.15	Remainder
5252	0.08	0.10	0.10	0.10	2.2-2.8	...	...	0.05	...	...	0.05	0.03	0.10	Remainder
5352	...	0.45 Si + Fe	0.10	0.10	2.2-2.8	0.10	...	0.10	0.10	...	...	0.05	0.15	Remainder
5552	0.04	0.05	0.10	0.10	2.2-2.8	...	...	0.05	...	...	0.05	0.03	0.10	Remainder
5652	...	0.40 Si + Fe	0.04	0.01	2.2-2.8	...	...	0.10	...	...	...	0.05	0.15	Remainder
5154	0.25	0.40	0.10	0.10	3.1-3.9	0.15-0.35	...	0.20	0.20	...	...	0.05	0.15	Remainder
5154A	0.50	0.50	0.10	0.50	3.1-3.9	0.25	...	0.20	0.20	...	...	0.05	0.15	Remainder
5154B	0.35	0.45	0.05	0.15-0.45	3.2-3.8	0.10	0.01	0.15	0.15	...	...	0.05	0.15	Remainder
5254	...	0.45 Si + Fe	0.05	0.01	3.1-3.9	0.15-0.35	...	0.20	0.05	...	...	0.05	0.15	Remainder
5354	0.25	0.40	0.05	0.50-1.0	2.4-3.0	0.05-0.20	...	0.25	0.15	...	...	0.05	0.15	Remainder
5454	0.25	0.40	0.10	0.50-1.0	2.4-3.0	0.05-0.20	...	0.25	0.20	...	...	0.05	0.15	Remainder
5554	0.25	0.40	0.10	0.50-1.0	2.4-3.0	0.05-0.20	...	0.25	0.05-0.20	...	...	0.05	0.15	Remainder
5654	...	0.45 Si + Fe	0.05	0.01	3.1-3.9	0.15-0.35	...	0.20	0.05-0.15	...	...	0.05	0.15	Remainder
5754	0.40	0.40	0.10	0.50	2.6-3.6	0.30	...	0.20	0.15	...	...	0.05	0.15	Remainder
5954	0.25	0.40	0.10	0.10	3.3-4.1	0.10	...	0.20	0.20	...	...	0.05	0.15	Remainder
5056	0.30	0.40	0.10	0.05-0.20	4.5-5.6	0.05-0.20	...	0.10	...	...	...	0.05	0.15	Remainder
5356	0.25	0.40	0.10	0.05-0.20	4.5-5.5	0.05-0.20	...	0.10	0.06-0.20	...	...	0.05	0.15	Remainder
5456	0.25	0.40	0.10	0.50-1.0	4.7-5.5	0.05-0.20	...	0.25	0.20	...	...	0.05	0.15	Remainder
5456A	0.25	0.40	0.05	0.7-1.1	4.5-5.2	0.05-0.25	...	0.25	0.15	...	...	0.05	0.15	Remainder
5556	0.25	0.40	0.10	0.50-1.0	4.7-5.5	0.05-0.20	...	0.25	0.05-0.20	...	...	0.05	0.15	Remainder
5556A	0.25	0.40	0.10	0.6-1.0	5.0-5.5	0.05-0.20	...	0.20	0.05-0.20	...	...	0.05	0.15	Remainder
5257	0.08	0.10	0.10	0.03	0.20-0.6	...	...	0.03	...	...	...	0.02	0.15	Remainder
5357	0.12	0.17	0.20	0.15-0.45	0.8-1.2	...	...	0.05	...	...	...	0.05	0.15	Remainder
5457	0.08	0.10	0.20	0.15-0.45	0.8-1.2	...	...	0.05	...	...	0.05	0.03	0.10	Remainder
5557	0.10	0.12	0.15	0.10-0.40	0.40-0.8	...	...	0.05	...	...	0.05	0.03	0.10	Remainder
5657	0.08	0.10	0.10	0.03	0.6-1.0	...	...	0.05	...	0.03	0.05	0.02	0.05	Remainder



REGISTERED COMPOSITIONS continued

AA No.	Si	Fe	Cu	Mn	Mg	Cr	Ni	Zn	Ti	Ga	V	Others		Aluminum Minimum		
												Each	Total			
5058	0.40	0.50	0.10	0.20	4.5-5.6	0.10	...	0.20	0.20	...	...	...	0.05	0.15	Remainder	
5180	...	0.35 Si + Fe	0.10	0.20-0.7	3.5-4.5	0.10	...	1.7-2.8	0.06-0.20	...	...	...	0.08-0.25 Zr	0.05	0.15	Remainder
5082	0.20	0.35	0.15	0.15	4.0-5.0	0.10	...	0.25	0.10	...	...	...	...	0.05	0.15	Remainder
5182	0.20	0.35	0.15	0.20-0.50	4.0-5.0	0.10	...	0.25	0.10	...	...	...	...	0.05	0.15	Remainder
5083	0.40	0.40	0.10	0.40-1.0	4.0-4.9	0.05-0.25	...	0.25	0.15	...	...	...	...	0.05	0.15	Remainder
5183	0.40	0.40	0.10	0.50-1.0	4.3-5.2	0.05-0.25	...	0.25	0.15	...	...	...	...	0.05	0.15	Remainder
5283A	0.30	0.30	0.03	0.50-1.0	4.5-5.1	0.05	0.03	0.10	0.03	...	...	...	0.05 Zr	0.05	0.15	Remainder
5283A	0.30	0.30	0.03	0.50-1.0	4.5-5.1	0.05	0.03	0.10	0.03	...	...	...	0.05 Zr	0.05	0.15	Remainder
5383	0.25	0.25	0.20	0.7-1.0	4.0-5.2	0.25	...	0.40	0.15	...	...	...	0.20 Zr	0.05	0.15	Remainder
5086	0.40	0.50	0.10	0.20-0.7	3.5-4.5	0.05-0.25	...	0.25	0.15	...	...	...	...	0.05	0.15	Remainder
5186	0.40	0.45	0.25	0.20-0.50	3.8-4.8	0.15	...	0.40	0.15	...	...	...	0.05 Zr	0.05	0.15	Remainder
5087	0.25	0.40	0.05	0.7-1.1	4.5-5.2	0.05-0.25	...	0.25	0.15	...	...	...	0.10-0.20 Zr	0.05	0.15	Remainder
5091	0.20	0.30	...	...	3.7-4.2	...	...	...	...	...	...	...	...	0.05	0.15	Remainder
6101	0.30-0.7	0.50	0.10	0.03	0.35-0.8	0.03	...	0.10	...	...	...	...	0.06 B	0.03	0.10	Remainder
6101A	0.30-0.7	0.40	0.05	...	0.40-0.9	...	...	...	...	...	...	...	...	0.03	0.10	Remainder
6101B	0.30-0.6	0.10-0.30	0.05	0.05	0.35-0.6	...	...	0.10	...	...	...	...	...	0.03	0.10	Remainder
6201	0.50-0.9	0.50	0.10	0.03	0.6-0.9	0.03	...	0.10	...	...	...	...	0.06 B	0.03	0.10	Remainder
6201A	0.50-0.7	0.50	0.04	...	0.6-0.9	...	...	...	...	...	...	...	0.06 B	0.03	0.10	Remainder
6301	0.50-0.9	0.7	0.10	0.15	0.6-0.9	0.10	...	0.25	0.15	...	...	...	...	0.05	0.15	Remainder
6401	0.35-0.7	0.04	0.05-0.20	0.03	0.35-0.7	...	...	0.04	0.01	...	...	...	...	0.01	...	Remainder
6002	0.6-0.9	0.25	0.10-0.25	0.10-0.20	0.45-0.7	0.05	...	...	0.08	...	...	...	0.09-0.14 Zr	0.05	0.15	Remainder
6003	0.35-1.0	0.6	0.10	0.8	0.8-1.5	0.35	...	0.20	0.10	...	...	...	...	0.05	0.15	Remainder
6103	0.35-1.0	0.6	0.20-0.30	0.8	0.8-1.5	0.35	...	0.20	0.10	...	...	...	...	0.05	0.15	Remainder
6004	0.30-0.6	0.10-0.30	0.10	0.20-0.6	0.40-0.7	...	...	0.05	...	...	...	...	...	0.05	0.15	Remainder
6005	0.6-0.9	0.35	0.10	0.10	0.40-0.6	0.10	...	0.10	0.10	...	...	...	...	0.05	0.15	Remainder
6005A	0.50-0.9	0.35	0.30	0.50	0.40-0.7	0.30	...	0.20	0.10	...	...	...	0.12-0.50 Mn + Cr	0.05	0.15	Remainder
6005B	0.45-0.8	0.30	0.10	0.10	0.40-0.8	0.10	...	0.10	0.10	...	...	...	...	0.05	0.15	Remainder
6105	0.6-1.0	0.35	0.10	0.15	0.45-0.8	0.10	...	0.10	0.10	...	...	...	...	0.05	0.15	Remainder
6205	0.6-0.9	0.7	0.20	0.05-0.15	0.40-0.6	0.05-0.15	...	0.25	0.15	...	...	...	0.50-0.15 Zr	0.05	0.15	Remainder
6006	0.20-0.6	0.35	0.15-0.30	0.05-0.20	0.45-0.9	0.10	...	0.10	0.10	...	...	...	...	0.05	0.15	Remainder
6106	0.30-0.6	0.35	0.25	0.05-0.20	0.40-0.8	0.20	...	0.10	...	...	...	...	...	0.05	0.15	Remainder
6206	0.35-0.7	0.35	0.20-0.50	0.13-0.30	0.45-0.8	0.10	...	0.20	0.10	...	...	...	...	0.05	0.15	Remainder
6306	0.20-0.6	0.10	0.05-0.16	0.10-0.40	0.45-0.9	...	...	0.05	0.05	...	...	...	...	0.05	0.15	Remainder
6007	0.9-1.4	0.7	0.20	0.05-0.25	0.6-0.9	0.05-0.25	...	0.25	0.15	...	...	...	0.05-0.20Zr	0.05	0.15	Remainder
6008	0.50-0.9	0.35	0.30	0.30	0.40-0.7	0.30	...	0.20	0.10	...	...	...	...	0.05	0.15	Remainder
6009	0.6-1.0	0.50	0.15-0.6	0.20-0.8	0.40-0.8	0.10	...	0.25	0.10	...	...	...	...	0.05	0.15	Remainder
6010	0.8-1.2	0.50	0.15-0.6	0.20-0.8	0.6-1.0	0.10	...	0.25	0.10	...	...	...	...	0.05	0.15	Remainder
6110	0.7-1.5	0.8	0.20-0.7	0.20-0.7	0.50-1.1	0.04-0.25	...	0.30	0.15	...	...	...	...	0.05	0.15	Remainder

REGISTERED COMPOSITIONS continued

AA No.	Si	Fe	Cu	Mn	Mg	Cr	Ni	Zn	Ti	Ga	V	Others		Aluminium	
												Each	Tonal	Minimum	Remainder
6110A	0.7-1.1	0.50	0.30-0.9	0.30-0.9	0.7-1.1	0.05-0.25	...	0.20	...	...	...	0.20 Ti + Zr	0.05	0.15	Remainder
6011	0.6-1.2	1.0	0.40-0.9	0.8	0.6-1.2	0.30	0.20	1.5	0.20	...	...	...	0.05	0.15	Remainder
6111	0.6-1.1	0.40	0.50-0.9	0.10-0.45	0.50-1.0	0.10	...	0.15	0.10	...	...	...	0.05	0.15	Remainder
6012	0.6-1.4	0.50	0.10	0.40-1.0	0.6-1.2	0.30	...	0.30	0.20	...	...	0.7 Bi, 0.40-2.0 Pb	0.05	0.15	Remainder
6013	0.6-1.0	0.50	0.6-1.1	0.20-0.8	0.8-1.2	0.10	...	0.25	0.10	...	...	...	0.05	0.15	Remainder
6113	0.6-1.0	0.30	0.6-1.1	0.10-0.6	0.8-1.2	0.10	...	0.25	0.10	...	...	...	0.05	0.15	Remainder
6014	0.30-0.6	0.35	0.25	0.05-0.20	0.40-0.8	0.20	...	0.10	0.10	...	0.05-0.20	...	0.05	0.15	Remainder
6015	0.20-0.4	0.10-0.30	0.10-0.25	0.10	0.8-1.1	0.10	...	0.10	0.10	...	...	...	0.05	0.15	Remainder
6016	1.0-1.5	0.50	0.20	0.20	0.25-0.6	0.10	...	0.20	0.15	...	...	...	0.05	0.15	Remainder
6016A	0.9-1.5	0.50	0.25	0.20	0.25-0.6	0.10	...	0.20	0.15	...	...	...	0.05	0.15	Remainder
6116	0.9-1.3	0.25	0.20	0.15	0.25-0.6	0.15	...	0.20	0.15	...	...	...	0.05	0.15	Remainder
6017	0.55-0.7	0.15-0.30	0.05-0.20	0.10	0.45-0.6	0.10	...	0.05	0.05	...	...	...	0.05	0.15	Remainder
6018	0.50-1.2	0.7	0.15-0.40	0.30-0.8	0.6-1.2	0.10	...	0.30	0.20	...	...	...	0.05	0.15	Remainder
6020	0.40-0.9	0.50	0.30-0.9	0.35	0.6-1.2	0.15	...	0.20	0.15	...	...	...	0.05	0.15	Remainder
6022	0.8-1.5	0.05-0.20	0.01-0.11	0.02-0.10	0.45-0.7	0.10	...	0.25	0.15	...	...	...	0.05	0.15	Remainder
X6030	0.40-0.8	0.7	0.15-0.40	0.15	0.8-1.2	0.04-0.35	...	0.25	0.15	...	...	0.05 Pb, 0.9-1.5 Sn	0.05	0.15	Remainder
6151	0.6-1.2	1.0	0.35	0.20	0.45-0.8	0.15-0.35	...	0.25	0.15	...	...	...	0.05	0.15	Remainder
6351	0.7-1.3	0.50	0.10	0.40-0.8	0.40-0.8	...	...	0.20	0.20	...	...	...	0.05	0.15	Remainder
6351A	0.7-1.3	0.50	0.10	0.40-0.8	0.40-0.8	...	...	0.20	0.20	...	...	...	0.05	0.15	Remainder
6951	0.20-0.50	0.8	0.15-0.40	0.10	0.40-0.8	...	...	0.20	...	...	...	...	0.05	0.15	Remainder
6053	...	0.35	0.10	...	1.1-1.4	0.15-0.35	...	0.10	...	...	...	...	0.05	0.15	Remainder
6253	...	0.50	0.10	...	1.0-1.5	0.04-0.35	...	1.6-2.4	...	...	...	...	0.05	0.15	Remainder
6056	0.7-1.3	0.50	0.50-1.1	0.40-1.0	0.6-1.2	0.25	...	0.10-0.7	...	...	...	...	0.05	0.15	Remainder
6060	0.30-0.6	0.15	0.10	0.10	0.35-0.6	0.05	...	0.15	0.10	...	...	...	0.05	0.15	Remainder
6160	0.30-0.6	0.15	0.20	0.05	0.35-0.6	0.05	...	0.05	...	...	...	...	0.05	0.15	Remainder
6061	0.40-0.8	0.7	0.15-0.40	0.15	0.8-1.2	0.04-0.35	...	0.25	0.15	...	...	...	0.05	0.15	Remainder
6061A	0.40-0.8	0.7	0.15-0.40	0.15	0.8-1.2	0.04-0.35	...	0.25	0.15	...	...	...	0.05	0.15	Remainder
6261	0.40-0.7	0.40	0.15-0.40	0.20-0.35	0.7-1.0	0.10	...	0.20	0.10	...	...	...	0.05	0.15	Remainder
6162	0.40-0.8	0.50	0.20	0.10	0.7-1.1	0.10	...	0.25	0.10	...	...	...	0.05	0.15	Remainder
6262	0.40-0.8	0.7	0.15-0.40	0.15	0.8-1.2	0.04-0.14	...	0.25	0.15	...	...	...	0.05	0.15	Remainder
6063	0.20-0.6	0.35	0.10	0.10	0.45-0.9	0.10	...	0.10	0.10	...	...	...	0.05	0.15	Remainder
6063A	0.30-0.6	0.15-0.35	0.10	0.15	0.6-0.9	0.05	...	0.15	0.10	...	...	...	0.05	0.15	Remainder
6463	0.20-0.6	0.15	0.20	0.05	0.45-0.9	...	...	0.05	...	...	...	...	0.05	0.15	Remainder
6463A	0.20-0.6	0.15	0.25	0.05	0.30-0.9	...	...	0.05	...	...	...	...	0.05	0.15	Remainder
6763	0.20-0.6	0.08	0.04-0.16	0.03	0.45-0.9	...	...	0.03	...	...	0.05	...	0.05	0.15	Remainder
6963	0.40-0.6	0.25	0.15-0.25	0.05	0.35-0.7	0.10	...	0.10	0.10	...	...	...	0.03	0.10	Remainder
6066	0.9-1.8	0.50	0.7-1.2	0.6-1.1	0.8-1.4	0.40	...	0.10	0.15	...	...	...	0.05	0.15	Remainder
6069	0.6-1.2	0.40	0.55-1.0	0.05	1.2-1.6	0.05-0.30	...	0.05	0.10	...	0.10-0.30	0.05 Sr	0.05	0.15	Remainder
6070	1.0-1.7	0.50	0.15-0.40	0.40-1.0	0.50-1.2	0.10	...	0.25	0.15	...	...	...	0.05	0.15	Remainder

## REGISTERED COMPOSITIONS continued

AA No.	Si	Fe	Cu	Mn	Mg	Cr	Ni	Zn	Ti	Ga	V	Others		Aluminum Minimum	
												Each	Total		
6081	0.7-1.1	0.50	0.10	0.10-0.45	0.6-1.0	0.10	...	0.20	0.15	...	...	0.05	0.15	Remainder	
6181	0.8-1.2	0.45	0.10	0.15	0.6-1.0	0.10	...	0.20	0.10	...	...	0.05	0.15	Remainder	
6082	0.7-1.3	0.50	0.10	0.40-1.0	0.6-1.2	0.25	...	0.20	0.10	...	...	0.05	0.15	Remainder	
6082A	0.7-1.3	0.50	0.10	0.40-1.0	0.6-1.2	0.25	...	0.20	0.10	...	...	0.05	0.15	Remainder	
6091	0.40-0.8	0.7	0.10	0.15	0.8-1.2	0.15	...	0.25	0.15	...	...	0.05	0.15	Remainder	
6092	0.40-0.8	0.30	0.7-1.0	0.15	0.8-1.2	0.15	...	0.25	0.15	...	...	0.05	0.15	Remainder	
7001	0.35	0.40	1.6-2.6	0.20	2.6-3.4	0.18-0.35	...	6.8-8.0	0.20	...	...	0.05	0.15	Remainder	
7003	0.30	0.35	0.20	0.30	0.50-1.0	0.20	...	5.0-6.5	0.20	...	0.05-0.25 Zr	0.05	0.15	Remainder	
7004	0.25	0.35	0.05	0.20-0.7	1.0-2.0	0.05	...	3.8-4.6	0.05	...	0.10-0.20 Zr	0.05	0.15	Remainder	
7005	0.35	0.40	0.10	0.20-0.7	1.0-1.8	0.06-0.20	...	4.0-5.0	0.01-0.06	...	0.08-0.20 Zr	0.05	0.15	Remainder	
7008	0.10	0.10	0.05	0.05	0.7-1.4	0.12-0.25	...	4.5-5.5	0.05	...	...	0.05	0.10	Remainder	
7108	0.10	0.10	0.05	0.05	0.7-1.4	...	...	4.5-5.5	0.05	...	0.12-0.25 Zr	0.05	0.15	Remainder	
7108A	0.20	0.30	0.05	0.05	0.7-1.5	0.04	...	4.8-5.8	0.03	0.03	...	0.15-0.25 Zr	0.05	0.15	Remainder
7009	0.20	0.20	0.06-1.3	0.10	2.1-2.9	0.10-0.25	...	5.5-6.5	0.20	...	...	0.05	0.15	Remainder	
7010	0.12	0.15	1.5-2.0	0.10	2.1-2.6	0.05	0.05	5.7-6.7	0.06	...	0.10-0.16 Zr	0.05	0.15	Remainder	
7011	0.15	0.20	0.05	0.10-0.30	1.0-1.6	0.05-0.20	...	4.0-5.5	0.05	...	...	0.05	0.15	Remainder	
7012	0.15	0.25	0.8-1.2	0.08-0.15	1.8-2.2	0.04	...	5.8-6.5	0.02-0.08	...	0.10-0.18 Zr	0.05	0.15	Remainder	
7013	0.6	0.7	0.10	1.0-1.5	...	...	...	1.5-2.0	...	...	...	0.05	0.15	Remainder	
7014	0.50	0.50	0.30-0.7	0.30-0.7	2.2-3.2	...	0.10	5.2-6.2	...	...	0.20 Ti + Zr	0.05	0.15	Remainder	
7015	0.20	0.30	0.06-0.15	0.10	1.3-2.1	0.15	...	4.6-5.2	0.10	...	0.10-0.20 Zr	0.05	0.15	Remainder	
7016	0.10	0.12	0.45-1.0	0.03	0.8-1.4	...	...	4.0-5.0	0.03	...	...	0.03	0.10	Remainder	
7116	0.15	0.30	0.50-1.1	0.05	0.8-1.4	...	...	4.2-5.2	0.05	0.03	0.05	0.05	0.15	Remainder	
7017	0.35	0.45	0.20	0.05-0.50	2.0-3.0	0.35	0.10	4.0-5.2	0.15	...	...	0.05	0.15	Remainder	
7018	0.35	0.45	0.20	0.15-0.50	0.7-1.5	0.20	0.10	4.5-5.5	0.15	...	0.10-0.25 Zr	0.05	0.15	Remainder	
7019	0.35	0.45	0.20	0.15-0.50	1.5-2.5	0.20	0.10	3.5-4.5	0.15	...	0.10-0.25 Zr	0.05	0.15	Remainder	
7019A	0.30	0.40	0.10	0.10-0.6	1.5-2.5	0.05-0.35	...	3.0-5.0	0.10	...	...	0.05	0.15	Remainder	
7020	0.35	0.40	0.20	0.05-0.50	1.0-1.4	0.10-0.35	...	4.0-5.0	...	...	...	0.05	0.15	Remainder	
7021	0.25	0.40	0.25	0.10	1.2-1.8	0.05	...	5.0-6.0	0.10	...	0.08-0.18 Zr	0.05	0.15	Remainder	
7022	0.50	0.50	0.50-1.0	0.10-0.40	2.6-3.7	0.10-0.30	...	4.3-5.2	...	...	0.20 Ti + Zr	0.05	0.15	Remainder	
7023	0.50	0.50	0.50-1.0	0.10-0.6	2.0-3.0	0.05-0.35	...	4.0-6.0	0.10	...	...	0.05	0.15	Remainder	
7024	0.30	0.40	0.10	0.10-0.6	1.0-1.0	0.05-0.35	...	3.0-5.0	0.10	...	...	0.05	0.15	Remainder	
7025	0.30	0.40	0.10	0.10-0.6	0.8-1.5	0.05-0.35	...	3.0-5.0	0.10	...	...	0.05	0.15	Remainder	
7026	0.08	0.12	0.6-0.9	0.05-0.20	1.5-1.9	...	...	4.6-5.2	0.05	...	0.09-0.14 Zr	0.03	0.10	Remainder	
7028	0.35	0.50	0.10-0.30	0.15-0.6	1.5-2.3	0.20	...	4.5-5.2	0.05	...	0.08-0.25 Zr + Ti	0.05	0.15	Remainder	
7029	0.10	0.12	0.50-0.9	0.03	1.3-2.0	...	...	4.2-5.2	0.05	...	0.05	0.03	0.10	Remainder	
7129	0.15	0.30	0.50-0.9	0.10	1.3-2.0	0.10	...	4.2-5.2	0.05	0.03	0.05	0.03	0.10	Remainder	
7229	0.06	0.08	0.50-0.9	0.03	1.3-2.0	...	...	4.2-5.2	0.05	...	0.05	0.03	0.10	Remainder	
7030	0.20	0.30	0.20-0.40	0.05	1.0-1.5	0.04	...	4.8-5.9	0.03	0.03	0.05	0.05	0.15	Remainder	

REGISTERED COMPOSITIONS continued

AA No.	Si	Fe	Cu	Mn	Mg	Cr	Ni	Zn	Ti	Ga	V	Others		Aluminium
												Each	Total	
7031	0.30	0.08-1.4	0.10	0.10-0.40	0.10	...	...	0.8-1.8	...	...	...	0.05	0.15	Remainder
7032	0.10	0.12	1.7-2.3	0.05	1.5-0.25	0.15-0.25	...	5.5-6.5	...	...	...	0.05	0.15	Remainder
7033	0.15	0.30	0.7-1.30	0.10	0.20	0.20	...	4.6-5.6	0.10	0.03	0.05	0.05	0.15	Remainder
7040	0.10	0.13	1.5-2.3	0.04	1.7-2.4	0.04	...	5.7-6.7	0.06	...	...	0.05	0.15	Remainder
7039	0.30	0.40	0.10	0.10-0.40	2.3-3.3	0.15-0.25	...	3.5-4.5	0.10	...	...	0.05	0.15	Remainder
7046	0.20	0.40	0.25	0.30	1.0-1.6	0.20	...	6.6-7.6	0.06	...	...	0.05	0.15	Remainder
7146	0.20	0.40	...	...	1.0-1.6	...	...	6.6-7.6	0.06	...	...	0.05	0.15	Remainder
7049	0.25	0.35	1.2-1.9	0.20	2.0-2.9	0.10-0.22	...	7.2-8.2	0.10	...	...	0.05	0.15	Remainder
7049A	0.40	0.50	1.2-1.9	0.50	2.1-3.1	0.05-0.25	...	7.2-8.4	...	...	...	0.05	0.15	Remainder
7149	0.15	0.20	1.2-1.9	0.20	2.0-2.9	0.10-0.22	...	7.2-8.2	0.10	...	...	0.05	0.15	Remainder
7249	0.10	0.12	1.3-1.9	0.10	2.0-2.4	0.12-0.18	...	7.5-8.2	0.06	...	...	0.05	0.15	Remainder
7349	0.12	0.15	1.4-2.1	0.20	1.8-2.7	0.10-0.22	...	7.5-8.7	...	...	...	0.05	0.15	Remainder
7449	0.12	0.15	1.4-2.1	0.20	1.8-2.7	...	...	7.5-8.7	...	...	...	0.05	0.15	Remainder
7050	0.12	0.15	2.0-2.6	0.10	1.9-2.6	0.04	...	5.7-6.7	0.06	...	...	0.05	0.15	Remainder
7050A	0.12	0.15	1.7-2.4	0.04	1.7-2.6	0.04	0.03	5.7-6.9	0.06	...	...	0.05	0.15	Remainder
7150	0.12	0.15	1.9-2.5	0.10	2.0-2.7	0.04	...	5.9-6.9	0.06	...	...	0.05	0.15	Remainder
7055	0.10	0.15	2.0-2.6	0.05	1.8-2.3	0.04	...	7.6-8.4	0.06	...	...	0.05	0.15	Remainder
7060	0.15	0.20	1.8-2.6	0.20	1.3-2.1	0.15-0.25	...	6.1-7.5	0.05	...	...	0.05	0.15	Remainder
7064	0.12	0.15	1.8-2.4	...	1.9-2.9	0.06-0.25	...	6.8-8.0	...	...	...	0.05	0.15	Remainder
7072	0.25	0.6	0.7 Si + Fe	0.10	0.10	...	...	0.8-1.3	...	...	...	0.05	0.15	Remainder
7472	0.25	0.6	0.05	0.05	0.9-1.5	...	...	1.3-1.9	...	...	...	0.05	0.15	Remainder
7075	0.40	0.50	1.2-2.0	0.30	2.1-2.9	0.18-0.28	...	5.1-6.1	0.20	...	...	0.05	0.15	Remainder
7175	0.15	0.20	1.2-2.0	0.10	2.1-2.9	0.18-0.28	...	5.1-6.1	0.10	...	...	0.05	0.15	Remainder
7475	0.10	0.12	1.2-1.9	0.06	1.9-2.6	0.18-0.25	...	5.2-6.2	0.06	...	...	0.05	0.15	Remainder
7076	0.40	0.6	0.30-1.0	0.30-0.8	1.2-2.0	...	...	7.0-8.0	0.20	...	...	0.05	0.15	Remainder
7277	0.50	0.7	0.8-1.7	...	1.7-2.3	0.18-0.35	...	3.7-4.3	0.10	...	...	0.05	0.15	Remainder
7178	0.40	0.50	1.6-2.4	0.30	2.4-3.1	0.18-0.28	...	6.3-7.3	0.20	...	...	0.05	0.15	Remainder
7278	0.15	0.20	1.6-2.2	0.02	2.5-3.2	0.17-0.25	...	6.6-7.4	0.03	0.03	0.05	0.03	0.10	Remainder
7278A	0.12	0.15	1.3-2.1	0.25	2.3-3.2	0.05	...	6.4-7.4	0.05	...	...	0.05	0.15	Remainder
7090	0.12	0.15	0.6-1.3	...	2.0-3.0	...	...	7.3-8.7	...	...	...	0.05	0.15	Remainder
7091	0.12	0.15	1.1-1.8	...	2.0-3.0	...	...	5.8-7.1	...	...	...	0.05	0.15	Remainder
7093	0.12	0.15	1.1-1.9	...	2.0-3.0	...	0.04-0.16	8.3-9.7	...	...	...	0.05	0.15	Remainder

## REGISTERED COMPOSITIONS continued

AA No.	Si	Fe	Cu	Mn	Mg	Cr	Ni	Zn	Ti	Ga	V	Others		Aluminum
												Each	Total	Minimum
8001	0.17	0.45-0.7	0.15	...	...	...	0.9-1.3	0.05	...	...	...	0.05	0.15	Remainder
8005	0.40-0.50	0.40-0.8	0.05	...	0.05	...	...	0.05	...	...	...	0.05	0.15	Remainder
8006	0.40	1.2-2.0	0.30	0.30-1.0	0.10	...	...	0.10	...	...	...	0.05	0.15	Remainder
8007	0.40	1.2-2.0	0.10	0.30-1.0	0.10	...	...	0.08-1.8	...	...	...	0.05	0.15	Remainder
8008	0.6	0.9-1.6	0.20	0.50-1.0	...	...	...	0.10	...	...	...	0.05	0.15	Remainder
8009	0.7-1.9	8.4-8.9	...	0.10	...	0.10	...	0.25	0.10	...	1.1-1.5	0.05	0.15	Remainder
8010	0.40	0.35-0.7	0.10-0.30	0.10-0.8	0.10-0.50	0.20	...	0.40	0.10	...	...	0.05	0.15	Remainder
8011	0.50-0.9	0.6-1.0	0.10	0.20	0.05	0.05	...	0.10	0.08	...	...	0.05	0.15	Remainder
8011A	0.40-0.8	0.50-1.0	0.10	0.10	0.10	0.10	...	0.10	0.05	...	...	0.05	0.15	Remainder
8111	0.30-1.1	0.40-1.0	0.10	0.10	0.05	0.05	...	0.10	0.08	...	...	0.05	0.15	Remainder
8211	0.40-0.8	0.50-1.0	0.10	0.05-0.20	0.10	0.15	...	0.10	0.05	...	...	0.06	0.15	Remainder
8112	1.0	1.0	0.40	0.6	0.7	0.20	...	1.0	0.20	...	...	0.05	0.15	Remainder
8014	0.30	1.2-1.6	0.20	0.20-0.6	0.10	...	...	0.10	0.10	...	...	0.05	0.15	Remainder
8015	0.30	0.8-1.4	0.10	0.10-0.40	0.10	...	...	0.10	...	...	...	0.05	0.15	Remainder
8016	0.20	0.7-1.1	0.10	0.10-0.30	0.10	...	...	0.10	...	...	...	0.05	0.15	Remainder
8017	0.10	0.55-0.8	0.10-0.20	0.10-0.40	0.10	...	...	0.10	...	...	...	0.03	0.10	Remainder
8018	0.50-0.9	0.6-1.0	0.30-0.6	0.30	0.01-0.05	...	...	0.05	0.006-0.06	...	0.04 B, 0.003 Li	0.05	0.15	Remainder
8019	0.20	7.3-9.3	...	0.05	...	...	...	0.05	0.05	...	...	0.05	0.15	Remainder
8020	0.10	0.10	0.005	0.005	...	...	...	0.005	...	...	0.05	0.03	0.10	Remainder
8021	0.15	1.2-1.7	0.05	...	...	...	...	...	0.05	...	...	0.05	0.15	Remainder
8021A	0.20	1.2-1.7	0.05	0.03	0.02	...	...	0.05	0.05	...	...	0.02	0.15	Remainder
8021B	0.40	1.1-1.7	0.05	0.03	0.01	0.03	...	0.05	0.05	...	...	0.03	0.10	Remainder
8022	1.2-1.4	6.2-6.8	...	0.10	...	0.10	...	0.25	0.10	...	0.40-0.8	0.05	0.15	Remainder
8130	0.10	0.30-0.8	0.15-0.30	...	0.05	...	...	0.05	...	...	...	0.03	0.10	Remainder
8030	0.15	0.40-1.0	0.05-0.15	...	...	...	...	0.10	...	...	0.001-0.04 B	0.03	0.10	Remainder
8040	1.0 Si + Fe	0.20	0.20	0.05	...	...	...	0.20	...	...	0.10-0.30 Zr	0.05	0.15	Remainder
8050	0.15-0.30	1.1-1.2	0.05	0.45-0.55	0.05	0.05	...	0.10	...	...	...	0.05	0.15	Remainder
8076	0.10	0.6-0.9	0.04	...	0.08-0.22	...	...	0.05	...	...	0.04 B	0.03	0.10	Remainder
8176	0.03-0.15	0.40-1.0	...	...	...	...	...	0.10	...	0.03	...	0.05	0.15	Remainder
8077	0.10	0.10-0.40	0.05	...	0.10-0.30	...	...	0.05	...	...	0.05 B	0.03	0.10	Remainder
8177	0.10	0.25-0.45	0.04	...	0.04-0.12	...	...	0.05	...	...	0.04 B	0.03	0.10	Remainder
8079	0.05-0.30	0.7-1.3	0.05	...	...	...	...	0.10	...	...	...	0.05	0.15	Remainder
8280	1.0-2.0	0.7	0.7-1.3	0.10	...	...	0.20-0.7	0.05	0.10	...	5.5-7.0 Sn	0.05	0.15	Remainder
8081	0.7	0.7	0.7-1.3	0.10	...	...	...	0.05	0.10	...	18.0-22.0 Sn	0.05	0.15	Remainder
8090	0.20	0.30	1.0-1.6	0.10	0.6-1.3	0.10	...	0.25	0.10	...	0.04-0.16 Zr	0.05	0.15	Remainder
8091	0.30	0.50	1.6-2.2	0.10	0.50-1.2	0.10	...	0.25	0.10	...	0.08-0.16 Zr	0.05	0.15	Remainder
8093	0.10	0.10	1.0-1.6	0.10	0.9-1.6	0.10	...	0.25	0.10	...	0.04-0.14 Zr	0.05	0.15	Remainder

# **Appendix 2**

## **Conversion factors for some common units**

An asterisk (\*) denotes an exact relationship

<i>Imperial unit</i>	<i>SI unit</i>	<i>Imperial unit</i>	<i>SI unit</i>
<b>Length</b>		<b>Velocity</b>	
*1 in	25.4 mm	1 ft/s	0.304 8 m/s
*1 ft	0.304 8 m	1 mile/h	0.447 04 m/s
*1 yd	0.914 4 m	<b>Volumetric flow</b>	
1 mile	1.609 3 km	1 ft <sup>3</sup> /s	0.028 316 m <sup>3</sup> /s
*1 Å (angstrom)	10 <sup>-10</sup> m	1 ft <sup>3</sup> /h	7.865 8 cm <sup>3</sup> /h
<b>Time</b>		1 UK gal/h	1.262 8 cm <sup>3</sup> /s
*1 min	60 s	1 US gal/h	1.051 5 cm <sup>3</sup> /s
*1 h	3.6 ks	<b>Mass flow</b>	
*1 day	86.4 ks	1 lb/h	0.126 00 g/s
1 year	31.5 Ms	1 ton/h	0.282 24 kg/s
<b>Area</b>		<b>Mass/area</b>	
*1 in <sup>2</sup>	645.16 mm <sup>2</sup>	1 lb/in <sup>2</sup>	703.07 kg/m <sup>2</sup>
1 ft <sup>2</sup>	0.092 903 m <sup>2</sup>	1 lb/ft <sup>2</sup>	4.882 4 kg/m <sup>2</sup>
1 yd <sup>2</sup>	0.836 13 m <sup>2</sup>	1 ton/mile <sup>2</sup>	392.30 kg/km <sup>2</sup>
1 acre	4046.9 m <sup>2</sup>	<b>Density</b>	
1 mile <sup>2</sup>	2.590 km <sup>2</sup>	1 lb/in <sup>3</sup>	27.680 g/cm <sup>3</sup>
<b>Volume</b>		1 lb/ft <sup>3</sup>	16.019 kg/m <sup>3</sup>
1 in <sup>3</sup>	16.387 cm <sup>3</sup>	1 lb/UK gal	99.776 kg/m <sup>3</sup>
1 ft <sup>3</sup>	0.028 32 m <sup>3</sup>	1 lb/US gal	119.83 kg/m <sup>3</sup>
1 yd <sup>3</sup>	4546.1 cm <sup>3</sup>	<b>Pressure</b>	
1 US gal	3785.4 cm <sup>3</sup>	1 lbf/in <sup>2</sup>	6.894 8 kN/m <sup>2</sup>
<b>Mass</b>		1 tonf/in <sup>2</sup>	15.444 MN/m <sup>2</sup>
1 oz	28.352 g	1 lbf/ft <sup>2</sup>	47.880 N/m <sup>2</sup>
*1 lb	0.453 592 802 3 kg	*1 standard atmos.	101.325 kN/m <sup>2</sup>
1 cwt	50.80 kg	*1 at (1 kgf/cm <sup>2</sup> )	98.066 5 kN/m <sup>2</sup>
1 ton	1016.06 kg	*1 bar	105 N/m <sup>2</sup>
<b>Force</b>		1 ft water	2.989 1 kN/m <sup>2</sup>
1 pdl	0.1382 6 N	1 in water	249.09 N/m <sup>2</sup>
1 lbf	4.448 2 N	1 in Hg	3.386 4 kN/m <sup>2</sup>
1 tonf	9.964 0 kN	1 mm Hg (1 torr)	133.32 N/m <sup>2</sup>
*1 dyn	10 <sup>-5</sup> N	<b>Power</b>	
<b>Temperature</b>		1 hP (UK)	745.70 W
*1 °F	5/9 °C (K)	1 hP (metric)	735.50 W
<b>Energy</b>		1 erg/s	10 <sup>-7</sup> W
1 ft lbf	1.355 8 J	1 ft lbf/s	1.355 8 W
1 ft pdl	0.042 14 J	1 btu/h	0.293 07 W
*1 cal	4.186 8 J	<b>Moment of inertia</b>	
1 erg	10 <sup>-7</sup> J	1 lbf <sup>2</sup>	0.042 140 kg m <sup>2</sup>
1 Btu	1.055 06 kJ	<b>Momentum</b>	
1 hp h	2.684 5 MJ	1 lb ft/s	0.138 26 kg m/s
*1 kW h	3.6 MJ	<b>Angular momentum</b>	
1 therm	105.51 MJ	1 lbf <sup>2</sup> /s	0.042 140 kg m <sup>2</sup> /s
1 thermie	4.185 5 MJ	<b>Calorific value</b>	
<b>Calorific value</b>		(volumetric)	
1 Btu/ft <sup>3</sup>	37.255 kJ/m <sup>3</sup>		

<i>Imperial unit</i>	<i>SI unit</i>	<i>Imperial unit</i>	<i>SI unit</i>
<b>Viscosity, dynamic</b>		<b>Heat flux density</b>	
1 P(poise)	0.1 N s/m <sup>2</sup>	1 Btu/hft <sup>2</sup> °F	3.154 6 W/m <sup>2</sup>
1 lb/ft h	0.413 38 mN s/m <sup>2</sup>	*1 kcal/h m <sup>2</sup>	1.163 W/m <sup>2</sup>
1 lb/ft s	1.488 2 N s/m <sup>2</sup>	<b>Heat transfer coefficient</b>	
<b>Viscosity, kinematic</b>		1 Btu/h ft <sup>2</sup> °F	5.678 3 W/m <sup>2</sup> K
1 S (stokes)	10 <sup>-4</sup> m <sup>2</sup> /s	<b>Specific enthalpy (latent heat etc)</b>	
1 ft <sup>2</sup> /h	0.258 06 cm <sup>2</sup> /s	*1 Btu/lb	2.326 kJ/kg
<b>Surface energy</b>		<b>Heat capacity</b>	
1 dyn/cm <sup>2</sup>	10 <sup>-3</sup> J/m <sup>2</sup>	*1 Btu/lb °F	4.186 8 kJ/kg K
<b>Surface tension</b>		(specific heat)	
1 erg/cm	10 <sup>-5</sup> J/m	<b>Thermal conductivity</b>	
<b>Mass flux density</b>		1 Btu/h ft <sup>2</sup> °F	1.730 7 W/m K
1 lb/h ft <sup>2</sup>	1.356 2 g/s m <sup>2</sup>	1 kcal/h m °C	1.163 W/m K



# **Appendix 3**

## **Temper designations**

**(a) Strain hardened alloys**

- F** As fabricated. No control over the amount of strainhardening; no mechanical property limits.
- O** Annealed, recrystallized. Temper with the lowest strength and greatest ductility.
- H1** Strain hardened.  
**H12, H14, H16, H18.** The degree of strain hardening is indicated by the second digit and varies from quarter-hard (H12) to full-hard (H18), which is produced with approximately 75% reduction in area.  
**H19.** An extra-hard temper for products with substantially higher strengths and greater strain hardening than obtained with the H18 temper.
- H2** Strain hardened and partially annealed.  
**H22, H24, H26, H28.** Tempers ranging from quarter-hard to full-hard obtained by partial annealing of cold worked materials with strengths initially greater than desired.
- H3** Strain hardened and stabilized.  
**H32, H34, H36, H38.** Tempers for age-softening aluminum–magnesium alloys that are strain hardened and then heated at a low temperature to increase ductility and stabilize mechanical properties.
- H112** Strain hardened during fabrication. No special control over amount of strain hardening but requires mechanical testing and meets minimum mechanical properties.
- H321** Strain hardened during fabrication. Amount of strain hardening controlled during hot and cold working.
- H323** Special strain hardened, corrosion-resistant tempers for aluminum–magnesium alloys.
- H343**

**(b) Temper designation system applicable to heat treatable alloys**

- F** As fabricated. Applies to wrought products that acquire some temper from shaping processes in which no special control is exercised over the amount of strain hardening or thermal treatment. For wrought products in this temper, there are no mechanical-property limits. Applies to castings in the as-cast condition if the alloy is also regularly produced in heat treated tempers.
- O** Annealed (wrought products only). Applies to the softest temper of wrought products.
- W** Solution heat treated. An unstable temper applicable only to alloys that age at room temperature after solution heat treatment. This designation is specific only when the period of natural aging is indicated; for example: W(0.5 hr). T9 Sa
- T** Heat treated to produce stable tempers other than F or O. Applies to wrought and cast products that are heat treated, with or without supplementary cold working to produce stable tempers.  
 The T is always followed by one or more digits. Numerals 1 through 10 indicate specific sequences of treatments:
- T1** Naturally aged to a substantially stable condition. Applies to products in which partial solution of alloying elements is provided by elevated-temperature, rapid-cool fabrication.
- T2** Annealed (cast products only). Designates a temper produced by a type of annealing treatment used to improve ductility and increase dimensional stability of castings.

- T3** Solution heat treated, cold-worked, and naturally aged to a substantially stable condition. Applies to products that are cold worked to improve strength, or in which the effect of cold work associated with flattening or straightening is recognized in applicable specifications. Different amounts of cold work are denoted by a second digit.
- T4** Solution heat treated and naturally aged to a substantially stable condition. Applies to products that are not cold worked after solution heat treatment, or in which the effect of cold work associated with flattening or straightening may not be recognized in applicable specifications.
- T5** Artificially aged only. Applies to products that are artificially aged after an elevated-temperature, rapid-cool fabrication process, such as casting or extrusion, to improve strength and/or dimensional stability.
- T6** Solution heat treated and artificially aged. Applies to products not cold worked after solution heat treatment, or in which the effect of cold work associated with flattening or straightening may not be recognized in applicable specifications.
- T7** Solution heat treated and overaged. Applies to products that are solution heat treated and artificially aged beyond the condition of maximum strength, to provide controlled special characteristics, such as dimensional stability, lower residual stresses, or improved resistance to corrosion.
- T8** Solution heat treated, cold worked, and artificially aged. Applies to products that are cold worked to improve strength, or in which the effect of cold work associated with flattening or straightening is recognized in applicable specifications. Different amounts of cold work are denoted by a second digit.
- T9** Solution heat treated, artificially aged, and cold worked. Applies to products that are cold worked as a final operation, to improve strength.
- T10** Artificially aged and cold worked. Applies to products that are artificially aged after an elevated-temperature, rapid cool fabrication process, such as casting or extrusion, and then cold worked to improve strength.

A period of natural aging may occur between the operations listed for tempers T3 through T10. Control of this period may be necessary to achieve the desired characteristics.

The following designations involving additional digits are assigned to stress-relieved tempers of wrought products:

- Tx51<sup>(a)</sup>** Stress relieved by stretching. Applies to products that are stress relieved by stretching the following amounts after solution heat treatment: plate – 0.5 to 3% permanent set; rod, bar and shapes – 1 to 3% permanent set. This designation applies directly to plate and rolled or cold finished rod and bar. These products receive no further straightening after stretching. Additional digits are used in the designations for extruded rod, bar, shapes and tube as follows: Tx510(a) applies to products that receive no further straightening after stretching; Tx511(a) applies to products that receive minor straightening after stretching to comply with standard straightness tolerances.
- Tx52<sup>(a)</sup>** Stress relieved by compressing. Applies to products that are stress relieved by compressing after solution heat treatment, to produce a nominal permanent set of 2.5%.
- Tx53<sup>(a)</sup>** Stress relieved by thermal treatment.

(a) The letter *x* represents digits 3, 4, 6, or 8, whichever is applicable.

# Index

- $\alpha$  solid solution, 74
- Accountability, 331
- Acicular morphology, 224
- Active extrusion ratio (CADEX), 344
- Aerospace alloys, 71, 72, 171
- Ageing and skip transports, 330
- Ageing, clustering behaviour in, 267
- Alloys
  - AA designation, 205–226
  - 1XXX, 205–7
  - 2XXX, 208–16
  - 3XXX, 216–19
  - 4XXX, 219–21
  - 5XXX, 221–6
  - 6005A, 265
  - 6351/6082, 264–5
  - 6XXX, 186, 253–322
  - 7075 – effect of homogenization, 244
  - 7XXX, 227–36
  - Al–4.5%Cu alloy, 70
  - Al–Cu, 70
  - Al–Cu–Mg, 70
  - Aldur, 76
  - Al–Fe, 106
  - Al–Li, 86, 236
  - Al–Li–Cu, 89
  - Al–Li–Cu–Mg, 90
  - Al–Li–Mg, 88
  - Al–Mg, 73
  - Al–Mg–Si, 76, 190
  - Al–Si, 72
  - Al–Zn–Mg, 81, 187, 227–32
  - Al–Zn–Mg–Cu, 82–3, 232–6
  - RR58, 71
- Ancillary equipment
  - automatic welding machine, 385
  - billet heating and die heating, 382
  - cooling table, 328
  - double puller system, 327
  - packing line, 330
  - stretcher and stretcher feeder, 328
  - stretcher headstock, 329
  - supporting run-out, 372
- Anneals; low temperature, 74
- As-cast structure; retained, 212
- Atom and activation, 112
- Atomic movements and diffusion, 95
- Avrami, 116
- Axisymmetric upper bound, 35
- $\beta'$ , and diffusionless transformation, 255
- $\beta'$ Mg<sub>2</sub>Si rods, 265
- Balanced alloy, 255, 263
- Billet preheating practice, 260
- Billet temperature control, 373, 240
- Billet-to-billet extrusion, 12, 311
- Breakthrough pressure, 144, 176, 242
- Bridge die extrusion, 148

- Cast state, 90
- Castability, 84
- Cell size, 27
- Cleaning,, 272
- Coalescence
  - in Al–Si alloys, 72
  - of voids, 174
- Coarse grains, 206
- Coarse intermetallic compounds, 174
- Complex shapes, classification of, 380
- Composition control in melting furnace, 381
- Concentrated in the die region, 139
- Concentration, 65
- Concentration dependence, 66
- Consistency, 331
- Constitutional equalization, 94
- Constitutive equations for some Al-alloys, 132
- Cooling, control of, 382
- Cooling period, 194
- Cooling rate, 188, 267
- Cooling rates/Heat-up rates, 131
- Cored dendritic structure, 93
- Corrosion resistance, 72, 78, 171, 197, 242
- Critical rate of change of  $Z$ , 184–5
- Critical strain, 175
- Crystal orientation, 301
- Curvature of the pressure line, 240
  
- DSC and the solvus temperature, 108
- DSC trace, 233
- Decomposition reactions, 172
- Defects
  - carbon originating from the pad, 309
  - dark (grey or black) rough patches, 319
  - defective longitudinal welds, 307
  - extrusion defect, 136, 138, 307
  - extrusion/back end defect, 307
  - hot spots, 319
  - longitudinal welds, 313
  - metallurgical defects visible after anodizing, 317
  - non-uniform appearance, 319
  - ‘piping’ defect, 47
  - scoring, 272
  - scouring effect, 281
  - streaking, 313, 317
  - streaking after anodizing, 309
  - tearing, 52, 272, 298
  - transverse weld defect, 307, 309, 311
  - weld streaks, 319
- Deformation and thermal activation, 113
- Dendrite cells, 99
- Dendrites and interdendritic eutectics, 74
- Dendritic structure, 208
- Dick, Alexander, 4
- Dies
  - and press as a unit, 371
  - aperture location, 371
  - apertures, 364
  - assembly, 372
  - backers, 374
  - basic die configurations, 358
  - bearing friction, 361
  - bearing lengths, 369
  - bearing width, height or length, 361
  - bolsters, 374
  - bridge dies, 359
  - bridge or porthole, 15
  - bridge widths, 364
  - carburization or decarburization, 375
  - choked area, 275
  - cleaning, 375
  - computer analysis of die stress, 383
  - computer-controlled die heating system, 383
  - contoured bolster, 373

- custom backer, 358
- deflection, 367
- dishing, 367
- distinct streams (in bridge dies), 15
- dimensional allowances, 367
- equal flow through each port, 368
- feedback on performance of die, 357
- feeder plate dies, 334
- feeding the die throat, 288
- flow at centre of die, 364
- improper seating of the die ring, 372
- land length, 283
- laying out sections, 364
- lubrication, 375
- minimization of die replacement, 384
- modernization of preparation and maintenance, 382
- modifications to die design, 383
- modifications to die temperature control, 383
- multi-hole dies, 148, 368
- opening the die, 371
- overall die stack, 360
- peening, 371
- port diameter increase, 383
- proper support, 374
- rotation of, 372
- section, 382
- section which 'wings in', 362
- separate dummy block, 12
- spider dies, 359
- standard range of backers, 358
- stiffness of core support, 368
- strength formula (bridge shear), 365
- tongue deflection, 359, 367
- tool failure, 374
- tool preheat, 374
- welding chamber, 15, 16, 369
- Die land/extrudate interaction, 281
- Die shuffle, 17
- Die-face slide, 17
- Differences in lengths; multi-hole extrusion, 377
- Difficulty of extrusion, 240
- Diffusion, 62, 95, 102
- Diffusion coefficient; concentration dependence, 66
- Dimensional accuracy of the section, 343
- Discard, minimization of, 385
- Dislocation, 7, 27
- Dislocation climb, 167
- Dislocation density, 27, 112, 117, 129, 166, 179, 185
- Dispersoid forming elements, 6
- Dispersoid particles, 75, 85, 106, 265
- Dissolution, 233, 237
- Distortion, 195
- Drag force of Mn particles, 166
- Driving force, 166, 179
- Dynamic balance, 135
- Dynamic recovery, 114
- Dynamic recrystallization, 114
- Dynamic restoration, 207
  - homogenization; effect of alloying elements, 228
- Extrusion of 6XXX alloys
  - effect of cooling rate, 258
- Effect of section shape, 146
- Electronic programmable limit switch, 336
- Electronic pump unloading, 337
  - forged steel cylinder, 334
  - fixed dummy block, 324
  - improvements in reliability, 384
  - indirect extrusion, 1
  - method of axial movement of the mandrel, 14
  - method of billet piercing, 14
  - method used for bleeding, 13
  - platen deflection, 333
  - press alignment, 370

- press hydraulic system, 336
- pressure ring or gate lock
  - inspection, 370
- prestressed press frame, 18, 332
- proportional relief valves, 336
- quick-action locking devices, 20
- rotating head, 17
- separate pumping system, 17
- specific pressure requirements, 305
- tie rod failure, 333
- 'X' guiding, 332
- Endurance life; Al-Zn-Mg alloys, 228
- Energy expended, 36
- Energy of migration, 97
- Energy savings, 187
- Entrapped air, 316
- Equalization of concentration
  - differences, 102
- Equivalent extrusion ratio, 149
- Eutectic, 47, 74
- Excess Mg<sub>2</sub>Si, 253
- Excess Si, 255
- Excess Si and Mg<sub>2</sub>Si, effect on
  - mechanical properties, 262
- Excessive speed and distortion, 370
- Exfoliation corrosion, 229
- Exit temperature, 50, 60, 190
- Expert system, 343, 351
- Exposure time and particle
  - coarsening, 108
- Extended soak, 211
- Extrudability, 194, 238, 258
- Extrudability; relative difficulty, 239
- Extrudate structure, 183-5
- Extruded length, imprecision of, 377
- Extruded subgrain size, 156
- Extrusion conditions, 206
  - pressure dependence on
    - homogenized condition, 212
- Extrusion press
  - accumulator, 3
  - checking for alignment, 371
  - compact presses, 23
  - container misalignment, 334
  - container sealing cylinders, 333
  - container size and available
    - pressure, 305, 371
  - direct extrusion, 1
  - discharge over relief valves, 335
  - electronic programmable limit
    - switch, 336
  - electronic pump unloading, 337
  - forged steel cylinder, 334
  - fixed dummy block, 324
  - indirect extrusion, 1
  - improvements in reliability, 384
  - method of axial movement of the
    - mandrel, 14
  - method of billet piercing, 14
  - method used for bleeding, 13
  - platen deflection, 333
  - press alignment, 370
  - press hydraulic system, 336
  - quick-action locking devices, 20
  - rotating head, 17
  - separate pumping system, 17
  - specific pressure requirements, 305
  - tie rod failure, 333
  - X guiding, 332
- Extrusion speed, optimum, 341
- Extrusion time reduction, 350
- Extrusion topology (limit) diagram, 292, 293
- Fatigue, 171
- Fibrous or 'cold worked' structure, 115, 156, 161, 177
- Fick's first law, 62
- Fick's second law, 67
- Flow lines, bending of, 146
- Flow stress
  - at the container/billet interface, 147
  - comparison of torsion flow stress
    - with compression, 130

- dependency on process
    - parameters, 127
  - discrepancies in, 127
  - evolution of kinetic laws, 129
  - from torsion testing, 129
  - function of the process
    - parameters, 128
  - interrelationship of  $A$ ,  $\Delta H$  and  $n$ 
    - 135
  - intrinsic limitations 127
  - response of 'weak' and 'hard'
    - alloys, 131
  - retarding softening, 206
  - steady state 128
  - structural events in development
    - 128
  - texture development, 128
- Flux of atoms (in diffusion), 62
- Fracture properties, 174
- Fracture surfaces, 173
- Fracture toughness, 71, 171, 237, 242
  - and processing, 174
- Freezing rate during casting, 108
- Friction, 48
- Friction coefficient,  $m$ , 48
- Fuel-fired furnaces, 19
- Fully dedicated press, 15
- Gas content reduction, 381
- Gas furnaces, 49
- GP zones, 75, 268
- Grain boundary phases; low melting
  - point, 6, 233
- Grain refiners, 71, 237
- Grain size, 27
- Grain structure and fracture
  - toughness, 174
- Heat-treatment cycle, basic kinetics,
  - 170
- Helical dislocation and ageing, 164
- Heterogeneity and ageing, 172
- Heterogeneous as-cast state, 93
- High stacking fault energy, 113
  - effect of higher Mg levels, 167
- Hollow sections, 368
- Homogenization,
  - advantages of, 93
  - air cooling in Al-Zn-Mg, 227
  - depth of penetration, 97
  - effect of alloying elements, 230
  - effect on extrudability, 244
  - equivalent times and temperatures,
    - 10
  - eutectic temperature differences,
    - 222
  - excessive void formation, 23
  - fast cooling rate, 236
  - fine precipitates, 225
  - grain boundary phases
    - spheroidized, 234
  - hardening constituents, 214
  - high temperature soak, 207, 221
  - higher extrusion speeds, 261
  - higher melting phases, 237
  - influence on ductility, 222
  - intermetallic phases, 94
  - interstitial position, 96
  - inverse segregation pattern, 221
  - iron phase transformation, 256
  - iso-0.2% proof stress (MPa), 256
  - Mg<sub>2</sub>Si precipitation, 257
  - nearest neighbour site, 96
  - nucleation, 114, 118
  - nucleation rate, 119
  - of dendrite cells, 98
  - particles, 212
  - producing brittle structure, 206
  - quick guide to dissolution times,
    - 97
  - sequence for 3004, 217
  - slow cooling (10°C/min), 236
  - solute concentration, 75
  - spheroidization, 221
  - stress relieving stage, 234
  - stringers, 212
  - structure and substructure, 204
  - structures, 214



- structures produced during
  - commercial homogenization, 258
- surface cracking in preheat cycle, 211
- temperature range for 7020, 227
- temperature sensitivity during working, 237
- temperatures, 205
- tensile failure mode, 250
- three-dimensional growth, 255
- time to homogenize, 100
- transition metal compounds, 225
- treatment, 6
- two-stage homogenization treatment, 222
- unsuitable for forming, 209, 2024, 212
- 6XXX alloys, 253, 257
- Hypoeutectic structure, 220
  
- Idle time, minimization of, 384
- Impurity elements, 69
- Incipient melting, 104, 198, 233, 296
- Indirect process, 137
- Induction furnaces, 19
- Inert atmosphere, 274
- Influence on strength; factors in 6XXX alloys, 256
- Interdendritic region, 207, 225
- Intergranular rupture, 174
- Intermediate size particles, 174
- Inverse segregation layer reduction, 381
  
- Kinetics
  - of dissolution, 190
  - of precipitation, 65
  
- Limit diagrams
  - and productivity, 240
  - extrusion of specific product, 249
  - inclusion of structural data, 292
  - inherent stiffness, 197
  - load limit, 241
  - loci for AA6082, 300
  - modified extrusion limit diagram, 296
  - pressure/temperature, 198
  - process variables, 198
  - productivity diagrams, 245
  - showing undesirable features, 198
  - specific metallurgical data, 199
  - surface acceptability criteria, 154
  - variation of temperature, 242
- Liner, 20
- Localized melting, 95, 150, 226
- Log heater, 327
- Lubricated extrusion, 135
- Lubrication of fixed dummy block, 326
  
- Machined billets, 12
- Mass-transfer, 7
- Mass-transfer problem, 113
- Material flow
  - cylinder wall shear, 177
  - dead metal zone, 137, 177
  - dead metal zone interfaces, 275
  - dead metal zone/deformation zone shear band, 151
  - deformation bands, 36, 179, 180
  - deformation; concentration in the die region, 140
  - development of structure in the extrusion container, 174–86
  - dislocation structure related to peak pressure, 184
  - effects of both temperature and ram speed, 139
  - equiaxed subgrain structure, 181
  - experimental methods to determine actual flow, 138
  - flow through commercial dies, 358
  - flow under differing conditions, 136–9
  - grain boundaries, 185
  - high friction forces, 136

- higher strains, 183
- incomplete recovery, 181
- indirect flow, 139
- internal dislocation density, 181
- lubricated, 136
- material/container interface, 144
- quasi-static deformation zone, 177
- shear bands, 174
- steady-state region, 141
- strain gradients, 181, 184
- zones of heavy shear, 136
- Maximum production rates, 248
- Maximum size of extrusion is limited, 21
- Maxwell–Boltzmann distribution, 112
- Mean equivalent stress, 26
- Measure of extrudability, 238
- Mechanical properties
  - attainment of mechanical properties, 306
  - UTS, 172
- Mechanical working, 172
- Medium strength alloys, 263
- Melting failure mode, 250
- Microsegregation, 93
- Microstructural damage, 105
- Microstructure, 115, 255
- Mixed mode fracture, 173
- Modern automated plant, 323
  - automated press set-up, 338
  - closed loop speed control, 335
  - comprehensive process optimization, 344
  - data acquisition, 339
  - data exchange with CADEX, 345
  - diagnostic systems, 338
  - expert systems
    - backward chaining, 352
    - base is supplied by human experts, 351
    - forward chaining, 352
    - IF–THEN rules, 351
    - inference engine, 352
    - simplified rung; ‘ram forward’, 355
  - feedback, 344
  - hierarchical structure of control systems, 332
  - intelligence, 332
  - isopressure, 344
  - isothermal extrusion, 55, 340, 343
  - layout of modern extrusion plant, 323
  - mathematical model, 344
  - microcomputers, 330
  - parameters in a simulation model, 330
  - planning, 331
  - planning of cut lengths, 303
  - press operator – no manual control, 344
  - process data file, 330
  - process optimization, 343
  - reliability, 331
  - repeatability, 332, 337
  - run-out system, 327
  - saw conveyor, saw and stacking unit, 329
  - self-monitoring, 332
  - sensors, 331
  - smart display, 354
  - supervisory computer, 338
  - three-man crew, 323
  - topping and tailing of billets, 334
  - transducer monitoring, 339
- Nitriding, 274
- Nonequilibrium melting, 103
- Notch sensitivity, 78
- Notch toughness, 259
- On-line prediction, 55
- Optimum soak; times/Ageing times, 157
- Ostwald ripening, 108
- Out-of-tolerance sections, 359
- Overheating, 260

- Overlap of Mg and Si in 6061 and 6082, 262, 264
- Overlengths of extruded profiles, 375, 377
- Oxide inclusions reduction, 381
- Oxidized billet skin, 307
- Partial segregation, 212
- Particle coarsening, 108
- Penetration curve in diffusion, 64
- Perfect lubrication, 48
- Peripheral ratio, 147
- Peripheral recrystallization, 47
- Periphery of shaped extrusions, 161
- Phase
  - changes, 108
  - diagram, 103, 253
  - transformations; 6XXX alloys, 296
  - transformations in Al–Mg–Si alloys, 80
- Phase diagram, restrictions imposed by, 103
- Phases
  - $\alpha$ -AlFeSi, 79, 188, 257
  - AlCrMg, 85
  - AlFeSi, 78
  - Al<sub>2</sub>CuMg (S), rapid formation of, 233
  - Al<sub>2</sub>CuMg-based S phase, 82, 83, 90
  - Al<sub>6</sub>CuMg<sub>4</sub>-based T phase, 90
  - Al<sub>7</sub>Cu<sub>2</sub>Fe, 82
  - Al–MgZn<sub>2</sub>, 81
  - AlMnSi, 85
  - Al<sub>6</sub>Mn, 165
  - $\beta$ -AlFeSi, 79
  - $\beta$ -Mg<sub>5</sub>Al<sub>8</sub>, 74
  - CrAl<sub>7</sub>, 85
  - Cr<sub>2</sub>Mg<sub>3</sub>Al<sub>8</sub>, 82
  - CuAl<sub>2</sub> ( $\theta$ -phase), 71, 91
  - CuFeAl<sub>6</sub> + Cu<sub>2</sub>FeAl<sub>7</sub>, 71
  - (CuFeMn)Al<sub>6</sub>, 71
  - (CuFeMn)<sub>3</sub>Si<sub>2</sub>Al<sub>15</sub>, 71
  - CuMgAl<sub>2</sub> (S-phase), 71
  - CuMg<sub>4</sub>Al<sub>6</sub>, 71
  - Cu<sub>2</sub>Mg<sub>8</sub>Si<sub>6</sub>Al<sub>5</sub>, 71, 210
  - $\delta$ (AlLi), 86
  - $\delta'$ (Al<sub>3</sub>Li), 86
  - FeAl<sub>3</sub>, 69, 206
  - FeAl<sub>6</sub>, 69
  - (Fe,Mn)SiAl<sub>12</sub>, 72
  - Fe<sub>2</sub>SiAl<sub>8</sub>, 206
  - Fe<sub>2</sub>Si<sub>2</sub>Al<sub>9</sub>, 69
  - Fe<sub>3</sub>SiAl<sub>2</sub>, 69
  - Fe<sub>3</sub>Si<sub>2</sub>Al<sub>15</sub>, 206
  - M(AlMgZnCu), 91
  - Mg(Zn,Cu,Al)<sub>2</sub>, 82
  - MgZn<sub>2</sub>, 81
  - Mg<sub>2</sub>Si, 76, 253
  - Mg<sub>2</sub>Zn<sub>11</sub>, 81
  - Mg<sub>3</sub>Zn<sub>3</sub>Al<sub>2</sub>, 81
  - Mg<sub>5</sub>Al<sub>8</sub>, 81
  - MnAl<sub>6</sub>, 85
  - (Mn,Fe)Al<sub>6</sub>, 72
  - S(Al–Cu–Mg), 84
  - S(Al<sub>2</sub>CuMg), 91
  - S'(Al<sub>2</sub>CuMg), 90
  - T(AlMgZnCu), 91
  - T(Al–Zn–Mg–Cu), 84
  - T1(Al<sub>2</sub>CuLi), 90
  - ZrAl<sub>3</sub>, 82, 85
  - Zr<sub>2</sub>O<sub>3</sub>, 274
- Plastic flow, 112
- Platelets, 106
- Power exponents, 117
- Precipitation, 6, 105, 119
  - ageing precipitates, 85
  - C-curve nose, 109
  - copious in homogenization, 225
  - dissolution of precipitate, 107, 188
  - globules, 106
  - hardening, 73
  - of  $\theta$  phase, 172
  - precipitate dissolution, 107, 189
  - precipitate free zone (PFZ), 75, 165, 174, 210, 224, 228, 263

- precipitate size, 77
- precipitate spacing, 27
- reaction, 253
- secondary precipitates in homogenization, 227
- TTP curves, 120
- Predominantly recrystallized structure, 161
- Press effect, 196–8
- Press heat treatment cycle, 120
- Pressure and temperature analysis
  - base pressure, 36
  - conservation of energy, 40
  - control volumes, 55
  - deformation zone, 36, 177
  - deformation zone semiangle, 142
  - effect of section shape, 145
  - finite-element techniques, 37
  - Galerkin procedure, 39
  - heat conduction, 56
  - increment of peak pressures, 57, 143, 144
  - integral profile, 55, 58, 200
  - interface temperature, 56
  - kinematic compatibility, 37
  - lower bound, 29
  - m* value, 48
  - mesh dependency, 42
  - mesh topology, 40
  - modified Feltham strain rate, 36, 143
  - peak pressure, 140
  - plane strain upper-bound, 34
  - pressure, 29, 30, 140
  - relaxation of the hydrostatic stress, 37
  - rise in temperature due to friction
    - in the die land, 60
  - simple compression, 55
  - steady state, 63
  - steady state equation, 144
  - stiffness matrix, 39
  - upper-bound theorem, 31
  - work of extrusion, 55
- Pressure/displacement diagram, smoothed, 140
- Pressure weld, 15
- Principal strengthening agent in 6XXX, 253
- Probability and thermal activation, 112
- Process parameters and properties, 170–176
- Process/structure relationships, 156–60
- Product tolerance, 382
- Properties, 170
- Pseudo phase diagram for Mg<sub>2</sub>Si, 254
- Pyrometer, 347
- Quality, 340
- Quenching
  - extrusion ram speed and quenching, 191
  - forced air and quenching, 192
  - increase in solubility and quenching, 187
  - influence of Cr, Mn and Zr on quench sensitivity, 269
  - Mg<sub>2</sub>Si heterogeneous nucleation sites, 190
  - quench sensitivity, 84, 120, 267, 270
  - quenching directly, 77
  - successful, 189
  - ram speed and quenching, 192
  - reheating and quenching, 189
  - tensile strength and median cooling time, *t*, 267
  - thermal aspects of quenching, 194
  - thermal considerations, 191
  - TTP diagrams, 193
  - various quench media, 195
  - water and quenching, 192
- Radiation pyrometer, 347
- Ram speed, 241
- Ram speed reductions, 77

- Rate controlling, 113
- Rate equation, 116
- Rate of diffusion, 98
- Rate of homogenization, 65
- Recrystallization
  - and limit diagrams, 161, 242
  - and recovery, 114
  - during solution soak, 162, 173
  - fraction recrystallized,  $X_v$ , 118
  - grain boundary nucleated
    - reactions, 116
  - inhibited, 79, 85, 237, 269
  - kinetics, 114, 116
  - Mg-vacancy interactions, 167
  - particle count, 167
  - pinning forces, 167
  - pseudo-internal variable equation, 117
  - strain-free recrystallized grains, 113
  - structure, 227
  - subgrain and recrystallized grain size, 159
- Rectangular extrudes, 52
- Reduced corrosion resistance, 268
- Redundant deformation, 146
- Reheating, 188
- Relative motion, 137
- Relaxation time and diffusion, 66
- Residual substructure, 173
- Retention of substructure, 164, 249
- Roll correction, 371
- Rosettes, 105
  
- Scalp, 137
- Schematic limit diagram for 6063, 303
- Scrap
  - billet scrap between foundry and press, 376, 379
  - billet scrap in the press, 378
  - billet scrap on the press, 376
  - hot shear or saw scrap, 375
  - material scrap during die changes, 378
  - 'no scrap', 334
  - raw material scrap, 376
  - sawing scrap, 376
  - stretcher scrap, 303, 375
- Second phase particles, 174
- Secondary dendrite arm spacing and time, 103
- Segregated globular particles, 224
- Segregation, 6, 233
- Self-diffusion, 134
  - activation energy for, 65, 97
- Separate solution treatment, 80
- Sequence of operation, 8
- Severe cracking, 151
- Shape factor, 118, 16
- Short mandrel, 15
- Simulated texture, 302
- Snake-like undulations, 372
- Software-based control systems, number of, 344
- Solid solution dendritic, 74
- Solid solution strengthening, 84
- Solidification sequence of minor element additions, 92
- Solidus, 206
- Solubility limit, equilibrium solid, 105, 253
- Solute; concentration of, 65
- Solute elements, 171
- Solution soak; desired structure after, 159
- Solution treatment, 167
- Solution treatment and extrusion, 186
- Solutionizing anneal, 158
- Speciality alloys, 266
- Specific metallurgical data, 198
- Specific product of fixed dimensions, 248
- Speed limits for rod extrusions, 298
- Speed profile, 343
- Spheroidize, 72
- Standard stress concentration factors, 161
- State variables, 27, 116

- Statistical process control, 340
- Steady-state conditions, 243
- Stepped heating procedure, 237
- Strain hardening, 47
- Strain rate, 141, 275
- Stray lubricant, 311
- Stress corrosion, 81
- Stress corrosion cracking, 228
- Stress relief treatments, 74
- Stress relieving of stems, 374
- Stretching, 268
- Structure after extrusion, 160–6
- Subcutaneous regions of the billet, 136
- Subgrain boundary, 165
- Subgrain coalescence, 159, 206
- Subgrain size, 242  
variation in, 156
- Subgrains, bands of, 179
- Submicron particles, 75
- Substitutional solid solution  
strengthening, 74
- Substructural strengthening, 170
- Substructural considerations, 179–83
- Substructural correlations, 184
- Surface oxidation, 94
- Surface quality  
acceptable surface quality, 154  
avoidance of surface defect, 303  
blistering, 233, 307, 316  
blistering in a 6082 extrusion, 316  
capillarity-driven diffusion  
processes, 287  
coarse-grain outer zone, 20  
combined tensile and melting  
failure, 249  
cavitation, 286  
continuous ‘virgin’ surface, 274  
cracking, 233  
cracking susceptibility, 251  
critical temperature for ‘pick-up’,  
260, 300  
debris, 277  
die design streaks, 319  
die lines, 152, 272, 278, 279  
division between acceptable/poor  
surfaces, 154  
dual pick-up mechanisms, 277  
effects of temperature on surface  
finish, 280  
elongated iron phase, 285  
evidence of division between  
acceptable/poor surfaces, 153  
extrusion defect streaks, 319  
fine score lines, 285  
fragmented iron phase particles,  
286  
fragments, 275  
fragments of larger precipitates,  
286  
grainy surface, 320  
hot cracking in alloy AA7150, 248  
in the extrudate, 151  
increase of iron phase fragments,  
290  
ingot structure streaking, 318  
ironing of the particles, 276  
low billet temperature, 298  
melting failure mode, 250  
metallurgical reactions and speed,  
299  
micro-die lines, 285, 288  
origin of spheroidal particles, 288  
pick-up, 79, 272, 274  
deposit, 275  
extrusion temperature, 275  
formation, 275  
peak, 300  
pure tensile failure, 249  
quality of the section surface, 343  
quantifying excessive pick-up, 278  
rapid transformation; fragmented  
precipitates, 287  
region of local weakness, 273  
run-out table ‘bridge up’, 372  
spall, 275, 298, 276  
spangle, 320  
shear and rolling type texture, 302

- surface features, 274
- surface finish, 279
- surface roughness, 281
- surface scoring, 151
- unacceptable surface quality, 153
- valleys of the die surface, 281
- Syalon, 274
  
- T5 and T6 strength, 173
- Temperature gradient for the billet, 349
- Temperature range, 226
- Temperature rise, 184
- Temperature-compensated strain rate, 151, 278
- Temperature measurement using infrared pyrometers, 347
- Texture developments, 127
  - modern extrusion plant, 323
- Theoretical productivities, 248
- Thermal activation, 109, 112
- Thermal softening, 47
- Thermomechanical balance, 37
- Thermomechanical process (TMP), 6
- Thermomechanical variables, 343
- Time/cycle diagram, 17
- Toughness, 78, 85, 270
- Transgranular, 173
- Transgranular dimpled rupture, 174
- Transient sticking, 277
- Transport of atoms, 96
- Typical dead metal zone, 138
  
- Underageing, 270
- Undesirable features, 197
- Uniformly dispersed Mg<sub>2</sub>Si, 77
- Unlubricated extrusion, 47, 136
- Unstable aluminium film, 281
  
- Vacancies, 7, 97, 113, 172
  - equilibrium number of, 109
- Vacancy diffusion, 135
- Variations in properties of Al–0.5Mg–0.65Si alloy, 191
- Velocity and temperature, 200
- Virtual work principle, 38
- Volatile lubricants, 316
- Volume% recrystallized, 165, 249
  
- Workability, 93
- Weld strengths, 313
- Welding response, 72
- Work hardening, 135
- Work softening, 135
- Wrought product, 6
  
- Yield criteria
  - hydrostatic stresses, 24
  - invariants, 24
  - Tresca, 26
  - Von Karman, 24
  - Von Mises criteria, 26
- Yield; definition of, 379
  - improvements in, 385
  
- Zener and Hollomon, 127
- Zener–Hollomon equation, 28
- Zirconium, 6, 237, 269